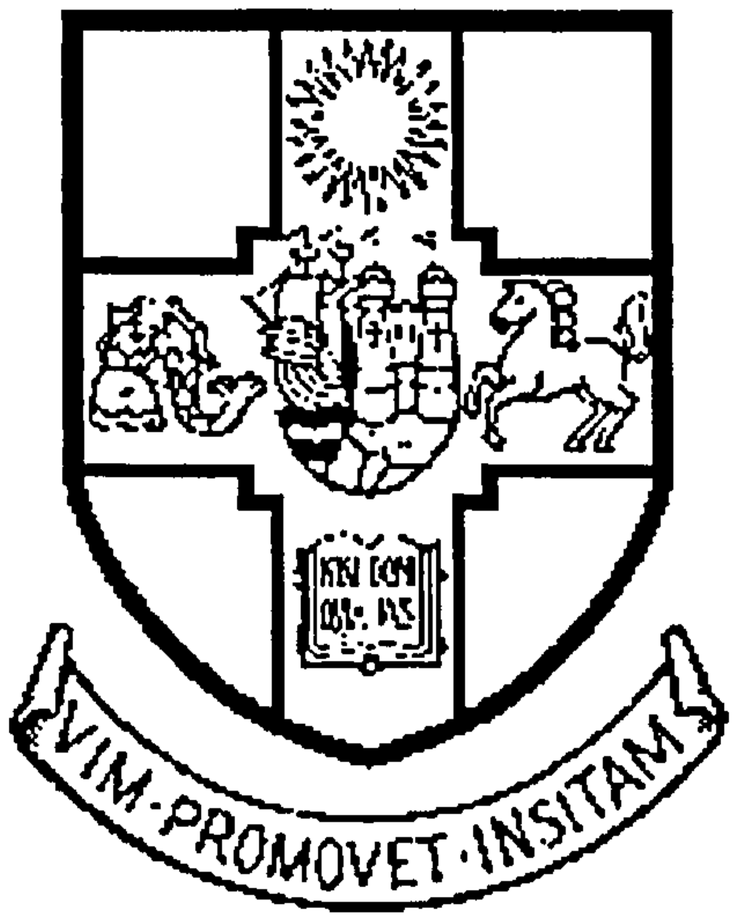

Pulse tests in soil samples

by

Marcos Arroyo

A dissertation submitted to the University of Bristol in accordance with the requirements of the degree of Doctor of Philosophy in the Faculty of Engineering, Department of Civil Engineering

November 2001

Abstract

This thesis contains analytical, numerical and experimental results concerning the measurement of elastic moduli of soils using pulse tests in laboratory samples. Particular emphasis is placed on the most frequently adopted configuration: bender-element transducers and propagation along the axis of cylindrical samples.

Arrival time selection in the received pulse is generally perceived as problematic and near field effects often quoted as the main cause of error. A bench test experiment with a progressively shortened sample of reconstituted Gault clay is performed to clarify the extent of the problem and test the near field hypothesis. The results reveal that current procedures are compatible with an uncertainty in moduli of circa 100% of the mean estimated value. Use of a non-dispersive propagation model is identified as the main conceptual error. New signal-independent criteria are developed to avoid near field effects. Their application to the bench test results reveals that this is not the cause of the observed dispersion. Material dispersion effects due to Biot-like fluid interaction are then examined, showing their irrelevance in the Gault case and giving clear relevance criteria for the general case. A transfer function approach is developed to deal with interference caused by end rebounds and bender length. A waveguide model of the effect of lateral boundaries is also developed. Both models are able to explain recurrent features of the recorded traces. Multimodal propagation is ill suited for measurement purposes but material constraints and transducer characteristics make it very likely for most current test configurations.

The effect of elastic anisotropy is also considered. An algebraic approach is used to show that all types of elastic anisotropy are possible in soils. The characteristics of anisotropic or directional dispersive propagation are illustrated with soil results. It is also shown that measured anisotropy does not support the assumption of elliptical wavefronts.

Dedication and Acknowledgements

This thesis is dedicated to the memory of Angel Uriel, who taught me.

This work was started thanks to a Needham Cooper Scholarship, granted to the author by the Department of Civil Engineering, University of Bristol. Later on the Fundación Entrecanales joined forces, granting one of its Beca Entrecanales to me for three consecutive years . Thanks are given to both institutions, to Mrs. Joyce Needham Cooper and to Professor Santiago Uriel.

David Muir Wood has been my advisor. I am still amazed by his ability to hear attentively my ranting, his patience with my zig-zagging track, his intelligent suggestions, his skilful steering. He has been vitally helpful.

Dr. Paul Greening performed the bench test series described in Chapter 3. Not only this, he became more and more of a confident as the data begun to unwield its significance. That was a role also played by my friend, Dr. Mohammed Rouainia, particularly during his time at the Department.

This work has benefited from numerous discussions with staff and colleagues in the Department of Civil Engineering. David Nash and Mike Pope dispelled my previous suspicions about the hidden dangers of laboratories. Martin Lings was helpful in many discussions about bender testing and anisotropy. Matt Dietz, Benson Hsiung and Aime Harrison, my geotechnical colleagues, have been particularly close. I am grateful to all of them and to many others working in the Department who, as a last favour, will forgive me for not listing them here.

Outside the Department I was helped in my research by discussions with Manolo Pastor, Stuart Crampin, Dimitrios Kolymbas, Roberto Nova, Andrés Saenz and Francisco Montero de Espinosa. Dr. Bruce Drinkwater facilitated his copy of Disperse. Dr Reiko Kuwano sent me her data files. Dr. Sebastiano Foti sent me a copy of his thesis. Professor H. Peregrine was fundamental by his teaching and amiable responses to my pedestrian enquiries in opening my eyes to some very basic aspects of elastodynamic problems. I am grateful to them all.

Too many persons have helped me through these years. My friends in Spain and Bristol. My family, my brother, my sister, my patient and loving parents. I am grateful to you all. It has been great.

Declaration

I declare that the work in this dissertation was carried out in accordance with the regulations of the University of Bristol. The work is original except where indicated by special reference in the text and no part of the dissertation has been submitted for any other degree.

Any views expressed in the dissertation are those of the author and in no way represent those of the University of Bristol.

The dissertation has not been presented to any other university for examination either in the United Kingdom of overseas.

Signed: 

Marcos Afroyo

Date: 10-11-2001

Contents

List of symbols and abbreviations

Symbols are also defined when introduced in the text. The following list presents only the most recurrent symbols and abbreviations used in this dissertation, with indication of their meaning -or meanings, if they have various in different sections of the text. In general bold characters –e.g. **u**, **Γ**- are used to represent multidimensional quantities i.e. vectors or tensors. Einstein convention is followed and, except where otherwise indicated, repeated indexes imply sum along the index range.

b	forcing vector at an isolated source
c	phase velocity vector
$\mathbf{D_0}$	elastic stiffness tensor
D_{ij}	generic elastic moduli
D	damping ratio
d	diameter
E	Young's modulus
e	void ratio
f	frequency
f	body force vector
GR	Green tensor
G	isotropic shear modulus
H	sample height
i	imaginary unit
k, **k**	wavenumber, wave vector
K_0	absolute permeability
L	transducer length
n	number, porosity
p	normalised slowness vector
p	mean stress
q	slowness vector
r	radius
r	spherical position vector
SWA	shear wave anisotropy
T	period, transducer thickness
t	time
u, **u**	displacement, displacement vector
v	phase velocity
v_g	group velocity
$\mathrm{v_S}$	isotropic bulk shear velocity
$\mathrm{v_P}$	isotropic bulk compressive velocity
x, **x**	position, position vector
α	attenuation coefficient

δ	Dirac's delta, Thomsem's anisotropic parameter
δ_{ij}	Kronecker's delta
Δ	increment
ε	Thomsem anisotropic parameter
ε	strain tensor
γ	Thomsem anisotropic parameter
η	kinematic viscosity
λ	Lamé coefficient, wavelength
Γ	Kelvin-Christoffel or acoustic tensor
μ	Lamé coefficient, viscosity
ν	Poisson ratio
Θ	phase function
θ	phase angle
ρ	density
σ	stress tensor
τ_α	tortuosity
Ψ	transfer function phase
ω	angular frequency

Subscripts

ap	apparent
CS	cross spectrum
cut	cut-off
H	relative to sample height
i	imaginary part of a complex quantity
LB	relative to bender length
max	maximum
min	minimum
mn	modal index
p	related to P-waves
r	real part of a complex quantity
s	related to S-waves
t	time derivative
SR	spectral ratio
x	space derivative

List of tables

List of figures

1 INTRODUCTION

"Elasticity, gravity, cohesion of parts, communication of motion by impulse; these are probably the ultimate causes and principles we shall ever discover in nature; and we may esteem ourselves sufficiently happy if , by accurate enquiry and reasoning, we can trace the particular phaenomena to, or near to, these general principles. The most perfect philosophy of the natural kind only staves off our ignorance a little longer: As perhaps the most perfect philosophy of the moral or metaphysical kind serves only to discover larger portions of our ignorance."

David Hume "*An enquiry concerning human understanding*"

1.1 MOTIVATION AND OVERVIEW

1.1.1 The small strain stiffness of soils

Perhaps the main developments in soil testing during the last twenty years have been those related to laboratory stiffness determination. The development of local measurement systems (e. g. Jardine et al. 1984) was crucial in achieving a much-improved picture of soil stiffness. Around 1980 laboratory equipment was only measuring strains bigger than 0.1% Resolution has been increased now by nearly three orders of magnitude (Lo Presti et al. 1999). Figure 1-1 illustrates how this affects test results.

As a consequence of this improved resolution, it was soon appreciated (Burland, 1989) that the higher stiffness values thus obtained in static tests were similar to those obtained in dynamic tests. The traditional distinction between dynamic and static stiffness disappeared and was substituted by another picture, by now already traditional -Figure 1-2. In this picture dynamic and static measurements are shown to collaborate in the determination of a unique, highly non-linear, strain-dependent, soil stiffness.

Another element of this picture is a certain threshold value beyond which the strain dependency of stiffness begins. This is easily identified with an elastic limit, and therefore the stiffness values measured before that threshold are identified as elastic moduli. As elastic moduli have been used generously as fitting parameters in soil mechanics literature, it has been customary to identify those threshold values adding some suffix to the elastic parameter being discussed. Here we partly follow the notation of Pennington (1999) and a 0 is employed, writing $\mathbf{D}_0$ when referring to the stiffness tensor of a general elastic material. However, we will generally drop the suffix when referring to specific moduli, writing for instance, G and E for the shear and Young modulus of an isotropic material;

The elastic $\mathbf{D}_0$ properties are far from being constants for any particular soil. They are best thought of as state functions, depending on state variables such as stress state and void ratio. During the last decade extensive research programmes have been carried on world-wide on different soils to measure them under a variety of conditions-see the symposia proceedings of Sapporo'94 (Shibuya et al. 1995) or Torino'99 (Jamiolkowski et al. 1999)-.

There are various reasons to justify this interest. First, it has been shown repeatedly (e.g. Burland 1989) that deformation analyses of geotechnical structures under monotonic loading require an accurate description of soil stiffness to be successful. The elastic $\mathbf{D_0}$ properties are a basic element in such a description. Secondly, if the elastic properties result from a complex function of state, inverting this function is one possible mean to infer state properties. This is particularly useful in the field where elastic measurements are relatively common, cheap and quick to perform, (for an application to obtain stress state, see Fioravante et al. 1998). Finally, a thorough understanding of state evolution is needed to formulate soil behaviour under complex loading paths, and measurement of elastic properties offers one plausible way to achieve that purpose.

One important result of this research has been (Stokoe et al. 1995, Pennington 1999) the recognition that in most cases the elastic properties show directional dependency or, in other words, that they are anisotropic. Widespread recognition of anisotropy in $\mathbf{D_0}$ is still relatively recent[1]. Measurement procedures developed under the assumption of elastic isotropy have been applied to recover anisotropic elastic constants without too much worrying about their appropriateness. In this thesis we will address this issue with a double objective in mind: as a necessary step to assess the evidence so far produced and as guidance to future experimental research. Regarding this last reason the ongoing geotechnical research programme at Bristol has been a particularly strong stimulus.

1.1.2 Stiffness measurements & pulse tests

The laboratory techniques now available to measure $\mathbf{D_0}$ are quite diverse (see Lo Presti et al. 1999). Basically, though, a substantial division can still be made between static and dynamic procedures. Dynamic procedures are those where inertia effects are explicitly taken into account to interpret the test results. Static procedures are those where inertia effects are disregarded. Although this definition is clear enough, two shades are worth adding. First, this excludes cyclic static tests (e.g. cyclic simple shear, cyclic triaxial) from the dynamic realm, as, due to the relatively low frequency of the applied load, they are interpreted without inertia effects. Second, it is possible -and indeed advantageous, as shown by recent research: Kuwano, 1999; Pennington, 1999- to use simultaneously static and dynamic procedures to measure $\mathbf{D_0}$ in soils.

Notwithstanding this, there is now a strong presumption that one particular kind of technique is due to play a major role in the future practice of soil testing. This technique is laboratory pulse testing, a particular type of dynamic procedure. Although other configurations are possible, the recent surge in popularity of these tests is built on the incorporation of piezoelectric transducers in standard static testing devices. Indeed, in his recent (2000) Rankine lecture, Atkinson signalled how both their usefulness and relative simplicity are quickly driving those tests into the realm of routine laboratory practice.

1Anisotropy might be seen as a second order modification of an isotropic property. Obviously, a sharper instrument will be more likely to detect anisotropy than a blunter one. It is then reasonable for older stiffness measurements to obtain an isotropic picture of elastic properties (e.g. Rowe, 1971)

It is also reasonable to suspect that laboratory pulse tests will be of some importance for geotechnical research. First, most of the research programmes on D_0 we have just alluded to use them already to a certain degree. Second, the relative robustness of piezoelectric transducers and perceived simplicity of pulse tests have made them very strong candidates for more complicated endeavours. For instance, of all the dynamic procedures employed in soils, only pulse tests have been used so far to measure elastic properties under the assumption of anisotropy.

This brilliant perspective does not mean, however, that there are no problems regarding either the performance or interpretation of laboratory pulse tests. This can be illustrated by reference to recent work at Imperial College: Figure 1-3 shows pulse test measurements by Kuwano (1999) on Ham River sand. Later on we will consider the possible meaning of these results, here it is enough to note that Jardine et al. (1999) felt compelled to abandon continuum-based models to explain them.

1.1.3 Thesis overview

In this thesis we share Atkinson's view about the central role that laboratory pulse tests will play in soil mechanics, therefore their present limitations and future possibilities are one of its major themes. The other theme, intertwined with the first, is that of elastic anisotropy, its measurement and importance for soil modelling purposes. Our approach will be mostly based on the theory of elastic wave propagation or elastodynamics. This deserves some comment.

Elastodynamics is a vast, long-researched subject (e.g. Achenbach, 1973, Graff, 1975). This theory forms the basis of nearby subjects such as seismology (e.g. Aki & Richards, 1980, Sheriff & Geldart, 1982, Udías, 2000) or ultrasonic testing of non-soil materials (e.g. Mason, 1958, Krautkramer & Krautkramer, 1990). Within the geotechnical literature the situation is somehow blurred for historical reasons.

Between approximately forty and ten years ago[2], the situation was clear: there were static properties, measured by static methods for static problems and there were dynamic properties, measured by dynamic methods for dynamic problems. Accordingly, a substantial corpus of dynamic and static soil research was conducted along different paths. Bluntly speaking, two communities grew side by side looking at the same object from differing viewpoints. As usually happens in these cases, they developed different conventions, worries and priorities; in short, they developed differing languages.

Although the divide between static and dynamic soil properties has fallen, the methodological barrier seems to still have some hold over the minds. This is manifest in the differing roles of elastic theory in both fields. Elasticity was and still is central to soil dynamics literature (e.g. Kramer 1996) but was generally regarded as of marginal interest for those involved in static problems (Wood, 1990), occupied by the modelling challenges of irrecoverable behaviour. There is even a tendency in current mechanical

---

[2]This is arbitrary, of course. But, on one hand, it seems reasonable to place the onset of the separation with the development of the resonant column test to measure "dynamic" stiffness (e.g. Hardin & Richart, 1963). On the other hand, the XI European Conference on Soil Mechanics held at Florence in 1991 might well be chosen to mark the end of this separation, at least for the geotechnical community at large (Uriel, 1992).

theories of soil behaviour to dismiss from the onset the possibility of elastic behaviour –e.g. hypoplasticity, Kolymbas 1989.

In the case of laboratory pulse tests this dubious theoretical status has been compounded with a certain lack of familiarity with dynamic problems. As we have said, laboratory pulse tests act, in most cases, as an extra measuring tool within some traditionally "static" instrument. Physically they represent a small modification to an otherwise familiar apparatus that is still performing its job. They are dynamic intruders in a static world. It should come then as no surprise that their theoretical treatment has been scarce and their interpretation more often than not based on rather sketchy models. This might be opposed to the situation of field pulse tests, a traditionally "dynamic" method, where the interpretative elastic-based models have reached a considerable degree of refinement –e.g. Foti, 2000.

It is our purpose here to fill, at least partially, this gap. This reliance on elastodynamics then makes it necessary to include some of its results. This is made in a stepwise manner, exposing the concepts as needed. We begin in this chapter, recalling the basic elements of elastodynamics and wave motion, making some emphasis on the different vestments of the superposition principle. The chapter ends with an exposition of plane elastic waves, with particular consideration of the isotropic case.

Isotropy is much simpler than anisotropy; however, we will see that, even within the restrictions imposed by isotropy, there is scope for some important interpretative issues regarding pulse tests. For expositive purposes it is thus very convenient to address first the subject within an isotropic context and leave the introduction of anisotropy for a second stage. There is also another reason for this two-step approach. As Chapter 2 will show, isotropic elasticity has been and still is the framework of most pulse test interpretation in soils. This is not due to some generalised forgetfulness about anisotropy but rather due to the limited scope of most equipment: if a property is measured just in one direction it is pretty much useless to wonder about some theoretical directional dependence.

The second chapter, therefore, will examine the current practice of pulse testing in soils, while exposing from a rather general viewpoint the material constraints that lie beneath this practice. One of them –fluid coupling- has made shear waves the tool of choice in most cases. Chapter 3 will describe a bench shear pulse test series on Gault clay whose results will be used to illustrate the limitations of the simpler interpretative models commonly adopted. Chapter 4 will introduce the concept of dispersion, which provides a very natural framework for most subsequent discussions. This will be shown there by reference to near field effects, an issue that has been recurrently discussed in the literature. Chapter 5 will address material dispersion due to viscous effects and the bi-phasic nature of soil. On Chapter 6 geometric dispersion will be addressed. All this will be made within the assumption of isotropy and focusing on shear wave measurements.

Soil anisotropy is a subject where the discussion can quickly become tangled. Chapter 7 will introduce a framework that will hopefully help to avoid some traps, and this will be illustrated with a brief excursion

into static measurements. The discussion there will also dwell on the justification and limitations of the elastic approach employed so far. Chapter 8 will then go back to dynamics, discussing anisotropic dispersion. Chapter 9 will finally recapitulate and offer some advice for future work. The appendixes contain either additional background information –I and II- or some lateral developments of the main discussion –III and IV.

1.2 BASIC CONCEPTS

1.2.1 Elasticity and elastodynamics

1.2.1.1 Stress-strain relations

Until further notice the results and concepts of elastic theory employed in this thesis will be based on the following three basic assumptions:

- The appropriate measure of deformation is the small strain deformation tensor, **ε**. This is related to the derivatives of the displacement vector, **u**, by the following linear relationship –where the familiar and compact comma notation is introduced for spatial derivatives

$$\boldsymbol{\varepsilon}_{ij} = \frac{1}{2}\left[\frac{\partial u_i}{\partial x_j} + \frac{\partial u_j}{\partial x_i}\right] = \frac{1}{2}\left[u_{i,j} + u_{j,i}\right] \qquad (1)$$

- Linearity is also predicated of the relation linking stress and strain, written by means of a fourth order stiffness tensor, $\mathbf{D_0}$, as

$$\boldsymbol{\sigma}_{kl} = \mathbf{D}_{0klij}\boldsymbol{\varepsilon}_{ij} \qquad (2)$$

- The stiffness tensor $\mathbf{D_0}$ has the following symmetries

$$\mathbf{D}_{0klji} = \mathbf{D}_{0klij} \quad \mathbf{D}_{0lkij} = \mathbf{D}_{0klij} \quad \mathbf{D}_{0ijkl} = \mathbf{D}_{0klij} \qquad (3)$$

The assumed symmetries of $\mathbf{D_0}$ imply that, at most, only 21 components are different. This allows the stress-strain relation (2) to be rewritten using a 6x6 symmetric matrix to represent the stiffness tensor and 6x1 vectors to represent stress and strain. This is sometimes convenient and is written using a convention carrying the name of Voigt:

$$\begin{Bmatrix} \sigma_{11} \\ \sigma_{22} \\ \sigma_{33} \\ \sigma_{23} \\ \sigma_{31} \\ \sigma_{12} \end{Bmatrix} = \begin{bmatrix} \mathrm{D}_{11} & \mathrm{D}_{12} & .. & .. & .. & \mathrm{D}_{16} \\ \mathrm{D}_{12} & \mathrm{D}_{22} & & & & \\ .. & & .. & & & \\ .. & & & .. & & \\ .. & & & & .. & \\ \mathrm{D}_{16} & & & & & \mathrm{D}_{66} \end{bmatrix} \begin{Bmatrix} \varepsilon_{11} \\ \varepsilon_{22} \\ \varepsilon_{33} \\ \varepsilon_{23} \\ \varepsilon_{31} \\ \varepsilon_{12} \end{Bmatrix} \qquad (4)$$

The number of independent components in $\mathbf{D_0}$ is further reduced when account is taken of the material symmetries. Chapter 7 will address this issue in some detail. Here we will just state that for the case of an isotropic material there are only two independent components and $\mathbf{D_0}$ takes the following form

$$D_{0ijkl} = \lambda\delta_{ij}\delta_{kl} + \mu\left(\delta_{ik}\delta_{jl} + \delta_{il}\delta_{kj}\right) \tag{5}$$

Where δ stands for the usual Kronecker symbol and λ and μ are Lamé's coefficients, whose relationships with other currently used moduli are collected in Table 1-1.

1.2.1.2 Dynamic equilibrium

From Newton's second law and the elastic constitutive relation (2) the basic differential equation of dynamic equilibrium follows –Udías, 2000- as

$$\rho\ddot{u}_m = f_m + D_{0mnpq}u_{p,qn} \tag{6}$$

These are three linear partial differential equations on u_m, where f_m and u_m stand, respectively, for the components of the force field and displacement vectors. Note that the absence of any forcing or loading term in the equation will make it valid only away from any such source of movement. In that case only movement propagation is dealt with, and not its generation. Substitution of (5) into (6) leads to the corresponding expression for homogeneous isotropic materials

$$\begin{aligned}\rho\ddot{u}_m &= f_m + (\lambda+\mu)u_{k,km} + \mu u_{m,kk} \\ &= f_m + (\lambda+\mu)\nabla(\nabla\cdot\mathbf{u}) + \mu\nabla^2\mathbf{u}\end{aligned} \tag{7}$$

From the second expression above and using Helmholtz potentials it can be shown–e.g. Bedford & Drumheller, 1994- that dilatational movement is uncoupled from shear movement. This result is only valid for isotropic solids and we will recover it later in a different guise. Now it is preferable to take a step back and introduce a different approach to our problem.

1.2.2 Linear systems

1.2.2.1 Superposition: unit response and transfer functions

Linearity is a requisite for superposition, and superposition is the basic tool to obtain solutions to linear problems. The idea is to build solutions to complex problems as linear combinations of solutions to simpler ones, something that is pretty intuitive when considering spatial dimensions and a little bit less so for the time dimension. Superposition in time, fundamental in dynamic problems, is presented in different ways in different contexts. In experimentally oriented work (e.g. Ewins, 2000, Doyle, 1989), there is a preference for the concepts of linear systems theory like transfer functions. On the other hand, theoretically oriented work (e.g. Graff, 1975, Aki & Richards, 1980) uses a more mathematical approach based in concepts like Green functions or fundamental solutions. In our case both approaches are useful and it is convenient to appreciate their relations.

From the abstract viewpoint of linear systems theory –e.g. Lynn, 1989- any dynamical process might be characterised by its time dependent inputs and outputs. In a linear system the response to a unit impulse is given by the unit response function h(t), a system characteristic. The role of this function can be clarified by reference to a simple, one-dimensional, linear system. Figure 1-4, taken from Brigham (1988) is helpful for this purpose. The response of the linear system to a unit impulse is given by h(t). The

response to a series of impulses acting at times τ0, τ1, τ2, is obtained by superposing responses shaped by h(t), but shifted in time and with amplitude proportional to that of the impulse. This process could be extended to a continuous input x(t) obtaining the corresponding response, y(t), as a convolution[3] of this input and the unit response function h(t). Thus the behaviour of a one-dimensional dynamical system can be concisely expressed as

$$y(t) = h(t) * x(t) \tag{8}$$

As explained in Appendix I, a time domain function might be alternatively represented in frequency domain by its Fourier transform. The frequency domain representation of the unit response function is known as its transfer function, H(f). In frequency domain convolution is a much simpler operation because it reduces to multiplication, and the behaviour of a one-dimensional dynamical system is expressed by

$$Y(f) = H(f) \cdot X(f) \tag{9}$$

Frequency domain representations are generally complex. Expressing them in polar form, the previous equation brings out the following amplitude and phase relations,

$$\begin{aligned} |Y| &= |H||X| \\ \theta_Y &= \theta_H + \theta_X \end{aligned} \tag{10}$$

The main attraction of this abstract approach is that it might be equally applied to very different elements involved in the measuring process: hardware like the transducers or software like a smoothing filter operator applied to the output signal. It is then very helpful to see the whole measuring process as a series combination of linear subsystems and an example of this with laboratory pulse tests in mind is shown in Figure 1-5. The global transfer function will be product of all the partial subsystem transfer functions, whose contributions might be separately studied.

From this viewpoint the role of elastodynamics is to provide a transfer function for the elastic subsystem – for instance the soil sample in Figure 1-5. In fact, the decomposition idea might be also applied to the elastic subsystem, separating, for instance source and various path effects as it is commonly done in exploration geophysics –Sheriff & Geldart, 1982. Accordingly, various elastodynamic and phenomenological models might be employed together according to the purpose of the modelling exercise and/or the characteristics of the measuring system.

Elastodynamic transfer functions might then take different forms. In some cases they will relate the input force history at some point and the output displacement history at some other point; in other cases the sought output will be the velocity or acceleration history[4]. Yet in other circumstances the needed transfer

---

[3] This concept is explained in Appendix I.

[4] In experimental vibration analysis these varied possibilities have brought a specific nomenclature for each transfer function: if the output is displacement receptance, if the output is velocity it is called mobility and accelerance if the output is acceleration (Ewins, 2000).

function should relate the recorded displacements of two points –that is the case, for instance, in many seismological applications.

1.2.2.2 Spectral analysis

Based on superposition, harmonic or spectral analysis is a very useful tool to obtain transfer functions for all kind of linear systems. The idea is to solve the problem for a single harmonic time dependency and then use the frequency as parameter to synthesise the total response. That is, for a single time-harmonic input we have a frequency dependent output, with identical harmonic time dependence

$$\exp(i\omega t) \xrightarrow{S} r(\omega)\exp(i\omega t) \tag{11}$$

The frequency dependent coefficient, r(ω), is the transfer function of the system. To see that, consider an input where all the frequencies are equally represented and sum their corresponding responses

$$\int_{-\infty}^{\infty} \exp(i\omega t)\, d\omega \xrightarrow{S} \int_{-\infty}^{\infty} r(\omega)\exp(i\omega t)\, d\omega \tag{12}$$

Using the Fourier transform definition given in Appendix I the input –left hand- represents a unit impulse, consequently the output –right hand- is the unit response function and r(ω) its Fourier transform or transfer function. A general input-output relation will be obtained introducing the input Fourier transform, say a(ω), within the integral sign.

In the elastodynamic case this approach is also valid but two extensions are needed. The first one is to consider input and output as vectors; each force component –for instance- will generally induce movement in three directions. This generalisation can be dealt with using some matricial housekeeping and presents no further problem. A more fundamental question is posed by the extra required generalisation: spatial dependency. The elastodynamic transfer function is generally a double function of position: the input and output locations are not indifferent. This can be appreciated by reference to the scheme in Figure 1-6, representing a cantilevered plate with some load history acting at $\mathbf{x_0}$. It is pretty intuitive that the response –say, displacement- recorded at point **x** near the loaded corner will be different from that recorded at **y**, near the free corner. Hence, in analogy to (11) above we will now write

$$\exp(i\omega t) \xrightarrow{S} r_{pq}(\omega, \mathbf{x}, \mathbf{x_0})\exp(i\omega t) \tag{13}$$

The subindex indicate that this is a matricial transfer function relating the q-input component with the p-output component. This expression naturally brings about the question of how can this spatial dependency of the transfer function be established. Postponing briefly the answer to that question, it is now more interesting to write the complex transfer function in exponential form, to give

$$\exp(i\omega t) \xrightarrow{S} A_{pq}(\omega, \mathbf{x}, \mathbf{x_0})\exp\left(i\left(\omega t - \Psi_{pq}(\omega, \mathbf{x}, \mathbf{x_0})\right)\right) \tag{14}$$

If the output is considered as a function of space and time, the right hand side can be seen as describing some kind of motion, with the frequency as parameter. There is a specific nomenclature readily available to describe this type of motion and its introduction is the subject of next section.

1.2.3 Wave motion

1.2.3.1 Definitions

A wave is a concept with strong intuitive appeal and no all-encompassing definition –Witham, 1974. For our purposes the following expression of harmonic waves is general enough

$$u(\mathbf{x},t) = a(\mathbf{x})\cos\left[\Theta(\mathbf{x},t)\right] = \mathrm{Re}\left\{a(\mathbf{x})\exp\left[i\Theta(\mathbf{x},t)\right]\right\} \tag{15}$$

There are considerable notational and operational advantages in using the complex exponential version, and that will be favoured throughout, with the implicit understanding that the real part is being considered. In the preceding expression a represents the amplitude of the movement whose space dependency allows for possible attenuation. The phase function is represented by Θ and holds the information about the periodic nature of the harmonic wave motion.

For any given time, t_0, all the points $\mathbf{x}$ where Θ has the same value form a surface of constant phase, $W(\mathbf{x})$, which is called a wavefront. Measured in radians per unit time, the angular frequency, ω, is defined as the time derivative of the phase function. The wave vector, $\mathbf{k}$, is defined as minus the spatial gradient of the phase function,

$$\begin{aligned} \omega(\mathbf{x},t) &= \dot{\Theta} \\ \mathbf{k}(\mathbf{x},t) &= -\nabla_{\mathbf{x}}\Theta \end{aligned} \tag{16}$$

Differentiating the constant phase condition a phase velocity vector, $\mathbf{c}$, parallel to the wave vector can also be defined

$$\dot{\Theta}dt + \nabla_{\mathbf{x}}\Theta\,\mathbf{dx} = 0 \Rightarrow \omega = \mathbf{k}\frac{\mathbf{dx}}{dt} = \mathbf{k}\,\mathbf{c} \tag{17}$$

Thus defined, the phase velocity vector is immediately identifiable with the wavefront velocity along its normal. The modulus of $\mathbf{k}$, k, is called wavenumber and the modulus of $\mathbf{c}$ is the phase velocity v. From (17) the following basic relation between angular frequency, wavenumber and phase velocity results

$$\omega = kv \tag{18}$$

The wavenumber has, consequently, units of radians per unit length and an equivalent expression can be written eliminating the radians and introducing the frequency f and wavelength λ,

$$\lambda f = v \tag{19}$$

These relations are familiar but it should be noted that, although not explicitly indicated in the last equations, all the quantities involved are generally functions of time and position, i.e. they have only local meaning.

There are a number of other vectors parallel to **k** that are found to be useful within the theory. They are the slowness vector **q** and the normalised slowness vector, **p**. The relations between them are the following:

$$\mathbf{k} = \omega \mathbf{q} = \frac{\omega}{v}\mathbf{p} = \frac{\omega}{v^2}\mathbf{c}$$
$$\|q\| = \frac{1}{v} \quad \|p\| = 1 \quad \|c\| = v \tag{20}$$

The slowness vector modulus is just the inverse of the corresponding phase velocity. The normalised slowness has unit modulus, i.e. the normalised slowness is the unit vector normal to the wavefront.

1.2.3.2 Wave motion and transfer functions

Comparing now equations (14) and (15) it is apparent that for any fixed harmonic input –i.e. fixed $\mathbf{x}_0$ and ω-, the output of an elastodynamic system is a frequency dependent harmonic wave. To be more precise, the complete output may comprise up to three different waves for each q-component of the input. If we consider a fixed input location the explicit reference to $\mathbf{x}_0$ is unnecessary, and the wavefront at time t_0, wave vector and phase velocity vector can be written in terms of a given transfer function phase

$$W(\omega, \mathbf{x}) = \frac{\Psi(\omega, \mathbf{x})}{\omega} = t_0$$
$$\mathbf{k}(\omega, \mathbf{x}) = \nabla_{\mathbf{x}} \Psi(\omega, \mathbf{x}) \tag{21}$$
$$\mathbf{c} = \frac{\omega}{\nabla_{\mathbf{x}} \Psi(\omega, \mathbf{x})}$$

This allows the interpretation of any measured transfer function in terms of wave properties. One advantage of using this wave nomenclature in elastodynamics is that it suggests analogies with other wave phenomena: mechanical –e.g. fluids- or non-mechanical –e.g. optics. Another is that in many circumstances the simplest approach to obtain an elastodynamic transfer function relating the movement at two points is to assume that it is transported by some specific wave motion –attenuation and wavefront shape. A simple and useful example of that is provided by harmonic plane waves.

1.2.3.3 Plane waves

Plane waves are characterised by a plane wavefront, something illustrated schematically in Figure 1-8. In this case the phase function of the harmonic wave has a rather simple expression

$$\Theta = \omega t - \mathbf{k} \cdot \mathbf{x} \tag{22}$$

In this case the wave vector, **k**, is independent of position although it may be dependent on frequency. Attenuation might be included allowing for a complex wave vector. If interest is focused on a single direction, plane wave propagation becomes a 1-D spatial problem as all that matters is what happens along the direction indicated by **p**. Using a Cartesian frame including **p**, the wave vector has only one component which coincides with the wavenumber, the one-dimensional nature of the movement is then clear and we can write the wave-induced transfer function relating movements at two points as

$$r(\omega,x)=\exp\left(-i(k_r(\omega)x+ik_i(\omega)x)\right)=e^{-i\bar{k}x} \tag{23}$$

The space dependent output corresponding to an arbitrary input of frequency domain expression $a(\omega)$, is then given by

$$u(x,t)=\frac{1}{2\pi}\int_{-\infty}^{\infty}a(\omega)r(\omega,x)e^{i\omega t}d\omega=\frac{1}{2\pi}\int_{-\infty}^{\infty}a(\omega)e^{-i\bar{k}x}e^{i\omega t}d\omega \tag{24}$$

It is then practical to place the coordinate origin at the input point to see that $a(\omega)$ is simply the Fourier transform of the movement at the input location

$$u(0,t)=\frac{1}{2\pi}\int_{-\infty}^{\infty}a(\omega)\,e^{i\omega t}d\omega \tag{25}$$

To establish the wavenumber-frequency relation the constitutive equation describing the propagating media needs to be enforced. This is done in the following section.

1.2.4 Bulk plane waves

1.2.4.1 General

We have just seen that a propagating plane wave offers an attractively simple transfer function between the recorded motion at two points. The question now is what kind of plane waves can propagate within the bulk of some elastic solid.

If the solid is isotropic there are a number of ways to proceed, but considering our interest in anisotropy it is best to keep some generality[5]. A harmonic plane wave may be then substituted in equation (6) with zero body forces. Using the normalised slowness to express its phase and considering that the wave-transported movement could take place –or be polarised- in any direction, **d**, this harmonic wave is written

$$\mathbf{u}(x,t)=\mathbf{d}\exp(i(\omega t-kx)) \tag{26}$$

after some simplifications, the following expression is retrieved

$$\rho v^2 d_n = D_{0nmpq}d_p p_m p_q \tag{27}$$

This equation relates the polarisation of the wave-like movement (**d**), its propagation direction (**p**) and its phase velocity (v). It can be arranged in the form of an eigenvalue problem

$$\begin{aligned}\Gamma_{ij}&=D_{0iljk}p_l p_k\\ \left[\Gamma-\rho v^2\mathbf{1}\right]\mathbf{d}&=\mathbf{0}\end{aligned} \tag{28}$$

As a tribute to its earlier proponents, this form is often known as the Kelvin-Christoffel equation and the tensor Γ as the Kelvin-Christoffel tensor or the acoustic tensor. Due to the symmetries of the elastic

---

[5] We follow here the presentation of this subject by Crampin (1981)

tensor Γ is also symmetric. Γ is also positive-definite as the elastic tensor is positive definite[6]. Consequently (see e.g. Landesman & Hestenes, 1992) the characteristic equation

$$\det\left[\Gamma_{ij} - \rho v^2 \delta_{ij}\right] = 0 \tag{29}$$

has three positive real solutions (eigenvalues), possibly different from each other, each one associated with a different direction (eigenvector). Moreover, these three eigenvectors form an orthogonal set. This means that for any given elastic tensor **C** and any given propagation direction **p** there are, in general, three possible plane waves, with phase velocities v_i and polarizations $\mathbf{d}_i$

1.2.4.2 Isotropy

All this has general validity but it is now time to introduce the assumption of isotropy. Using the isotropic stiffness (5) to form the acoustic tensor (28) and expressing it in a Cartesian frame with **p** as one of the basis vectors we obtain,

$$\Gamma_{ij} = (\lambda+\mu)p_i \otimes p_j + \mu(\delta_{ij} - p_i \otimes p_j) = \lambda p_i \otimes p_j + \mu \delta_{ij} \tag{30}$$

From this expression it is immediately recognisable that

- the preceding result is equally valid for every given direction **p** i.e. in the isotropic case plane wave propagation properties are isotropic[7].
- associated with the eigenvalue $\lambda+\mu$ there is one eigenvector along the direction given by **p** i.e. the wavefront normal. This is a wave oscillating along the propagation direction and is called a P wave.
- associated with the eigenvalue μ there are two eigenvectors perpendicular to **p**. These are waves oscillating on a plane orthogonal to the propagation direction and are called S waves.
- The P wave involves only volumetric strain, whereas the S waves involve no volumetric strain at all. This is plain if the general expression of the movement is considered.

$$\begin{aligned} \mathbf{u}_p &= \{a \quad 0 \quad 0\} e^{-i\omega\left(t-\frac{x_1}{v_p}\right)} \\ \mathbf{u}_s &= \{0 \quad b \quad c\} e^{-i\omega\left(t-\frac{x_1}{v_s}\right)} \end{aligned} \tag{31}$$

These are familiar results and are even more familiar if we write the phase velocities using the Young's modulus, *E*, Poisson's ratio, ν and shear modulus, G:

$$\begin{aligned} v_p &= \sqrt{\frac{\lambda+\mu}{\rho}} = \sqrt{\frac{E(1-\nu)}{\rho(1+\nu)(1-2\nu)}} \\ v_s &= \sqrt{\frac{\mu}{\rho}} = \sqrt{\frac{G}{\rho}} \end{aligned} \tag{32}$$

---

[6] Chapter 7 delves more into this issue

[7] This result will be generalised to anisotropic cases in Chapter 8

These are usually known as the compressional or primary velocity, v_p, and the shear or secondary velocity, v_s. The ratio between both velocities is only dependent on Poisson ratio.

$$v_s = v_p\sqrt{\frac{(1-2\nu)}{2(1-\nu)}} \tag{33}$$

Figure 1-9 illustrates this dependency for a range of Poisson ratios typical of soil. Honouring its name, the primary velocity v_p is always bigger than the shear or secondary velocity, v_s, by a factor between 1.5 and 3 for the most probable range of Poisson's ratio.

1.2.5 Elastodynamic transfer functions

The preceding strategy can be replicated in other cases, using differently specified waves -for instance with spherical or cylindrical wavefronts- or a different material model –viscoelastic for instance, see Chapter 5. But it is clear that it offers a rather limited answer to the search for elastodynamic transfer functions. Although bulk waves propagate according to the material properties they do not reflect the effect of loading or boundary conditions. A more general approach to obtain elastodynamic transfer functions is provided by the Green function concept.

1.2.5.1 Green functions

A Green function, **GR**, gives the time history of displacements when an instantaneous load is applied at an isolated point, say $\mathbf{x}_0$, in some elastic body. This is obtained as the solution of the elastodynamic equilibrium equation (6) subject to an specific set of boundary conditions. By a generalisation of the common concept of elastic reciprocity it can be shown –Achenbach 1973- that the response $\mathbf{u}(\mathbf{x},t)$ to a general input load history $\mathbf{f}(\mathbf{x},t)$, is given by

$$\mathbf{u}(\mathbf{x},t) = \int_V \mathbf{GR}_{\mathbf{x}_0} * \mathbf{f}_{\mathbf{x}_0} d\mathbf{x}_0 + \int_S (\mathbf{GR}_{\mathbf{x}_0} * \mathbf{t} - \mathbf{u} * \mathbf{t}_{\mathbf{GR}_{\mathbf{x}_0}})\, ds \tag{34}$$

where **t** denotes the surface traction and the symbol * indicates time convolution. The elastic body is assumed quiescent before the application of $\mathbf{f}(\mathbf{x},t)$ and with known boundary conditions. The first term on the r.h.s. gives the response due to loads inside the body, the second term the contribution of the boundary. As it is apparent, the unknown response, **u**, also features in the second term. If this second term is null then we can identify directly the Green function with the sought-after unit response function. In principle the Green function boundary conditions should be chosen to satisfy this criterion in accordance with the problem boundary conditions. In practice the catalogue of available Green functions is rather limited, simple geometry being a basic requirement. This opens various possibilities.

1.2.5.2 Fundamental solutions

The first and simplest is to ignore the influence of the boundaries altogether, dropping the second term in (34). Mathematically this is equivalent to obtaining the Green function for a body of infinite extent. This is called a fundamental solution –Bonnet, 1995- and such solutions are known for a variety of material models. Physically, this may be an adequate approximation if the points **x** whose response is sought after are far away from the boundaries. The scheme of Figure 1-7 represents a cantilevered plate with some

load acting at $\mathbf{x}_0$. A fundamental solution might be adequate to evaluate the response at points such as $\mathbf{x}_1$, $\mathbf{x}_2$ or $\mathbf{x}_3$ but is rather unlikely to do so at points such as $\mathbf{x}_4$ or $\mathbf{x}_5$. The fundamental solution approach is then useful to incorporate the effect of loading but not that of boundary conditions. An example of this approach is studied in Chapter 4.

1.2.5.3 Modal solutions

A second possibility is to obtain all the solutions of the homogeneous unforced case for given boundary conditions. These solutions are called modes and each one represents a possible type of elastodynamic transfer function for the system. The particular transfer function corresponding to some specific loading may then be obtained as a combination of modal solutions. The potential of this approach is illustrated in Chapter 6.

1.2.5.4 Spatial discretization

The third possibility is to solve the problem through some spatial discretization scheme. Finite elements are perhaps the most popular, although the modelling requirements of dynamic problems with rapidly varying loads are rather subtle and computationally intensive–Hitchings, 1992. Boundary element techniques whose starting point is equation (34) above, offer an interesting alternative –Domínguez, 1992. Obviously, the drawback of this approach is that no analytical formulation is explicitly available for the obtained transfer function. If the purpose of the exercise is to evaluate some material property by comparison with an experimentally obtained transfer function we face a rather cumbersome inverse matching problem.

1.3 SUMMARY

The small-strain stiffness is one of the fundamental properties of soils. Laboratory pulse tests are one of the most popular and promising tools available for its measurement. This thesis deals with the interpretation of laboratory pulse tests in soils. Elastodynamics offers an ample theoretical bosom and is here adopted as a heuristic guide. Its basic hypotheses have been recalled and its relationship with the less theoretically committed lineal systems framework has been outlined. As an application the case of bulk plane waves in isotropic solids has been developed.

1.4 TABLES

	λ, μ	G, ν	E, ν	K, G
λ	λ	$\frac{2G\nu}{1-2\nu}$	$\frac{\nu E}{(1+\nu)(1-2\nu)}$	$K-\frac{2}{3}G$
μ =G	μ	G	$\frac{E}{2(1+\nu)}$	G
K	$\frac{(3\lambda+2\mu)}{3}$	$\frac{2G(1+\nu)}{3(1-2\nu)}$	$\frac{E}{3(1-2\nu)}$	K
E	$\frac{(3\lambda+2\mu)}{\lambda+\mu}$	$2(1+\nu)G$	E	$\frac{9KG}{3K+G}$
ν	$\frac{\lambda}{2(\lambda+\mu)}$	ν	ν	$\frac{3K-2G}{2(3K+G)}$

Table 1-1 Relations between isotropic elastic moduli

1.5 FIGURES

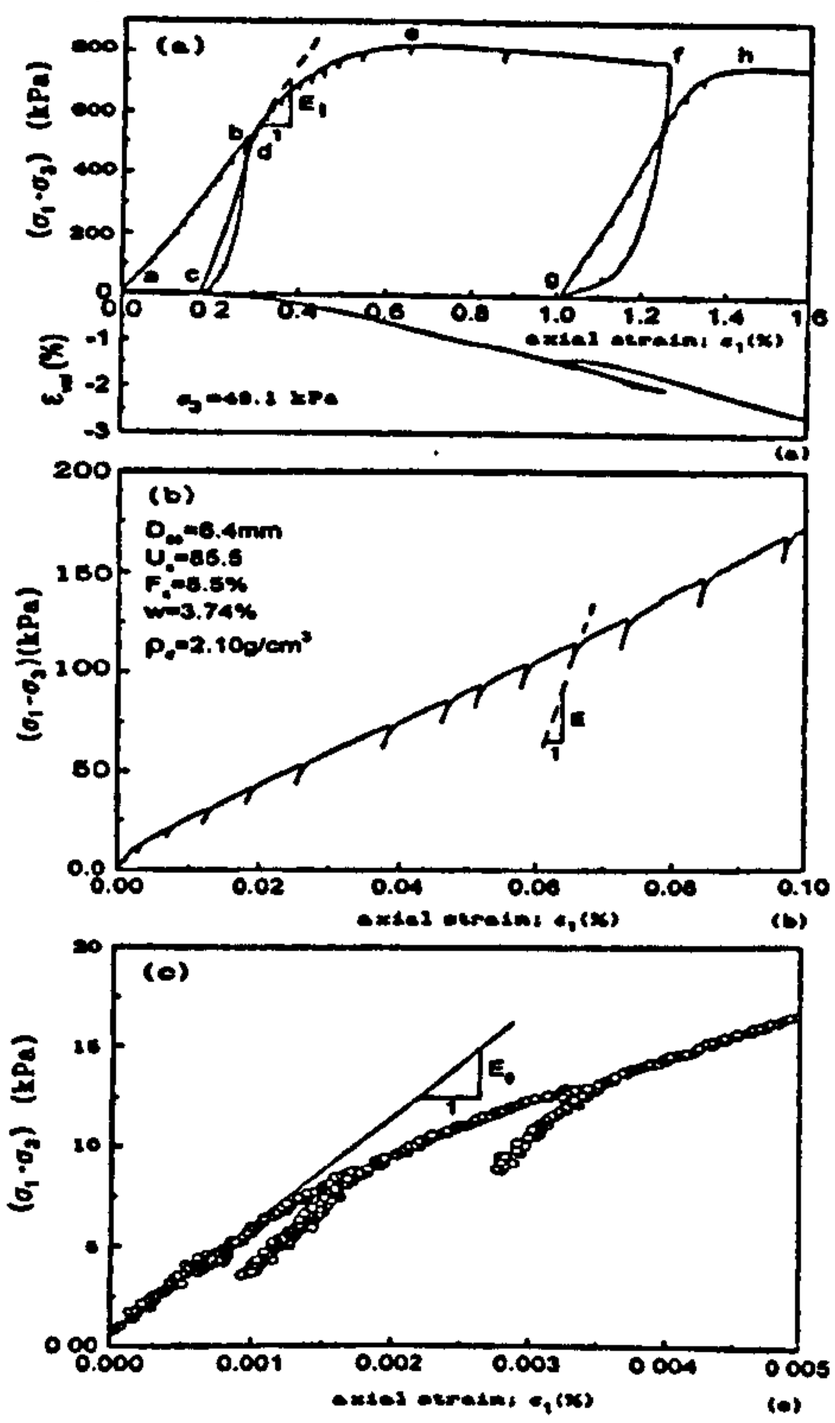

Figure 1-1 Increased resolution in stiffness measurements. Chiba gravel results by Jiang & Kohata (1996) as quoted by Tatsuoka (1999).

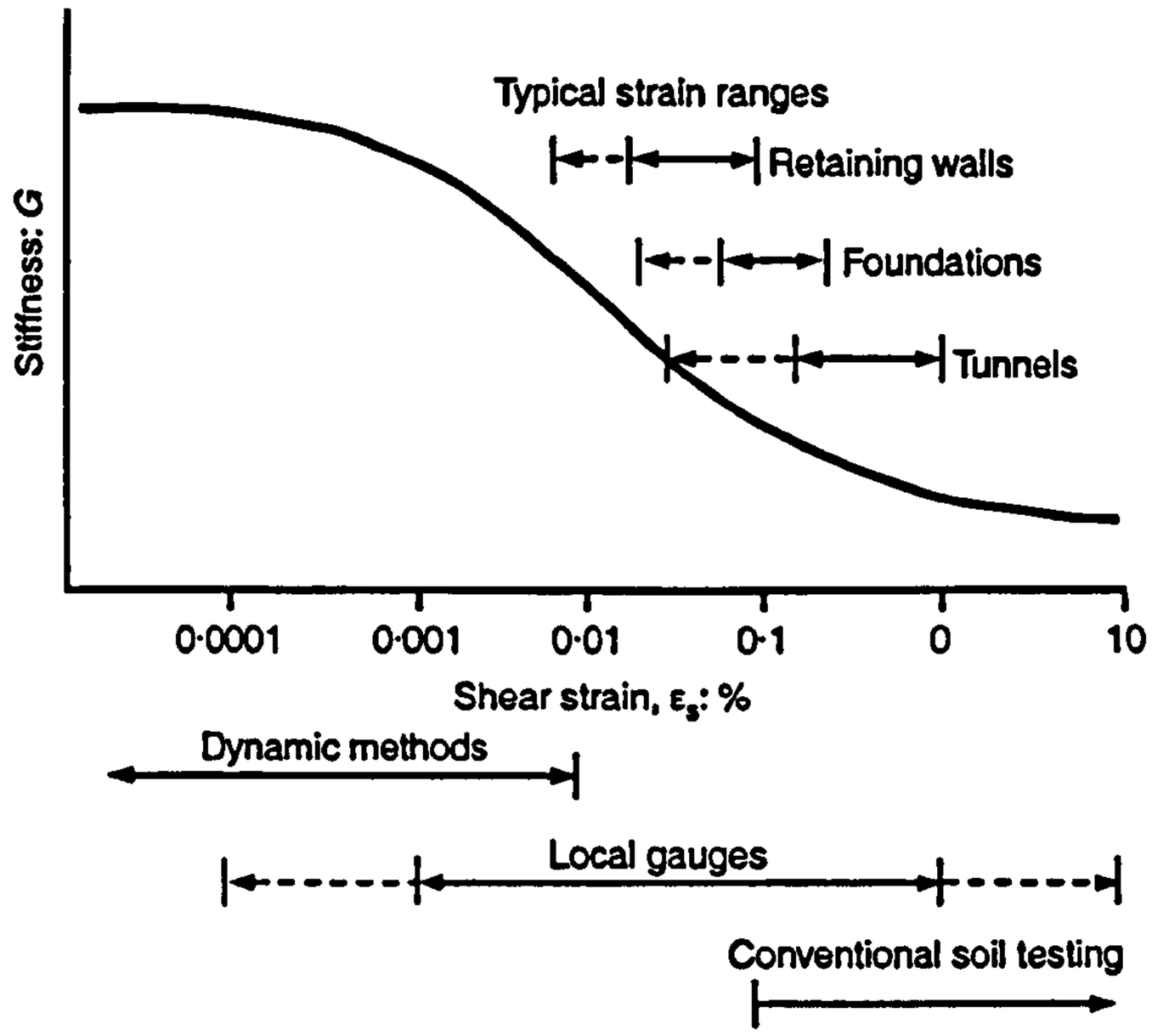

Figure 1-2 Stiffness-strain behaviour of soils with typical strain ranges for laboratory tests and structures (after Atkinson, 2000)

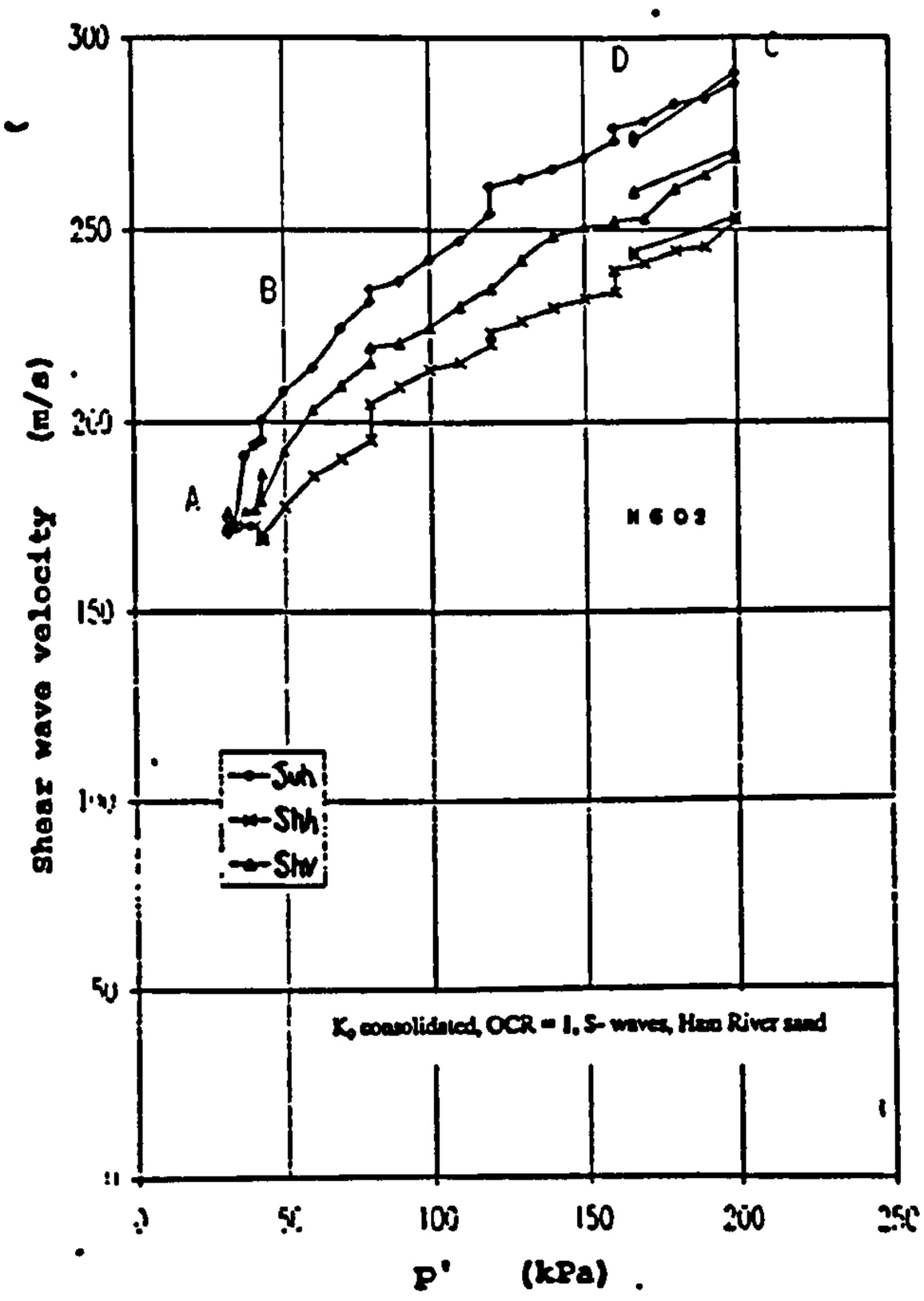

Figure 1-3 Anisotropic velocity measurements using bender elements in a sample of Ham River sand (after Jardine et al. 1999)

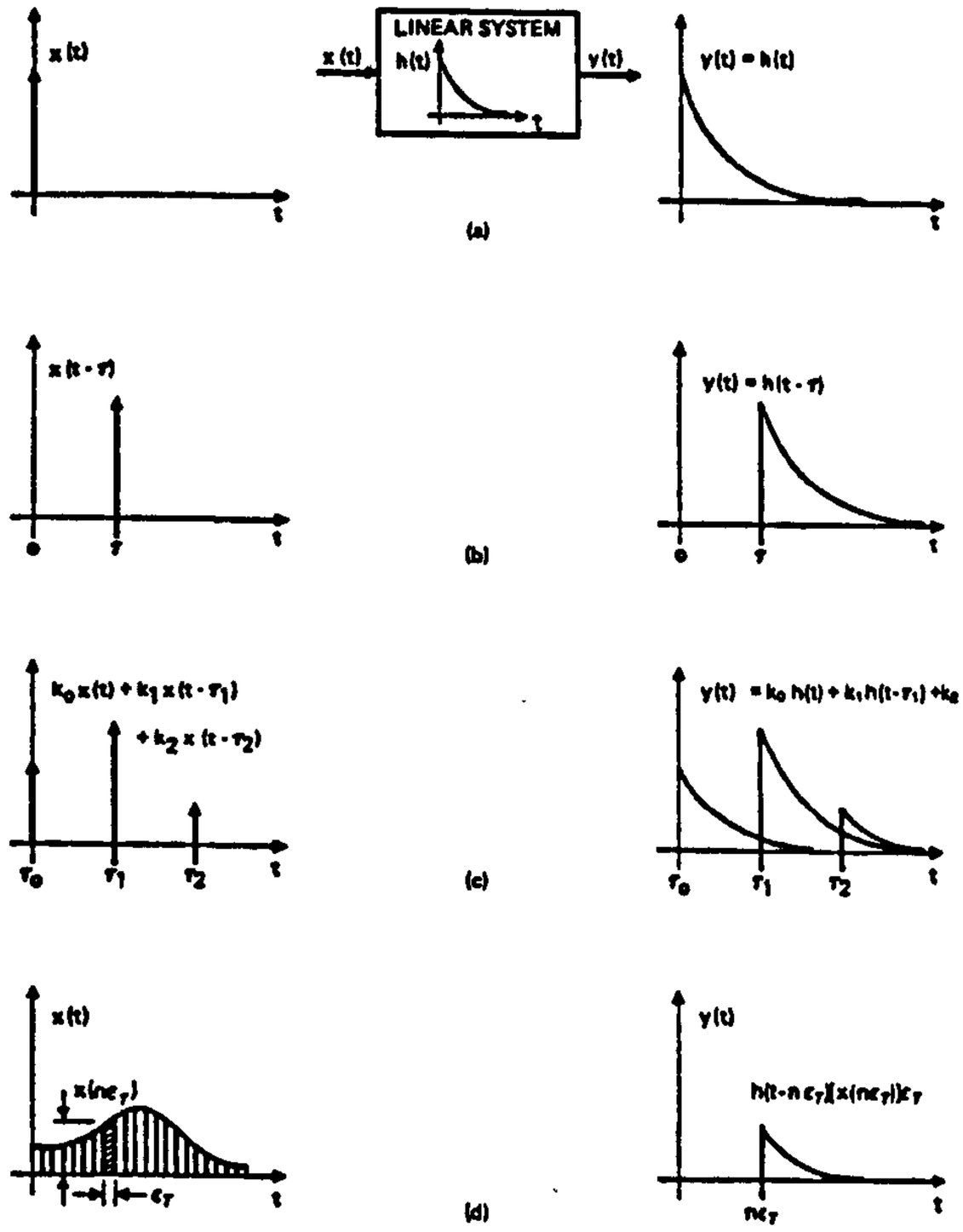

Figure 1-4 Time superposition in linear systems. From Brigham (1988)

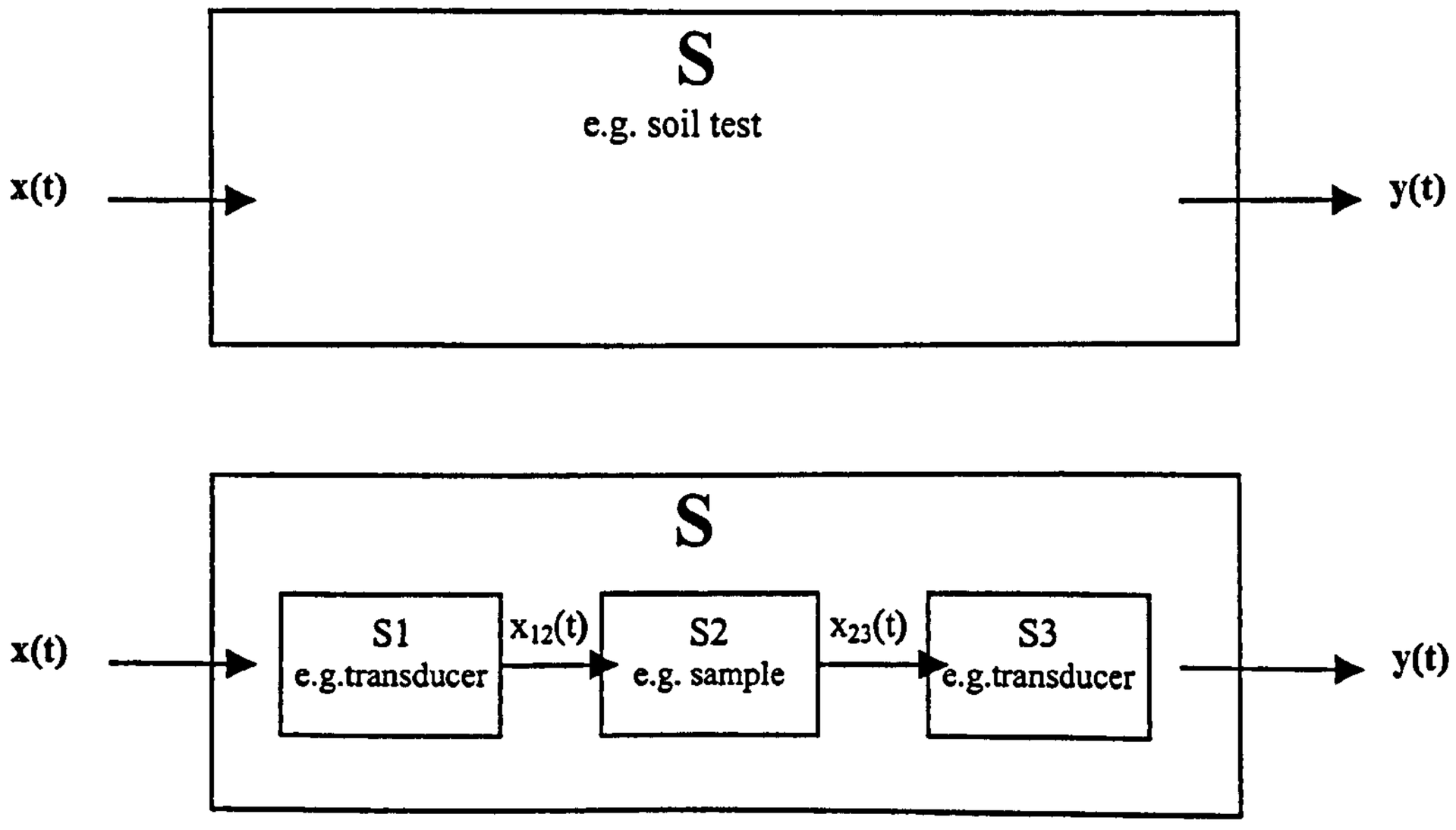

Figure 1-5 Dynamical systems: a gradable black-box approach

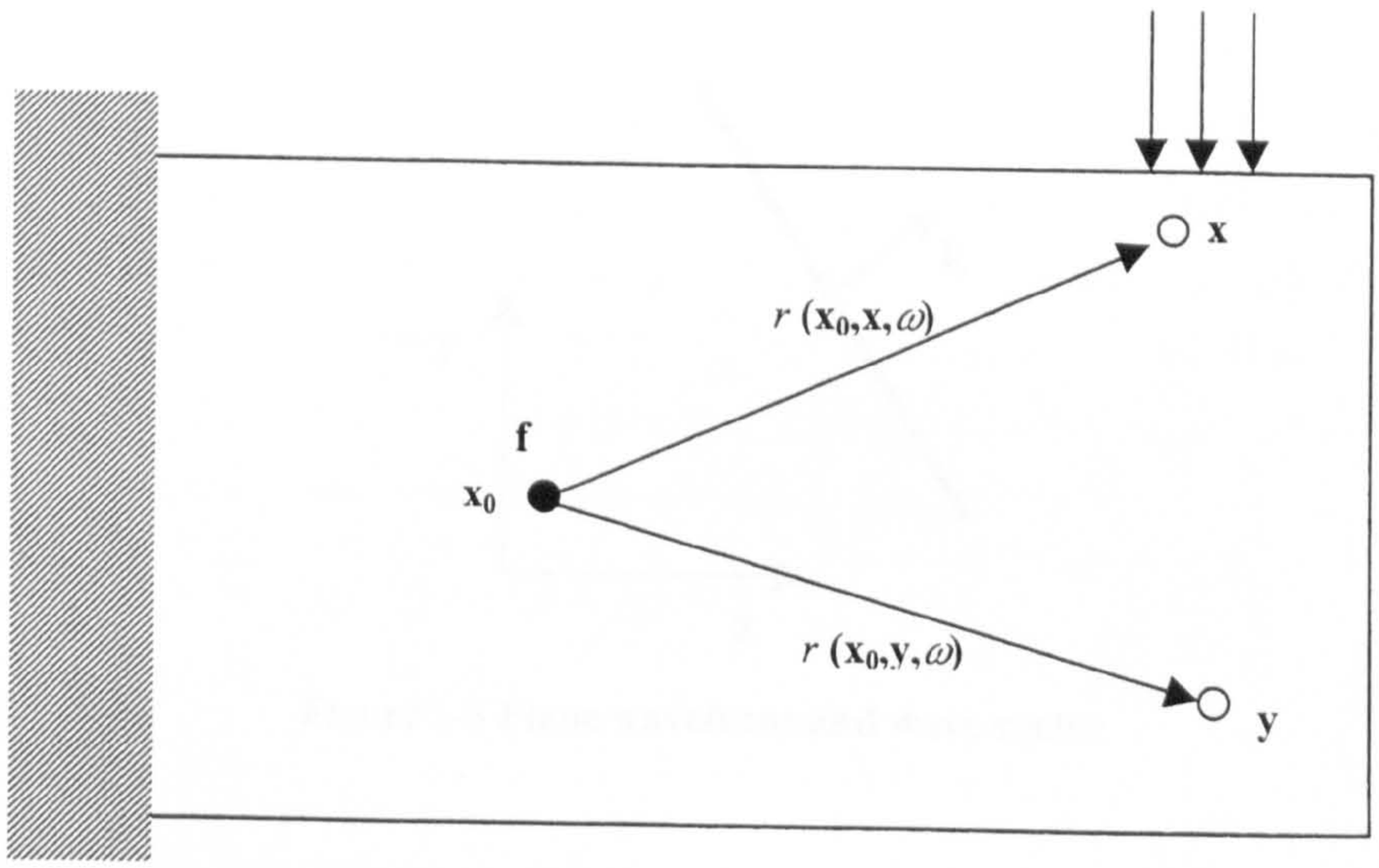

Figure 1-6 Transfer functions in elastodynamics

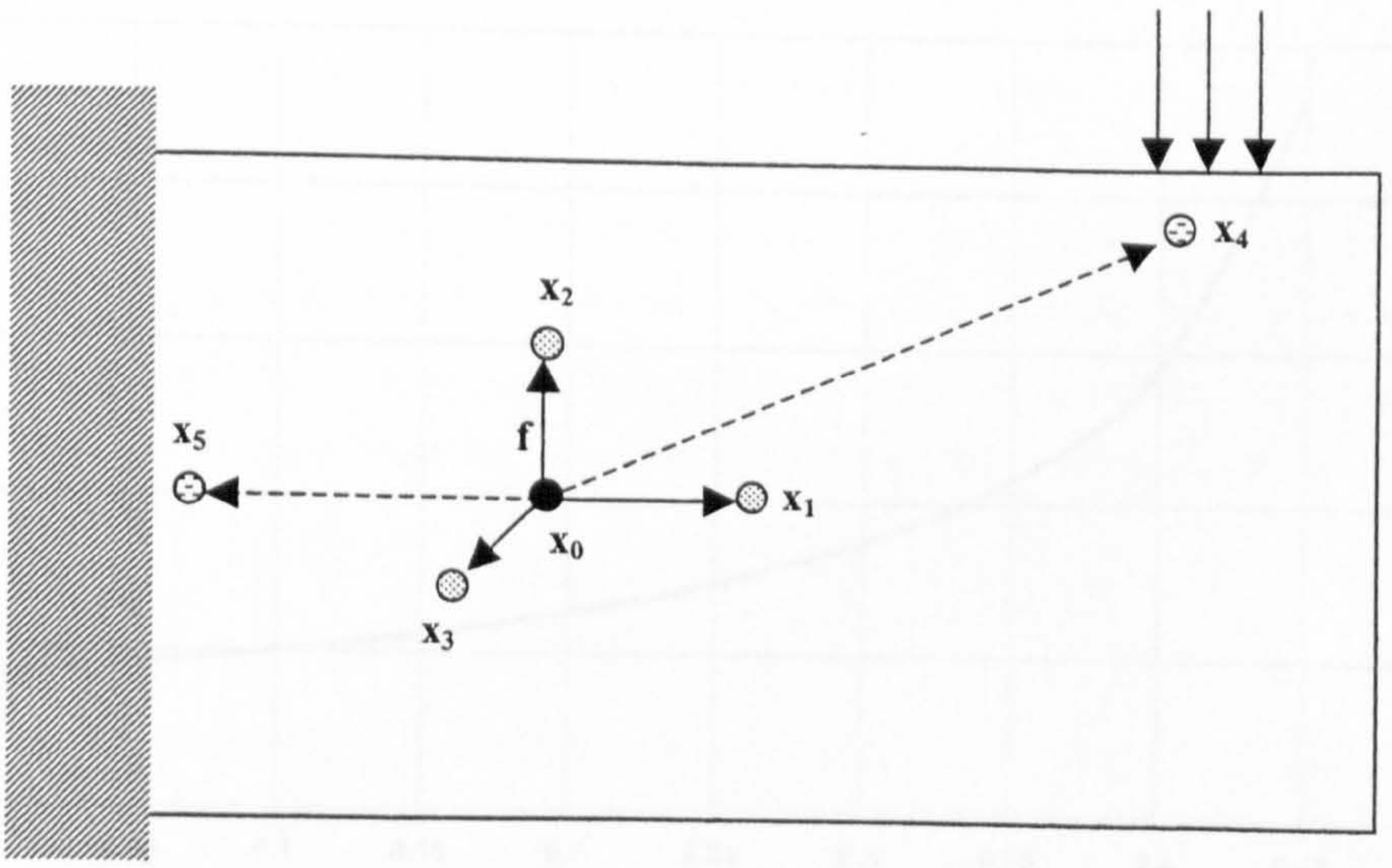

Figure 1-7 Fundamental solutions and boundary conditions

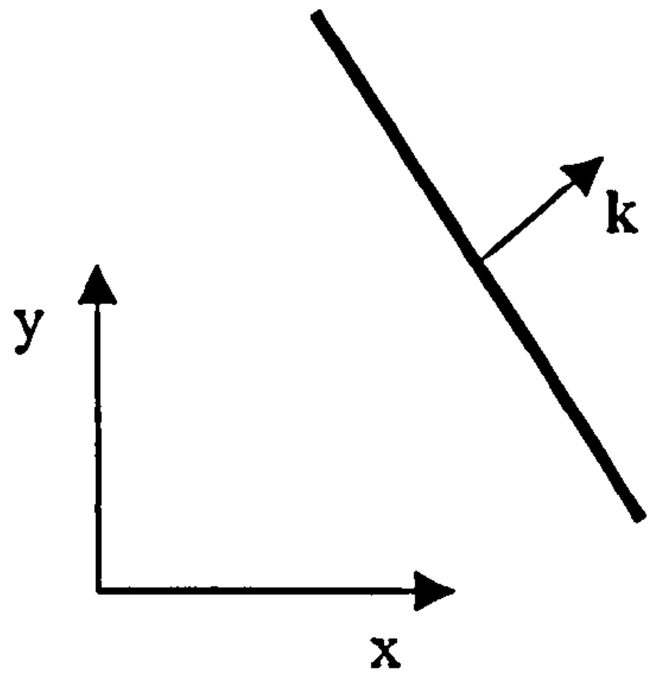

Figure 1-8 Plane wavefront and wave vector

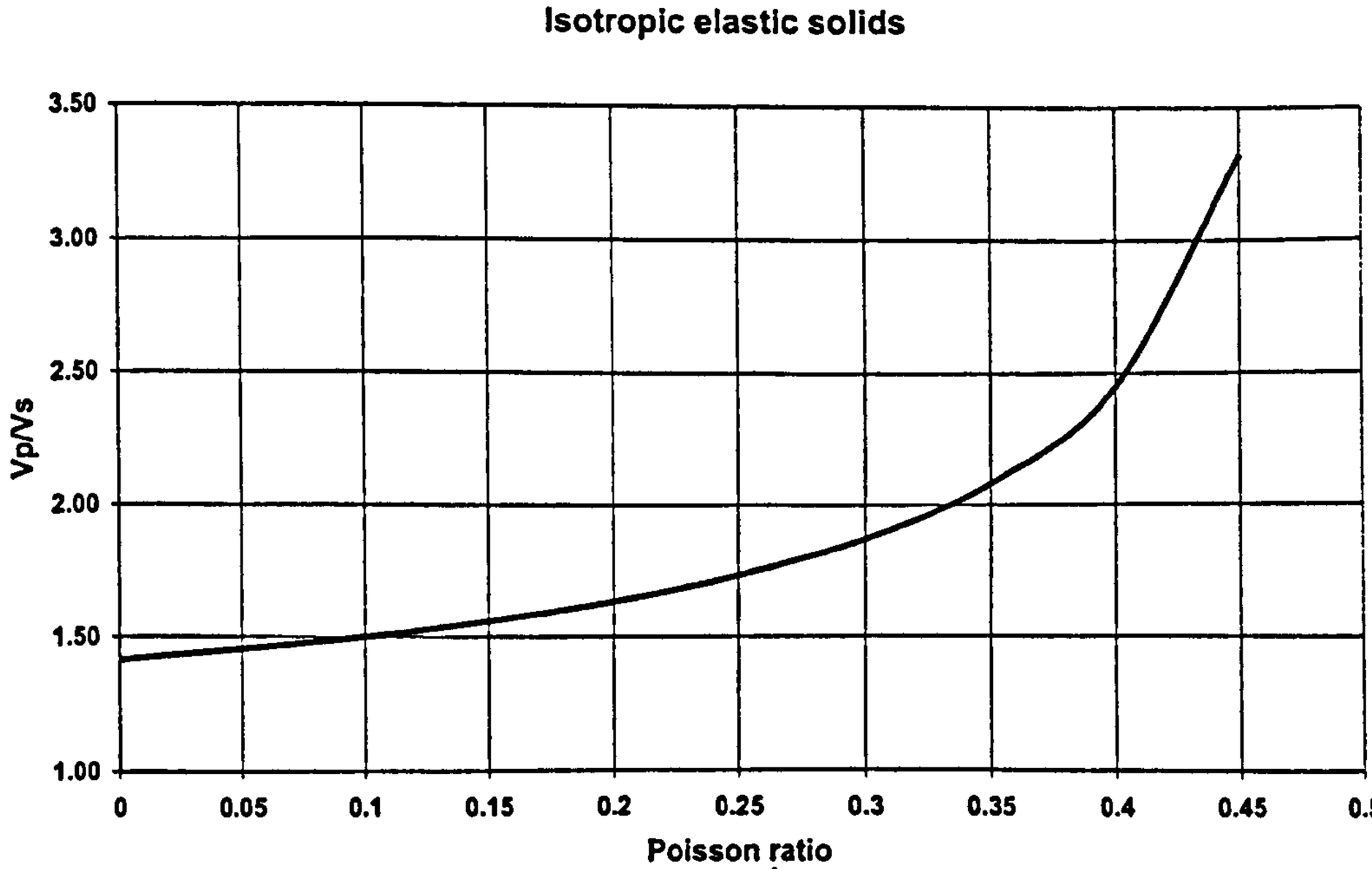

Figure 1-9 Ratio of bulk velocities in isotropic elastic solids

2 CONTEXT AND PRACTICE OF PULSE TESTS IN SOILS

2.1 THE CONTEXT OF PULSE TESTING

2.1.1 Dynamic testing

It is useful to distinguish various conceptual steps in the dynamic procedures employed to measure elastic properties. First, a movement is generated in the elastic body under consideration and some particularities of this movement are recorded: for instance the time history of movement at some points, $\mathbf{u}_i(t)$. Second, taking account the geometry of the test set-up, those movement particularities are combined to obtain some characteristic dynamic properties of the body, (e.g. characteristic velocities $\mathbf{v}_i$). Finally, some theoretical relations between the elastic properties and the characteristic dynamic properties are employed to obtain the elastic $\mathbf{D}_0$ properties. Formally this can be expressed as follows

$$\begin{aligned} \mathbf{v}_i &= F(\mathbf{u}_j(t), test\ set-up) \\ \mathbf{v}_i &= S(\mathbf{D}_0) \end{aligned} \qquad (35)$$

It is clear that dynamic tests require, in general[8], a more involved interpretation procedure than static tests. In particular, explicit expressions such as F could not always be obtained even if the test set-up is carefully designed; moreover, there is no guarantee that the relations between $\mathbf{D}_0$ and $\mathbf{v}_i$, symbolised by S, would be explicitly invertible[9]. These are important inconveniences of dynamic procedures.

Their advantages, on the other hand, are well known. Dynamic procedures have a wider scope than static procedures, and similar techniques could be employed in the field and the laboratory, thus providing a very direct way to transfer results between both. Most dynamic techniques are non-intrusive (e.g. SASW), or very mildly intrusive (e.g. cross-hole or bender element testing) and non-destructive, thus allowing repeated testing of the same sample or site at will. This makes them ideal for control purposes as a change-tracking tool. Dynamic tests have also the potential to map inhomogeneities of the tested elastic body and this is, in fact, a main application of field geophysics. In contrast, static procedures are always relying in local measurements and, therefore, place more strict interpretative constraints on the homogeneity of the test element.

2.1.2 Types of dynamic tests

The dynamic procedures employed for soil testing are usually classified into field and laboratory methods –see Kramer 1996 for a general review. Another possible classification might be established if we focus on the interpretation procedure employed. Figure 2-1 - adapted from Pollard 1977- illustrates such a classification. Two categories are employed in it, both related to important characteristics of the movement being measured. The kind of input: continuous excitation will be employed to generate steady state movements, whereas pulse input will generate some transient movements. End effects involve

---

[8] In the anisotropic case there are, nevertheless, some difficulties even for static tests: see Chapter 7

[9] Such is the case for Rayleigh waves, and there, on the inversion procedures, lies one of the prominent difficulties of methods using them, like the SASW (Foti, 2000).

reflection and/or refraction of the waves and the test interpretation procedures might allow for them or not.

Figure 2-1 also includes an indication of where the most important geotechnical procedures could be fitted. In many cases this classification is rather obvious. The resonant column is the classical dynamic laboratory test and a neat example of resonance analyses. Cross-hole and down-hole are field tests where the input is some sort of impulsive loading and they are interpreted without account for any reflection or refraction[10].

The inclusion of the spectral analysis of superficial waves (SASW) method within the pulse methods seems reasonable as the load is impulsive and the waves measured are propagating over an unlimited surface. The steady state Rayleigh-wave method on the other hand is a a clear example of travelling-wave type analyses.

Bender element testing has also been included within the pulse category. Contrary to the previous, this is a laboratory test. This is interesting, because, at least in principle, discounting of end effects is harder to achieve within the laboratory, as they require either a perfectly absorbing boundary or a very big distance to the boundaries.

In geotechnical practice the methods beneath the echo heading are not really employed[11] for the measurement of elastic properties but rather to locate discontinuities –rock substrata or pile flaws. This is, also, an interesting peculiarity of soil mechanics, because the use of echoes from specimen ends is the most commonly employed procedure for measurement of elastic constants in most industrial materials, like metals or ceramics, -Papadakis 1990- but also in rock core measurements in the laboratory – Schreiber et al. 1973-

2.1.3 Dynamic testing of soils: material constraints

Soil Mechanics as a discipline might be placed on the crossroad between Geology and Materials Science. It is therefore to be expected that the application of dynamic testing procedures to soils will have much in common with analogous activities in both sciences. This is, in fact, the case. Field techniques are, although sometimes different in configuration and purpose, strongly linked to those employed in seismology and geophysical prospecting. Within the laboratory, most procedures employed to obtain elastic parameters were borrowed or adapted from previous material science techniques.

In general, seismic applications of elastic wave propagation theory preceded those of acoustic testing of materials, but this trend was reversed for the particular case of elastic anisotropy. Within the material science community, anisotropic wave propagation received much attention from the beginning, (e.g. Mason, 1958) as crystalline materials under study were obviously anisotropic. It took around three

---

[10] At least in the propagation direction
[11] But see below on a proposal by Arulnatham et al. (1998)

decades more for seismologists (see Crampin, 1984) to make systematic consideration of this property. Previously anisotropy was regarded as a second order effect, partly because the focus was set on other complex propagation problems, like those posed by inhomogeneous layered media (Aki & Richards, 1980); and partly because the data acquisition techniques did not favour its observation. This situation has changed dramatically in the last twenty years, and now the consideration of elastic anisotropy plays a key role in many seismic studies (e.g. Crampin, 1999).

Although there is much to be learned from those related fields, direct extrapolation is not granted. Elastic waves in soils have some peculiarities that affect considerably the performance and interpretation of dynamic tests. It is worthwhile to address them in general before going into more detail.

The first peculiarity to note is that soils have lower wave propagation velocities than most other materials of engineering interest. This, of course, is a consequence of their relatively low stiffness: Figure 2-2 illustrates the isotropic velocities corresponding to a typical range of soil stiffness. Soils are perhaps the softer materials were shear wave propagation is possible: velocities as low as 3m/s have been measured on marine sediments. As for the faster, compressive velocity, only for the stiffer soils (dense sands) will it reach above 1 km/s. Most other solids are well above this limit, and the same happens with many liquids. Water, for instance, has a v_p of circa 1.5 Km/s a value substantially higher than the corresponding one in most soils. This is particularly interesting because soils are porous materials and, in many instances, they are saturated with water.

It is then to be expected that porewater will cause great interpretative difficulties to dynamic measurements of v_p in saturated soils. Roughly, most energy will travel at velocities which bear more relation with the stiffness of water than with that of the solid skeleton. There is a complex dynamic coupling between porewater and soil skeleton –Biot, 1956- and Gajo & Mongiovi –1994- have illustrated how this coupling precludes an easy measurement of the bulk modulus of soils in saturated samples. We will be back on this issue later, here its enough to say that this problem has induced most geotechnical researchers to work on dry granular materials (e.g. Moncaster, 1997) or/and to concentrate on shear velocity measurement (e.g. Kuwano, 1999).

Another interesting consequence of low propagation velocities is most easily seen if we consider the basic relationship between wavelength, frequency and velocity of propagation.

$$\lambda f = v \tag{36}$$

Figure 2-3 represents this relationship for an interval of velocities typical of shear waves in soils and in other materials like rocks (Simmons, 1964), ceramics or metals (Krautkramer & Krautkramer, 1990). In the figure it is also indicated the range of frequencies typically employed in soil pulse testing in the laboratory and in the field, as well as the corresponding one for ultrasonic testing of materials (Krautkramer & Krautkramer, 1990) and exploration geophysics (Teldorf et al., 1990). These frequency ranges give in turn a range of characteristic wavelengths, λ_{char}, for each case.

It is worth noting at this juncture that the frequencies of interest in seismology and earthquake engineering are generally below 100 Hz (Kramer, 1996). The classical dynamical laboratory test for soils, resonant column, usually proceeds below 100 Hz and, therefore, is testing directly within that range of interest. Field pulse tests, like cross-hole, are not very far away either. Laboratory pulse tests, on the other hand, work at relatively much higher frequencies, although unlike in most materials not high enough to qualify them as ultrasonic –the common hearing range is 20Hz to 20kHz (Lighthill, 1978).

In most aspects of wave theory the comparison of the characteristic wavelengths with some characteristic length of the problem, $d_{set\text{-}up}$, is key to the modelling problem. For instance, considering the propagation of waves within a finite body we can safely ignore the effects of its finite size as long as this is substantially higher than the wavelengths involved. A number of useful simplifications depend on the achievement of movement frequencies, f, high enough to make the corresponding wavelength, λ, far smaller than $d_{set\text{-}up}$.

For most laboratory tests on soils the characteristic dimensions of the sample range between 2 cm (e.g the wall thickness of a hollow cylinder) and 20 cm (height of samples in large triaxial apparatuses). Now, looking at Figure 2-3 it appears that similarly sized wavelengths are typical of most lab tests. Following the previous discussion one might wonder why test set-ups for soils are not modified, allowing for bigger distances, or, if this looks unpractical, why then are not soils tested with higher frequencies. This possibility is hindered by a second important peculiarity of soils: they rank among the highest attenuating materials.

There are many possible measures of wave attenuation (Kramer, 1996). For our purposes here, is useful to look at it as the coefficient[12] relating the amplitude of a wave at two points, spaced at a distance d, i.e.

$$A_2 = A_1 e^{-\alpha d} \tag{37}$$

Furthermore, it is also useful to consider now this attenuation coefficient, α, as a sum of three different factors, whose meaning is explained below,

$$\alpha = \alpha_g + \alpha_{sc} + \alpha_a \tag{38}$$

The attenuation or damping of elastic waves is a concept whose neat experimental appearance - Figure 2-4- contrasts with its many interpretative difficulties. In principle, elastic materials are meant to be conservative i.e. they should not dissipate energy and the movement should continue indefinitely. For

[12]Attenuation is usually expressed in dB/unit length or like in the formula (37) above in neper/unit lenght. Decibels are obtained as $20\log(A_2/A_1)$. One neper is 20/ln10 dB or 8.686 dB.

elastic homogeneous materials the only cause for amplitude attenuation of elastic waves should be the geometrical spread of energy in expanding wavefronts. This is known as geometrical attenuation and is represented above by the factor α_g. But the fact is that all elastic waves die out, even when confined to small laboratory samples; moreover, for a given test geometry, different materials will show a different, characteristic, material attenuation. The presence of attenuation as a factor in test designed to measure elastic properties is a reminder, if needed, of the limited scope of the elastic idealisation.

There are two different aspects of these limitation; the first is related with the assumption of homogeneity. At some scale or another, all materials are inhomogeneous. Inhomogeneity results in scattering of elastic waves i.e. partial reflection and deviation of energy. Wave scattering is heavily dependent on the relation between the wavelength of the impending wave and the size of the obstacle or inhomogeneity. This introduces a frequency dependence on attenuation and imposes a practical higher limit to the movement frequency.

The frequency applied should be low enough to make the corresponding wavelength, λ, bigger enough than a characteristic length, d_{sc}, which represents the size of typical inhomogeneities within the material. At this respect, Krautkramer & Krautkramer (1990), summarises the experience obtained in ultrasonic testing of materials. He suggests the following relation for scattering related attenuation, α_{sc},

$$\begin{aligned} &\lambda > 100\, d_{sc} \rightarrow \alpha_{sc} \approx 0 \\ &100\, d_{sc} > \lambda > 10\, d_{sc} \rightarrow \alpha_{sc} \propto \left(\frac{d_{sc}}{\lambda}\right)^3 \\ &\lambda < 10\, d_{sc} \rightarrow \alpha_{sc} \approx \infty \end{aligned} \qquad (39)$$

Hence, for $\lambda > 100\ d_{sc}$ scattering is negligible, whereas for $\lambda < 10\ d_{sc}$ scattering is high enough to make ultrasonic testing almost impossible. Between them attenuation by scattering grows quickly, with the third power of the frequency. For soils d_{sc}, the characteristic size of inhomogeneities, might well be identified with grain size. Figure 2-5 its obtained when Krautkramer & Krautkramer limits are applied with this criteria. It shows clearly that for granular soft materials the operating frequency range has a pretty low ceiling – frequencies above 20 kHz will pose serious attenuation problems even for fine sands.

Finally, the factor α_a represents the true material absorption, the energy loss due to the material anelastic properties. In soils two major mechanisms of material attenuation are present. The first is fluid coupling; the second hysteretic or frictional "dry" losses that appear on soils even within the "elastic", very low strain amplitude range. This hysteretic losses represent, therefore, the minimum material attenuation to be expected when testing soils. A value of 0,16 dB per wavelength is typical for most soils and rocks (Teldorf et al. 1990). For laboratory pulse tests this will correspond to values of circa 16 dB/m. The loss due to fluid coupling depends on a number of parameters (frequency, granulometry...), but values above 50 dB/m are common in the range of interest (Stoll & Brian 1969).

2.2 PULSE TESTING PRACTICE

2.2.1 Overview

Pulse transit tests are perhaps the most popular dynamic procedure in use today. One main reason for this is their relative conceptual simplicity. Pulse tests are conceptually simpler than echo or resonance tests as they are idealised as an experiment on wave propagation in a boundless homogeneous medium (see Figure 2-6). A mechanical disturbance is created at some point (source) and its arrival is measured at a different point (receiver). Measuring the distance between source and receiver and the time of travel of the disturbance between them, a velocity of propagation, **V**, could be assessed.

As we have said, this idealisation is applied to very different configurations. In the field to cross-hole tests where sources and receivers are placed in boreholes, to down-hole or up-hole tests where one of them is placed in the surface and to Rayleigh wave-based tests[13], where all receivers are placed on the surface....But this research focuses on laboratory tests and there also pulse tests have been performed on a variety of set-ups. Some have been performed on calibration chambers, (Lee, 1993; Bellotti et al., 1996) with sources and receivers buried within the sample. Nevertheless in most cases laboratory pulse testing has been achieved by placing source and receiver on the surface of a sample that is being simultaneously tested on some static apparatus.

Bigger set-ups, like those provided by calibration chambers, permit a variation on the scheme shown in Figure 2-6. In it, various receivers are placed along the same direction and the time measured refers to the disturbance travel time between aligned receivers. This modified scheme has also been applied in field tests, although there cost considerations may sometimes impose the basic scheme. When measuring on static apparatus, this aligned multiple receiver scheme has not been yet employed.

2.2.2 Instrumentation

Between the years 1940 to 1960 ultrasonic testing of materials took off both as a scientific and an industrial tool for testing materials (Mason, 1958). The publication of "Physical acoustics" (Mason, 1964) offered and overview of an already well established technique that had been by then extensively applied to metals, crystals, ceramics and, within the geological materials, rocks (Anderson & Liebermann, 1968). A variety of methods were already developed: those based on resonance but also, and perhaps even more, those based on elastic pulses, under various forms: through transmission, echo and interferometry. The elastic constants of all those materials were being measured with infinitesimal precision under a variety of conditions of pressure and temperature. For soils, nevertheless, the story was rather less successful.

In 1963 Hardin & Richart published the first systematic work on soils with a resonant column apparatus of modern design. Whitman and Lawrence (1963) made a contribution in written discussion, describing

---

[13] Of course, in the case of Rayleigh waves the boundless media is a surface.

an application of the pulse transmission technique to soils[14]. The apparatus presented was able to measure both compressional and shear waves, although the results there shown related only to compressional waves and compared poorly with those presented by Hardin & Richart.

The general scheme of the apparatus employed by Lawrence was similar to that shown in Figure 2-7. A pulse generator sends simultaneously one electrical signal to the sample and another to the oscilloscope. The signal sent to the sample is transduced to a mechanical input, and, after traversing the sample, is picked up by another transducer whose output is also plugged into the oscilloscope, possibly after some amplification and filtering.

This scheme was devised more than 50 years ago (Mason ,1958) and has remained almost unchanged since. The only major modification, systematic in the last 10 years, has been the incorporation of computers for storage and analysis of the digital records of output and input signals. The instrumentation scheme is valid also for cases where multiple receivers are used, with the only difference that each receiver will provide a new signal to be plugged into the oscilloscope, which, of course, will need more channels[15].

By the mid 70's (Hampton, 1974, Richart, 1978) there was general agreement on the limitations of pulse tests in soils. Compressional wave measurements were numerous, but, as Biot theory explained, they were strongly affected by porewater and of little use to characterise the stiffness of soils. For the same reason, shear wave measurements were recognised as most interesting, but remained elusive. The problem, as it happened, was related to transducer design.

The transducers used so far (e.g. Withman & Lawrence, 1963) were similar to those used for other ultrasonic measurements, i.e. piezoelectric displacement transducers. For shear wave measurement they took the form of shear plates –Figure 2-8. In them, (Mason, 1958) the displacement of the transducer (D) and its resonant frequency (f_T) are related to the transducer material (k_i) and dimensions (L, length, T, thickness) and the input voltage (V) by

$$D = L\tan\left(\frac{k_1}{T}V\right)$$
$$f_T = \frac{k_2}{L} \qquad (40)$$

This resulted in high frequencies and small displacements, which, combined with the high attenuation typical of soils made the shear waves almost undetectable –Stephenson, 1978, provides an example of these problems-

---

[14] Hardin & Richart (1963) quote some earlier work of Matsukawa & Hunter (1956) on pulse transmission through soils. They were not controlling the pressure on the specimen. Interestingly, in their apparatus sand was contained within a cylinder lined with sponge rubber, an absorbing material. The pulse frequency was 20 kHz.

[15] Alternatively, (Lee, 1993), the oscilloscope might be suppressed and the signals directly plugged in to the computer via some ADC.

The introduction of bender elements (Shirley, 1977; Shirley and Hampton, 1977) represented a major breakthrough. Within bender elements the piezoelectric transducers were arranged as a deflecting beam[16] –see Figure 2-9- thus increasing substantially their flexibility, and allowing a much bigger mechanical output for a given voltage and a much lower resonant frequency, namely:

$$D = \frac{3}{2} k_3 \left(\frac{L}{T} \right)^2 V$$
$$f_T = k_2 \frac{T}{L^2} \qquad (41)$$

Working with the same piezoelectric material they achieved a ten fold increase in displacement magnitude and a twenty fold decrease in resonant frequency. This arrangement effectively overcome the limitations posed by high attenuation as they proved installing the transducers in and oedometer-like box and measuring shear velocities as low as 3.6 m/s.

Shirley and Hampton developed the bender elements as logging instruments, to be mounted on drilling rigs for off-shore exploration of soft marine sediments. Their laboratory tests, employing variously shaped calibration chambers, were designed to prove the viability of the concept and not as an standalone objective. It was Schultheiss –1983- who first installed bender elements as transducers on standard soil testing equipment, namely an oedometer and two different triaxial apparatuses. The elements were built in into the end and top platens and cantilevered into the sample in a design illustrated in Figure 2-9. With minor modifications[17], this design became a model for most subsequent work. Table 2-1 resumes the information available on various bender element transducers employed to date. A tendency to reduce the size of the instruments is noticeable.

The use of shear plates for stiff soils was advocated by Brignoli et al. (1996), but the idea does not seem to have had many followers. The system employed by Nakagawa et al. (1996) is an interesting exception, showing the problems associated with this design. Testing medium stiff soils (v_s 100 to 300 m/s) they experienced highly attenuated reception. That required using four transducers in parallel, high voltage inputs (500 V against 10 V in many bender based tests), strong amplification, signal averaging and filtering, to produce more or less interpretable traces.

Test in calibration chambers have used different transducer types. For example, Lee (1993), uses accelerometers and geophones (velocity transducers), whereas Bellotti et al. (1997) used geophones both as sources and receivers.

---

[16] Sometimes called a bimorph

[17] Mostly concerning aspects related with the achievement of a satisfactory electrical insulation of the transducers: resin coating procedures, cable choice ...Pennington (1999) gives more details about bender element fabrication.

2.2.3 Bender element response

Their mounting procedure separates bender elements tests from most usual arrangements of ultrasonic tests. The hardness of most materials tested in shear was enough for the ultrasonic probe to be placed completely outside the sample, on its surface. As Schultheiss -1983- reports, the initial arrangement of bender elements respected this approach, and the newly developed beam-like piezoelectric transducers were placed within the container walls of the testing chamber. This soon proved unpractical, due to the imperfect isolation of transducers and container. As the elements bent they rang against the wall, thus transmitting a good deal of energy via the box itself. This being metallic, a fast, high frequency disturbance manifested itself on the trace of the received signal. On the short term problems were solved (?) filtering out the high frequencies from the trace. But on the long term a simpler solution was devised and the transducers were installed inside the sample, first as a pinned beam on a platform and then cantilevered.

For most external transducers the relevant basic model for transducer operation was and still is the radiating piston or baffle –Mason, 1958. In this model the transducer radiates plane waves through an aperture on a rigid wall. This aperture has a size corresponding to the contact face within the transducer and the sample. The radiated field is diffracted into the sample and a wave beam results. The characteristics of the radiated field have been thoroughly explored. Coupling problems made this model only approximate but transducers are now tailored to radiate much closely to its specification -Hutchins & Hayward, 1990.

The situation with bender elements is far less satisfactory and little is known about their detailed behaviour. Usually bender probes are specified by their resonant frequency. This is obtained -e.g. Morgan Matroc 1999- as the first resonant frequency for a free cantilever beam. Of course a free cantilevered beam has other, higher, resonant frequencies. They correspond to modes where the curvature of the beam changes sign along its length. In operation, bender probes are surrounded to a higher or lesser degree[18] by soil. This will change their dynamic response. Qualitatively, it will add damping to the system thus lowering somehow the resonant frequencies.

Huot –1999- has investigated this problem. He modelled the soil constraint as a viscoelastic support distributed along the beam. For the case of a relatively rigid soil (E = 900 MPa) he observed that when the higher modes were excited the signal was richer in v_p travelling energy.

It is not known how this relates to the "overshooting" described by Jovicic et al. (1996). Using the self-monitoring technique proposed by Schultheiss they observed that the input signal was not followed by the transducer when the frequency was increased. A self-monitoring piezoelectric transducer has an input band and an output band on its surface, mechanically joined but electrically isolated. This allows to measure the output from the source bender, thus determining its response to the electrical input when mounted within the sample. Although this technique seems very well suited to establish the transfer

function F_B it does not seem to have been systematically exploited. Recent laser observations by Greening (2001) indicate however that their performance is poor.

2.2.4 Arrival time identification

Two measurements are needed to obtain a velocity value from a pulse test: distance between source and receiver and travel time. Distance is by far the less problematic: the only uncertainty is related with the finite size of source and receiver. The usual approach to this has been to obtain travel times at varying distances and then extrapolate the results to zero travel time. By so doing, a number of investigations (e.g. Schultheiss, 1983) have shown that the best distance estimate for bender elements is given by the tip-to-tip distance between instruments.

The scheme shown in Figure 2-6 is an obvious idealisation. One particular aspect of it may be strongly misleading: the propagating mechanical disturbance is represented as a line, therefore suggesting an unequivocal, easily identifiable, arrival. That might be the case for materials with good acoustic properties i.e. materials transmitting fast, with low attenuation or distortion. An example of the kind of result there available is shown in Figure 2-4. For soils this is not at all the case.

The input signals employed in pulse testing might be more or less controlled in shape. For instance, in field tests impact sources are common, thus producing a rather uncontrolled input. An example of this practice, as presented by Mancuso et al. (1989), is shown in Figure 2-11. In the laboratory, on the other hand, the general practice is to specify more tightly the input signal. As can be checked in Table 2-2 the pulse shapes favoured by most researchers have been either square –e.g. Jamiolkowski et al. (1995) Figure 2-12- or sinusoidal –e.g. Shirley (1978) Figure 2-13-. Occasionally, there have been more imaginative proposals, such as the distorted half-sine postulated by Jovicic (1997) and reproduced in Figure 2-14 as applied by Pennington (1999). Nevertheless, what is clear from this figures and from all the similar ones published to date is that what appears on the output is not very similar to what has been used as input. Even for aligned multiple-receiver set-ups, as in Figure 2-11, the comparison between their respective outputs still shows appreciable differences.

Therefore it seems that pulse test in soils should cope not just with a slow, highly attenuated transmission, but also with an important distortion of the transmitted signal. This, of course, creates problems of interpretation. If a signal, however complicated, travels undistorted between two points, any particularity of its shape might well be taken as reference of its arrival. But when this is not the case some other criteria needs to be applied.

As the output pulses, even distorted, are finite in extent, one possible approach would be to ignore the problem and select any point in the pulse as indicating the arrival. If the pulse is short enough compared with the theoretical travel time the error will be small. Consider the distorted transmission represented in

---

[18] They have to go also through the end porous stones employed in triaxial testing.

Figure 2-15. If there is complete uncertainty about which point to select within the arrival signal[19], the maximum possible error will be

$$\varepsilon_{MAX} = \frac{T_{ap}(1+n)}{T_i} \tag{42}$$

Here T_{ap} represents the duration -or apparent period- of the input. The arriving signal is not only distorted, but longer than the input –something which is observed on all the traces registered in soils- This extra length is represented by a factor n. Finally T_i represents the ideal arrival time for an undistorted signal. This ideal arrival time will be given by the characteristic velocity of the medium, V and d, the distance between source and receiver. Introducing those values in (34) the following expression results

$$\varepsilon_{MAX} = \frac{V(1+n)}{d\ f_{ap}} = \frac{\lambda_{ap}}{d}(1+n) = \frac{(1+n)}{n_{ap}} \tag{43}$$

where an apparent frequency and wavelength of the pulse have been introduced with obvious meaning. The resulting adimensional apparent normalised distance, n_{ap}, is an important parameter of pulse tests. It represents the number of apparent wavelengths between source and receiver. In soils, its value is strongly limited by their characteristically high attenuation. A value of 10 is a reasonable upper limit, representative of most current practice. In fact, for reasons that will be explained below, most researchers try to obtain a value of n_{ap} between 2 and 4. The value of n, on the other hand, is more difficult to establish on a general basis, but, judging from reported cases like the one shown in Figure 2-13 a value of n = 0.5 would seem a reasonable lower bound. Figure 2-16 is a plot of equation (2) using these values. In soils the problem posed by signal distortion is potentially very important.

Note that this problem is closely related to the limited range of n_{ap} in soils. In materials with better acoustic properties, such as rocks, pulse transmission tests are inherently more precise. For instance, the shear wave measurements by Simmons (1964) were made with an apparent normalised distance of around 40. For the case represented in Figure 2-16 this will bound the error to a few percentage points. If the signal distortion is less intense the improvement will be even higher. In fact, with an experience mostly based in rocks, Schreiber et al. (1973) gave a value of 1% as the expected precision of pulse transmission tests when the arrival time was directly established by inspection of the trace on the oscilloscope[20]. The arrival was identified as the first arrival point i.e. the point where the trace of the received signal first departs from zero.

The same method was applied by Shirley (1978), and, as Table 2-3 shows, this has been and remains the most popular method of time arrival identification in soil mechanics. Although conceptually simple, this method requires a fair amount of interpretative skill –e.g. Figure 2-17 Thomann & Hryciw 1990-, and

---

[19] To simplify the discussion we assume here that there is no uncertainty on the input signal.
[20] And one order of magnitude more if some visual reference was introduced on the oscilloscope, for instance by means of a mercury delay line.

perhaps the most extended agreement among practitioners is about the important role that subjectivity and expertise plays on it (e.g. Viggianni, 1992, Brignoli et al., 1996, Pennington, 1999, Lo Presti, 1999, Kuwano, 1999).

Another possible approach is to establish the arrival selecting comparable, easily identifiable points, on two traces. This is most easily applied to aligned receiver set-ups and thus was used first in the context of field cross-hole testing (Sánchez-Salinero et al. 1986, Mancuso et al. 1989). First peak, first crossing and first through have been proposed as candidates for an easy identification.

In source to receiver set-ups this approach has also been used. Sinusoidal or sinusoidal-like input pulses offer peaks and throughs so they seem suitable for this criteria. But even when, for instance because of being square, the first signal has not any characteristic point, there may be advantages in establishing as arrival a characteristic point (first peak, first crossing,...) of the second signal. A major one is that easiness of identification might ensure a more repeatable procedure. If pulse testing is used as a change-tracking tool during a different test this is the essential requirement. Even if a systematic error is present, it would be the same in all the measurements. Therefore change trends will be more reliable than isolated measurements. This is a common sense argument and, in the context of pulse testing has been put forward a number of times (e.g. Weidner, 1987, Viggianni, 1992, Kuwano, 1999).

Of course, the problem is that different researchers might use different characteristic points and comparison between their respective results will be then subject to the uncomfortable background of Figure 2-16. Some researchers have indeed measured the differences arising from assigning the arrival time to one or another point in the trace. Bodare & Massarsch –1984- in a series of cross-hole essays in clay with an impact source registered differences of 50% between measurements based on different characteristic points. Viggiani and Atkinson -1995- using bender elements in clay showed differences of 30% for the case of a low frequency square wave.

Another easily repeatable criteria to identify arrival times is given by the cross-correlation[21] maxim of the first and second signal. Again this was applied first to cross-hole testing with multiple receiver set-ups. (Sánchez-Salinero et al. 1987, Mancuso et al. 1989) Then Viggianni & Atkinson (1995) applied it to bender element tests. In all those works arrival times obtained by cross-correlation are shown to be different than those obtained from characteristic points. Viggianni & Atkinson (1995) proclaimed it "the most accurate", but curiously, in subsequent work by the same group (Jovicic et al. 1996) this method was deemed too complicated and abandoned. Maybe because of that it has not had many followers[22], and only Arulnathan and co-workers have made systematic use of it (Arulnathan et al. 1998, Boulanger et al. 1998).

---

[21] A brief reminder of this and other signal treatment concepts is given in Appendix I

[22] Cross-correlation and other FFT based signal treatment procedures are now built-in most common laboratory equipment like oscilloscopes, and they are also heavily used in many fields, either very close (e.g. geophysics) or unrelated but pervasive (e.g. image analysis). This can hardly be seen as "complex numerical analysis" (Jovicic et al. 1996).

Another interesting variation has been proposed by Boulanger et al. (1998). They used also visual identification of characteristic points and cross-correlation, but comparing the first and second arrival of the signal. In fact, this is an echo-based method. Echo methods are known since long (e.g. Schreiber et al. 1973) to require samples with higher acoustic quality than through transmission methods. One reason is that attenuation makes hard to detect the echo. Another is that if the signal is distorted and the path is relatively short (low n_{ap}) first and second arrivals may overlap. Those problems were also recognised by Arulnathan et al. (1998).

All the arrival identification methods described so far have one point in common: they work on the time record of the signal. An alternative procedure is to work on the frequency domain and obtain a velocity value examining the phase of the cross-spectrum. Details of how this is actually done are left for later. Here it is enough to say that again this was first proposed to interpret field tests either with a single (Bodare & Massarsch, 1984), or multiple aligned receivers (Mancuso et al. 1989). Again it was applied to bender element testing by Viggiani and Atkinson (1995) and later discarded as being too complicated by Jovicic et al (1996). This frequency domain approach has had even less followers than cross-correlation: Arulnathan et al. (1998) did not use it on grounds that it produced almost the same results as cross-correlation. This was based on a single test by Viggiani and Atkinson (1995) showing indeed a close result. On the other hand, results by Mancuso et al. (1989) showed far more disagreement between this cross-spectrum value and the cross-correlation one.

2.2.5 Interpretation models

As pointed out by Jovicic (1997) the dominant model for pulse test interpretation is that of a shear bulk plane wave travelling between source and receiver. Hence the test result is simply related to the shear modulus by equation (32). This is straightforward, but has an important disadvantage. As explained in chapter 1, this model offers no cue whatsoever about why there is any signal distortion at all and hence it is unhelpful to rank the various results obtained with different arrival time identification methods.

A new perspective was introduced by Sánchez-Salinero working at the University of Texas, Austin (Sánchez-Salinero et al. 1986). As his work has permeated most of later approaches to this problem it is worth considering it in some detail. With a multiple aligned receiver, field cross-hole set-up in mind, he performed a systematic sensibility analysis of the propagation of a single sinusoidal pulse in isotropic elastic media. His attention was focused on the peculiarities of the movement near its source. For reasons that will be made clear in chapter 4, plane bulk waves are a good approximation to this problem only when the normalised distance between source and receiver is above some limit value. This value marks the end of what is known as the "near field" of the movement[23].

Salinero produced clear graphic evidence of how near field effects could affect the recorded shear movement, taking also into account hysteretic damping. He did that by numerically generating and

analysing synthetic wave records, and compared methods of time arrival selection based on direct inspection of the simulated signals, methods based on their time cross correlation, and methods based on frequency spectra analysis.

One of his main results was that if the receiver is placed within the near field range of the test the precise measurement of velocity could be very problematic, particularly in time domain. Having thus established the importance of proper receiver placement, he gave recommendations for it, proposing the following limits:

$$2 < \frac{r}{\lambda_{ap}} = n_{ap} < 4 \qquad (44)$$

$$\lambda_{ap} = v_s T_{ap}$$

where T_{ap} is the apparent period of the single sinusoidal pulse he was employing. The upper limit was introduced to make allowance of signal attenuation via damping, the lower limit for near field effects.

It is important to note that Salinero was working with a multi-receiver set-up in mind. The signals he was comparing, correlating, etc were theoretical records from two receivers, placed at different distances. This has not discouraged other researchers from applying its results in source to receiver experiments and, in fact, they have been extensively used, almost to the point of becoming standard (e.g. Viggiani, 1992; Brignoli et al., 1996; Jovicic, 1997; Pennington, 1999; Lo Presti et al, 1999; Kuwano, 1999).

A good corroboration was seemingly obtained by Brignoli et al (1996). They made source to receiver experiments with simultaneous measurement of compressive and shear motion. Results showed the simultaneous appearance of movement in both traces and also how an increased n_{ap} resulted in a more clear arrival in the shear trace -Figure 2-18-, in accordance with Salinero's results.

Following Salinero's recommendations has not been a recipe for unalloyed success. Gajo et al. (1997), Moncaster (1997), Pennington (1999) and Kuwano (1999), amongst others have reported difficulties in obtaining clear arrivals even when abiding by these rules. The fact that Salinero's work was made within an isotropic single-phase elastic theory might point to the origin of some discrepancies when his work is used within different assumptions, like anisotropy (e.g. Pennington, 1999) or fluid-solid interaction (Gajo et al. 1997). Moreover, Salinero only used one input waveform shape, a sinusoidal single cycle. It is not clear to what point his recommendations extend to different waveshapes, like those recommended by Jovicic (1997) or to the -still in use- square signal.

There are other intriguing aspects. Sometimes -Table 2-3- signal polarity inversions are used to help interpretation in shear movement traces. The idea is that shear waves change polarity while compressive waves do not. Salinero et al. (1987) showed that this technique was useless while working in the near

---

[23] This is an usage taken from geophysics (Aki & Richards, 1980, Udías, 2000). Note that "near fields" with different characteristics appear also in the proximity of a diffracting obstacle. This is the main usage of the term in ultrasonics literature (Mason, 1958,

field. This was, nevertheless, the technique used by Dyvik and Madshus (1985) at the NGI to interpret the arrival of a low-frequency square signal -Figure 2-19.

Dyvik and Madshus results are important, because they installed bender elements in a resonant column, thus obtaining a direct comparison of the shear modulus obtained with both systems. Their results for Drammen clay are shown in Figure 2-20. This almost perfect agreement was reproduced, -with slightly less impressive neatness-, by Thomann and Hryciw (1990) working with sand. In apparent contradiction with them, Jamiolkowski et al. (1995) reported an average difference of circa 25% between bender and RC shear modulus for clay. Later, Nakagawa et al. (1996) obtained similar differences, albeit their transducers were of the shear plate type. Disagreements between RC and bender element results have also been found in recent work at Imperial College: moderate while benders were installed in solid samples –Kuwano, 1999, Figure 2-21- they became much more impressive (up to 300% of shear modulus estimates) when using hollow cylinder samples –Conolly & Kuwano, 1999.

It is difficult to tell what lies beneath these discrepancies. As we have seen, the detailed interpretation procedure of pulse test in soils is far from settled. Different researchers develop different recipes for the task with a pick and mix approach. Even where an apparently optimal tradition should exist it is changed if need comes. An example is provided by work at the NGI–Figure 2-22, BRE, 1997. In the figure 1st and 2nd choice refer to pulse test with bender elements. The 1st choice corresponds to arrival points selected with the criteria established by Dyvik and Madshus. The 2nd choice to a new criteria developed -again- with the help of resonant column testing. Overall, it is difficult to disagree with Arulnathan et al. (1998) when they ended their study of the subject claiming for more "experimental and analytical research".

2.3 SUMMARY

Although conceptually more complicated than static methods, dynamic procedures offer powerful tools to measure D_0. There are a variety of methods available, but in later times pulse tests have become very popular in geotechnics because of their versatility. In soils, pulse tests, like any other dynamical methods, have to cope with a slow and highly attenuated transmission. Shear waves are of higher interest, because they are less affected by pore fluids. Their measurement in the laboratory required the development of low-frequency highly compliant transducers: piezoelectric bender elements. Then transmission was possible, but this revealed another problem: the transmitted pulse was substantially distorted on reception. This affects the interpretation procedure, introducing considerably uncertainty in the process. A number of suggestions have been introduced to ease the problem, but their following its not unanimous and their results sometimes contradictory.

Krautkramer, 1990).

2.4 TABLES

Reference	Material	Fixity	Set-up	L (mm)	W(mm)	T (mm)
Shirley & Hampton (1978)	Ceramic	Pinned	C. chamber	25.4		12.7
Schultheiss (1983)	PZT	Cantilevered	Oedometer	10	5	3
Schultheiss (1983)	PZT	Cantilevered	Small TX	15	15	13
Schultheiss (1983)	PZT	Cantilevered	Big TX	18	18	3
Dyvik & Madhus (1985)	Ceramic	Cantilevered		14.5	12	1
Brignoli et al (1996)	PZT 5HN	Cantilevered	TX	20	10	1.1
Jovicic (1997)	PZT 5B	Cantilevered	TX	13	10	3
Arulnathan et al. (1998)	Ceramic	Cantilevered	TX	15	15	1
Pennington (1999)	PZT 5B	Cantilevered	TX (belt)	3.5	5	0.5

Table 2-1 Some characteristics of bender-type transducers employed in previous research

Reference	Type	Apparatus	Signal shape	fap(kHz)
Shirley & Hampton (1978)	BE	Calibration chamber	Sine	0,338
Shirley (1978)	BE	Calibration Chamber	Sine	4
Schultheiss (1983)	BE	Oedometer	Square	
Schultheiss (1983)	BE	Triaxial	Square	< 40 Hz
Dyvik & Madshus (1985)	BE	Resonant column	Square	< 0.1
Thomann & Hryciw (1990)	BE	Oedometer Resonant column	Square	?
Viggiani (1992)	BE	Triaxial	Sine	1 – 10
Jamiolkowski et al. (1995)	BE	Oedometer	Square	0.1
Brignoli et al. (1996)	BE SP	Triaxial	Sine	1 – 20
Nakagawa et al. (1996)	SP	Triaxial	Sine/Sawtooth	3 – 5
Jovicic (1997)	BE	Triaxial	Distorted half-sine/Sine burst	< 20
Boulanger et al. (1998)	BE	Triaxial	Sine	1.1
Zeng (1999)	BE	Oedometer	Square	?
Pennington (1999)	BE	Triaxial	Sine/Distorted half-sine	3 – 20
Kuwano (2000)	BE	Triaxial	Sine	4 –10
BE = Bender element SP = Shear Plate				

Table 2-2 Laboratory shear pulse tests: transducer and input signal in previous research

Reference	Method	Point	Auxiliary criteria
Shirley & Hampton (1978)	Visual identification	First arrival	
Shirley (1978)	Visual identification	First arrival	
Schultheiss (1983)	Visual identification	First arrival	
Dyvik & Madshus (1985)	Visual identification	First arrival	Polarity inversion
Thomann & Hryciw (1990)	Visual identification	First arrival	
Viggiani (1992)	Visual identification	First peak	
Lee (1993)	Visual identification	First arrival	Polarity inversion
Jamiolkowski et al. (1995)	Visual identification	First arrival	
Brignoli et al. (1996)	Visual identification	First arrival	P measurements Salinero's NFL
Nakagawa et al. (1996)	Visual identification	First arrival	P measurements
Jovicic (1997)	Visual identification	First arrival	Salinero's NFL
Boulanger et al. (1998)	Visual identification	Characteristic	First and second

Reference	Method	Point	Auxiliary criteria
		points	arrival
Boulanger et al. (1998)	Cross-correlation	Maximum value	First and second arrival
Zeng (1999)	Visual identification	First arrival	Polarity inversion
Pennington (1999)	Visual identification	First arrival	Salinero's NFL
Kuwano (2000)	Visual identification	First arrival	Salinero's NFL
NFL = Near Field Limit ; P measurements = simultaneous measurement of compressive waves available			

Table 2-3 Laboratory shear pulse tests: arrival identification in previous research

2.5 FIGURES

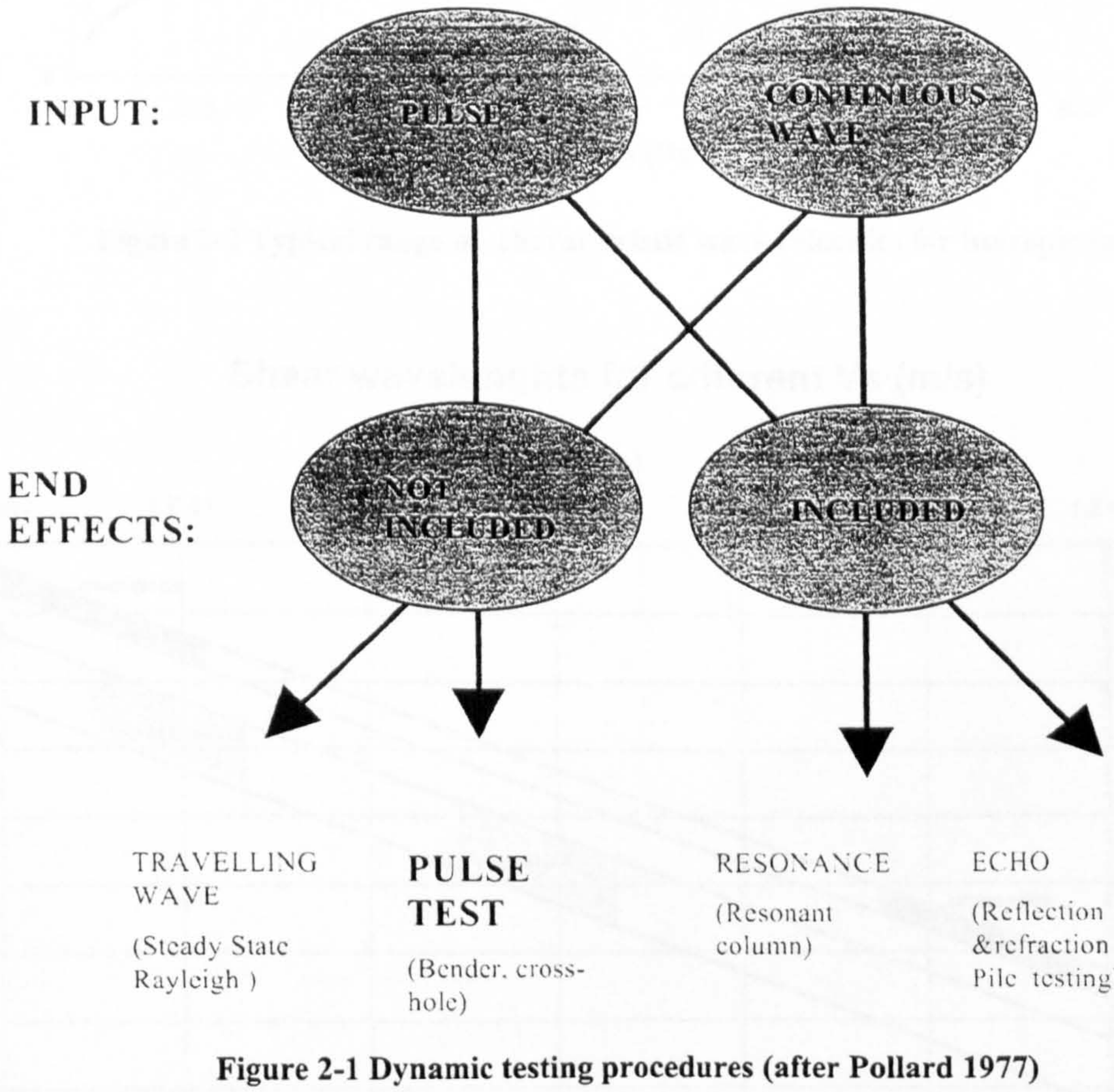

Figure 2-1 Dynamic testing procedures (after Pollard 1977)

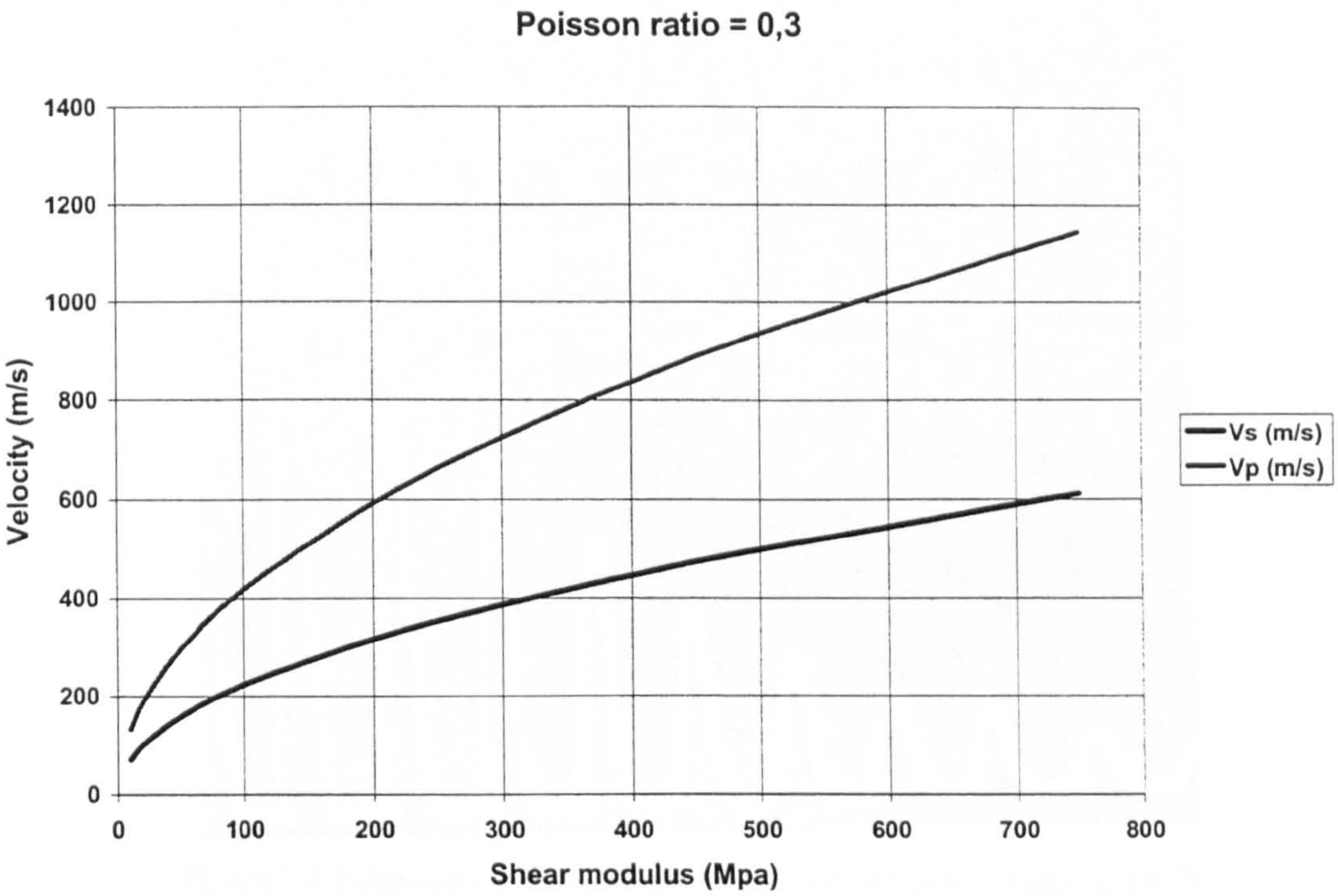

Figure 2-2 Typical range of characteristic wave velocities for isotropic soils

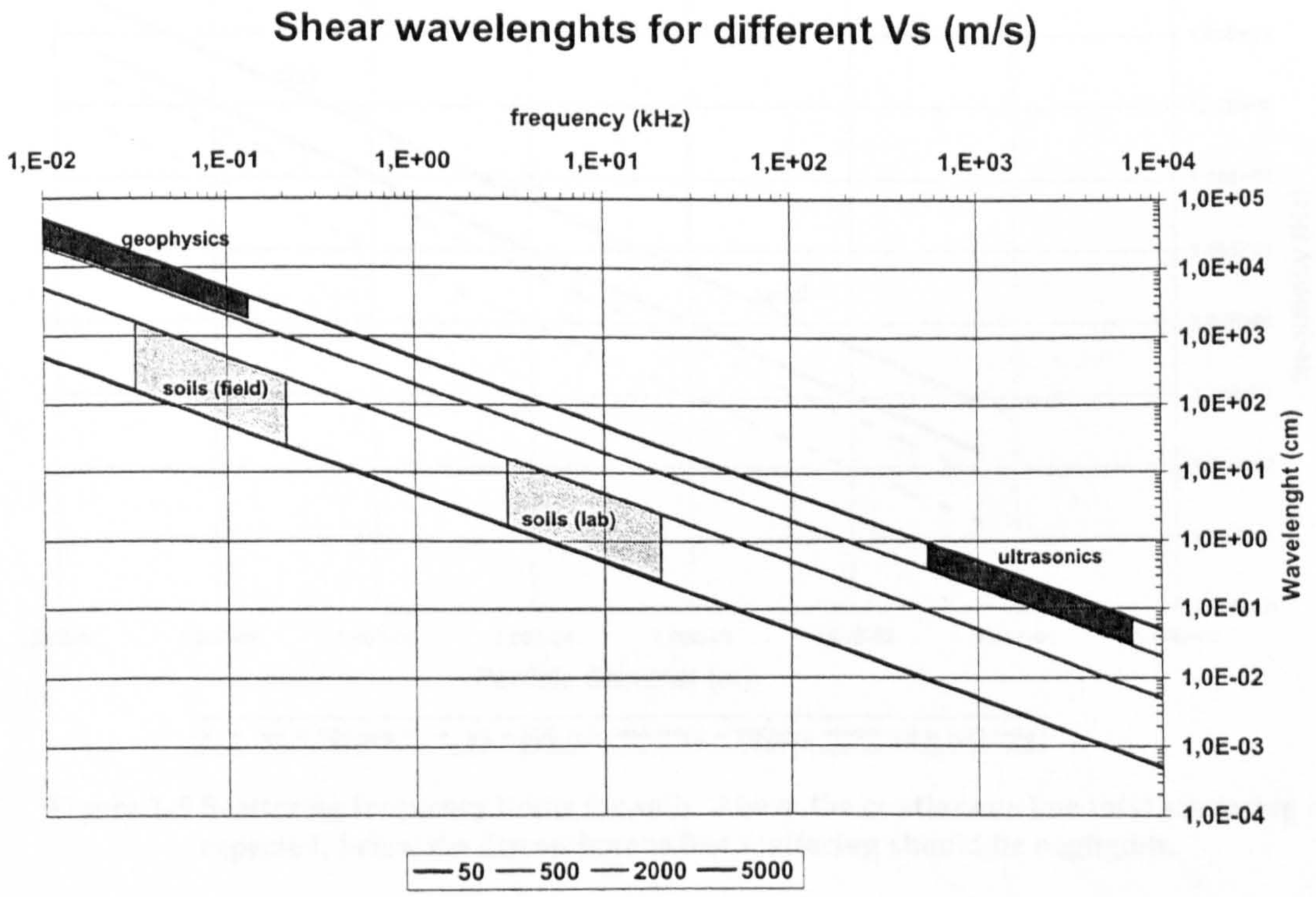

Figure 2-3 Comparative ranges of pulse tests in geotechnics and some related fields

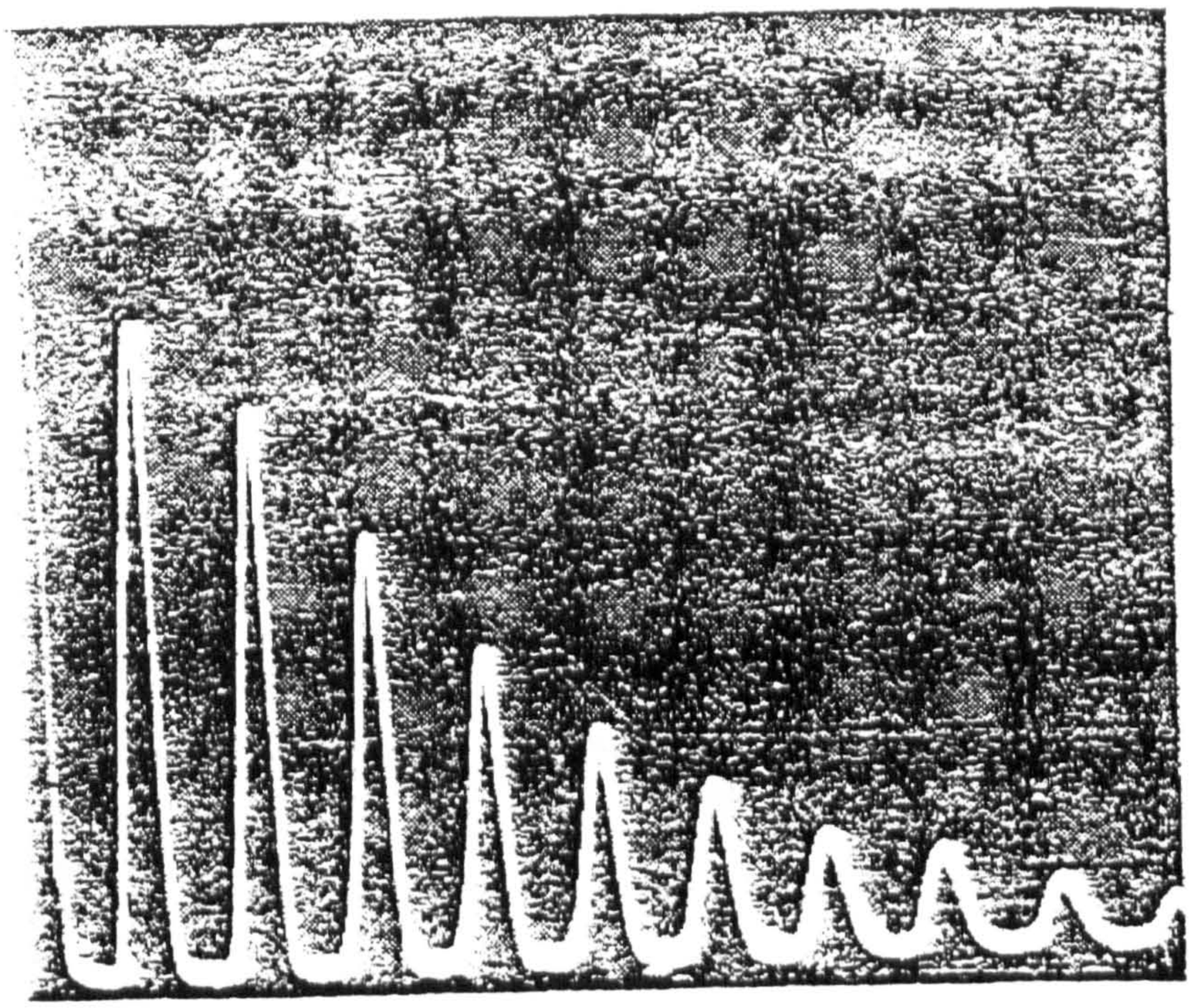

Figure 2-4 Pulse-echo test in a single cystal of NaCl (after Pollard, 1977)

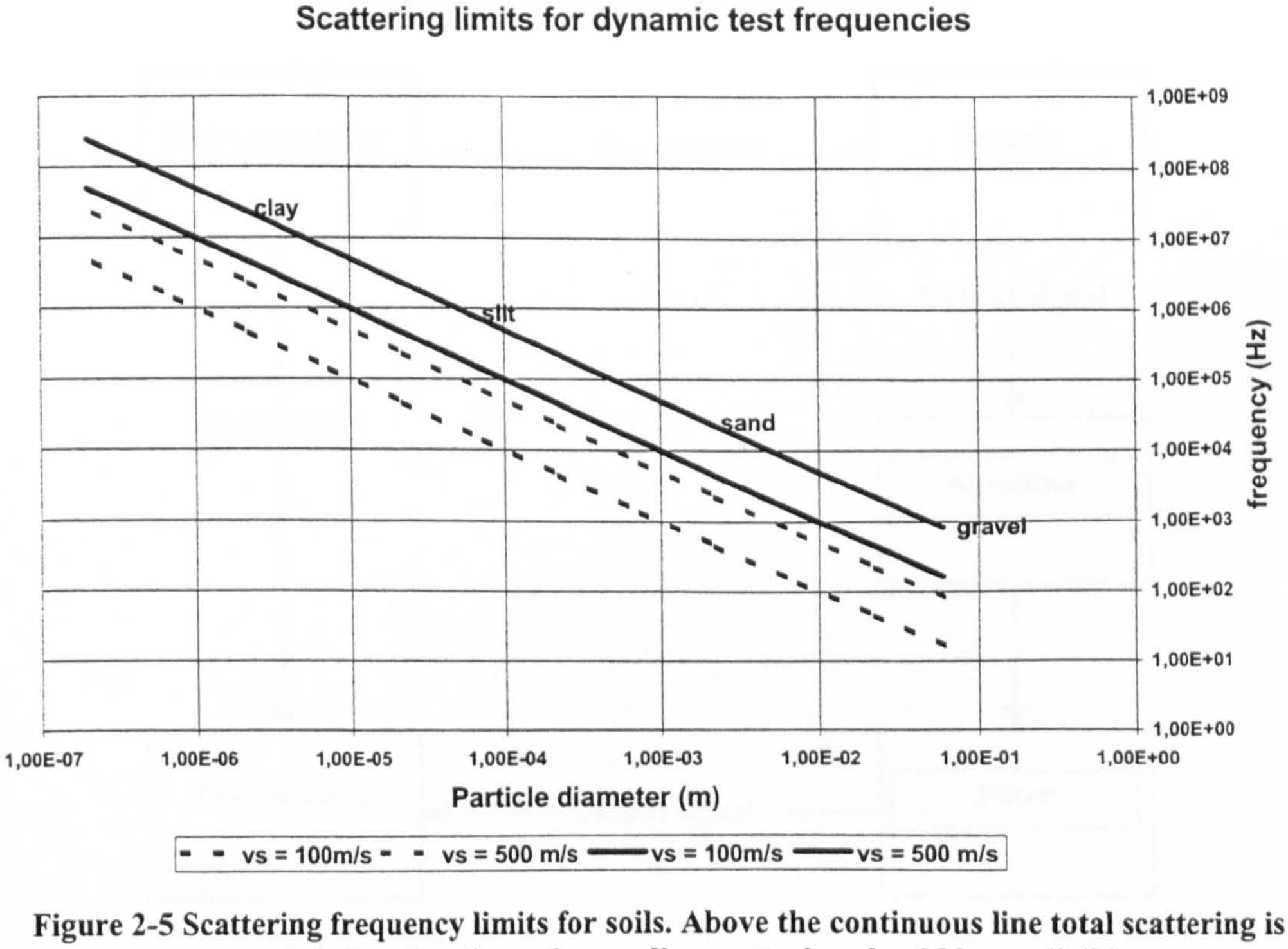

Figure 2-5 Scattering frequency limits for soils. Above the continuous line total scattering is expected; below the discontinuous line scattering should be negligible.

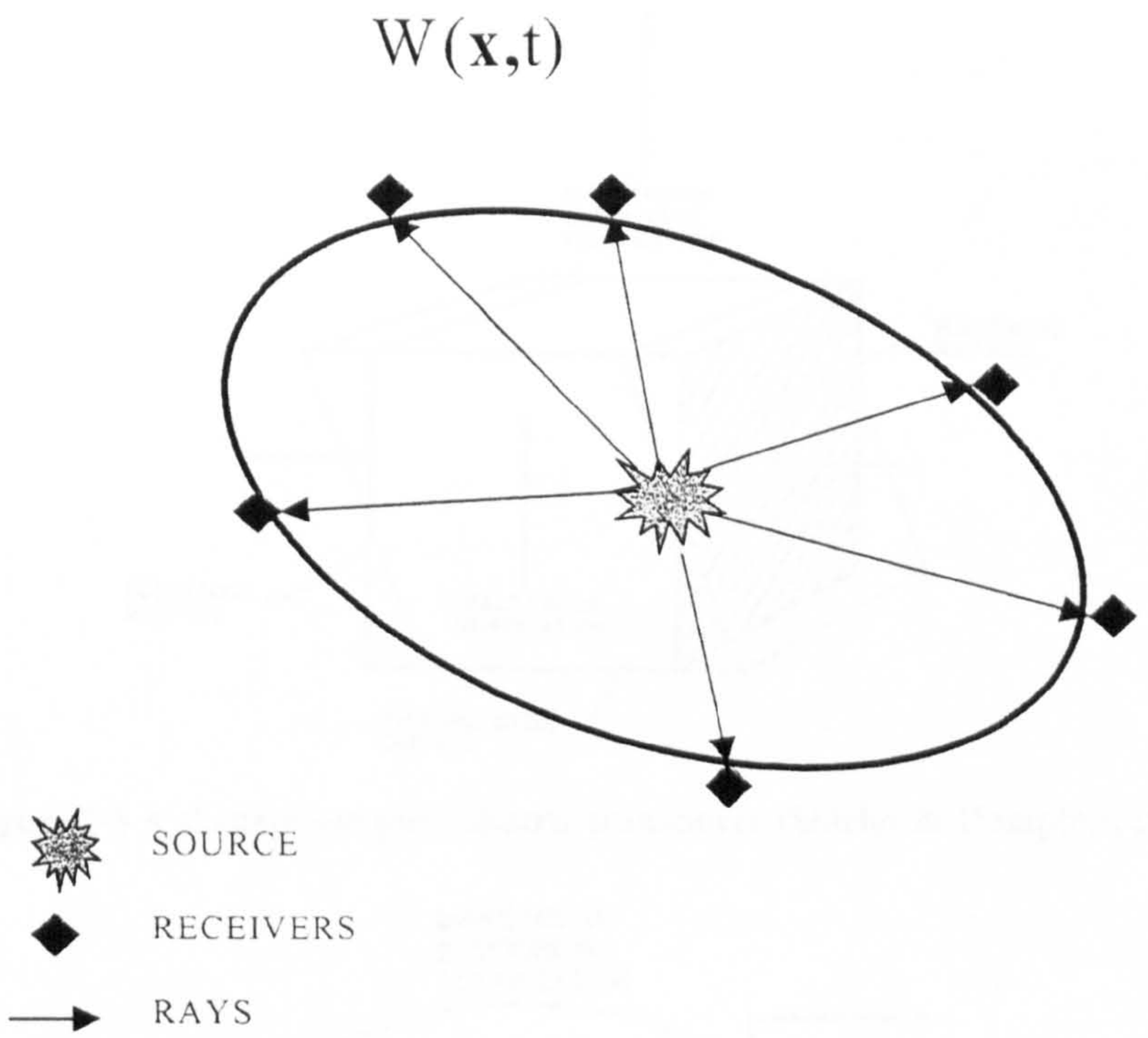

Figure 2-6 Pulse tests; conceptual scheme.

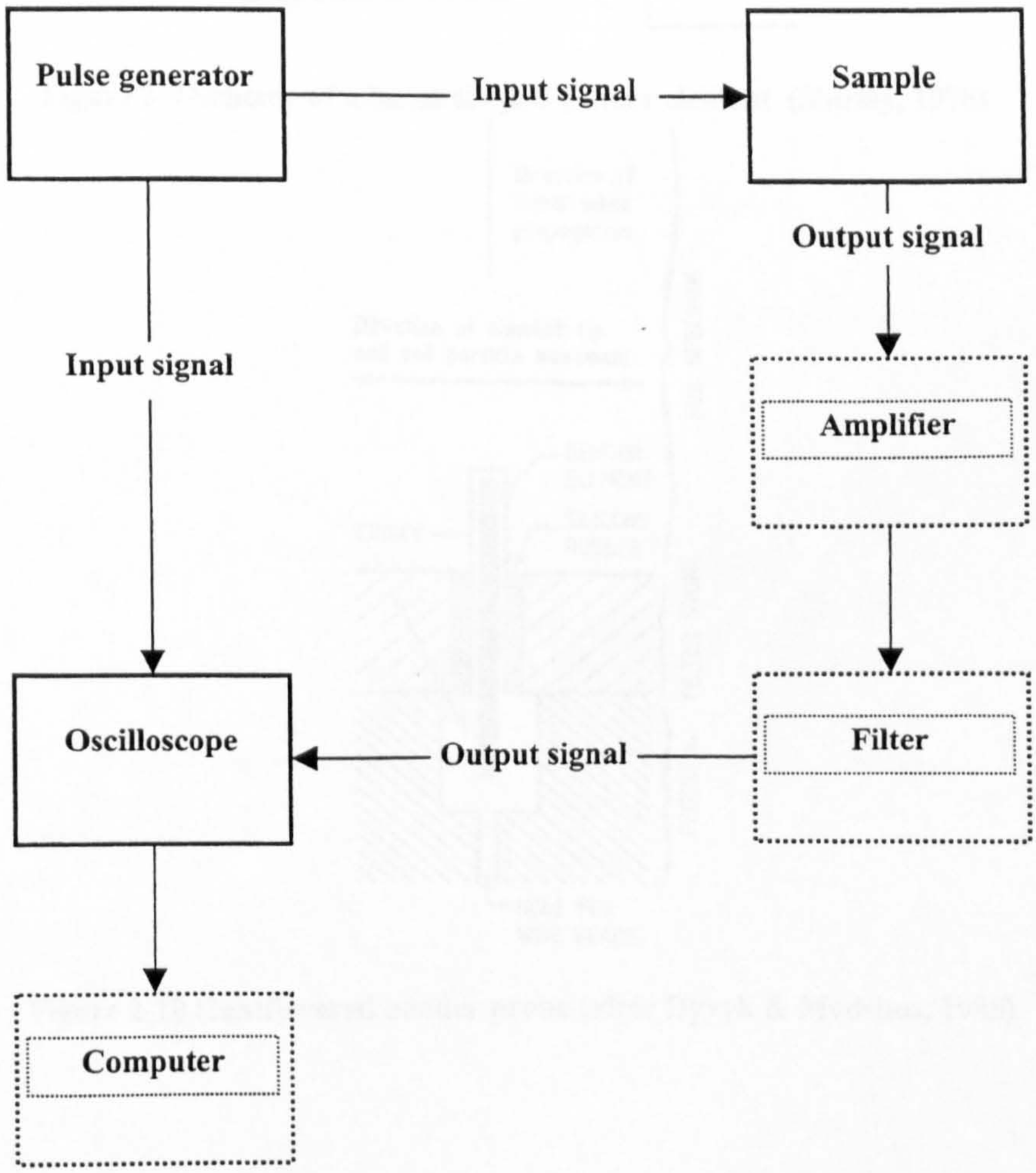

Figure 2-7 Instrumentation scheme for pulse tests in soils

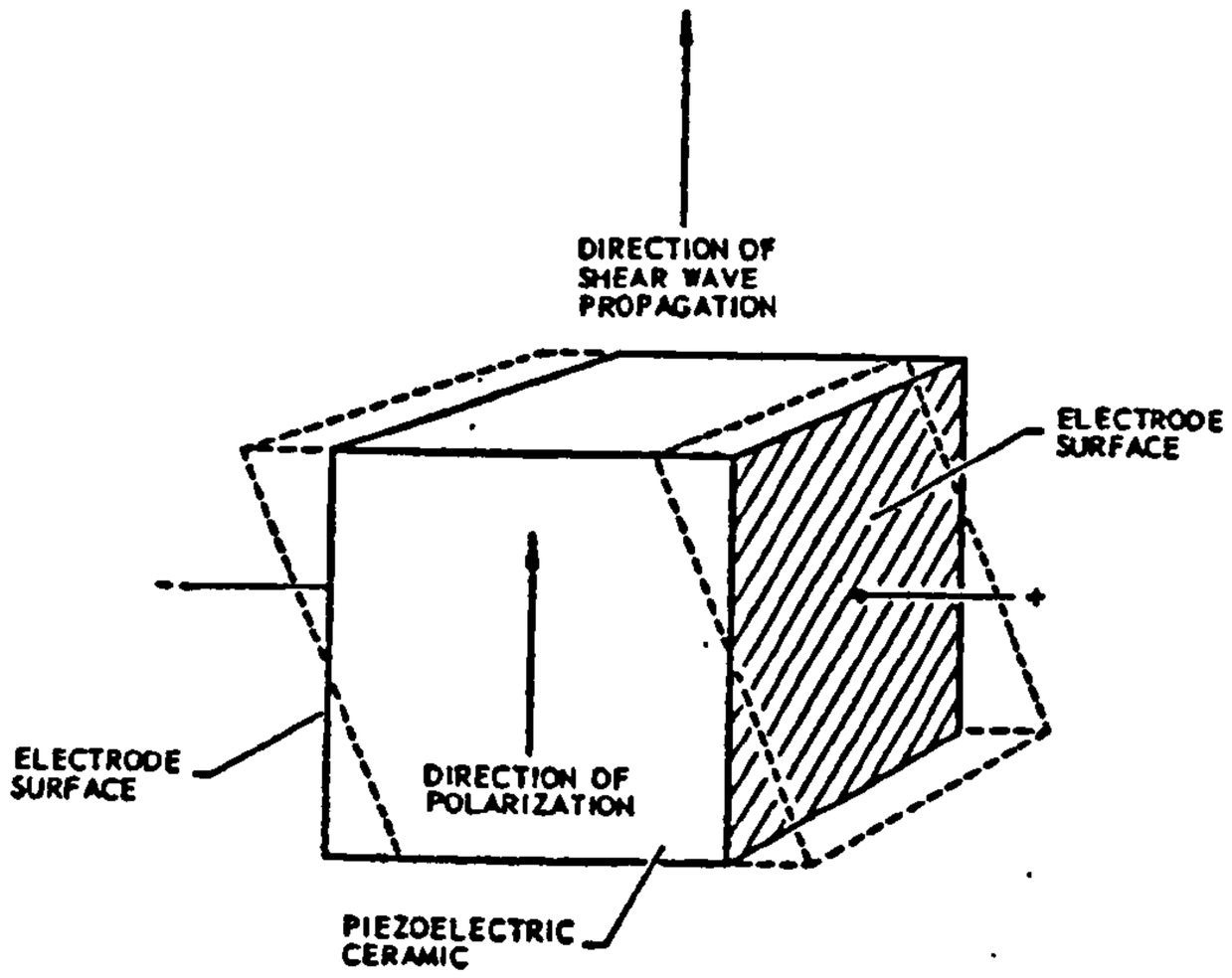

Figure 2-8 A shear-plate piezoelectric transducer (Shirley & Hampton, 1978)

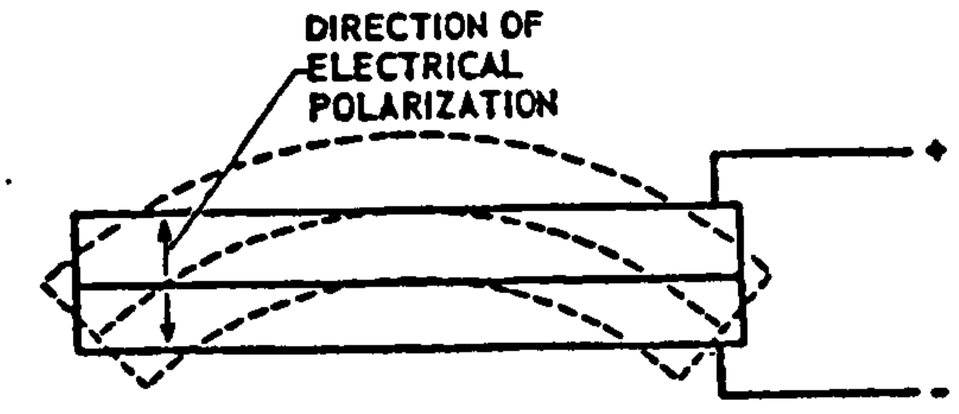

Figure 2-9 Scheme of a beam shaped bender element (Shirley, 1978)

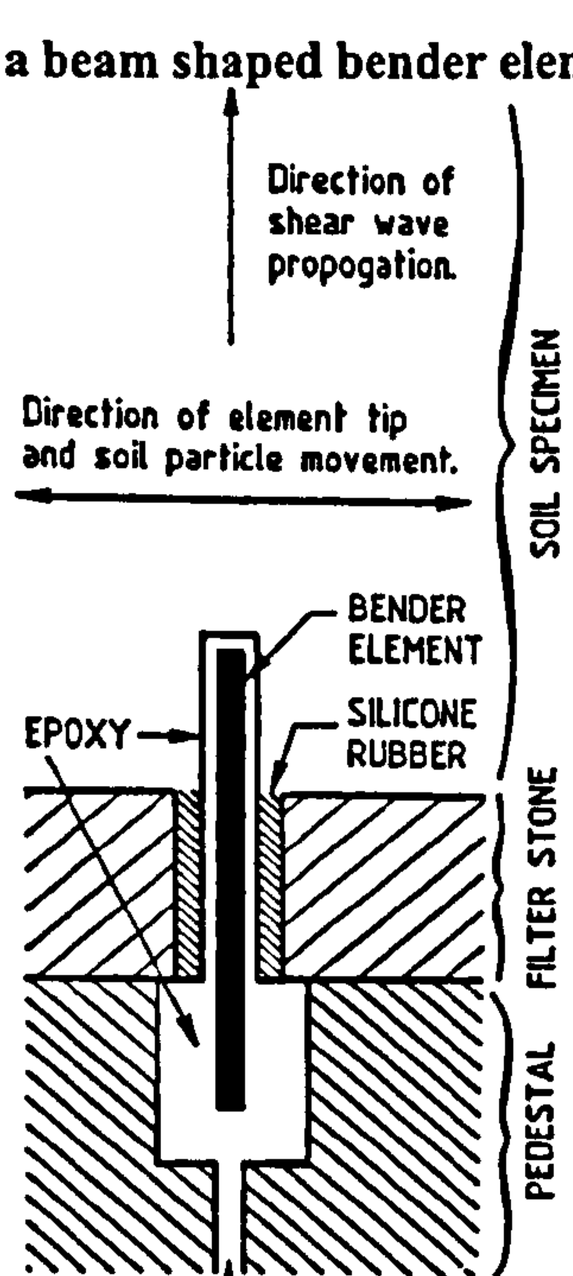

Figure 2-10 Cantilevered bender probe (after Dyvyk & Madshus, 1985)

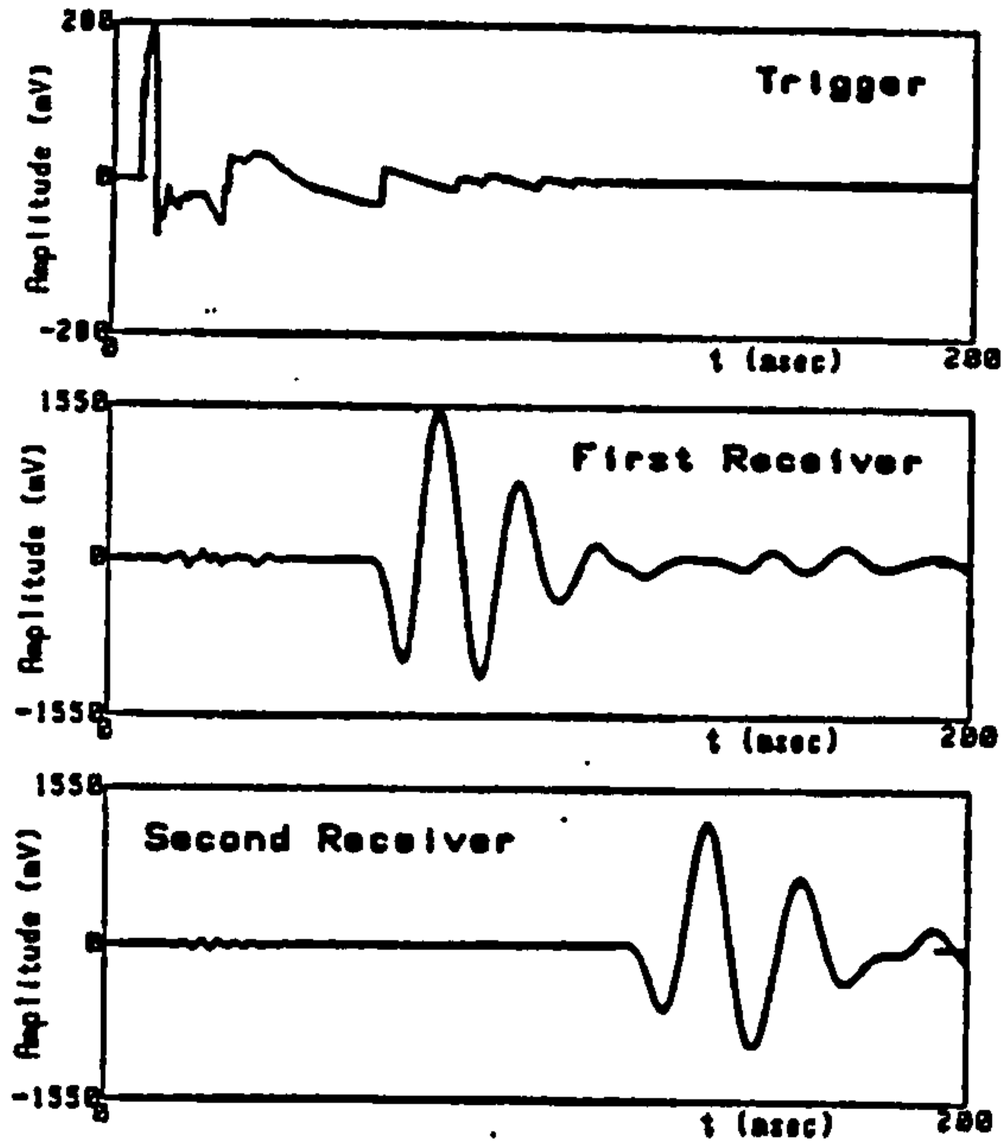

Figure 2-11 Impact source in a cross-hole pulse test in clay (Mancuso et al. 1989)

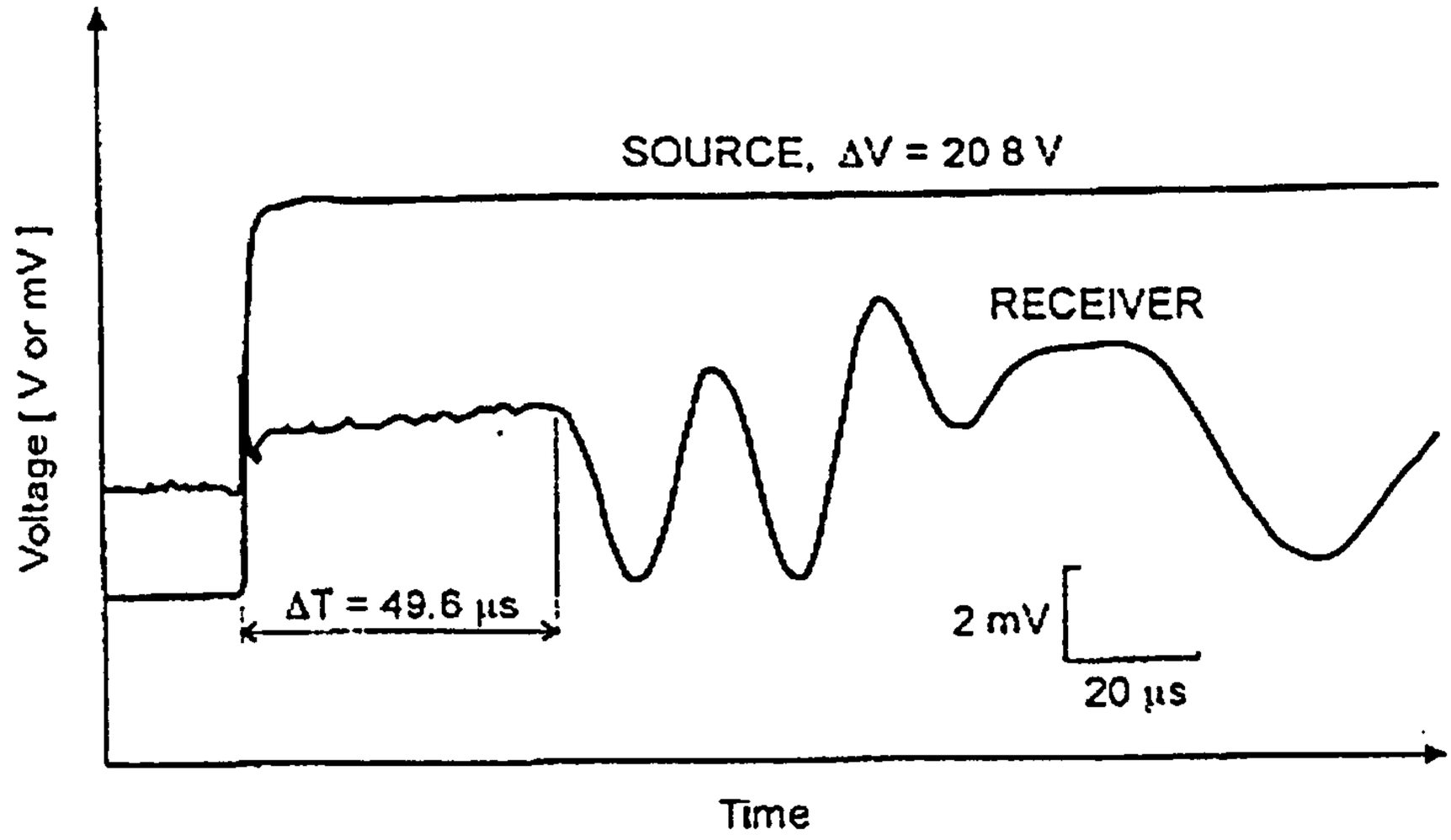

Figure 2-12 Pulse test in clay with an square input signal (Jamiolkowski et al. 1995)

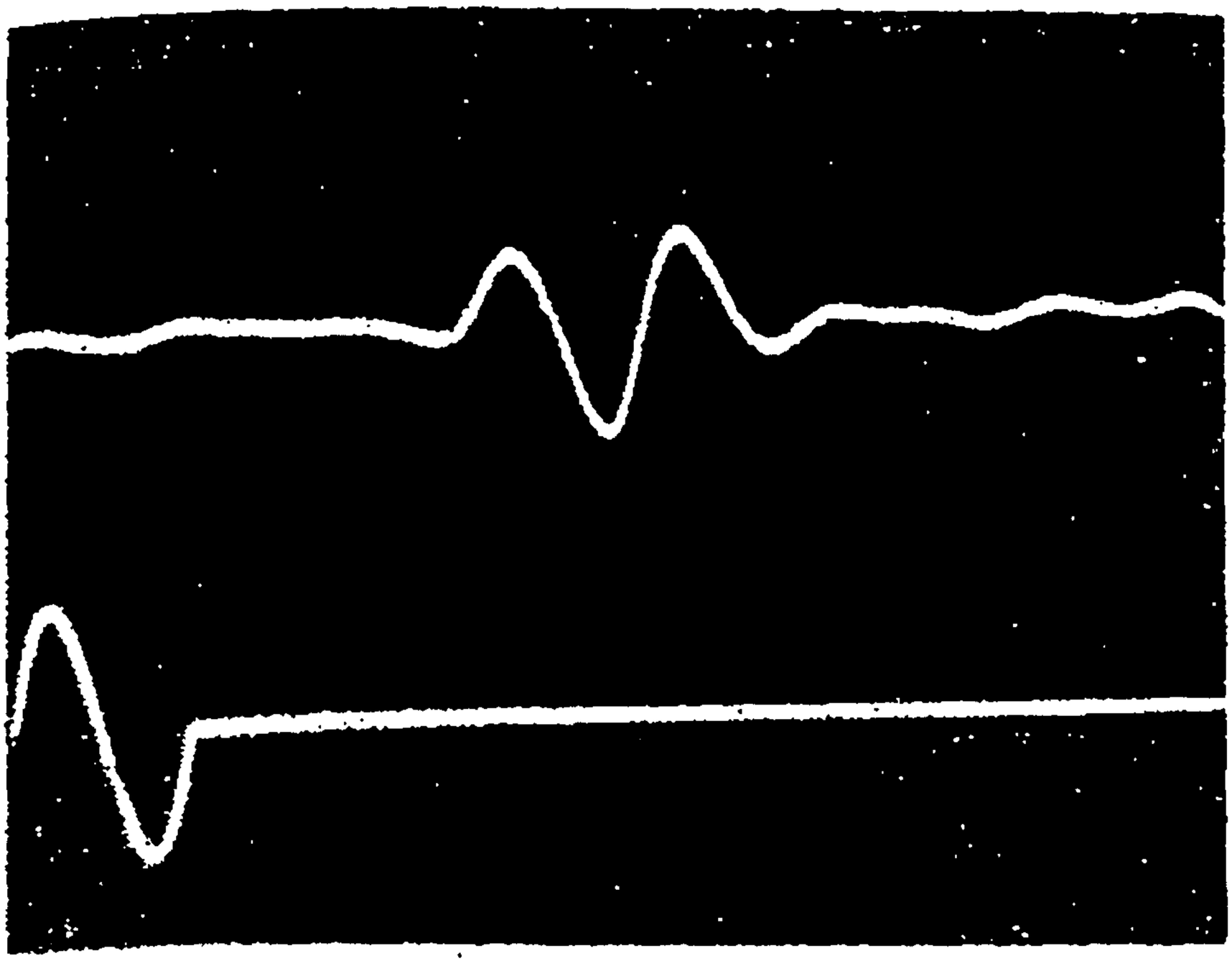

Figure 2-13 Sinusoidal source. Oscilloscope images of a pulse test in sand (Shirley, 1978).

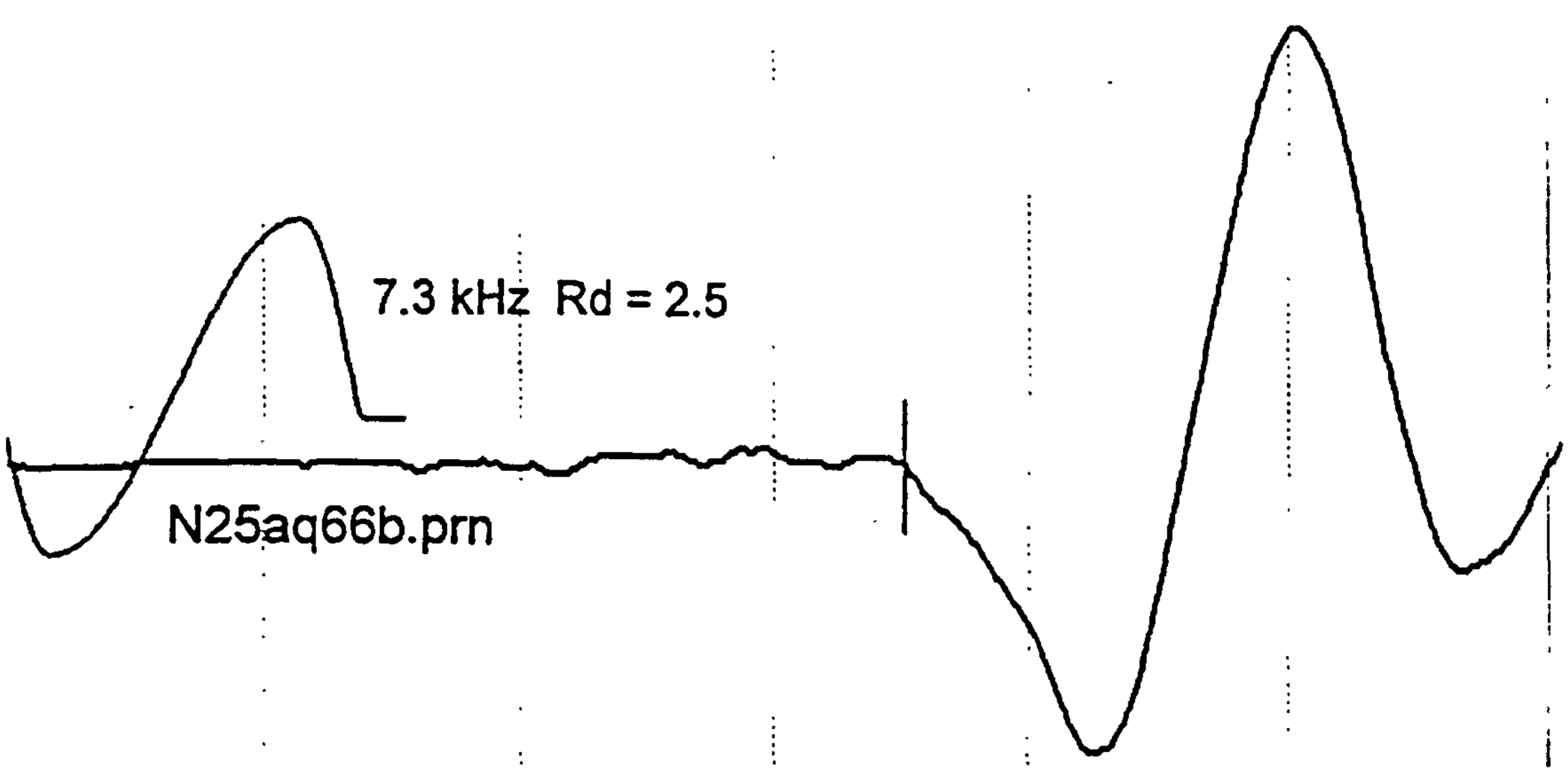

Figure 2-14 Distorted sine as input to pulse test in clay (Pennington, 1999). The receiver signal has been truncated.

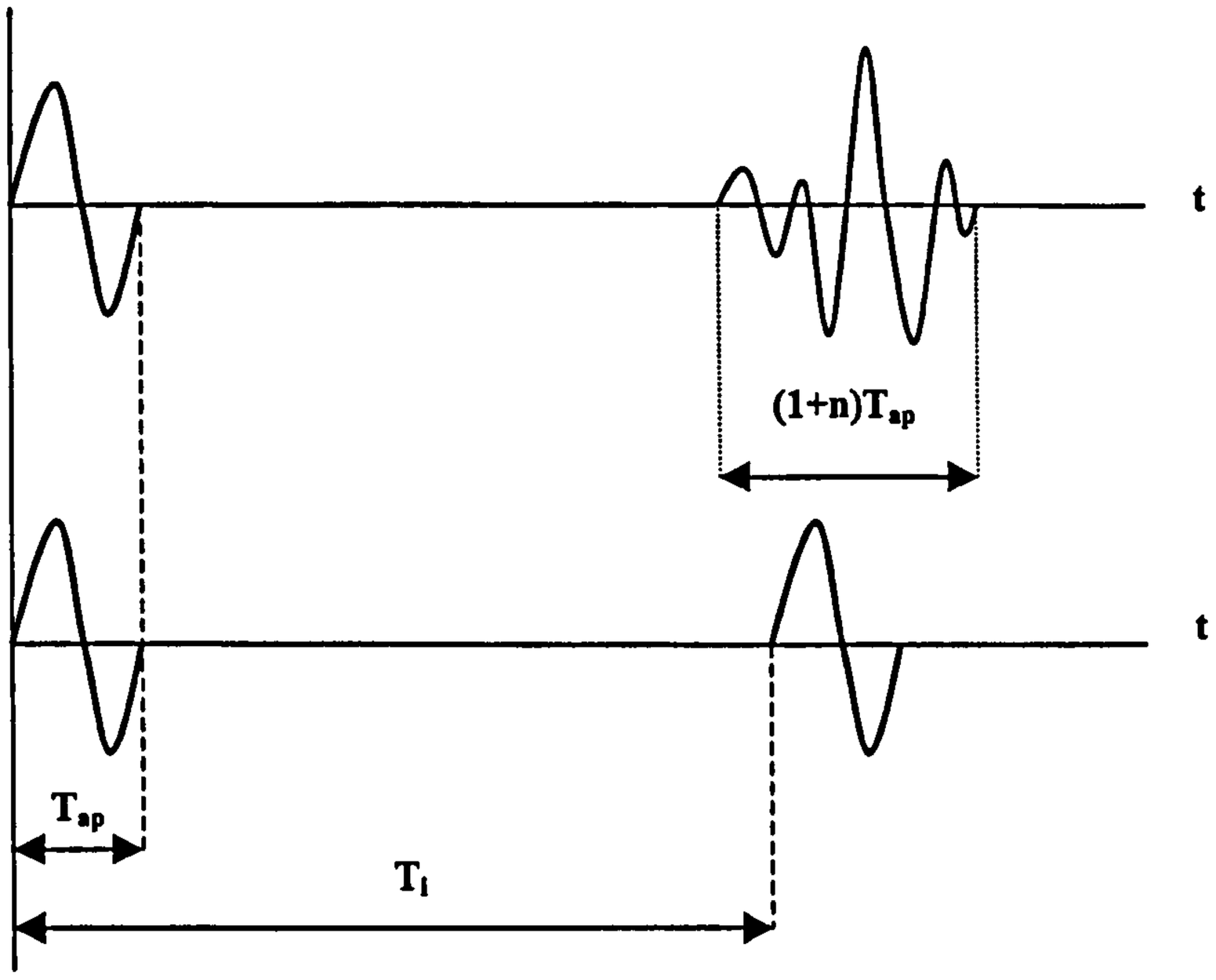

Figure 2-15 Pulse transmission with and without distortion

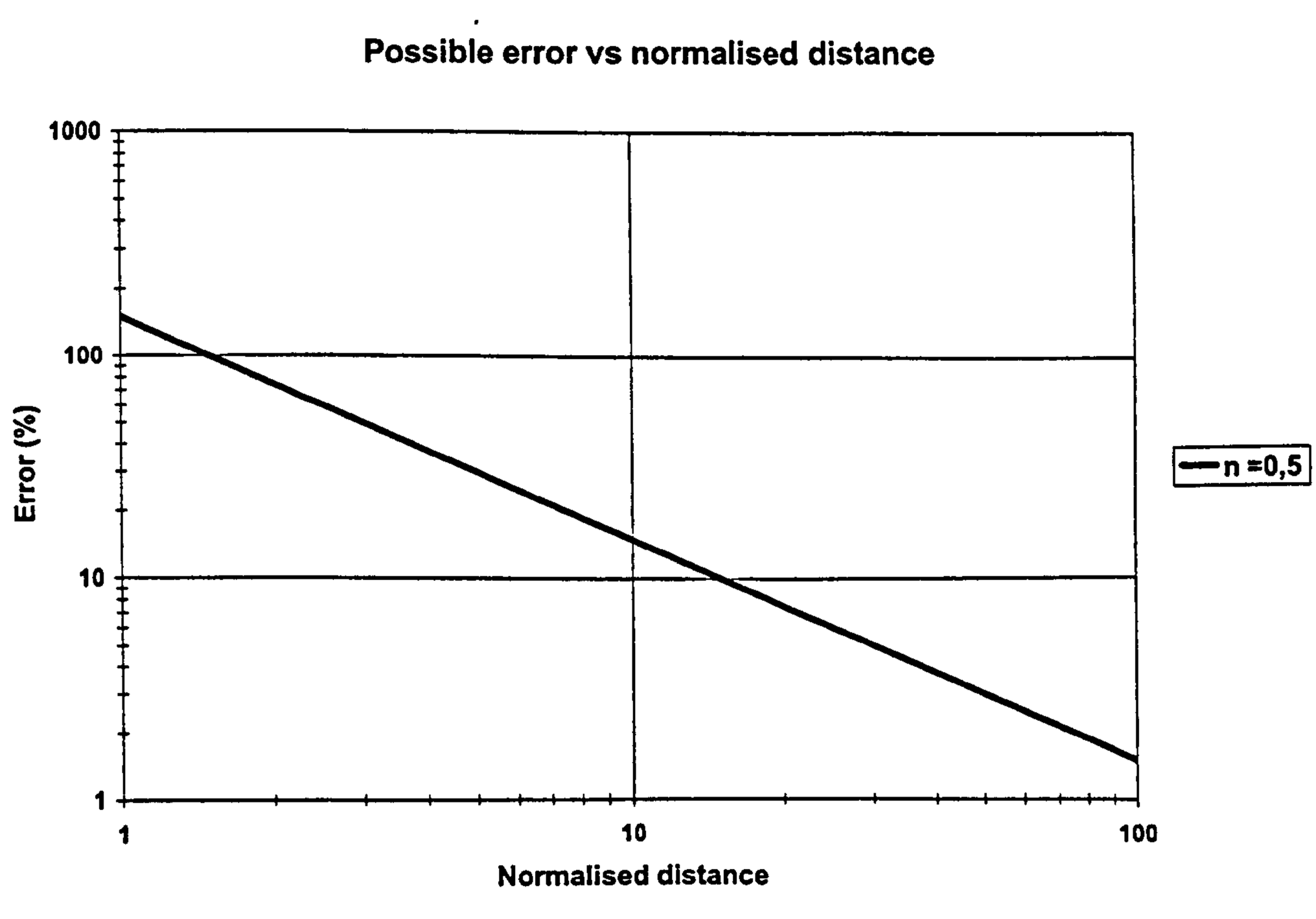

Figure 2-16 Possible error in travel time when the output signal is distorted and enlarged 50%

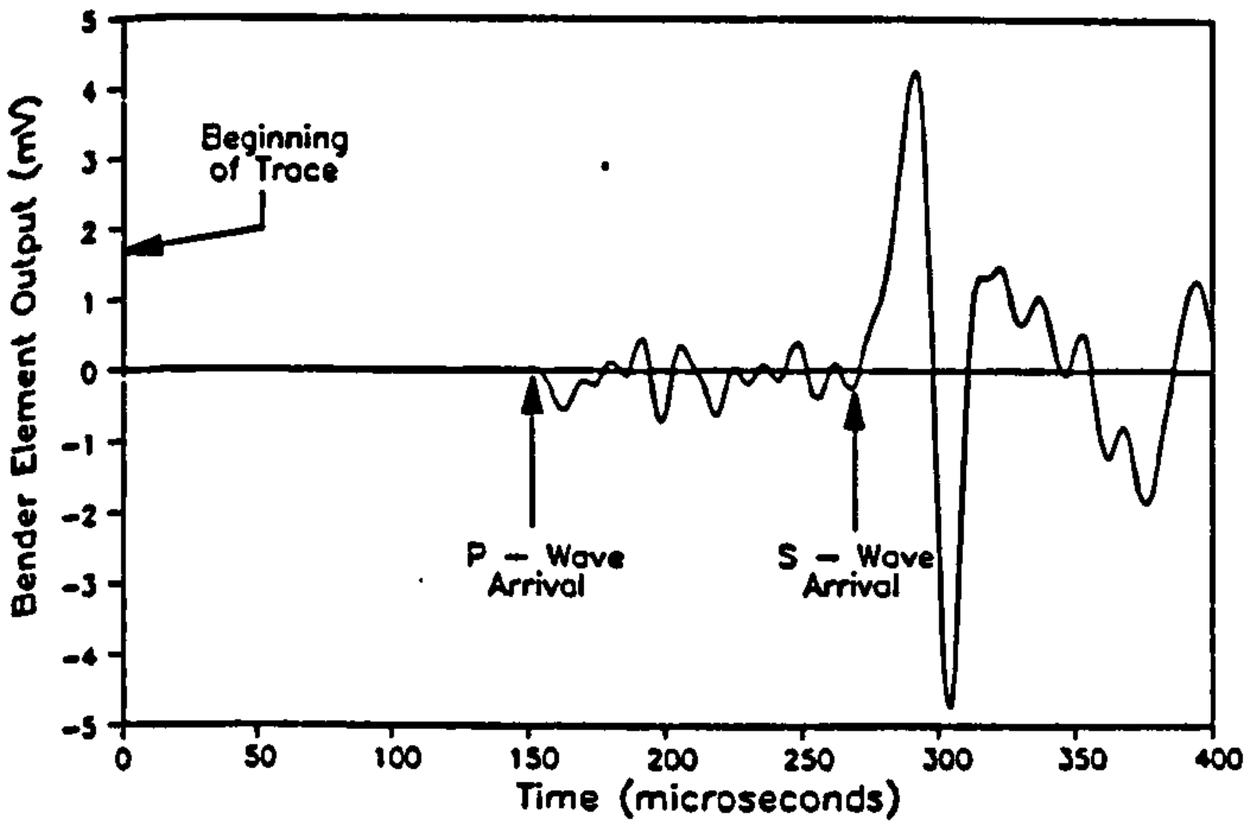

Figure 2-17 Visual identification of arrival time in pulse tests (Thomann & Hryciw, 1990)

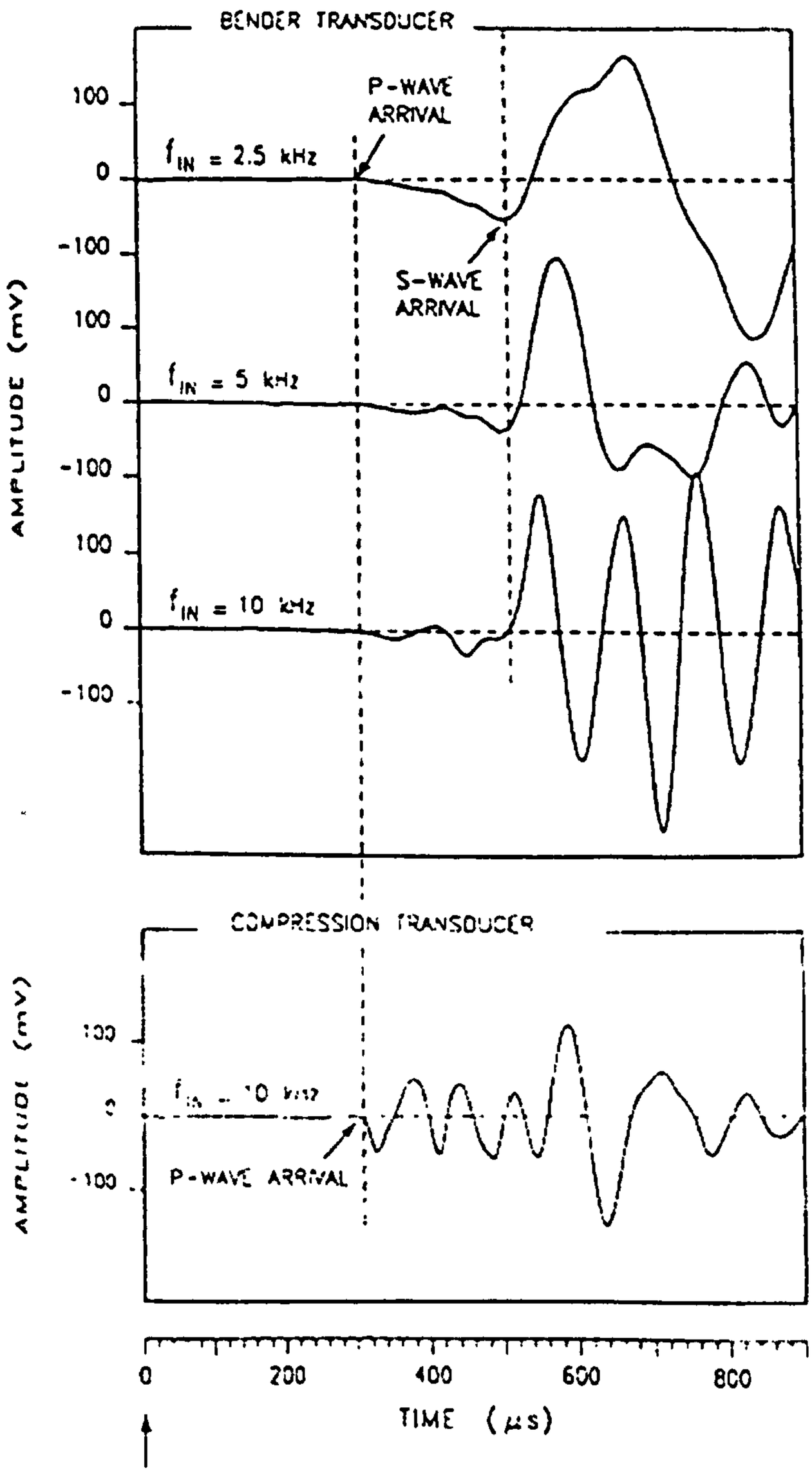

Figure 2-18 Simultaneous measurement of shear and compressive movements in Pontida clay (Brignoli et al. 1996)

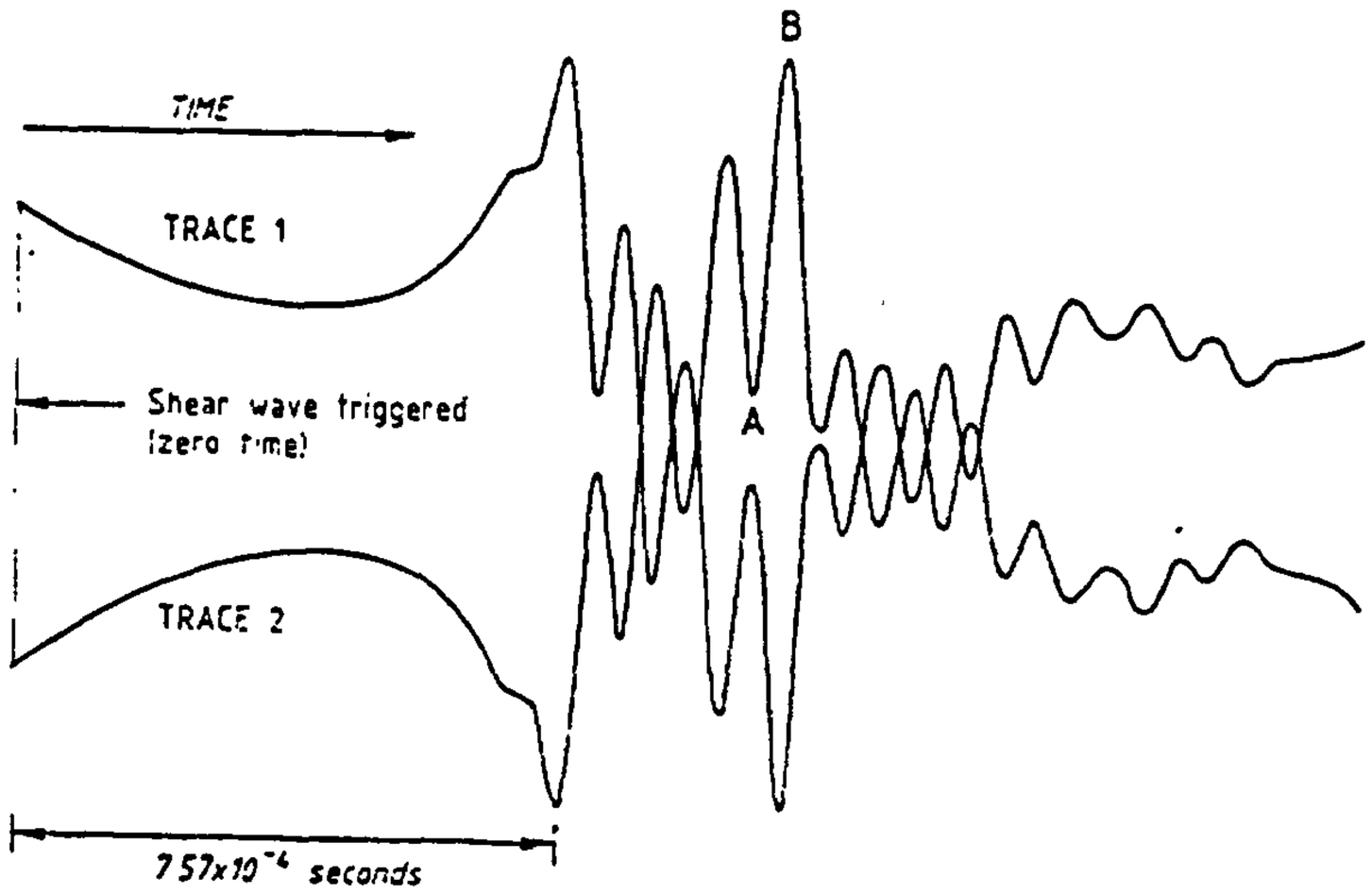

Figure 2-19 Polarity inversion as an aide to identify arrival times in pulse tests (after Dyvik & Madshus, 1985)

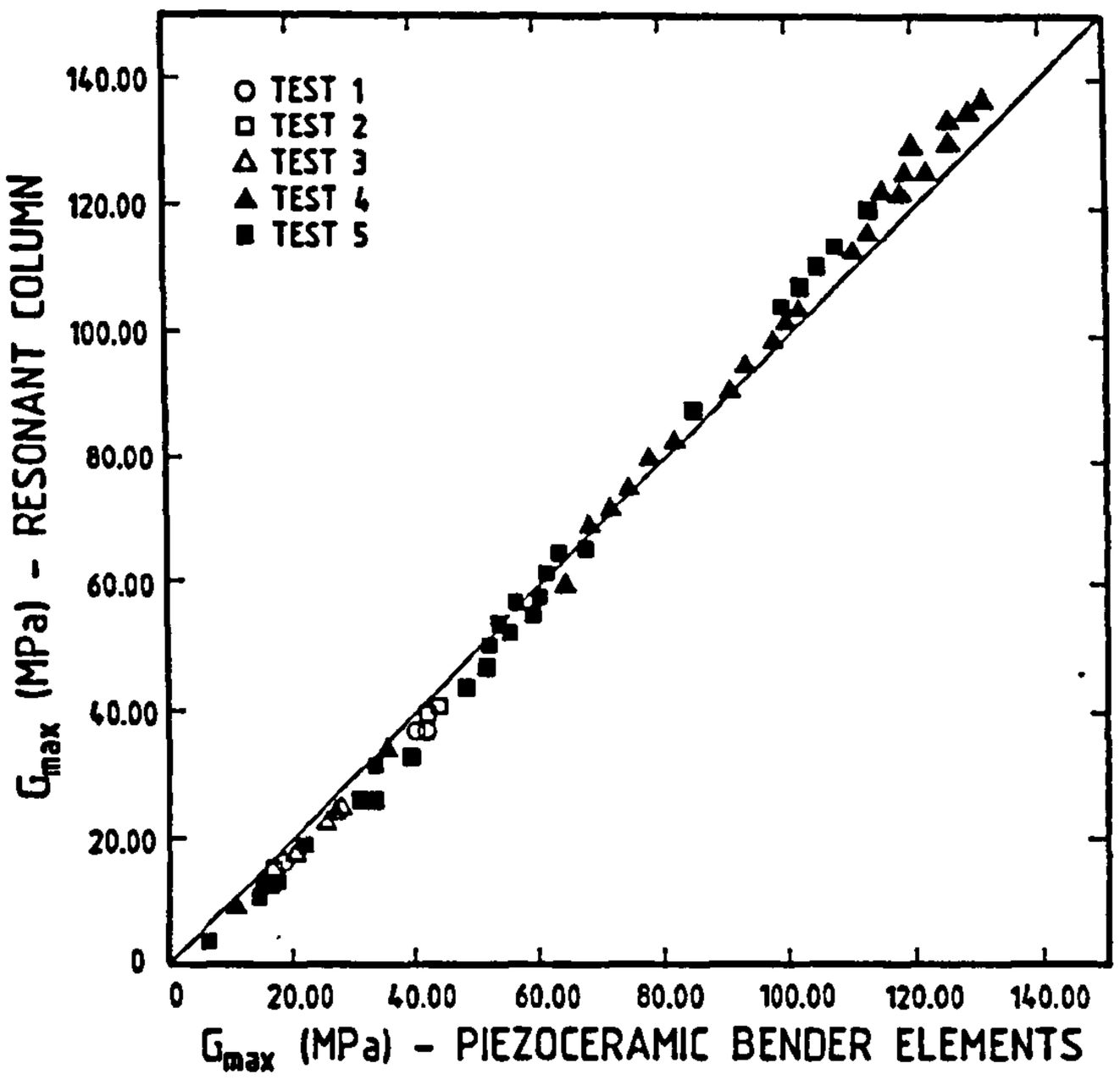

Figure 2-20 Agreement between pulse test and resonant column results (Dyvik and Madshus, 1985)

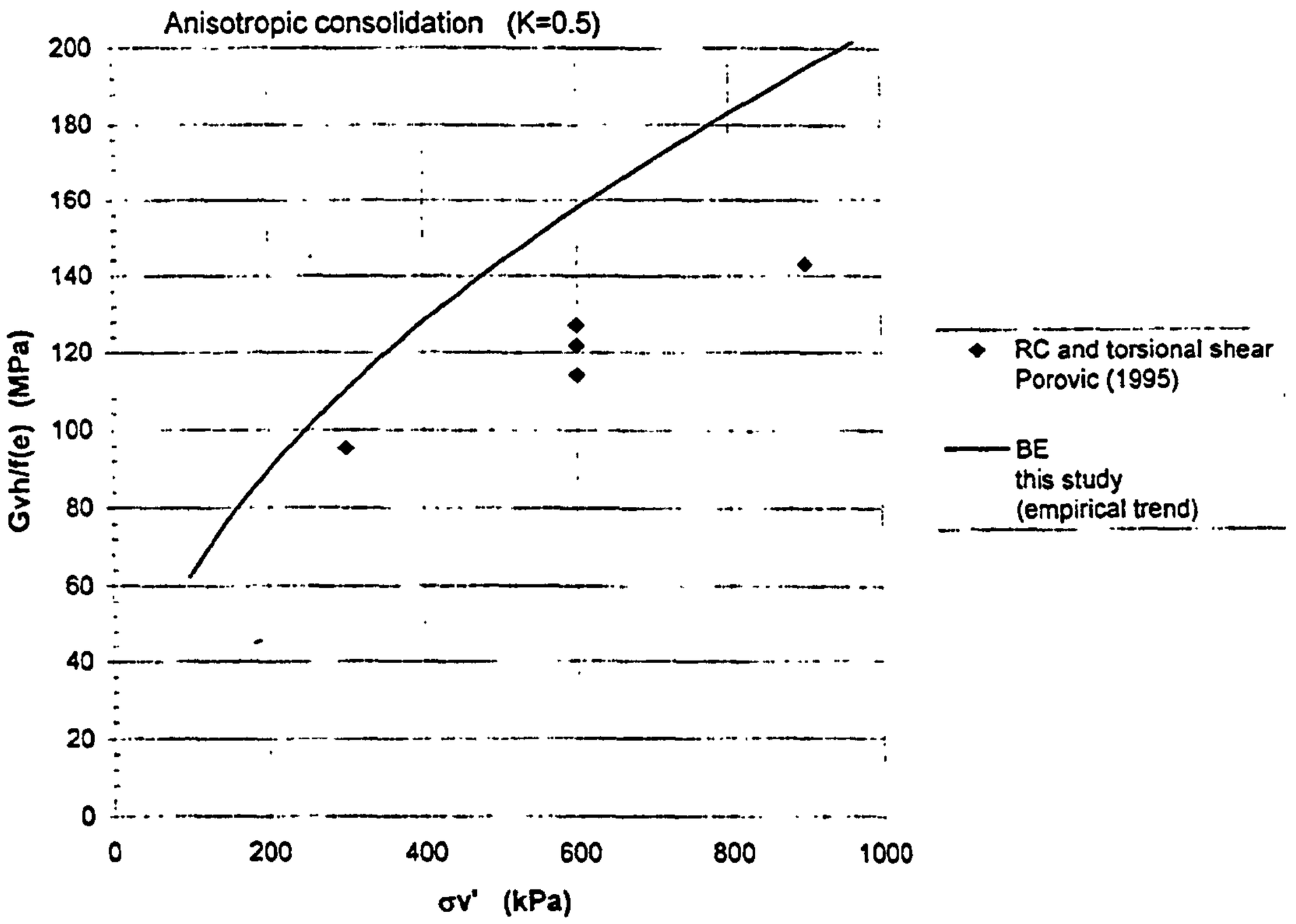

Figure 2-21 Disagreement between pulse tests and resonant column test results. Ham River Sand. (Kuwano, 1999)

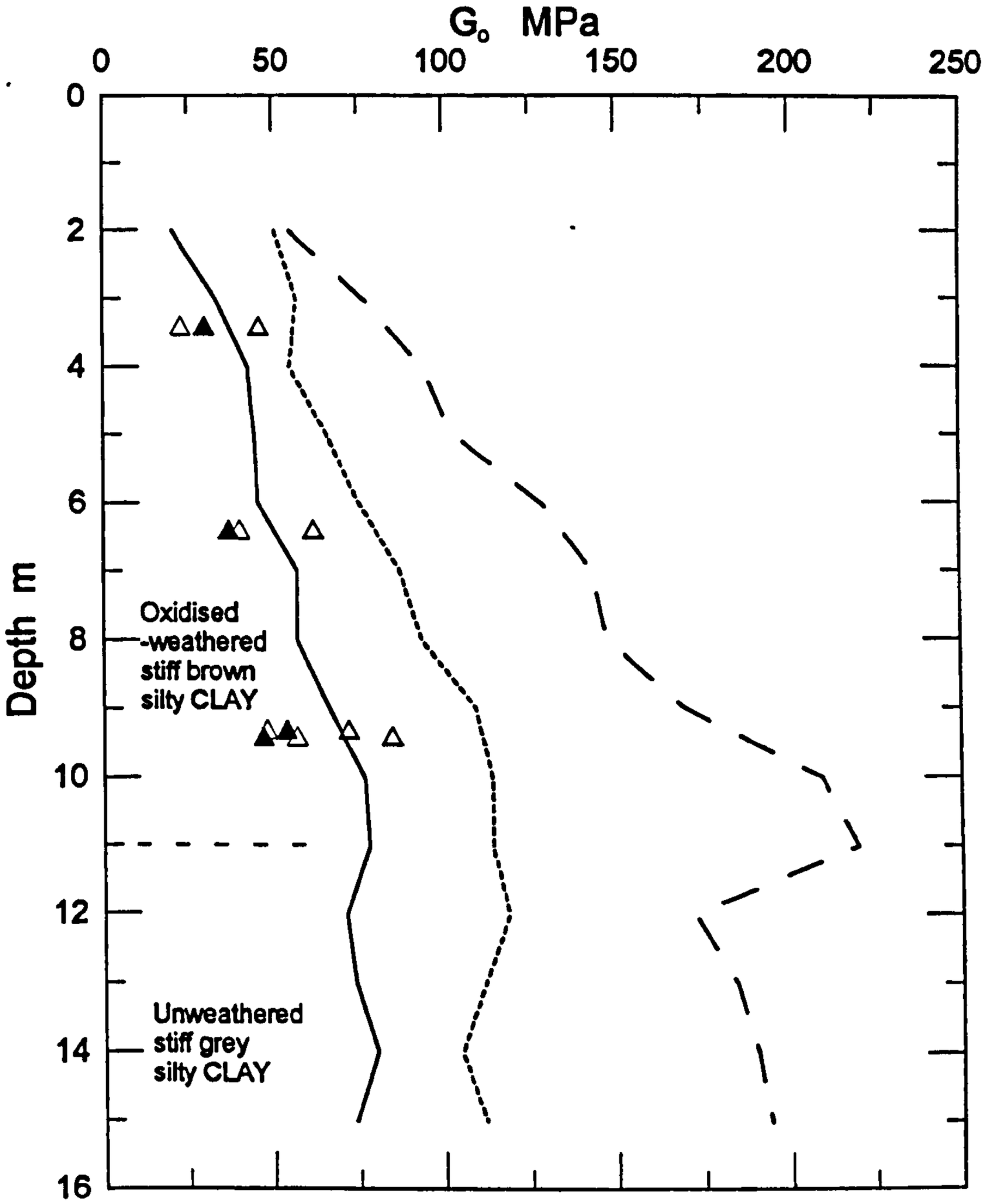

Figure 2-22 Pulse test interpretation difficulties. Test on overconsolidated clay by the NGI.

3 A BENCH TEST SERIES ON GAULT CLAY

3.1 INTRODUCTION

The previous chapter made clear that there is ample room for improvement in the interpretation of laboratory pulse tests in soils. This has been noticed before, and works by Brignoli et al (1996), Viggiani & Atkinson (1995), Jovicic et al. (1997), Arulnatham et al. (1998) and Blewett et al. (1999) have been specifically devoted to this subject. It is nevertheless a curious feature of this literature the paucity of published data on the comparative performance of the proposed methods. Viggiani & Atkinson, for instance, base their arguments on the results of two tests. Arulnatham et al. include more results, but most of them correspond to simulated rather than measured traces. More data is available on related work by Bodare & Massarsch (1984) and Mancuso et al. (1989), although those results correspond to field tests and, therefore, they are not directly comparable with laboratory tests.

It was felt necessary to generate a more ample database with a double objective in mind:

- To have a statistically more sound estimate of the actual uncertainty associated with the current practice of pulse test interpretation
- To have a background against which explore current and alternative interpretative hypotheses

What follows is a description of how this database was generated and what responses did it offer to the first item above.

3.2 TEST DESCRIPTION

3.2.1 Material

The material employed in this test series was Gault clay. Gault clay was selected because of its ready availability, but had the extra advantage of being a material already employed by previous researchers at the University of Bristol, particularly Ng (1992) and Pennington (1999). Pennington work is particularly relevant as he has obtained already a substantial amount of data on the elastic E0 properties of Gault clay. Relevant basic data from this previous work is summarised in Table 3-1.

3.2.2 Sample preparation

A reconstituted sample was formed out of slurry in a consolidometer of internal diameter 98.5 mm. The procedure has been described by Pennington (1999). It involves a K_0 consolidation up to a vertical nominal stress of 150 kPa, equivalent, because of wall friction, to 100 kPa effective vertical stress. Suction measurements by Pennington indicate an isotropic confining stress after extrusion from the consolidometer tube of 25 kPa. He measured also a void ratio of 1.38, or equivalently a porosity, n, of 0.58.

3.2.3 Equipment

3.2.3.1 Bender elements

The piezoelectric bender probes employed in this test series were made at Bristol University by Dr. P. Greening, following a procedure detailed by Pennington (1999). Their main characteristics are resumed in Table 3-2 and illustrated in Figure 3-1. The compliance, free deflection and free resonant frequency quoted there are based on information provided by the bimorph producer (Morgan Matroc).

3.2.3.2 Data acquisition and treatment

The equipment used for data acquisition included an oscilloscope -Textronik TDS 3014. The apparatus has an upper limit sampling rate of 1 MHz. During the tests this variable was adjusted with the purpose of having a sampled time history of no more than 10000 data points. Each reading was repeated a number of times for averaging or stacking purposes. The total number of readings thus stacked varied between 128 and 512, with 256 being the most common setting.

In some cases the oscilloscope was substituted by a function analyser –Advantest R9211C- who, apart from sampling, displaying and averaging had also the possibility of computing the coherence of the averaged signal[24].

The averaged signal record was then transferred to a computer. The initial 10000 data record was deemed too long for the subsequent analysis and it was then reduced by sampling to 2500 data points. The sampling interval was varied between 4e-3 and 4e-4 ms. These values, as well as the total sampling time, resultant frequency step and Nyquist frequency[25] for each test are collected in Table 3-5.

3.2.3.3 Others

A programmable function generator TG 1010 was employed to produce the input signal on the transmitter bender. In some cases a charge amplifier (Kistler 5011) was introduced in the connection between receiver and oscilloscope. This device induced a 90 degree phase shift in the received signal. More worryingly, it did also introduce a substantial amount of low-frequency noise in the received signal. As explained below this made necessary to filter the output, thus affecting the uniformity of the test series. Partly because of that and partly because the non-amplified received signal was clear enough, its use was restricted to a fraction of the tests -see Table 3-5.

3.2.4 Testing procedure

A total of 96 bender traces were initially recorded. The main factors identifying each test are the source to receiver configuration and the characteristics of the input signal. Table 3-6 collects these data for each test in the series. Some explanations are given below.

---

[24] See Appendix I for a definition of coherence.
[25] See Appendix I

3.2.4.1 Source to receiver configuration

After consolidation the sample was isolated with wax and placed on a laboratory bench, simply supported on its larger side. Then six bender probes were installed in the sample following again a procedure described by Pennington. This sample had initial length of circa[26] 18 cm and a diameter of approximately 9 cm. Two probes were installed on the opposite ends of the sample and the other four on the lateral surface. All of them were installed in the same meridian plane, their disposition being illustrated in Figure 3-2.

After a number of tests with this initial configuration, the sample was modified, slicing out one end, waxing it again and reinstalling the instrument in the same position. This process was repeated four times in total as indicated in Figure 3-2. The tip to tip distances between instruments were calculated by subtracting the total length of the probe pair from the distance measured across the back of the probes. These distances are collected in Table 3-3. This table also shows how only two transducers –A and C, Figure 3-2- were used as sources. The rest were used as receivers.

From the dimensions given in Figure 3-1 and the measured distances an azimuth can be computed for each source-receiver pair. These azimuths are collected in Table 3-4. Note that angles are measured from the consolidation axis of the sample.

3.2.4.2 Input signals

A variety of input signals were employed. They can be classified within two different categories on the basis of their spectral characteristics:

- Wide-band single cycle signals. Mostly two different shapes were used: a sine cycle or an square pulse. A few tests employed the distorted half-sine cycle proposed by Jovicic (1997).
- Narrow-band multiple sine cycle signals. Two shapes were employed, one including four successive cycles, the other ten.

The wide-band square, single sinusoidal pulses or distorted sinusoidal pulses were selected because of their traditional use within the soil-testing community. Narrow-band burst signals have had less success in soil mechanics, although they have been favoured in other areas of ultrasonic testing -Schreiber et al. 1973.

The time domain shape of these signals is represented in Figure 3-3 for a nominal unit amplitude and apparent period. Note that the apparent period corresponds to the total duration of the signal in single-cycle cases and to the duration of one cycle in the multiple cycle cases. The input amplitude to the source was fixed at 10 V.

---

[26] There is some uncertainty about the exact dimensions of the sample, as it was covered with wax. This, nevertheless, does not apply to the distance between instruments which is the relevant one for test interpretation and well known.

The spectra of these signals are shown in Figure 3-4, again for a unit nominal apparent frequency, f_{ap}. In the test series here described f_{ap} was varied between 2.7 and 9 kHz. Table 3-6 includes all the data

3.2.4.3 Other factors

The whole testing took place in eight different sessions. The sample remained in the bench laboratory for 26 days. The bench-time days for each test are also indicated in Table 3-6.

The quality of the traces was generally good, although some high frequency noise was generally present. A typical result is shown in Figure 3-5. Note that in this and all the subsequent figures both input and output traces normalised to a nominal peak amplitude of 1. The inverse of the normalising factor gives the amplification applied to the output signal, it was recorded and its shown in Table 3-7.

Rather more inconvenient was the presence of low frequency noise in 18 traces, causing an apparent drift on the signal -Figure 3-6. This noise was always present when using the amplifier, but appeared also on other occasions. These traces were subjected to a low pass filter with a pass frequency of 1kHz. This is also indicated in Table 3-7.

3.3 ARRIVAL TIME IDENTIFICATION PROCEDURES

3.3.1 Time domain

All the test traces were first examined in time domain to obtain arrival times. A variety of methods were employed to select the arrival time: visual identification, automatic identification and cross-correlation. These methods are described below.

3.3.1.1 Visual identification

The operator selected the arrival time by inspection of the trace, looking for the first "significant" deviation from zero. The operator was aware of possible near field effects, and those were approximately taken in account, disregarding minor initial deviations in the trace. The inspected trace was recorded and closely examined with the help of MATLAB. This permits a more leisurely identification than what is possible with a direct inspection on the oscilloscope. This procedure corresponds fairly well with that described by Pennington (1999) or Kuwano (1999). These times are believed to represent the current research practice of bender element testing. In what follows this arrival time is identified as T_E[27].

3.3.1.2 Automatic identification

A program was written to select the following characteristic points on the trace:

- Time were the trace first deviates from zero or T_0. Deviations from zero of less than 10% of the maximum value were discarded
- Time were the trace reaches its first peak or T_1
- Time were the trace has its second zero i.e. the first crossing after the first peak. In what follows this time is called T_2

[27] In this as well as in all subsequent methods the corresponding velocity is identified with the same subindex as the arrival time.

- Time were the trace reaches its first through or T_3

The automatic procedure involved some extra steps. The original trace was too irregular so it was necessary to smooth it out. This was achieved substituting the original trace by a moving average of between 10 and 30 data points, depending on how noisy the signal appeared to be –the actual value for each test is collected in Table 3-7- In Figure 3-7 one original trace is shown along the corresponding filtered trace: it is clear that the alteration of the time-domain signal is minor[28]. Figure 3-8 does show an example of the automatically identified arrival points T_i as well as the visually identified T_E. This example is representative of the generally good-looking performance of the automatic procedure.

3.3.1.3 Cross-correlation.

The input trace was cross-correlated with the output trace. The cross correlation function was normalised and the maximum value identified. This gave another arrival time T_{CC}. An example of the cross-correlation result is plotted along the corresponding input and output signals in Figure 3-9.

The cross-correlation was performed on the frequency domain through a FFT-based algorithm. More details about the characteristics and implementation of this and other signal treatment procedures can be found in Appendix I.

3.3.2 Frequency domain: Cross-spectrum phase

As it is shown in Appendix I, the cross-correlation of two signals in the frequency domain receives the name of cross-spectrum. Within the context of pulse test in soils, Mancuso et al. (1989) for cross-hole and Viggiani and Atkinson (1995) for bender element test have applied this method to establish the arrival time using the cross-spectrum between the input and output signals of source and receiver[29].

To obtain an arrival time they fitted a line to the unwrapped plot of the cross-spectrum phase against frequency -Figure 3-10. If the slope of this line is called *a* then a travel time is obtained as

$$T_{CS} = \frac{a}{2\pi} \qquad (45)$$

Note that *a* is a ratio of phase (adimensional) and frequency, and has therefore the proper time dimension. The arrival time T_{CS} is called a group travel time by Mancuso et al and Viggiani and Atkinson. The rationale for this name will be made clear in the next chapter, the important thing here is to note that however this arrival time was called, it was used exactly as any of the time domain values presented before.

This procedure was again implemented by means of an Excel-VBA program and applied to the bench-test records. The cross spectrum of input and output is obtained from the FFT of both signals. To fully

---

[28] A moving average is equivalent to a rather rustic high pass filter. Note that this modified signal was used only for methods based on identification of characteristics points on the trace. Cross-correlation and cross-spectra used the original trace in all cases except the low-filtered ones indicated in Table 3-7.

automatise the procedure a couple of extra criteria need to be specified: how to select the range of frequencies where the linear fit is applied and how to unwrap the phase of the cross-spectrum.

Some indication regarding the first criteria was given in the literature. Mancuso et al. suggested that the fitting interval should be established by reference to the cross-spectrum module, selecting only the frequency range where this is significant -i.e. high enough. They also suggested employing the coherence function of repeated measurements as a complementary tool. Viggiani and Atkinson employed only the cross-spectrum module. No particular indication was given by any of them about the procedure employed to unwrap the phase.

Coherence was measured a number of times but not systematically recorded. A typical result, nevertheless, is that shown in Figure 3-11. It was very high (i.e. above 90%) for frequencies between 0.5 and 10 kHz and very low (i.e. below 20%) for frequencies outside this range. The figure also shows a recurrent feature of the observed coherence: an isolated zone of low values (around 5,25 kHz in this case). This is a typical manifestation of high peaks in the spectra.

It was hence the module criteria the one employed to establish the range of frequencies available for the linear fit, establishing the significative level at 10% of the maximum cross spectrum power. The unwrap procedure assumed that the phase was always increasing and that each apparent reversal on the unwrapped phase corresponded to a single missing cycle. A round-off of $\pi/100$ was also included in the algorithm, which may be synthetically expressed as

$$\theta_i^u = \theta_i^w + 2\pi \sum_{j=2}^{i} \left\langle \theta_j^w - \theta_{j-2}^w \right\rangle \qquad (46)$$

Where the superindex indicate the wrapped or unwrapped angle and the subindex i goes throughout the values of the discrete spectra. Figure 3-12 exemplifies the performance of the unwrapping procedure, Figure 3-13 the fitting criteria and in Figure 3-8 the arrival time thus obtained is displayed along the other estimates.

3.4 AN ESTIMATE OF UNCERTAINTY IN CURRENT PRACTICE

3.4.1 Preliminaries

The systematic application of the methods described above produced seven different estimates of arrival time for each of the 92 tests available[30]. The estimates were represented on the trace and all of them were inspected to pick any obvious errors. Some 13 cases were discarded as unsuitable for analysis, most of them because of substantial low frequency noise was present even after filtering[31]. These cases are indicated in Table 3-7 and included all those were the amplifier was used which, unfortunately, corresponded also to all the shots for the A-D source to receiver configuration. Results from these tests

---

[29] Two receivers in the case of Mancuso et al. (1989)
[30] Except the visually identified V_E who was only available for the 49 tests along the sample axis.

are included in Table 3-8, where all the velocity estimates are collected, but they will not be considered further.

Even after this purge there are more than 500 different estimates of velocity available for the same sample. Displaying all this data together, like in Figure 3-14 offers a rather daunting picture. The apparent variability is enormous: there is a factor of five between the lowest and highest measurements.

3.4.2 Anisotropy and time effects

To account for this spread there are, in principle, five different factors to be considered –azimuth, distance, frequency, signal type and bench time- Of all them only two come within the usual interpretative framework of pulse tests in soils: azimuth and bench time.

Stiffness variations ascribed to the source to receiver azimuth are best explained in terms of anisotropy. Indeed, Pennington clearly showed both that the elastic behaviour of remoulded Gault clay is anisotropic and that pulse tests were able to detect it. The measured velocities seem to support this view. Figure 3-15 portrays the influence of azimuth in measured velocities. Even through the blurred lens of this greatly dispersed data some influence seems visible. A more technical assessment might be obtained using the statistical package SPSS –George & Mallery, 2000- to perform Analysis of Variance (ANOVA). The results –see Table 3-9- show variable but relatively high –83% to 100%- support for anisotropy for all methods employed[32]. To explore this issue further some familiarity with anisotropic effects in wave propagation is needed. As this is the subject of later chapters we postpone any further consideration of anisotropy until then.

Once recognised the anisotropy, it is best to concentrate now on a simpler case, that of tests made along the axis of the sample i.e. tests with zero azimuth or, briefly, vertical tests[33]. There are near 50 tests under this condition, more than 300 arrival time estimates and some statistical analysis is still warranted. From now onwards, all the results presented in this chapter will be based on them.

The second factor who may explain the variability of the results is time. As we mentioned before testing took place during a period of 26 days. There are two possible ways in which time might have affected the results: sample creep or drying. Creep (i.e. direct time effect on stiffness) is known to affect pulse tests in clay (Nash, 2000). But this creep effect is known to depend on the stress level applied to the sample, which is pretty low on these tests. The effect, if present, should be one of stiffening.

Consider now dissication: although protected with wax, the sample might have dried while in the bench. The cutting operations were regarded as particularly tricky on this respect, as the new face of the sample was then unprotected for a while. Mechanically, drying will results on increased suction. Although there

---

[31] Raising the filter low pass setting above 1kHz would have dented too much in spectral regions of high coherence and magnitude.
[32] Bare the expert visual appreciation who was only available for vertical tests.
[33] This "vertical" makes reference to axis position during sample forming. While testing the sample lied on its side and the axis was horizontal.

is lack of experience on its particular effects on pulse tests, suction is known to affect the stiffness of soils in general and Gault in particular (Pennington, 1999). At the low levels of dissication expected it can be treated simply as an increased confining pressure. The effect, if present, will again be a stiffening one.

Again, simply plotting all the results against benchtime does not offer a very clear picture -Figure 3-16. Statistical analysis, -Table 3-10-, would seem to preclude any discernible time effect on velocity for most methods involved, with the notable exception of the hand-picked expert times, who strongly support some effect. But, if we explore this presumed effect by plotting the means of V_E against time -Figure 3-17 a pattern inconsistent with an increasing tendency appears. We conclude then that some other spurious effect must be acting and that no proper time effect should be considered in further analyses.

3.4.3 Variability in axial measurements

The first thing to note then are the solid differences between methods. Table 3-11 presents some summary results for each method: the mean, the standard deviation, the coefficient of variation. A few things are noticeable:

There are substantial differences in mean value between the methods. This is not surprising for the V_0 to V_3 time domain values: after all we tried to select different arrival points in the trace. It is more interesting to see that V_{CC} is below V_3 and V_{CS} is even below V_{CC}. It is interesting also to notice that the expert estimate of first arrival V_E is quite close in mean to V_0. In fact, this is the only non-significant mean difference, the rest being pretty consistent as shown in Table 3-12. Using the difference between the two extreme values (i.e. V_0 and V_{CS}) this result may be interpreted as follows: the velocities obtained by two researchers making one measurement with their favourite method in Gault might well differ on more than 60m/s. This represents 50% of the global average value. In other words, the global uncertainty in moduli determination approaches 100%

When adhering firmly to one method the uncertainty is substantially reduced. The coefficient of variation might be used as an estimate and lies between 10% and 20% Still, this represents an uncertainty in moduli between 20% and 40% From this point of view the velocities given by the first peak (V_1), first crossing (V_2) or first through (V_3) seem to be the more consistent. First arrival is somewhat less so, with no difference between the manual (V_E) or automatic procedure (V_0). Cross-correlation and cross-spectra perform notably worst.

Mean and variance do not exhaust the observed differences between methods. Figure 3-18 presents the corresponding histograms of measured velocities. The distributions are fairly varied: only V_3 and V_{CS} approach consistently a normal distribution, whereas V_0 and V_1 look bimodal, V_2 nearly uniform and the others are skewed in opposite directions. From the statistical viewpoint a normal centred distribution is attractive and therefore this is an argument in favour of V_{CS}.

It is appropriate to wonder about the robustness of the methods employed. The visually picked times are subjectively satisfactory and this is the end of the affair: there is no adjustment parameter to play with. The automatically picked characteristic times will depend on the threshold value used to determine meaningful departures from zero and more importantly on the moving average setting. This being true, we have already stated that posterior inspection of the traces offered intuitive satisfaction about the performance of the method: peaks, crossings and throughs were indeed selected. There is no adjustment parameter available for the cross-correlation method. Cross-spectrum estimates, on the other hand, are affected by the criteria employed to select the fitting range for the phase. Table 3-13 shows how as the limit for significative modulus increases so does the performance of the method. To explain this phenomena will need a more in depth look at the basis of the method, something that is left for next chapter.

3.4.4 Distance and signal effects

Discarded time and postponed anisotropy only source-to-receiver distance and signal characteristics -type and apparent frequency- are left to explain the results. Considering first signal type, there is again a method-dependent effect -Figure 3-19. For characteristic-point methods there is a noticeable difference between shortband and broadband results, the latter giving higher readings than the former, with square signals coming on top. But this difference wanes out as the arrival times are selected deep into the trace, becoming non-significant from V_3 onwards -Table 3-14.

This difference between methods persist when we look at the effect of the other variables. Figure 3-20 represents the mean velocity values as a function of measurement distance. An intriguing and robust -Table 3-15- oscillatory pattern, which is apparent in the faster[34] methods, fades away in the slowest. The effect of apparent signal frequency seems to be an slight increase in velocity -Figure 3-21-, but again cross-correlation and cross-spectra offer a different image[35].

3.4.5 Discussion

The uncertainty suggested by the results just described seems really high. It is then comforting to find that Bodare & Massarch results[36] do not stray far away from ours –ratio range/mean between 30% and 50% Figure 3-22-. Viggianni & Atkinson present two results: if it is true that they found 64% uncertainty for a low frequency square wave[37] they also obtained a much lesser value namely 7% for a sinusoidal wave of moderately high frequency. Looking at the distribution of values here obtained -Figure 3-23- this last value seems far less probable than the first.

Closer examination of other reported data also supports this view. The NGI results shown in the last figure of Chapter 2 show an spread –range over mean- of up to 73% in bender-based shear module estimates. Resonant column values fall always near the lower bound. Figure 3-24 taken from Arulnatham

---

[34] I.e. those methods giving higher velocities
[35] As the figure represent mean values only frequencies at which more than two tests were available are included
[36] It is true that they are isolated i.e. they are probing each time a different site or they are made at different heights in a borehole. This may add to their uncertainty; on the other hand they are made at fixed distances and with a fixed source.

et al. (1998) shows various arrival times picked on the same trace by various methods, characteristics point selection –points A to C-, direct cross-correlation -point D- and output autocorrelation –point E. They span a range of circa 1ms for a medium arrival time which is also close to that value.

It is also interesting to note that the results obtained fit well with the distortion argument given in the previous chapter – Figure 2-15- If we consider again the traces presented for instance in Figure 3-8: it is clear that the output trace is many times larger than the input one. Establishing an equal weight criteria to identify arrival in the trace will produce even bigger uncertainty. Cold comfort, anyway, as this still leaves us with a very imprecise tool.

It may be argued, quite reasonably, that no self-respecting researcher will ever use a single, unspecified method to measure velocity. Or else, that if only agreement was reached about what method to use the uncertainty amongst researchers will be greatly reduced. Or even better, if this agreement were to be extended at the kind of signal to be employed and the distance between source and receiver then the measured velocity would be much reliable....These arguments are certainly valid and they may offer a normative way forward to extend the use of pulse tests to routine geotechnical work as recently suggested by Atkinson (2000).

However, this approach is hardly satisfactory from a broader viewpoint. The need to deal with a complicated and/or strict testing procedure is really a hindrance for the sort of systematic use that pulse test do potentially have. Laboratory pulse testing cannot be contrived without losing versatility, one of its main appeals. For instance, a hidden distance dependency on the results does not bode well to comparisons between results from instrumented oedometer and triaxial apparatus, neither does for the extrapolation of triaxial procedures to true triaxial or hollow cylinder apparatuses. But this practical arguments again beg the main question. Why there is such a big uncertainty? Why the output signals are so heavily distorted? Why factors such as pulse type or source-to receiver distance affect the results? What is obviously needed is a more deep understanding of the factors affecting the performance of pulse tests in soils. An explanatory attempt begins in the following chapter.

[37] And that only with T_0, T_1 and T_2.

3.5 SUMMARY

A series of pulse tests were performed in an unconfined sample of remoulded Gault clay. Three aspects were investigated: the influence of the arrival time selection method, the influence of source to receiver configuration –azimuth and distance- and the influence of input signal characteristics –type and apparent frequency- As expected, anisotropy was revealed. More of a surprise was the very high variation registered in axial measurements. The main variance factor relates to differences between methods, but even for a fixed method there is substantial uncertainty –between 20% and 40% in moduli- Both distance and signal characteristics seem to affect the recorded time.

3.6 TABLES

Property	Value	Source
Void ratio (e) / porosity (n)	1.25 / 0.54	Pennigton (1999)
Plastic limit	26 – 32 %	Pennington (1999)
Liquid limit	75 – 80 %	Pennington (1999)
E_V / p'	550	Pennington (1999)
E_H / p'	2186	Pennington (1999)
ν_{VH}	0	Pennington (1999)
ν_{HH}	-0.041	Pennington (1999)
G_{HV} / p'	507	Pennington (1999)
At rest earth pressure (K_0)	0.6	Ng (1992)
Engineering permeability (k)	$3x10^{-10}$ m/s	Ng (1992)

Table 3-1 Properties of reconstituted samples of Gault clay

Property	Value
Length (mm)	10
Thickness (mm)	2.5
Width (mm)	12
Piezoelectric material	PZT 5A
Free resonant frequency (Hz)	2300
Compliance (m/Nw)	4,3E-5
The dimensions quoted include the epoxy cover	

Table 3-2 Properties of the piezoelectric bender probes used in this study

	Source	
Receiver	A	C
B	0,17524	-
D	0,094	0,06912
E	0,0435	-
F	0,151	-
G	0,1494	-
H	0,1209	-
I	0,09696	-
J	0,07276	-

Table 3-3 Distances (m) between transducers

	Source	
Receiver	A	C
A	.	-
B	0	-
C	-	.
D	21.57	90
E	52.6	-
F	13.23	-
G	0	-
H	0	-
I	0	-
J	0	-

Table 3-4 Azimuthal angle of propagation in degrees

TEST	Time step (s)	Duration (s)	Nyquist f (kHz)	freq step (Hz)	Amplifier	TEST	Time step (s)	Duration (s)	Nyquist f (kHz)	freq step (Hz)	Amplifier
1	4E-06	0.01	125	50	out	52	4E-06	0.01	125	50	out
2	4E-06	0.01	125	50	out	53	4E-06	0.01	125	50	out
3	4E-06	0.01	125	50	out	54	4E-06	0.01	125	50	out
4	4E-06	0.01	125	50	out	55	4E-06	0.01	625	250	out
5	8E-07	0.002	625	250	out	56	4.00E-07	0.001	625	250	out
6	8E-07	0 002	625	250	out	57	1.6E-06	0.004	625	250	out
7	8E-07	0.002	625	250	out	58	1.6E-06	0.004	625	250	out
8	8E-07	0.002	625	250	out	59	1.6E-06	0.004	625	250	out
9	8E-07	0.002	625	250	out	60	1.6E-06	0.004	625	250	out
10	8E-07	0.002	625	250	out	61	1.6E-06	0.004	625	250	out
11	8E-07	0.002	625	250	out	62	1.6E-06	0.004	625	250	out
12	8E-07	0.002	625	250	out	63	1.6E-06	0.004	625	250	out
13	8E-07	0.002	625	250	out	64	1.6E-06	0.004	625	250	out
14	8E-07	0.002	625	250	out	65	1.6E-06	0.004	312.5	125	out
15	1.6E-06	0.004	312.5	125	out	66	4E-06	0 01	312.5	125	out
16	1.6E-06	0.004	312.5	125	out	67	4E-06	0.01	312.5	125	out
17	1.6E-06	0.004	312.5	125	out	68	4E-06	0.01	125	50	out
18	4E-06	0.01	125	50	out	69	4E-06	0.01	125	50	out
19	4E-06	0.01	125	50	out	73	1.6E-06	0.004	125	50	out
20	4E-06	0.01	125	50	out	74	1.6E-06	0.004	125	50	out
21	4E-06	0.01	125	50	out	75	1.6E-06	0.004	312.5	125	out
22	1.6E-06	0.004	312.5	125	out	76	1.6E-06	0.004	625	250	out
24	8E-07	0.002	625	250	out	77	1.6E-06	0.004	625	250	out
25	8E-07	0.002	625	250	out	78	1.6E-06	0.004	625	250	out
26	8E-07	0.002	625	250	out	79	1.6E-06	0.004	625	250	out
27	8E-07	0.002	625	250	out	80	4E-06	0.01	625	250	out
28	8E-07	0.002	625	250	out	81	4E-06	0.01	625	250	out
29	8E-07	0.002	625	250	out	82	4E-06	0.01	625	250	out
31	8E-07	0.002	625	250	out	83	1.6E-06	0.004	625	250	out
32	8E-07	0.002	625	250	in	84	1.6E-06	0.004	625	250	out
33	8E-07	0.002	625	250	in	85	1.6E-06	0.004	625	250	out
34	8E-07	0.002	625	250	in	86	1.6E-06	0.004	625	250	out
35	8E-07	0.002	625	250	in	87	1.6E-06	0.004	625	250	out
36	8E-07	0.002	625	250	in	88	4E-06	0.01	625	250	out
39	8E-07	0.002	625	250	in	89	4E-06	0.01	625	250	out
40	8E-07	0 002	625	250	in	90	4E-06	0.01	625	250	out
41	8E-07	0.002	625	250	in	91	4E-06	0.01	312.5	125	out
42	1.6E-06	0.004	312.5	125	out	92	4E-06	0.01	312.5	125	out
43	1.6E-06	0.004	312.5	125	out	93	4E-06	0.01	312.5	125	out
44	1.6E-06	0.004	312.5	125	out	94	4E-06	0.01	312.5	125	out
45	1.6E-06	0.004	312.5	125	out	95	1.6E-06	0.004	312.5	125	out
46	1.6E-06	0.004	312.5	125	out	96	1.6E-06	0.004	312.5	125	out
47	1.6E-06	0.004	312.5	125	out	97	1.6E-06	0.004	312.5	125	out
48	1.6E-06	0.004	312.5	125	out	98	4E-06	0.01	312.5	125	out
49	1.6E-06	0.004	312.5	125	out	99	4E-06	0.01	312.5	125	out
50	1.6E-06	0.004	312.5	125	out	100	4E-06	0.01	125	50	out
51	4E-06	0.01	125	50	out	101	4E-06	0.01	125	50	out

Table 3-5 Signal processing settings for each test

TEST	bench time (days)	Angle (degrees)	Distance (cm)	Signal	fap (Hz)	TEST	bench time (days)	Angle (degrees)	Distance (cm)	Signal	fap (Hz)
1	0	90	6.912	10*sine	4000	52	21	52.6	4.35	sine	4000
2	0	90	6.912	10*sine	3000	53	21	52.6	4.35	sine	6000
3	0	90	6.912	10*sine	5000	54	21	52.6	4.35	square	4000
4	0	90	6.912	10*sine	6000	55	21	52.6	4.35	square	6000
5	0	90	6.912	sine	5000	56	21	52.6	4.35	square	9000
6	0	90	6.912	sine	3000	57	21	13.23	15.1	sine	4000
7	0	90	6.912	sine	4000	58	21	13.23	15.1	sine	6000
8	0	90	6.912	sine	6000	59	21	13.23	15.1	square	4000
9	0	90	6.912	Jovicic	8000	60	21	13.23	15.1	square	6000
10	0	90	6.912	Jovicic	6000	61	21	13.23	15.1	square	9000
11	0	90	6.912	Jovicic	4000	62	21	0	14.94	square	4000
12	0	90	6.912	square	1050	63	21	0	14.94	square	6000
13	0	90	6.912	square	3000	64	21	0	14.94	square	9000
14	1	90	6.912	square	4000	65	21	0	14.94	sine	4000
15	1	90	6.912	4*sine	5000	66	21	0	14.94	4*sine	4000
16	1	90	6.912	4*sine	4000	67	21	0	14.94	4*sine	6000
17	1	90	6.912	4*sine	4000	68	21	0	14.94	10*sine	6000
18	1	0	17.524	4*sine	3000	69	21	0	14.94	10*sine	4000
19	1	0	17.524	4*sine	4000	73	26	0	12.09	square	4000
20	1	0	17.524	10*sine	4000	74	26	0	12.09	square	6000
21	4	0	17.524	10*sine	4000	75	26	0	12.09	square	9000
22	4	0	17.524	sine	2700	76	26	0	12.09	sine	4000
24	5	90	6.912	4*sine	5000	77	26	0	12.09	sine	6000
25	5	90	6.912	4*sine	5000	78	26	0	12.09	4*sine	6000
26	5	90	6.912	4*sine	5000	79	26	0	12.09	4*sine	4000
27	5	90	6.912	4*sine	5000	80	26	0	12.09	10*sine	4000
28	5	90	6.912	4*sine	5000	81	26	0	12.09	10*sine	6000
29	5	90	6.912	4*sine	5000	82	26	0	9.696	square	4000
31	5	90	6.912	4*sine	5000	83	26	0	9.696	square	6000
32	5	21.57	9.4	square	6000	84	26	0	9.696	square	9000
33	5	21.57	9.4	square	9000	85	26	0	9.696	sine	5000
34	5	21.57	9.4	square	9000	86	26	0	9.696	sine	4000
35	5	21.57	9.4	square	9000	87	26	0	9.696	sine	6000
36	5	21.57	9.4	square	9000	88	26	0	9.696	4*sine	4000
39	5	21.57	9.4	square	4000	89	26	0	9.696	4*sine	6000
40	5	21.57	9.4	sine	6000	90	26	0	9.696	10*sine	4000
41	5	21.57	9.4	sine	4000	91	26	0	9.696	10*sine	6300
42	18	0	17.524	4*sine	3000	92	26	0	9.696	10*sine	6000
43	18	0	17.524	4*sine	4000	93	26	0	7.276	square	4000
44	18	0	17.524	4*sine	5000	94	26	0	7.276	square	6000
45	18	0	17.524	4*sine	6000	95	26	0	7.276	square	9000
46	18	0	17.524	4*sine	7000	96	26	0	7.276	sine	4000
47	18	0	17.524	4*sine	8000	97	26	0	7.276	sine	6000
48	18	0	17.524	4*sine	9000	98	26	0	7.276	4*sine	4000
49	18	0	17.524	4*sine	10000	99	26	0	7.276	4*sine	6000
50	18	0	17.524	4*sine	3000	100	26	0	7.276	10*sine	4000
51	21	52.6	4.35	sine	5000	101	26	0	7.276	10*sine	6000

Table 3-6 Test variables

TEST	Amplif.	Low Pass (Hz)	n moving average	Errors	TEST	Amplif.	Low Pass (Hz)	n moving average	Errors
1	179		10	no	52	745		30	no
2	357		10	no	53	908		20	no
3	301		10	no	54	594		20	no
4	297		10	no	55	607		20	no
5	479		10	no	56	477		50	yes
6	449		10	no	57	2654		30	no
7	431		10	no	58	3550	1000	30	no
8	565		10	no	59	1538		30	no
9	537		10	no	60	1597		30	yes
10	449		10	no	61	991		30	no
11	404		10	no	62	975		30	no
12	389		10	no	63	887		30	no
13	351		10	no	64	1179		30	no
14	297		10	no	65	1073		30	no
15	301		10	no	66	858		30	no
16	186		10	no	67	1293	1000	30	no
17	659		10	yes	68	1189		10	no
18	912		10	no	69	660		10	no
19	1915		30	no	73	651		10	no
20	1305		10	no	74	804		10	no
21	1369		10	no	75	1110		20	no
22	2268		20	no	76	870		20	no
24	9		10	no	77	1285		20	no
25	294		10	no	78	945		20	no
26	11		10	no	79	592		20	no
27	19		10	no	80	597		20	no
28	18		10	no	81	938		20	no
29	11		10	no	82	513		20	yes
31	2		10	no	83	563		20	no
32	71	1000	30	yes	84	638		20	no
33	4	1000	30	yes	85	1427		20	no
34	3	1000	30	yes	86	819		10	no
35	56	1000	30	yes	87	1967	1000	30	no
36		1000	30	yes	88	797		10	no
39	25	1000	30	yes	89	1566		10	no
40	22	1000	30	yes	90	827		10	no
41	17	1000	30	yes	91	1919		30	no
42	1006		10	no	92	1630		10	no
43	86	1000	30	no	93	297		10	no
44	36	1000	30	no	94	320		10	no
45	8235	1000	30	no	95	414		10	no
46	156	1000	30	no	96	406		10	no
47	219	1000	30	no	97	647		10	no
48	318	1000	30	yes	98	195		10	no
49	3178	1000	30	yes	99	758		10	no
50	16		10	no	100	178		10	no
51	729		10	no	101	600		10	no

Table 3-7 Output signal treatment settings

TEST	VE (m/s)	V0 (m/s)	V1 (m/s)	V2 (m/s)	V3 (m/s)	VCC (m/s)	VCS (m/s)	TEST	VE (m/s)	V0 (m/s)	V1 (m/s)	V2 (m/s)	V3 (m/s)	VCC (m/s)	VCS (m/s)
1	81	141	125	117	106	81	81	52	0	130	113	100	89	81	46
2	0	138	124	114	102	80	79	53	0	200	155	136	118	83	42
3	0	145	129	120	109	64	59	54	0	182	154	130	115	81	37
4	0	145	130	122	112	76	91	55	0	189	156	132	119	82	38
5	0	142	128	120	109	79	73	56	*0*	*194*	*149*	*136*	*123*	*83*	*108*
6	0	138	125	115	103	119	68	57	0	164	158	129	121	102	107
7	0	141	126	117	106	80	69	58	0	172	160	132	124	102	106
8	0	147	131	121	111	118	74	59	0	161	146	127	120	102	81
9	0	131	118	112	103	119	74	60	0	*294*	*179*	*165*	*160*	*102*	*88*
10	0	151	133	127	114	118	71	61	0	169	138	131	123	102	98
11	0	143	128	122	109	119	67	62	149	158	137	126	110	84	79
12	0	148	132	120	110	58	64	63	152	164	137	130	111	85	87
13	0	145	130	120	109	61	67	64	152	158	139	132	122	85	88
14	0	144	130	121	107	119	68	65	105	115	109	105	100	85	87
15	0	144	128	120	109	64	63	66	104	105	100	94	90	86	61
16	0	139	126	118	105	82	81	67	108	118	114	108	106	108	61
17	*0*	*-9095*	*1160*	*525*	*108*	*81*	*80*	68	124	124	121	116	112	97	104
18	102	114	106	101	97	85	92	69	104	126	110	104	100	67	74
19	133	150	140	133	127	88	69	73	149	149	137	126	122	75	74
20	133	134	127	120	107	88	79	74	153	151	137	130	125	75	77
21	136	138	131	125	116	73	77	75	153	156	139	131	126	75	81
22	143	144	131	118	111	89	91	76	150	148	136	128	121	75	78
24	0	152	133	125	114	75	71	77	158	151	137	132	125	75	87
25	0	150	134	127	114	85	71	78	159	131	125	120	115	118	95
26	0	153	134	125	114	75	71	79	153	152	137	128	121	76	75
27	0	152	134	125	114	75	71	80	151	128	122	114	103	76	62
28	0	156	134	125	114	75	71	81	158	133	126	120	116	118	118
29	0	154	134	125	114	75	71	82	*38*	*38*	*36*	*34*	*32*	*30*	*27*
31	0	154	134	126	114	75	71	83	141	129	122	115	108	89	72
32	*0*	*810*	*500*	*299*	*244*	*125*	*100*	84	150	149	138	131	122	88	78
33	*0*	*742*	*590*	*353*	*340*	*124*	*97*	85	142	130	120	114	107	89	82
34	*0*	*649*	*588*	*356*	*340*	*124*	*97*	86	143	127	118	111	105	89	90
35	*0*	*3431*	*1331*	*348*	*341*	*124*	*100*	87	138	128	121	115	109	89	81
36	*0*	*616*	*449*	*362*	*340*	*58*	*57*	88	116	113	106	100	94	89	100
39	*0*	*298*	*249*	*202*	*185*	*58*	*56*	89	114	129	122	115	109	66	54
40	*0*	*594*	*425*	*364*	*317*	*125*	*99*	90	113	113	106	100	94	90	113
41	*0*	*545*	*403*	*318*	*236*	*125*	*102*	91	116	120	112	105	100	113	42
42	129	129	121	113	108	94	95	92	143	127	121	115	109	66	68
43	144	129	121	116	111	105	107	93	155	158	136	123	111	74	67
44	146	133	122	117	113	104	83	94	153	167	137	125	116	75	61
45	146	147	142	136	133	103	71	95	163	161	137	128	118	74	69
46	152	155	145	138	136	103	73	96	149	156	132	122	111	75	72
47	120	163	144	138	136	103	94	97	153	160	135	127	116	100	68
48	*150*	*107*	*103*	*100*	*98*	*53*	*55*	98	157	123	111	102	93	75	84
49	*0*	*63*	*57*	*55*	*50*	*53*	*55*	99	148	151	135	127	117	60	47
50	149	158	137	126	119	86	96	100	152	123	111	102	93	75	82
51	0	174	142	124	111	81	66	101	159	155	135	127	117	60	64

Table 3-8 Measured velocities (discarded tests in italics)

ANOVA

		Sum of Squares	df	Mean Square	F	Sig.
V0	Between Groups	8096.831	3	2698.944	12.110	.000
	Within Groups	16938.558	76	222.876		
	Total	25035.389	79			
V1	Between Groups	3182.335	3	1060.778	9.141	.000
	Within Groups	8819.074	76	116.040		
	Total	12001.408	79			
V2	Between Groups	480.364	3	160.121	1.708	.172
	Within Groups	7124.706	76	93.746		
	Total	7605.070	79			
V3	Between Groups	548.358	3	182.786	2.041	.115
	Within Groups	6806.611	76	89.561		
	Total	7354.969	79			
VCC	Between Groups	1365.023	3	455.008	1.811	.152
	Within Groups	19346.189	77	251.249		
	Total	20711.212	80			
VCS	Between Groups	7542.509	3	2514.170	14.155	.000
	Within Groups	13676.795	77	177.621		
	Total	21219.304	80			

Table 3-9 Statistical test (ANOVA) for anisotropic effects

ANOVA

		Sum of Squares	df	Mean Square	F	Sig.
VEXPERT	Between Groups	3785.407	4	946.352	3.863	.009
	Within Groups	10535.006	43	245.000		
	Total	14320.413	47			
V0	Between Groups	644.530	4	161.132	.557	.695
	Within Groups	12444.163	43	289.399		
	Total	13088.692	47			
V1	Between Groups	623.942	4	155.986	1.090	.374
	Within Groups	6155.347	43	143.148		
	Total	6779.289	47			
V2	Between Groups	544.650	4	136.162	1.090	.373
	Within Groups	5371.014	43	124.907		
	Total	5915.663	47			
V3	Between Groups	991.349	4	247.837	2.208	.084
	Within Groups	4825.874	43	112.230		
	Total	5817.223	47			
VCC	Between Groups	1775.634	4	443.908	2.455	.060
	Within Groups	7775.702	43	180.830		
	Total	9551.336	47			
VCS	Between Groups	860.349	4	215.087	.859	.496
	Within Groups	10765.225	43	250.354		
	Total	11625.574	47			

Table 3-10 Statistical test (ANOVA) for time effects on vertical shots

	VE	V0	V1	V2	V3	VCC	VCS
N	48	48	48	48	48	48	48
Mean	140.1	139.1	126.8	119.4	112.3	85.9	79.4
Stdv	17.5	16.7	12.0	11.2	11.1	14.3	15.7
Cv	0.12	0.12	0.09	0.09	0.10	0.17	0.20

Table 3-11 Basic statistics of measurements along the sample axis

Paired Differences	Mean	Std. Dev.	LL 95%CI	UL 95%CI	t	df	Sig. (2-tailed)
VEXPERT - V0	0.9	14.0	2.0	5.0	0.5	47	0.64
V0 - V1	12.3	6.7	1.0	14.3	12.7	47	0.00
V1 - V2	7.4	2.1	0.3	8.0	24.2	47	0.00
V2 - V3	7.1	3.5	0.5	8.1	14.0	47	0.00
V3 - VCC	26.4	17.4	2.5	31.4	10.5	47	0.00
V3 - VCS	32.9	19.7	2.8	38.6	11.6	47	0.00
VCC - VCS	6.5	16.5	2.4	11.3	2.7	47	0.01
V0-VCS	59.7	24.8	3.6	66.9	16.7	47	0.00

Table 3-12 Mean difference between various methods of arrival time selection (T test)

Limit	5%	10%	20%
Mean	76.72	79.40	83.19
Stdv	16.21	15.56	14.94
Cv	0.21	0.20	0.18

Table 3-13 Influence of module criteria on cross-spectrum method performance

ANOVA

		Sum of Squares	df	Mean Square	F	Sig.
VEXPERT	Between Groups	2380.011	3	793.337	2.923	.044
	Within Groups	11940.403	44	271.373		
	Total	14320.413	47			
V0	Between Groups	3935.078	3	1311.693	6.305	.001
	Within Groups	9153.615	44	208.037		
	Total	13088.692	47			
V1	Between Groups	1461.051	3	487.017	4.029	.013
	Within Groups	5318.237	44	120.869		
	Total	6779.289	47			
V2	Between Groups	1060.168	3	353.389	3.202	.032
	Within Groups	4855.495	44	110.352		
	Total	5915.663	47			
V3	Between Groups	738.228	3	246.076	2.132	.110
	Within Groups	5078.995	44	115.432		
	Total	5817.223	47			
VCC	Between Groups	897.714	3	299.238	1.521	.222
	Within Groups	8653.622	44	196.673		
	Total	9551.336	47			
VCS	Between Groups	203.183	3	67.728	.261	.853
	Within Groups	11422.391	44	259.600		
	Total	11625.574	47			

Table 3-14 Statistical test (ANOVA) for signal type effects on vertical velocities

ANOVA

		Sum of Squares	df	Mean Square	F	Sig.
VEXPERT	Between Groups	6269.246	4	1567.312	8.371	.000
	Within Groups	8051.167	43	187.236		
	Total	14320.413	47			
V0	Between Groups	3202.308	4	800.577	3.482	.015
	Within Groups	9886.385	43	229.916		
	Total	13088.692	47			
V1	Between Groups	1597.668	4	399.417	3.315	.019
	Within Groups	5181.620	43	120.503		
	Total	6779.289	47			
V2	Between Groups	1259.623	4	314.906	2.908	.032
	Within Groups	4656.040	43	108.280		
	Total	5915.663	47			
V3	Between Groups	1554.641	4	388.660	3.921	.008
	Within Groups	4262.582	43	99.130		
	Total	5817.223	47			
VCC	Between Groups	1953.908	4	488.477	2.765	.039
	Within Groups	7597.428	43	176.684		
	Total	9551.336	47			
VCS	Between Groups	1714.474	4	428.618	1.860	.135
	Within Groups	9911.101	43	230.491		
	Total	11625.574	47			

Table 3-15 Statistical test (ANOVA) for distance effects on vertical velocities

3.7 FIGURES

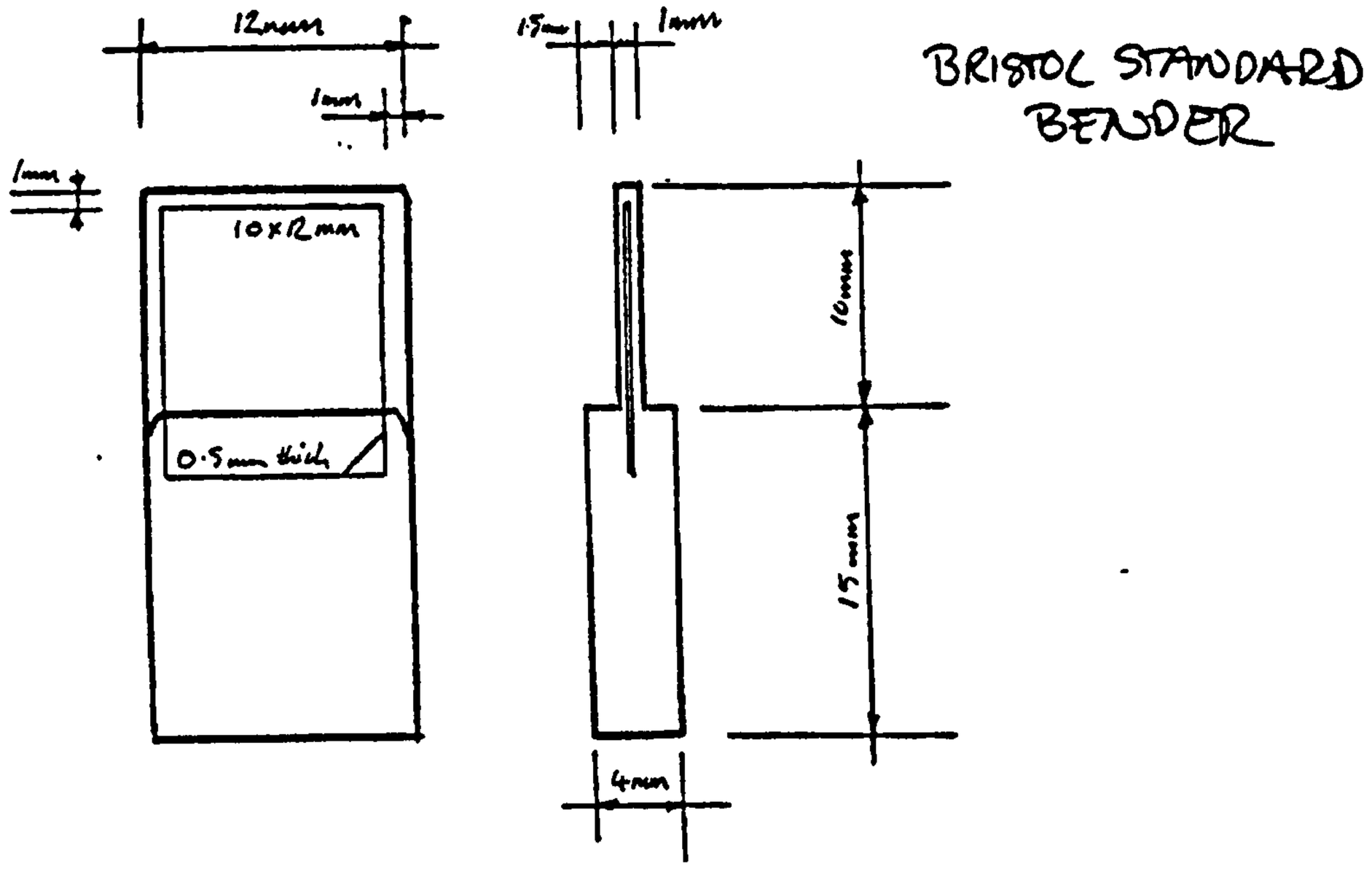

Figure 3-1 Bender probe used in this study (drawing by P. Greening)

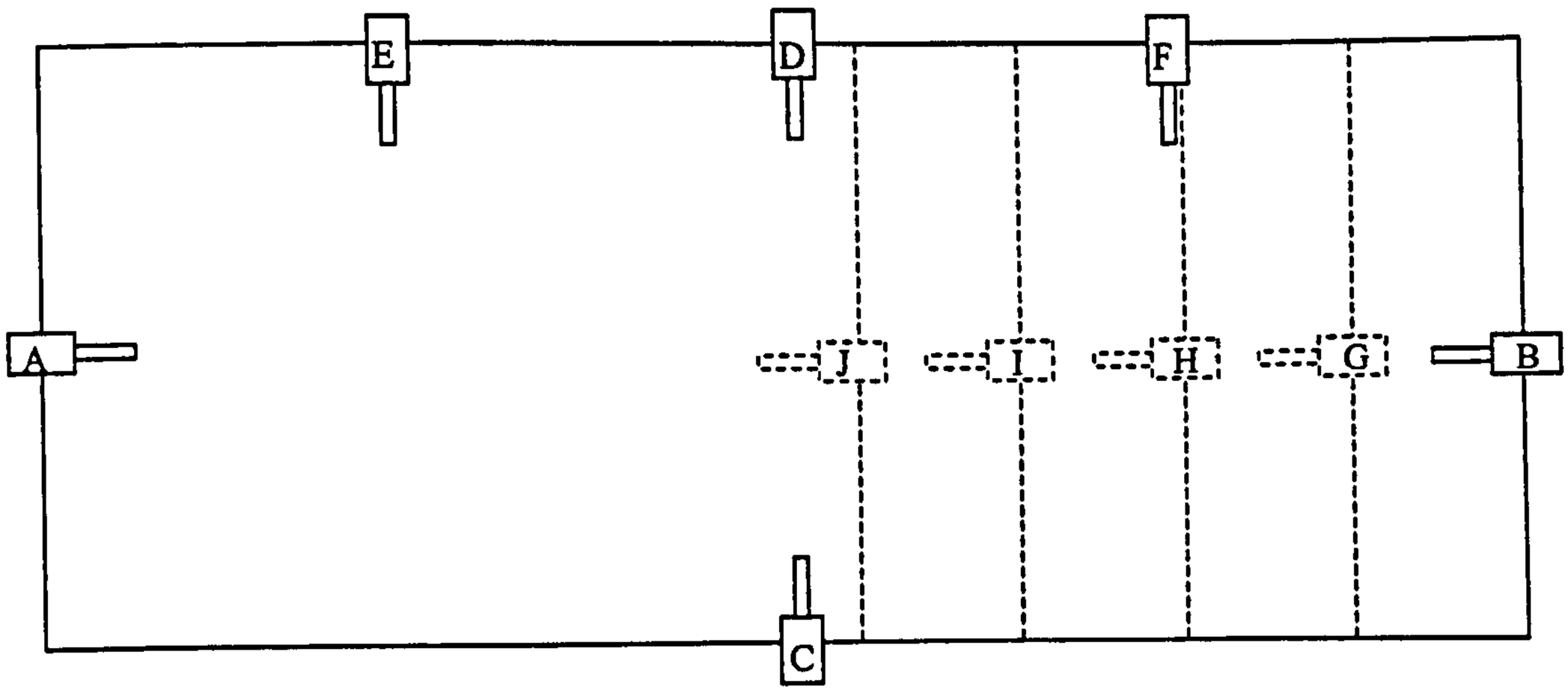

Figure 3-2 Sample instrumentation plan

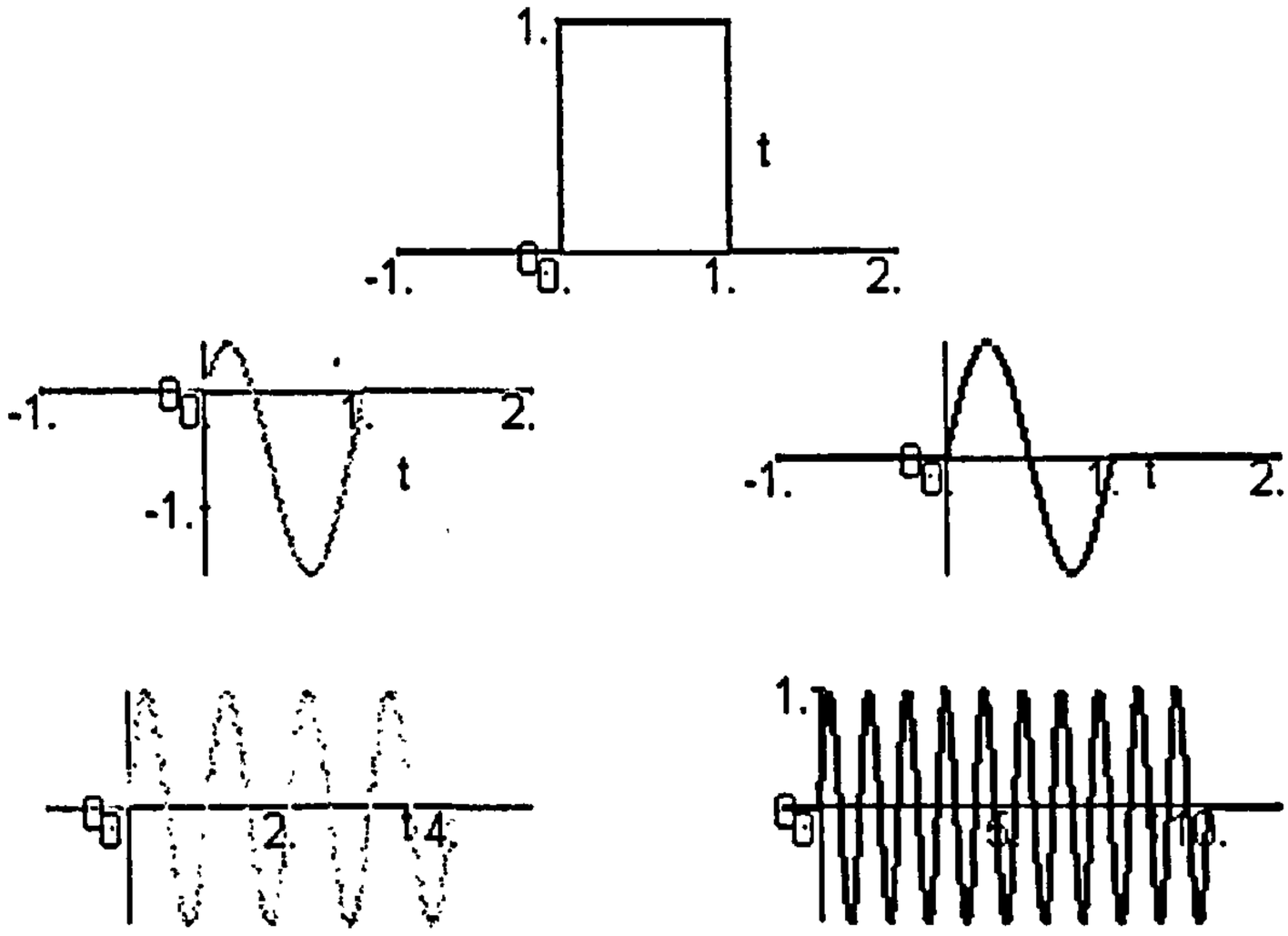

Figure 3-3 Nominal driving signals employed in bench pulse tests

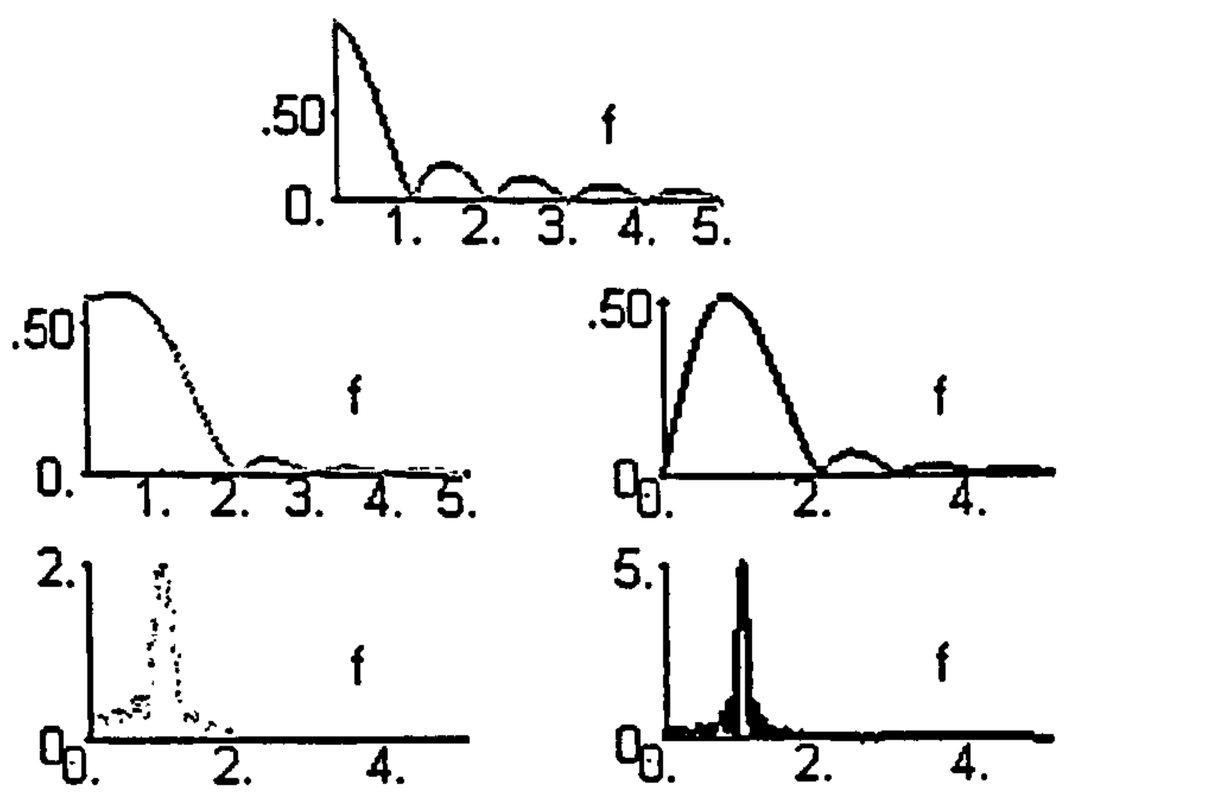

Figure 3-4 Amplitude spectra of the precedent

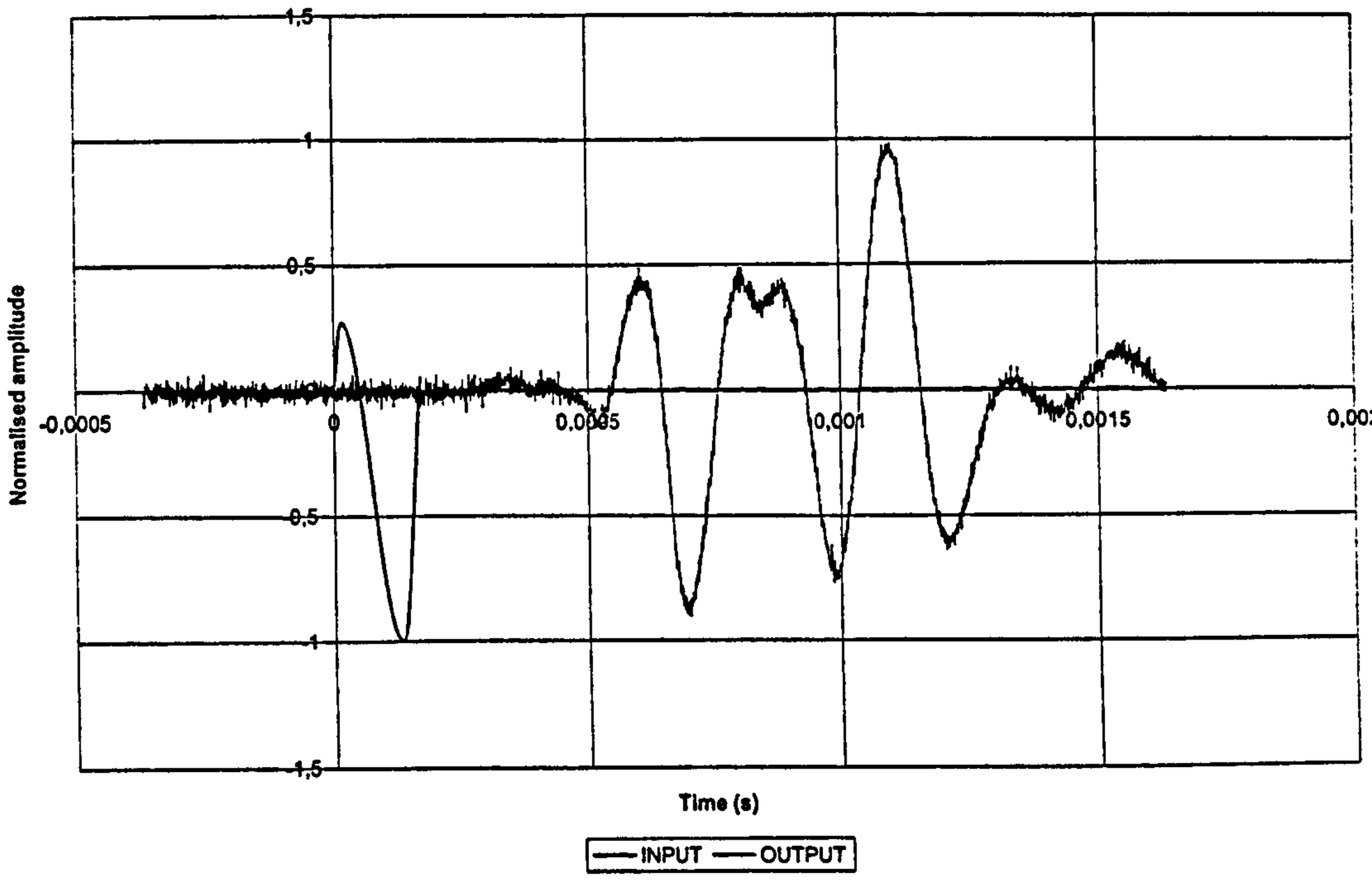

Figure 3-5 Typical test result showing moderate high frequency noise

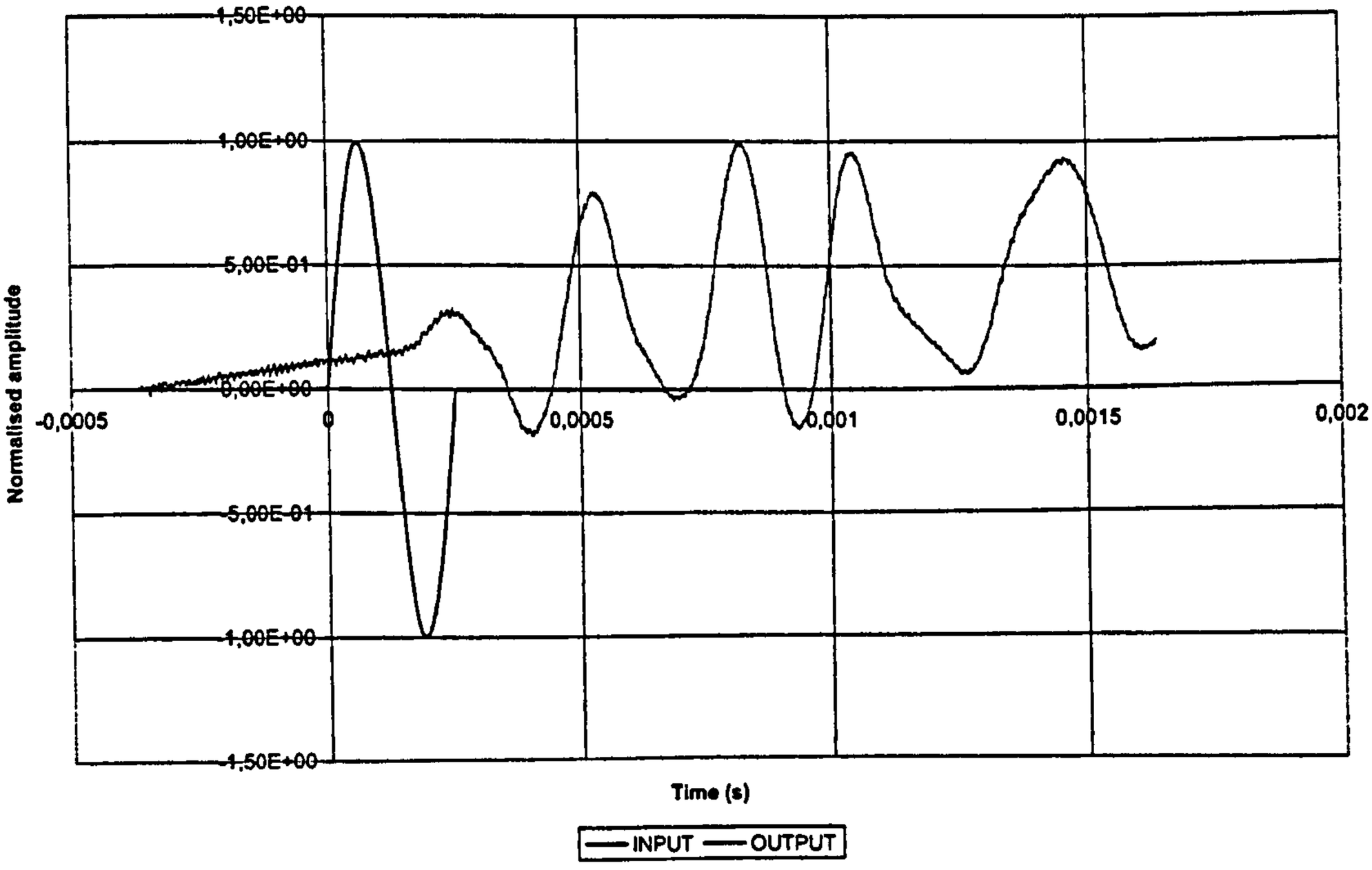

Figure 3-6 Low frequency noise in receiver trace

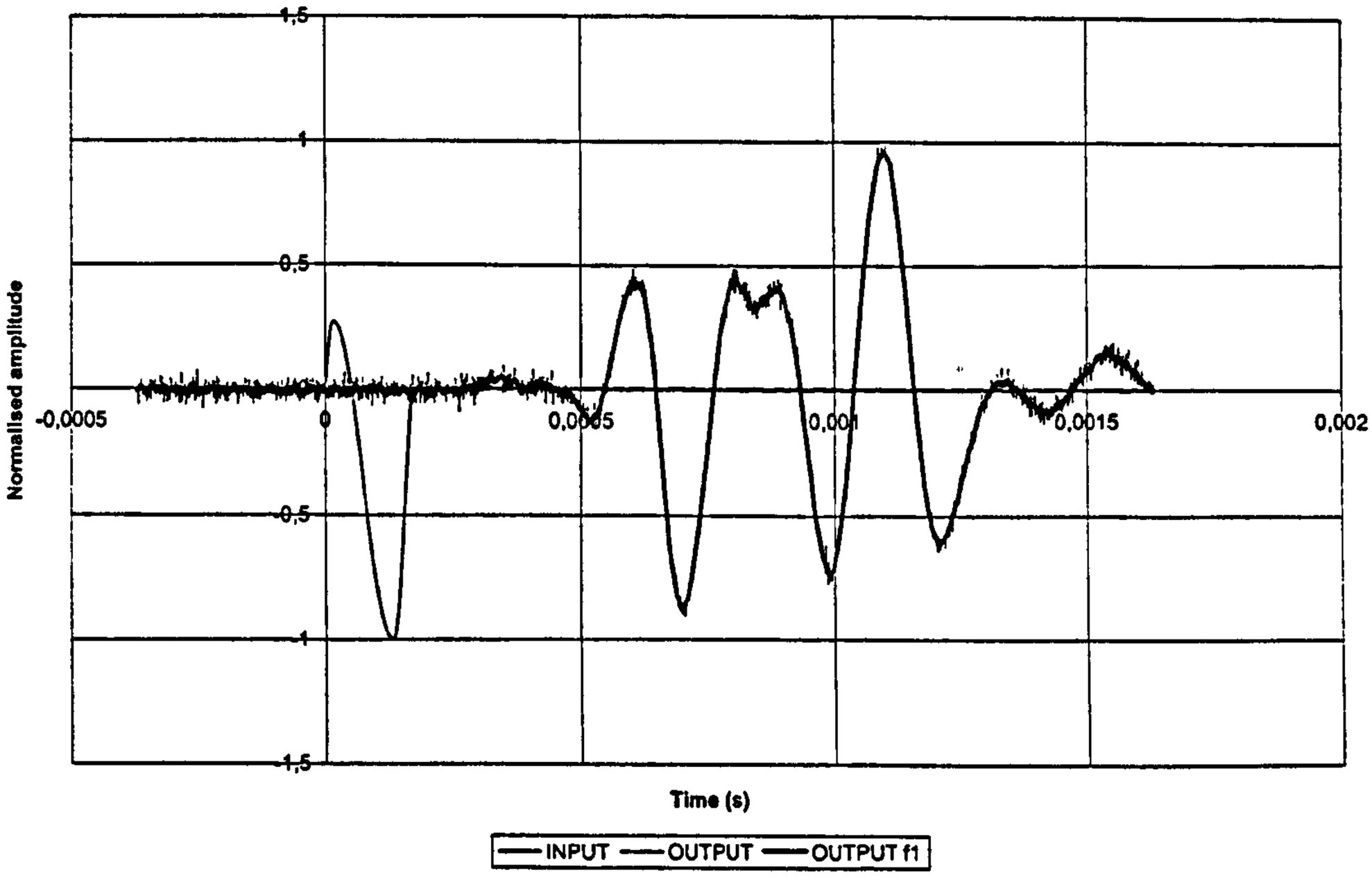

Figure 3-7 Original and smoothed output traces

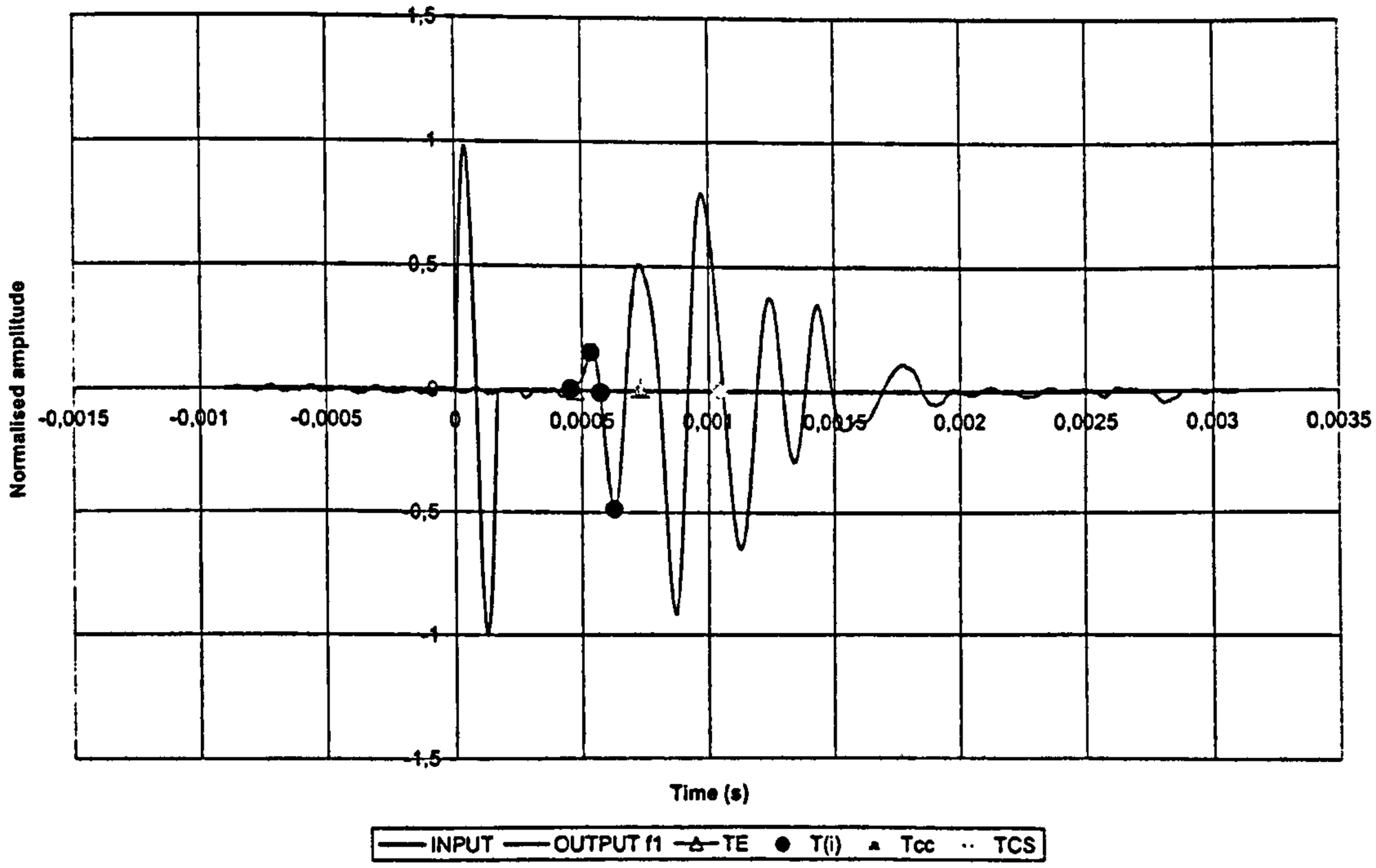

Figure 3-8 An example of arrival point selection

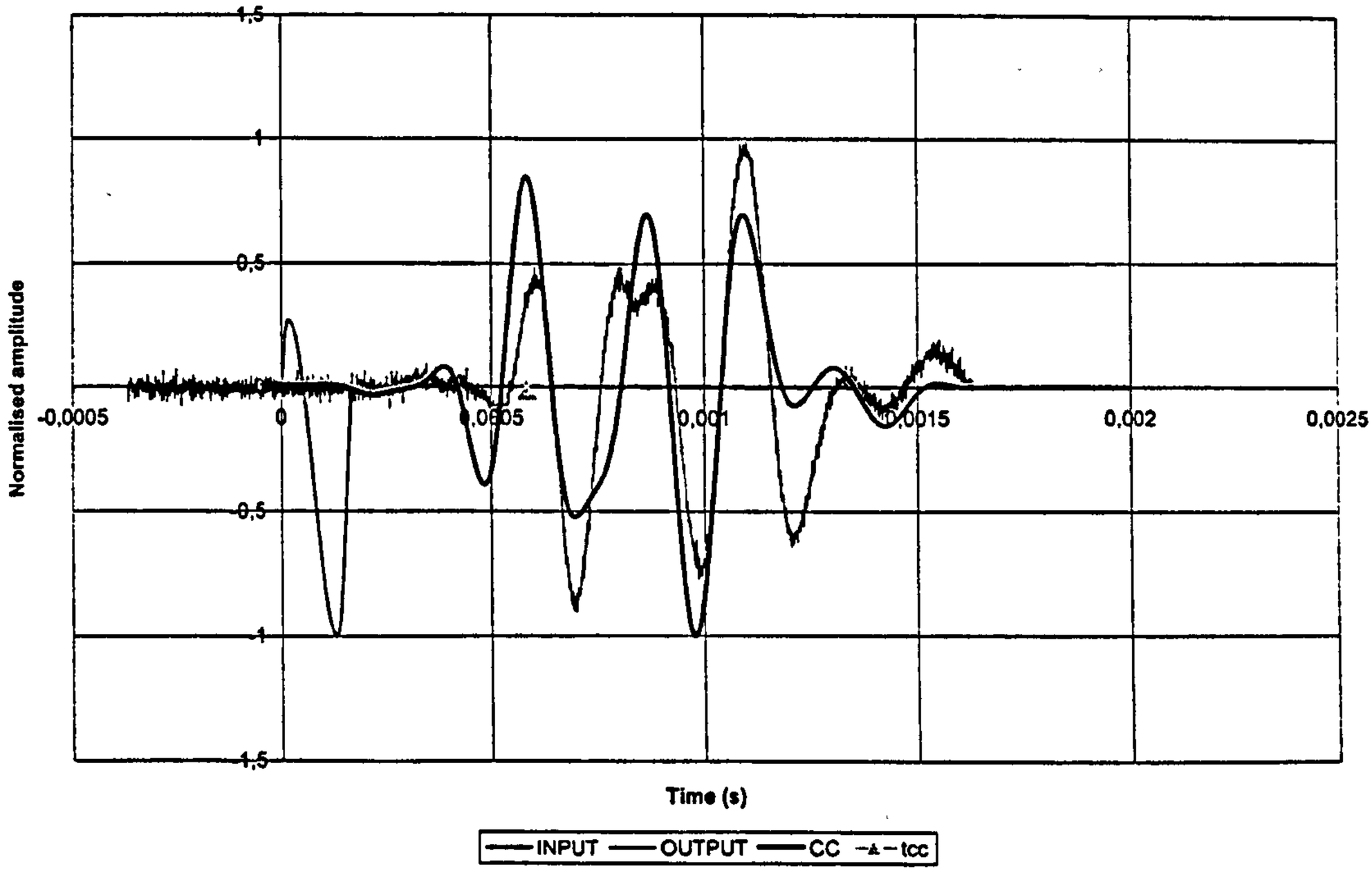

Figure 3-9 Arrival time by cross-correlation

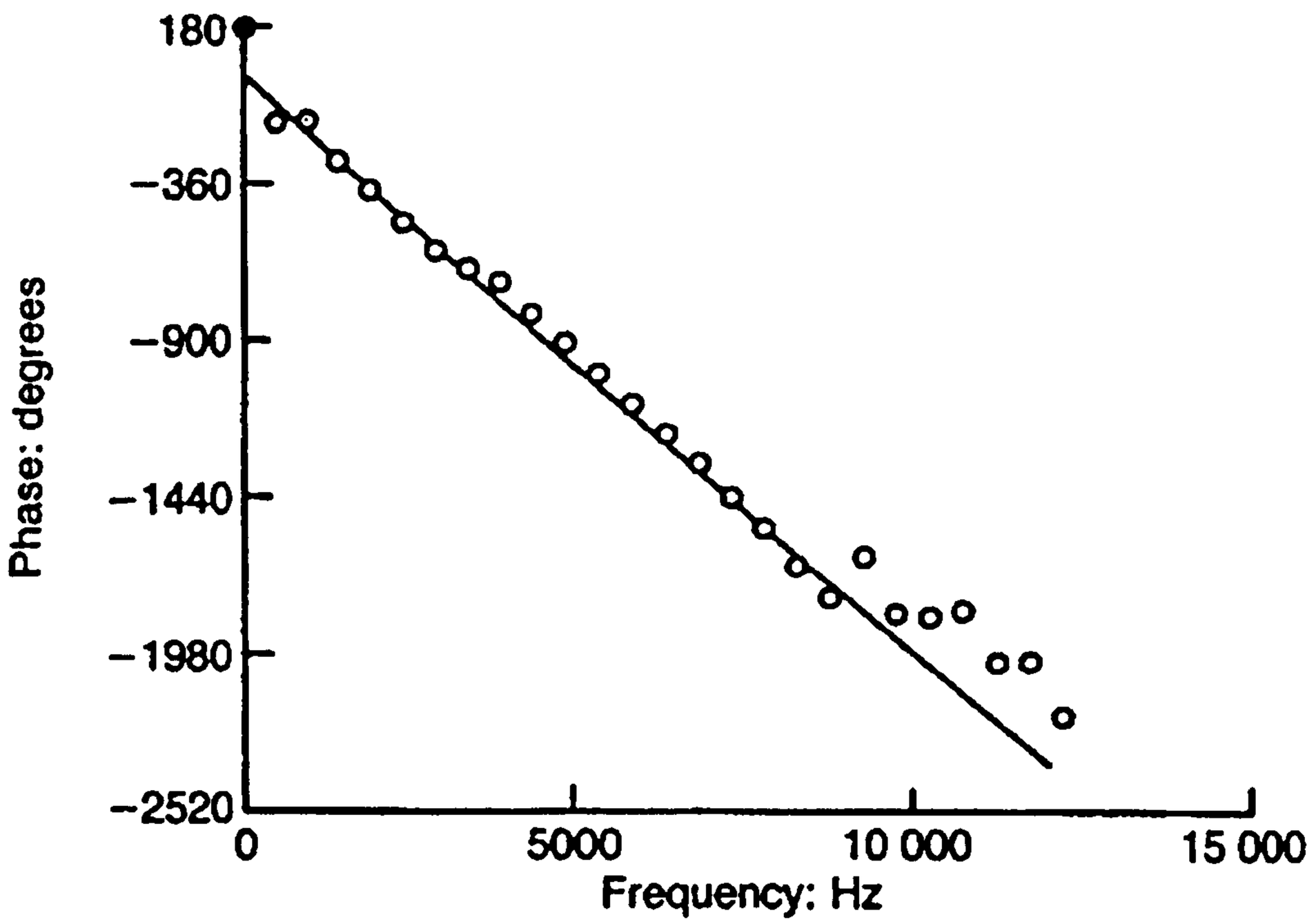

Figure 3-10 Viggiani & Atkinson illustration of the cross-spectrum method

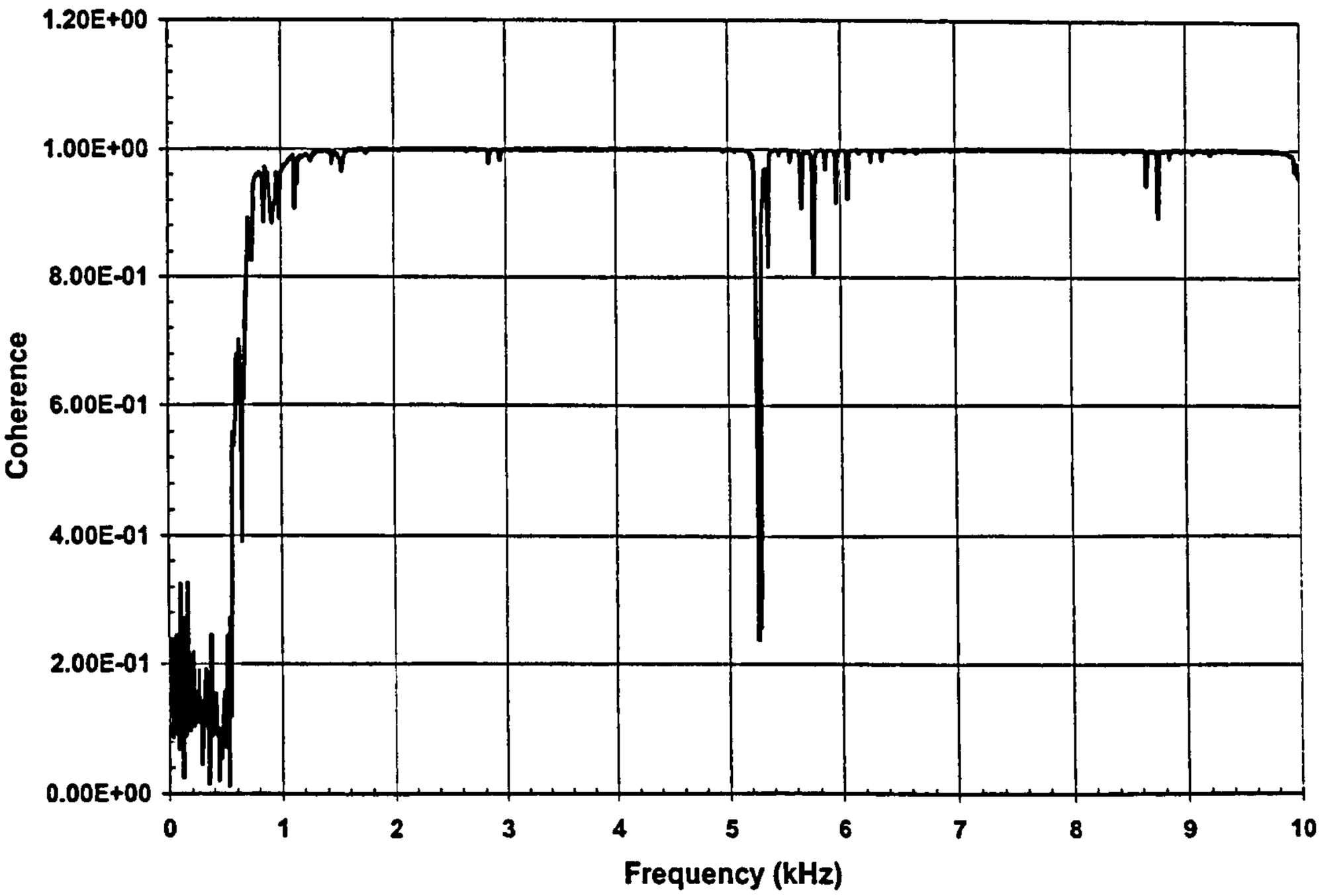

Figure 3-11 Typical coherence of recorded output

Output Test 97

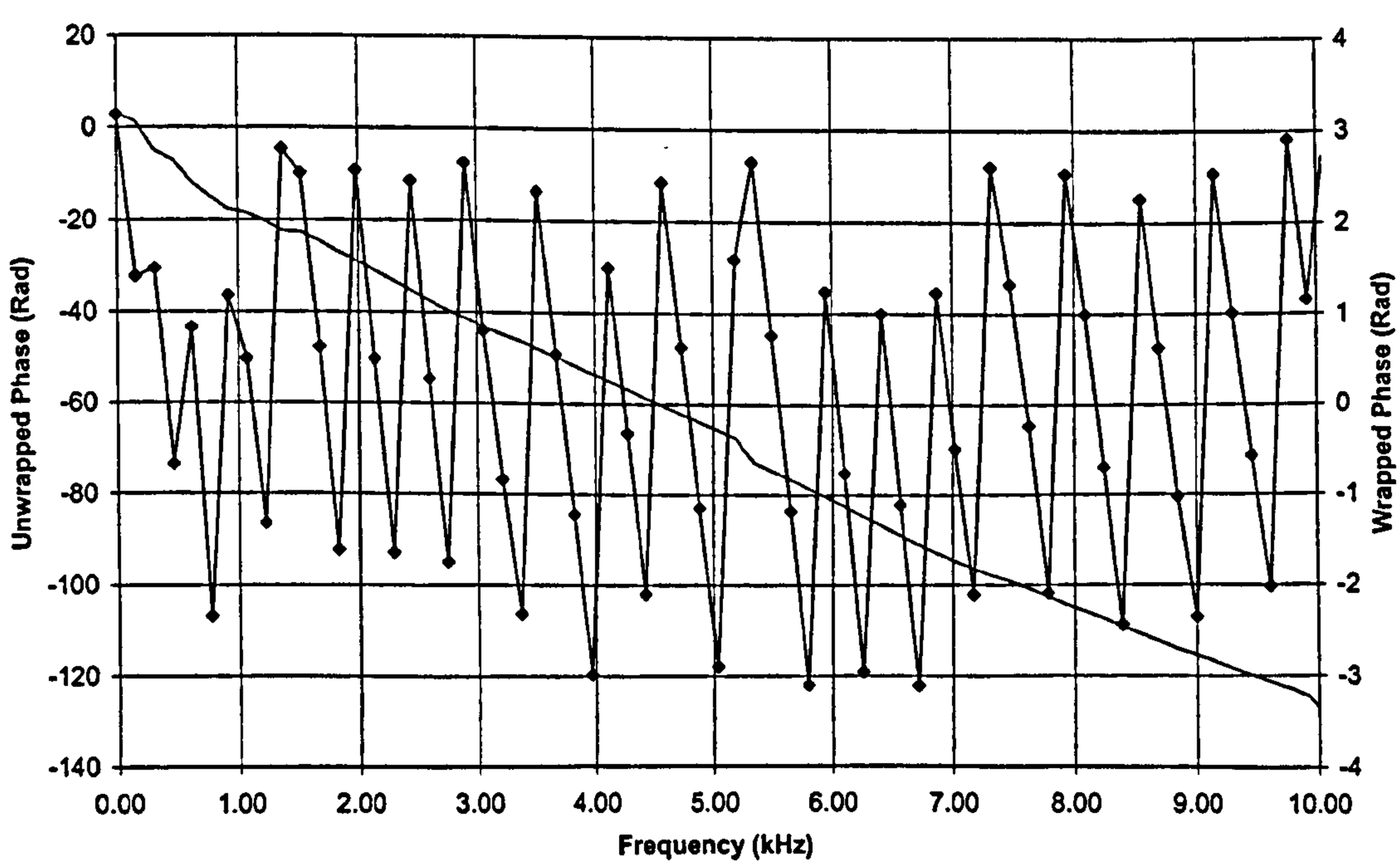

Figure 3-12 Phase unwrapping example

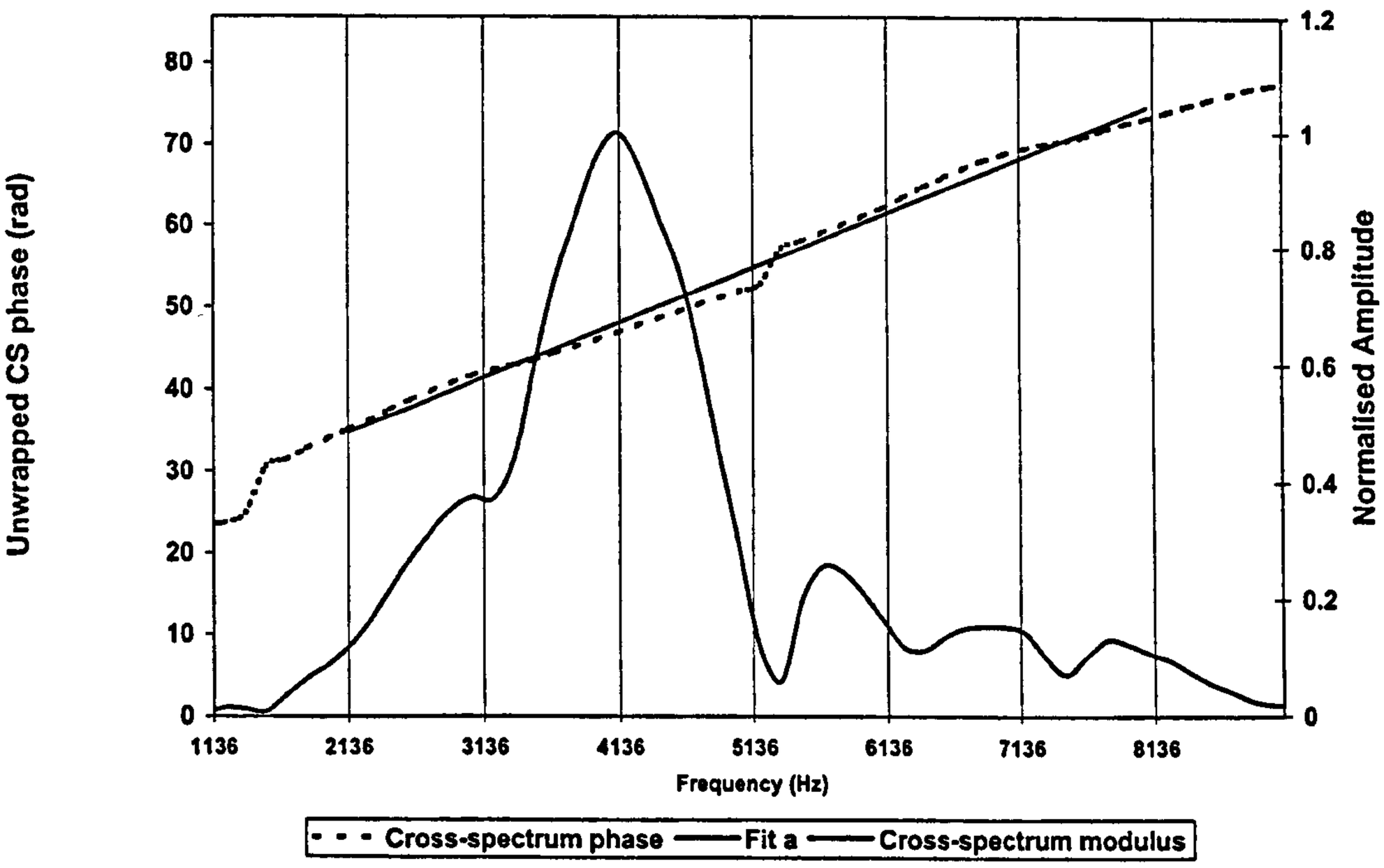

Figure 3-13 Fitting procedure for cross-spectrum phase

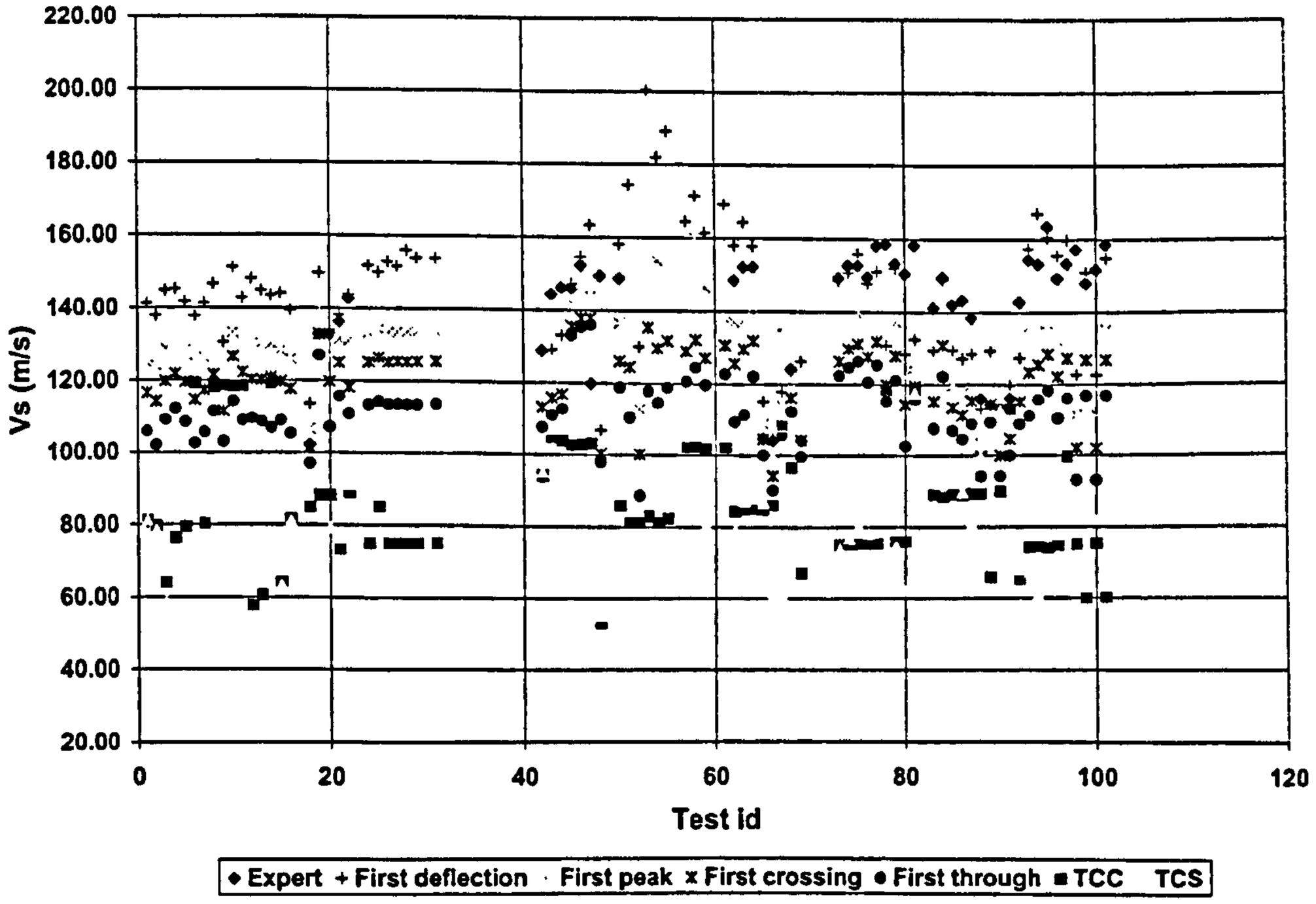

Figure 3-14 Arrival time estimates for all tests

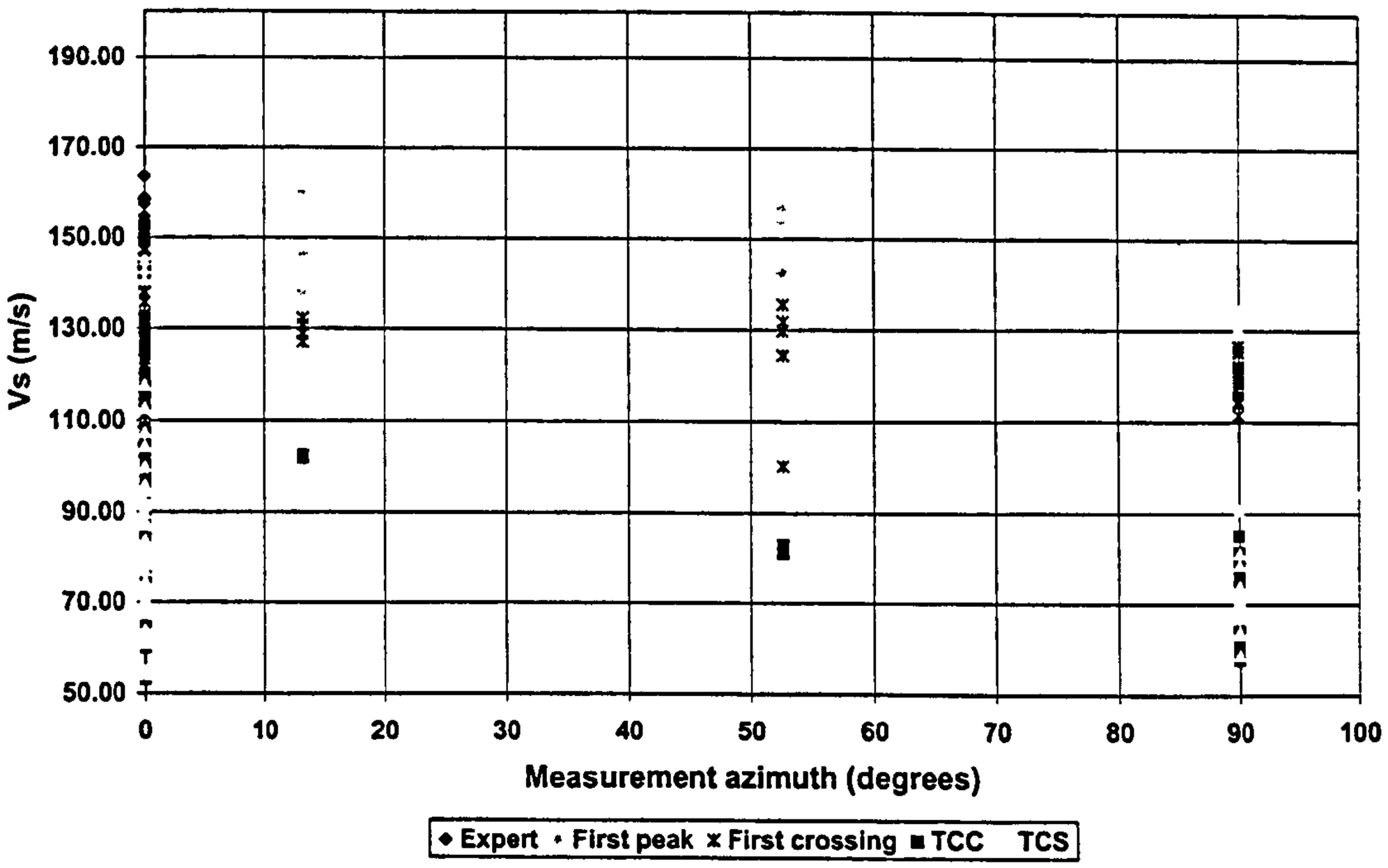

Figure 3-15 Anisotropy in measured velocities

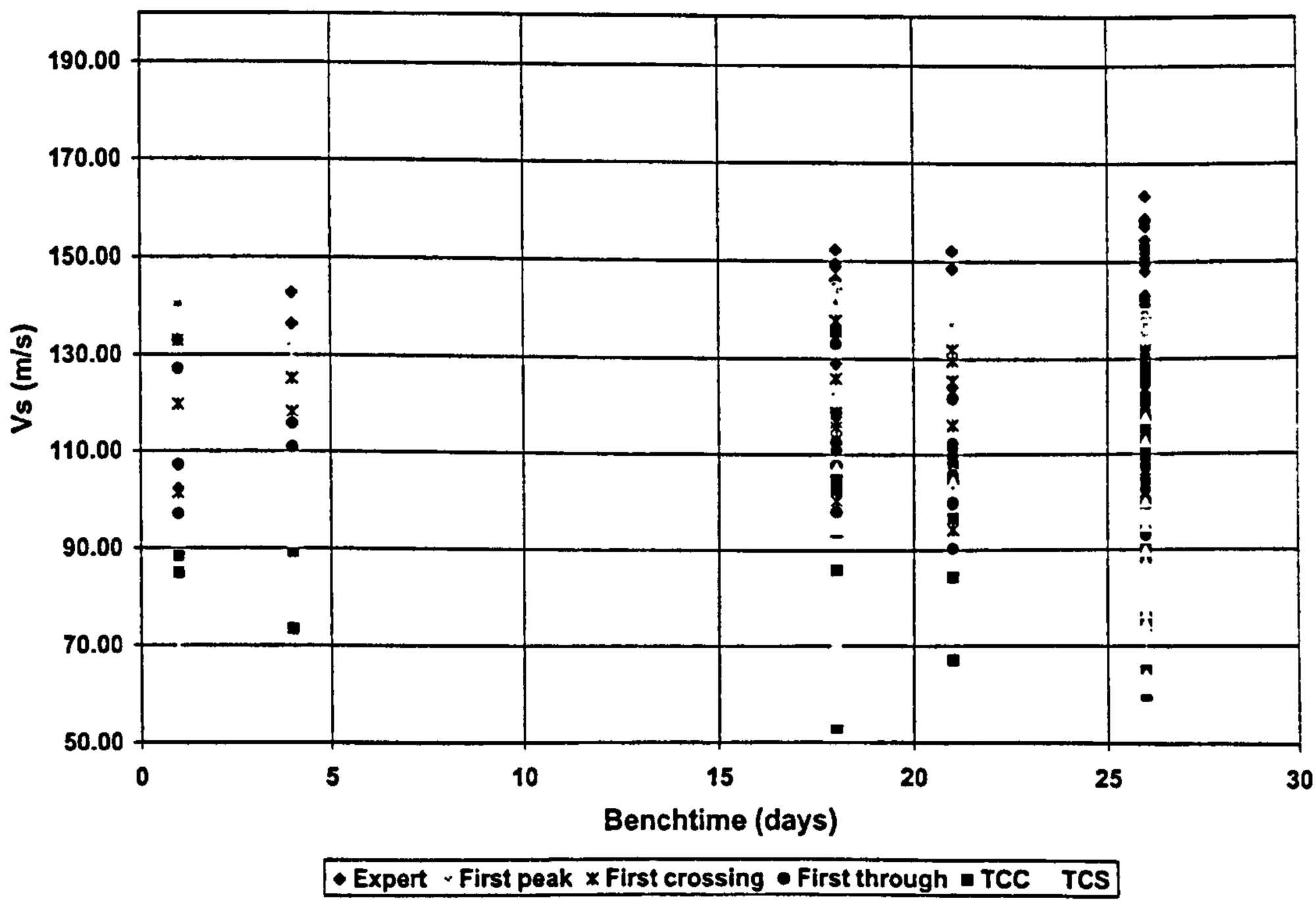

Figure 3-16 Time effect on measured vertical velocities

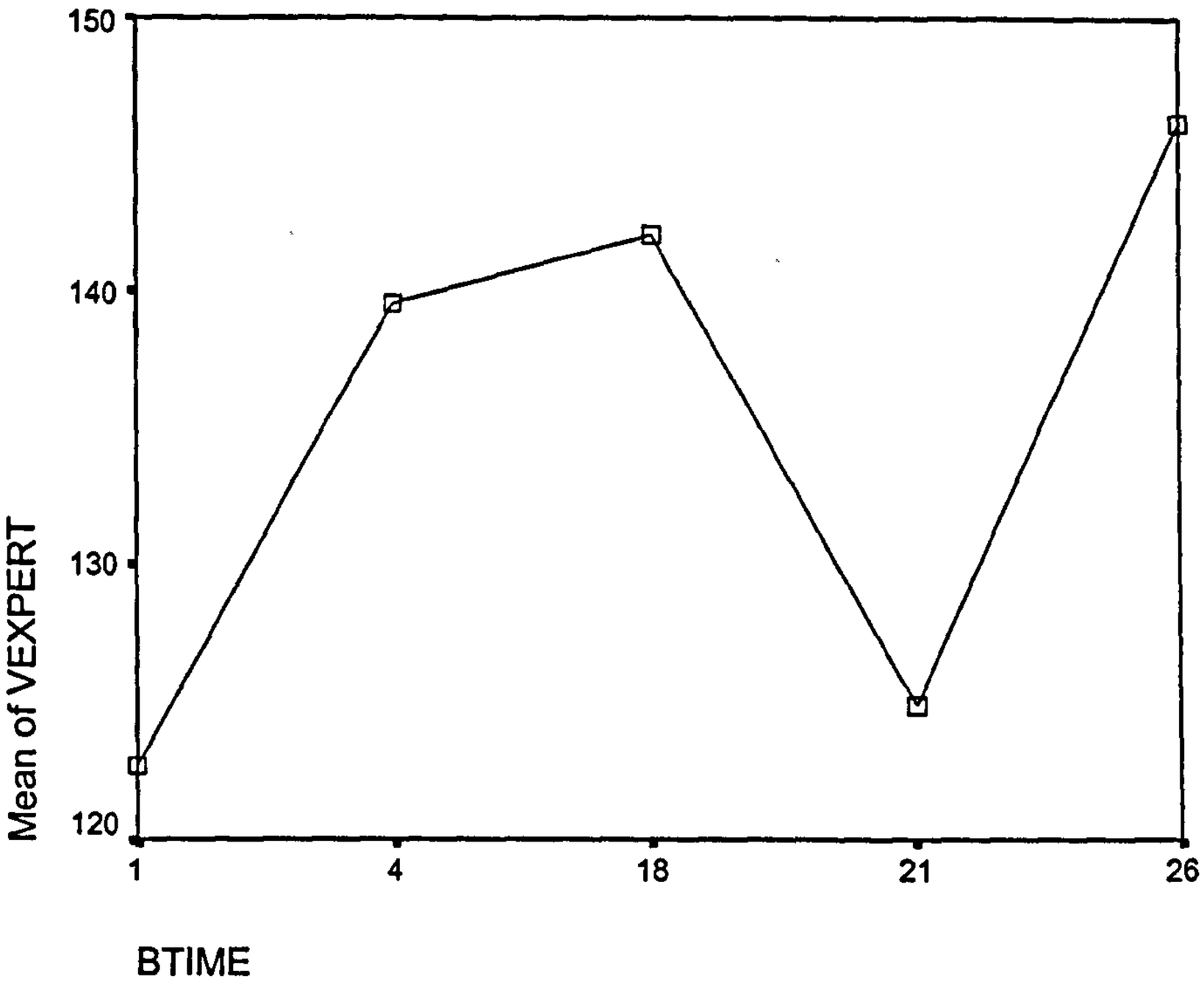

Figure 3-17 Time effect on manually identified arrival times

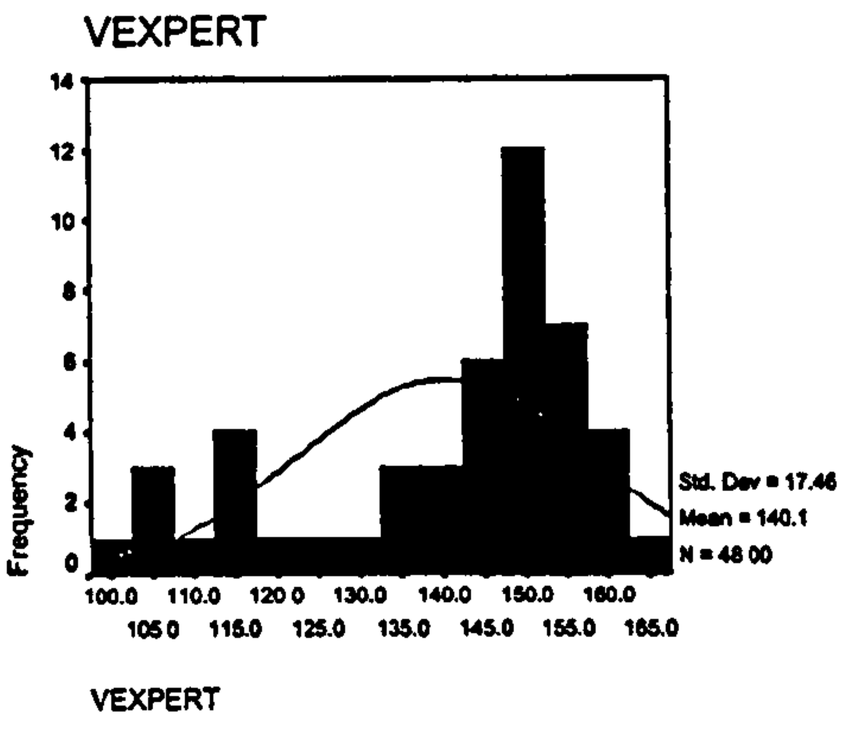

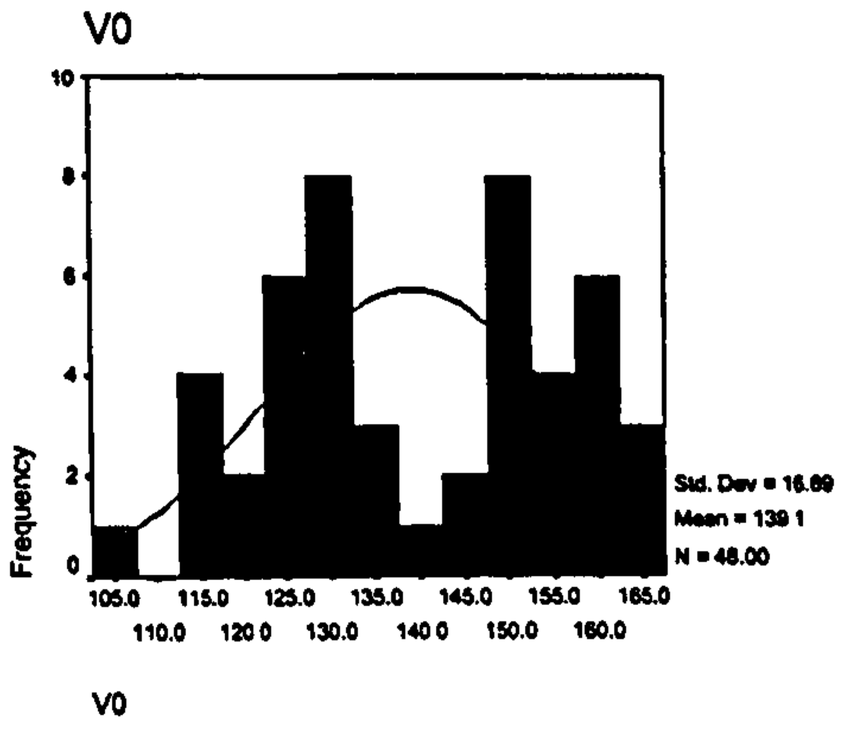

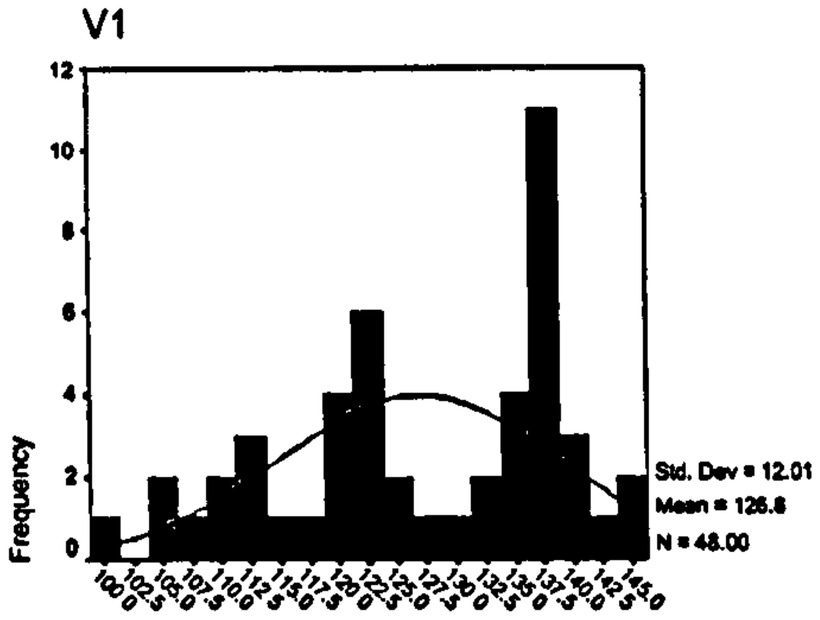

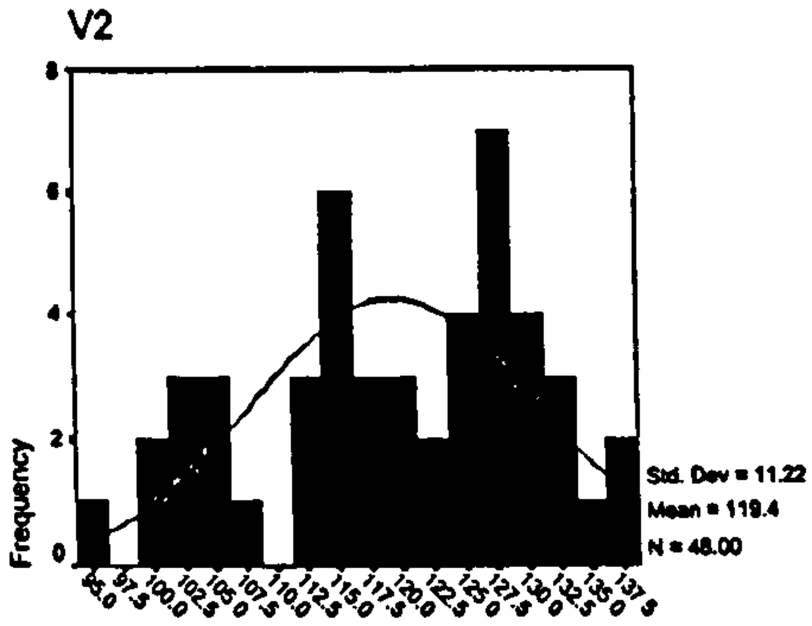

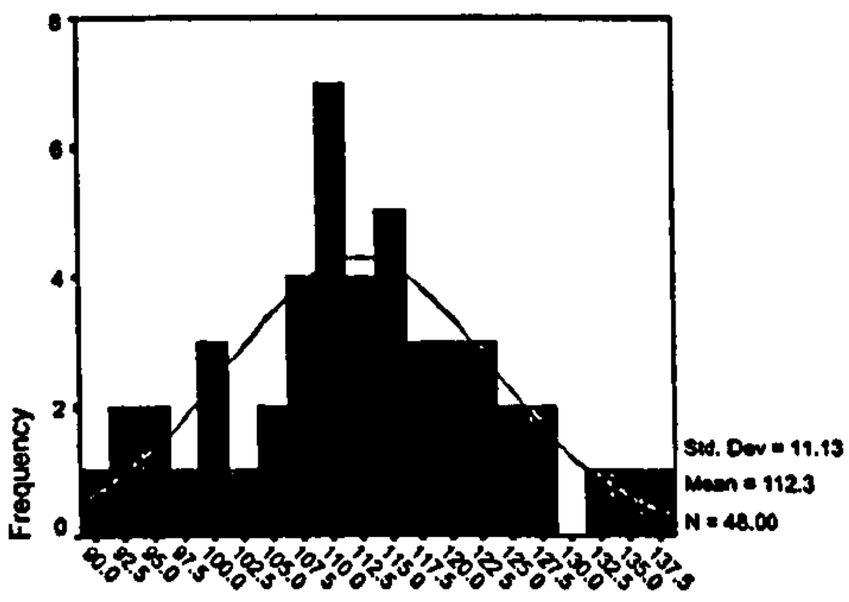

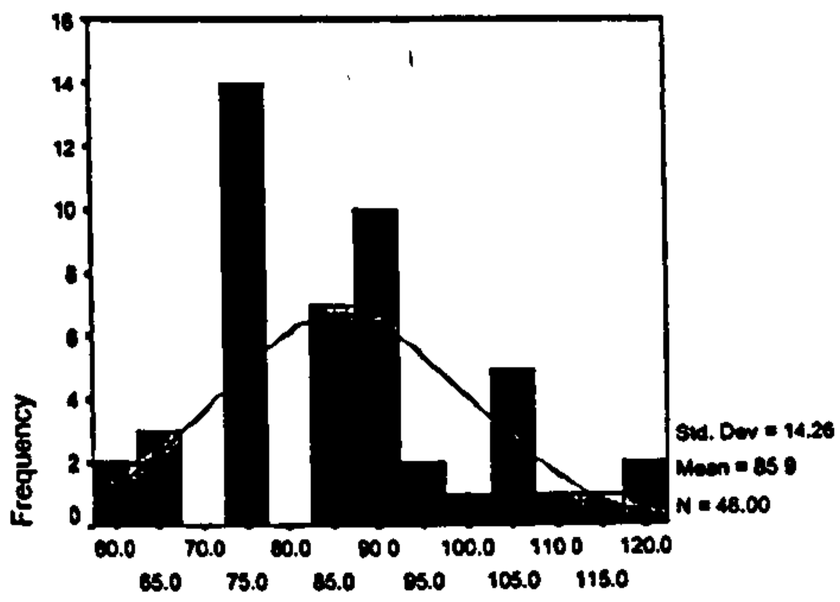

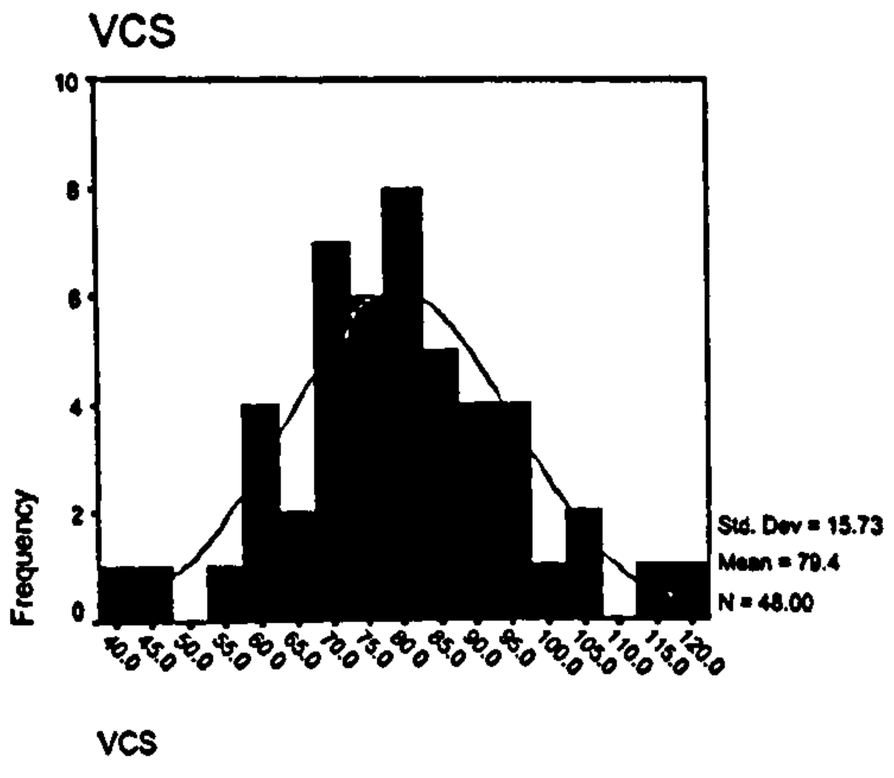

Figure 3-18 Histograms of estimated vertical velocities

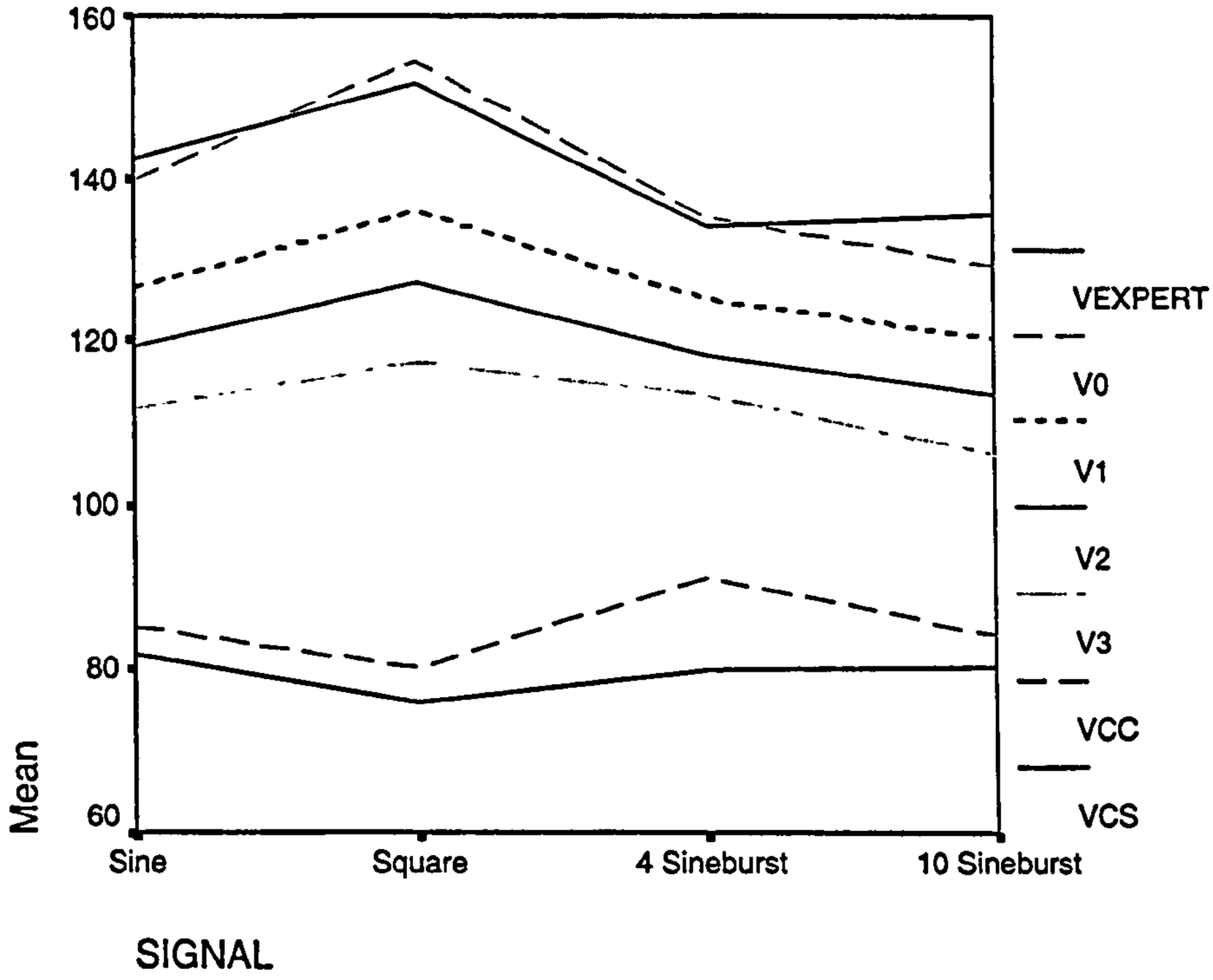

Figure 3-19 Effect of input signal type in measured vertical velocity. Mean values (m/s)

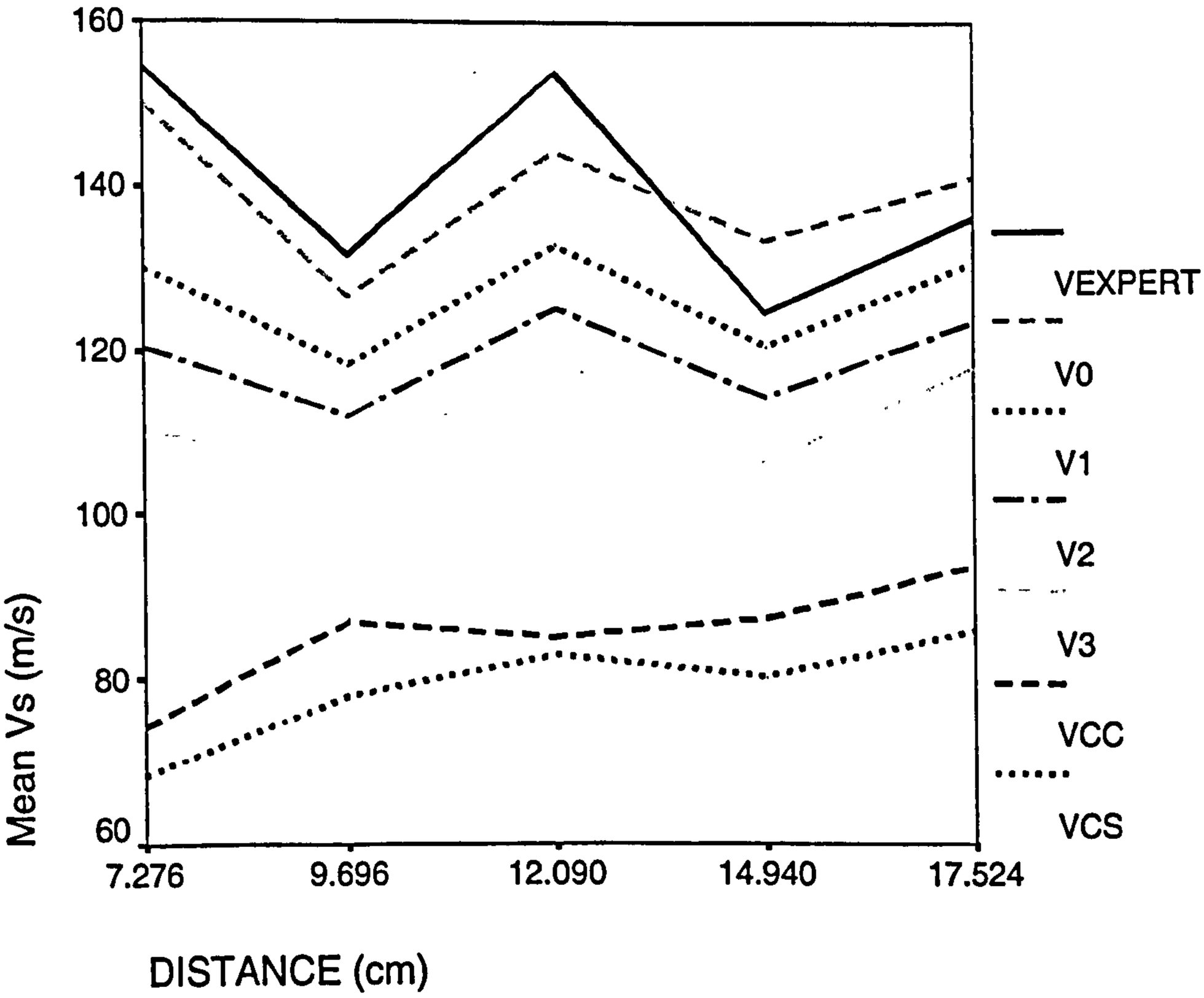

Figure 3-20 Effect of measurement distance on vertical velocities. Mean values (m/s).

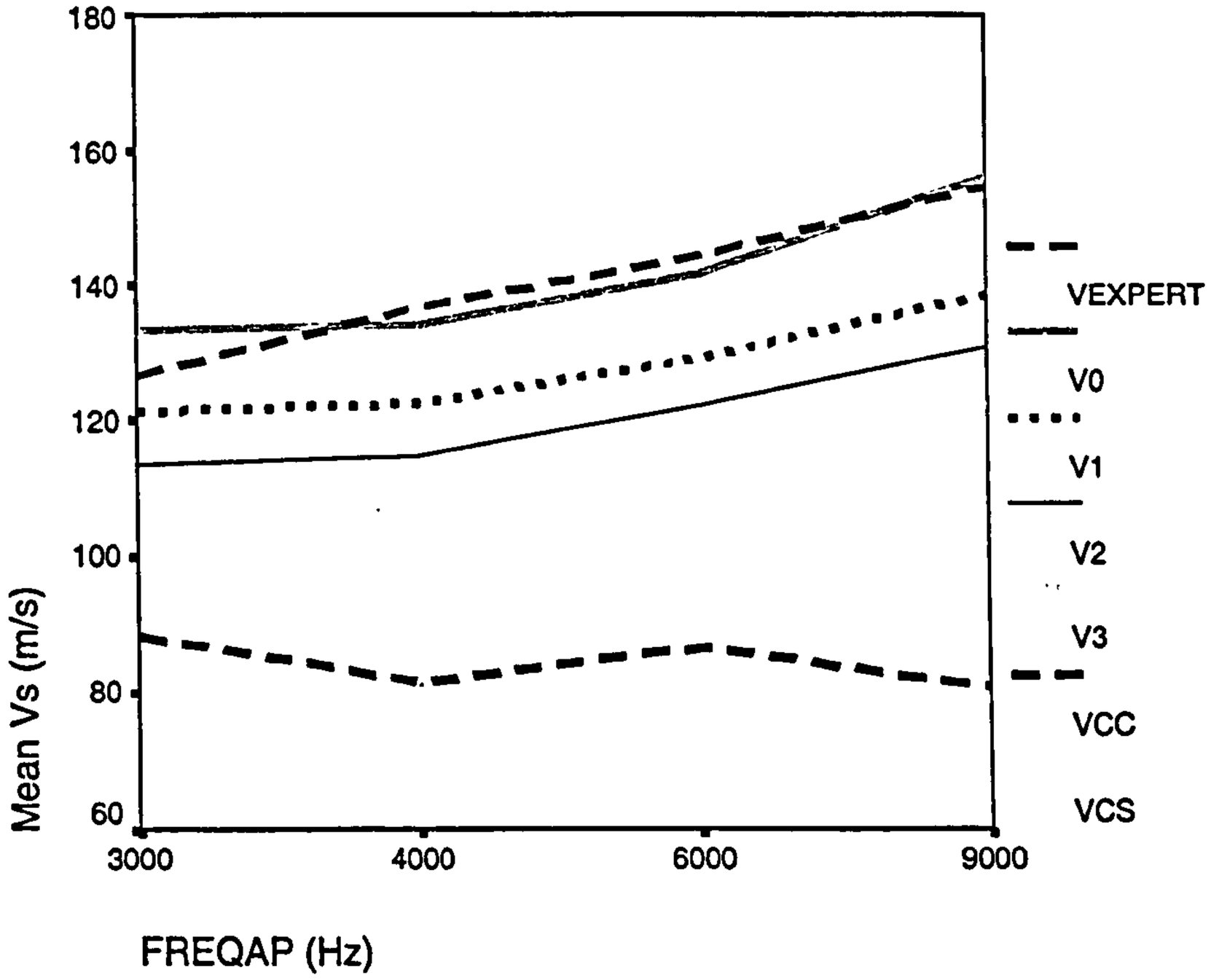

Figure 3-21 Effect of input apparent frequency on vertical velocities Mean values (m/s).

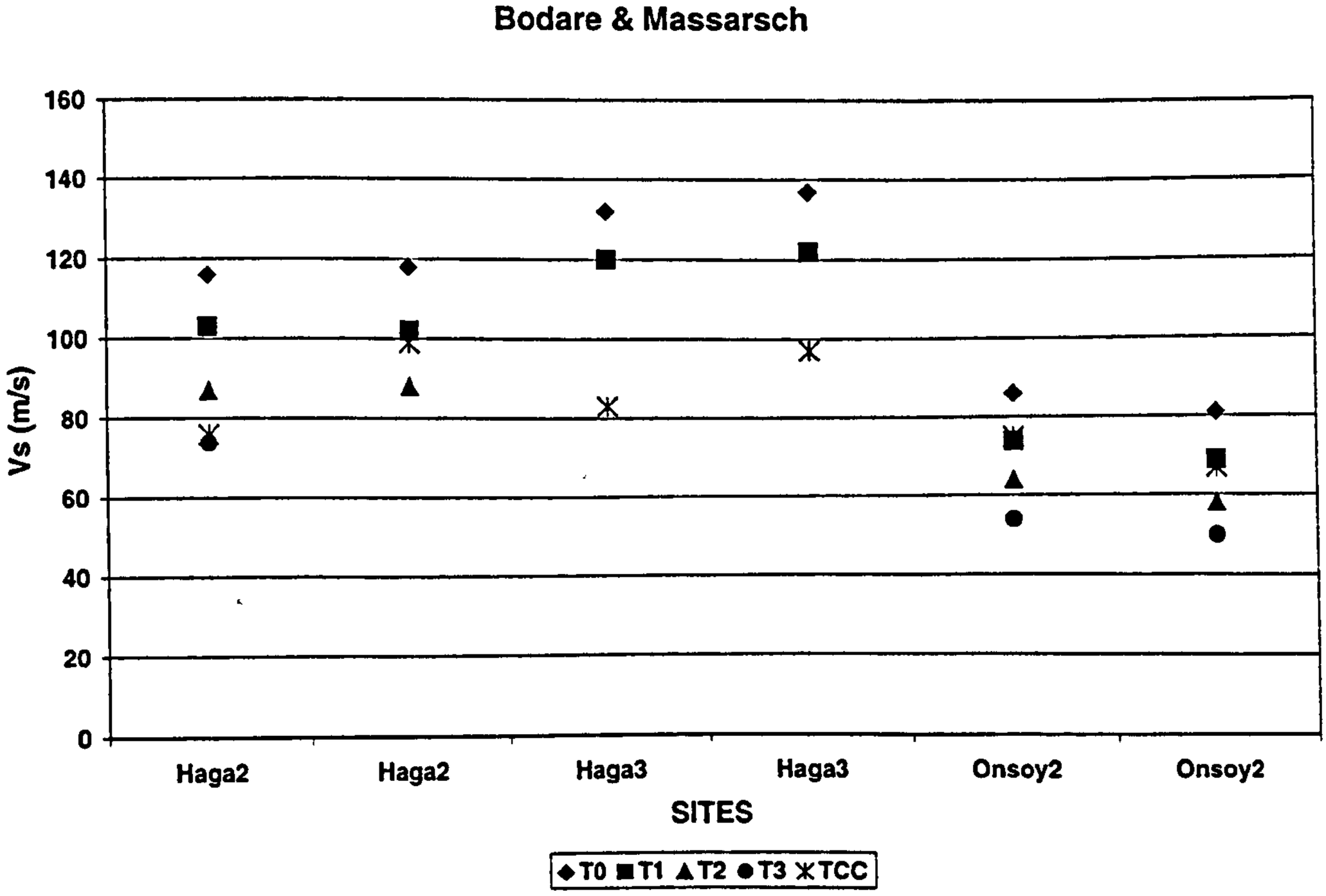

Figure 3-22 Cross-hole measurements by Bodare & Massarsch

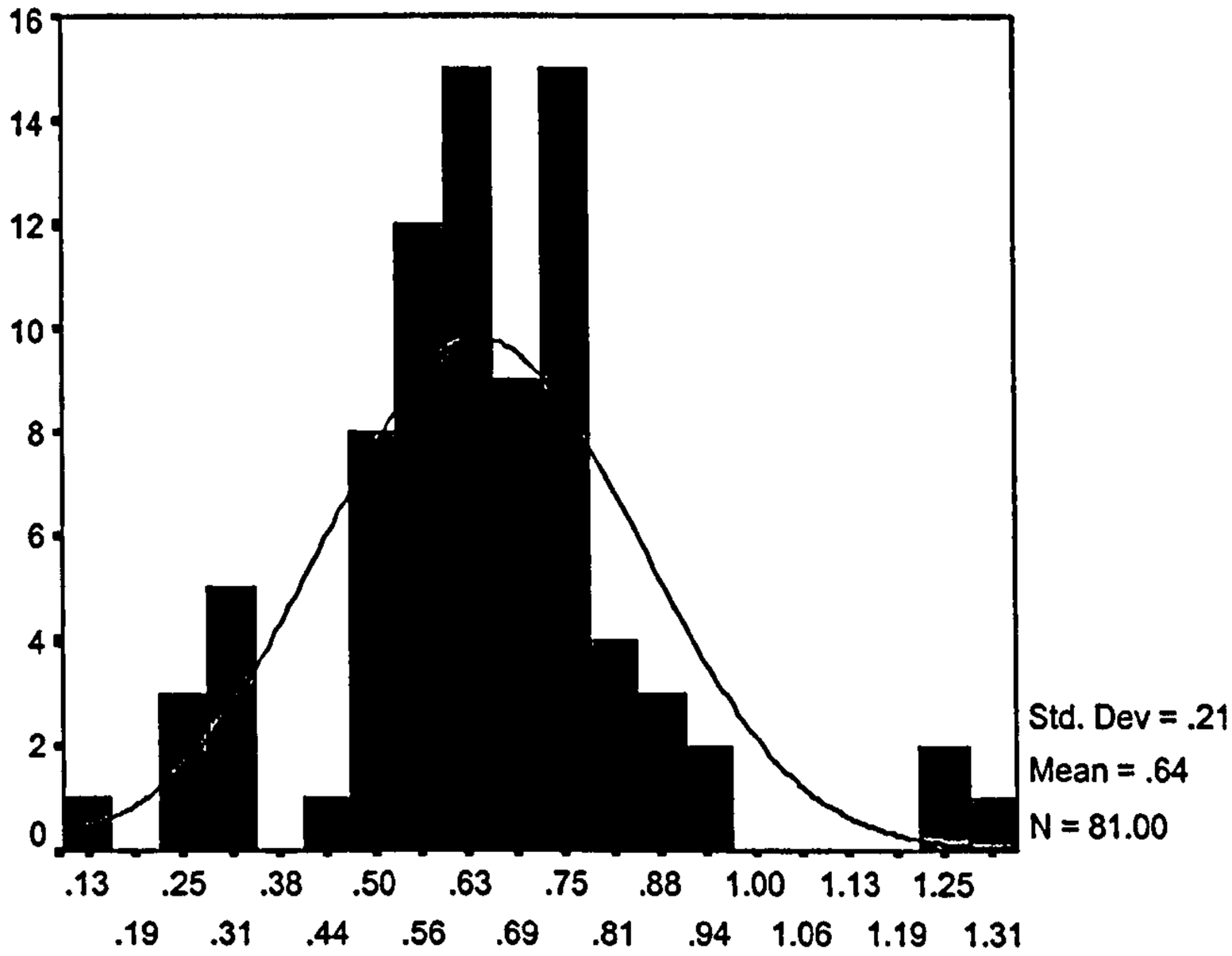

Figure 3-23 Uncertainty (range/mean) distribution for all tests

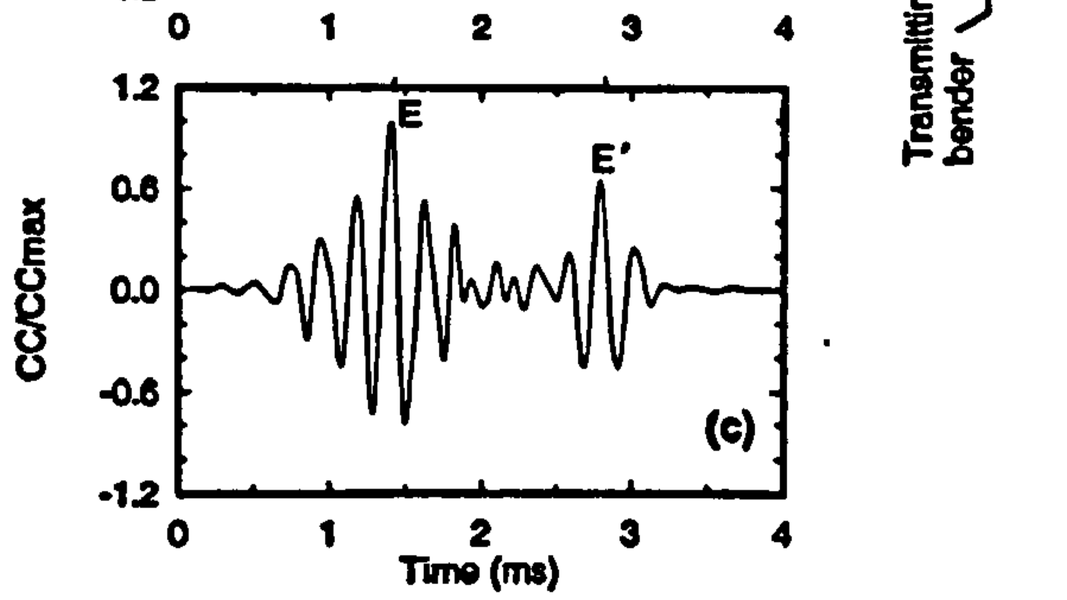

Figure 3-24 Alternative arrival points in a bender trace as indicated by Arulnatham et al. (1998)

4 ISOTROPIC DISPERSION AND NEAR FIELD EFFECTS

4.1 WAVE DISPERSION

4.1.1 General concept

Dispersion is one of the key concepts in wave propagation. Waves are dispersive when the frequency has a non-linear relationship with the wave vector. This can be written generally –Whitham, 1974- as:

$$\omega = \omega(\mathbf{k})$$

$$\det\left|\frac{\partial^2 \omega}{\partial k_i \partial k_j}\right| \neq 0 \tag{47}$$

Using the relation between the wave vector and frequency above, the wavenumber k might be expressed as a function of frequency and phase velocity as a function of either wavenumber or frequency.

$$\mathbf{c} = \frac{\omega}{\mathrm{k}}\mathbf{k} \Leftrightarrow \mathrm{v}(\omega) = \frac{\omega}{\mathrm{k}(\omega)} \tag{48}$$

All these relations are different, equally valid, expressions of dispersion, but the one with perhaps most intuitive appeal for our problem is that linking phase velocity and frequency. In a pulse or signal each frequency component will travel with different phase velocity. Therefore the pulse or signal will spread out or change shape as it travels; in a word: it will disperse. The converse statement also holds: if distortion is observed in a travelling pulse the propagation is necessarily dispersive.

4.1.2 Group velocity

Whenever dispersion occurs the concept of signal velocity becomes problematic. On the one hand a monotone single frequency signal would have a clearly defined phase velocity, but neither beginning nor end, thus no proper "arrival". On the other hand any finite signal would necessarily have components at multiple frequencies and a number of differing phase velocities will be involved. It is nevertheless almost intuitive that the problem should be more substantial for shapes that contain many frequencies than for shapes whose frequency content is very limited; in other words, dispersion would distort more wide-band signals than narrow-band signals. Looking at results from our bench test series there is certainly more distortion in wide band pulses -Figure 3-8- than in narrow band pulses -Figure 4-1- performed in the same conditions.

It can be proved analytically -e.g. Graff, 1975- that narrow band pulses centred at ω_0 will travel almost undistorted but with a velocity, $v_g(\omega_0)$ called **group velocity** which is generally different from the corresponding phase velocity $v(\omega_0)$. This is a somehow counterintuitive result that, nevertheless, has had extensive confirmation in many circumstances where dispersive waves appear: light –Brillouin, 1960-, the sea - Lighthill, 1978-, the earth's surface –Udías, 2000. Wide band pulses will cover an ample range of group velocities and their frequencies will order themselves in time domain according to their

respective v_g values. In general, (Whitham, 1974), group velocity is defined as the gradient of the dispersion relation, i.e:

$$\mathbf{c}_g = \nabla_{\mathbf{k}} \omega \tag{49}$$

For one-dimensional problems direction is not an issue and wave vector, phase velocity and group velocity might be represented by their moduli. The corresponding definitions of phase and group velocity are then

$$v = \frac{\omega}{k}$$
$$v_g = \frac{d\omega}{dk} \tag{50}$$

And both might be expressed as functions of either the wavenumber or the frequency by means of the dispersion relation. When this relation is plotted as in Figure 4-2 it is possible to identify phase and group velocity as the secant and tangent to the dispersion relation, respectively[38]. It is convenient to have an explicit relation between both quantities and a straightforward development of (50) leads to

$$v_g = v + k\frac{dv}{dk}$$
$$v_g = \frac{v}{1 - \frac{\omega}{v}\frac{dv}{d\omega}} \tag{51}$$

The expression to choose will depend on either wavenumber or frequency being considered the independent variable. It is clear also from these expressions that the slope of the phase velocity function will control the relative size of phase and group velocity at any given frequency or wavenumber –Figure 4-3. Phase and group velocity will be only equivalent when the change in phase velocity is very small, that is, when dispersion is negligible or, locally, at extrema of the phase velocity function.

4.1.3 Dispersion measurements

A dispersion curve relates, for instance, wavenumber and frequency. Such a curve can be obtained experimentally from time records of a travelling pulse. Recall that, in Chapter 1, it was shown that an experimental wavenumber field might be obtained from a transfer function field as

$$\mathbf{k}(\omega, \mathbf{x}) = \nabla_{\mathbf{x}} \Psi(\omega, \mathbf{x}) \tag{52}$$

where ψ is the measured phase of the transfer function, coincident with the cross-spectrum phase of the input and the output at **x**. This, as shown in Appendix I, may be obtained numerically from the cross-correlated time records by means of a discrete Fourier transform. In practice the measurements are only taken at discrete locations and that introduces one further approximation. Assume, for argument's sake, a

---

[38] This offers a cue to understand why narrow-band pulses travel at the group velocity. Within a narrow range, the tangent is a good linear approximation to the curved dispersion relation, whereas, generally, the secant is not. A linear k-ω relation involves no dispersion.

one-dimensional problem where measurements are available at two different locations, say x_1 and x_2. We can then obtain a lineal approximation to the x-dependent dispersion curve as

$$k(\omega,x) \approx \frac{\Psi(\omega,x_2)-\Psi(\omega,x_1)}{x_2-x_1} \tag{53}$$

Moreover, if x_1 is taken as the coordinate origin and the time record there is defined as the input, the preceding expression simplifies[39] to

$$k(\omega,x) \approx \frac{\Psi(\omega,x_2)}{x_2} \tag{54}$$

And from this estimated dispersion curve other relevant quantities like phase or group velocity might be deduced, for instance using (50). Obviously if the spatial dependency of the wavenumber field is lineal equations (53) and (54) involve no approximation. This is the case when the registered motion is due to a plane wave.

Apparently this FFT based technique was employed first for seismological applications (Bolt 1974) and then adopted for ultrasonic testing of dispersive materials, like composites (Sachse & Pao, 1978). It may also be applied to a single location record of a pulse and its reflection, provided that the reflections are distinguishable and the reflector distance is known (Pialucha et al. 1989). In geotechnics it is commonly applied to obtain the experimental dispersion curve in the SASW method (Foti, 2000) and it has been applied to laboratory tests by Fratta & Santamarina (1996).

4.1.4 Group velocity, phase velocity and elastic moduli

From what has just been said it is apparent that the dispersion concept is extremely relevant to our problem[40]. All the time records of pulse tests in soils shown in Chapters 2 and 3 show dispersion to a minor or major degree. We know also that a non-dispersive elastodynamic model -plane bulk wave propagation- performed very poorly when confronted with real data. This now seems perfectly reasonable. Moreover, using the unwrapped cross-spectrum phase we can tentatively compute phase and group velocity for each test using (50) above. An example of the results thus obtained is shown in Figure 4-4.

The phase velocity values seem to be low and that can be explained because of the sensitivity of the chosen unwrapping algorithm to trace noise. Phase velocity is based on the whole unwrapped curve -is the secant of the dispersion relation- and therefore is affected by all the accumulated unwrapping errors. A low value implies excessive unwrapping by the chosen algorithm. Other algorithms are available in the literature, but no one seems to offer complete guarantee (Shatilo, 1992). The group velocity values are less affected by errors in the unwrapping algorithm, as they are based on local values –the tangent of the

---

[39] The frequency domain autocorrelation or autospectrum of a signal has zero phase (Lynn, 1989).

[40] This has been recognised for a long time in the field of ultrasonic testing of materials –Elices & García-Moliner, 1968- although with the high frequency techniques and low dissipation materials initially employed researchers avoided the problem in most cases – Schreiber et al. 1973

dispersion relation. Its values within the range of significative spectral energy –indicated by the cross-spectrum moduli in Figure 4-4- are well within the range of velocities estimated in chapter 3 and, therefore, are more reliable. The variations in group velocity are important. We can see now that the cross-spectrum method proposed by Viggiani & Atkinson and applied in Chapter 3 was actually averaging those values –i.e. it was fitting a single line where local tangents show an ample range of variation[41]. This procedure seems now to be unnecessarily opaque.

Although these results are interesting they are just another way of presenting what was already evident at the end of the previous chapter, namely, that the bulk wave model is perfectly inadequate to make sense of pulse tests in soil samples. The final objective of laboratory pulse tests is to measure $\mathbf{D_0}$, not to obtain a dispersion curve. What is now clear is that some other model is needed than that provided by bulk waves: a different elastodynamic transfer function, and a dispersive one at that. That function should provide a better alternative to the now tenuous link between $\mathbf{D_0}$ and the measured propagation properties.

When a wave traverses a solid, dispersion can arise for a variety of causes (Sachse & Pao, 1978): frequency dependent material properties, inhomogeneity, boundary effects, non-linearity...Rayleigh waves are perhaps the best known example of dispersive elastic waves with geotechnical relevance, and for them dispersion appears as a consequence of layering on the testing sites (Foti, 2000). In this and following chapters we will examine a variety of possible dispersion-inducing mechanisms relevant to pulse tests in soil samples.

4.2 NEAR FIELD EFFECTS

As explained in chapter 2 near field effects have been prominent in the discussion about pulse test interpretation in soils since the issue was introduced by Sánchez-Salinero and co-workers (1986). This tradition alone justifies a detailed consideration of near field effects in our search for possible causes of uncertainty in pulse test interpretation. It is less traditional to discuss this problem as an example of dispersion[42]. From our point of view this has two distinct advantages: it brings the discussion in line with other problems to be next investigated and offers a relatively simple ground to put to work the concepts just introduced. There are some additional benefits from this approach. It was also noted in Chapter 2 that even if Salinero's work contains copious insight into the problem it lacks some generality, as it was based on numerical analyses of a transmitted single sinusoidal pulse. Although that particular pulse shape is not central to the argument, this point seems to have been lost in later research. The general viewpoint here adopted permits us to clarify this. We shall then begin with some theoretical background.

4.2.1 Source near field: theoretical aspects

In the geophysical literature that inspired Salinero's work, near field is a shorthand for the peculiarities of the movement field near its source. The discussion then goes beyond the propagation of some assumed

---

[41] The value obtained in this case was 68 m/s, fitting a line between 2 and 8 kHz

wavefront shape –planar, say- to its generation, hence its starting point will always be the inhomogeneous equilibrium equation, that is, for the isotropic case,

$$\rho\ddot{\mathbf{u}} = \mathbf{b} + (\lambda + \mu)\nabla(\nabla \cdot \mathbf{u}) + \mu\nabla^2\mathbf{u} \qquad (55)$$

As we know, the possibilities offered by superposition make the solution for the case of a single isolated impulsive force extremely important. Stokes obtained the solution describing the movements generated by a unit impulsive force isolated in an infinite elastic medium in 1849 –Aki & Richards, 1980. According to the terminology introduced in chapter 1 this will be a "fundamental solution". Stokes proof of the fundamental solution is reproduced and explained in many books, for instance Dominguez (1993), and there is no need to reproduce it again here. It is nevertheless interesting to appreciate one aspect of it: as the elastic space is assumed infinite and the load isolated the problem is naturally posed in spherical coordinates centred at the load.

Stoke's fundamental solution is indeed fundamental. Analytically it has been used to obtain solutions to more complicated source problems, implying moment or distributed sources (Achenbach, 1973, Aki & Richards, 1980). Numerically it lies at the heart of boundary element solutions to general elastic wave propagation problems (Dominguez, 1993). A rather less ambitious use of the fundamental solution, albeit still an interesting one, is as transfer function for arbitrarily oriented dynamic load histories within an infinite elastic body. That is a transfer function[43] linking the "output" -displacement vector u(t)- to the "input" –the source force vector **b**(t). That was the use made by Salinero and co-workers and that is also the use here investigated.

As this transfer function relates two vectors matricial notation is convenient. The relation linking an isolated force and the generated displacement field is then expressed as

$$\mathbf{u} = \mathbf{GR} * \mathbf{b} \qquad (56)$$

Where the * symbol indicates convolution in time. **GR** its known as the Green tensor. It is a matrix, GR_{ij}, where each element is the unit displacement along the axis i corresponding to a unit impulsive force acting along the axis j. We will first inspect its general structure before going into more detail. Emphasising then its structure, the Green tensor could be written as follows,

$$\begin{aligned} \mathbf{GR} &= N(r,t)[3\mathbf{A} - \mathbf{1}] + F_P(r,t)\mathbf{A} - F_S(r,t)[\mathbf{A} - \mathbf{1}] \\ \mathbf{A} &= \nabla\mathbf{r} \otimes \nabla\mathbf{r} = \vec{\mathbf{r}} \otimes \vec{\mathbf{r}} \\ \|\vec{\mathbf{r}}\| &= 1 \end{aligned} \qquad (57)$$

---

[42] The use of the concept by Salinero et al. is rather subdued. Later contributions –e.g. Brignoli et al. 1996, Jovicic et al. 1996, Arulnathan et al. 1998- tend to ignore it altogether.

[43] We will be referring to it as a transfer function all along even if, strictly speaking, when used in time domain it is a unit response function. In the terminology of structural modal testing (Ewins, 2000) this particular transfer function will be called receptance or admittance.

Vector **r** indicates position relative to the source, and, formed by its director cosines, makes **A** only dependent on the angular coordinates. Figure 4-5 presents a scheme, identifying this vector, as well as **b** and **u**. The tensorial coefficients, depending only on time and distance from the source, are the far field term (F_p) travelling at velocity v_p, the far field term, (F_s), travelling at velocity v_s and the near field term (N) travelling at some intermediate velocity. These affirmations will be justified later; it is first desirable to obtain some consequences out of the fundamental solution structure. The first thing to note is that the character of the movement –what is propagated- depends only on the angular coordinates i.e. on the propagation direction. On the other hand, propagation takes place in the same form in all directions, as the propagation characteristics depend only on the radius.

An important question is to establish when and where is the movement parallel to the propagation direction, and when and where is it perpendicular to the propagation direction. As we know, the first type of movement is that associated with a compressive plane wave travelling at v_p the second with a shear plane wave travelling at v_s. Some algebraic manipulation of the fundamental solution offers a clear answer to this question. The general expressions of movement parallel ($\mathbf{u}_p$) and perpendicular ($\mathbf{u}_s$) to the propagation direction are given by:

$$\begin{aligned} \mathbf{u}_p &= (\mathbf{u}\cdot\vec{\mathbf{r}})\vec{\mathbf{r}} = (\vec{\mathbf{r}}\cdot\mathbf{b})*\left[2N+F_p\right]\vec{\mathbf{r}} \\ \mathbf{u}_s &= \mathbf{u}\wedge\vec{\mathbf{r}} = (\vec{\mathbf{r}}\wedge\mathbf{b})*\left[F_s-N\right] \end{aligned} \tag{58}$$

Important consequences of these expressions are:

- When the propagation direction is chosen parallel to the source, there is no s-like movement as $(\mathbf{r}\wedge\mathbf{b}) = \mathbf{0}$
- When the propagation direction is contained in a plane perpendicular to the source there is no p-like movement as $(\mathbf{r}\cdot\mathbf{b}) = 0$.
- In general, it will be only when far field coefficients -F_i- are much bigger than the near field one, i.e. only when $N / F_i \rightarrow 0$, that p-like movement will be associated with v_p, and s-like movement will be associated with v_s

The last point above can also be understood as stating under which conditions plane wave propagation will be a good model for the movement[44]. As this condition depends on the coefficients of equation (57) it is now desirable to take a closer look at them. The expression of these coefficients in the time domain, using H for the Heaviside step function and δ for the Dirac delta function, is given by –Dominguez, 1993-

[44] At least with respect to its velocity, attenuation due to geometrical spreading is a peculiarity that cannot be modelled by plane waves.

$$N = \frac{kt}{r^2}\left(H\left(t - \frac{r}{v_p}\right) - H\left(t - \frac{r}{v_s}\right)\right)$$

$$F_p = \frac{k}{v_p^2}\delta\left(t - \frac{r}{v_p}\right) \qquad F_s = \frac{k}{v_s^2}\delta\left(t - \frac{r}{v_s}\right) \tag{59}$$

$$k = \frac{1}{4\pi\rho r} \qquad r = \|\mathbf{r}\|$$

From those time domain expressions it can be appreciated that, as stated above, F_p and F_s correspond to an instantaneous disturbance passing through r at times given by r/v_p and r/v_s respectively, whereas N corresponds to a disturbance acting at r between those two times. Also the presence of r^2 in N indicates that the attenuation of this factor with distance is two orders of magnitude higher than F_p and F_s, which attenuate with r.

It seems that we have already found a good justification for the terminology "far field" and "near field". Far will mean simply distances from the source where $1/r^2$ is small enough. This is quite reasonable in itself -we would expect that at large radius spherical wavefronts might well be approximated by their tangent planes- but, nevertheless, it is not the end of the story. Our radius criterion is blatantly dimensional, surprisingly suggesting that it would be possible for a single limit distance to be equally valid for all kinds of loading and all isotropic elastic materials. In fact, our reasoning has conveniently forgotten that squared velocities divide the far field factors, and has also forgot that a time factor multiplies the whole near field coefficient, suggesting that for large times this coefficient would also become large. On the other hand, as time passes, the disturbance will travel further and the radius will increase...surely some compensation might occur between those two phenomena, but at what rate? To obtain an answer to all these questions it is necessary to turn now to the frequency domain expression of the fundamental solution.

In the frequency domain the structure of the Green tensor given by equation (57) does not change, only the time-dependent coefficients have a new, frequency-dependent, expression. This expression might be obtained, for instance, applying a Fourier transform to (59). After some rearrangements we can write an expression equivalent –albeit more compact- to one given by Aki & Richards (1981):

$$N = N_S - N_p$$

$$N_S = \frac{k}{v_s^2}\frac{\sqrt{1+n_s^2}}{n_s^2}e^{-i[n_s - arctan(n_s)]}$$

$$N_P = \frac{k}{v_p^2}\frac{\sqrt{1+n_p^2}}{n_p^2}e^{-i[n_p - arctan(n_p)]} \qquad (60)$$

$$F_p = \frac{k}{v_p^2}e^{-in_p} \qquad F_p = \frac{k}{v_s^2}e^{-in_s}$$

$$k = \frac{1}{4\pi\rho r}$$

where we have emphasised the symmetry between the terms where each respective bulk velocity $-v_s$ or v_p- intervenes, expressing the near field coefficient as a difference of two components, N_S and N_P, one of each kind. All the coefficients are expressed using two dimensionless ratios, whose definitions are given by

$$n_p = \frac{\omega}{v_p}r = 2\pi\frac{r}{\lambda_p} = 2\pi\bar{n}_p$$

$$n_s = \frac{\omega}{v_s}r = 2\pi\frac{r}{\lambda_s} = 2\pi\bar{n}_s \qquad (61)$$

As we see these ratios are proportional –with scaling factor 2π- to the normalised distances that measure the distance between source and evaluation point against the corresponding characteristic wavelengths. Looking at expression (60) it is clear that the difference between corresponding near and far field terms – N_p and F_p, say- is exclusively dependent on the corresponding dimensionless ratio. The exponential form chosen makes it very simple to separately compare modulus and phase for paired terms.

Looking first at the modulus it can be appreciated that the quotient of corresponding Near and Far field terms has the general form

$$\frac{N_i}{F_i} = \frac{\sqrt{1+n_i^2}}{n_i^2} \qquad (62)$$

In Figure 4-6 this quotient is plotted against the normalised distance. The ratio is only higher than 0.25 within the first wavelength of the source. At distances bigger than two wavelengths the near field modulus is less than 10% of the corresponding far field term. This gives a more precise meaning to the terminology: the term "far field" refers to big distances measured against the corresponding wavelength.

Considering now the phase it can quickly be appreciated that near field terms have a more complicated form than corresponding far field terms. Figure 4-7 represents their phase as a function of normalised distance. The difference between them is also represented and quickly stabilises as $\arctan(n) \rightarrow \pi/2$.

Velocity information is contained in the phase. As the only spatial coordinate is r, we can obtain the wavenumber as the phase derivative with respect to r. The phase velocity for corresponding near and far field terms is then given by

$$V_{PH}^{FF_i} = v_i$$
$$V_{PH}^{NF_i} = v_i\left(1+\left(\frac{v_i}{\omega r}\right)^2\right) = v_i\left(1+\frac{1}{n_i^2}\right) \qquad (63)$$

As expected, the phase velocity of the far field term is constant and equals the corresponding bulk velocity. On the other hand, the phase velocity of the near field term is not constant but frequency and distance dependent. This is bad news, as it means that near field terms are dispersive and, for given distance between source and receiver, every frequency will propagate with a different velocity. But there is also good news: as the normalised distance increases dispersion fades and the phase velocity of near field terms quickly approaches the corresponding bulk velocity.

4.2.2 Near field limit and shear-like movement

Although the term-by-term comparison just made is illustrative it does not address directly our concern. This is mostly related to shear tests, where there is a certain possibility of the near field term travelling at v_p causing premature detection. Considering now the complete expression for $\mathbf{u_s}$ -equation (58)- it could be seen that the relevant transfer function is given by the difference between the far field term, F_s, and the whole near field term. Using (60) this can be written explicitly as:

$$S = F_s - N_s + N_p$$
$$S(\omega,r) = k\left\{\frac{e^{-in_s}}{v_s^2} - \frac{\sqrt{1+n_s^2}}{v_s^2 n_s^2}e^{-i[n_s-\arctan(n_s)]} + \frac{\sqrt{1+n_p^2}}{v_p^2 n_p^2}e^{-i[n_p-\arctan(n_p)]}\right\} \qquad (64)$$
$$k = \frac{1}{4\pi\rho r}$$

This expression is equivalent to one used by Salinero et al. (1984) and quoted by Jovicic et al (1997). We will refer to it as the S transfer function. There are two different dimensionless ratios in it, n_p and n_s, as well as two bulk velocities, v_p and v_s. Some insight is gained if the p-related quantities are expressed in terms of the s-related quantities, using the Poisson-ratio dependent speed ratio v_R

$$S(\omega,r) = k\left\{\frac{e^{-in_s}}{v_s^2} - \frac{\sqrt{1+n_s^2}}{v_s^2 n_s^2}e^{-i[n_s-\arctan(n_s)]} + \frac{\sqrt{1+v_r^2 n_s^2}}{v_s^2 n_s^2}e^{-i[v_r n_s-\arctan(v_r n_s)]}\right\} \qquad (65)$$
$$v_r = \frac{v_s}{v_p} = \sqrt{\frac{1-2\nu}{2-2\nu}}$$

To interpret this expression, apart from the already examined quotient between N_S and F_S it is interesting to consider also the moduli quotient between N_P and F_S. This shows a slight dependence on Poisson ratio, -Figure 4-8- but also declines quickly as n_s increases. It is already clear that the relative magnitude of the

whole near field and the far field term would be very small at some wavelengths from the source. To be more precise both near field terms should be combined taking account of their respective phases. This has been done and the corresponding result is plotted in Figure 4-9. It shows a different pattern, remaining below 10% after 3 normalised distances.

Still, our main interest lies elsewhere, as the time delay between input and output and, consequently, the wave velocity, are not controlled directly by the modulus but by the phase of the transfer function. It is possible to obtain an exact expression for the phase of (64) but it is cumbersome and the resultant phase and group velocity are expressed in terms of trigonometric functions and need unwrapping. Numerical evaluation is possible and that was the road followed by Salinero et al. (1986). But it is now relatively simple and perhaps more interesting to obtain directly an upper bound for phase and group velocity.

Figure 4-10 represents the effect of the near field term in the phase of the S transfer function as a correction on that given by the F_S term. This term has a phase directly related to the bulk shear velocity by (63). The actual near field would generally form a variable angle with F_S, depending on their relative phases. The $\pi/2$ angle assumed in the figure gives the highest delay[45] for given moduli and therefore bounds the phase correction $d\Theta$ and, consequently, the corresponding phase velocity, v. We have then that

$$v_s = \frac{\omega r}{\theta_{F_S}} \qquad v = \frac{\omega r}{\theta_{F_S} - d\theta}$$

$$d\theta \le \frac{|N|}{|F_S|} \tag{66}$$

$$\frac{v}{v_s} = \frac{\theta_{F_S}}{\theta_{F_S} - d\theta} \le \frac{\theta_{F_S}}{\theta_{F_S} - \frac{|N|}{|F_S|}}$$

Figure 4-11 represents this last ratio against normalised distance. As the slope is always negative this also represents an upper bound for the S group velocity. It appears that if phase or group velocity is measured at more than about 1.6 normalised distances from the source the possible excess over the shear bulk velocity, v_S, will stay below 5%

In general, given a constant wave speed, there are two possible methods of achieving far-field conditions: either by separating source and receiver, thus increasing r, and/or by specifying a high frequency. Whereas in field applications like cross-hole it may be possible –attenuation permitting- to place source and receiver as far apart as needed, in laboratory conditions this is not the case. The dimensions of the sample being tested limit the distance between source and receiver, and those dimensions are machine-dependent, with little scope for change once the apparatus has been built. Therefore, the adjustment has to be made via frequency and the near field influence limit just suggested will translate into

[45] Note that with our Fourier transform conventions a phase delay signifies a time advance.

$$f_{min} = \frac{V_s}{\lambda} > \frac{V_s}{1.6d} \qquad (67)$$

This minimum frequency has been plotted in Figure 4-12 for a range of shear stiffness typical of sands (Jovicic & Coop, 1999) and for several distances typical of usual laboratory configurations. As we know, testing with bender probes usually proceeds between 2 and 20kHz; it can be appreciated how, for the smaller distances, corresponding, for instance to hollow cylinder walls or small triaxial diameters tests might proceed well within the near field. On the other hand, bigger distances, corresponding for instance to the height of samples in big triaxial cells, will give some allowance to test even relatively stiff materials.

4.2.3 Near field limit and pulse test interpretation procedures

The question now is how to apply the frequency limit just established when interpreting pulse tests in soils. This has two different answers, depending on whether this interpretation proceeds in frequency or in time domain. In the former case the answer is pretty simple and direct, as a frequency limit is directly enforceable there. For instance, if we measure velocity fitting a line to the cross-spectrum phase it is only necessary to take care and begin the fitting range beyond an appropriately selected f_{min}. This selection taking account of the measurement distance and estimating the soil stiffness can be performed with the help of diagrams such as Figure 4-12. This idea is also valid if more elaborated use of the spectral information is needed; an example is given by its application to dispersion curve inversion in the nearby technique of SASW -Foti, 2000.

In time domain the answer is less clear cut. This is natural as time domain procedures do not deal directly with the transfer function but with the recorded output, i.e. a convolution of the transfer function and input signal. It is then to be expected that the character of the input signal will also play an important role. There are a number of features, nevertheless, that are valid for any input signal:

- The near field term attenuates faster than the far field term.
- First arrival of the near field term happens at d/v_p that of the far field term at d/v_s
- In time domain the far field term translates the input without distortion whereas the near field term produces a transposed and distorted replica of the input.

All these aspects are illustrated in Figure 4-13 where the effect of both terms has been computed[46] separately for a distorted sine –or "Jovicic"- input. The amplitudes have been scaled and its clear that, for this particular case the near field term has a very mild effect on the total output. To be more precise, the initial bump due to the near field term represents just 5% of the output peak. Hence, in this particular case, the automatic procedure employed in chapter 3, which ignored peaks below 10%, will have successfully identified the first arrival of the signal as that corresponding to the bulk shear velocity[47].

---

[46] Using a FFT with 2048 samples at 0.002 ms

But this very same procedure will have failed with other input shapes. Figure 4-14 compares four signals propagated under the same conditions. The figure is represented for an apparent normalised distance, n_{ap}, of 2. It is important to note that the normalising factor here is taken to be the apparent frequency of the input signal, f_{ap}, i.e. the inverse of its apparent period. This is only a convenient shorthand to characterise signals that, as Figure 3-4 illustrated, may have quite wide spectra. Of course, for a given signal, the higher the apparent frequency the smaller the energy it would have below a particular frequency and, consequently, the lower its proportion of near field energy. But this argument is not helpful to rank signal shapes when time domain output is considered.

Back to Figure 4-14 it can be seen how the near field term causes again initial bumps in all the transmitted signals. But, while it attains a height of 5% in the Jovicic shape, it is 10% in the single sinusoidal and the sine burst and almost 30% in the square signal. At least in the latter case, the automatic procedure of Chapter 3 will have picked an arrival time corresponding to the compressive bulk velocity. Evidently, such a minor program setting might be modified to cater for the signal in use. But the key point here is that no single criterion is valid for all kinds of input. Figure 4-15 represents how the near field induced bump height falls as normalised distance increases for various signal shapes.

This figure suggests that the choice of input signal might be important if time domain procedures are used to select the arrival time. It is apparent that the square-shaped signal is the least favourable shape and the distorted sine the most favourable, as suggested by Jovicic[48]. Also, the sine and sine-burst signals behave very similarly in this respect, although the burst has a much narrower spectrum than the single sine. This result extends what Salinero found for the single sine shape. We can see now that his limit of $n_{ap}= 2$ for the single sine corresponds roughly to a policy of ignoring bumps of 10% maximum height. Remembering that the values of T_E obtained in chapter 3 were very similar to the automatically obtained T_0 this seems to be what a trained "expert" eye will do for any kind of input shape.

Salinero also introduced the effect of hysteretic damping in his simulations and, for reasonable values, observed that his criteria still held. Although it will be simple now to do the same for other shapes, we will not follow this route here for various reasons. First, it would seem more sensible for future research to employ the unequivocal frequency domain criteria established above. Second, the introduction of damping modifies the material model, something that has some extra consequences and for our purposes is best addressed separately –Chapter 5. Finally, it may turn out to be that near field effects are only of secondary importance. It is time now to check our bench test results.

4.2.4 Application to bench test results

So far we have obtained clear rules that may be used to avoid and/or estimate near field influence in pulse tests. However, the question remains about the possible relevance of this problem in actual soil test configurations. Recall that, for sine pulses, we have recovered very similar limits to those proposed by

---

[47] In the figure the time is scaled so as to make the theoretical arrival time equal to 1.

Salinero et al. Recall also that, even when using sine pulses and abiding by those limits, various researchers have signalled problems in arrival time identification –e.g. Moncaster, 1997, Pennington, 1999, Kuwano, 1999. We have also seen –Chapter 3- that these problems are indeed substantial. We are now able to explore how much of the uncertainty there discovered can be attributed to this near field problem.

Beginning with the time domain estimates it is clear that near field effects will be most visible in first arrival-based velocity estimates. In Figure 4-16 we represent this estimate against the apparent normalised distance of each test. This last value is computed assuming that vertical shear velocity for our sample is –say- 120 m/s[49]. In the figure we represent separately results corresponding to square signals and to sinusoidal signals – as according to Figure 4-15 there is no need to distinguish single-cycle and bursts. The results are interesting, as the square signals systematically show higher values than the sinusoidal ones. That was already observed in Chapter 3 and near field effects might explain this bias, as most normalised distances are below the value needed for the 10% limit to be effective for square signals -around 9- but above that working for sinusoidal shapes –around 2.5. Still, the substantial dispersion of results within both categories remains unexplained. This want is even more apparent if we consider cross-spectrum results.

In the frequency domain our search for near field influence is simpler as it is not affected by signal shape. On one hand, we have obtained, as subproduct of the algorithm estimating the cross-spectrum velocities, the frequency interval –say f_{min} to f_{max}- where the normalised cross-spectrum modulus was over 10% On the other hand using (2) and again assuming an v_s of 120 m/s we can obtain f_{lim} for each source to receiver distance. It is then possible to define a near field spectral ratio as

$$NF_{SR} = \frac{f_{max} - f_{lim}}{f_{max} - f_{min}} \tag{68}$$

And this ratio represents the near field influence in the cross spectrum velocity estimate. Negative values mean that all the testing frequencies were in the near field, for values between 0 and 1 the near field overlap progressively decreases, values above 1 correspond to tests performed well within the far field. Plotting this ratio against v_{CS} we will expect a clear relation to appear, namely an increase in the measured velocity with the ratio, as opposed to time domain results. This increase should be expected because we know now that the cross-spectrum method measures an average group velocity, and, considering the negative slope of phase velocity in Figure 4-11, group velocity should approach v_s asymptotically from below. Figure 4-17 supports this view. If some effect is there at all, it is a decrease of the estimated velocity as NF_{SR} increases: that is, tests that are within the near field, show lower v_s than those well out of it. But the figure also shows that measurements outside the near field do not quietly approach any asymptote, but instead show a much higher variation than those inside the near field.

---

[48] However, this result is strongly dependent on the amount of distortion introduced. This signal is given by $I = A\,(\sin(\pi(2tf_{sp} + di/2)) - \sin(\pi di/2))$. The results correspond to a distortion factor, di, of 1/3.

[49] Were the normalised distance to be computed using the estimated velocity for each test the effect looked for would be introduced twice in the graph.

It seems then that source near field effects are not able to explain on their own the disparate results described in Chapter 3. Also, the complaints of previous researchers about the inability of Salinero's criteria to deliver clear non-ambiguous results seem now perfectly reasonable. Neither these criteria, nor the more comprehensive analysis developed above will be of much help if near field effects are not the culprits of the observed dispersion. Of course, this does not means that all efforts should not be made to work outside the near field, and the criteria given above might help in this respect. It means rather that working in the far field , desirable as it may be, would not be generally enough.

Other dispersive phenomena should then be taken into account and this –relative- failure might point us in the right direction. Remember that Salinero's work was prompted by concerns about field pulse tests, particularly cross-hole, and only later, and after apparent success, was applied to laboratory tests. This suggests the model of field pulse tests should not be directly translated to the laboratory and that some major element is lost in the intent. One obvious difference is that in the field source and receivers are minute elements placed in the middle of a rather large extent, whereas in the laboratory –with the possible exception of tests within calibration chambers- source and receiver are smaller than those in the field, but much more so is the sample in whose surface they are placed.

4.3 SUMMARY

Dispersive waves spread out and change shape as they travel. The dispersion relation is a non-linear functional dependence between the wave vector and frequency. Phase velocity is then frequency dependent and not directly related with time-domain signal propagation. A new quantity, the gradient of the dispersion relation, called group velocity, is more relevant. Dispersion characteristics can be measured in pulse tests analysing the results in frequency domain. An elastodynamic dispersive model is needed to interpret pulse tests. There are a variety of mechanisms that may cause dispersion. In this chapter we have explored near field effects, that is, dispersion caused by proximity to the source of movement. Clear criteria have been obtained to evaluate the influence of this effect in time and in frequency domain. However, using the Gault bench test results we have shown that near field effects cannot account for the major part of the observed dispersion.

4.4 FIGURES

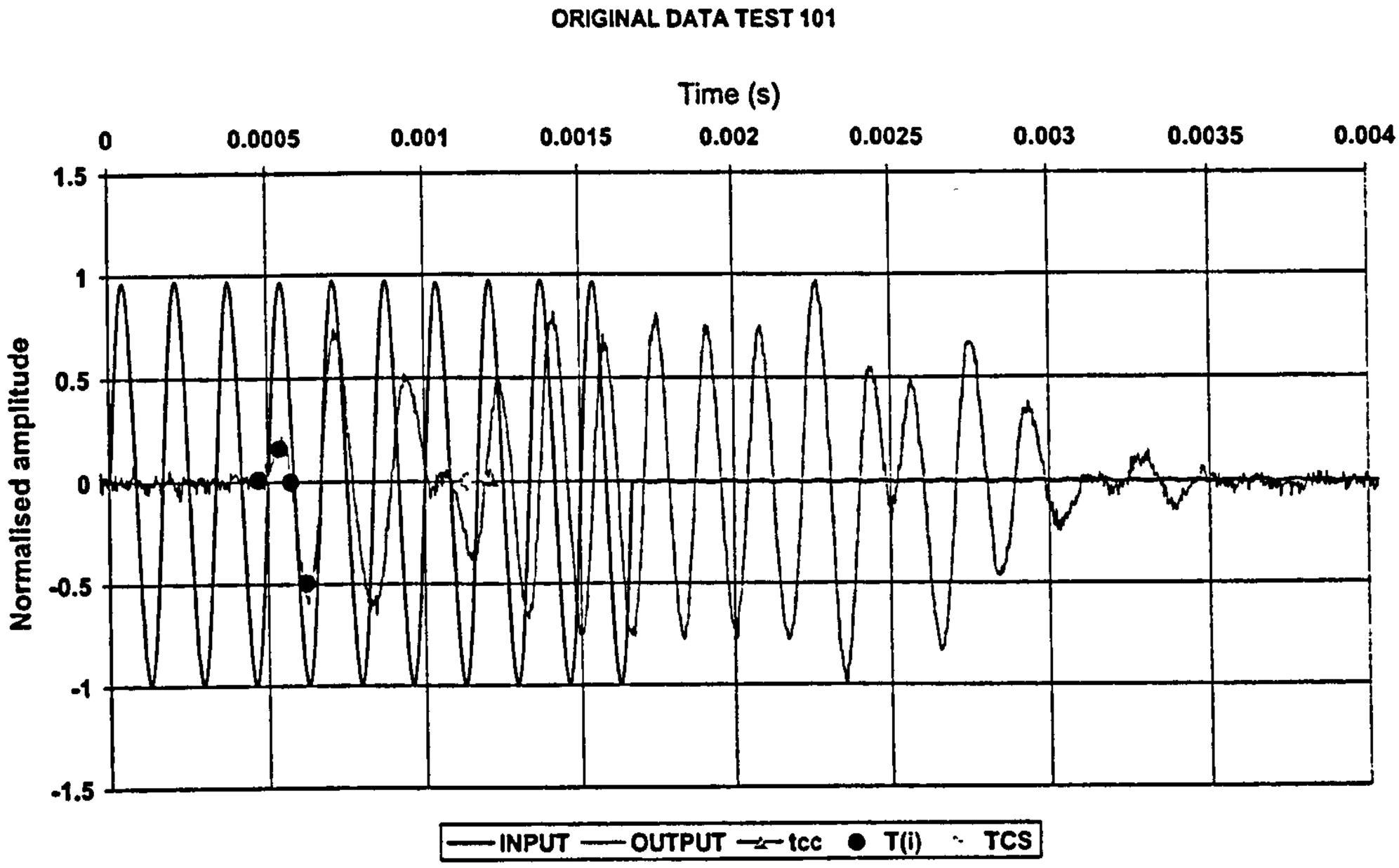

Figure 4-1 Distorted narrow band signal from bench test

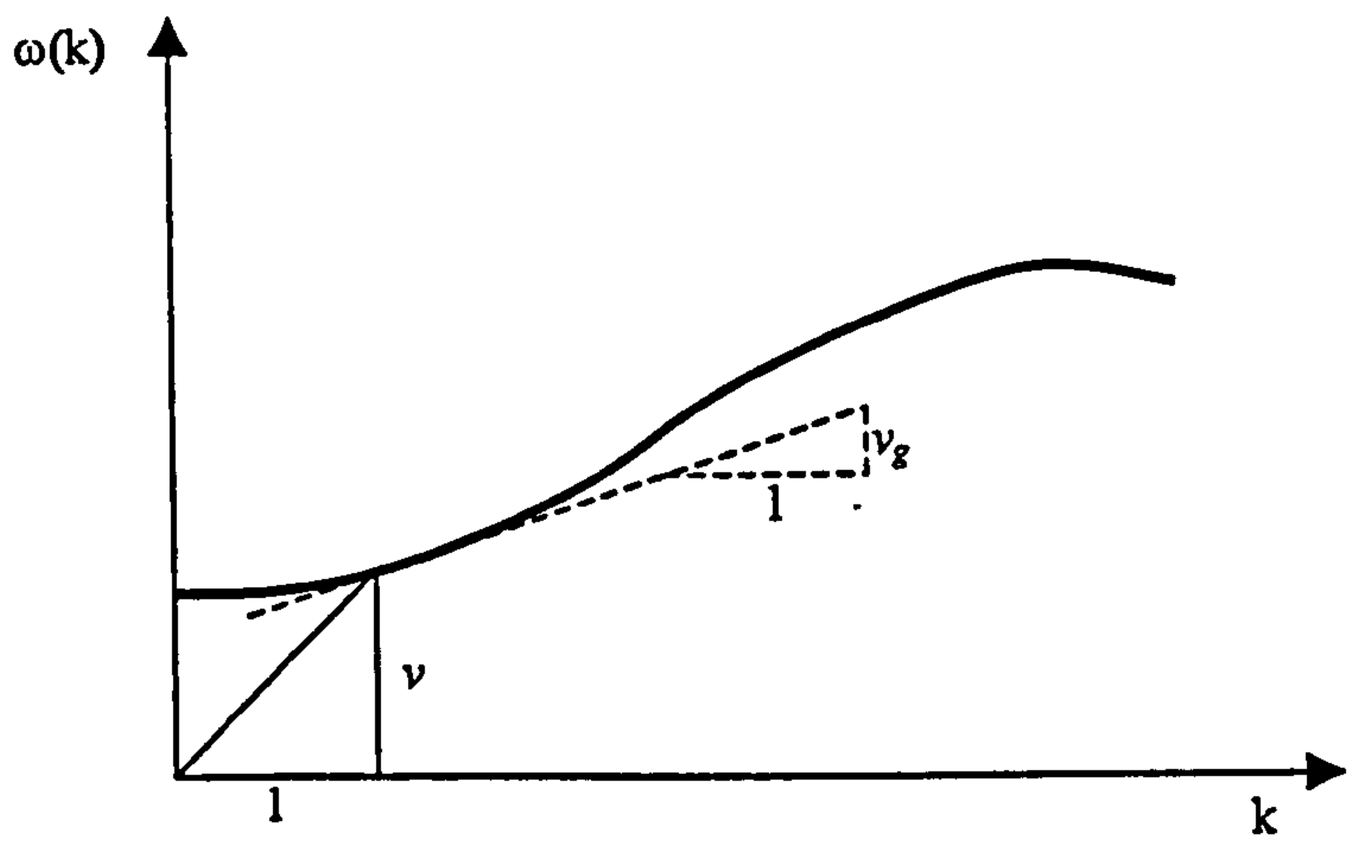

Figure 4-2 Phase and group velocity on a frequency-wavenumber plot

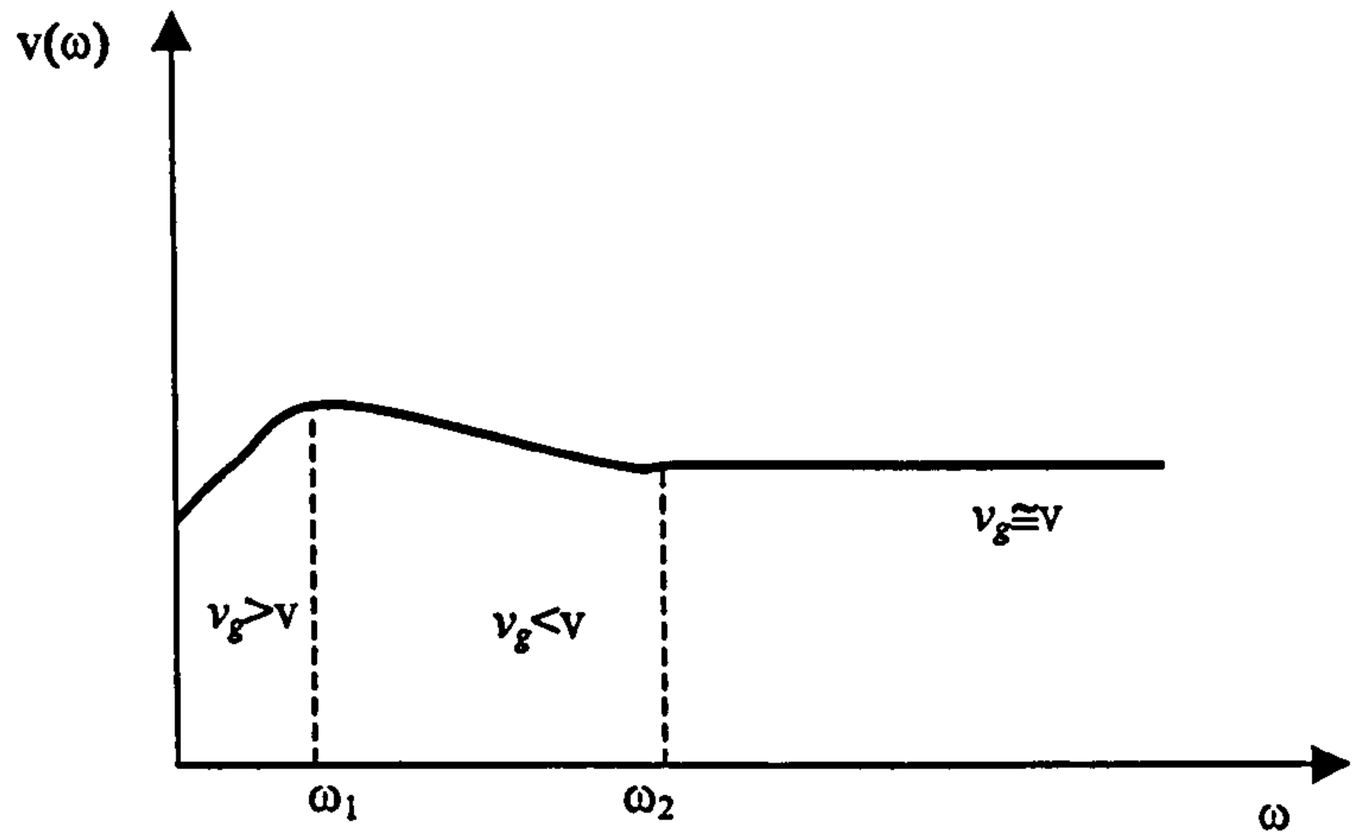

Figure 4-3 Dispersion relation and relative size of group and phase velocities

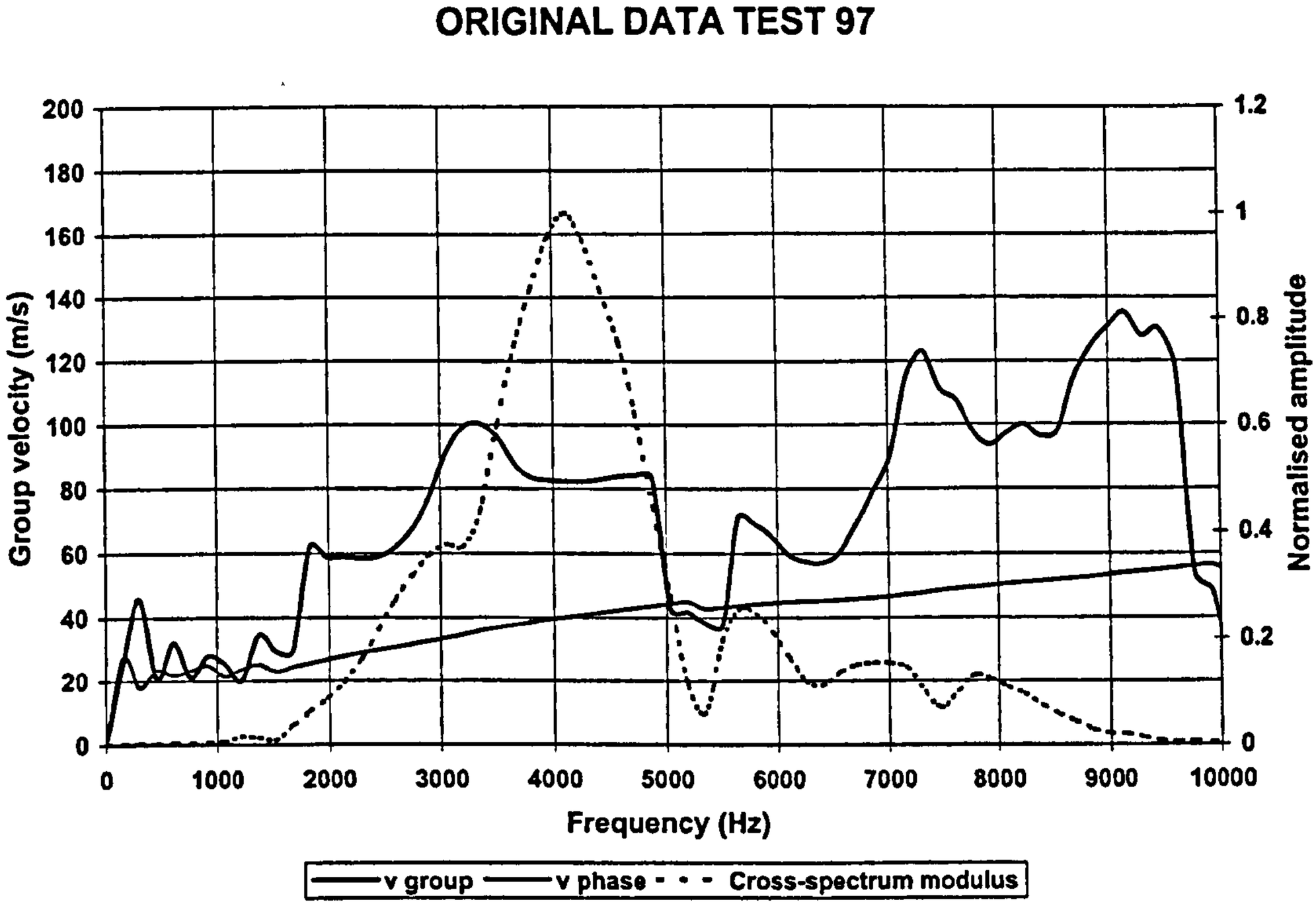

Figure 4-4 Pulse test in Gault clay: numerical evaluation of phase and group velocities

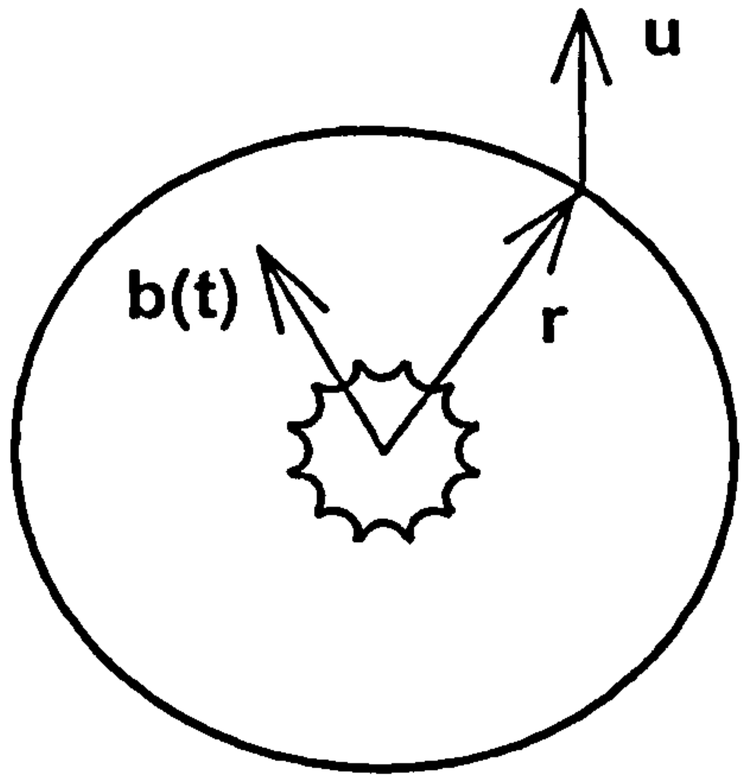

Figure 4-5 Fundamental solution: vector nomenclature

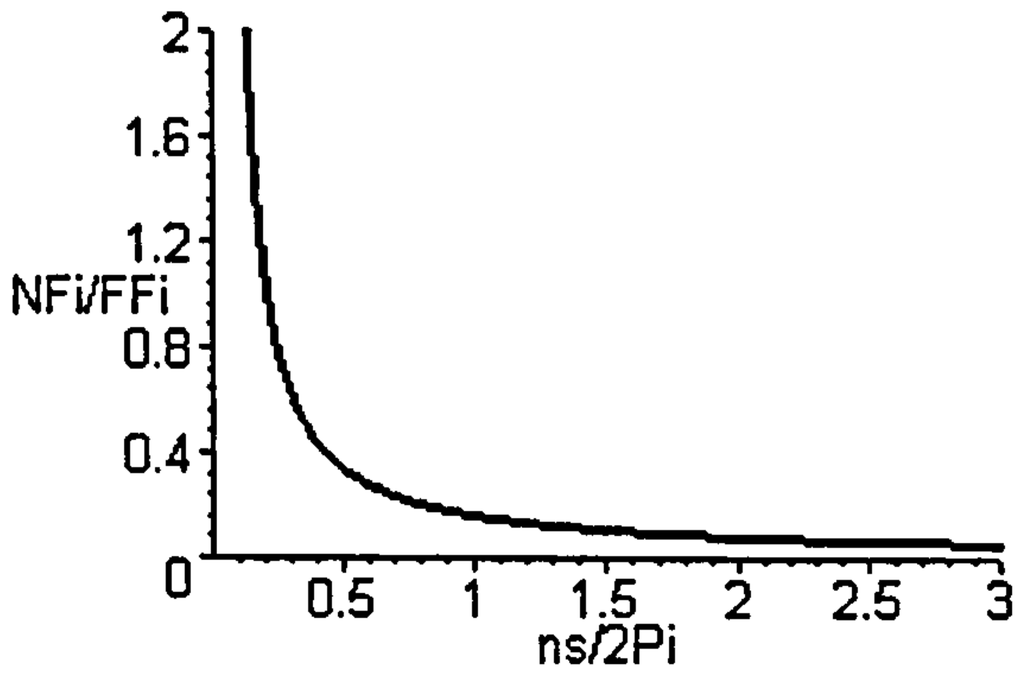

Figure 4-6 Moduli ratio of corresponding near and far field terms vs normalised distance

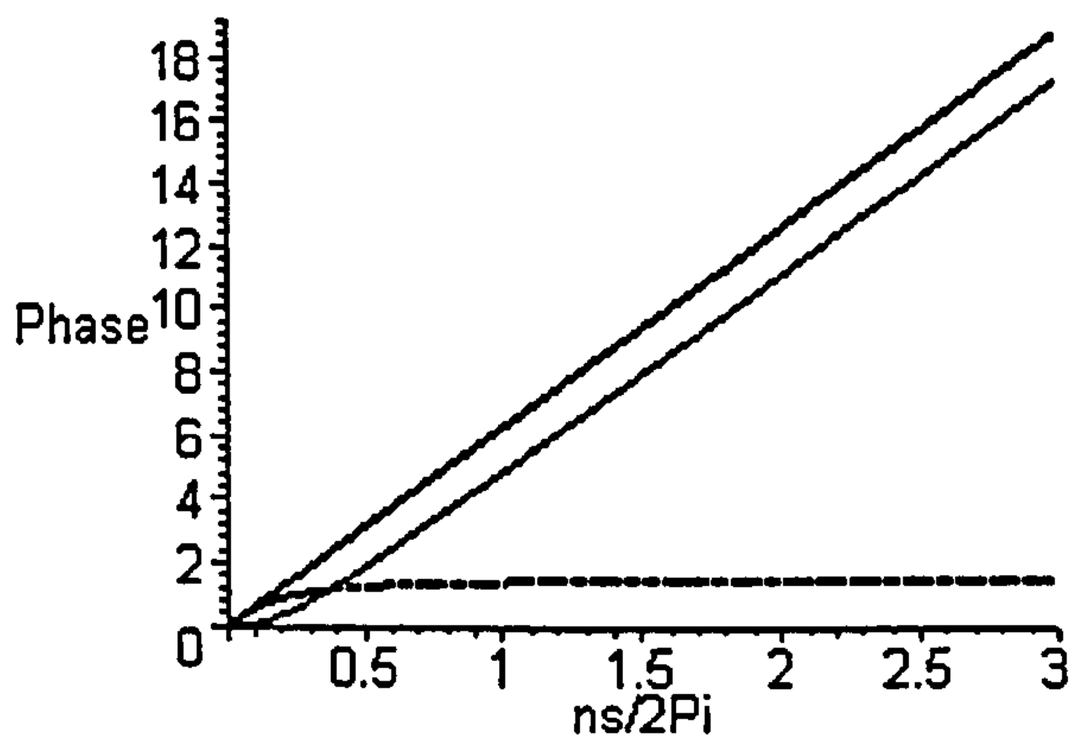

Figure 4-7 Phase and phase difference(dashed) of corresponding near and far field terms against normalised distance

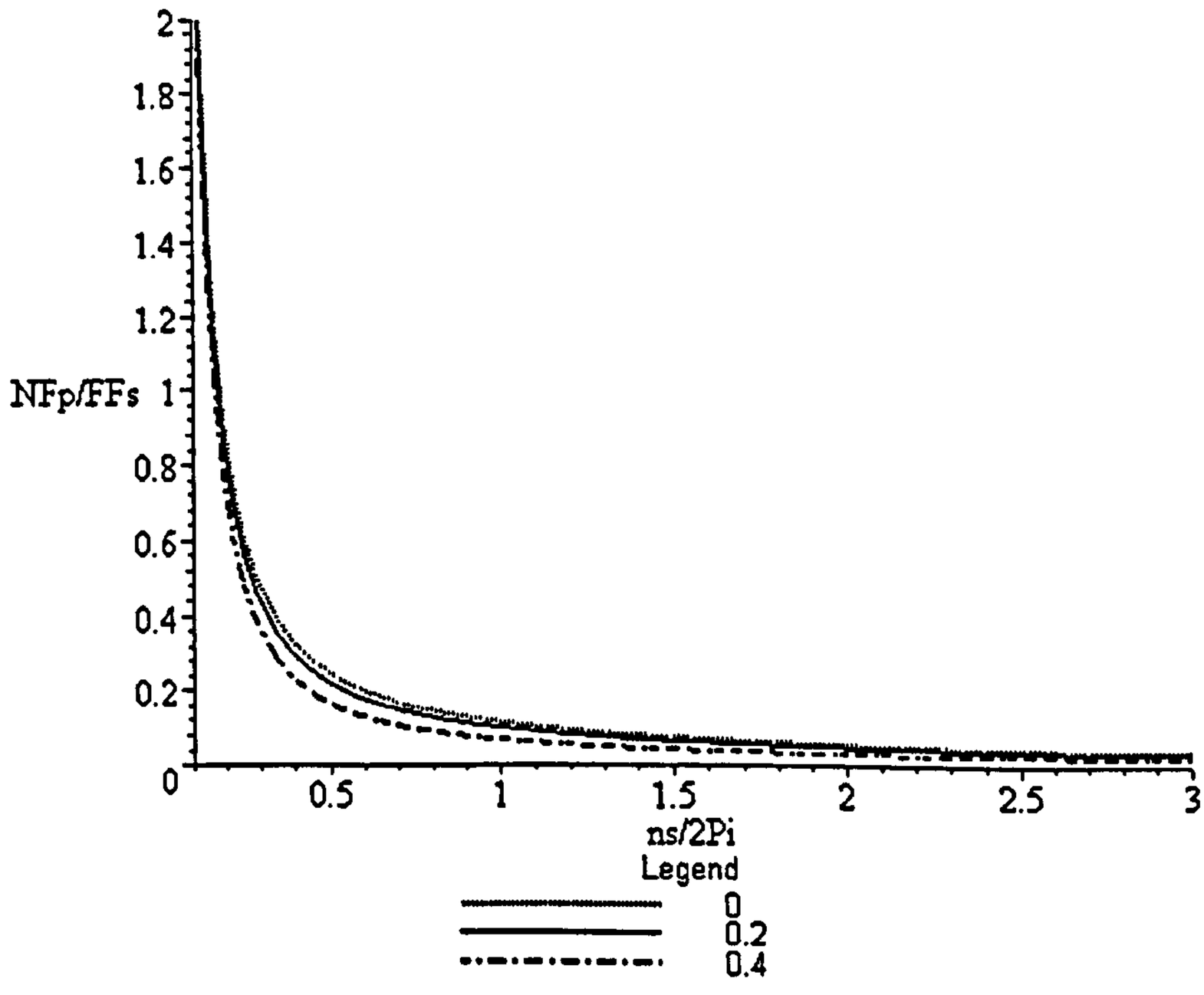

Figure 4-8 Moduli ratio NFp/FFs for Poisson ratio 0, 0.2, 0.4

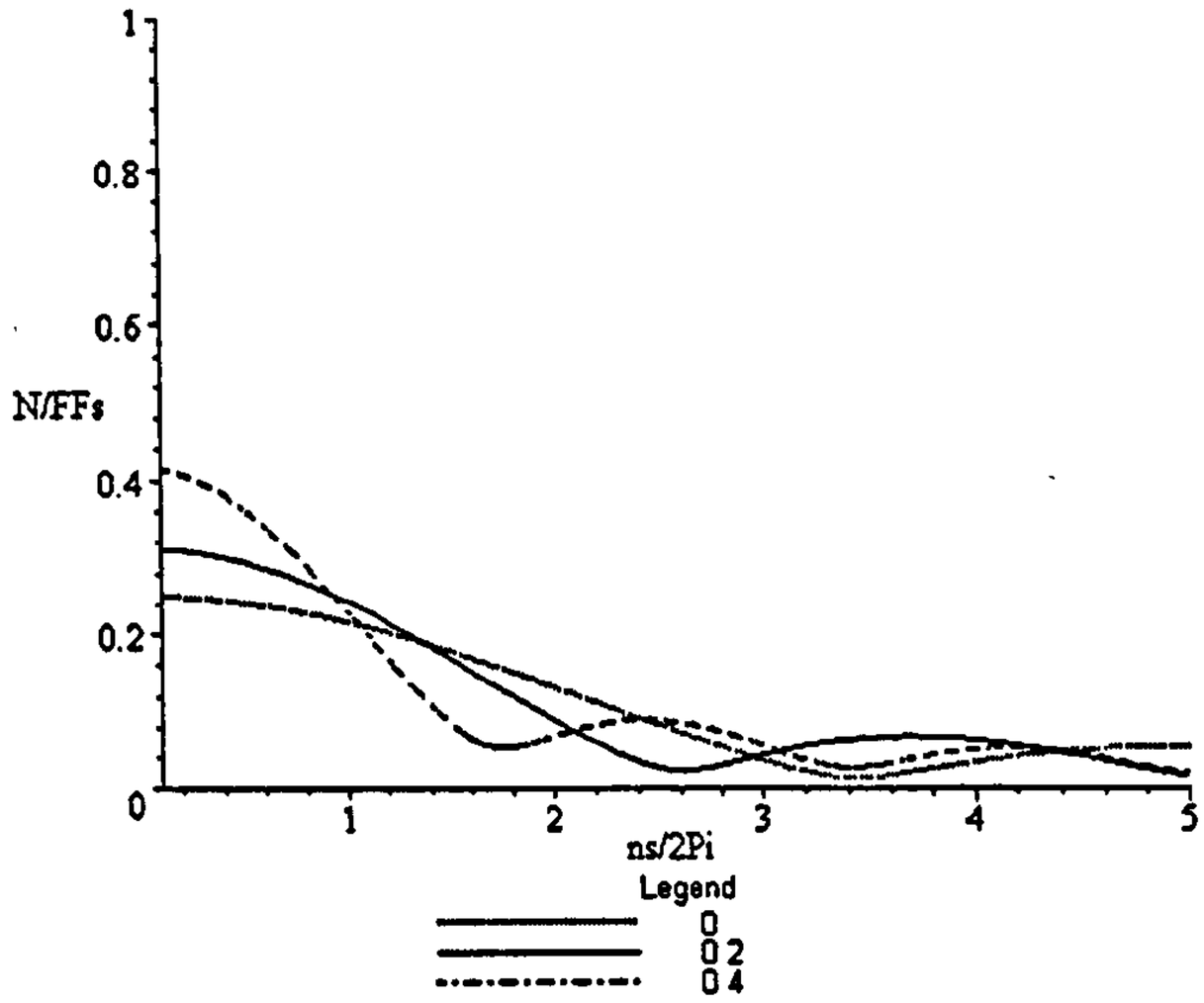

Figure 4-9 Moduli ratio N/FFs. Poisson ratio 0, 0.2, 0.4

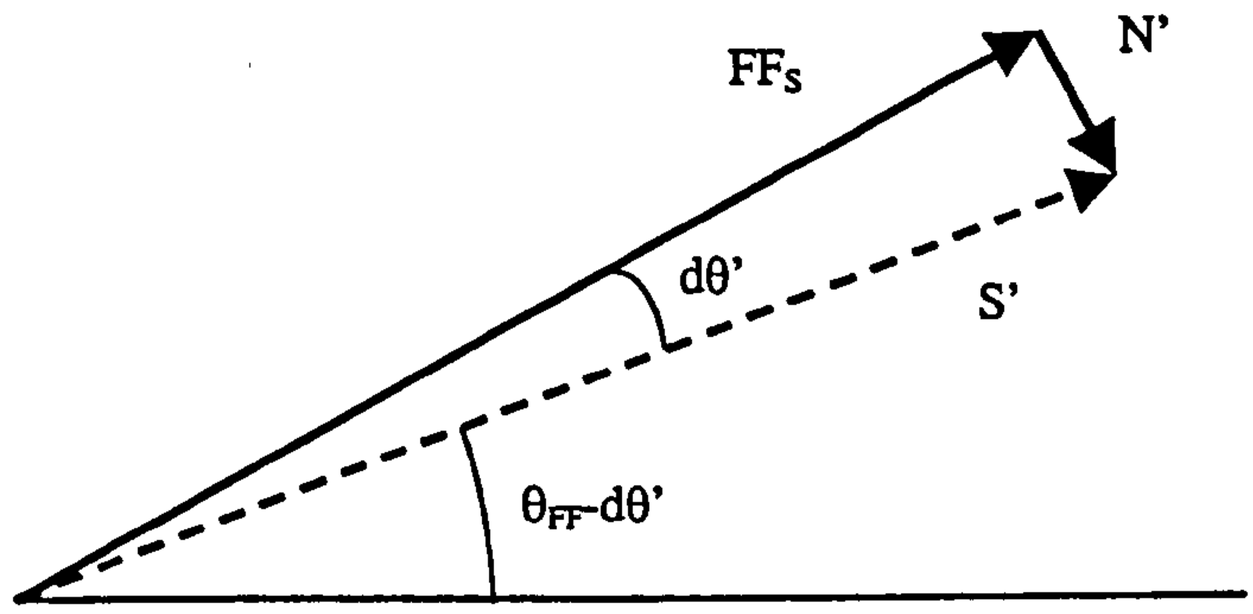

Figure 4-10 Phase delay due to the near field in S-like movement

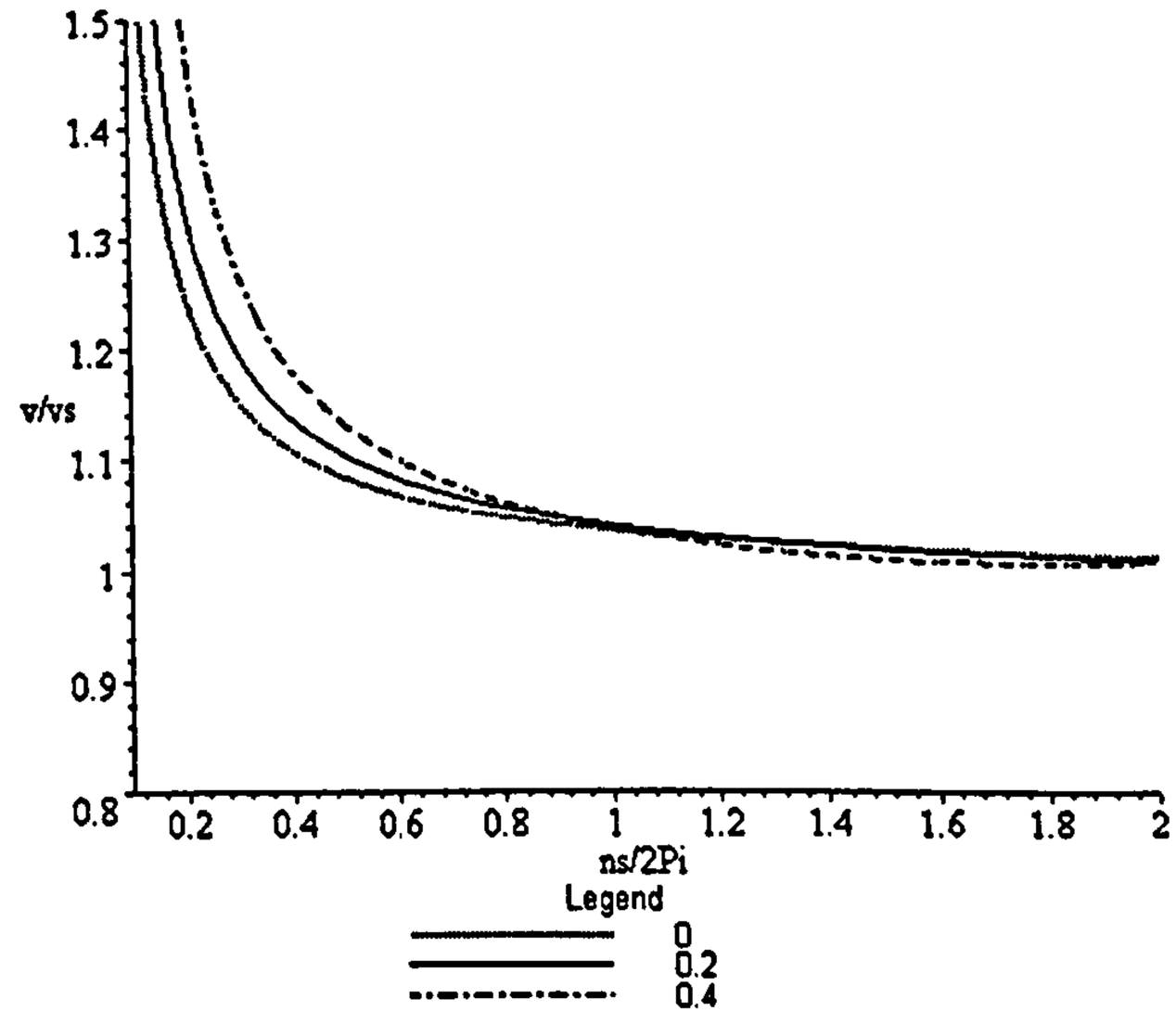

Figure 4-11 Upper limit of S phase velocity versus normalised distance. Poisson ratio 0, 0.2, 0.4

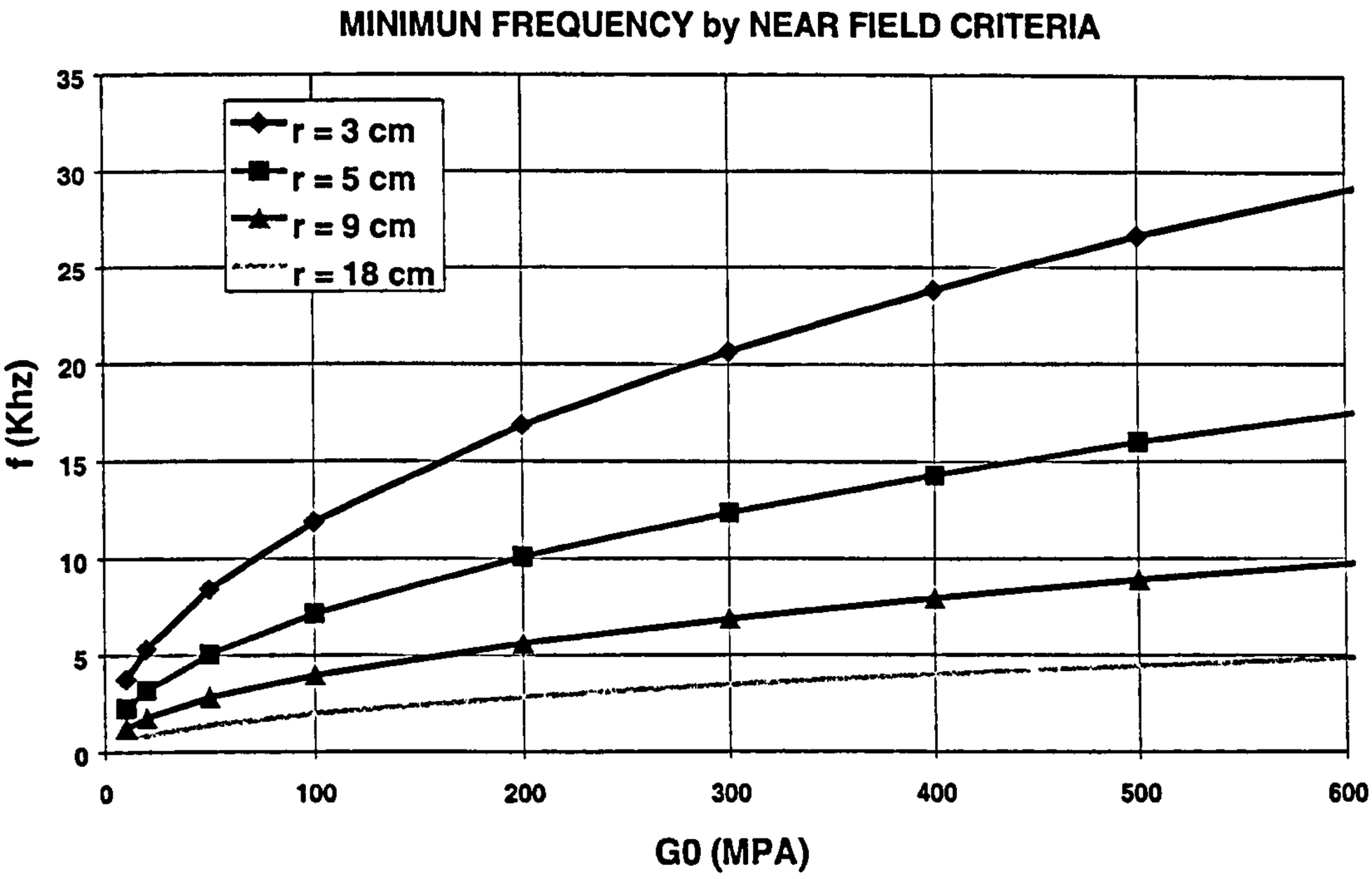

Figure 4-12 Near field frequency limit vs sand stiffness for varying source to receiver distances

$n_{sp} = 2$

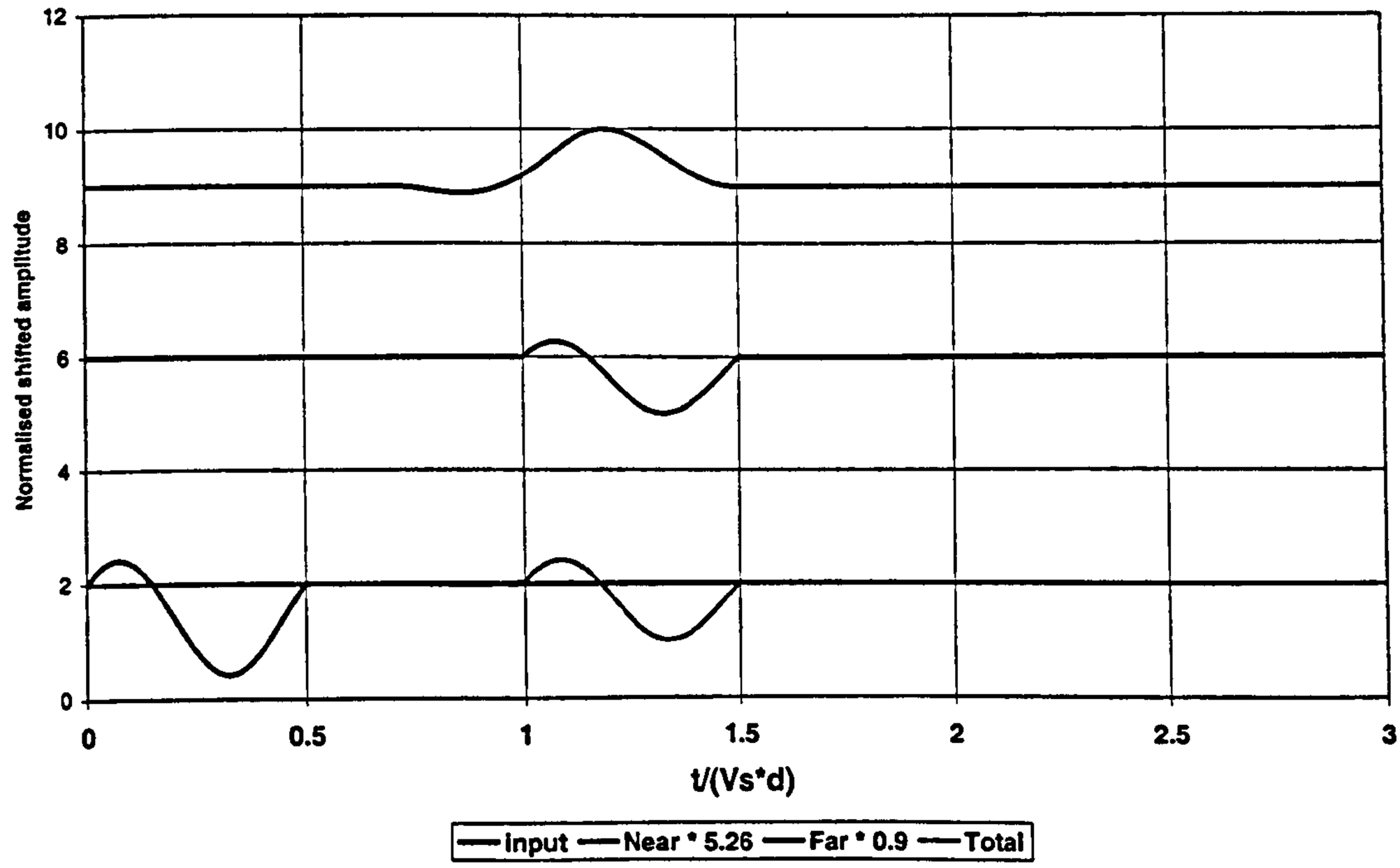

Figure 4-13 Stokes propagation of a distorted sine pulse

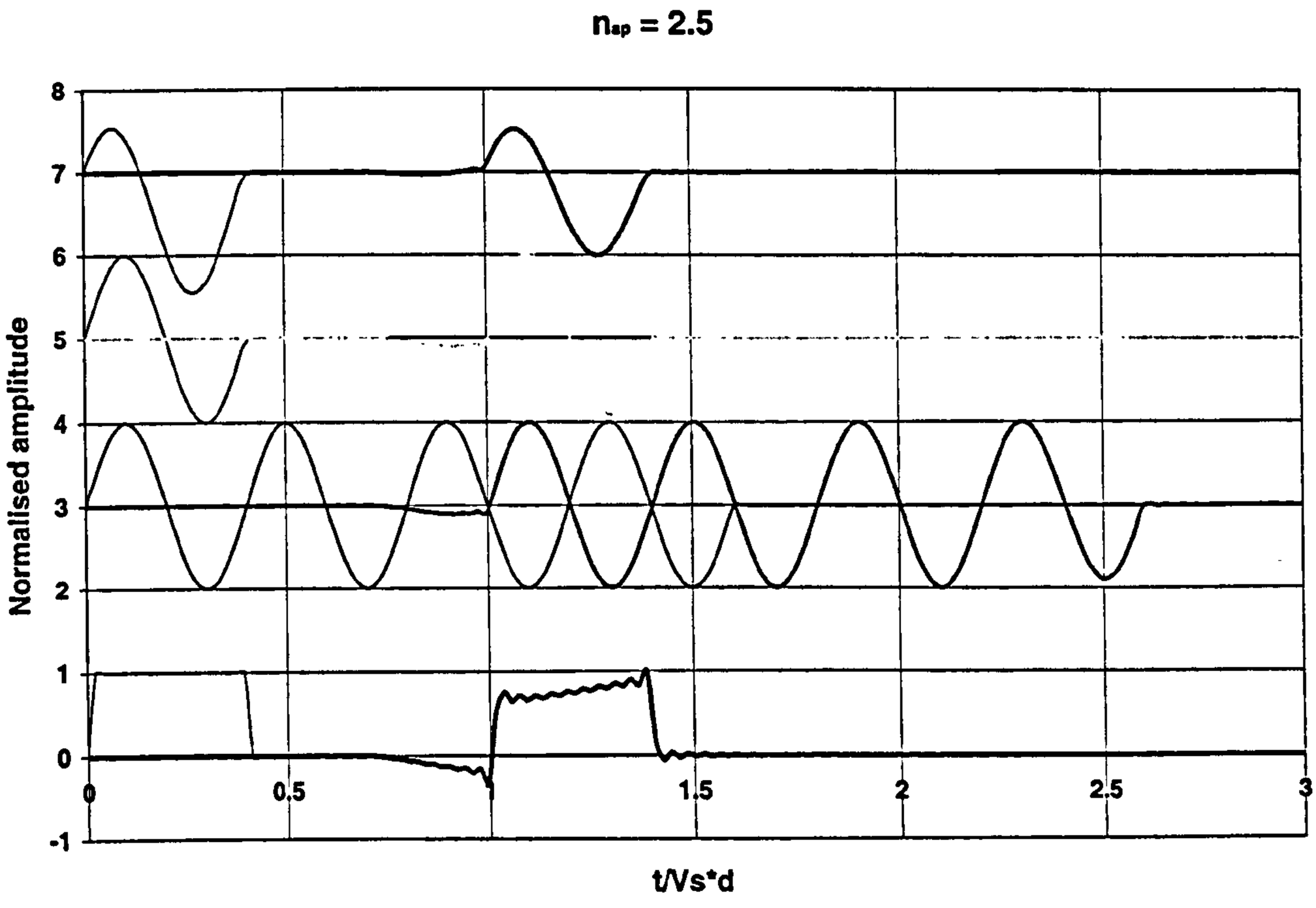

Figure 4-14 Input shape and near field effect in time domain

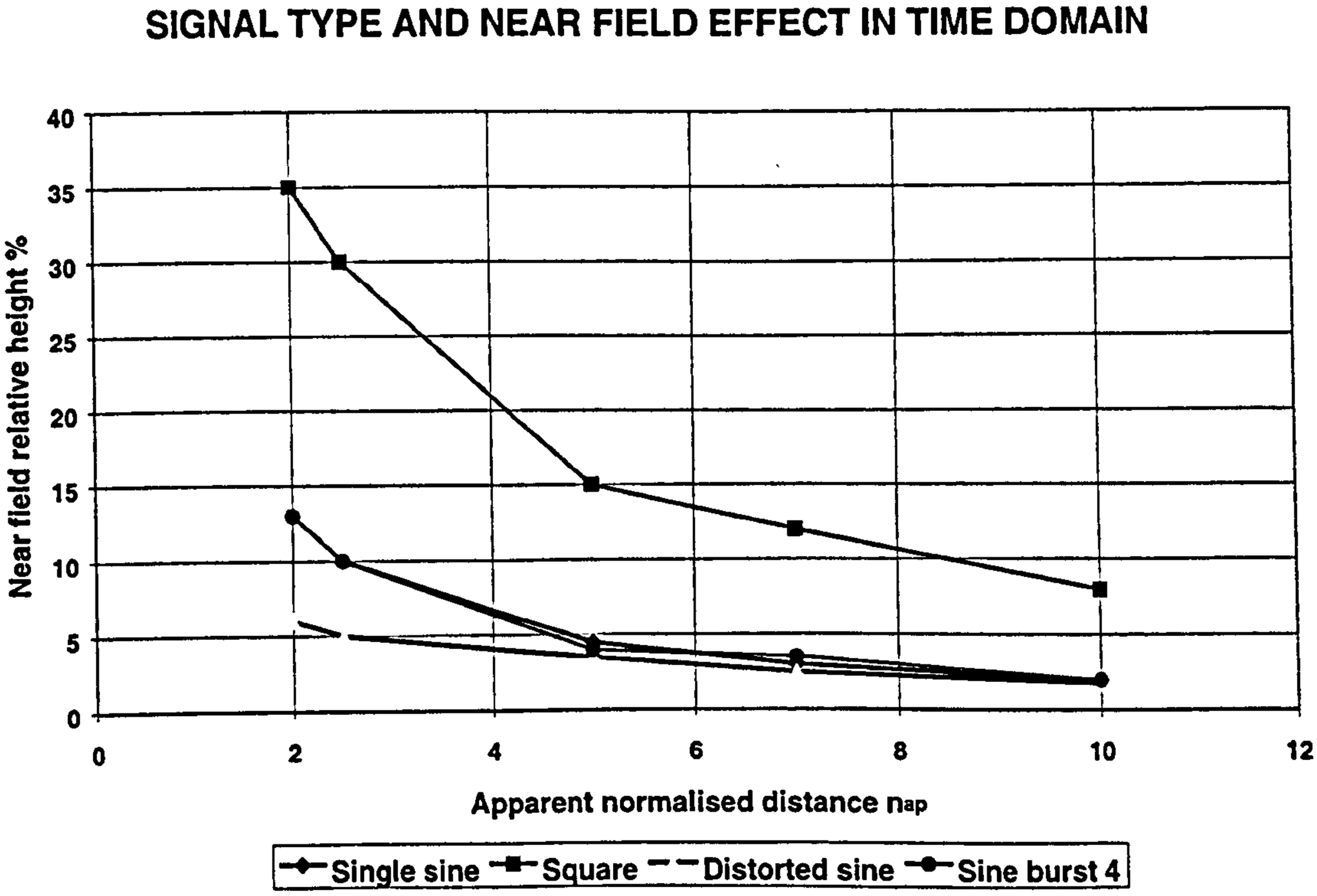

Figure 4-15 Effect of input signal type on the percentage height of the near field

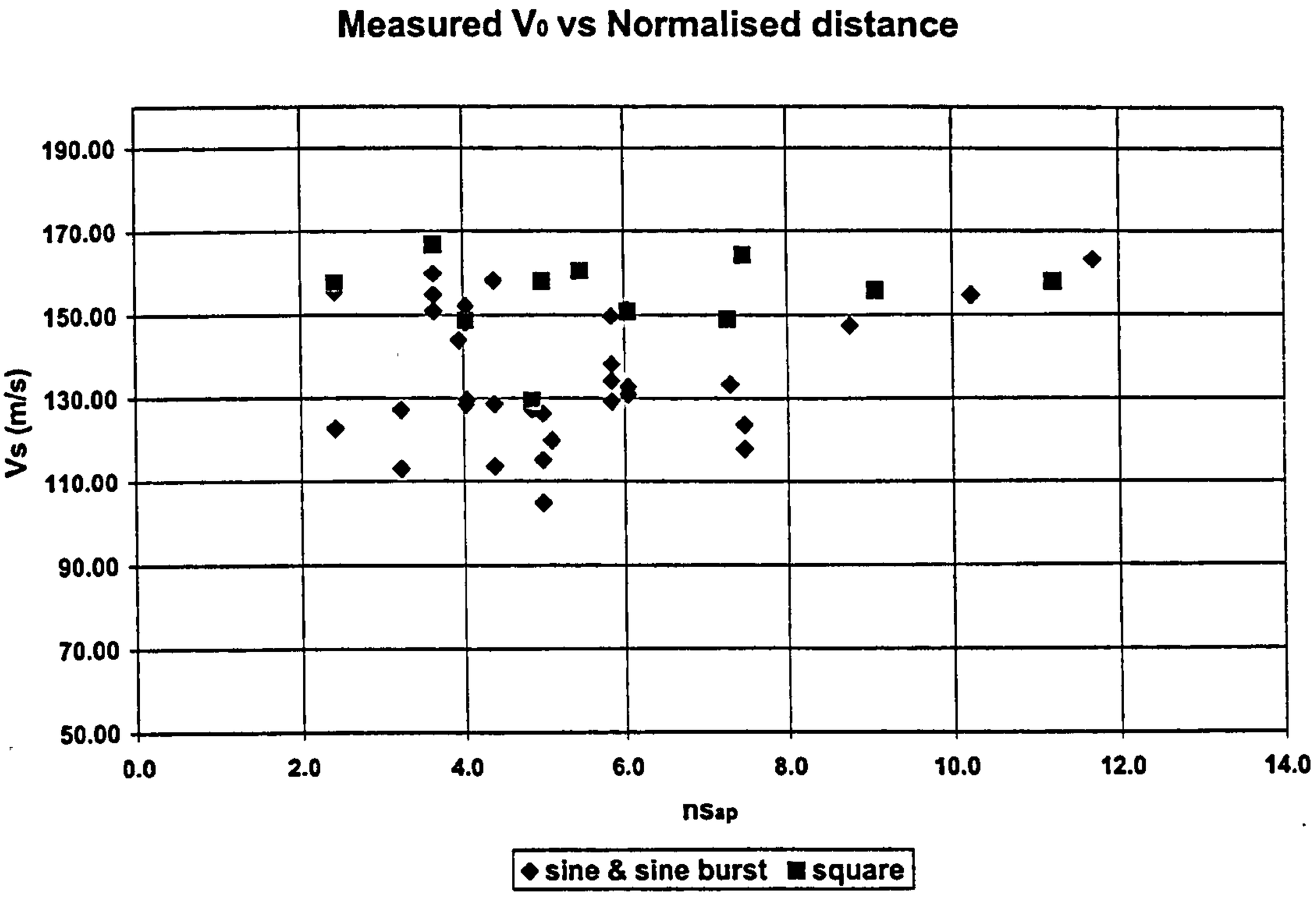

Figure 4-16 Bench tests on Gault clay. Influence of near field on first-arrival estimate of Vs

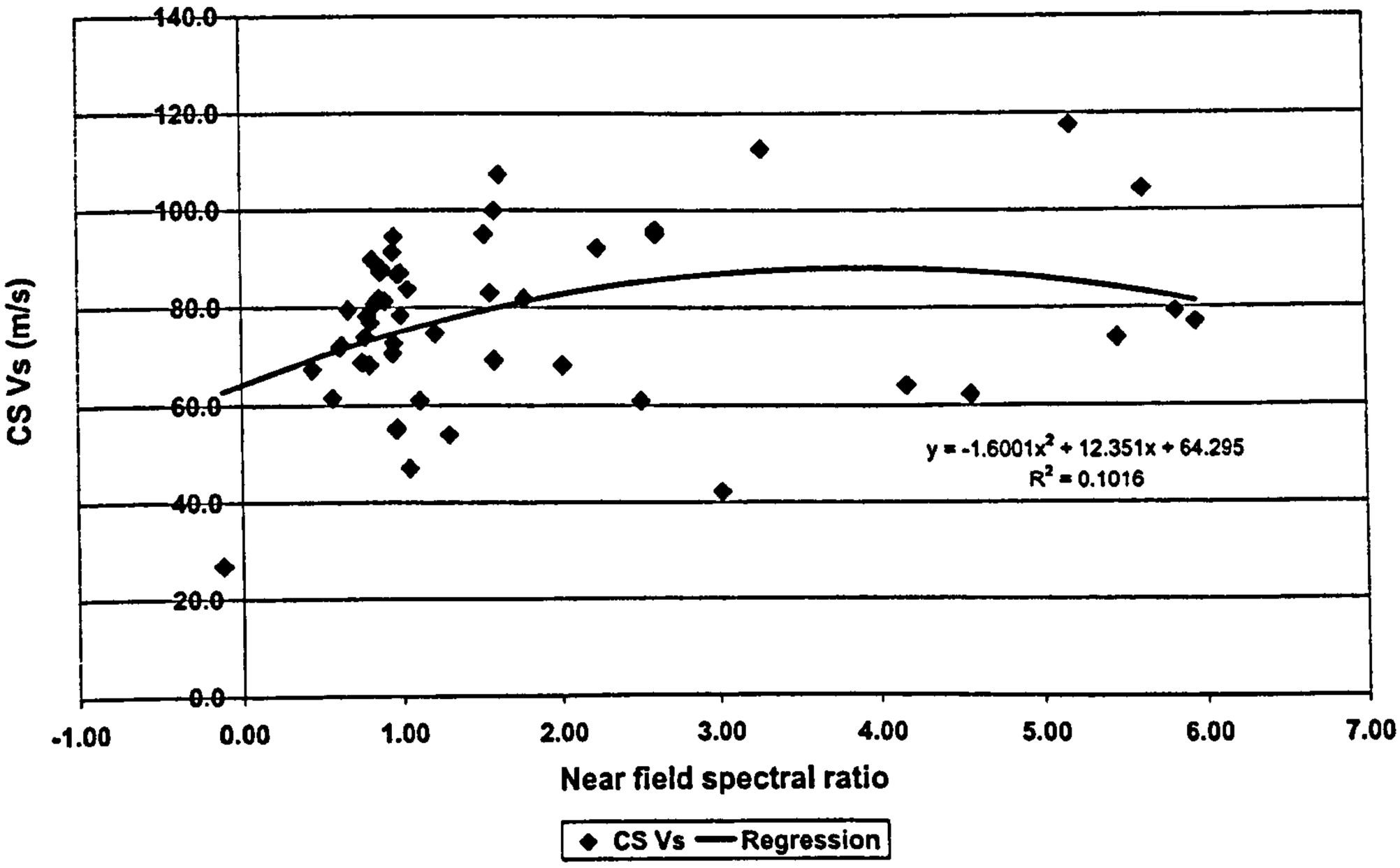

Figure 4-17 Bench tests on Gault clay. Influence of near field on cross-spectrum estimate of Vs

5 MATERIAL ISOTROPIC DISPERSION

Continuing our search for dispersive elastodynamic models for shear pulse tests in soils we address in this chapter two different possibilities. First we will consider a modification to the elastic material model we have been employing so far. Then we will consider the dispersive effects induced by the heterogeneous bi-phasic nature of soils. Following a terminology suggested by Sachse & Pao (1979) these effects will belong in the category of material dispersion.

5.1 VISCOSITY AND DISPERSION

Without leaving the linear realm an obvious possibility to introduce dispersion is to employ a viscoelastic material model. Viscoelastic constitutive relations can be written in a differential form relating the time derivatives of the stress and strain tensors (Christensen, 1971)

$$\mathbf{a}_0\boldsymbol{\sigma}+\mathbf{a}_1\frac{\partial\boldsymbol{\sigma}}{\partial t}+\mathbf{a}_2\frac{\partial^2\boldsymbol{\sigma}}{\partial t^2}+\ldots+\mathbf{a}_k\frac{\partial^k\boldsymbol{\sigma}}{\partial t^k}=\mathbf{b}_0\boldsymbol{\varepsilon}+\mathbf{b}_1\frac{\partial\boldsymbol{\varepsilon}}{\partial t}+\mathbf{b}_2\frac{\partial^2\boldsymbol{\varepsilon}}{\partial t^2}+\ldots+\mathbf{b}_i\frac{\partial^i\boldsymbol{\varepsilon}}{\partial t^i} \qquad (69)$$

All the a_k and b_i coefficients have tensorial nature, and therefore each term included in the equation may increase considerably the complexity of the material description. Notwithstanding this complexity the relationship is still linear and the superposition principle still applies. One of the simplest viscoelastic material models is the Kelvin-Voigt material, whose constitutive relationship may be written as

$$\boldsymbol{\sigma}=\mathbf{D}_0\boldsymbol{\varepsilon}+\mathbf{D}'_0\frac{\partial\boldsymbol{\varepsilon}}{\partial t} \qquad (70)$$

where $\mathbf{D}'_0$ is the tensor of viscous coefficients. For an isotropic material the elastodynamic equilibrium equation will now be written[50]

$$\rho\ddot{u}_m=f_m+(\lambda+G)u_{k,km}+Gu_{m,kk}+(\lambda'+G')\dot{u}_{k,km}+G'\dot{u}_{m,kk} \qquad (71)$$

Wave propagation in such a material is generally dispersive, as can be seen in the simple one-dimensional example of a plane harmonic shear wave. Disregarding source terms, naming x the direction of propagation and u the y-directed single non-zero movement component, elastodynamic equilibrium takes the form

$$\rho u_{tt}=Gu_{xx}+G'u_{xxt} \qquad (72)$$

where G is the shear modulus and G' is the viscous counterpart. Substituting the general expression of harmonic plane wave a dispersion equation results

$$\rho\omega^2=Gk^2+iG'\omega k^2 \qquad (73)$$

This is often written using a complex modulus notation, to emphasise the formal analogy with the elastic case

---

[50] We write here G instead of the usual Lamé symbol μ to avoid confusion with fluid viscosity appearing later on this chapter.

$$\rho\omega^2 = G^* k^2$$
$$G^* = G(1+i\omega\delta) \tag{74}$$

where δ symbolises the ratio G'/G and is handy to express the wavenumber solutions of (72).This solutions are complex, with the real part belonging to the wave phase and the imaginary part to the wave magnitude.

$$k_r^2 = \frac{\rho\omega^2}{2G(1+\delta^2\omega^2)}\left\{(1+\delta^2\omega^2)^{1/2}+1\right\}$$
$$k_i^2 = \frac{\rho\omega^2}{2G(1+\delta^2\omega^2)}\left\{(1+\delta^2\omega^2)^{1/2}-1\right\} \tag{75}$$

The phase velocity v is given by the ratio ω/k_r. Rearranging the first equation above, its ratio to the elastic shear velocity may be expressed as

$$\frac{v}{v_s} = \left[\frac{2(1+\delta^2\omega^2)}{(1+\delta^2\omega^2)^{1/2}+1}\right]^{1/2} \tag{76}$$

where the dispersive nature of the model is patent. Only for low frequencies and small moduli ratio (δ) would the phase velocity be equal to the elastic one. Figure 5-1 plots the resulting dispersion relations for two moduli ratios: an almost negligible 0.1% and 5%. Even for the lower value, the range of phase velocities implied for typical pulse test frequencies seems excessive. Moreover, the phase velocity is unbounded and its slope implies an even higher group velocity. That would be enough to dismiss the model, but it is nevertheless instructive to consider also the predicted damping ratio.

The damping ratio D is a basic dynamic concept used to measure the ratio of energy loss per cycle ΔE to the maximum cycle energy E. It is defined (Kramer, 1996) by

$$D = \frac{\Delta E}{4\pi E} \tag{77}$$

For the case of a propagating plane wave it can be shown -e.g. Udías, 2000- that the damping ratio is given by the ratio between the imaginary and real parts of the wavenumber. Using (75) above this leads to

$$D = \frac{k_i}{k_r} = \frac{\delta\omega}{(1+\delta^2\omega^2)^{1/2}+1} \tag{78}$$

which has been plotted in Figure 5-2, for the same moduli ratios as above. It can be appreciated that the predicted damping ratio is sigmoidal, and hence approximately linear within a certain frequency range. It is this characteristic that gives the model some appeal when the problem at hand is restricted to a narrow

frequency range[51] and the main concern is with movement amplitude. But this is not generally the case for pulse tests on soils.

Damping ratio is, precisely, one of the basic parameters measured and commonly employed by "soil dynamics" practitioners (Kramer, 1996). Most of these data have been obtained either measuring the hysteresis loop in static cyclic apparatus –like triaxial, direct simple shear or hollow torsional cylinders- or the resonance bandwidth of resonant column tests. Consequently, these results relate to relatively low frequencies (below 100 Hz). Figure 5-3 reproduced from Kim, Stokoe & Roesset, (1991), presents results that may be considered typical (see for instance Toki et al. 1995).

The results for dry sand are frequency independent over the range explored. This is usually introduced in models assuming that δ -or equivalently G'- is inversely proportional to frequency. This is what is usually known as hysteretic or structural damping -Kramer, 1996; Ewins, 2000. A quick perusal of expressions (75) and (76) confirms that the resulting damping ratio is indeed constant but so also is the phase velocity, thus precluding any dispersion.

Hysteretic damping does not involve dispersion and it is therefore useless for our purposes. It may be argued, however, that the frequency range of interest in pulse tests is rather higher than that explored by Kim et al. Directly relevant data are scarce. For reasons that will be explored later on, the usual arrangement of shear pulse tests employing bender elements is not generally used to measure attenuation. An exception is offered by Brocanelli & Rinaldi (1998), who, employing benders in a somewhat different arrangement, have obtained attenuation data at 2.5 kHz for dry sand. The measured D values are similar to those depicted in Figure 5-3. Even more strong support for the hysteretic approach for dry sand is offered by Prasad & Meissner (1992) who again obtained very similar shear damping values testing at 100 kHz.

At this juncture, it may be worth noting that although hysteretic damping may be favoured in dynamic models –e.g. Salinero et al. 1984- it has an intrinsic "ad hoc" character that fits badly within the linear theory. For vibration problems, Crandall (1970) shows how this results in non-causal model behaviour i.e. in output preceding the input. Within a wave propagation context Aki & Richards (1980) also show that the introduction of attenuation without dispersion results in instantaneous wave arrivals. The model performs quite well for small amounts of damping and when used for a restricted frequency range, but this characteristic has prompted the search for more elaborate viscoelastic models. Although there are proposals in the seismic literature (see Aki & Richards 1980) that might be applied to soil mechanics this issue will not be considered further here. It will be only pointed out that recognition of direct time effects in the mechanical response of dry sands is very recent and that these are usually interpreted within a non-linear viscoplastic framework (Imposimato, 1998; Di Benedetto, 2001).

---

[51] Crandall, 1970, gives a thorough discussion of this issue within the closely related context of vibration theory.

The previous discussion has dealt only with dry sands. Looking again at Figure 5-3 it may be noticed that clay does indeed show some damping increase in the higher frequency range. This should not be taken as a vindication of the Kelvin-Voigt model. Clays are never tested dry but with a rather high degree of saturation. For all kinds of soils, the presence of water introduces a different mechanism of viscous dissipation and a new source of dispersion. This mechanism does again involve a modification in the material model, albeit a different one: the soil is still treated as elastic but is not anymore supposed to be homogeneous.

5.2 FLUID COUPLING: BIOT'S THEORY

5.2.1 General

The interaction between solids and pore fluid in saturated soils is commonly described within the framework proposed by Biot. He addressed the problem of elastic wave propagation in porous solids in a series of classical papers (1956a, 1956b, 1992). There he predicted that three different modes of plane wave propagation were to be found in them: one shear mode and two compressive, one fast P-wave and a slower one which is now usually referred to as the Biot wave.

His results (1956a, 1956b) indicated that for soils[52] the fast P-wave would travel between two and five times faster than the compressive velocity that would be predicted from static moduli disregarding interaction; the slow mode will show less difference (between one and two) but will be strongly attenuated and thus very hard to measure. The shear velocity was less affected, its increase remaining below 30% of the elastic value. Biot shows that the wavenumbers obtained from the dispersion equation are complex, with both real and imaginary parts showing frequency dependence.

These predictions have had extensive confirmation. Saturation produced a substantial increase in the measured compressive velocity of soils (Whitman & Lawrence, 1963). Attenuation showed a pattern in good correspondence with the prediction (Stoll & Brian, 1969). Acoustic measurements in marine sediments (Hampton, 1974) repeatedly showed the fast arrivals that Biot predicted for the first wave. The measurement of the second compressive wave in soils[53] has proved more elusive, but during the last decade enough experimental evidence has finally appeared, both in field tests (Chotiros, 1995) and in the laboratory (Nakagawa et al. 1997).

Biot theory has another important consequence: the relation between the wave velocities and the elastic moduli of the soil skeleton ceases to be a simple one. Apart from the elastic moduli of the soil skeleton, a number of different material parameters appear in the relation: porosity, viscosity and compressibility of the fluid, compressibility of the soil grains, permeability plus some extra parameters measuring the geometrical characteristics of the pore network. Recently, Gajo and coworkers (Gajo & Mongiovi, 1994; Gajo, 1995; Gajo, 1996; Gajo, Fedel & Mongiovi, 1997) made an extensive study of this problem. They

---

[52] An assumption about the relative magnitude of fluid and frame bulk moduli is necessary to interpret Biot adimensional results.
[53] The first measurements (e.g. Johnson & Plona, 1982) took place in artificial materials -sintered glass beads-

showed how sensitive is the relation between $\mathbf{D_0}$ and velocity measurements to incorrect assumptions about other parameters. The problem is extreme for measurements based on compressive velocities, and less so for measurements based on shear velocities.

Gajo's work being comprehensive in aim, devotes more space to the more peculiar and important effects of Biot's theory: those affecting the transmission of compressive waves[54]. Our aim here is more specific: we are only interested in the dispersive characteristics of shear propagation within Biot's theory. This is obviously motivated by the restricted character of our Gault clay database, where only shear results are present. But certain disagreements in recent experimental work provide some extra interest. Jovicic (1997) or Kuwano (1999) working with granular materials –various sands, glass ballotini- decided after some consideration of Gajo's results not to take into account fluid interaction effects in the interpretation of their measurements. On the contrary, Blewett et al. (2000) pointed to these as a major cause of dispersion in their own measurements in Levenseat sand and advocated for their systematic consideration.

5.2.2 Biot shear wave

Biot presented a theory that considered the interacting movement of an elastic solid skeleton and the pore fluid filling its pores. The basic field variables are then two movements, that of the fluid, U and that of the solid skeleton, u. They are coupled through two field equations that express dynamic equilibrium. These equations can be written in a number of ways[55]; we use here the emphatically symmetric form presented by Gajo et al. (1997)

$$\begin{aligned} \rho_{11}u_{tt} + \rho_{12}U_{tt} + bu_t - bU_t &= c_{11}u_{xx} + c_{12}U_{xx} \\ \rho_{12}u_{tt} + \rho_{22}U_{tt} - bu_t + bU_t &= c_{12}u_{xx} + c_{22}U_{xx} \end{aligned} \tag{79}$$

These equations contain no source term and rule 1-D movements such as those produced by plane waves. The ρ_{ij} are density-like coefficients affecting the inertia terms, the c_{ij} are moduli-like coefficients affecting the stiffness terms and b is a coefficient affecting viscous terms. There are three kinds of coupling between fluid and solid movements: mechanical, inertial and viscous, given respectively by c_{12}, ρ_{12} and b.

The stiffness coefficients are very simple for the shear case: there is no mechanical coupling and all are zero except for c_{11} that is equal to G, the usual shear modulus of the soil. The inertia coefficients can be rewritten (Biot, 1956a) in terms of the soil solid and fluid densities -ρ_s and ρ_f- the porosity n and a new parameter, the added mass, ρ_a.

---

[54] This emphasis on compressive waves is also a quasi-unanimous feature of most geophysical and material research on the subject, even in recent times (e.g. Moussatov et al. 1998, Hickey & Sabatier, 1997, Chotiros, 1995).

[55] The main difference between formulations has to do with the choice of stress variables (total stress, effective stress, solid stresses...). There is no unanimity in this particular. Biot himself presented his equations in a number of ways and all have had some following. Also the material parameters appearing in the stiffness and inertia terms are rather freely combined by different authors.

$$\rho_{11} = (1-n)\rho_s + \rho_a$$
$$\rho_{22} = n\rho_f + \rho_a \qquad (80)$$
$$\rho_{12} = -\rho_a$$

The viscous coupling coefficient can be written as

$$b = b_0 F(\omega) = \frac{\mu n^2}{K_0}(F_r + iF_i) \qquad (81)$$

Where the symbol μ denotes the viscosity[56] of the pore fluid, K_0 the absolute permeability[57] and F(ω) is a dynamic correction factor, generally complex.

Substitution of a harmonic plane wave expression for the solid and fluid movements in (79) leads to a dispersion equation, that is, to an equation relating wavenumber and frequency. This development is presented for instance in Biot (1956a, 1956b); here we just write the resulting wavenumber solution

$$k_r = \frac{\omega}{v_s\sqrt{2}}\left\{\left(E_r^2 + E_i^2\right) + 2E_r\right\}^{1/2}$$
$$k_i = \frac{\omega}{v_s\sqrt{2}}\left\{\left(E_r^2 + E_i^2\right) - 2E_r\right\}^{1/2} \qquad (82)$$

The real and imaginary part are expressed in terms of

$$v_s = \frac{G}{n\rho_f + (1-n)\rho_s}$$
$$E_r = \frac{(r_1\kappa + F_i)(r_2\kappa + F_i) + F_r^2}{(r_1\kappa + F_i)^2 + F_r^2} \qquad (83)$$
$$E_i = \frac{F_r\kappa n\rho_f}{(r_1\kappa + F_i)^2 + F_r^2}$$

By v_s we denote the base shear velocity; this is the one usually employed in pulse test interpretation when fluid interaction is disregarded (e.g. Jovicic 1997, Pennington, 1999, Kuwano, 1999). Three adimensional ratios have been employed to shorten the notation; the first two are mass –or density- ratios

$$r_1 = \frac{\rho_{22}}{\rho_{22} + \rho_{12}}$$
$$r_2 = \frac{\rho_{11}\rho_{22} - \rho_{12}^2}{(\rho_{11} + \rho_{22} + 2\rho_{12})(\rho_{22} + \rho_{12})} \qquad (84)$$

and the third one is a normalised frequency

---

[56] We adhere here to a fluid mechanics convention, no confusion should arise with the equally named Lamé coefficient which does not appear in this section. Viscosity has dimensions M/LT and it is related to the kinematic viscosity through $\eta = \mu/\rho_f$

[57] Which has dimensions of L^2 and is related to the engineering permeability or hydraulic conductivity k_H by $K=(\mu/\gamma_w)k_H$ with γ_w being the specific weight of water.

$$\kappa = \frac{\omega}{\omega_c}$$
$$\omega_c = \frac{b_0}{\rho_{22} + \rho_{12}} = \frac{\eta}{nK_0} \qquad (85)$$

Careful consideration of the previous expressions will reveal that only two unfamiliar material properties have been introduced: the added mass density, ρ_a, responsible for inertial coupling and the dynamic correction factor F(ω) appearing in the viscous coupling coefficient. These properties need to be further specified before the theory can be applied.

Research by Johnson and co-workers (1982, 1987, 1994) has shown that both properties are related to the same physical phenomena: the frequency-dependent characteristics of the fluid flow through the pore network. This frequency dependency is expressed in F(ω), given by

$$F(\omega) = \left\{1 - i\frac{4\tau_\infty^2 K_0^2}{\eta n^2 \Lambda^2}\omega\right\}^{1/2} \qquad (86)$$

This expression guarantees that the low-frequency quasi-static interaction is ruled by the viscous term –a term where the permeability K_0 is the fundamental parameter- whereas the high-frequency interaction is ruled by the inertial term –and hence ρ_a. The added mass appears slightly disguised in the previous expression, as it is related to the newly introduced tortuosity τ_∞ by

$$\tau_\infty = \frac{\rho_a}{n\rho_f} + 1 \qquad (87)$$

Tortuosity can be measured using electrical conductivity measurements or deduced from acoustic high frequency measurements –see below. An empirical alternative was proposed by Gajo (1997):

$$\tau_\infty = \frac{1}{\sqrt{n}} \qquad (88)$$

This relation with porosity was based on measurements on a range of granular materials, most of them artificial; it was shown to give a reasonable fit for the intermediate range of porosity –0.2 to 0.6- usually relevant in geotechnical problems. It is plotted in Figure 5-4, where some new results for sand have been added. These results were either directly measured (Moussatov et al. 1998) or obtained by back-analysis of field and laboratory measurements. It seems that Gajo's relation will offer a fair estimate of tortuosity for any soil modelling exercise.

An extra parameter, Λ, appears in (6). It has length dimension and it measures the average size of the dynamically connected pore network (Johnson et al, 1987). Its direct measurement is possible although

rather involved[58]. A common alternative (e.g. Gajo 1997) is to assume M equal to 1, where M is defined by the relation

$$M = \frac{8\tau_\infty K_0}{n\Lambda^2} \tag{89}$$

M equal to 1 is the exact result for a cylindrical non-intersecting pore network and seems to hold within an order of magnitude for real materials (Smeulders et al. 1992). As an alternative one might use an empirical relation suggested by Johnson et al. (1994)

$$\Lambda = \frac{2nd}{9(1-n)} \tag{90}$$

This relation was shown to offer good results for sandstone and fused glass beads; a result for sand by Moussatov et al. (1998) would suggest that this relation underestimates Λ.

5.2.3 Shear dispersion characteristics

Although the Biot model looks complex its shear dispersion characteristics are relatively simple. Figure 5-5 represents the dispersion curves that correspond to some typical permeable soils, Gault clay and Levenseat sand. These curves represent the normalised phase velocity as a function of frequency, that is

$$\frac{v}{v_s} = \frac{\omega}{k_r(\omega)\sqrt{G/\rho}} \tag{91}$$

The parameters employed are collected in Table 5-1. The permeability of typical soils has been taken from Mitchell (1991); data for Levenseat sand are given by Blewett et al (2000), Gault data are repeated here for ease of reference. Tortuosity is estimated using (88); M is assumed 1 in all cases; no G value is quoted as the normalised values are independent of its value. The dispersion curves are all similar: they have two plateaux at low and high frequencies and a transition zone in between, where the dispersion proper takes place. This zone is frequently known as the crossover range (e.g. Johnson & Plona 1982). Regarding this shape two important questions related to our problem arise.

The first question is about the magnitude of the velocity variation. How far from one another are the two plateaux? The low frequency velocity is just v_s, the high frequency limit is given by (Biot, 1956b; Gajo, 1996)

$$v_H^2 = \frac{G}{\rho_{11}\left(1-\frac{\rho_{12}^2}{\rho_{11}\rho_{22}}\right)} = \frac{G}{\left(1-\frac{1}{\tau}\right)n\rho_f + (1-n)\rho_s} \tag{92}$$

Using again (88) and assuming some standard values for fluid and grain density[59] we can plot the ratio v_H/v_s as a function of n -Figure 5-6. As we have said the common practice in soil mechanics is to use the

---

[58] Johnson et al. (1994) use acoustical measurements with superfluid HeII as saturant. Tizianel et al. (1999) use regular He but they need to consider the coupled thermal losses.

low frequency formula to obtain G; if the high frequency value is measured instead the induced error in G might lie above 25% for loose materials[60]. This error will overestimate the stiffness, something that would be unsafe for foundation design purposes.

The second question relevant to our problem asks about the frequency range where the dispersion takes place; this range is sometimes known as the crossover zone (Johnson et al. 1994). As can easily be inferred from Figure 5-5, and is more emphatically shown in Figure 5-7, permeability has a fundamental role in this respect. As the permeability decreases the crossover zone is pushed into higher frequencies. For low permeability materials the high frequency limit may be unattainable because of scattering. The presence of a scattering upper limit to wave propagation was commented upon in the second chapter. This limit was explicitly stated by Biot when the theory was proposed (1956a) and was later recognised experimentally by Johnson & Plona (1982) –testing at 500 kHz no low velocity arrivals, i.e. shear or Biot, were obtained in immersed refraction tests[61] of fused glass beads.

The controlling role of permeability in the position of the crossover zone was noted by Gajo (1996, 1997) who stated the problem in terms of the relation between the viscous and inertial coupling terms. That this approach is equivalent to the one here adopted stems from the fact that in the frequency domain time derivatives on the ruling equations translate into powers of frequency. High frequency behaviour is dominated by inertial terms – or ω^2 terms-, low frequency by viscous terms – or ω terms.

It is useful to normalise the frequency scale using the crossover frequency ω_c defined above (17); the effect of permeability is accounted by the normalisation –Figure 5-8- and a simple criterion for the limits of the crossover zone then becomes available.

$$0.1 f_c \le f \le 10 f_c$$
$$f_c = \frac{1}{2\pi}\frac{n\eta}{K_0} \qquad (93)$$

However, this neat result has a flaw. The size and shape of the crossover zone is not controlled only by the parameters within the crossover frequency. M has also some influence on it as Figure 5-9 illustrates. As equation (2) shows M is directly related to the dynamic pore size parameter Λ; the hardest one to measure. We have already commented that M = 1 is a common assumption; M = 4 is close to the value measured by Tizianel et al. (1999) on quarry sand; M = 0 is equivalent to ignoring the effect of the dynamic correction factor $F(\omega)$ and was also the value adopted by Gajo (1997) for his time domain analysis of transmitted pulses. It is apparent that the crossover range size is somehow dependent on M; an increasing M extends its span into higher frequencies but leaves its low frequency onset almost

---

[59] Namely ρ_f=1000 kg/m^3 and ρ_s=2650 kg/m^3. The first value is that of water and it is relevant for fully saturated materials; Gajo & Mongiovì (1994) have explored the possible variability of this parameter and its influence on the high frequency limit shear velocity. It is rather minor, and the same happens with grain density.

[60] Corresponding to a 12.5% error on V_s

[61] A technique commonly employed in ultrasonic testing. The sample is immersed in water and source and receiver are placed in the water tank away from the sample. See Krautkramer (1993) for details.

unchanged. This result is also supported by a similar sensitivity analysis of Biot's equations carried out by Huot (1999) with a different dynamic correction formulation.

5.2.4 Consequences for shear pulse tests

From the preceding exploration of Biot shear dispersion characteristics we can infer some consequences for bender based pulse tests. In general, the influence of Biot dispersion will depend on the relative position of the frequency testing range and the crossover range, where dispersion takes place. This overlap may be quantified through the following ratio

$$R = \frac{(f_h - f_l) - \langle f_h - f_H \rangle - \langle f_L - f_l \rangle}{(f_h - f_l)} \qquad (94)$$

where f_h and f_l are the high and low frequency limits of the testing range and f_H and f_L those of the crossover range. R is 1 when the overlap is complete and negative when there is no overlap at all[62]. Using (93) above, assuming water as saturating pore fluid and M = 1 it is easy to plot this ratio as a function of porosity and permeability for any testing frequency range. Figure 5-10 does just that for the range 1-10kHz, relevant for the bench tests described in chapter 3, and also for the tests described by Blewett et al (2000) and Kuwano (1999). There are three distinct zones:

- Low permeability materials are tested in the low frequency range. This is, for instance, the case of Gault clay, with n =0.44 and k_H =3e-9 m/s. This justifies the approach adopted by Pennington (1999) and leaves us with no insight into the observed dispersion in our bench tests.
- High permeability materials are tested in the high frequency range. This may have been the case of the materials tested by Kuwano[63].
- Intermediate, medium permeability materials, are affected by Biot shear dispersion. This is the case of the Levenseat sand -n =0.44, k_H =1e-4 m/s- tests described by Blewett et al. (2000).

When the objective is the evaluation of the shear modulus the ideal testing situation is that in the low frequency range because there the relation between the measured velocity and the modulus is only dependent on rather well-known parameters[64] –n, ρ_f, ρ_s. Measurement in the high frequency range is a second best, because the relation between modulus and velocity (92) is also mediated by the tortuosity. Direct tortuosity measurement is not easy, but figures such as Figure 5-6 may be used to correct the excess velocity. Finally, when measurements are made in the crossover range the inversion depends on an extra, poorly known, parameter, M –or Λ-; still, figures such as Figure 5-8 may be of some help in this case.

There is an optimistic counterpoint to this panorama of intrusive unknown parameters, and that is the possibility of obtaining extra information from shear tests. It is obvious, for instance, that if shear

---

[62] Recall the meaning of the Macaulay brackets <x> = 0 for x<0 and <x> = x for x>0.
[63] No direct permeability measurement is available, but with a medium grain size above 0.2 mm and no fines one might expect a conductivity above 1e-3 m/s

measurements are available in both the high and low frequency range tortuosity may be inferred from the difference. If not only the limit values are established but the whole dispersion curve over the crossover range, the situation is even better. Not only M, but the crossover frequency and hence the permeability might be estimated from dynamic shear measurements.

From the preceding discussion it is clear that a precise knowledge of the frequency range of velocity measurement is highly desirable. We have described in the preceding chapter how it is possible to obtain experimental dispersion curves from bender measurements. It is worth noticing that in this case of Biot shear dispersion the group velocity goes rather close to the phase velocity -Figure 5-11. This will help to establish the dispersion curve even if unwrapping problems affect the phase velocity measurements. It is nevertheless true that the crossover range extends over at least two orders of magnitude of the frequency. Current bender equipment might have problems to cover such an extension with adequate definition. The low frequency range may be affected by noise and other dispersive phenomena –e.g. near field[65]. On the other hand the higher frequency range may be affected by excessive scattering attenuation.

As in the case of near field effects, time domain interpretation of pulse measurements is less direct and powerful. If the whole spectrum of the input signal is located in the low or high frequency range, then any arrival selection criterion is equally valid to obtain the velocity. If, however, it is located over the crossover range then any time domain method will be similarly uncertain. This is illustrated in Figure 5-12 where a sine input has been propagated[66] through three increasingly permeable materials. The time scale has been normalised by the arrival time corresponding to the low frequency range velocity. The low frequency test arrives undistorted at its time. The high frequency test arrives earlier, with the 7% increase in velocity that will correspond to n = 0.4 in Figure 5-6. The test on the crossover range has a more imprecise arrival.

One extra possibility should be mentioned. To obtain the crossover frequency and hence to measure permeability, it may be simpler to measure attenuation. This is based on the fact that the crossover frequency approximately coincides with a maximum of the damping ratio vs frequency relationship. Turgut (2000) has recently explored this idea with compressive waves in mind, but this also applies to shear waves –Figure 5-13 illustrates this aspect, although the considerable effects of tortuosity are not shown. The problem with this approach is that attenuation measurements using bender elements are still poorly understood –see next chapter. Note also that the study of attenuation usually includes also hysteretic damping within the solid frame (e.g. Stoll & Bryan, 1971); we have not considered this here because, as shown previously, hysteretic damping is immaterial for dispersion.

The analysis just presented is based on the transmission of plane waves. It is then a far-field analysis, where mode separation is assumed from the outset. The results of chapter 4 indicated that this assumption

---

[64] See Gajo & Mongiovì (1994).
[65] One possibility of extending the low frequency range will be to use field pulse tests or laboratory resonant column tests
[66] Using the Biot wavenumber to construct a plane wave transfer function and using the same FFT algorithm as in the previous chapter. This method has been applied a number of times to simulate Biot signals –e.g. Van der Grinten & Van Dongen (1987).

might not be appropriate in all cases relevant for bender testing. Like Stokes for the elastic case there is also a fundamental solution available for the poroelastic problem, obtained by analogy with thermoelasticity (Dominguez, 1993). This solution describes the coupled movement of the three modes – shear, P, Biot- and its study is beyond the scope of this dissertation. However, the results of chapter 4 are still likely to be relevant, at least while testing on the low and high frequency range. This is based on the fact that the Biot wave is often disregarded in such cases –e.g. Morochnick & Bardet, 1996. Left with just one fast compressive velocity an analogy with the elastic case might be done, with the only caution of including a very high Poisson ratio, but, as shown in Chapter 4, Poisson ratio was scarcely relevant to the near field limit.

5.3 SUMMARY

Material dispersion can be introduced in soils while keeping the linear description of their behaviour. One possibility is through viscoelastic models but simple viscous models in use produce either too much dispersion –Kelvin-Voigt- or none –hysteretic. A more fertile possibility is offered by the consideration of fluid interaction through Biot theory. The amount of shear dispersion in pulse tests predicted by the model may be considerable for permeable materials. If not properly taken into account this will introduce a systematic shear stiffness overestimation; some guidance to avoid this problem is here included. On the other hand, if correctly interpreted, bender measurements may be used to evaluate permeability, which may be practical in medium permeability materials. For impermeable materials, like Gault clay, Biot dispersion takes place in a frequency range above that tested with bender elements. Therefore this phenomena is not directly relevant for the interpretation of the bench test results included in Chapter 3.

5.4 TABLES

Material	K0	M	porosity	rhof	rhos	viscosity
	m2			kg/m3	kg/m3	kg/ms
Gault	3.E-16	1	0.58	1000	2650	1.E-03
loose sand	1.E-09	1	0.5	1000	2650	1.E-03
dense sand	1.E-11	1	0.25	1000	2650	1.E-03
soft clay	1.E-15	1	0.5	1000	2650	1.E-03
compact clay	1.E-16	1	0.25	1000	2650	1.E-03
Levenseat	1.E-11	1	0.44	1000	2650	1.E-03

Table 5-1 Base parameters for Biot computations

5.5 FIGURES

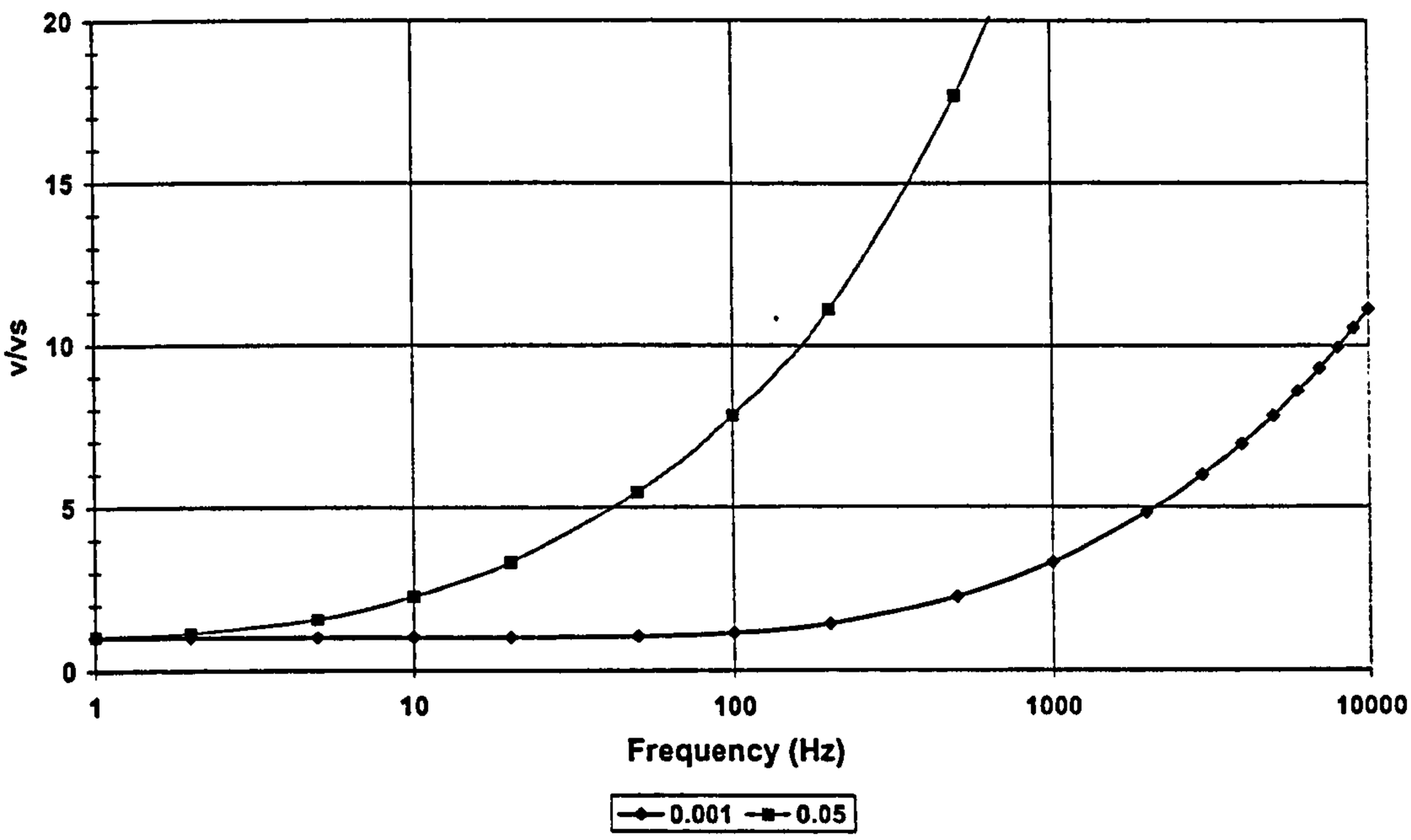

Figure 5-1 Effect of moduli ratio on the normalised phase velocity of a Kelvin-Voigt material

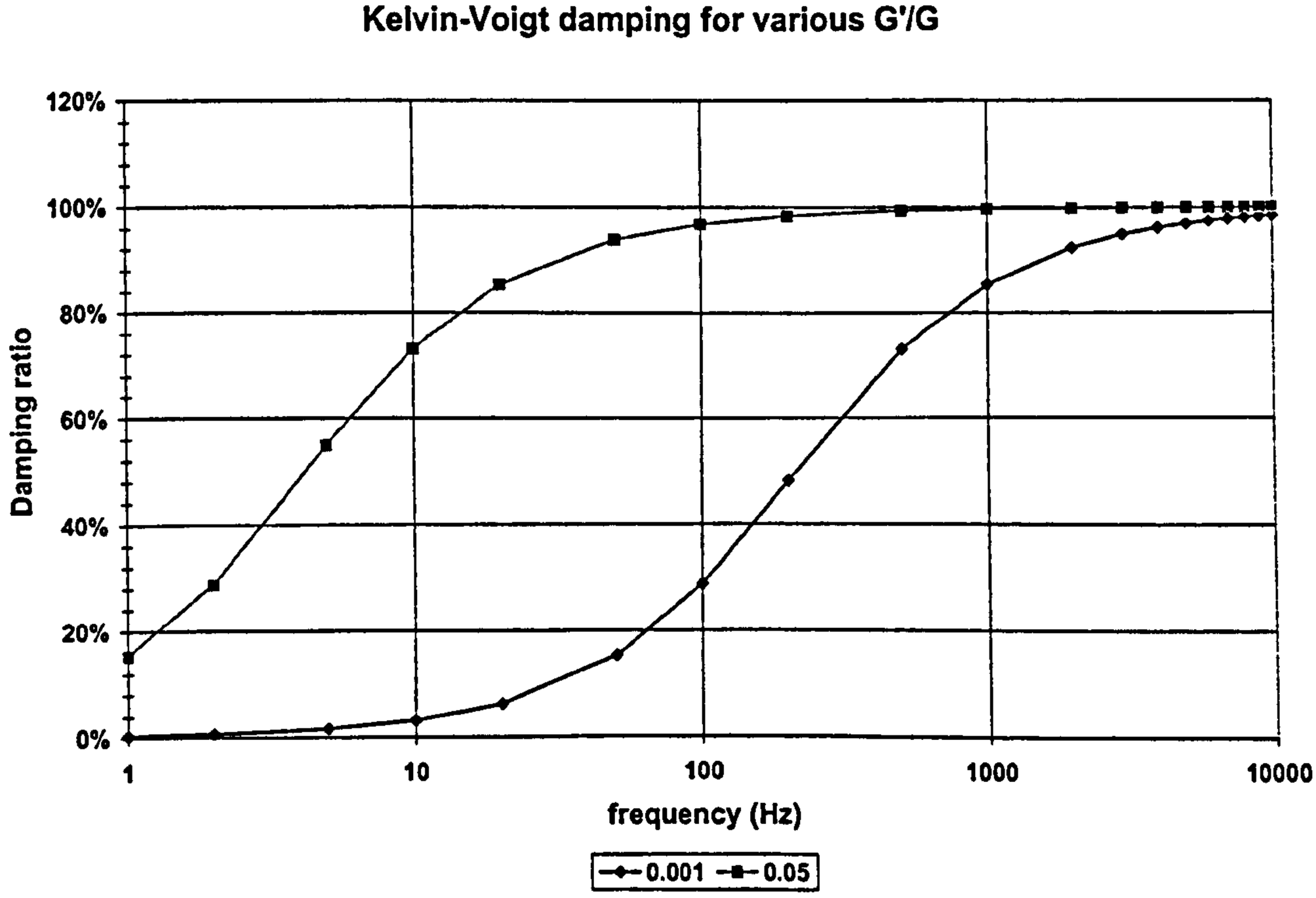

Figure 5-2 Effect of moduli ratio on the damping ratio of a Kelvin-Voigt material

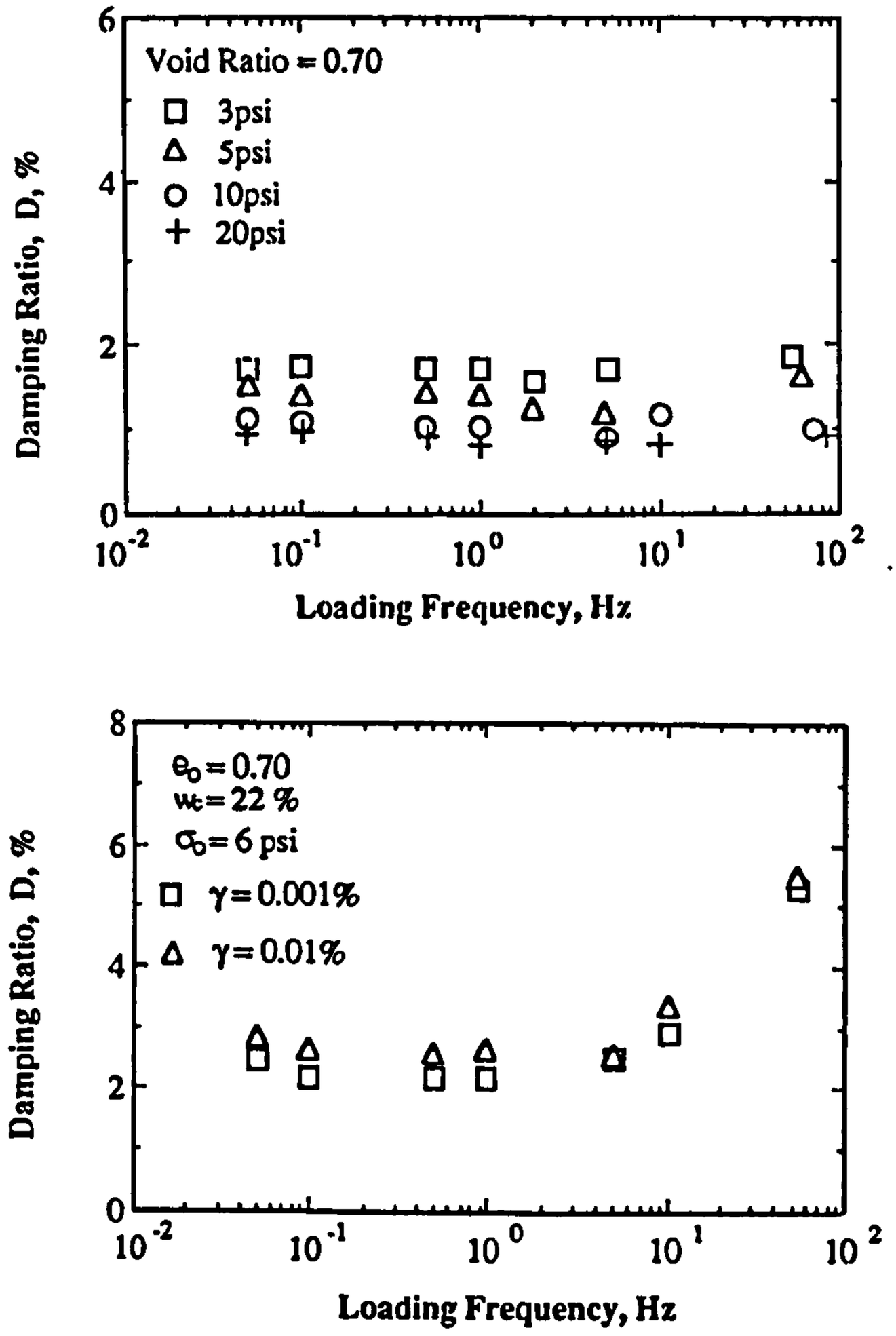

Figure 5-3 Damping vs frequency in dry sand (above) and clay (below). From Kim et al. (1991)

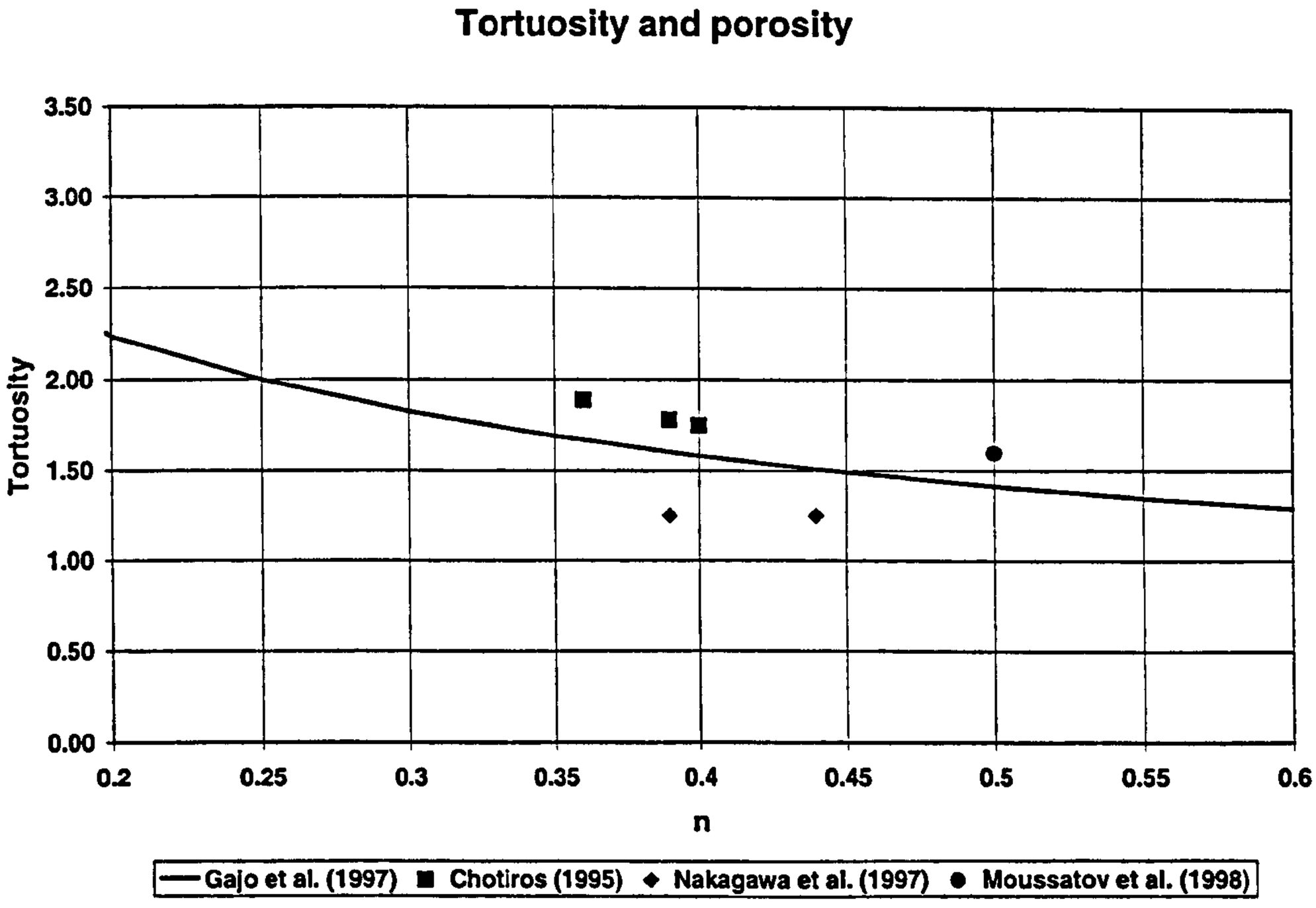

Figure 5-4 Gajo's relation between tortuosity and porosity and some sand results

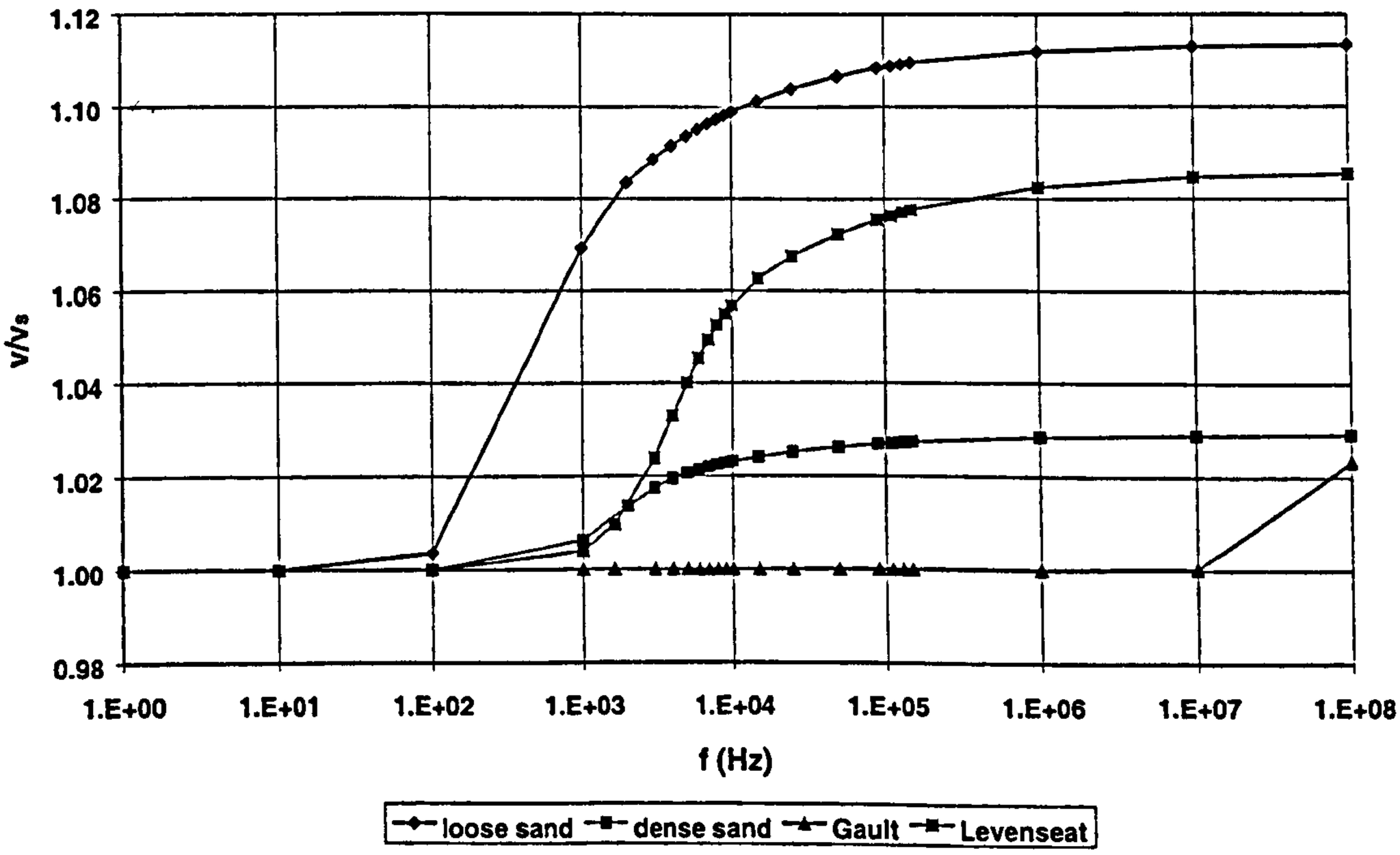

Figure 5-5 Normalised Biot shear dispersion curves of typical permeable soils, Levenseat sand and Gault clay.

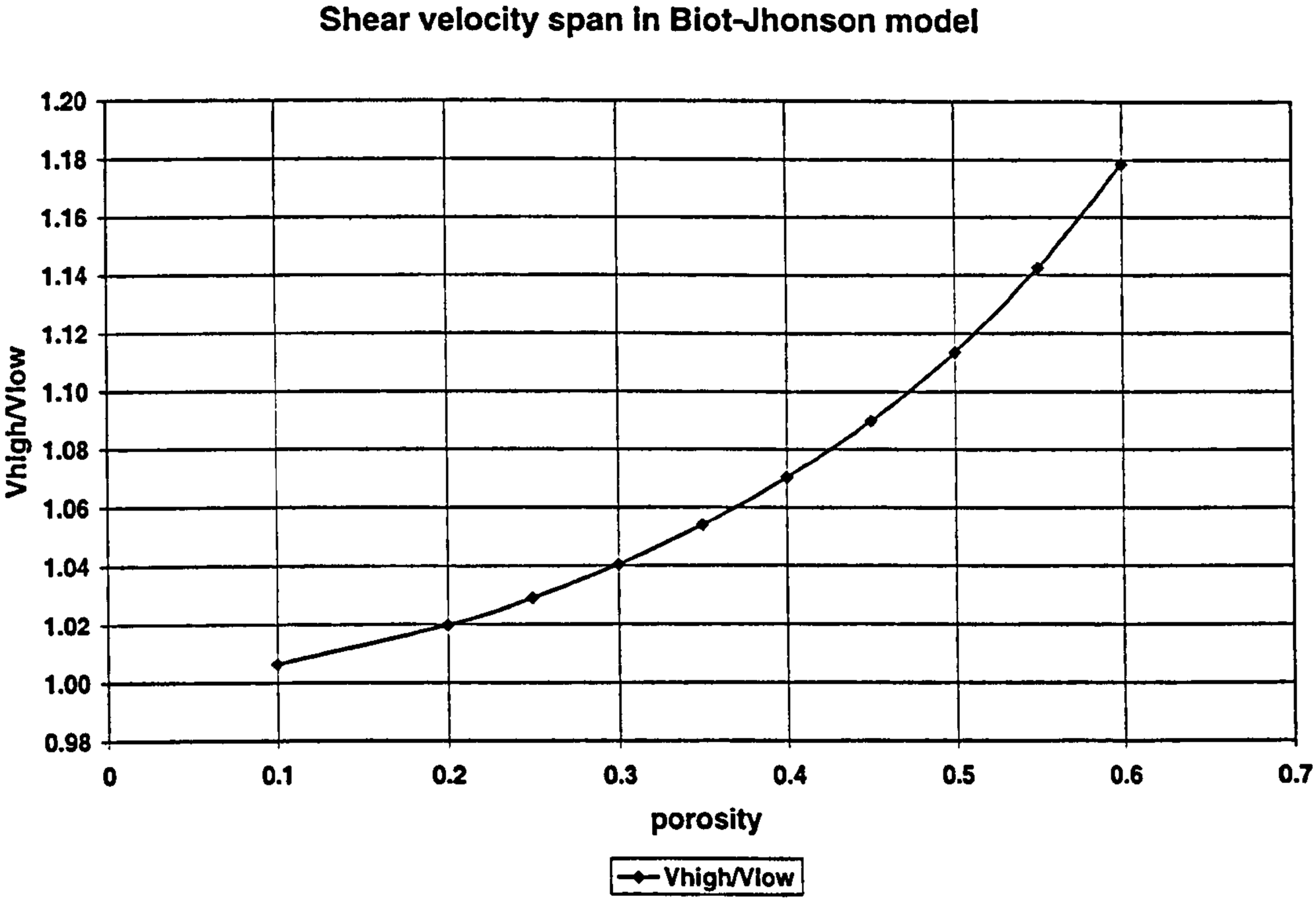

Figure 5-6 Ratio of high to low frequency Biot shear velocities as a function of porosity

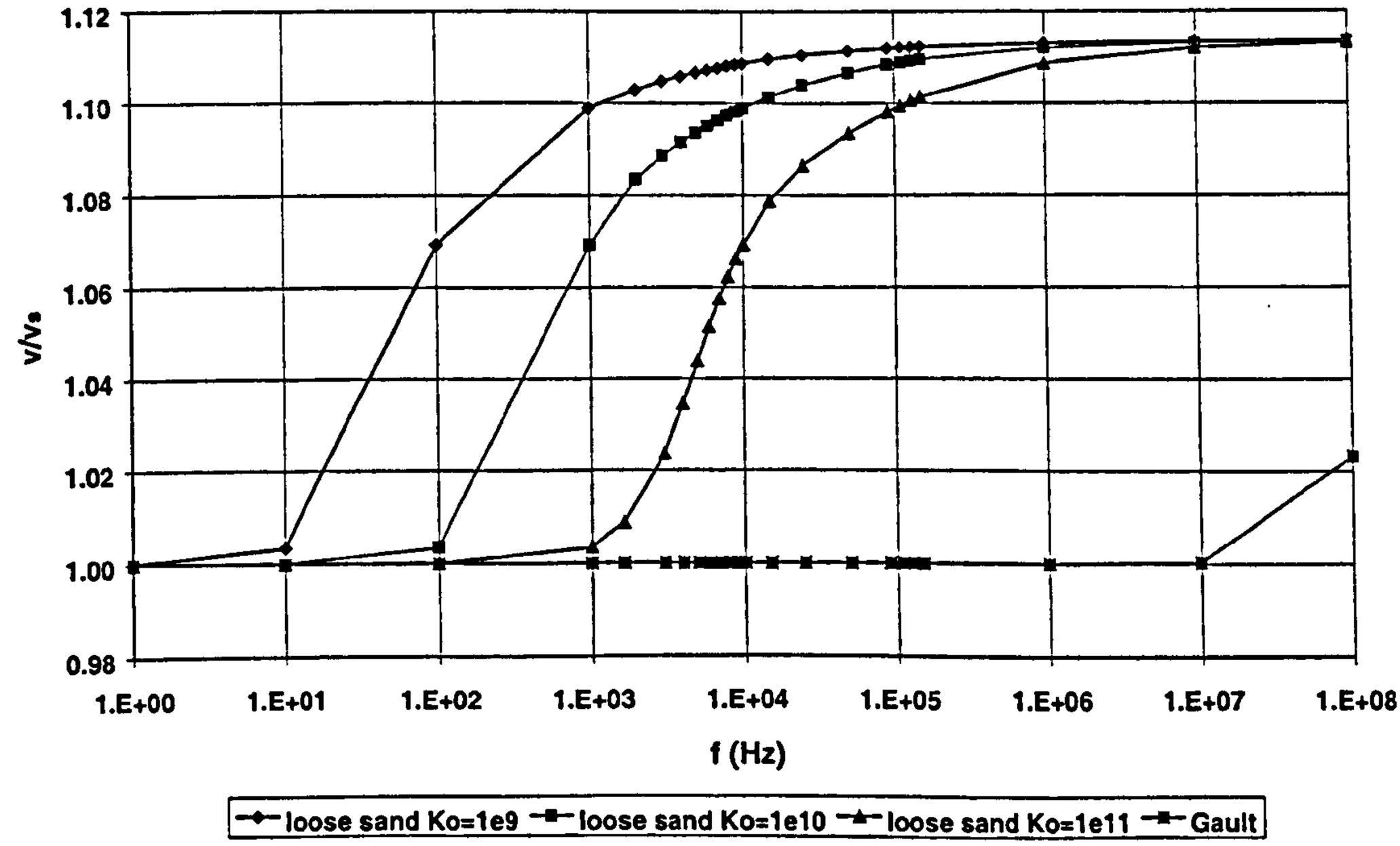

Figure 5-7 Influence of permeability in Biot shear dispersion. Ko in m^2.

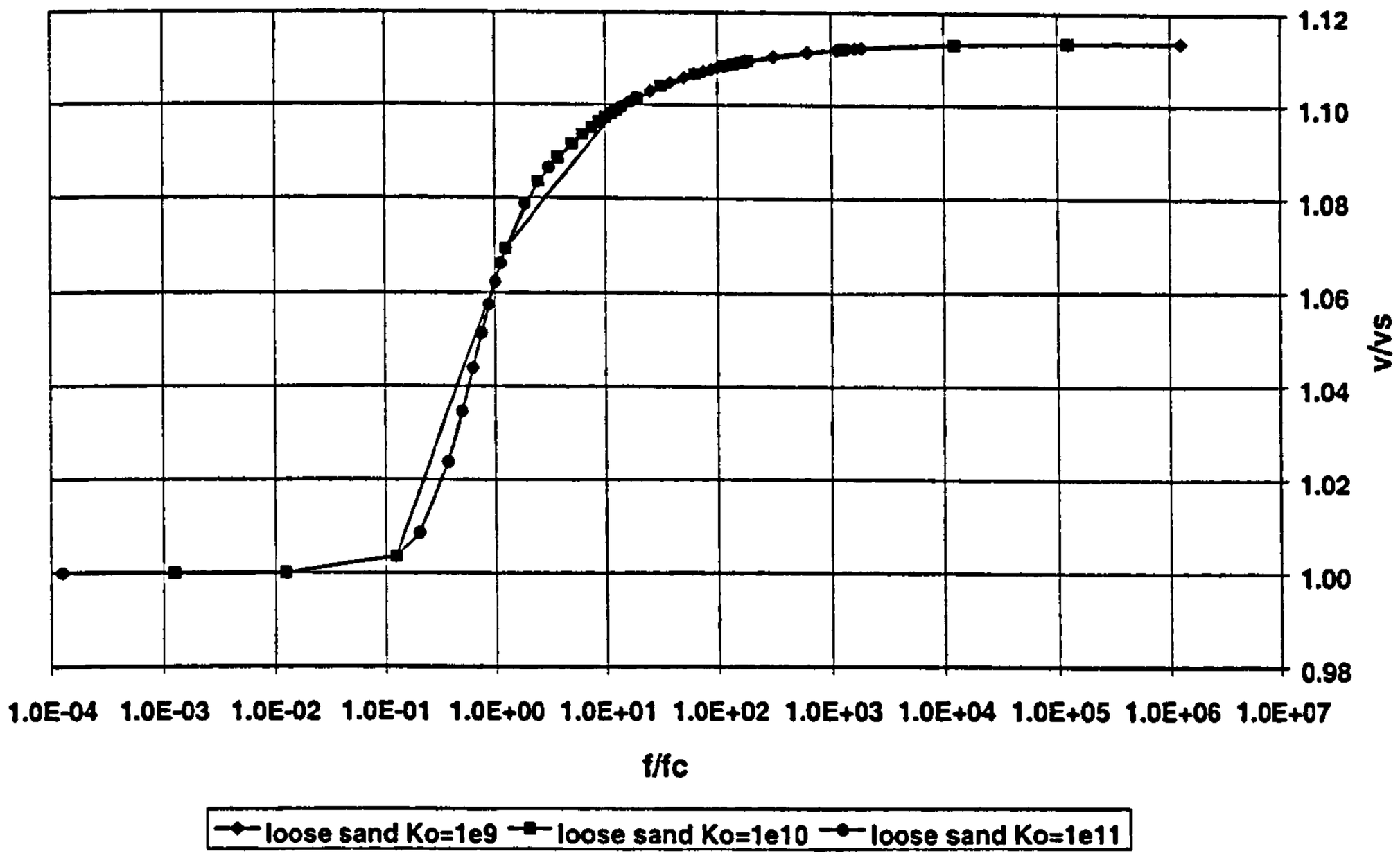

Figure 5-8 Normalised Biot shear dispersion curve

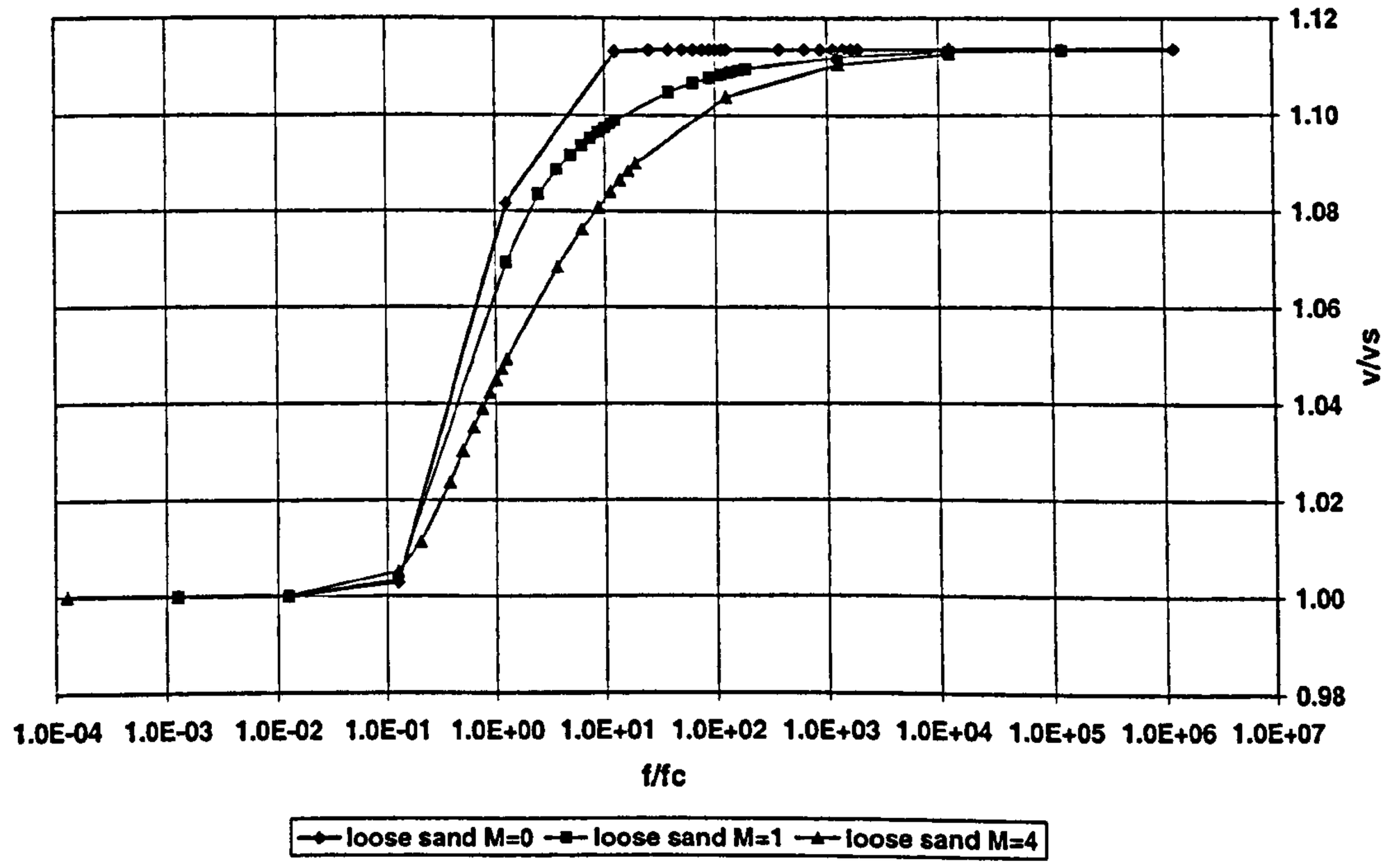

Figure 5-9 Influence of dynamically connected pore size in Biot shear dispersion

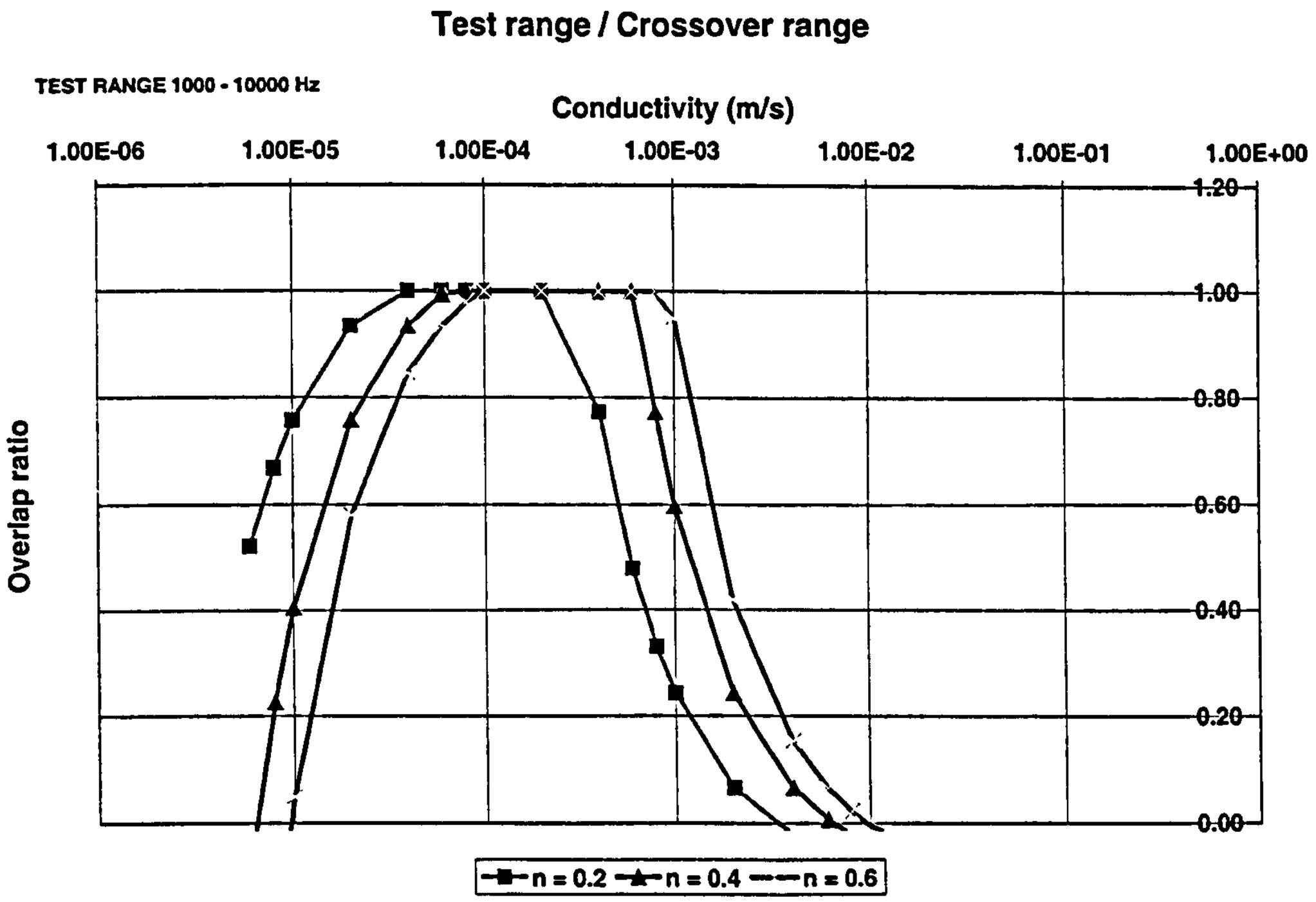

Figure 5-10 Overlap of bender frequency range and Biot crossover frequency range

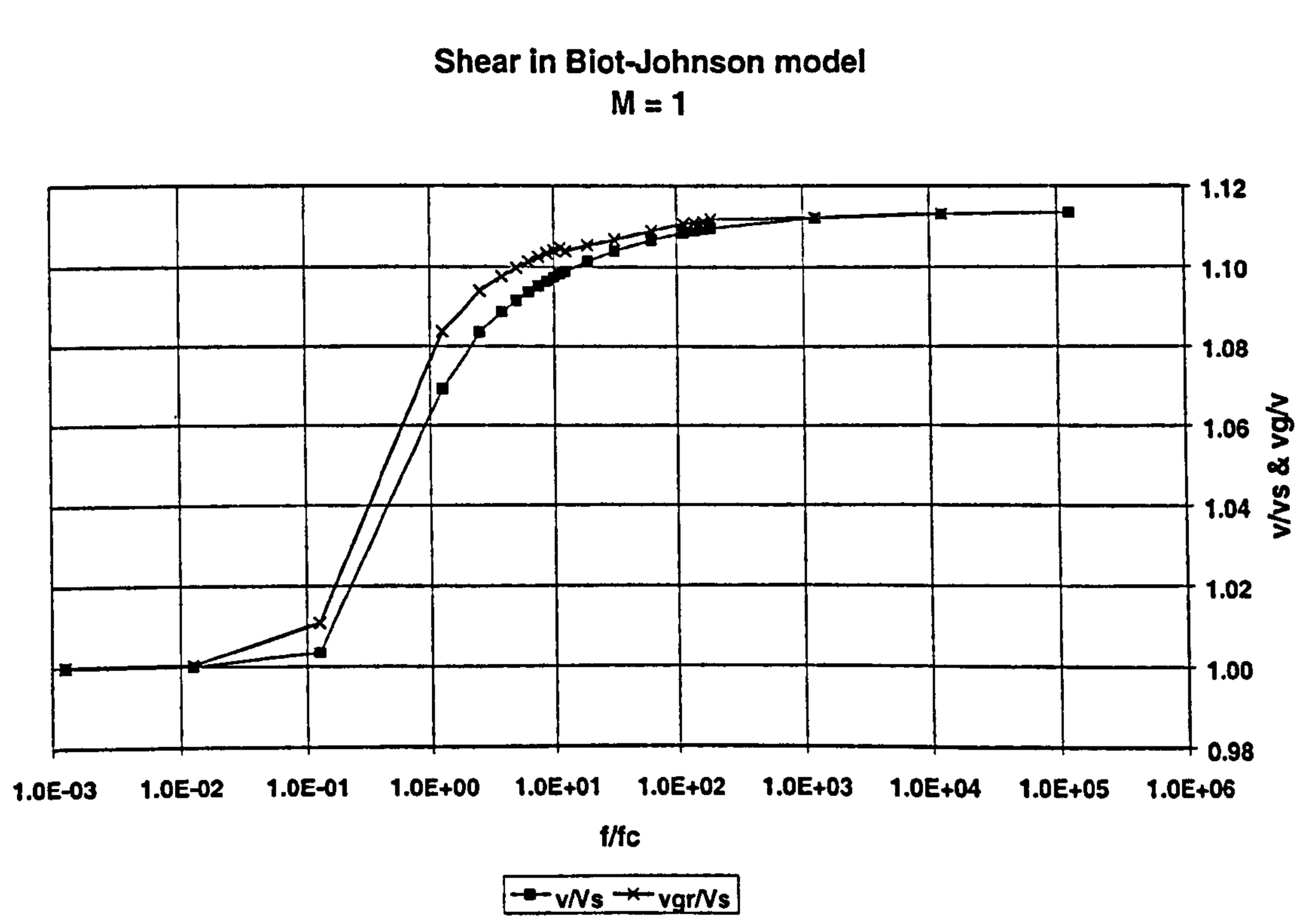

Figure 5-11 Normalised phase and group shear velocity

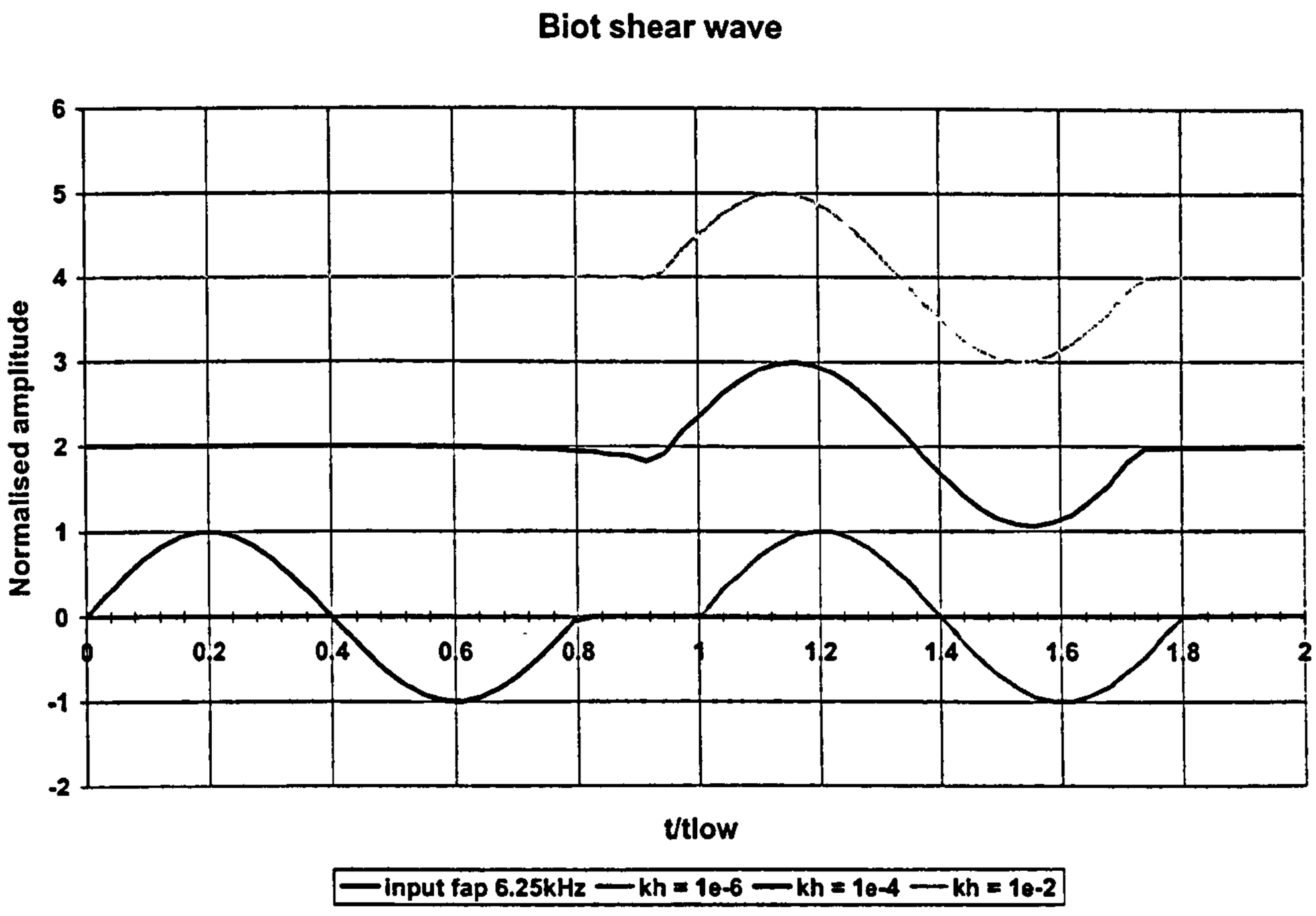

Figure 5-12 Time domain Biot shear propagation. M = 1, n = 0.4.

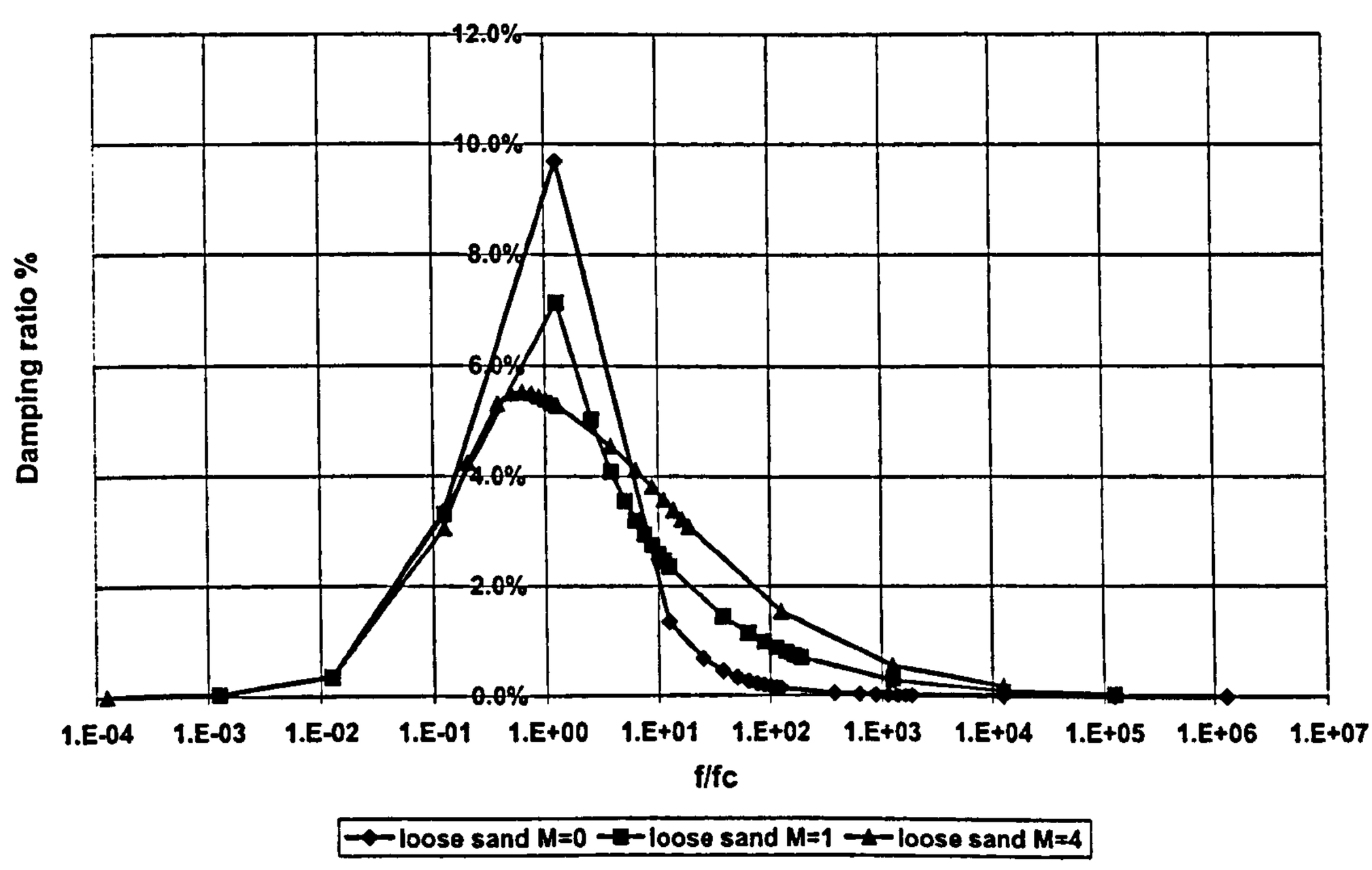

Figure 5-13 Biot shear damping ratio. Influence of dynamically connected pore size

6 ISOTROPIC GEOMETRIC DISPERSION

Up to this moment we have been faithful to a boundless interpretation of pulse testing. We have explored the consequences of being near the source and we have also considered alternative, richer, descriptions of soil elastic behaviour. But in both cases we have just considered the elastodynamic equilibrium equation without any reference to boundary conditions. We have remained in an agreeable, undefined, presumably vast, elastic body where the signal introduced by the source goes directly to the receiver. Looking again at Figure 2-6, chapter 2, we see that, although we don't accept anymore that the wavefront propagates as a neat, clearly defined line, the ideal, direct source-to-receiver path depicted there still lingers on.

The inadequacy of this free-space idealisation was already suggested in Chapter 2, when we compared the expected wavelength range of laboratory pulse tests with usual sample sizes. A considerable overlap was expected and, for instance, this is indeed the case for the Gault sample described in Chapter 3. An assumed vertical velocity of 120 m/s implies a wavelength range between 1.2 and 12 cm for the frequencies of interest –between say 1 and 10 kHz. This compares with a diameter of nearly 10 cm and length[67] varying between 9 and 19 cm. General principles of wave motion –Lighthill, 1978- would suggest already an important influence of sample size and shape on the motion. To study those effects further it is necessary to be more specific.

We will focus here on the particular sample shape used for the bench test series described in Chapter 3, that is a cylindrical unconfined sample whose slenderness –diameter to length ratio- varies between 1.9 and 0.9. This is less restrictive than it may first seem. Table 2-2collects information about sample size and shape in previous research. It is apparent that the cylinder has been the most common shape, which is logical considering the obvious benefits of using pre-existing equipment for pulse testing[68]. Excluding the "waveguide device" developed by Fratta & Santamarina, slenderness spans a range from 0.25 (Schultheiss, 1983) to nearly 6 (Jamiolkowski, 1995), with 2 being the most popular value.

We will first address end effects as those may still be treated within a 1-D propagation model, then we will move on to the more complicated models needed to take account of section shape effects.

6.1 END REBOUNDS AND INTERFERENCE

6.1.1 Introduction

The most common arrangement for pulse tests in soil samples has the transducers embedded on the top and bottom caps of a triaxial apparatus. Less frequent but –at least, in this respect- conceptually similar arrangements have benders placed vertically at the top and bottom ends of a hollow cylinder (e.g. Di Benedetto et al. 1999) or an oedometer (e.g. Zeng, 1999). In our bench test sample the situation is

---

[67] Note that this amount includes 1 cm at each side of bender length on top of the tip-to-tip distances quoted in chapter 3. This 1 cm is an estimate as probe penetration inside the sample was not controlled systematically on the experiments. At the time it did not appear to be important, as long as the tip-to-tip distance was known.

similar, the only difference being that the end walls are not confined but free. A simple modelling approach to these situations, introducing two end walls at the place of source –S- and receiver –R- is represented in Figure 6-1.

When an elastic wave arrives at a boundary between two elastic media part of the energy it carries is transmitted and part is reflected back. In the confined media depicted in Figure 6-1 this will happen at both ends, and therefore part of the signal from the source will reach the receiver again after being reflected twice. In the figure we have named the first arrival as A, and indicated front and back reflections through asterisks and apostrophes, respectively. Bouncing will happen again and again, and at the receiver we will have a sum of all successive reflections, or

$$O = A + A^{*'} + A^{*'*'} + A^{*'*'*'} \ldots\ldots \tag{95}$$

Explicit mention of reflections in soil pulse test traces can be traced back to Schultheiss (1983) who, called them "multiples", in analogy with similar phenomena in geophysical reflection surveys. Subsequently the problem did not seem to cause much concern until Arulnathan et al. (1998) made it central in their analytical study of bender element tests. This long lapse may be explained by a general proclivity to forget the dispersive character of the propagation.

When dispersion is not present the potential problem caused by reflections is relatively minor. A qualitative explanation of this is given in Figure 6-2. The upper diagram shows the first and second arrivals of a pulse in the non-dispersive case. T_{ap} is the apparent period –or duration- of the pulse and T_{rt} the time elapsed between the first and second arrival, or round-trip time. A non-overlap condition for those two arrivals can be written as

$$\frac{T_{ap}}{T_{rt}} < 1 \tag{96}$$

For a plane shear wave in the ideal conditions of Figure 6-1 this is easily translated as a relationship between the apparent wavelength and sample length

$$\frac{v_s}{2Hf_{ap}} = \frac{\lambda_{ap}}{2H} < 1 \tag{97}$$

As illustrated in Figure 6-3 this relation is not very exigent. H =10 cm and f_{ap}=5kHz will be enough except for the stiffer soils; for the case of our Gault sample all the single pulse tests described in Chapter 3 are above the 100 m/s line. With the notable exception of those who use square slow pulses –the "step" loading- most practitioners have abided by this rule –see Table 2-2- even if unconsciously. Besides, if dispersion is excluded then there is no need to worry excessively about any possible overlap, as the first arrival will never be affected.

---

[68] Interesting exceptions are the "oedometers" used by Jamiolkowski et al. (1995), whose only similitude with the conventional apparatus is the presence of rigid side walls.

Add in dispersion and the overlap problem becomes not only more acute but also more important. Back to Figure 6-2 and the lower diagram shows why overlap is increasingly possible. To a first approximation each frequency in a pulse will travel at a different group velocity, spreading the pulse in the time axis as the travel distance increases. There is a clear possibility for the fastest travelling frequencies in the second arrival to overtake the slowest in the direct signal. Within the frequency range spanned by the pulse group velocity will itself range between, say, V_{max} and V_{min}, and the overlap condition can now be written as

$$T_{ap} + \frac{H}{V_{min}} < \frac{3H}{V_{max}} \tag{98}$$

this can be rearranged to write

$$\frac{V_{max}}{Hf_{ap}} = \frac{\lambda_{max}}{H} < 3 - \frac{V_{max}}{V_{min}} \tag{99}$$

As it should, when $V_{max} = V_{min}$ we recover the non-dispersive case (97). It is clear that as the span in group velocity increases overlap becomes more possible. As an illustration Figure 6-4 represents (5) for a group velocity ratio of 2.5 and a range of V_{max} similar to that in Figure 6-3; now the non-overlap testing limit looks distinctly less comfortable than before. In fact, when the ratio of maximum to minimum group velocity is 3 or more, overlap will happen whatever the apparent frequency or sample height.

A consequence of the previous argument is that the Biot shear dispersion explored in Chapter 5 is generally not enough to produce interference. Considering Figure 5-6 there it appears that the ratio of maximum to minimum group velocity will remain below 1.2. This will leave room enough for most current tests to proceed in the non-overlap range. Another dispersion cause is needed for interference to be a problem.

In the dispersive case the possibility of overlap is also more worrying. When dispersion takes place the first absolute arrival is not anymore the only important result; instead, the complete dispersion curve will generally be sought after. The cross-spectrum technique described in chapter 4 will not work as intended, as the distance travelled by the mixed signal cannot be assigned with certainty –see equation (54).

As we mentioned before most geotechnical research has ignored the possibility of overlap interference. Arulnathan et al (1998) did not ignore it although they did ignore the extra problem caused by dispersion. Hence they insisted on time domain methods and used cross-correlation between first and second arrivals. To distinguish both in the trace some arbitrary limit was specified as end of the first arrival. That may well be applied to the cross-spectrum procedure, but the rationale for doing that is dubious as the transform of the arbitrarily selected arrival will be different from that of the assumed non-interfered signal. Although other factors come into play, this limitation partly explains the ambiguous results obtained by Arulnathan et al.

Fortunately, reflection interference is not a problem exclusive to geotechnical testing. It is prominent in exploration seismology, and has since long received considerable attention –Silvia & Robinson, 1979. More recently -Pialucha et al. 1989-it has also been studied in ultrasonic testing as it affects tests in thin layers, like adhesives. Inspired by this work we propose a new approach in the following section.

6.1.2 End reflections and transfer functions

It is interesting to recast the reflection interference phenomenon using the language of linear systems. Figure 6-5 does this, relating the input signal at the source, I, with the first arrival, A, the first rebound, A' and the second arrival, A'^*. The subsystems indicated are of two kinds. Wave propagation trough the sample, forwards and backwards, is represented by W^+ and W^-, respectively. Rebound is represented by B' and B^* at the receiver and source wall, respectively. Using those symbols now to represent the unit response of each subsystem we can, for instance, rewrite the first three terms as

$$\begin{aligned} A &= I * W^+ \\ A'^* &= I * W^+ * B'^* W^- * B^* * W^+ \\ A'^*'^* &= I * W^+ * B'^* W^- * B^* * W^+ * B'^* W^- * B^* * W^+ \end{aligned} \tag{100}$$

Substituting convolution for multiplication and unit response for transfer function the same equations would hold in the frequency domain. But the frequency domain representation has here one important advantage, appreciable when considering the total output

$$\begin{aligned} O &= A + A'^* + A'^*'^* + A'^*'^*'^* .... \\ &= A + AB'W^-B^*W^+ + A\left(B'W^-B^*W^+\right)^2 + ... \\ &= A\left(1 + B'W^-B^*W^+ + \left(B'W^-B^*W^+\right)^2 + ...\right) \end{aligned} \tag{101}$$

Transfer functions are just frequency-dependent complex numbers. Using the shortcut $S=B'W^-B^*W^+$ the output might be written –and summed- as a geometrical series

$$O = A\left(1 + S + S^2 + S^3 + ...\right) = \frac{A}{1-S} = I\frac{W^+}{1-S} \tag{102}$$

And a rather simple expression has been obtained for the complete system transfer function. It is well-known –e.g. Needham, 1997- that the sum is only valid when the modulus of S is less than 1. To see that this is true in our case it is necessary to specify more the subsystem transfer functions that form S.

Elastic rebound of plane waves at plane boundaries is usually dealt with using the so called transmission and reflection coefficients. These generally depend on the type of incident wave and angle of incidence – see, for instance, Udías, 2000. For the case of plane shear waves at normal incidence Miklowitz (1978) gives the following transmission and reflection coefficients

$$\begin{aligned} R &= \frac{Z_1 - Z_2}{Z_1 + Z_2} \qquad T = \frac{2Z_1}{Z_1 + Z_2} \\ Z_1 &= \rho_1 v_1 \qquad Z_2 = \rho_2 v_2 \end{aligned} \tag{103}$$

The quantities Z_i are the characteristic impedances of the two media. Impedance is a common concept in wave problems, representing a ratio between forcing and flow variables –Blackstock, 2000. For the case of shear waves those variables may be identified with the shear stress and particle velocity. With this in mind, the expression given by Miklowitz for elastic media may be easily generalised to other material descriptions –Biot poroelastic, for instance- using as impedance

$$Z_i^{\pm} = \mp \frac{k_i G_i}{\omega} \tag{104}$$

Where k_i represents the wavenumber of the medium and the sign depends on the forward or backward propagating character of the incident wave. This will make the impedance complex and frequency dependent.

To write the propagation transfer functions W^+ and W^- we need now to recall that plane wave solutions of wave propagation always come in pairs, forward and backward travelling[69]. Then, in general, we will write the x-dependent transfer function for waves originating at x_0 as

$$\begin{aligned} W^+(x,x_0) &= e^{-ik(x-x_0)} \\ W^-(x,x_0) &= e^{ik(x-x_0)} \end{aligned} \tag{105}$$

The wavenumber k in these expressions might be linear or non-linear in frequency, in other words non-dispersive or dispersive. In general it may be also complex or real, that is the propagation might be attenuating or not. The latter case is not realistic but might be adequate when most losses are due to transmission at the ends. When the ends are free or completely rigid there is no transmission and attenuating propagation is necessary for the series in (102) to converge.

6.1.3 Sample length effect

As a first example of this approach we address now the case depicted in Figure 6-1 where source and receiver are located at the sample ends. We also assume that both ends are similar and both either free or completely rigid. In that case the reflection coefficient is obtained from (103) with Z_2 either zero or infinite, resulting in R of either 1 or –1. We can then write the transfer function of the first arrival A and that of the rebound cycle S as follows

$$\begin{aligned} A &= I\,W^+(H,0) = I\,e^{-ikH} \\ S &= B^*W^-(0,H)B'W^+(H,0) = e^{ik(-H)}e^{-ikH} = e^{-i2kH} \end{aligned} \tag{106}$$

The sum in equation (102) is then given by

$$O = I\,F_H = I\frac{e^{-ikH}}{1-e^{-i2kH}} \tag{107}$$

---

[69] This may be appreciated for instance in the Kelvin-Christoffel equation we employed in chapter 1, where the eigenvalues were identified with the squared phase velocity, v^2. Also in the previous chapter we expressed the plane wave solution for a Kelvin-Voigt material in terms of a squared wavenumber. In both cases the positive root corresponds to a forward propagating wave, the negative to a backward propagating one.

Substituting the appropriate wavenumber in the second term we have a transfer function F_H that directly includes the effect of all end rebounds. It is interesting to explore it for the simple case of hysteretic –i.e. frequency independent- damping. In that case we can write the modulus, M_H, and phase, θ_H, of the transfer function above as follows

$$M_H = \frac{Q}{\sqrt{1-2Q^2\cos(4\pi n_H)+Q^4}}$$
$$\theta_H = arctan\left(\frac{Q^3+Q}{Q^3-Q}tan(2\pi n_H)\right) \qquad (108)$$

where we have introduced the normalised sample length n_H and the attenuation factor Q, related to the wavenumber real and imaginary parts through

$$Q = e^{-Hk_i} = e^{-2\pi D n_H}$$
$$n_H = \frac{Hk_r}{2\pi} = \frac{H}{\lambda} = \frac{Hf}{v} \qquad (109)$$

We have plotted M_H against the normalised sample length in Figure 6-6 for a damping coefficient D of 2%, typical, as we know, of soils below the Biot cross-over range. In the logarithmic scale employed the hysteretic damping of the first arrival plots as a straight line. The reflection series shows a clear interference pattern, where maxima and minima are given by

$$max(M_H) \Leftrightarrow n_H = 0, \frac{1}{2}, 1, \frac{3}{2}.....$$
$$min(M_H) \Leftrightarrow n_H = \frac{1}{4}, \frac{3}{4}, \frac{5}{4}..... \qquad (110)$$

This is the key to the amplitude spectrum method of phase velocity measurement proposed by Pialucha et al. (1989). When a series of reflections cannot be separated in time domain the frequency spectra of the complete record can still be employed to measure the phase velocity. For a known sample height, identifying the frequency and order of the extrema gives discrete measurements of phase velocity. In the normalised scale of Figure 6-6 the extrema of the transfer function are equally spaced. Phase velocity can be seen as a transformation from this axis to that of frequency. If the propagation is non-dispersive the extrema will also be equally spaced on the frequency axis, if dispersion is present, their spacing will reveal its character.

Interference makes the amplitude spectra meaningful, as not only attenuation, but also phase velocity can be read on it; on the other hand it makes the phase almost unintelligible. Figure 6-7 represents the wrapped phase of the first arrival along with θ_H. The added curvature between phase jumps at low n_H is due to the Q-dependent factor in θ_H. If the cross-spectrum method described in Chapter 4 is applied to an interfered signal as if it was a first arrival –that is, obtaining the wavenumber as the ratio between phase and H- this curvature will introduce a spurious fluctuation around the theoretical phase velocity. It will

also make very hard any numerical attempt to unwrap it, as contiguous samples on the very steep segments will be taken for jumps.

Is interesting to look now again at some bench test traces. End interference will be most clearly observed for the shortest samples; wide-band single-cycle signals are also interesting as they explore a larger range of the spectra. Figure 6-8 corresponds to a test –96- with a single sine with f_{ap} 4000 Hz travelling on a sample of circa 9 cm. The first arrival occurs near 0.5 ms, and by itself this suggest that, at least, part of what arrives after 1.5 ms has been already through a round-trip of the sample. In fact the record goes up to 3 ms, enough to add another reflection. Interestingly, the arrival time estimated by cross-correlation or cross-spectrum, circa 1 ms, will exclude any significant interference.

The amplitude ratio of the input signal and the whole output record is an estimate[70] of the soil transfer function. For test 96 the result of this operation appears on Figure 6-9. There are indeed a number of extrema, quite irregularly distributed on the frequency axis, which is an indication –another- of dispersive propagation. It is clear, however, that the gradual attenuation predicted in Figure 6-6 is not present. It is true that above 10 kHz the magnitude of the extrema may be dominated by noise in the signal; but even below that range there is no clear attenuation pattern in the spectra. This impression is reinforced by Figure 6-10 where we have plotted together the spectral ratios of tests 93 and 96. Test 93 was performed under similar conditions –H, f_{ap}- as test 96, only the input signal was square. Instead of some gentle decline of the spectral extrema, they show rather some kind of mean undulation spiked with local extrema. We are fortunate to have a possible explanation for this characteristic.

6.1.4 Bender length effect

We have commented in previous chapters that a commonly accepted criterion in bender element testing interpretation is to take as the distance of wave travel that between source and receiver tips. In a triaxial sample tested along the vertical axis this will place the ideal source and receiver at a certain distance from the top and bottom ends –see Figure 6-11.

Arulnathan et al. (1998) were quick to indicate that if the tip is taken as the source one should expect that both forward and backward plane waves would be generated within the soil sample. This is interesting but it is even more so when the effect of the end walls is introduced in the model. As indicated in Figure 6-12, four different kinds of path between source and receiver are now possible. Their degree of overlap would not be anymore a simple function of the sample length, but also of the distance between the bender tip and the wall, l_b

As shown in Appendix III, this problem is easily framed in the same scheme as before. The sum that includes the effect of rebounds and bender length is there shown to be

---

[70] This assumes that instrumental effects at source and receiver cancel out.

$$O = I\frac{e^{-ikH}}{1-e^{-i2kH}}\frac{\{\cos(2kl_b)+1\}}{2} = I\,F_H F_{LB} \tag{111}$$

Where is clear that the joint transfer function is now the product of a sample length dependent term, F_H and a bender length dependent term, F_{LB}. For the simple case of hysteretically damped propagation the modulus and phase of the newly introduced term can be written as

$$M_{LB} = \frac{\cos(4\pi n_H n_{LB})+\sinh(4\pi D n_H n_{LB})}{2}$$
$$\theta_{LB} = arctan\left(\frac{\sin(4\pi n_H n_{LB})\sinh(4\pi D n_H n_{LB})}{1+\cos(4\pi n_H n_{LB})\cosh(4\pi D n_H n_{LB})}\right) \tag{112}$$

where a new adimensional ratio has been introduced, n_{LB}, defined as the ratio of bender length, l_B to sample height H. The new term does add some extra complications to the phase, in the form of more spurious jumps. However it is the modifications on the amplitude spectra that are of more practical interest. Figure 6-13 represents the product $M_H M_{FB}$ for a damping ratio of 2% and various n_{LB} ratios. The effect is quite considerable. It can be seen that the term M_{FB} introduces a longer oscillation, modulating the interference pattern given by M_H. Global extrema correspond to extrema of M_{FB} and they happen at greater n_H as the n_{LB} ratio decreases.

This may be confirmed by the results shown in Figure 6-14, where the spectral ratio has been plotted for test 96 and test 22. We do not know the n_H scale, as the phase velocity is not known, but assuming that it remains the same for both tests, we have used the product height per frequency as substitute. Test 22 was performed on the largest sample, and n_{LB} was about a half that of test 96. It can be seen that, as predicted, the global extrema of the spectral ratio –indicated with arrows- are shifted backwards as the sample shortens. This phenomena is less clear at low n_H but at low frequencies the signals are masked by noise.

One conclusion is firm at this stage. End rebounds can disguise themselves as dispersion in the phase, but, for non dispersive propagation they offer a regular magnitude pattern. In our bench test the pattern is completely irregular, indicating, again, the presence of dispersive propagation. We have still to find the source of these irregularities and this is the subject of the next section.

6.2 WAVEGUIDE EFFECTS

6.2.1 Introduction

The term waveguide is used to describe situations where a wave is propagated in structures, like rods, plates or geological strata, whose shape directs the motion along a favoured dimension of the structure – for instance the length of a rod or the plane of the strata. When this dimension is assumed infinite the situation is amenable to mathematical analysis and constitutes a good model of how the propagation is affected by the sectional characteristics of the structure. We will use this approach to explore the effects of the radial dimension when propagating along the axis of cylindrical soil samples.

In our bench test series the fact that the propagated wave interacts with the sample lateral boundaries was rather obvious. As we were able to register the movement originating from an axially placed probe with receivers placed on the lateral perimeter of the sample –see Figure 3-2-, the radiated wave should indeed reach these boundaries. This issue is often dealt with in the ultrasonics testing literature under the heading of probe directionality (e.g. Krautkramer & Krautkramer, 1990). Although, as we have already remarked, bender probes are not very similar in their operation to the radiating piston model commonly used for external probes, we can still gain some insight considering the directional characteristics of the latter.

For the plane piston model the aperture of the radiating sound beam is directly related to the ratio between wavelength and a characteristic dimension of the transducer face (Krautkramer & Krautkramer, 1990). For the simple but important case of circular transducer and isotropic medium Mason (1958) gives the following relation for the beam angle:

$$sin\beta = 1.22\frac{\lambda}{D} \tag{113}$$

which shows that for wavelengths bigger than 0.82 D there is no beam effect whatsoever and the transducer radiates a hemispherical field into the sample.

If we consider now bender probes and their movement it is perhaps reasonable to identify either the element thickness, t, or its width, w, as the characteristic dimension of the diffracting aperture. The original bender elements were more sturdy, but they have grow thinner. Looking at Table 2-1, it will appear that for most designs employed all the energy contained in wavelengths above a few mm will not be beamed at all. As we have seen, this wavelength is below what is currently used in most soil pulse testing –Figure 2-3- and even below what, on account of scattering, would be possible to transmit in granular soils[71].

6.2.2 Guided waves in cylinders: modes and modal decomposition

Cylindrical structures are one of the most important cases of waveguide –think of rods and bars for the mechanical case, circular ducts for fluids or optic fibre cables- and they have received considerable attention –Graff, 1975, Miklowitz, 1978- partly prompted by their use as delay lines in communication systems -Thurston, 1978, 1992- but also for their implications regarding ultrasonic test procedures – Meeker and Meitzler, 1963.

Adopting a system of cylindrical coordinates, guided waves in this case can be synthetically expressed as motions given by

$$\mathbf{u}(r,\theta,z,t) = \mathbf{A}(r,\theta)\cos[\omega t - kz] \tag{114}$$

---

[71] Huot (1999) discusses this problem for P-waves and triaxial samples and arrives at a similar conclusion. Note that his arrangement for P-waves is more favourable, as the frequencies are two orders of magnitude higher than for benders (100 – 400 kHz) but the measured velocity is only about one order of magnitude higher than shear velocity.

where the first term describes the shape of the movement within the circular section of the cylinder and the second term how this shape propagates along the cylinder axis with a phase velocity given by

$$v(\omega) = \frac{\omega}{k(\omega)} \tag{115}$$

Generally, the phase velocity is frequency dependent and, therefore, propagation is dispersive. For given sectional characteristics and boundary conditions there are infinite motions like (114) satisfying the elastodynamic homogeneous equilibrium equation in a rod. Each of these motions is usually termed a mode, M_{mn}, and is characterised by its modal shape A_{nm} and modal dispersion curve $k_{nm}(\omega)$. In general the modal shape might also be wavenumber dependent and therefore we have

$$\mathbf{M}_{mn}(r,\theta,z,t) = \mathbf{A}_{nm}(r,\theta,k_{nm})\cos[\omega t - k_{nm}z] \tag{116}$$

Again, the assumed linearity of the problem is here very useful. The modal functions of a waveguide form an orthogonal functional base for the problem. This means –Lighthill, 1978- that a propagating solution corresponding to some loading **f** can be expressed as a linear combination of all modes

$$\mathbf{u}(r,\theta,z,t) = C_{mn}\,\mathbf{M}_{mn}(r,\theta,z,t) \tag{117}$$

and the weighting coefficient for each mode, C_{mn}, is formally given by

$$C_{mn} = \frac{\langle \mathbf{M}_{mn}, \mathbf{f} \rangle}{\langle \mathbf{M}_{mn}, \mathbf{M}_{mn} \rangle} \tag{118}$$

Where the brackets indicate a suitably defined functional inner product. The definition of this inner product is based on elastic reciprocity (Auld, 1973; McKenna & Simpkins, 1985) and is best written in the frequency domain

$$\begin{aligned} \langle \overline{\mathbf{M}}_{mn}, \overline{\mathbf{M}}_{mn} \rangle &= \int_S \left[\bar{\mathbf{u}}_{mn} \bar{\mathbf{t}}^{*}_{zmn} - \bar{\mathbf{u}}^{*}_{mn} \bar{\mathbf{t}}_{zmn} \right] dS \\ \langle \overline{\mathbf{M}}_{mn}, \bar{\mathbf{f}} \rangle &= \int_S \bar{\mathbf{u}}^{*}_{mn} \bar{\mathbf{f}}\, dS \end{aligned} \tag{119}$$

The bars indicate a transformed variable and the asterisks conjugation, $\mathbf{t}_{zmn}$ is the traction vector in a section induced by mode mn and S indicates the section of the waveguide. For any given frequency the modal coefficient is proportional to the spatial correlation along the cylinder section of the applied load and the modal shape. In other words, at any given frequency the propagating modes induced by some loading will be those whose shape is more akin to the load shape[72].

6.2.3 Guided waves in cylinders: mode typology

We need then to examine the modal characteristics relevant to our problem. Even for the simplest case of a homogeneous isotropic bar in free space the process of obtaining the modal characteristics -dispersion curve and modal shape- is rather involved, as the relevant functional base is expressed in terms of

---

[72] The loading considered here is applied within the guide, not at the boundaries, where other relations hold. Also, the loading is assumed to be concentrated at some fixed z, i.e. its variations along the guide are ignored.

transcendental Bessel functions. Its evaluation for a given problem –known material constants and bar diameter- necessarily resorts to numerical procedures. This has prompted the development of dedicated programs and here we will use Disperse, a program developed at Imperial College –Pavlakovic & Lowe, 2000- with ultrasonic testing applications in mind. Although some results for a cylindrical waveguide are available in the literature –e.g. Thurston 1978, 1992- and might have been applied directly, using Disperse offers a much wider range of results.

Disperse was then used to explore the modal characteristics of a problem tailored to approximate the Gault clay sample employed in chapter 3, that is a cylinder of an isotropic elastic material whose shear velocity is set to 120 m/s and whose Poisson ratio to[73] 0.1. To suit the usual range of operation of the program and avoid numerical problems lengths and frequencies were scaled by a factor of 100, hence a cylinder of radius 0.5 mm represented the 5 cm sample radius and 0.1MHz in the program output is equivalent to 1kHz in the sample; velocities being the product of length and frequency, they are not affected by the scaling[74]. This ideal Gault cylinder will produce all the results shown in this and next section.

The indexes n and m appearing in (6) serve to classify the modes according to general features of the movement they describe. For solid cylinders there are three mode categories: longitudinal, torsional, and flexural. This nomenclature is best understood if we write the mode solutions as follows

$$\begin{aligned} u_r &= g_1(r,k_{nm})e^{in\theta}\,e^{-i(\omega t-k_{nm}z)} \\ u_\theta &= g_2(r,k_{nm})e^{in\theta}\,e^{-i(\omega t-k_{nm}z)} \\ u_z &= g_3(r,k_{nm})e^{in\theta}\,e^{-i(\omega t-k_{nm}z)} \end{aligned} \qquad (120)$$

Torsional modes, T(0,m), are modes where $n = g_1 = g_3 = 0$, so the movement is independent of the angle and only its angular component is non-zero. They have the simple feature of a frequency-independent modal shape, where the m index indicates the number of counter-rotating sections found along a radius. This feature is illustrated in Figure 6-15 where the angular displacement is plotted as a function of radius. In the fundamental mode T(0,1) the whole section rotates in the same direction. As it happens, this is the basic assumption of the elementary theory of torsional vibration in a rod. A well-known consequence of that theory –e.g. Kramer, 1996- is that torsional waves propagate without dispersion at the shear bulk velocity. This is indeed the case of the first torsional mode, T(0,1), which is the only non-dispersive mode.

Higher order modes are dispersive and do not propagate at all frequencies. Figure 6-16 presents the dispersion curves of torsional modes obtained by Disperse. The phase velocity has an asymptote at a frequency characteristic of each mode, the cut-off frequency f_{cut}. It is apparent that their shape is

---

[73] Although Pennington (1999) measured 0 this value caused numerical problems. The effect of this change is the modal characteristics is minor.

[74] Phase velocity is not scaled, but for some reason the group velocity plots are also scaled

relatively simple and that some scaling looks possible. This is indeed the case and Thurston –1978, 1992- shows that these curves can be written as hyperbolae in v-f space

$$\left(\frac{v_s}{v}\right)^2+\left(\frac{f_{cut}}{f}\right)^2=1 \qquad (121)$$

Longitudinal modes, L(0,m), are motions where n =g_2= 0 and, therefore, have no angular displacement and radial and axial displacements are θ-independent or axisymmetric. Figure 6-17 illustrates the r-z section of the modal shapes for L(0,1) and L(0,2) at low and high frequencies. There is no available explicit form for their dispersion curve but Figure 6-18 show those computed by Disperse for our Gault bar.

The lowest order or fundamental mode L(0,1) is the only one covering the whole frequency range. At low frequencies it has an almost constant velocity that is called bar velocity, v_b, dropping at high frequencies to the Rayleigh velocity, v_R. These two velocities can be computed through

$$v_B=\sqrt{\frac{E}{\rho}} \qquad (122)$$
$$v_R\approx 0.9 v_S$$

The bar velocity is indeed familiar, as is the wave velocity of compressional pulses obtained for the elementary thin rod model –Graff, 1975. This is reasonable as in the low frequency range, where L(0,1) has the bar velocity, the axial displacement is almost uniform in the section and the radial displacement almost null, a situation well described by the elementary model. The Rayleigh velocity is also familiar as the velocity of surface waves. Its appearance here is related to the fact that at high frequencies the modal shape of L(0,1) reveals a motion constrained to the cylinder surface.

At high frequencies the phase velocity of all higher longitudinal modes tends to v_S; in between their dispersion curves are not monotonic, but have a ladder shape, with a marked echelon at v_p.

In flexural modes, F(n, m), all the movement components are non-zero. The first index, n, controls the angular variation of the modal shape: it represents the number of wavelengths round the circumference or circumferential order. The first order circumferential modes F(1,m) are the best known and Figure 6-19 represents the corresponding dispersion curves for our basic case.

Again the lowest order or fundamental mode F(1,1) has some important peculiarities. It is the only one which extends to zero frequency. Its dispersion curve is asymptotic to the Rayleigh velocity, approaching from below. It can be shown –Thurston, 1992- that this dispersion curve is coincident with that predicted by simpler theories of beam flexure –Bernouilli-Euler for the low frequency range and Timoshenko for the whole frequency range. Like in the L(0,1) case these propagation characteristics are best understood looking at the modal shape at different frequencies -Figure 6-20. At low frequencies flexure is almost

homogeneous and plane sections perpendicular to the axis remain almost plane, at high frequencies the movement migrates to the cylinder surface.

The dispersion curve of higher order modes is asymptotic to the bulk shear velocity. Some of them have plateaux near v_p like longitudinal modes, whereas others do fall more steadily to v_s. The modal shape is increasingly complicated as the modal order increases –Figure 6-20- but, contrary to what happens with the first mode, the movement does not migrate towards the surface at higher frequencies.

6.2.4 Guided waves in cylinders: pulse propagation

As we have remarked except for the fundamental torsional mode, T(0,1), all modes are dispersive. Figure 6-21 shows the group velocity curves of some flexural modes. Torsional modes –not shown- increase steadily up to the asymptotic v_s value. Flexural and longitudinal modes have more varied features. Before reaching the asymptote –at v_S or v_R- they go through various local extrema. The plateaux appearing near v_p, correspond to the same feature in the phase velocity curves. In general, at any given frequency there will be modes whose group velocity is close to v_p, others whose group velocity is close to v_S, a number in between and some below v_S.

In principle then, if a pulse is propagated along a cylinder and the mode of propagation is not specified the only certainty about its velocity is that it would remain below v_p. This may be illustrated with the help of a pulse propagation feature built-in in Disperse. With the numerically computed modal dispersion curves the program can propagate pulses using a FFT in much the same way as we have done in previous chapters, building a modal transfer function like

$$T_{mn}(\omega, x) = e^{-ik_{mn}(\omega)x} \tag{123}$$

and applying it to any specified input shape –see Pavlakovic & Lowe, 2000, for details.

Any computed mode can be used as propagator and –for reasons that will be soon clear- we have used several of the flexural modes computed for the Gault cylinder. Figure 6-22 shows the result of propagating a relatively narrow band pulse similar to those used in our bench test –10 cycles sineburst with f_{ap} 4 kHz. The time scale is normalised by the travel time of a shear bulk wave. It is apparent that the signal will travel at substantially different velocities in different modes. The arrival ordering might be helpfully interpreted with the aid of the group velocity curves shown in Figure 6-21. The fastest arrival corresponds to mode F(1,6) which at 0.75 is slightly below the time that will correspond to a v_p-travelling signal –0.67 for the specified $\nu = 0.1$. The second arrival corresponds to F(1,2) and its closeness to 1 might be explained by the dispersion curve being near the v_S asymptote at the central frequency of the pulse. Similarly, the belated arrivals of modes 3, 1 and 4 correspond to the increasingly low crossing of their group velocity curves with the 4kHz abscissa. Note that the arrival of the fundamental F(1,1) mode corresponds well to that of Rayleigh waves –1.12 for the specified $\nu = 0.1$.

The previous computation is illustrative but not very representative of the situations that may be encountered in soil pulse testing. To begin with the propagating distance was chosen long enough –12 m- to allow clear mode separation. A shortened distance will expand the relative time interval spanned by each mode and they will overlap. This is illustrated in Figure 6-23 where the same pulse is looked at just 12 cm from the input. The mode arrival ordering is the same as before, but now the overlap is substantial and the modes are indistinguishable in the total trace. The situation will be even more confused for a wide band input signal -Figure 6-24. As the input frequency range broadens, we cannot easily assign a single group velocity for each mode. All the modes are more heavily distorted and so is their sum, where the theoretical arrival time of a bulk shear wave is completely obscured.

Multimode propagation causes also problems for simple frequency domain approaches. For the case of two simultaneously propagating modes their combined transfer function can be written as

$$T(\omega, x) = C_1 e^{-ik_1 x} + C_2 e^{-ik_2 x} = C e^{-ik x} \qquad (124)$$

Cross-spectra or amplitude-spectra methods will measure the frequency dependence of the combined wavenumber, k. Simple complex algebra shows that this has a non-linear relation to k_1, k_2, C_1 and C_2. The phase and group velocity obtained from $k(\omega)$ will not correspond to any single mode[75].

6.2.5 Bender loading and modal selectivity

Now that the modal panorama is clear we will consider what modes might be excited by bender based pulse tests in soils. Two different aspects need to be considered: the frequency range of the forcing and its spatial distribution. We have seen in Chapter 3 that for our bench tests the frequency range of interest lies between 1 and 10 kHz and this is why the Disperse results presented so far have been computed in that range. The spatial distribution of bender loading is not known, although the results by Huot (1999) and others commented upon in Chapter 2 offer some clues.

A rigorous approach will proceed to compute the modal coefficients corresponding to a particular test arrangement using (118). This being basically a product will need two terms: a precise description of the mechanical excitation applied by the test and of the modal shape. Even if the first term would have been available the format of Diperse is not favourable to this approach, as it offers no easy numerical access to the modal shapes[76]. However, some insight may still be offered by an approximate computation.

For the usual bender arrangement we might then assume a simplified distribution of loading on the section such as that illustrated in Figure 6-25. The forcing there indicated is zero outside the face of the bender and –ignoring bender thickness- this is reduced to a segment of length w_B centred on the sample axis. On this segment the motion is directed along the angular coordinate, that is, only f_θ is assumed non-zero. The transition is abrupt, with f_θ being uniform along the whole length of the segment and zero outside.

---

[75] In fact, the near field problem discussed in Chapter 4 may be seen as a relatively simple instance of this problem.
[76] At least to those –longitudinal, transversal- which are frequency dependent.

The product (5) of such a forcing distribution and modal shapes it is relatively simple to compute. Is zero for all the longitudinal L(0, m) modes, as these are motions with no angular component. It is also null for all the torsional T(0,m) modes, as the angular component of these motions is odd about the cylinder axis whereas the assumed forcing distribution is even. This leaves only the flexural modes F(n,m).

The angular component of the F(n,m) modes is even along any diameter. Disperse offers graphical access to the motion components for any mode at any frequency. Figure 6-26 and Figure 6-27 represent the u_θ component of the F(1,m) modes present at 2 and 4 kHz in our ideal Gault cylinder. It is apparent that the motion varies with frequency and, for instance, that of the fundamental mode F(1,1) becomes more concentrated near the surface, as might be expected of its Rayleigh like behaviour at high frequencies. It is also clear that the inner product of the forcing represented in Figure 6-25 and these modal u_θ distributions is proportional to the integral of u_θ below $w_B/2$ or

$$\langle \overline{\mathbf{M}}_{mn}, \bar{\mathbf{f}} \rangle \propto \int_0^{D/2} f_\theta u_\theta \, dr = \int_0^{w_B/2} u_\theta \, dr \qquad (125)$$

With a 14 mm effective bender width w_B, and a 10 cm diameter we have computed the previous integral for all the F(1,m) modes present at 2kHz, 4kHz and 6 kHz. We have then normalised the result so as to make the coefficient sum for all modes equal to 1. The normalised coefficients are shown in Figure 6-28. As the frequency increases the number of modes to consider also increases and the modal contributions seem to be more evenly distributed. An exception is the fundamental mode, whose contribution declines as frequency increases; a consequence of its progressive confinement to the sample surface.

We have then shown that flexural modes are those which count[77]. It is tempting at this stage to go a little bit further and use the coefficients just obtained to weight Disperse computed signals such as those in Figure 6-23 and use equation (117). Two problems appear. First the weighting modal coefficients are frequency dependent, second we have only obtained the numerator, but not the denominator in equation (118). Selecting a narrow band signal the first problem is minimised; the second is at this stage unavoidable. Still, in one of our bench tests –test 80- the input was a 4kHz 10 cycle sine burst, and the output was registered at a distance of 12 cm. Figure 6-29 shows these traces as well as a Disperse simulated signal where the first eight L(1,m) modes were weighted with the values shown in Figure 6-28 for 4 kHz. There are substantial differences between the simulated and measured trace, however the result is encouraging: at least qualitatively, the similitude now achieved is far higher than what was obtained in previous chapters with other dispersion models like near field or Biot.

More experimental support from the multimodal propagation hypothesis is offered from cross-spectral group velocity estimates such as those described in Chapter 3. The irregular nature of the observed pattern may well be interpreted as the varying influence of different modes. Support for the presence of

waveguide effects can also be gathered from the experiments presented by Blewett et al. (2000). They performed bender-based pulse tests in Levenseat sand. The sand was deposited in a large container (0.5 m x 1 m) and source and receiver were closely placed – at less than 8 cm distance- near the middle of the sample. Tests were performed in that configuration and then repeated after a cylindrical metallic casing of 10 cm diameter was placed surrounding the installed probes. Figure 6-30 shows how this change affects the measured amplitude spectrum. The unique peak first apparent splits into various peaks, a known feature in other instances of multimodal transmission (Alleyne & Cawley, 1992).

6.2.6 Consequences for soil pulse tests

It seems then that for our sample of unconsolidated Gault clay pulse tests with bender probes produce a multimodal excitation. We have also shown above that in such circumstances time domain interpretation of pulse traces is inherently uncertain and that simple frequency domain approaches are not useful either. As our tests were representative of the current practice described in Chapter 2 in terms of bender characteristics, input signals and sample shape we might suspect that this problem is rather general. The question now is what strategies might be more successful in dealing with this problem. Two approaches are possible, either alone or in combination: the first is to tinker with the forcing so as to make the propagation problem simpler; the second is to admit some degree of complication and use more suitable test interpretation procedures.

6.2.6.1 Transducer arrangement

Keeping in use bender elements as sources and receivers modal selectivity can only be achieved via frequency. Only the extreme frequency ranges are attractive. At frequencies low enough only the fundamental F(1,1) mode will be excited. Although this mode is still dispersive it is well described by the Timoshenko beam flexure theory[78] and, therefore, a relatively simple interpretation is possible. Brocanelli & Rinaldi (1998) used this approach in their modified triaxial apparatus. However, they preferred to interpret their bender tests as a steady state resonance problem and, to limit the extra resonances induced by reflections, they had to shorten their sample.

The critical parameter here is the cut-off frequency of the lowest non-fundamental flexural mode. According to Thurston –1992- that mode is F(1,2) and the cut-off frequency is independent of Poisson ratio and given by the relation between shear velocity and cylinder diameter

$$f_{cut}^{L(1,2)} = 0.5681\frac{v_S}{D} \qquad (126)$$

Testing at higher frequencies fits well with conventional ultrasonic wisdom. At very high frequencies ultrasonic shear pulses travel at the bulk shear velocity (Mason, 1958; Thurston, 1992). This may be explained as follows: many modes are excited with almost equal intensity, only a few are still undergoing

---

[77] Higher order flexural modes will also be excited. Their motion is like that of F(1,m) scaled by a cos nθ factor. As our ideal loading is concentrated at θ = 0 it will excite all flexural modes equally.
[78] For a description of this theory see, for instance, Graff -1975.

the transition to their asymptotic behaviour, most of them are already travelling at v_s and their contribution dominates. Our previous computation -Figure 6-28- showed that, with our simplified bender loading scheme, modal contributions tend to equalise at high frequencies. This bodes well for this approach but, as we have remarked many times attenuation and bender response do limit closely the practical upper-frequency range. A limit for this quasi-bulk behaviour may be expressed as

$$\frac{D}{\lambda_S} > K_{qb} \tag{127}$$

In a classic study of this problem McSkimin (1956) proved experimentally that high frequency conditions were attained with D/λ_S ratios over 66. Thurston (1982) showed an example of how quasi-bulk propagation was achieved for K_{qb} over 53. These values are probably too high. The cut-off frequencies for flexural modes not only depend on v_S and D, but also on the Poisson ratio. However Sittig & Coquin (1970) explored that dependency for modes L(n,m) with n<10, m<10, and from their tables one can conclude that for D/λ_S above 10 there will be more than 15 active L(1,m) modes. Until further study we might suggest then a value of 15 K_{qb} as a practical compromise.

For a given shear velocity equations (126) and (127) might be used to obtain a frequency-diameter band where multimodal propagation will take place. This is shown in Figure 6-31, where for each velocity the zone contained between the continuous and dashed line will be that of multimodal propagation. Taking account of the usual range of diameters in triaxial apparatus the chart seems to indicate that only very soft materials are accessible to quasi-bulk testing with current bender probes. For stiff materials the low frequency limit seems more accessible. Still, it seems that a large number of tests to date and, particularly our bench test, have proceeded in the intermediate, hard to handle, range.

A more radical alternative will involve a different arrangement of the piezoelectric sources, able to produce a different, simpler excitation. Torsional modes are substantially simpler than flexural modes; amongst other favourable properties their group velocity is always below v_S, their dispersion relation is explicitly known and their modal shapes are frequency independent. Moreover, they include the only completely non-dispersive mode, T(0,1). This is the mode excited by resonant column-type tests and, was also excited by piezoelectric driven pulses by Fratta & Santamarina (1996). These authors did not gave any detail of the type of transducer they were using, however an arrangement of shear plates like the one employed by Nakagawa et al. (1996) -Figure 6-32- seems a good candidate for that purpose, as its symmetry suggests that input energy will be almost exclusively channelled into torsional modes[79].

6.2.6.2 Test analysis

As the previous paragraph suggests multimode transmission may be hardly avoidable. If this is known or suspected from the outset the analysis of test results should proceed accordingly. We have suggested before –Chapter 5- that when dispersion takes place the measurement of material properties requires some inverse analysis: for instance adjustment of Biot parameters to a measured dispersion curve. Facing

[79] This has been also observed by Huot (1999)

a multimodal transmission problem this is even more so, simulation and numerical analysis of the experiments are both necessary and the key is where to place the matching point.

Here we cannot develop any such scheme, but just make some observations inspired by analogous situations in nearby fields. Perhaps the nearest case is that of SASW -see Foti, 2000 and references therein- where multimode propagation is common when the strata stiffness does not increase monotonically with depth. But similar problems also arise in ultrasonic techniques developed to inspect adhesive joints, laminates or tendons –Alleyne & Cawley, 1992.

Let us consider first the backward or data analysis part of the problem. In the trace time record all modes are mixed. The same applies, as we have seen, to its frequency domain counterpart. Cross-spectra with the input will produce a local dispersion curve, which will not correspond to any particular mode. For inversion it will be very helpful to separate the different mode contributions to the trace. The only seemingly reasonable alternative[80] will be to do some kind of time-frequency analysis of the trace. These techniques were developed by seismologists –Dziewonski & Hales, 1972- to separate Rayleigh earth wave modes on earthquake traces. Basically, they looked at how the varying frequency content within the trace by doing a Fourier transform of successive trace portions. That worked well for recordings at long distances from the source, where the modes were well separated, but did not prove that useful for Al-Hunaidi –1994- who tried to apply the same methods for typical, short-range, SASW configurations. Similar problems have recently prompted ultrasonic practitioners to use a different kind of transform, the wavelet transform. Results by Veroy et al. –1999- and others seem encouraging in this respect.

The interest in obtaining separated dispersion curves for the modes is clear when we turn to the forward or predictive part of the problem. We have seen above that current possibilities to reach this stage are relatively good. It is much harder, though, to go further and simulate the forced problem to obtain a trace that might be adjusted to the recorded one. A mode expansion approach seems attractive, but, as our previous work may have clarified two major obstacles appear. The first is to model accurately the modal excitation by bender elements. The second is to take into account end effects.

Soil samples are not infinite cylinders. A previous section has shown how end effects have important consequences for simpler, single-mode propagation. In the case of waveguide propagation the same reasoning might be applied but the building blocks of the transfer function will be far more involved. For any given mode the propagator block in Figure 6-5 will be given by its own dispersion characteristics, but reflection will be more complicated as other modes will be generated. For instance, at a free end the torsional family is uncoupled –Thurston, 1978- but longitudinal and flexural modes are cross-coupled. Moreover, near the ends non-propagating modes –that is modes with complex wavenumbers, attenuating

---

[80] A much favoured alternative is based on a 2D Fourier transform. For ultrasonic applications Alleyne & Cawley –1991- have successfully applied it to resolve the different modal dispersion curves. Foti –2000- has done the same for SASW results. A 2D transform swaps time for frequency and distance along the guide for wavenumber. In the transformed ω-k domain the modes separate. However, this is a technique that can only be applied if the movement has been registered at different x locations. The number of registered traces is crucial for the success of the technique and is commonly over 20. With current pulse test configurations the movement is registered at just one location and this approach becomes impossible.

along the waveguide- will also be present. Although some theoretical work has been done –McKenna & Simpkins, 1985- practical problems involving reflection of flexural modes are not routinely solved – Aime & Brissaud, 2001.

Detailed finite element or discrete element models may be used with advantage to clarify these two problems. For the somewhat simpler case of Lamb waves in plates Moulin et al. (2000) have used with success a finite element model to clarify mode generation by an embedded bimorph, source of obvious similarity to bender elements. The use of finite elements to obtain modal reflection coefficients is exemplified by Lowe et al. –2000- again for Lamb waves and Pavlakovic et al. –1999- who have looked at longitudinal modes in embedded bars -L(0,1) and L(0,4), to be precise.

Discrete models may also be employed for the whole problem, but this is a very exacting approach and might lead astray. Usually, some simplifications will be introduced and if they are not guided by some higher level model –like waveguide theory- they may be rather misleading. Two examples of this are provided by Jovicic et al. (1997) and Arulnathan et al. (1998), who both used FEM to model a triaxial bender test. Arulnathan et al. decided to model the problem in 2-D to achieve a manageable model, this, in fact, transforms the cylinder in a slab. Slabs also guide waves, but the relevant modes –antisymmetric Lamb modes- are different from the Flexural cylindrical modes and the observed dispersion will be consequently affected. Jovicic et al. also used 2D and 3D FEM models. The model details are not very clear, the result was: the received waveshapes were equal to those predicted by Stokes fundamental solution for the unconfined space. This, as we have seen, is against all experimental and theoretical expectations.

6.3 SUMMARY

Soil samples have dimensions commensurate with the wavelengths typically employed in shear pulse tests. As a result sample size effects plague test interpretation and obscure the effects of material properties. We have explored here that problem for axis-directed tests with geometries typical of triaxial samples. The flat end boundaries provoke interference and signal overlap. The cylindrical perimeter acts as a waveguide inducing dispersion. Both problems reinforce one another, as dispersion facilitates end interference and end interference complicates the phase signature of dispersion. Details of transducer arrangement have an important bearing on the characteristics of the interference pattern and the induced dispersion. In this respect, current arrangements of cantilevered bender elements are far from optimum, if precise elastic measurements are sought after.

6.4 TABLES

Reference	Apparatus	Section	B (mm)[1]	H (mm)	l_B (mm)
Schultheiss (1983)	Oedometer	Circular	75	19	2
Schultheiss (1983)	Triaxial	Circular	50	101	10
Dyvik & Madshus (1985)	Resonant column	Circular	*50*	*100*	4
Thomann & Hryciw (1990)	Oedometer	Circular	177	76	*4*
Jamiolkowski et al. (1995)	Oedometer A	Square	44	300	*4*
Jamiolkowski et al. (1995)	Oedometer B	Square	67	400	*4*
Brignoli et al. (1996)	Triaxial	Circular	50	100	1.5
Nakagawa et al. (1996)	Triaxial	Circular	50	100	0[3]
Fratta & Santamarina (1996)	Waveguide	Circular	100	1600	
Boulanger et al. (1998)	Triaxial	Circular	71	170	5
Brocanelli & Rinaldi (1998)	Triaxial	Circular	63	28	4.5
Zeng (1999)	Oedometer	Circular	152	102	15 -18
Pennington (1999)	Triaxial	Circular	100	200	2
Kuwano (1999)	Triaxial	Circular	100	200	3
Huot (1999)	Triaxial	Circular	50	100	5
Chapter 3	Bench test	Circular	98	195	10
Chapter 3	Bench test	Circular	98	169	10
Chapter 3	Bench test	Circular	98	140	10
Chapter 3	Bench test	Circular	98	116	10
Chapter 3	Bench test	Circular	98	92	10

[1]Characteristic dimension of the section: diameter –circle- or side –square-
[2]Numbers in italic are dimensions only indicated by the authors (i.e. referred to previous work)
[3]Test performed with shear plates

Table 6-1 Laboratory shear pulse tests: sample geometry in previous research and this dissertation

6.5 FIGURES

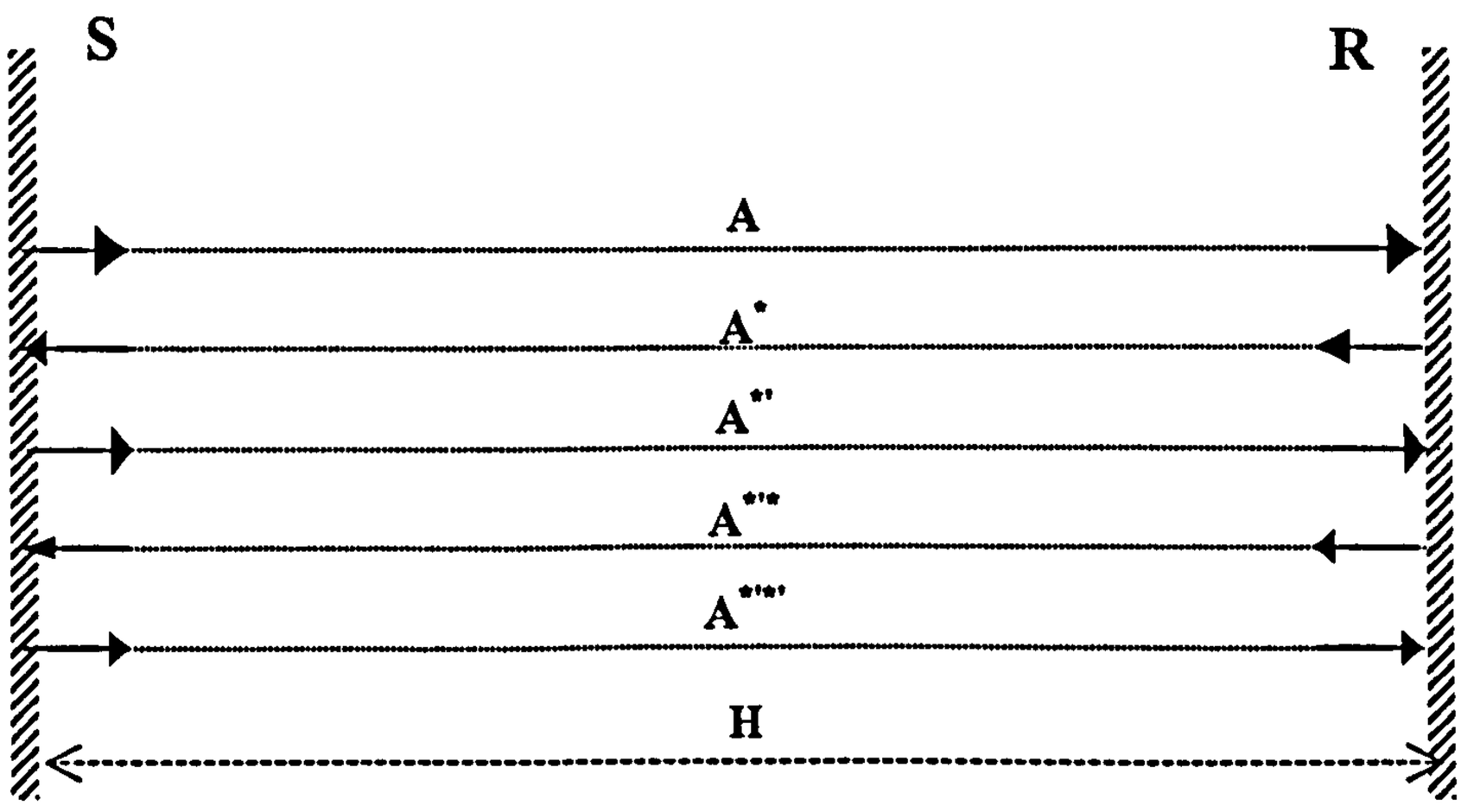

Figure 6-1 1-D wave propagation in a confined space

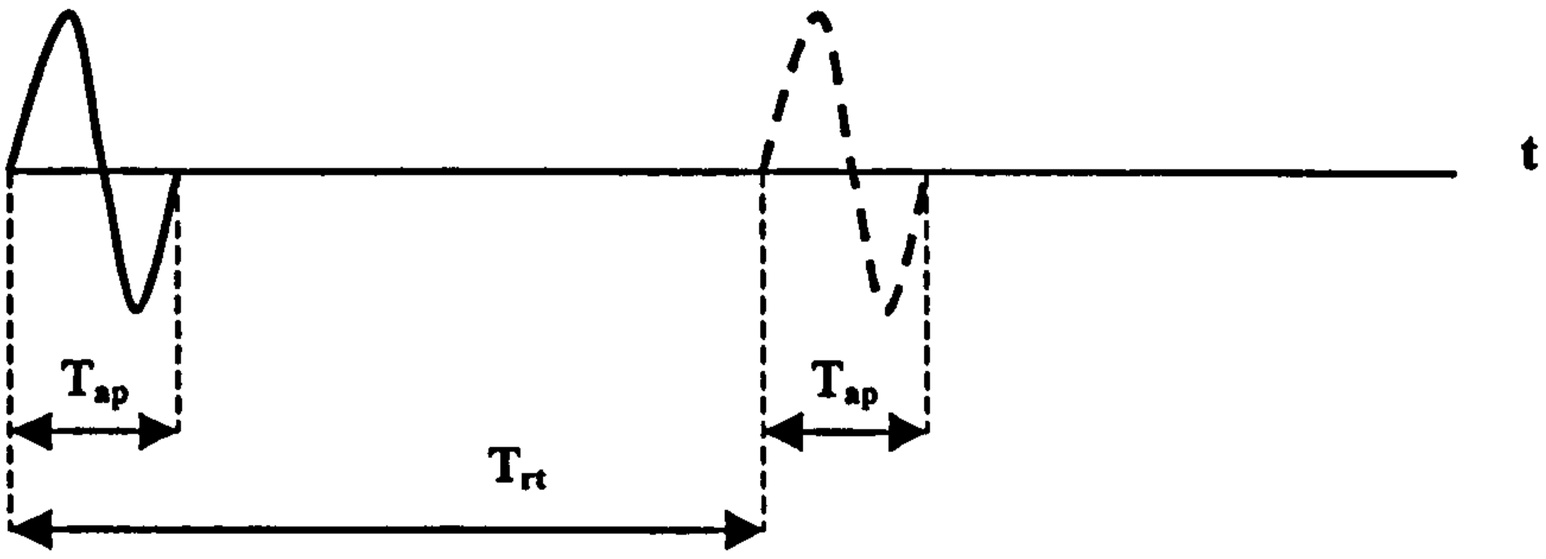

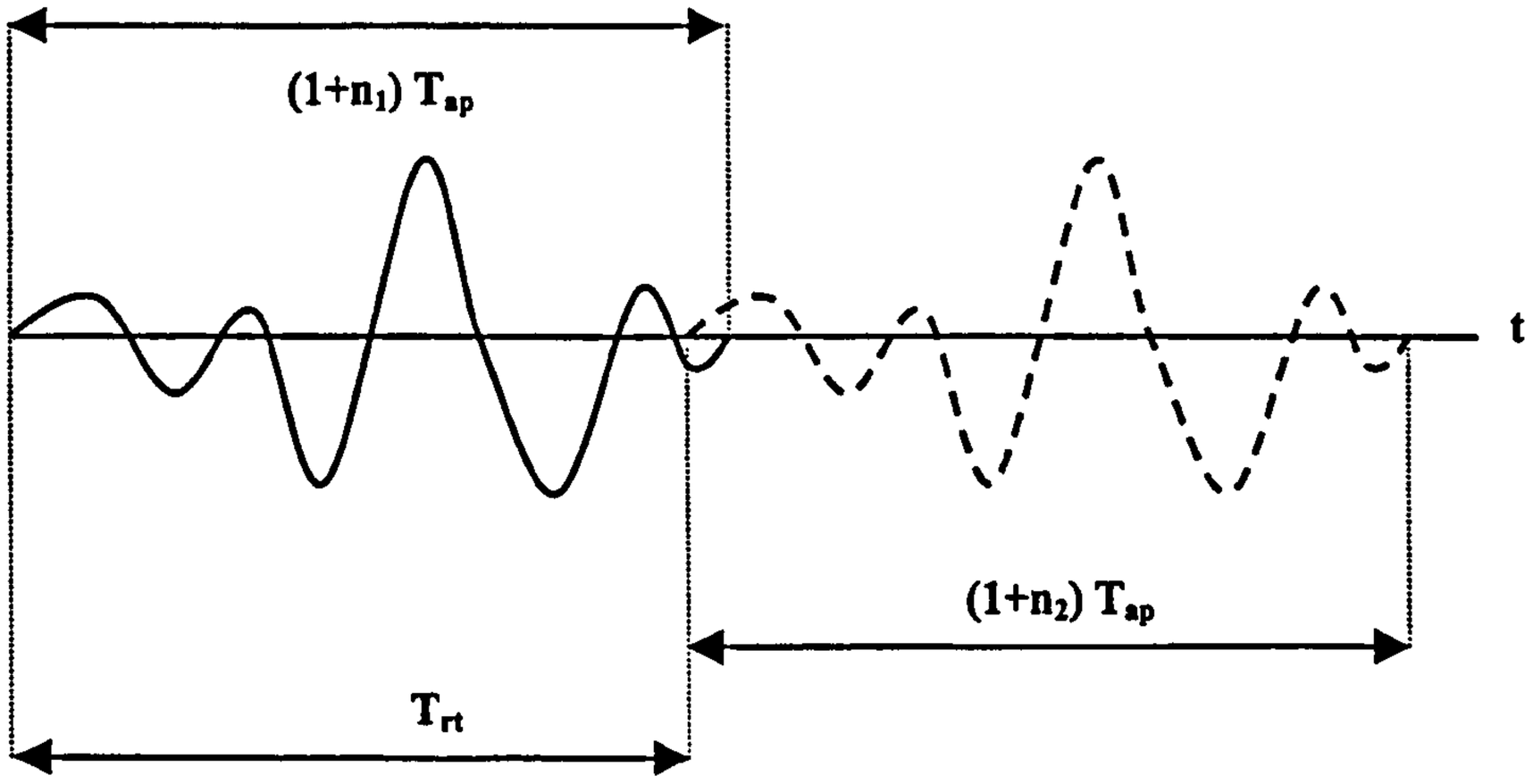

Figure 6-2 First and second arrival in a non-dispersive and dispersive situation

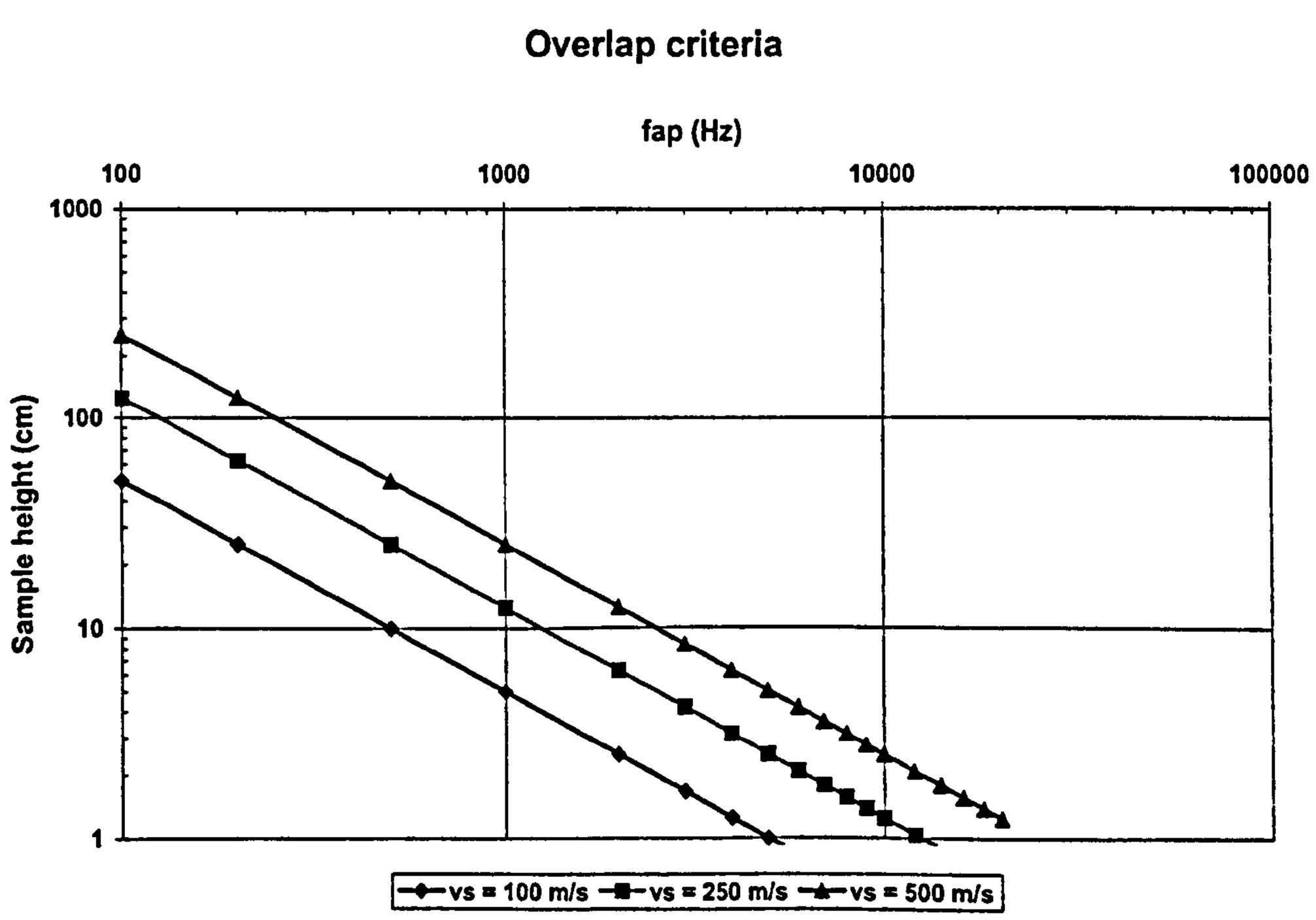

Figure 6-3 Minimum sample height for non-overlap in a non-dispersive case

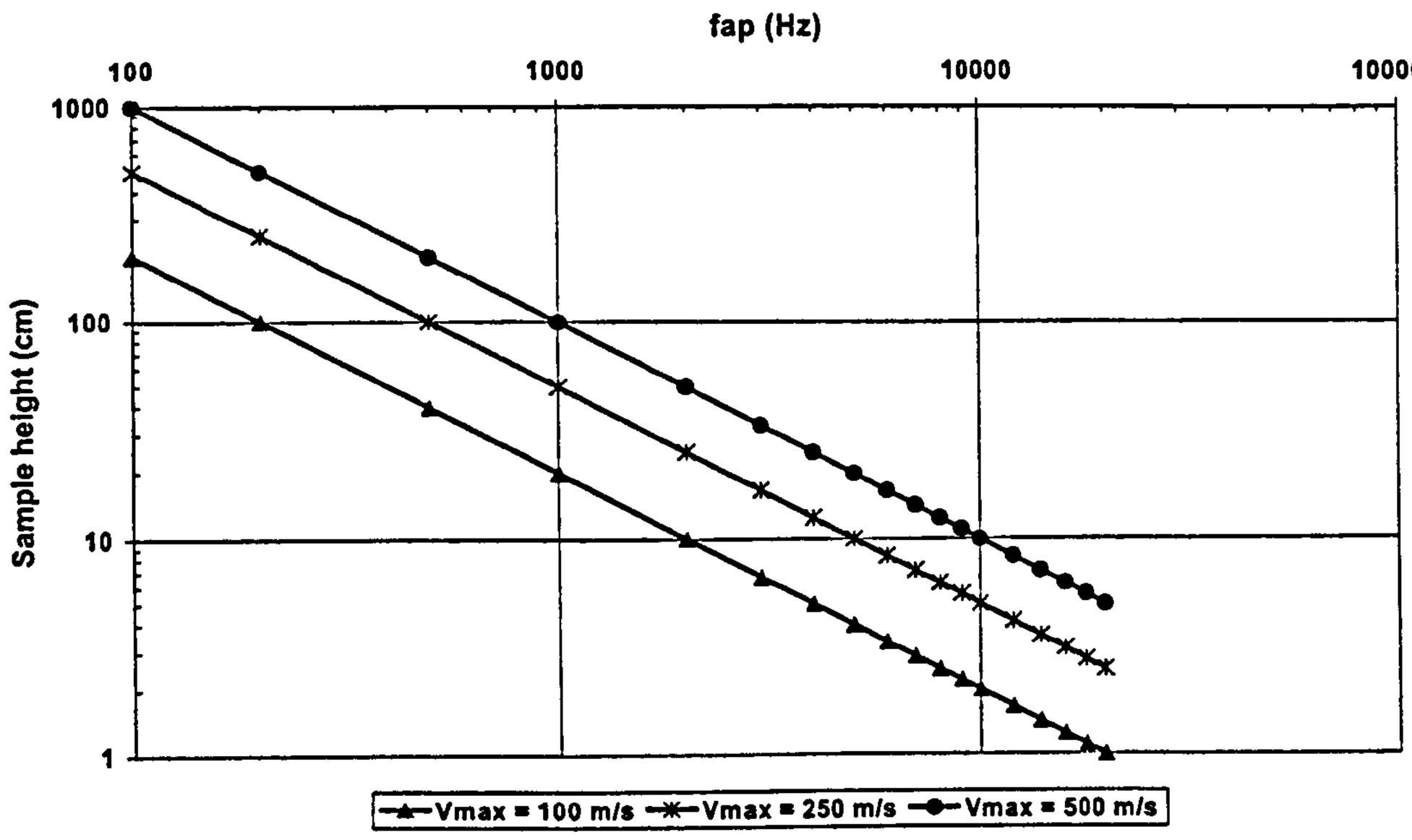

Figure 6-4 Minimum sample height for non-overlap in a dispersive case

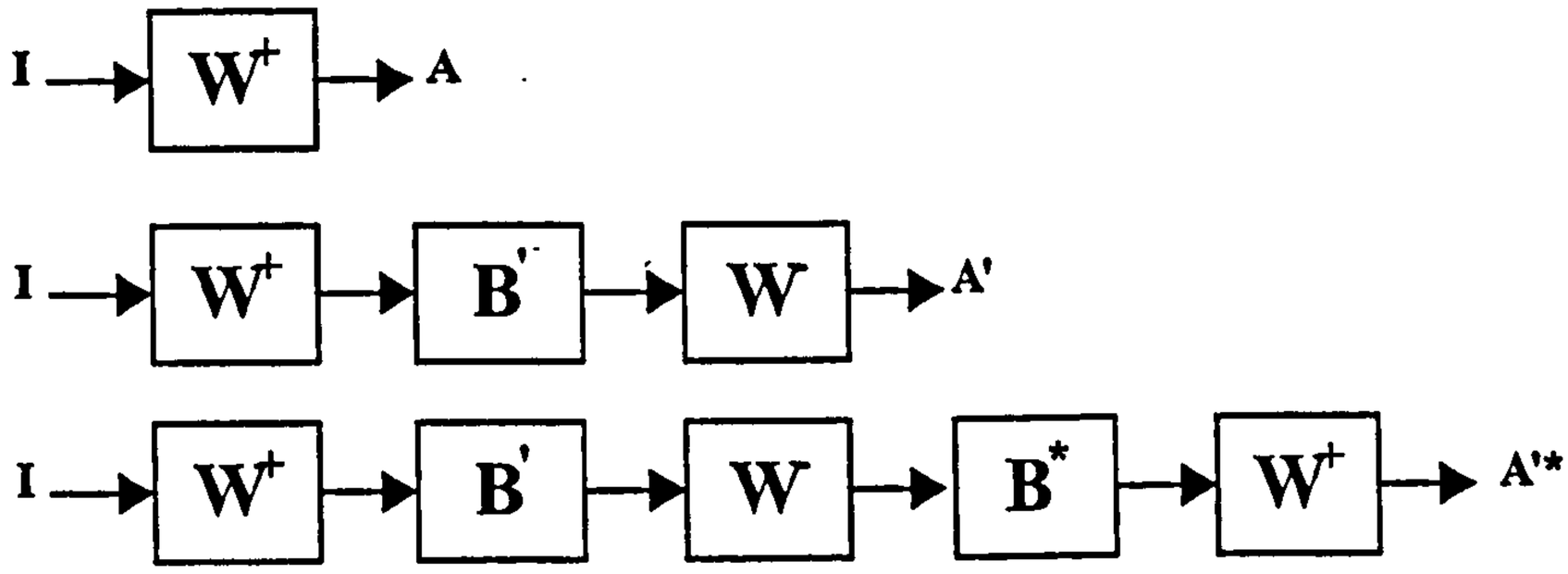

Figure 6-5 Linear system representation of reflected signals

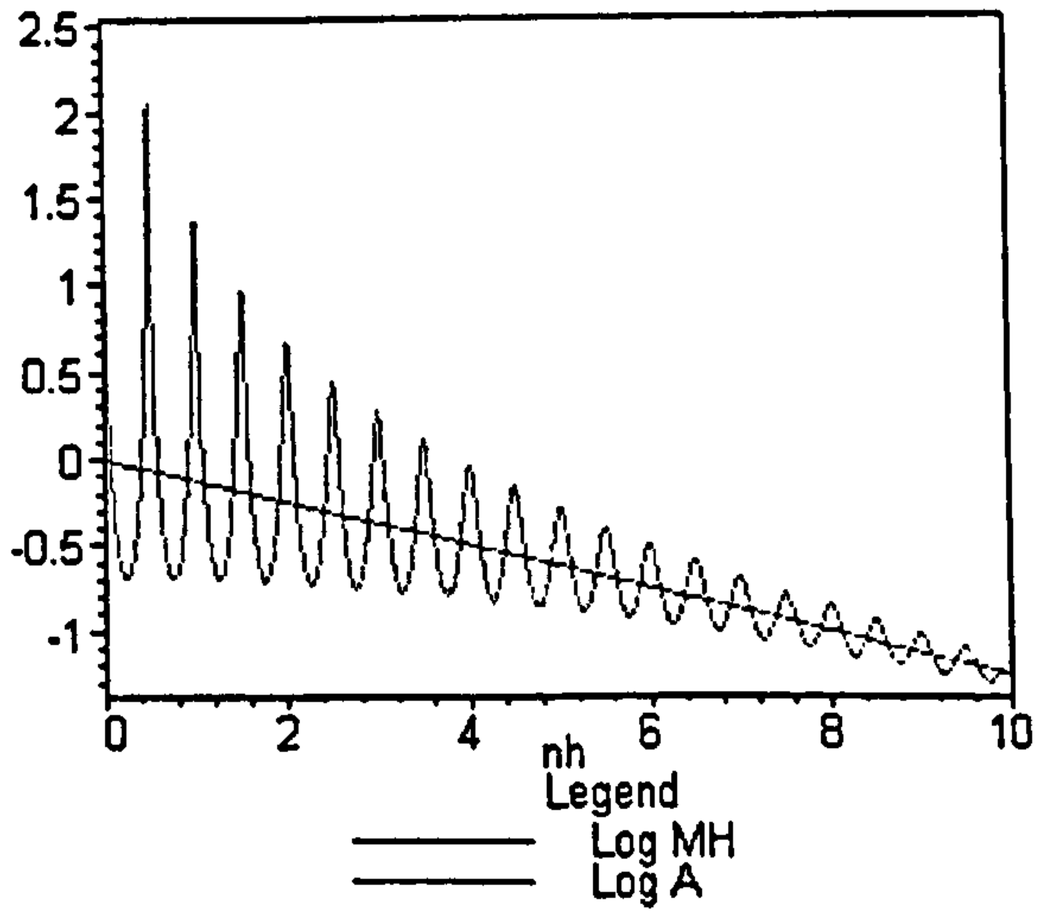

Figure 6-6 Moduli of first arrival (A) and complete reflection series (MH). Damping D = 2%

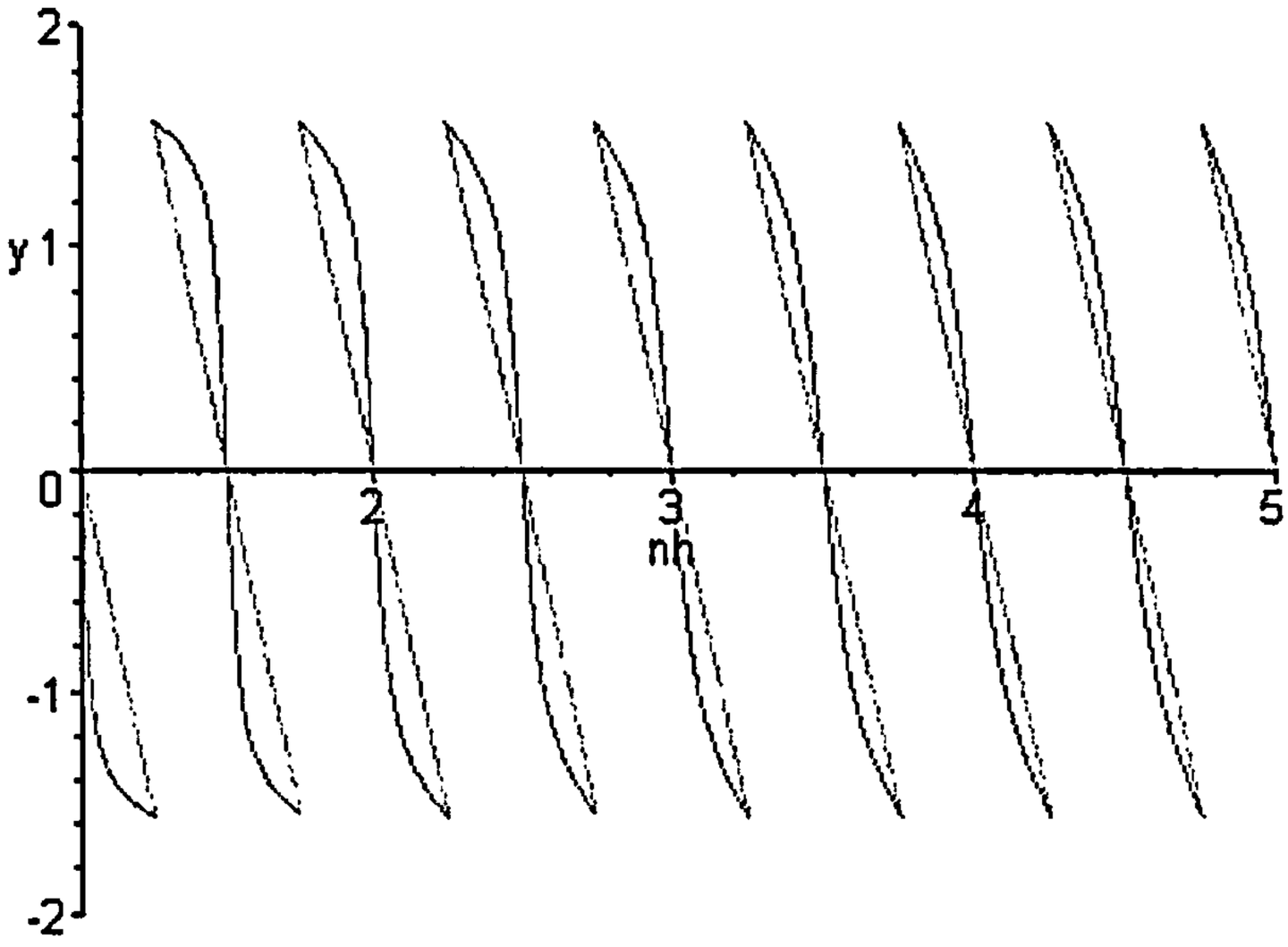

Figure 6-7 Wrapped phase of the first arrival transfer function –straight lines- and of the rebound series –curved lines.

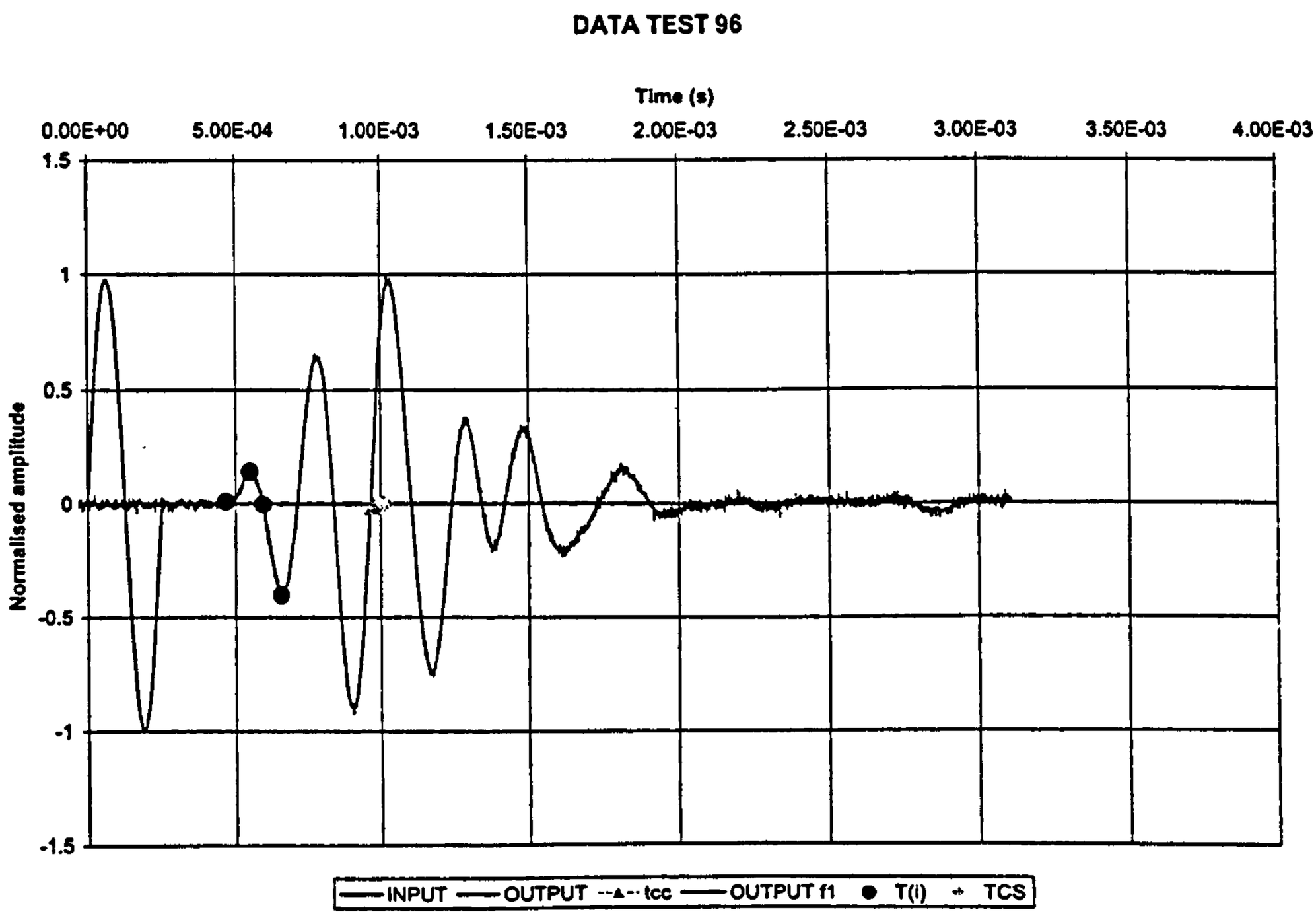

Figure 6-8 Bender trace for bench test 96 H ≅ 9.27cm f_{ap}= 4kHz

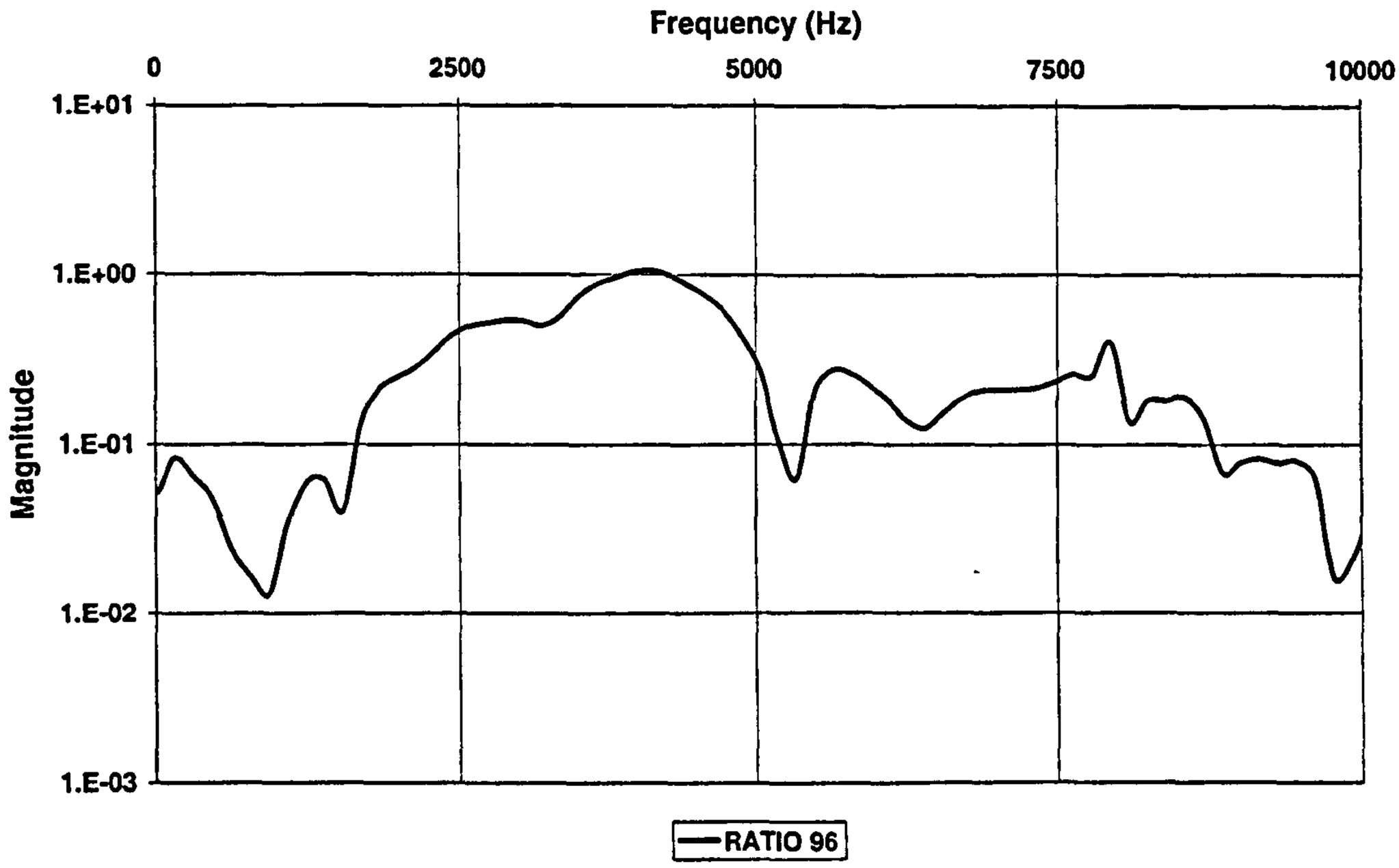

Figure 6-9 Spectral ratio for bench test 96

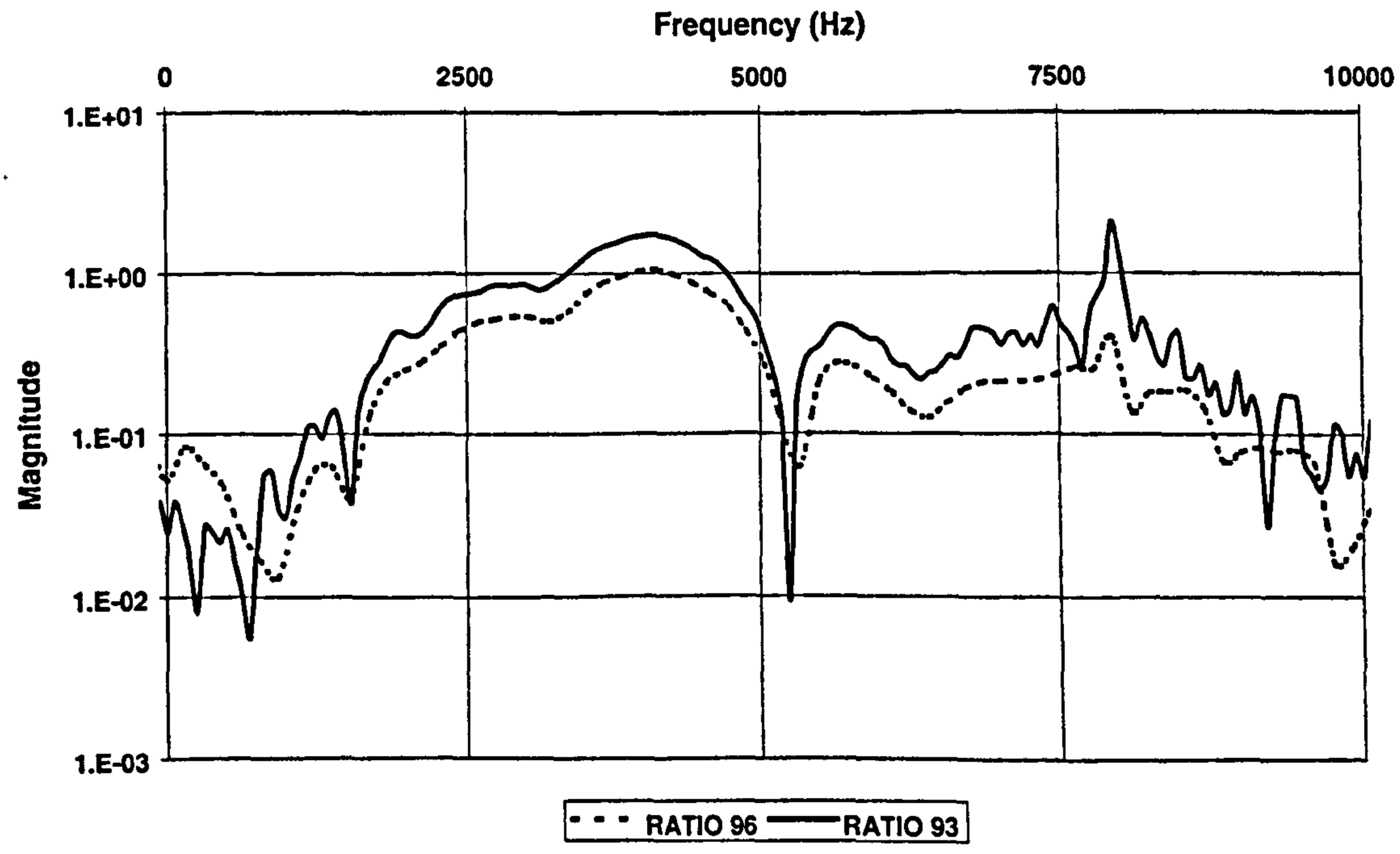

Figure 6-10 Spectral ratio for bench test 96 and 93

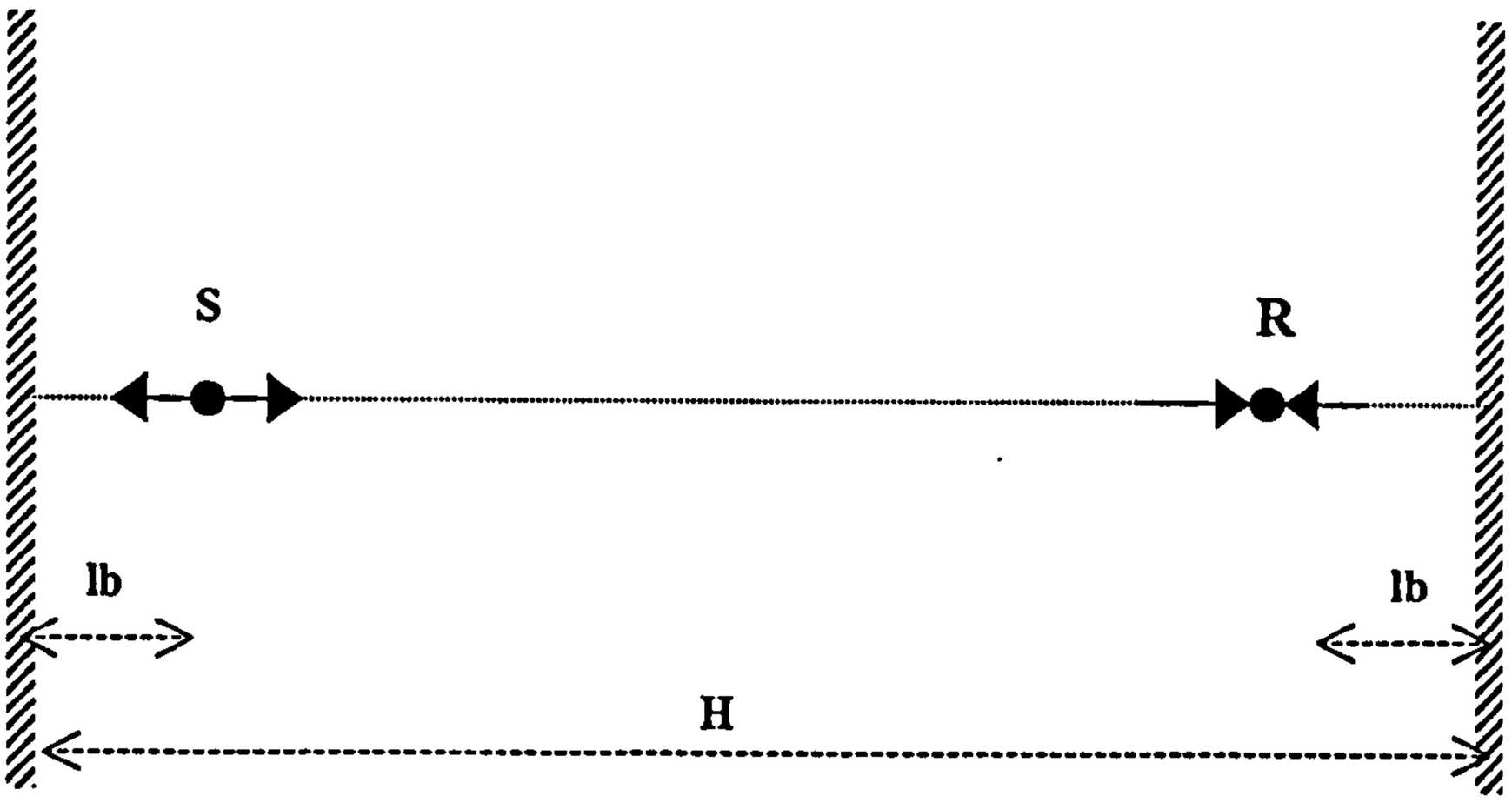

Figure 6-11 Bender elements as off-wall source and receiver

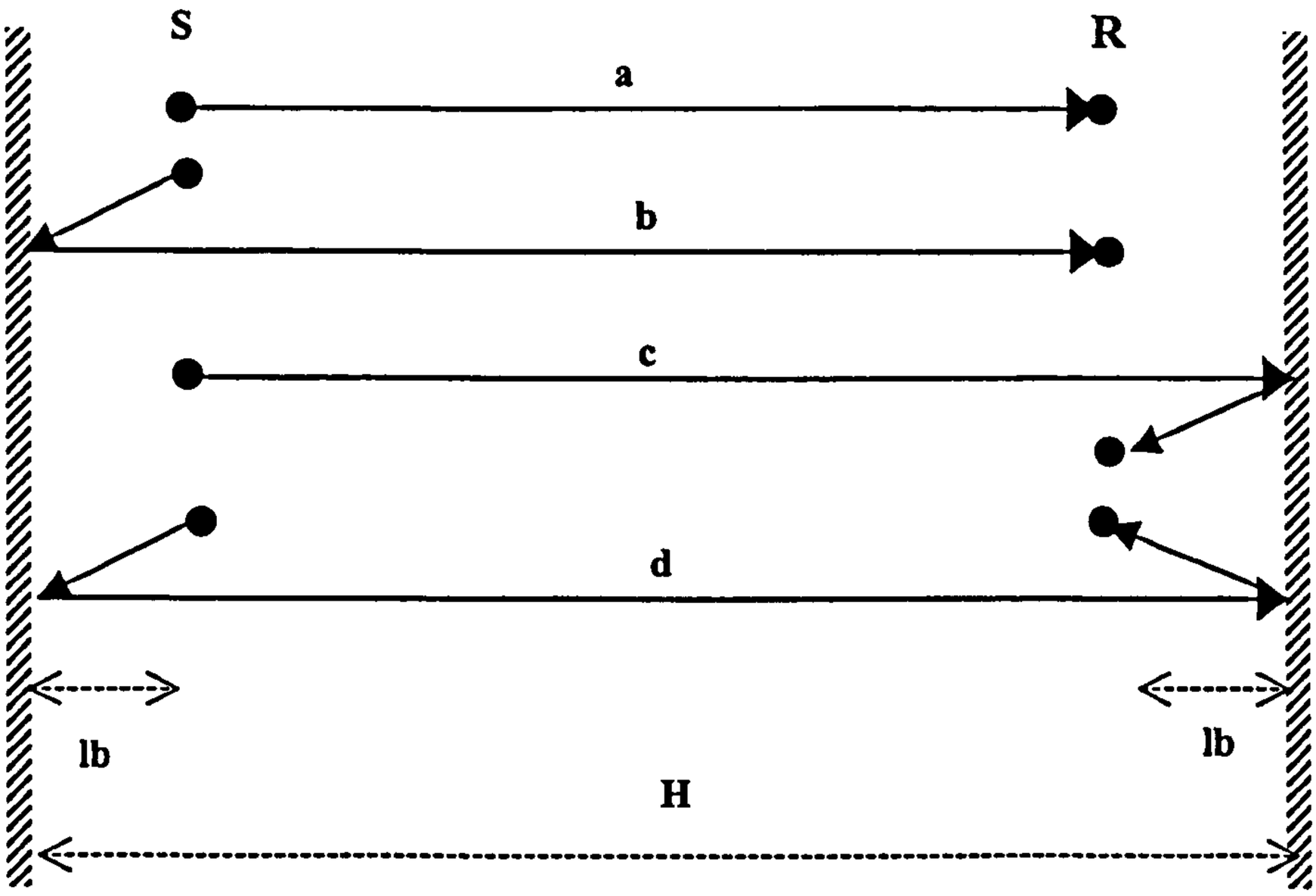

Figure 6-12 First arrival paths between off-wall source and receiver. Different paths are separately drawn for clarity in the figure.

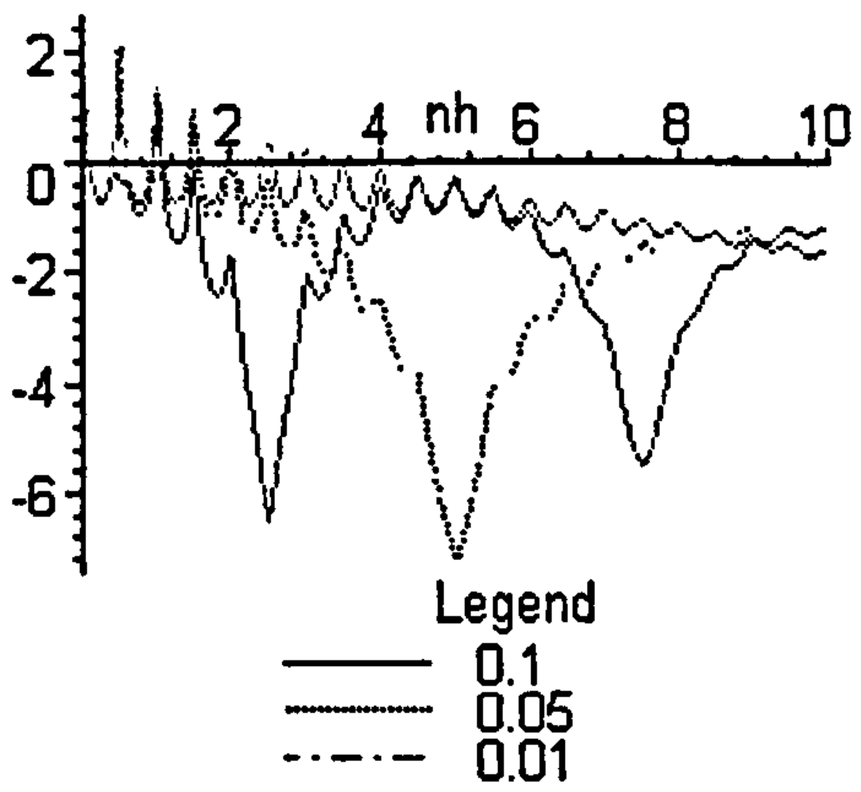

Figure 6-13 Moduli of a complete reflection series when bender length effects are included. Plots for varying n_{LB}

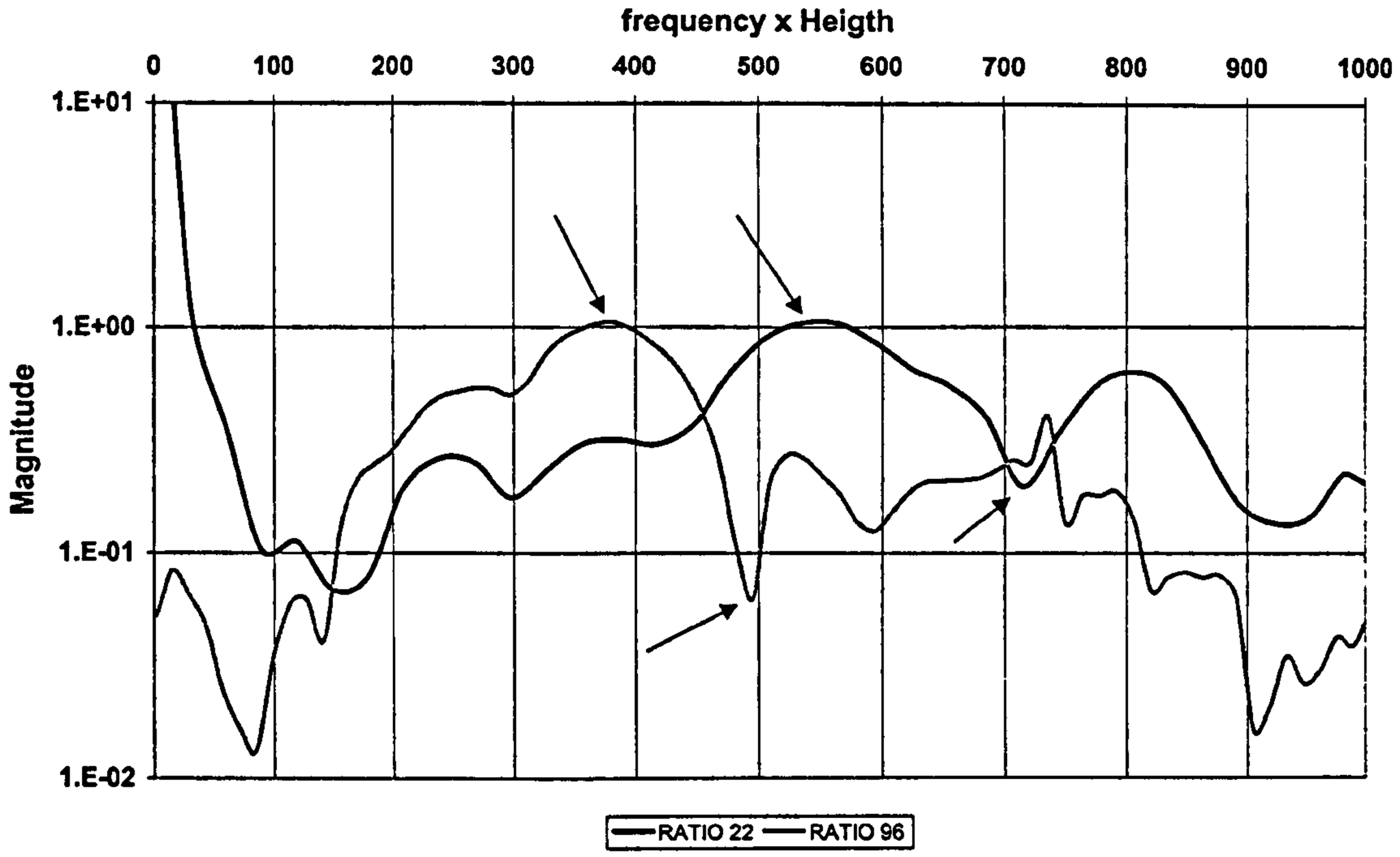

Figure 6-14 Spectral ratio dependence on H*f for bench test 22 and 96 .
Estimated $n_{LB} \cong 0.05$ –test 22- and $n_{LB} \cong 0.11$ –test 96-

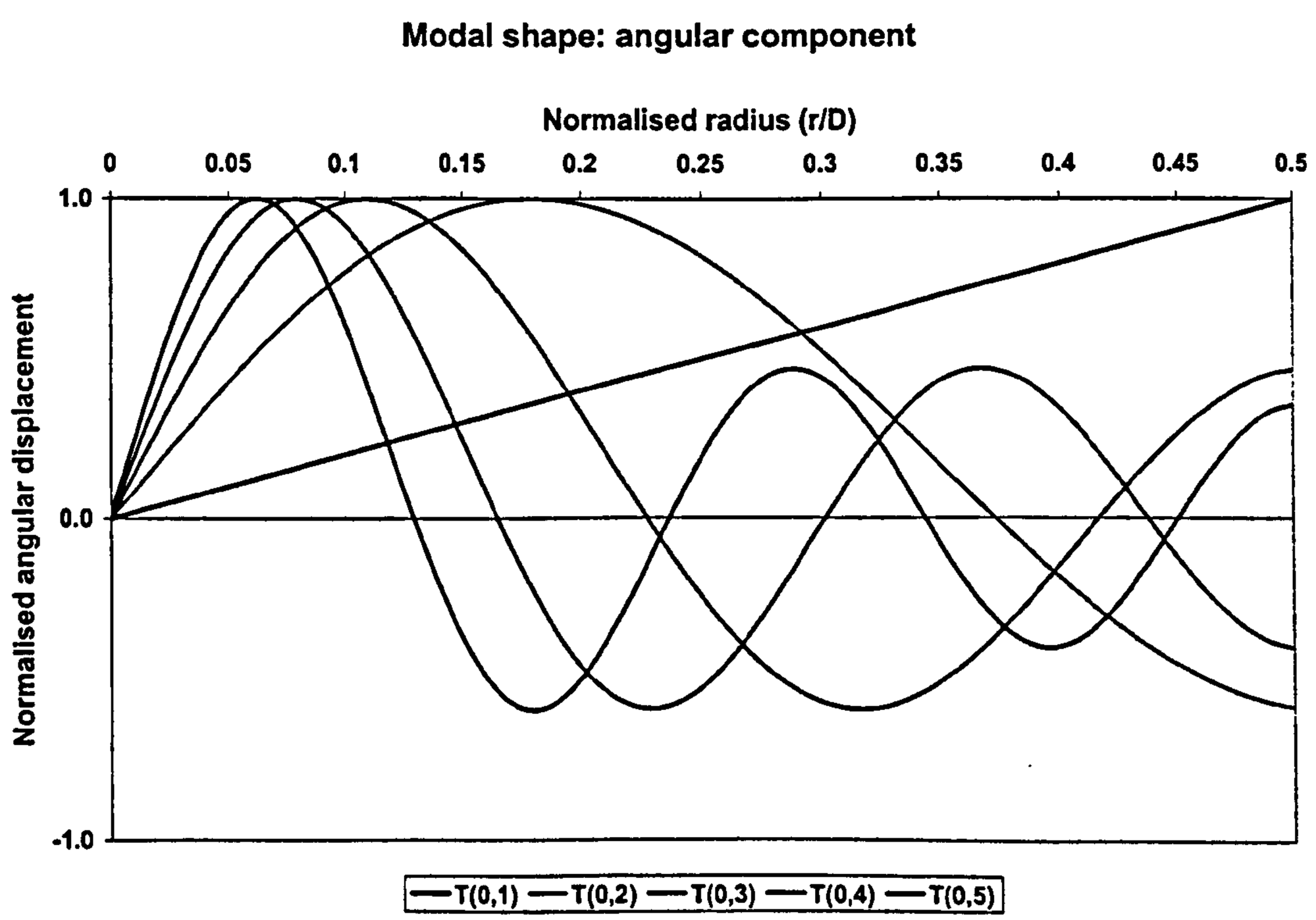

Figure 6-15 Torsional modes: normalised angular displacement

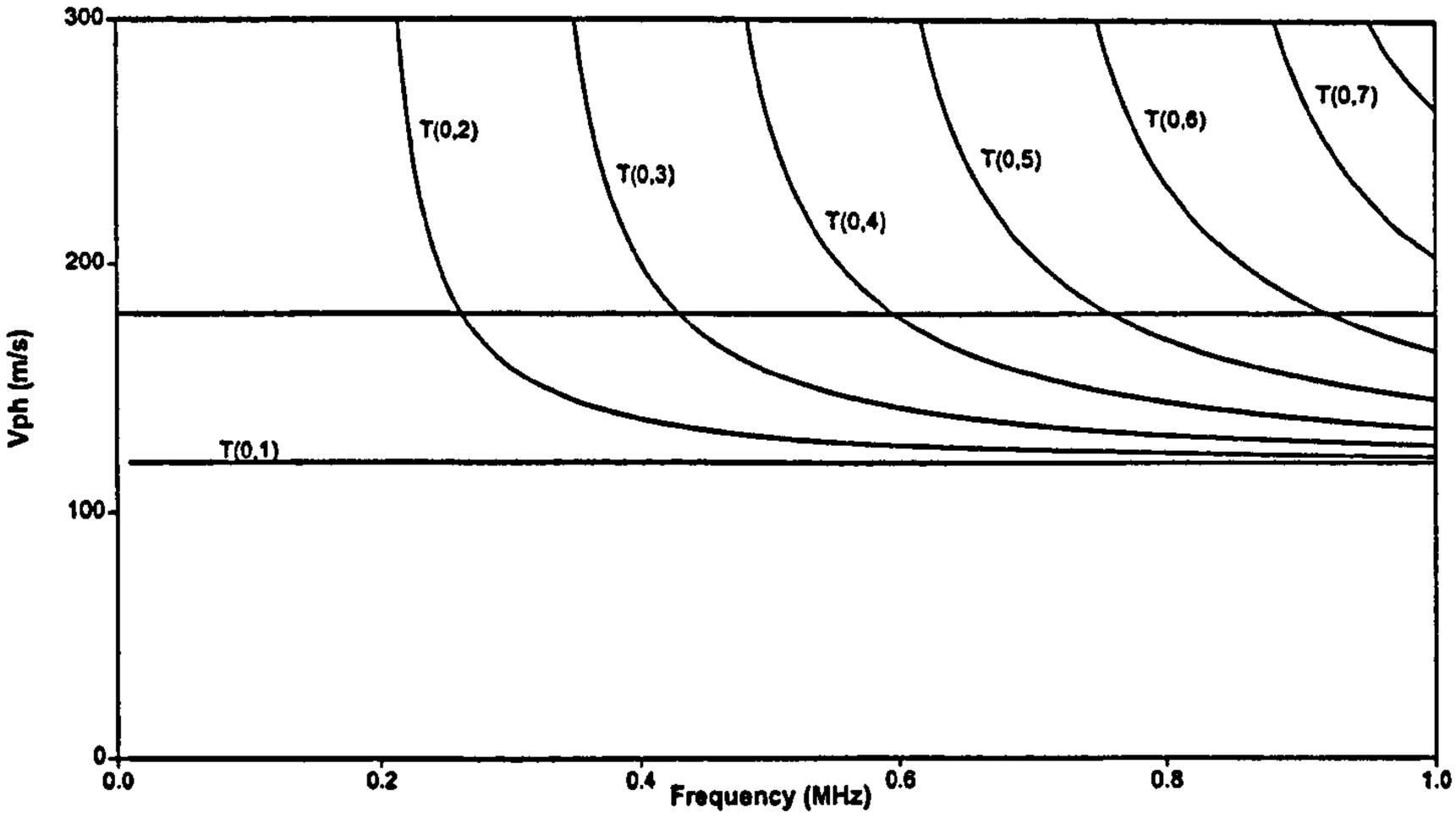

Figure 6-16 Torsional modes for a Gault clay cylinder. Scaled frequency 1MHz=10Khz

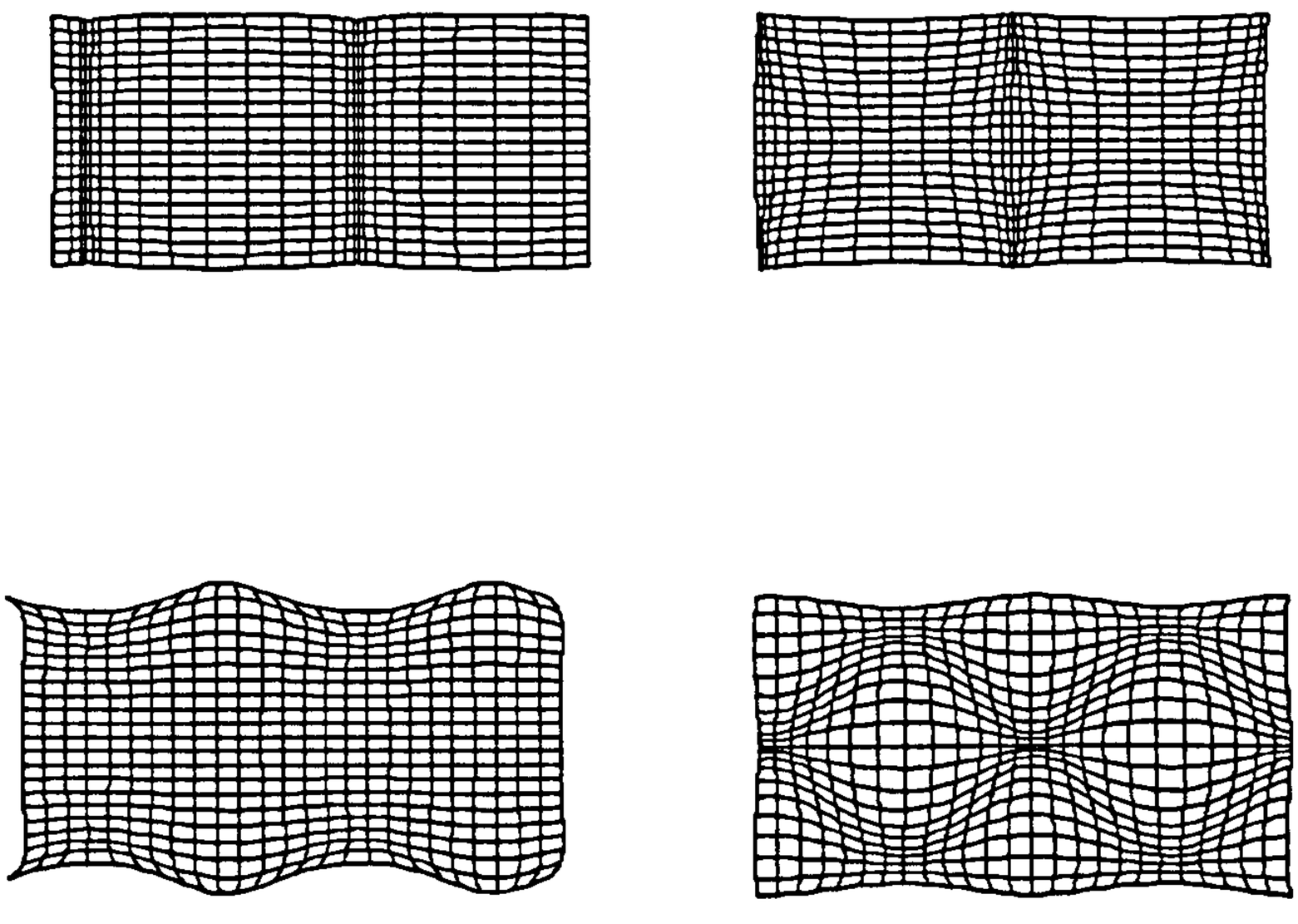

Figure 6-17 Modal shapes: lateral view of L(0,1) –left- and L(0,2) –right. Low frequencies –above- and high frequencies –below.

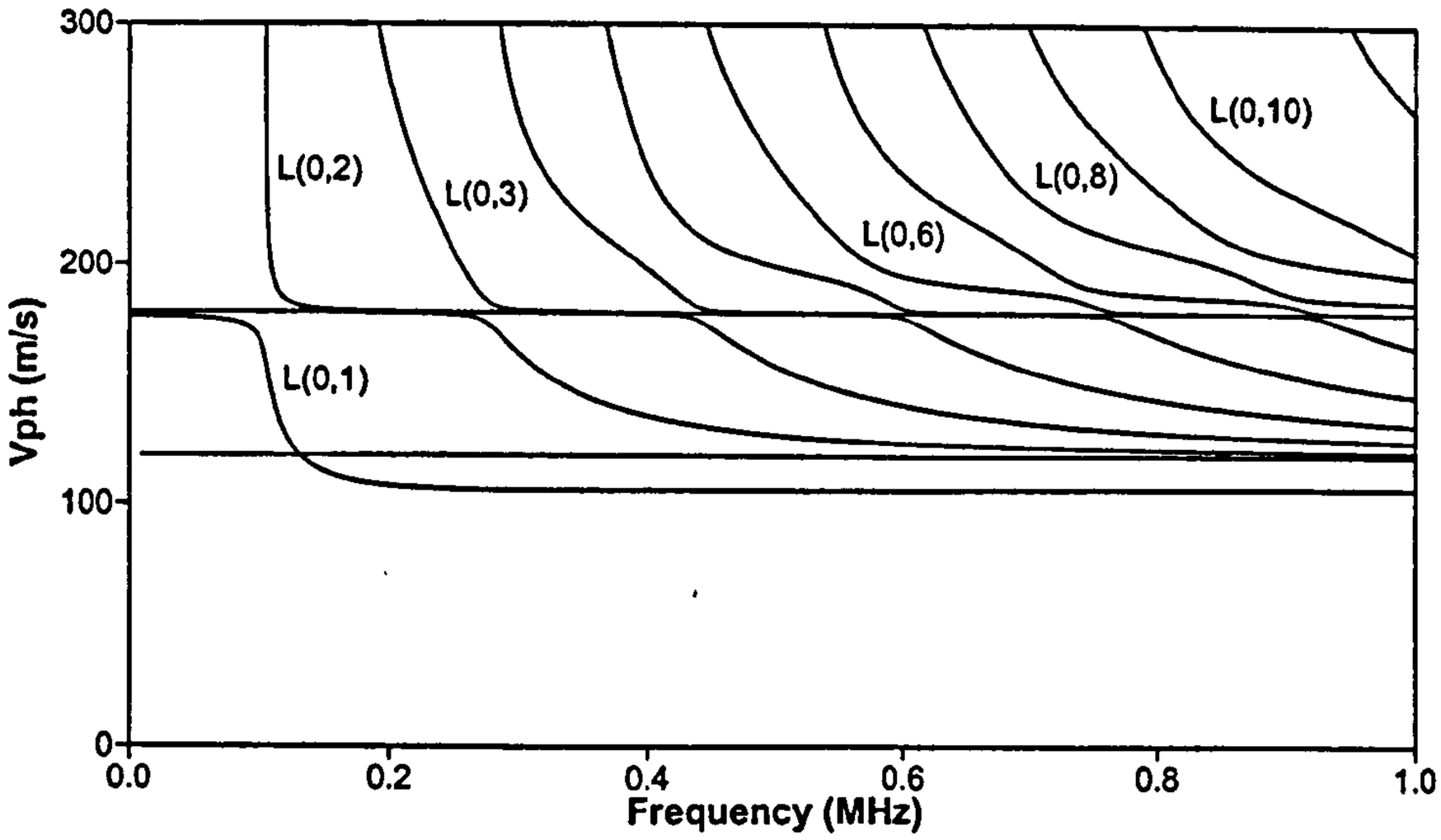

Figure 6-18 Longitudinal modes for a Gault clay cylinder. Scaled frequency 1MHz=10 kHz

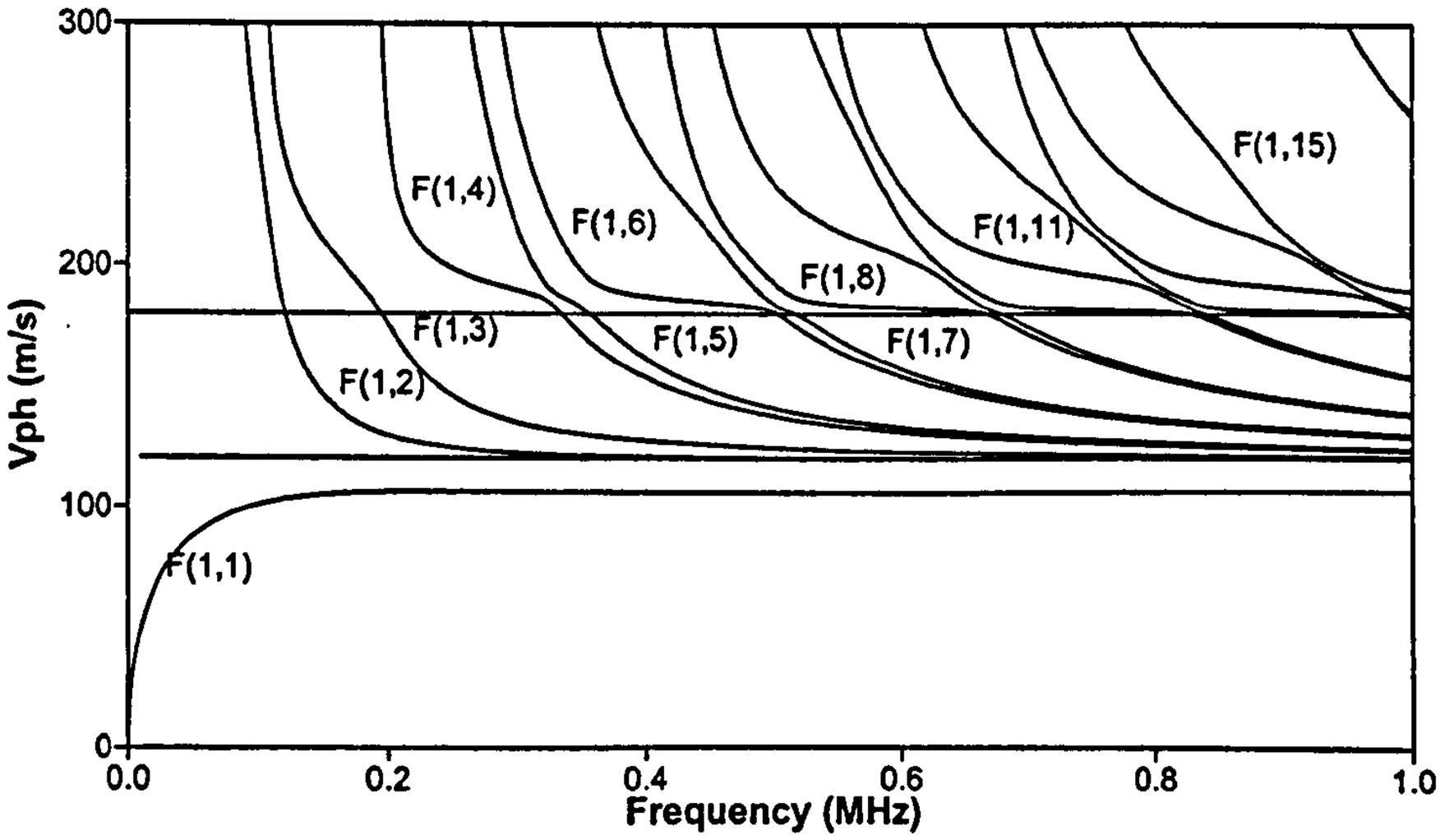

Figure 6-19 Flexural modes in a Gault clay cylinder. Scaled frequency 1MHz =10 kHz

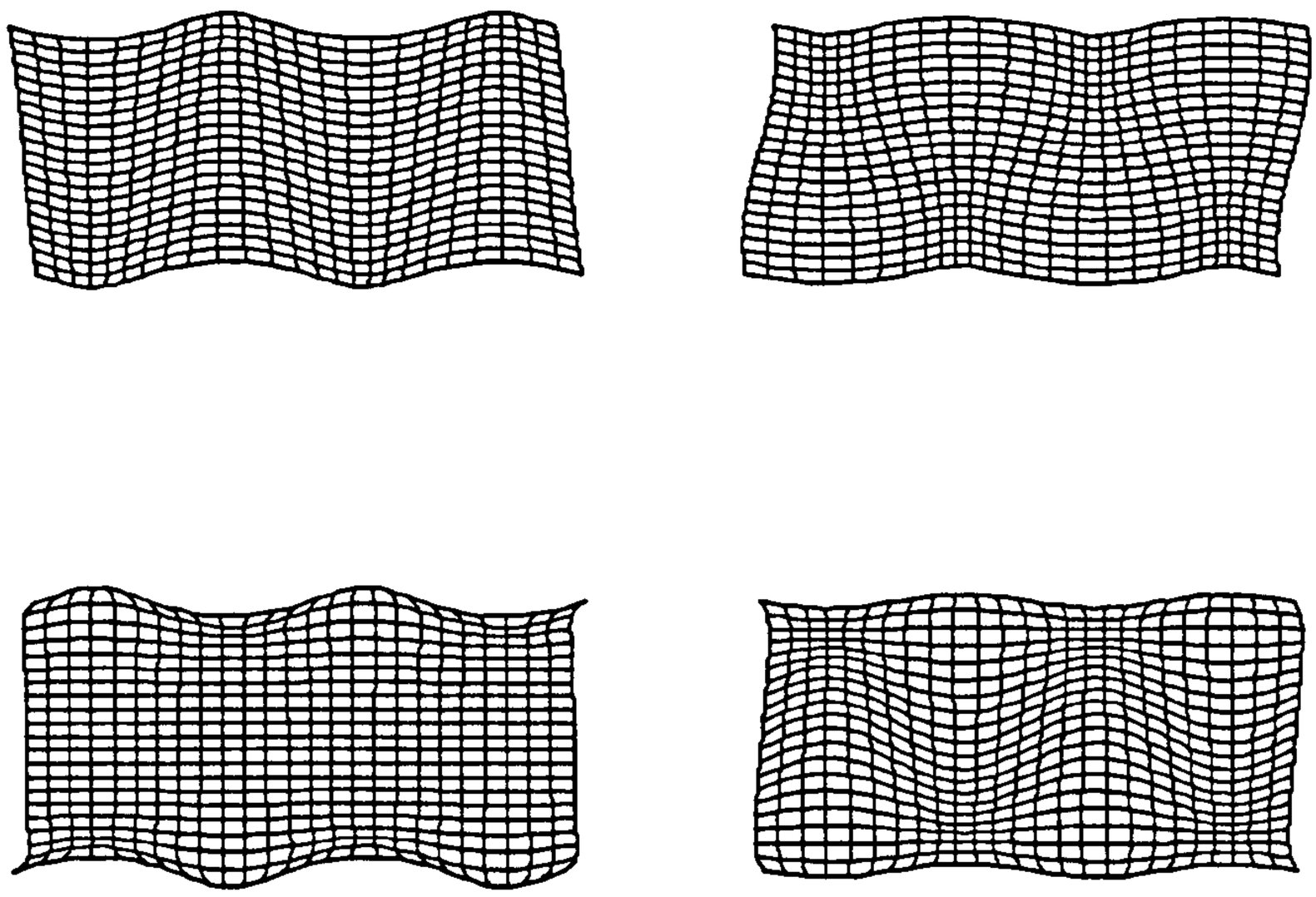

Figure 6-20 Modal shapes: lateral view of F(1,1) –left- and F(1,2) –right. Low frequencies –above- and high frequencies –below.

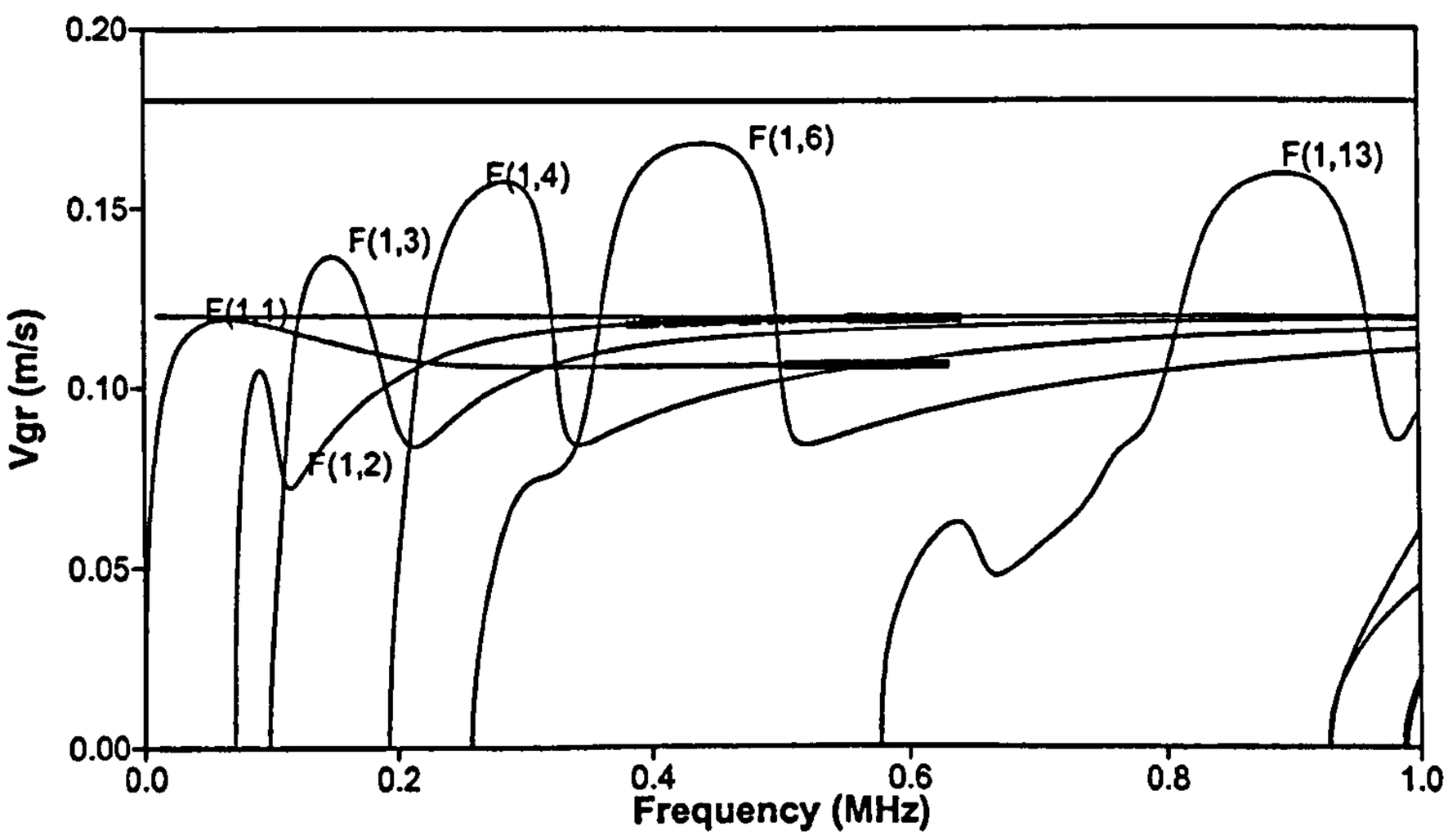

Figure 6-21 Group velocity curves in first order flexural modes. Scaled frequency 1Mhz =10kHz and velocity 0.1 = 100 m/s

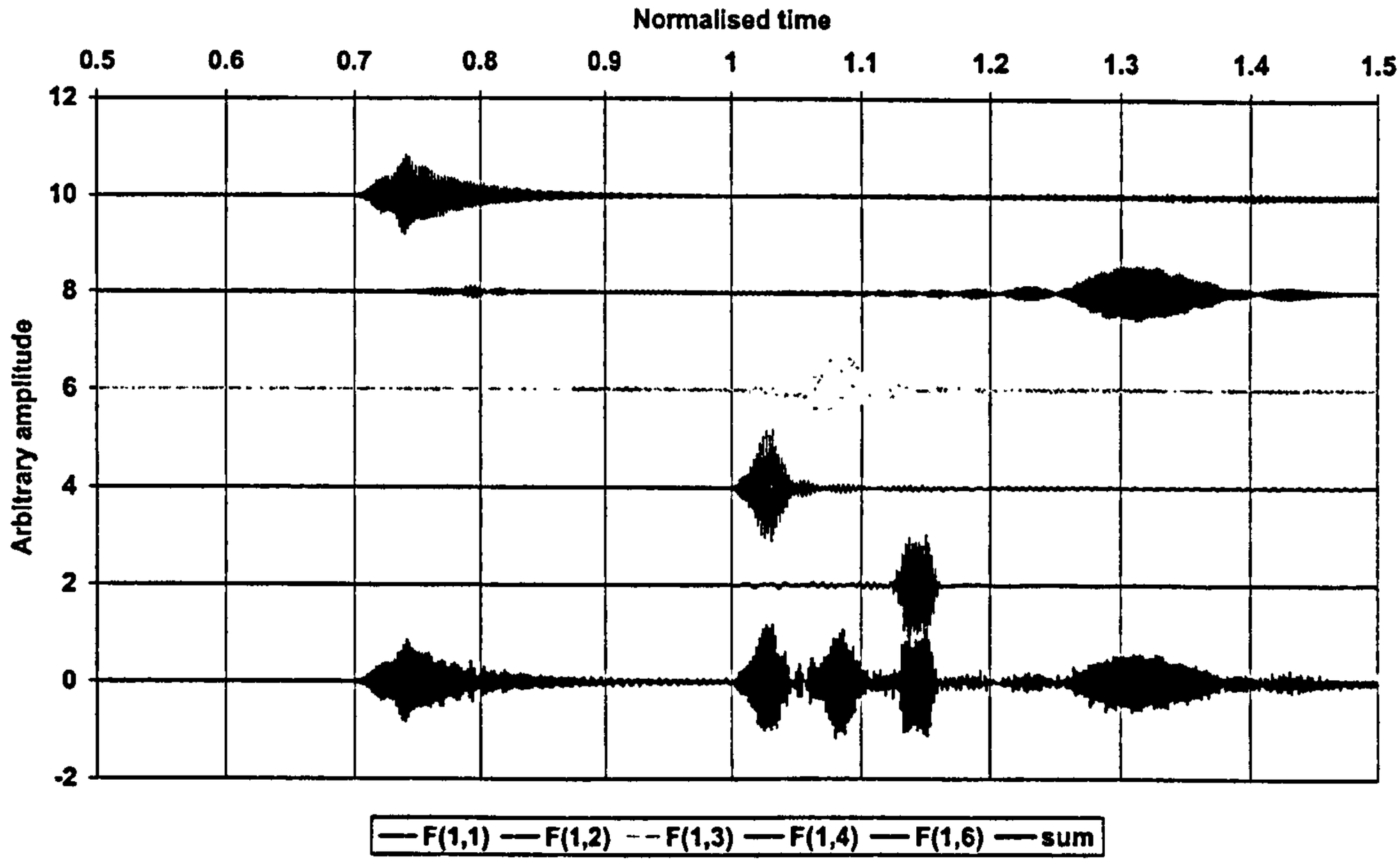

Figure 6-22 Pulse propagation on a Gault cylinder. Narrow band signal. Long (12 m) propagation distance

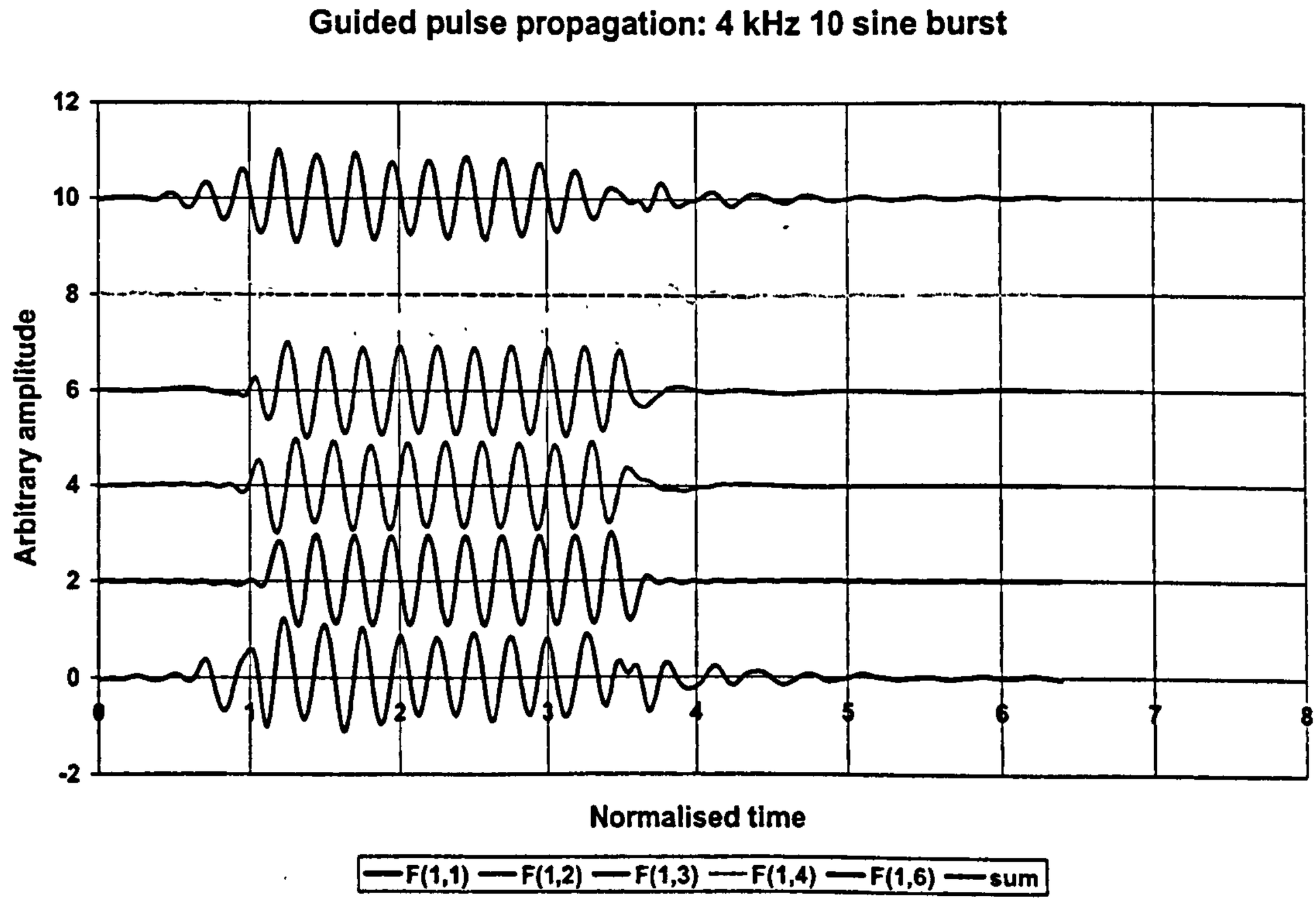

Figure 6-23 Pulse propagation on a Gault cylinder. Narrow band signal. Short (12 cm) propagation distance

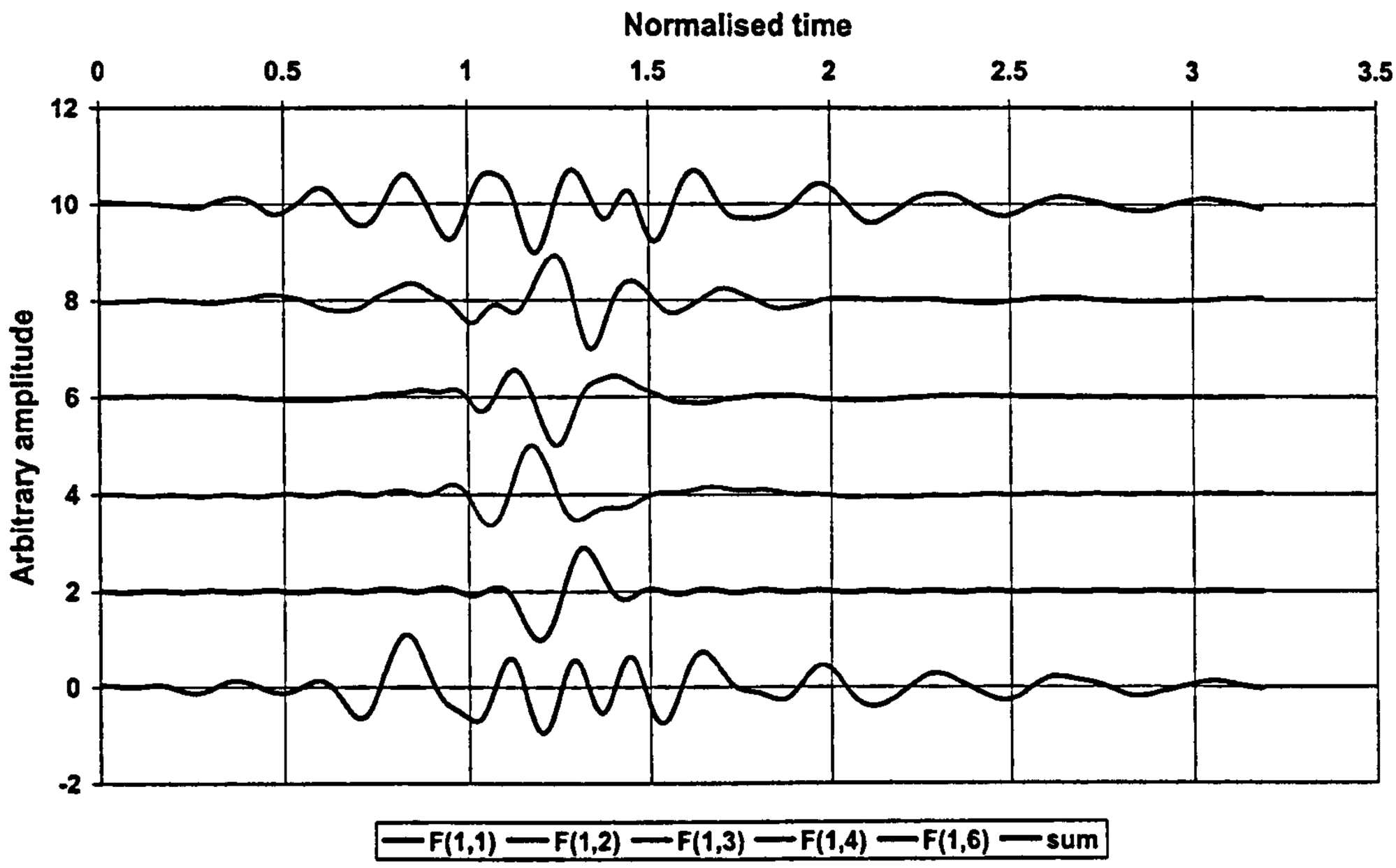

Figure 6-24 Pulse propagation in a Gault cylinder. Wide band signal. Short (12 cm) propagation distance

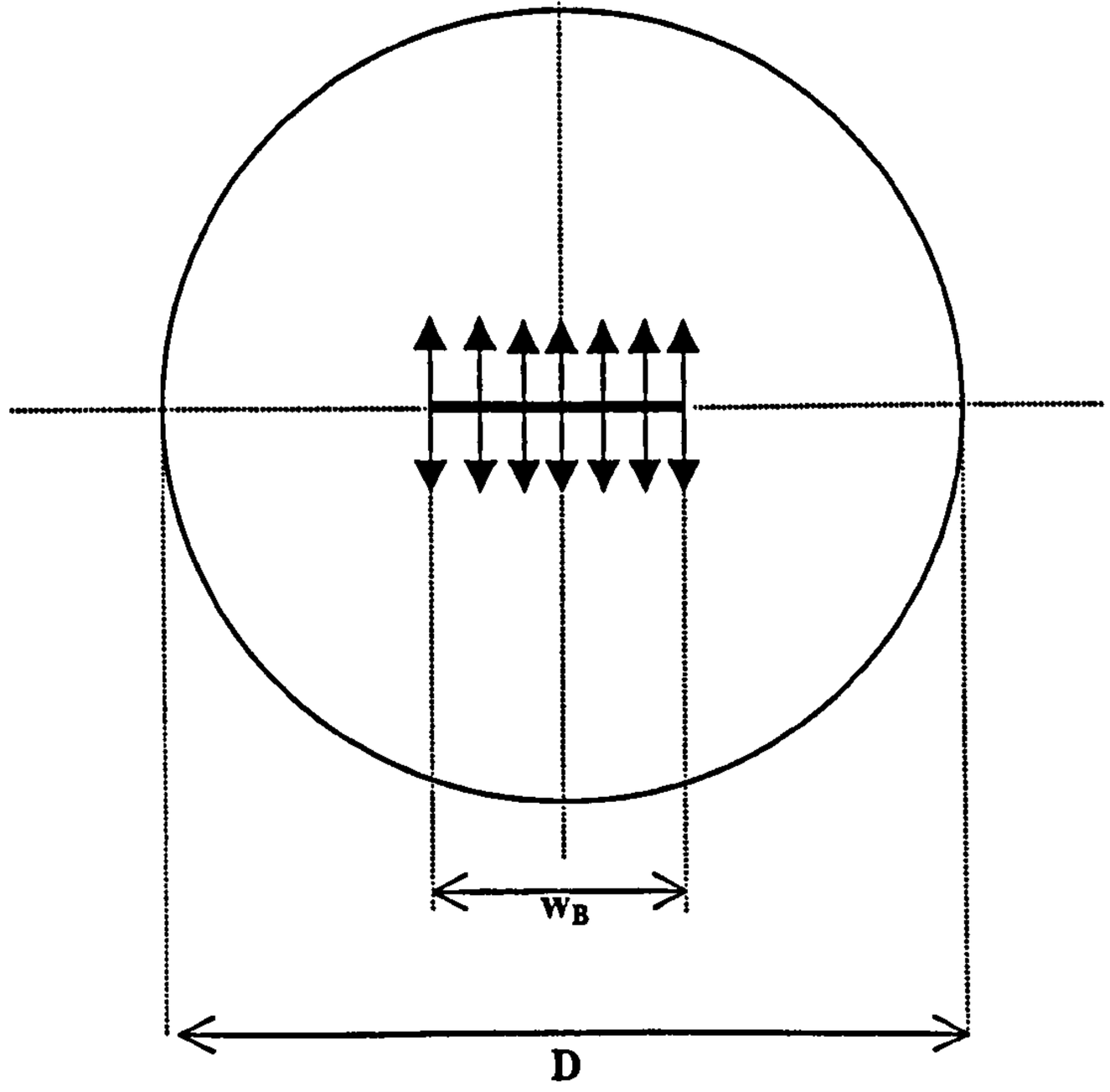

Figure 6-25 Schematic representation of bender loading on a cylinder section

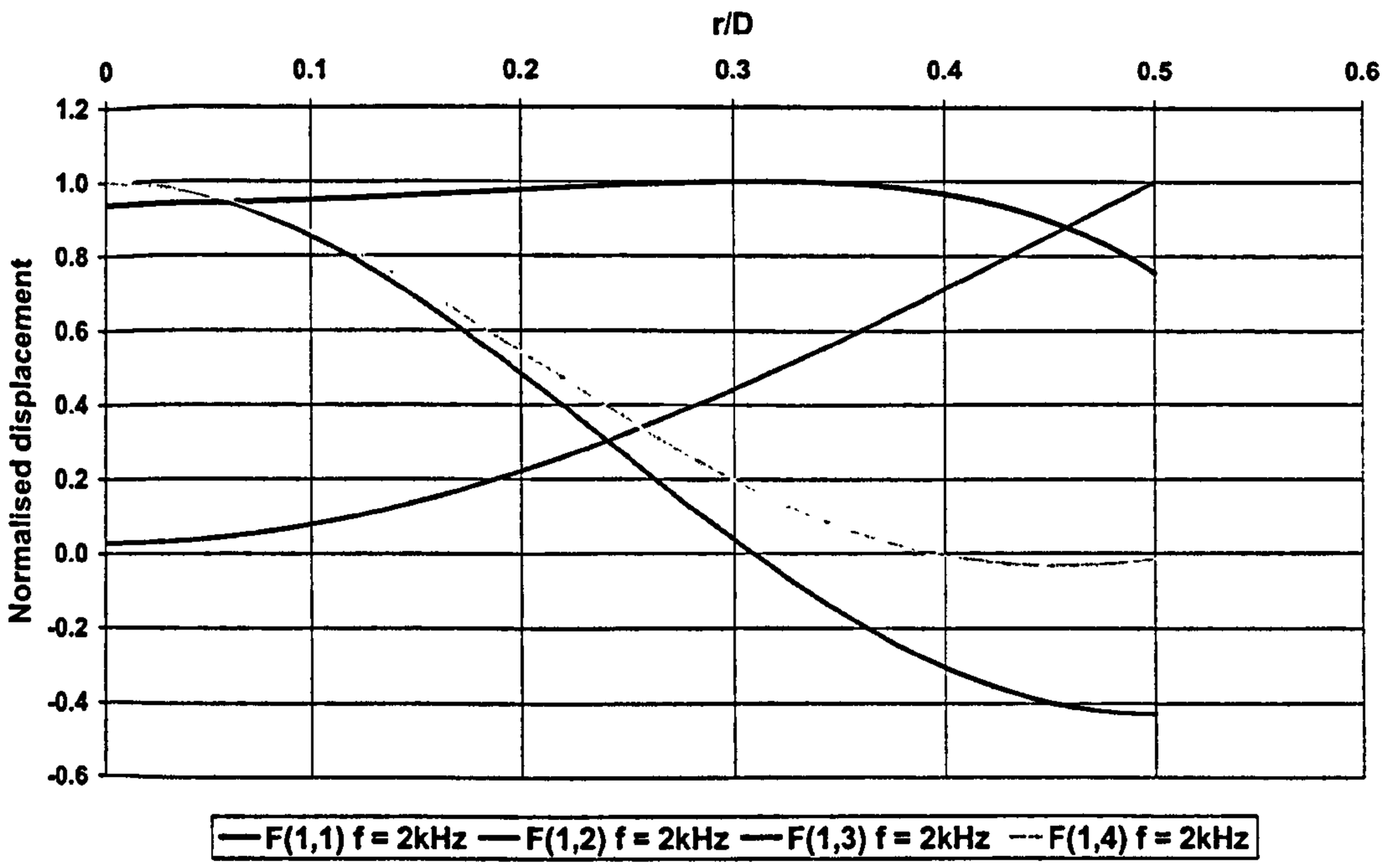

Figure 6-26 Gault cylinder: u_θ at $\theta=0$ for flexural F(1,m) modes at 2kHz

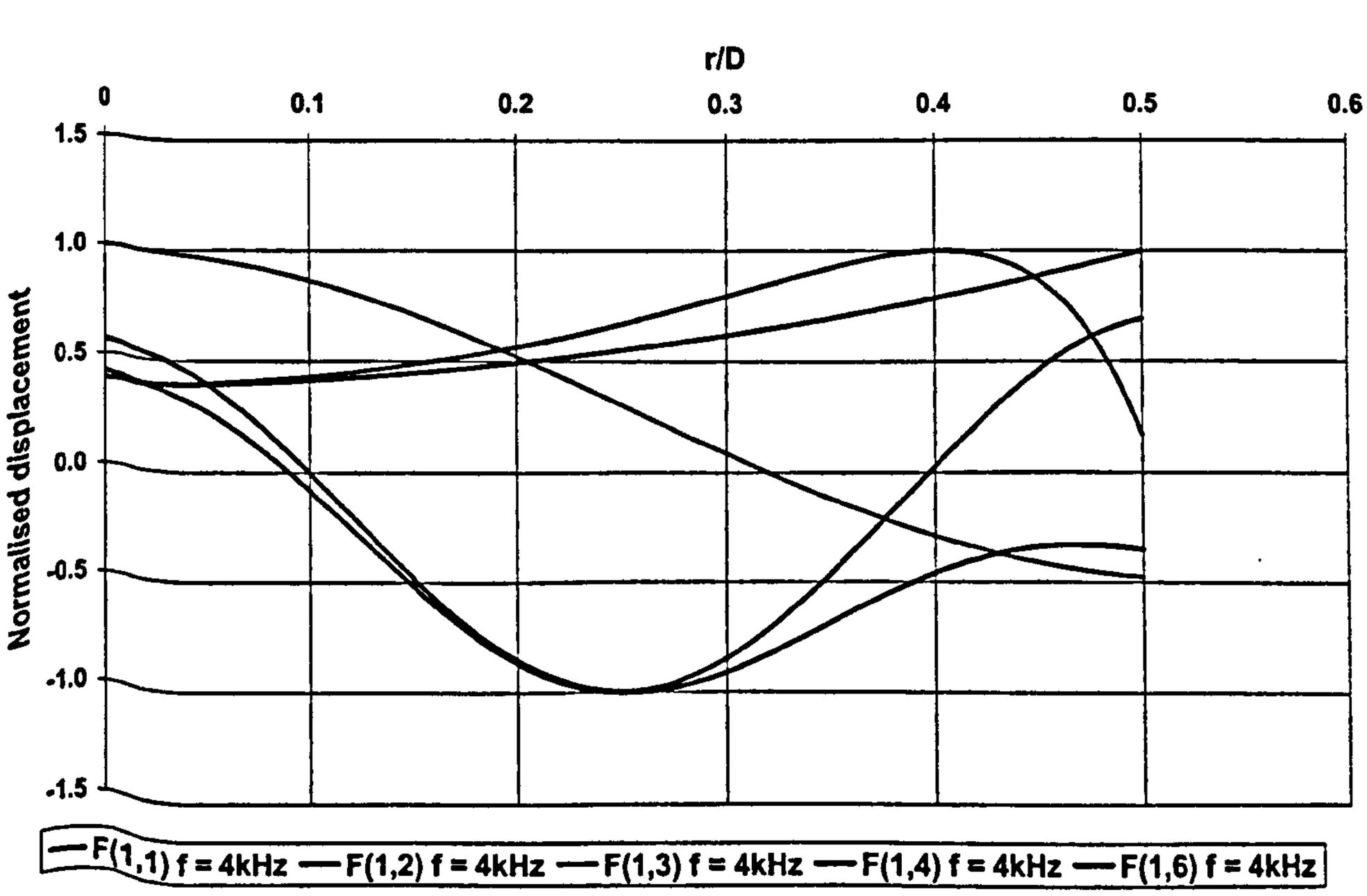

Figure 6-27 Gault cylinder: u_θ at $\theta=0$ for flexural F(1,m) modes at 4kHz

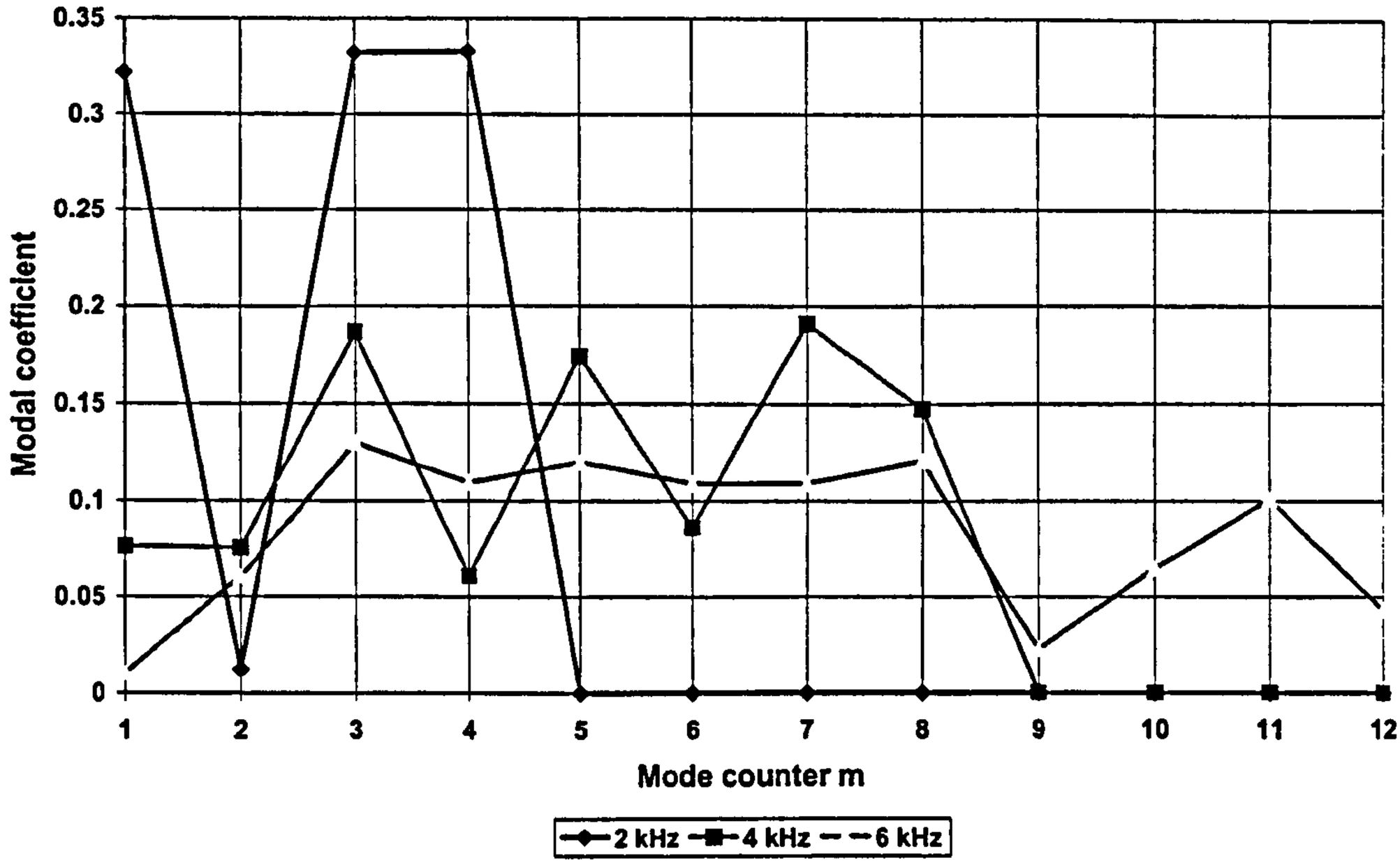

Figure 6-28 Gault cylinder: frequency effect on flexural mode weighting by bender elements

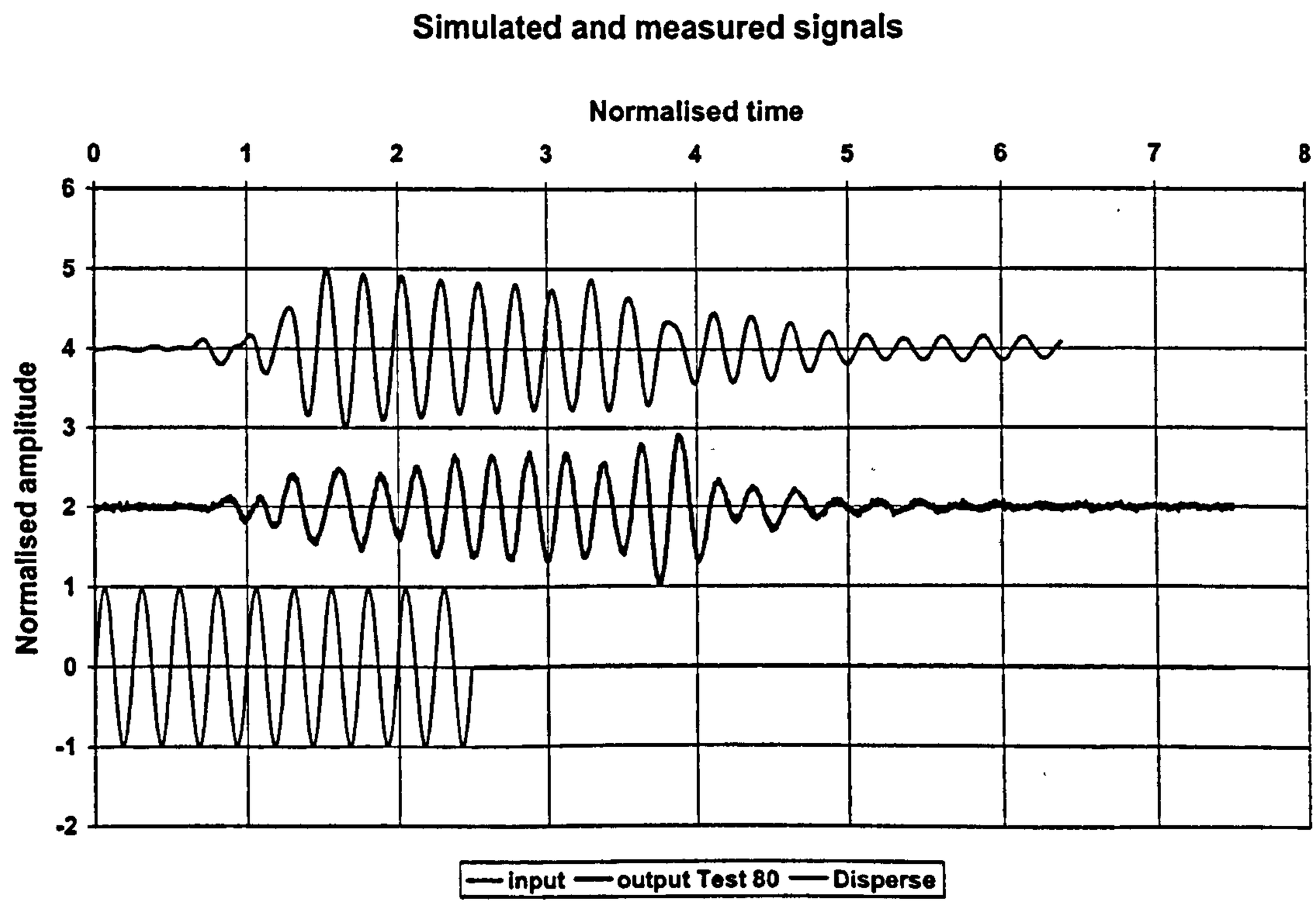

Figure 6-29 Measured trace and Disperse weighted output.
Input 4kHz 10 sine burst Assumed v, 120 m/s

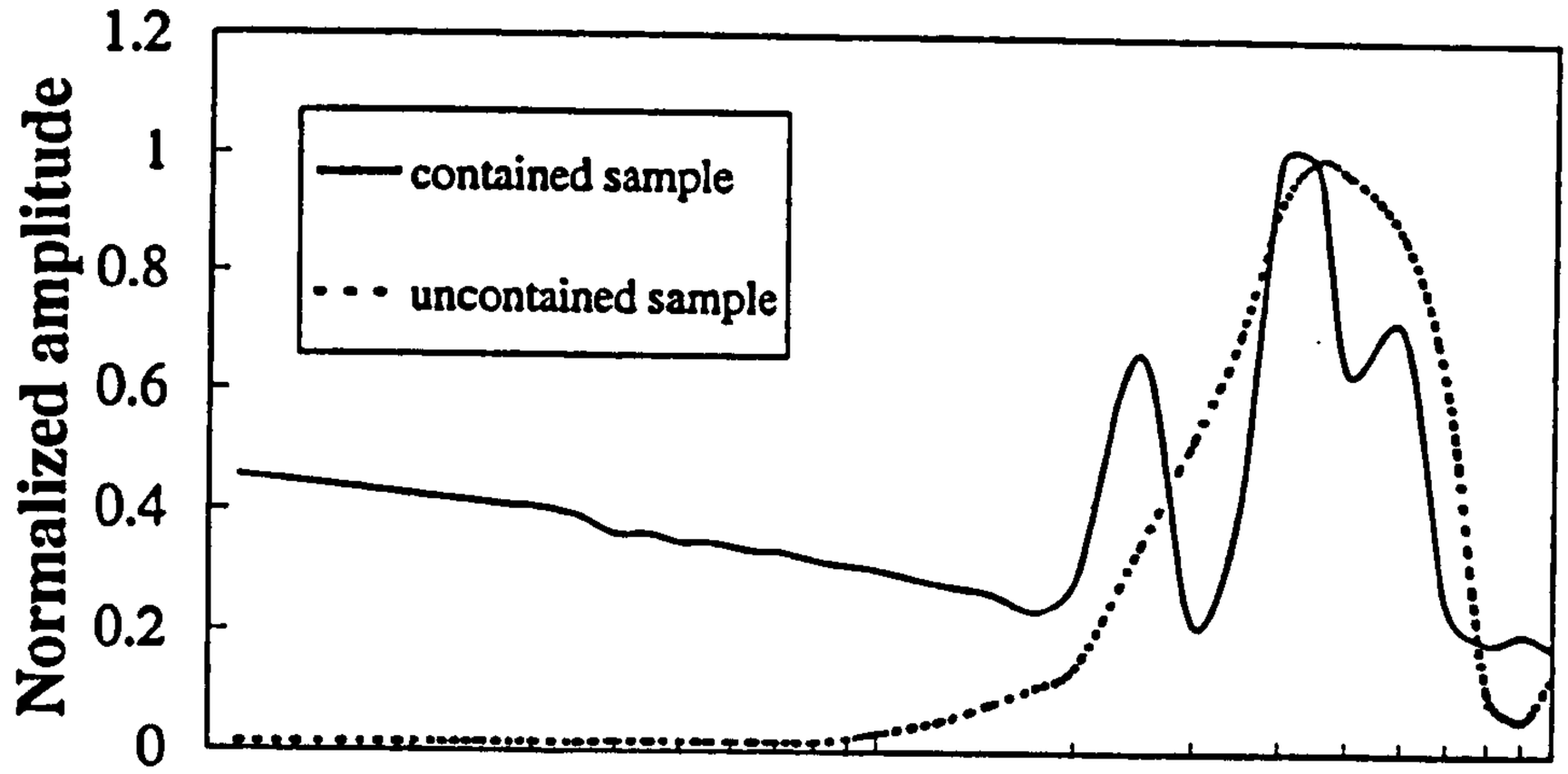

Figure 6-30 Effect of constrained cylindrical propagation on Levenseat sand (after Blewett et al. 2000)

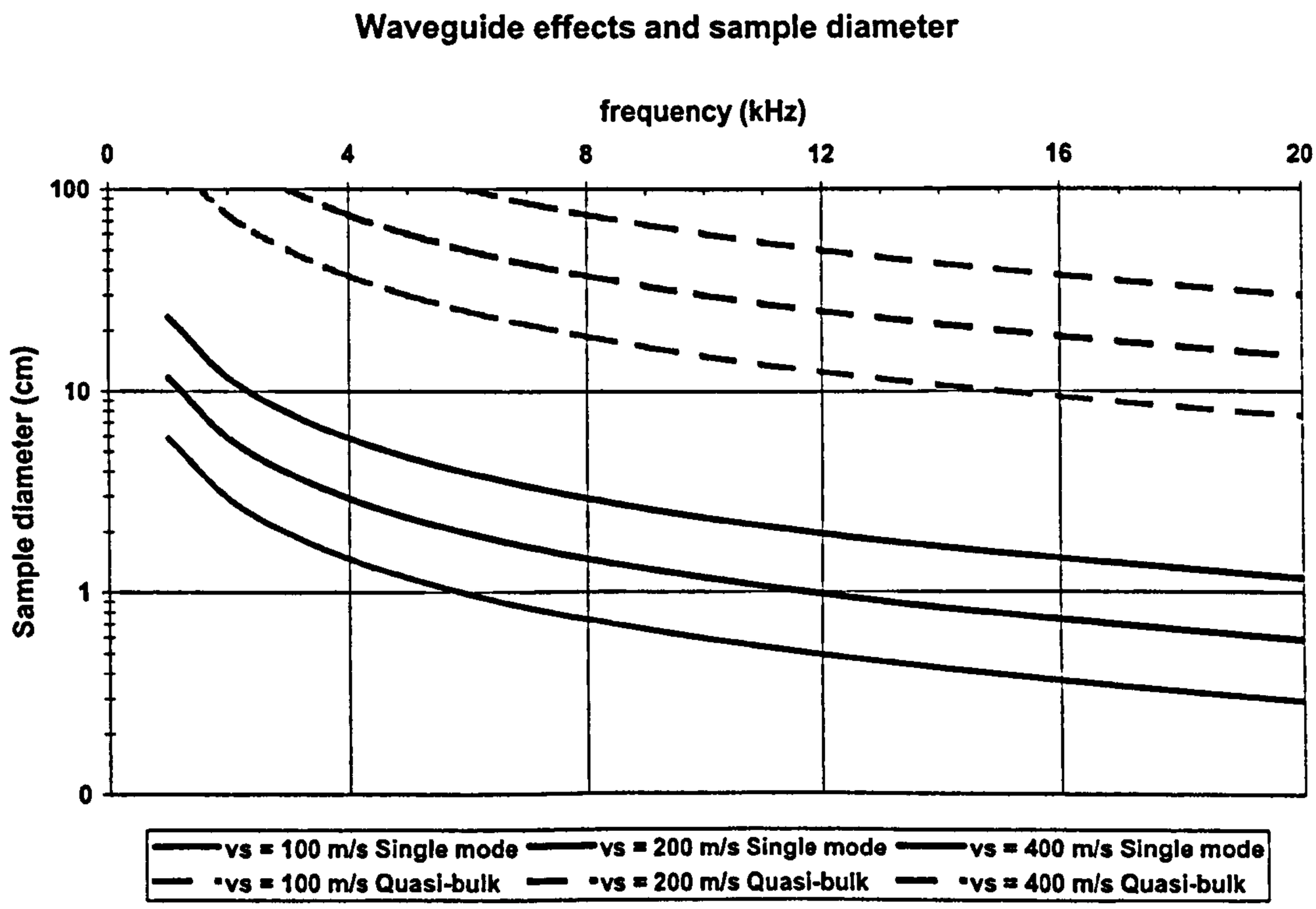

Figure 6-31 Operation limits of bender elements to avoid multimodal dispersion

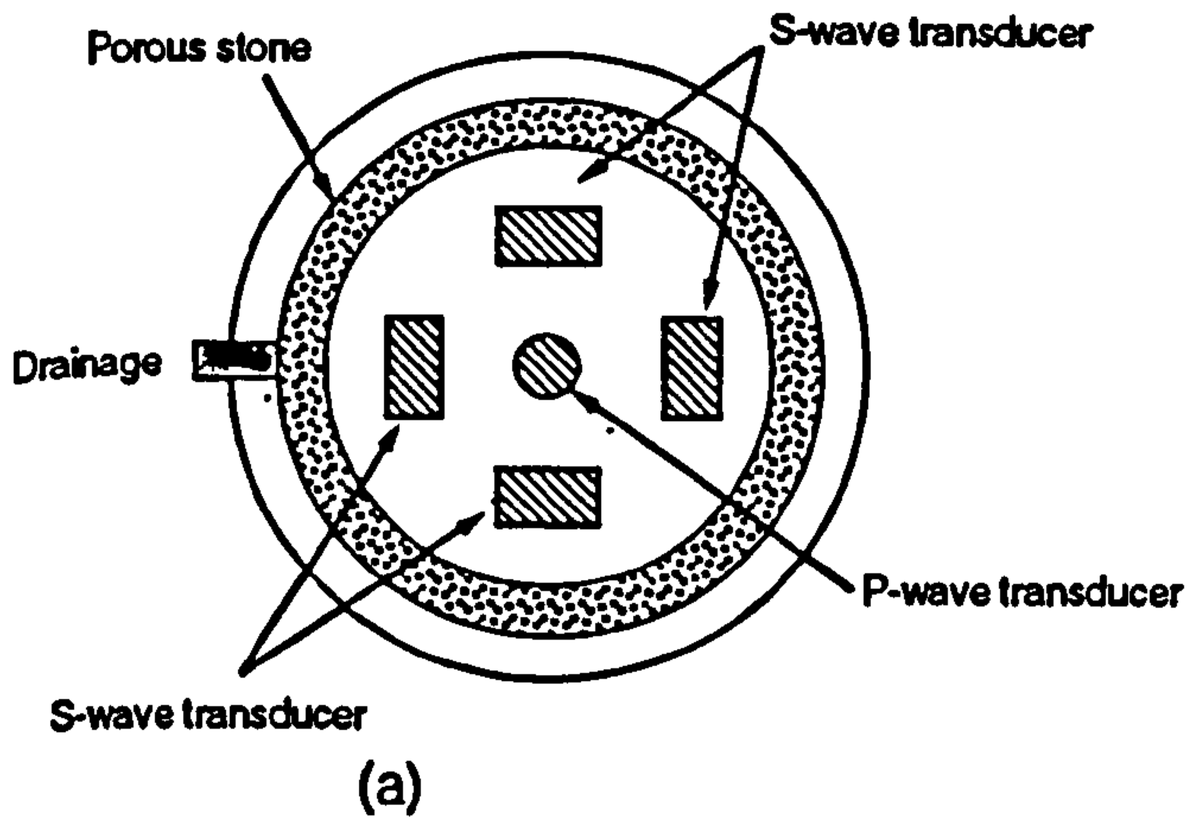

(a)

Figure 6-32 Alternative transducer arrangement in the triaxial plattens (after Nakagawa et al. 1996)

7 ELASTIC ANISOTROPY

"Having different properties in different directions". This is how an introductory text on materials science (Askeland, 1996) defines anisotropy. The bench test measurements on Gault presented in Chapter 3 were directionally dependent and the sample behaviour was then suspect of anisotropy. That was hardly surprising since Pennington (1999) had obtained the same result for Gault clay under a much wider variety of conditions in the triaxial cell. In fact, as we did mention in the introduction, the small strain stiffness of soils is now generally admitted to be anisotropic.

In soil mechanics literature, anisotropy or isotropy are usually predicated of different things. Depending of the context, researchers could refer to

A. The physical structure of the material being described
B. The models describing some aspect of the material behaviour
C. The stress or other tensorial variables entering the formulations

Oda (1972) gives an example of the first use, describing the symmetry of contact orientations between sand grains in triaxial samples. Pennington (1999) employs a cross-anisotropic elastic model to interpret stiffness measurements on Gault clay, and thus offers a nice example of the second use. The third use might be exemplified by Hansen & Gibson (1948), who studied the undrained strength of anisotropically consolidated clays, i.e. of clays whose stress states before undrained shearing were non isotropic.

Of course, one should expect those three aspects to be closely related. A material whose physical structure is anisotropic would be described with anisotropic state variables, interrelated through an anisotropic model. This might well be the case but some caution is guaranteed, because this relationship, based on how different symmetries interact, is not always immediate.

Symmetry is a subject where geometric intuition is greatly enhanced by algebra[81]. The symmetry of any geometrical figure is characterised by the rotations and reflections that may undergo without changing its appearance. The set of all rotations and reflections has group structure[82]. More restricted types of symmetry are qualified by subgroups i.e. specific parts of this group retaining the group structure. Groups may be used to describe the symmetry of materials, equations and tensorial variables as follows.

The symmetry group $\mathbf{G_A}$ of a tensor **A** is formed by those transformations that do not change its components –tensor transformations are recalled in Appendix II[83]. To define material and physical

---

[81] In fact Stewart & Golubistsky (1992) explain convincingly how dealing with symmetries geometry –almost- became algebra.
[82] A group is a set where one operation has been defined that composes two elements of the set to obtain another –i.e. is closed. For other properties see Jordan & Jordan (1994).
[83] Whilst simple material properties, as density, are well catered by single numbers, complex properties, (strength, stiffness), need multidimensional quantities. Furthermore, anisotropy deals with directional variations of properties, and directions in the plane or the space are also specified by multidimensional quantities. The usual way of dealing with multidimensional quantities requires

symmetry using groups we follow Zheng & Boehler -1994. Material symmetries are the symmetries of the material element. Physical symmetries are the symmetries of the physical laws describing the behaviour of the material.

The material element is the basic unit of a material model. To be observed, the material element should be defined by a characteristic size (e.g. radius of a small ball). Inside the material element, different physical features (atoms, crystals, dislocations, sand grains) might be observed. Their disposition must be described geometrically, and this is called the material structure. The symmetries of this structure are the material symmetries. This subgroup might be called the **material group**, and denoted by $\mathbf{G_M}$.

While material symmetries are properties of figures representing the material structure, physical symmetries are properties of the mathematical expressions describing the material behaviour. The basic mechanical variables like stress and deformation being tensors, the mathematical expressions employed in soil mechanics take the form of tensorial functions. As explained in Appendix II, the symmetries of tensorial functions are described also by groups, called symmetry groups this **symmetry group** would be generically denoted by $\mathbf{G_F}$.

The problem of how the three uses of anisotropy relate to one another can then be restated as one of establishing the relations between $\mathbf{G_A}$, $\mathbf{G_M}$ and $\mathbf{G_F}$. This approach to soil anisotropy is relatively new and will be explained in the last section of the chapter. Of course mathematical neatness is not here an objective in itself. In the first section we will describe a more classical approach to elastic anisotropy, developed for linear elastic materials. We will then move on to describe the current status of anisotropic elastic measurements in soil. We will finally show that the new approach advocated here makes easier both to interpret previous results and to plan new experiments.

7.1 ELASTIC ANISOTROPY: CLASSICAL APPROACH

Elastic anisotropy has been subject of study since long (Love, 1927; Lekhnitskii 1963). It is the classical framework of crystal mechanics and plays also of fundamental role on the study of composites, both artificial and natural –like wood or bones. In soil mechanics elastic anisotropy was a relatively fashionable idea circa 1970 -e.g. Uriel & Cañizo, 1971. Then it was somehow eclipsed by the emphasis on the plastic side of elasto-plastic models[84]. This, of course, was guided by a commendable effort to reduce model parameters and by the relatively minor role that lineal soil behaviour was supposed to play in static problems.

7.1.1 Elastic moduli and thermodynamics

In Chapter 1 we did put forward three basic hypotheses that underlie all developments presented so far: a pair of linearity assumptions -strain-displacement and stress-strain- and a set of constitutive symmetries.

---

tensors. It might be thus expected that the language employed to describe anisotropy uses intensively the concepts of tensor algebra. An Appendix is provided to remind those concepts, and reference to it is made when needed.

The constitutive symmetries are directly involved in any discussion of anisotropy and is therefore appropriate to take now a closer look at them. Let us then recall the two basic assumptions of interest

$$\boldsymbol{\sigma}_{kl} = \mathbf{D}_{0\,klij}\boldsymbol{\varepsilon}_{ij}$$
$$\mathbf{D}_{0\,klji} = \mathbf{D}_{0\,klij} = \mathbf{D}_{0\,lkij} = \mathbf{D}_{0\,ijkl} \tag{128}$$

Once the linear stress strain relationship is postulated the two first symmetries follow from the symmetry of the stress and strain tensors. Therefore only the third symmetry –sometimes called the major symmetry- and material linearity need some justification and this is classically provided by thermodynamics.

The basic thermodynamical assumption of elasticity is that materials are conservative i.e. they do not dissipate energy. Disregarding thermal effects[85] this means that the internal energy is given by an scalar function depending only on strain, say F. It follows from this condition – e.g. Nemat-Nasser & Hori 1999- that

$$G(\boldsymbol{\sigma}) + F(\boldsymbol{\varepsilon}) = \boldsymbol{\sigma} : \boldsymbol{\varepsilon} \tag{129}$$

where G stands for a complementary energy function, dependent only on stress. In that case stress, strain and their rates are interrelated through

$$\boldsymbol{\sigma}_{ij} = \frac{\partial F(\boldsymbol{\varepsilon})}{\partial \varepsilon_{ij}} \qquad \boldsymbol{\varepsilon}_{ij} = \frac{\partial G(\boldsymbol{\sigma})}{\partial \sigma_{ij}}$$
$$\dot{\boldsymbol{\sigma}}_{ij} = \frac{\partial^2 F(\boldsymbol{\varepsilon})}{\partial \varepsilon_{ij}\partial \varepsilon_{pq}}\dot{\boldsymbol{\varepsilon}}_{pq} \qquad \dot{\boldsymbol{\varepsilon}}_{ij} = \frac{\partial^2 G(\boldsymbol{\sigma})}{\partial \sigma_{ij}\partial \sigma_{pq}}\dot{\boldsymbol{\sigma}}_{pq} \tag{130}$$

The first pair of equations state that F is a potential function for the stress and G is a potential function for the strain. The second row serves as definition of the elastic stiffness and compliance tensors.

$$\mathbf{D}_{0ijpq} = \frac{\partial^2 F(\boldsymbol{\varepsilon})}{\partial \varepsilon_{ij}\partial \varepsilon_{pq}} \qquad \mathbf{D}^{-1}_{0\ ijpq} = \frac{\partial^2 G(\boldsymbol{\sigma})}{\partial \sigma_{ij}\partial \sigma_{pq}} \tag{131}$$

One being inverse of the other guarantees the uniqueness of the incremental relation between stress and strain. It is clear that the third constitutive symmetry follows directly from the symmetry of the derivatives.

Linear elasticity goes one step further and assumes that all stiffness coefficients are constant –i.e. independent of strain. In that case is possible to integrate directly the energy expressions to obtain

$$F = \boldsymbol{\varepsilon}_{ij}\mathbf{D}_{0ijpq}\boldsymbol{\varepsilon}_{pq} \qquad G = \boldsymbol{\sigma}_{ij}\mathbf{D}^{-1}_{0ijpq}\boldsymbol{\sigma}_{pq} \tag{132}$$

---

[84] Lade & Nelson (1987), for instance, argue very convincingly against any anisotropy in elastic soil behaviour.
[85] Schreiber et al. (1973) point out that whilst static tests are isothermal dynamic measurements are adiabatic. They also point that the distinction is irrelevant for shear tests.

As the energy is meant to be positive stating the previous expression in matrix-vector form makes clear that both elastic stiffness and compliance are positive definite. Being positive definite is of some consequence as all the principal minors of the matrix shall be positive

$$|D_{11}|>0 \quad \begin{vmatrix} D_{11} & D_{12} \\ D_{21} & D_{22} \end{vmatrix}>0 \quad \begin{vmatrix} D_{11} & D_{12} & D_{13} \\ D_{12} & D_{22} & D_{23} \\ D_{13} & D_{23} & D_{33} \end{vmatrix}>0 \qquad (133)$$

$$\begin{vmatrix} D_{11} & \dots & D_{14} \\ \dots & \dots & \dots \\ D_{14} & \dots & D_{44} \end{vmatrix}>0 \quad \begin{vmatrix} D_{11} & \dots & D_{15} \\ \dots & \dots & \dots \\ D_{15} & \dots & D_{55} \end{vmatrix}>0 \quad \begin{vmatrix} D_{11} & \dots & D_{16} \\ \dots & \dots & \dots \\ D_{16} & \dots & D_{66} \end{vmatrix}>0$$

This of course constraints the values of the moduli or compliance constants[86]. It is more restrictive than invertibility –which would only require the whole determinant of the matrix to be non zero. It also guarantees that the Kelvin-Christoffel tensor Γ is definite positive[87]. This, in turn, guarantees that the squared phase velocities of harmonic plane wave propagation are real and positive. All this makes the positive definite character of the elastic matrix very convenient and it is generally assumed to hold also for the more general case of non-constant moduli[88].

7.1.2 Physical symmetries in linear elastic materials

As we said in chapter 1 the index symmetries of both elastic stiffness and compliance reduce the number of independent components to 21. Further reduction is possible if some extra symmetries are imposed. Lekhnitskii (1963) does that for the case of lineal elasticity using the integral expression of the complementary energy function (129) . The procedure is always the same, he applies the symmetry-defining transformation to the stress tensor and forces the equality of the original and transformed energy expressions, thus constraining the compliance matrix. We can rephrase this procedure saying that he was enforcing various symmetry groups G_F on the energy equation, something that can be written as

$$G(\boldsymbol{\sigma}) = G\left(\mathbf{Q}\boldsymbol{\sigma}\mathbf{Q}^{T}\right) \quad \forall \mathbf{Q} \in G_F \qquad (134)$$

With this technique he explores the effects of various kinds of symmetry: reflections on a plane, reflections on three perpendicular planes and axysymmetry of various orders[89]. Figure 7-1 reproduces some of the reduced elastic compliance he thus obtains. An exactly similar procedure will apply to stiffness.

Immediately after obtaining these reduced matrices, Lekhnitskii explains that they are only valid on certain reference frames. In a general reference frame the simplifications are lost and the matrices are

---

[86] Pickering (1970), Uriel & Cañizo (1971) and more recently Lings (2001) have explored the consequences of this condition for the case of transverse isotropy.
[87] Technically this condition is known as strong ellipticity
[88] See for instance Bigoni & Loret (1999) who consider this issue from a very different perspective.
[89] The number of equivalent directions found in a plane orthogonal to a symmetry axis gives the order n of the axis. Axysymmetry of order 6 or superior implies isotropy in the plane perpendicular to the symmetry axis.

full[90]. However, for frames that respect the symmetries in G_F the matrices retain their simplified form. These frames define what he sometimes call principal directions of elasticity. They are fundamental: to fully specify any elastic symmetry we need then to specify both the elastic moduli and these principal directions.

7.1.3 Material and physical symmetries: Neumann's principle

Anisotropic elasticity was not developed for its own sake but as a model of material behaviour. The choice of one type or another of elastic symmetry should be guided by the material at hand. This is expressed classically by Neumann's principle. Neumann's principle was proposed as an axiom of crystallography: physical properties of crystals shall have the same kind of symmetry as the crystallographic form . It is now generally believed to apply to non-crystalline materials as well - Lekhnitskii 1963, Zheng and Boehler 1994. It can be stated more precisely using group terminology: the symmetry group of any constitutive law of the material must include its material group, that is

$$G_M \subseteq G_F \tag{135}$$

The symmetry of the material structure must then be present in the symmetries of the formulations employed to describe its behaviour, although these formulations might have greater symmetries[91]. This is an important result, for it suggests the following programme to obtain meaningful formulations:

a) Identify the material element
b) Measure its symmetries i.e. identify its material group
c) Enforce this symmetries on the formulations

This was easily done with crystals. At least since 1848 the complete catalogue of the 32 crystalline G_M was known –Stewart & Golubitsky, 1992. It turn out to be that a lesser number of elastic G_F were necessary, only nine. Figure 7-2 collects the elastic compliance in principal axis of four crystal systems.

As we said Lekhnitskii and others extended this approach to non-crystalline materials. The material structure was rather obvious in some cases. A wooden log has cylindrical symmetry at first approximation. Is also easy to see three perpendicular planes of symmetry on a fibre reinforced laminate. These material symmetries lead to elastic symmetries who were equal to those obtained for some crystal classes but where distinctly named. Figure 7-3 collects the elastic compliance for the symmetries most often discussed when non-crystalline materials are considered.

In our figures we have adhered to a rather self-explanatory naming convention for moduli and compliance constants -D_{ij} and d_{ij} respectively. There are other possibilities, of course, the most common being a generalisation of the {E, ν, G} notation of isotropic elasticity. In soil mechanics the case of

---

[90] Is not always that bad, but it is quite bad: for instance rotation around one axis leaves an originally hexagonal-form matrix in monoclinic form. A second rotation around a different axis and the whole matrix is full.
[91] The greatest symmetry of all being isotropy, this will mean that for any material Neumann's principle is compatible with an isotropic model. The model would not be very precise, however.

transverse isotropy has received much attention and two usual forms of the compliance matrix in this notation are written in Figure 7-4 for ease of reference. Note that the asymmetric form is that only on writing, as one Poisson ratio is redundant. The relation of this engineering moduli to those appearing in the matricial notation is given in Appendix III.

7.1.4 Measurement: test symmetries and elastic symmetries

Static test designs are poorly adapted to obtain anisotropic elastic constants. Element testing is the principle behind static test interpretation. In available soil mechanics configurations only some elements of the strain and stress vectors are directly controlled and measured. Two in triaxial tests, three in true triaxial apparatuses, four in some hollow cylinder designs and the plane strain directional shear cell. This is a well known limitation but there is another, more insidious. Each one of these test designs has its own in-built symmetry and it needs to be compatible with that subject to test.

When this is not the case, anisotropy may lead to inhomogeneous deformation fields within the sample, turning the presumed element test into a complex boundary value problem, where the dimensions of the sample might play a decisive role. Pagano & Halpin (1968) beautifully illustrated this issue in a classic paper. Figure 7-6 is taken from that paper and shows the response of a reinforced rubber to plane stress traction when the orientation of the reinforcement varies with respect to the loading. Inhomogeneous deformation appears on the specimen to the right where the specimen material axis were misaligned with those of the testing system. In that case, a naïve interpretation of axial stress and strain measurements will produce an incorrect estimate of the deformation modulus. This problem is known as off-axis testing and reduces considerably the testing scope of existing apparatuses.

Consider, for instance, the case of the triaxial test. The testing procedure has cylindrical symmetry around the axis of the apparatus and the sample being tested should have the same symmetry. This is achieved, for instance, if cylindrical samples are taken from a transverse isotropic material with the sample axis perpendicular to the plane of isotropy. If the sampling axis is oblique to that plane the symmetry is lost. The cylindrical sample may still be placed on the apparatus but with respect to the testing axis its elastic matrix has monoclinic[92] form even if is still dependent on just five moduli. A brief consideration of Figure 7-2 shows that the relevant relation between stress and strain will be

$$\begin{Bmatrix} \varepsilon_{11} \\ \varepsilon_{22} \\ \varepsilon_{33} \\ \varepsilon_{23} \\ \varepsilon_{31} \\ \varepsilon_{12} \end{Bmatrix} = \begin{bmatrix} d_{11} & d_{12} & d_{13} & 0 & 0 & d_{16} \\ d_{12} & d_{22} & d_{23} & 0 & 0 & d_{26} \\ d_{13} & d_{23} & d_{33} & 0 & 0 & d_{36} \\ 0 & 0 & 0 & d_{44} & d_{45} & 0 \\ 0 & 0 & 0 & d_{45} & d_{55} & 0 \\ d_{16} & d_{26} & d_{36} & 0 & 0 & d_{66} \end{bmatrix} \begin{Bmatrix} \sigma_{11} \\ \sigma_{22} \\ \sigma_{33} \\ \sigma_{23} \\ \sigma_{31} \\ \sigma_{12} \end{Bmatrix} \tag{136}$$

---

[92] As we mentioned before this follows from applying a rotation to the elastic tensor. It can also be appreciated directly noting that the off-axis cylindrical sample is left with just one plane of symmetry –that formed by the material symmetry axis and the sampling axis. One plane of symmetry is also the only material symmetry of a monoclinic crystal.

Shear and volumetric deformation are not anymore independent, an axial load will induce shear strain and the response in a plane perpendicular to the loading ram is not anymore isotropic. Moreover, in most triaxial testing implementations shear deformation is constrained by the top and end platens, resulting on shear stress under axial loading that will not be equilibrated on the lateral sides. The consequence is that deformation ceases to be homogeneous. This was observed long ago by Boehler and Sawczuk (1977) working with stratified rock –Figure 7-7.

For a true triaxial apparatus the situation is similar. The apparatus has three axis of symmetry and, therefore, is suitable to study samples with orthotropic or higher symmetry. An orthotropic or transverse isotropic material sampled off-axis will be subject to shear stress on the end platens. If these are not measured a systematic error will affect the measured moduli.

The symmetries of a hollow cylinder apparatus are more subtle. When inner and outer pressure are equal and no torque is applied the situation is very similar to that in a triaxial apparatus, and the test is axysimmetric. When the torsional torque is applied global axial symmetry is lost –the wall shear stress is antimmetric and the radial stress symmetric- but locally there is still symmetry about the plane dθ-dz. If this is coincident with the symmetry of the sample, a monoclinic cylindrical matrix can be measured. This may correspond, for instance, to a transverse isotropic material whose axis is contained in that plane. Finally if the inner and outer pressures are different even that symmetry is lost. The test is not anymore a single element test –radial stress varies along the wall- and some homogenisation assumption is needed. It is not known how this issue affects the measured elastic moduli.

It is then apparent that for static tests some knowledge of the kind of elastic anisotropy to be measured shall precede the measurement phase. It is also apparent that the most anisotropic cases pose formidable problems of test design. As we will see in next chapter dynamic tests allow more latitude in the first respect and –under certain conditions- pulse tests might be employed to measure all kinds of anisotropy. It is not strange then to find that dynamic tests have been since long the tool of choice for elastic measurements on fully anisotropic materials such as crystals –Schreiber et al. 1973. But our concern here is with soil and we need now to consider what has been discovered as yet from its elastic anisotropy.

7.2 ELASTIC ANISOTROPY IN SOILS

7.2.1 Testing conditions

Both static and dynamic procedures have been employed in studies of soil elastic anisotropy. Table 7-1 contains a selection of references describing static determination of $\mathbf{D_0}$ elements. Of course, the old cases used external measurements and, by today's criteria it is clear that they were not measuring within the elastic range. But even if the measurements were off-limit the interpretative framework employed was the same. The design of triaxial and true triaxial apparatus only allows investigation of the submatrix $\mathbf{D_0}$ relating normal stresses and strains. The elastic anisotropy investigated with these apparatus was transverse isotropy so the off-axis testing problem was not an issue. In the triaxial case only three values can be recovered and, as Graham & Houlsby (1982) carefully explained, only two of them correspond

directly to single moduli $-D_{33}$ and D_{13} in our notation- the third being a combination of D_{12} and D_{11}. From a pragmatic point of view if triaxial is the only measurement available there are some advantages in using differently defined moduli and various proposals in that sense have been put forward –Graham & Houlsby, 1982, Lings et al. 2000.

Small strain testing in hollow cylinders has, in principle, greater potential that in triaxial apparatus. Figure 7-5 taken from Di Benedetto et al. (1997) shows that up to four independent components of the stress and strain tensors may be measured. The results presented to this date have been more limited. The applied elastic loading has been always either strictly axial - where $d\sigma_z$ is the only non zero component- or strictly torsional – only $d\tau_z$ is non zero. Di Benedetto et al. (1999) measured the four strain components and therefore the eight compliances in the last two columns in the matrix. Yamashita & Suzuki (1999) measured just the two diagonal terms. None of them made very clear statements about the type of elastic anisotropy being measured.

Fully dynamic procedures remain scarce, mostly because they do require the measurement of compressive velocities and fluid interaction effects are then hard to handle. Some available data sets have nevertheless been obtained with dry granular materials -Table 7-2. This data has been mostly obtained in calibration chambers, of triaxial –Bellotti et al. 1996- and true triaxial design –Lee 1993, Stokoe et al. 1995. Both teams have presented results in terms of a transverse isotropic model, although Stokoe et al. pointed that an orthotropic model was more adequate for the true triaxial case. Argawal (1992) thought the same while using a true triaxial apparatus but was half successful and only recovered diagonal terms of the stiffness matrix . All this researchers tested in-axis and off-axis, but the consequences of this condition are different for dynamic tests as next chapter will explain.

A more common approach restricts the dynamic exploration of elastic anisotropy to shear waves. Velocities can be measured in different directions using various transducers in one sample (e.g. Jamiolkowski et al. 1995) or using similar but rotated samples in one apparatus (Jovicic & Coop, 1998). The first approach has numerous advantages and has taken new impetus with the advent of horizontally mounted bender elements, developed by Pennington (1999) and also employed by Kuwano (2000). Shear elastic anisotropy so measured is interesting in itself but is even more potent when combined with static strain measurements. Pennington (1999) and Kuwano (1999) have thus obtained five different elastic moduli of a transverse isotropic model. Their dynamic tests were in-axis, although dynamic off-axis tests is equally possible in samples –Jamiolkowski et al. 1995, Zeng, 1999.

7.2.2 Observed dependencies

Ever since it has been measured –e.g. Hardin & Richart 1963- the small-strain stiffness of soils has shown stress-dependency. Independently of the varied elastic symmetry assumptions and the increasing number of moduli, stress-dependency always appears. As we have just explained the stress space thus far explored remains overwhelmingly dominated by triaxial and true triaxial conditions. For this conditions the observed stress dependency has been generally summarised through exponential expressions like

$$X_{ii} = C_{ii}\tilde{\sigma}_{ii}^{n_i} \quad i = 1,2,3$$
$$Z_{jk} = C_{jk}\tilde{\sigma}_{jj}^{n_j}\tilde{\sigma}_{kk}^{n_k} \quad j \neq k \;\; j = 1,2,3, \;\; k = 1,2,3 \tag{137}$$

where repeated indexes do not imply sum. X_{ii} is a placeholder for axial loading properties like Young modulus –e.g. Hoque & Tatsuoka, 1998- or P-wave velocities –Stokoe et al. 1996, Bellotti et al. 1996- and Z_{jk} for shear properties, be it velocity –Kuwano, 1999- or shear modulus –Pennington, 1999- Stresses are normalised and the varying factor C contains other influences that will be examined later.

Two main observations distil from this research. The first is that shear properties are affected only by stresses on the plane of shear and axial loading properties only by stresses along their axis. The second is that the regressions usually find exponents implying a near square root stress-dependency of moduli.

The scope of this correlations is, however, limited. Even in the very limited stress space explored by the triaxial apparatus they seem unable to summarise all the data. Belloti et al. –1996-, for instance, note that their shear exponents depend on the stress ratio[93] for K<0.5. Hoque & Tatsuoka –1998- also observe the failure of isotropic correlations when K<0.5, but now for the case of Young modulus. The clearest result in that respect is due to Kuwano, who obtained her correlations with data from isotropic and anisotropic compression test stages and then noticed how the obtained correlations fared rather poorly on shear stages –Figure 7-8.

It is also generally accepted that void ratio affects small stiffness measurements. This is generally accounted for including a single[94] void ratio function in all the C factors of (137). Pennington (1999) is an exception as he proposed a different void ratio function for every direction, something tantamount to an anisotropic void ratio function.

There is more contention about the effects of the overconsolidation ratio on unload-reload consolidation paths. A common view is that tests on sand show almost no effect, but those on clay generally do –see Pennington 1999, for a resigned view on that issue. A single exponential dependency on OCR is then included on the C factors. Creep under the static applied load might affect measurements as Moncaster (1997) has shown recently. No account of this effect is generally introduced in the correlations and it might be avoided if enough waiting time is left for the creep period to end.

Finally there are effects which remain unexplained after account is taken of stress state, void ratio and OCR. These are included in the C factor and have to be directionally dependent to account for the general observation that even under isotropic stress states stiffness remains anisotropic. This are generally known as structure or fabric dependent factors. Pennington (1999) has shown that they are different in intact and reconstituted samples of Gault clay, and therefore they are not explainable only by composition.

---

[93] Ratio of horizontal to vertical stress in a triaxial apparatus.
[94] Single but not unique, there have been quite a few proposals and Kuwano (1999) offers an interesting review of them.

7.2.3 Which symmetry?

How did those researchers establish the type of elastic symmetry that they were measuring? A recurrent argument favouring transverse isotropy mentions the geological features of deposition basins. Horizontal stratification under a vertical force seems to be a good argument for transverse isotropy of samples from vertical borings. But, as any practising engineer knows too well this is most often than not a pious desire. The symmetry of the forming process for reconstituted samples offers a more sound argument, particularly for clay, where awkward processes like tamping or lateral vibration never enter into play.

All this considerations are really educated guesses about material symmetries. Based on Neumann principle we suggested above a three-step approach to anisotropic formulations: identify the material element, measure its symmetries, enforce them. The fabric factors introduced in the correlations may well be a measure of the material symmetries. This is, however, hard to tell, as in soils direct measurement of material symmetries is rather problematic.

The geometrical richness of soil microstructure is well described by Mitchell (1991, Cap. 8). In soils there is no equivalent to the repetitive unit cells of crystallography, nor there is to the unambiguous choice of atoms as basic units. Physical units of very different scales are identifiable e.g. clay aggregates, sand grains, laminations, even strata[95] ...There might be then different choices of material elements, employing different characteristic sizes and thus producing different material structures, possibly with different symmetries[96].

In granular soils like sands the elementary unit seemed obviously identifiable with the sand grain and a number of researchers since Oda (1972) have proposed different measures of grain arrangements –e.g. spatial distribution of contact unit normals. Measurement however requires inspection of thin sections of the sample, a rather daunting task even for medium sized materials.

Oda's patience was rewarded with the discovery of a different problem. The material symmetry thus measured was not fixed during a test but varying. This obviously meant that to keep track of the material symmetry a new measurement was needed at each test point. Even if automated image analysis of sections is now available (e.g. Muhunthan et al. 2000) the procedure is destructive and still requires a new sample –and a new test- at every measurement point. Apart from this practical difficulty Oda's discovery left one question open. The material symmetry was affected by the external load, but this had a symmetry of its own. What was the relationship between both? How do they affect measured response symmetries? This is directly relevant to the question of how many different elastic moduli might be measured or, in other words, what types of elastic anisotropy are possible in soils. The question is of

---

[95] Indeed. For instance Kirkgaard & Lade –1991- discovered that the San Francisco bay mud test samples taken from a trial pit were traversed by thin lenses of silt whose plane was at an angle with the sample axis.

[96] This, of course, leaves room to many important questions: what should be the relation between two different models of the same material and how coarse models might be related to finer ones? Are all macro-properties –e.g. permeability, stiffness- related to the same set of micro-structural features? What is the relation between externally imposed length scales –e.g. elementary test sample dimensions- and the appropriate level of material structure definition? This is a vast subject whose bearing extends well beyond soil mechanics and will not be addressed here -see e.g. Krajcinovic 1998.

some interest, both from a general viewpoint and –as next chapter will make clear- from the more restricted of pulse test interpretation.

For the case of elastic measurements this multiplicity of influences is generally framed within a dichotomy between inherent and induced anisotropy. This terminology has been used in geotechnical research since Casagrande & Carrillo (1944). However this long tradition does not mean that there is general agreement about its meaning. Quite the contrary, almost every researcher involved in the field feels compelled to propose a definition of its own. It is worth quoting some of them.

Lee (1993) defines inherent anisotropy as that "due to the material itself" and "not affected by imposed stress", a "result of deposition processes and grain characteristics". This is opposed to "stress-induced anisotropy" which includes that caused by "strain associated with stress" and is "a function of strain history" but "not an intrinsic property of sand". Three years later Belloti et al (1996) define "strain induced anisotropy" as "changes on the inherent anisotropy", which they describe operationally as that measured under isotropic stress; both are different from "stress-induced anisotropy", now redefined as that "due to anisotropic stress states". Two years later Hoque & Tatsuoka (1998) define "inherent anisotropy" as that "produced when deposited in air or water, or when compacted" which is similar to Lee, but there the similitude ends as they make the distinction between "stress state-induced anisotropy" and "strain history-induced anisotropy". This seems to agree with Belloti et al. but for them the first is that "developed as the stress state becomes anisotropic" and the second that "produced by dominant shear strain in a certain direction".

All these researchers were studying sand –but similar examples might be quoted from clay research. All of them were using apparatus with similar loading capabilities[97]. All of them described a transverse isotropic elastic stiffness. The paragraph above suggests that the abilities of natural language to deal with this issue quickly become exhausted. A more formal approach might offer some advantages, amongst them that of answering the question posed above about which types of elastic anisotropy might be measured in soils.

Numerical simulations have been employed. The elastic behaviour of an assembly of elastic balls has been subject of research since long ago–see Santamarina & Cascante, 1996, for a review. But analytical solutions were necessarily limited to simple cases, with very regular geometry, the typical model being that of identical spheres homogeneously packed. Numerical simulation via discrete element codes –Serrano & Rodriguez-Ortiz, 1973- had open the way to analyse more realistic granular assemblies –more numerous, multiple sized, with richer packing descriptions and non-elementary contact laws.

In discrete element simulations elastic loading is equivalent to fixed contact loading –Thornton, 2001. That is, for a given assembly the contacts between particles are frozen artificially, not allowing any slippage, and hence not allowing any contact to disappear or to be formed anew. This is then a fixed

fabric stress probe. One can argue then that, if discrete element models are able to recover reasonable soil-like elastic stiffness under this conditions, then the experimental values will also correspond to a substantially constant-fabric situation.

Actually, achieving soil-like stiffness has not been easy. Goddard (1990) pointed out how one main problem was that simulations of granular assemblies recovered a stress dependency close to that of Hertz spherical contacts –an exponent of 1/3. Meanwhile, in real granular materials the stress dependency showed exponents much closer to ½. Recently –2000- Yimsiri & Soga have shown that a realistic stress-dependency is possible if the contact laws are reformulated to account for particle roughness.

This is an important success but should not obscure the big picture. What has been achieved is to prove that an adequately specified fixed particle network may have realistic soil-like stiffness. In the case studied the network had a transverse isotropic structure and it was loaded on-axis. Quite a different problem is that of how material anisotropy evolves and how it can be related to the load evolution. This question remains fully open. In fact to this date discrete element simulations have failed even to reproduce the quantitative behaviour of soil samples tested in conventional apparatus –Thornton, 2001.

7.2.4 Coaxiality

In geotechnics the off-axis testing problem does not seem to have stirred much concern. There are probably two main reasons for this indifference. The first one is that most testing of soils has been performed in conditions where the axes of material anisotropy are coincident with the test axes[98]. The second one is that, unlike composites, soils do not have a fixed anisotropy, but a changing one. When this is due to features not immediately apparent as strata –e.g. sand grains- it is therefore hard to tell, in any particular configuration, if they are being tested off-axis or not.

Indeed, an interesting possibility is that material anisotropy and stress are always coaxial. Material anisotropy is often described by second order tensors as well as stress. Being coaxial means that they share principal axes. In a sense to be precised later second order tensors might be isotropic, transverse or orthotropic and this offers a seemingly good reason to expect the same kind of stiffness anisotropy.

Plane strain devices and hollow cylinders can be used to test this hypothesis. Saada (1970) was an honourable exception, who pointed to this effect as a primary cause of error when testing non-vertically formed clay samples in the triaxial apparatus. He went further and proposed hollow cylinder testing as a way out of this problem. In them, he reasoned, the stress can be aligned with the inclined material axis.

Hollow cylinders may be employed to test the coaxiality hypothesis for sand. As discrete element result suggest elastic probing should leave the material unaltered. Yamashita & Suzuki (1999) measured the vertical modulus of Toyoura sand in a hollow cylinder apparatus, under different orientations of the

---

[97] The calibration chamber used by Lee (1993) had the possibility of true triaxial loading, but most of his tests were in fact biaxial.

principal stress axis. They kept inner and outer pressures equal thus ensuring that radial and circumferential stress were the same. Hoque & Tatsuoka (1998) and Shibuya et al. (1991) had previously given enough information from coaxial apparatus to estimate four moduli of a transverse isotropic D_θ for given principal stresses[99]. Figure 7-9 represents the measured vertical modulus (E_V), the estimated modulus along the principal stress directions (E1, E3) and the vertical modulus consistent with a rotated transverse isotropic material (Ev^*). The results seem to disprove the hypothesis of perfect stress-induced anisotropy. The comparison is somehow flawed in that the stress state in the hollow cylinder was not strictly transverse, and three principal stresses were different. However the difference between the radial principal stress and the closest in-wall principal stress was always below 14%

7.3 ALGEBRAIC APPROACH TO SOIL ELASTIC ANISOTROPY

7.3.1 Isotropy of space and anisotropic materials

Adding to the practical difficulties just outlined, a theoretical inconsistency haunted for long the research in anisotropic materials. It is related to a basic principle of continuum mechanics, known as the principle of material frame-indifference or isotropy of space. This principle simply states that the properties of materials described by constitutive equations must be equally valid on any reference frame, i.e. constitutive equations must be objective[100] (see Malvern (1969) or Spencer (1980) for details).

Considering the particular case of changes of reference given by rotations, it follows that any material property expressed as a tensorial equation must be defined by an isotropic tensorial function of all it's arguments. This condition may be written as

$$T = F(A_1, A_2, \ldots A_n) \Rightarrow \bar{T} = F(\bar{A}_1, \bar{A}_2, \ldots \bar{A}_n) \quad \forall Q \in Orth \tag{138}$$

where the bar over a symbol indicates a tensorial transformation through the generic rotation Q.

Is straightforward to apply the principle of space isotropy for isotropic materials. Classically this will be done as a check in objectivity. In a formulation whatsoever, a general reference transformation is applied to its variables, and, after some manipulation, the original form should be recovered in the new reference. The traditional approach to anisotropic formulations apparently precludes this. Why this is so is illustrated in some detail in Appendix III using the Mises failure criteria. But the same reasoning employed there affects the classical approach to anisotropic elasticity.

Recall that Lekhnitskii (1963) obtained anisotropic formulations enforcing on the energy function a symmetry condition . The complementary statement of (2) is given by

$$F(S) \neq F(\bar{S}) \quad \forall Q \notin G_F \tag{139}$$

---

[98] Or rotated 90° as in Atkinson 1975. It can be proved that for a transverse isotropic material this rotation does not result in off-axis testing.

[99] The correlations given by Hoque & Tatsuoka were claimed valid for K > 0.5 or q/p < 0.75. Yamashita & Suzuki were always below that limit.

Employing the terminology of Appendix II, it could be said that the function F is in a class characterised by the argument T and the symmetry group G_F, $F \in \Im \{T, G_F\}$. This seems to stand in contradiction with the general principle of space isotropy (5).

Objectivity and anisotropy are then left as uneasy companions. The application of the principle of material indifference to anisotropic formulations has often proved difficult and misleading. Explicit testimony of that, within the soil mechanics literature, could be found in Gutierrez and Lacasse (1991) or in Roy and Campanella (1997). The talent of Boehler was to find a response to this problem.

7.3.2 Structural tensors

The key proposal of Boehler to get out of the muddle consists in adding explicit "structural tensors", characterising the anisotropy of G_F, to any anisotropic formulation. A structural tensor of G_F, ξ, is a tensor whose components are left unchanged by all the transformations included in G_F.

The extended set of variables thus obtained complies with the requirements of space isotropy. This idea receives the rather unattractive name of "Isotropicization theorem" and, as explained in Appendix II, could be formally written as

$$F(L_A, G_F) \equiv F(\{L_A, \xi_{G_F}\}, Orth) \qquad (140)$$

Where L_A for the list of arguments of the function F. The theorem could be interpreted as establishing a trade-off between the number of tensorial variables appearing in the formulation and the range of its symmetry group.

Another important result (Zheng & Boehler 1994) is that the number of possible types of symmetry is limited. Zheng (1994) gives a classification of all possible symmetry groups in two and three dimensions, list that is completed with single structural tensors characterising each symmetry group. This single structural tensor represents the most compact way in which a symmetry group may be characterised. Other tensors might be used for the task, but they will be more or less simple. It is important to note that these single structural tensors are not always second order symmetric tensors.

In fact, the abilities of a structural second order symmetric tensors are rather limited. This can be seen by a simple argument. Is known from algebra (e.g. Landesman & Hestenes, 1992) that the eigenvectors of second order symmetric tensors define an orthonormal reference frame. Furthermore, the eigenvalues define a geometrical figure attached to this frame, an ellipsoid or hyperboloid, depending on their sign. Those figures, with respect to the eigenvector frame, have:

- orthotropic symmetry if they have three distinct eigenvalues
- axial symmetry if they have two distinct eigenvalues

---

[100] As most engineering students know well, stresses and strains are not needed to deal with rigid-body movements. As changes of reference frame describe rigid-body movements, rigid-body motions must not alter the stress state of a body.

- isotropy if they have a single eigenvalue

These are exactly the types of symmetry that may be characterised by a second order symmetric tensor. Zheng (1995) explains that a single second order non-symmetric tensor is able to characterise monoclinic, triclinic and conic symmetry. To characterise cubic symmetry with a single tensor it has to be fourth order.

7.3.3 Induced & inherent anisotropy revisited

The structural tensor approach is directly related to the question of what may be the relationship between the symmetry group of the equation and the different symmetry groups of the tensorial variables involved, G_F and G_A in our terminology. This, in turn, gives a new, more precise, meaning to the expressions "induced" and "inherent".

If a constitutive equation F relates various tensorial variables the observed character of its symmetry group G_F will change according to which variables are fixed by the experimental procedure. Imagine a constitutive relationship of the form

$$\mathbf{X} = F(\mathbf{A},\mathbf{B},\mathbf{C}) \tag{141}$$

where the variable **X** is a function of three tensors whose symmetry groups are respectively G_A, G_B and G_C. If all three variables are under control we can observe different symmetries in F by fixing any of them. For instance

$$\begin{aligned}
&\mathbf{X} = F(\mathbf{A},\mathbf{B},\mathbf{C}_0) \Rightarrow G_F \equiv G_{C0} \\
&\mathbf{X} = F(\mathbf{A},\mathbf{B}_0,\mathbf{C}) \Rightarrow G_F \equiv G_{B0} \\
&\mathbf{X} = F(\mathbf{A},\mathbf{B}_0,\mathbf{C}_0) \Rightarrow G_F \equiv G_{B0} \cap G_{C0}
\end{aligned} \tag{142}$$

where a suffix 0 is employed to indicate which variables are fixed during a certain experimental program. Of course this reasoning works the other way round: if an experimental program is meant to leave a variable fixed, say $\mathbf{C} = \mathbf{C}_0$, the observed physical symmetry with respect the other variables will be also fixed. Any observed change will be an indication that $\mathbf{C} \neq \mathbf{C}_0$, a proof that **C** has been affected by the changes in the other variables.

Note also that in the third case shown above the physical symmetry is given by the intersection of the two tensorial symmetry groups. If the two groups G_{B0} and G_{C0} are the same then in the three cases shown above G_F is identical. This is not such an strange event as it may seem: it is exactly what would happen if the two variables are coaxial.

We see then that from the algebraic viewpoint all anisotropy is, strictly speaking, induced. Induced through the presence of tensors in the formulation. The only meaningful difference is that between fixed or evolving anisotropy, that is between fixed or variable tensors. The anisotropy induced by fixed tensors might well be called inherent. Elastic theory may serve as an example of the usefulness of this approach.

7.3.4 Elastic anisotropy revisited

Consider again the stress-strain relations of elasticity given by (130). Indicating the derivatives of the energy function with suffixes to reduce clutter we will write

$$\begin{aligned} \boldsymbol{\varepsilon} &= G_{\sigma}(\boldsymbol{\sigma}) \\ \dot{\boldsymbol{\varepsilon}} &= G_{\sigma\sigma}(\boldsymbol{\sigma}) : \dot{\boldsymbol{\sigma}} \end{aligned} \tag{143}$$

From the algebraic viewpoint the first equation ensures that stress and strain are collinear. The incremental stress-strain relation has stress-induced anisotropy[101]. Stress is a second order symmetric tensor and, therefore, incremental elastic anisotropy will be orthotropic at most.

Introduce now a material-based fixed structural tensor, **m**. We will have instead

$$\begin{aligned} \boldsymbol{\varepsilon} &= G_{\sigma}(\boldsymbol{\sigma}, \mathbf{m}) \\ \dot{\boldsymbol{\varepsilon}} &= G_{\sigma\sigma}(\boldsymbol{\sigma}, \mathbf{m}) : \dot{\boldsymbol{\sigma}} \end{aligned} \tag{144}$$

Even for the strictly linear case, where compliance does not depend on stress, every type of anisotropy is possible in both relations, depending on the characteristics of **m**. Let us assume that this **m** is also a second order symmetric tensor –like so many fabric measures so far introduced- and, to fix ideas, that this **m** has transverse isotropy.

The principal axes of this transverse isotropy will be termed $\{m_1,m_2,m_3\}$, with m_1 being the axis of symmetry. The incremental stress-strain relation will be generally anisotropic, of type depending on the principal values and directions of the stress tensor. If the principal directions are also $\{v_1,v_2,v_3\}$ and the principal stresses associated with $\{v_2,v_3\}$ are equal, then the stress tensor $\boldsymbol{\sigma}$ will be in the same symmetry group as **m** –coaxial-, the incremental relation will be transversely isotropic. If this is not the case but, nonetheless, they share some symmetry (reflection on the v_3 axis, for instance), this shared symmetry will characterise the anisotropy of the incremental relation. In a more general case, the symmetries of $\boldsymbol{\sigma}$ and **m** would be completely different, and a fully anisotropic relation might be expected.

Hence full coaxiality between the fabric and stress tensor reduces again the possible elastic symmetries to just three types: orthotropy, transverse isotropy and isotropy. When this is not the case all kinds of elastic anisotropy become possible. We seem to have here an answer to the question about the possible kinds of elastic anisotropy in soils.

7.3.5 Elasto-plastic coupling

So far, so good, but the precedent approach has some moot points. To begin with, we are still left with all the half answers that micromechanical analysis might provide about what this inherent **m** might be.

---

[101] Houlsby (1985) observed that this was indeed a consequence of his elastic "isotropic" models, where stress-dependent elastic shear and bulk moduli were introduced through a potential based formulation.

Second and more importantly, the experimental evidence reviewed before seems to point in a different direction.

Quite apart from their modest performance in general stress paths the stress dependency in (137) is incompatible with the elastic theory presented above. As shown in equation (131) the elastic compliance is the second order derivative of the complementary energy function G. With expressions like (137) we will have

$$\left.\begin{aligned}\frac{\partial^2 G}{\partial^2 \sigma_{11}} &= \frac{1}{C_{11}\sigma_{11}^{n_1}} \\ \frac{\partial^2 G}{\partial^2 \tau_{12}} &= \frac{1}{C_{12}\sigma_{11}^{n_1}\sigma_{22}^{n_2}}\end{aligned}\right\} \Rightarrow \frac{\partial^4 G}{\partial^2 \tau_{12}\partial^2 \sigma_{11}} \neq \frac{\partial^4 G}{\partial^2 \sigma_{11}\partial^2 \tau_{12}} \tag{145}$$

Thus any model based on exponential expressions such as these seems incompatible with elastic potentials depending only on stress, or in stress plus some other constant tensor. In fact the most serious attempt to formalise this expressions into a fully fledged elastic model for soils is that due to Hardin & Blandford –1989. Their model is unashamedly incompatible with potential-derived elasticity as they propose an elastic stiffness where the major symmetry is lost. The consequences of such approach are, however, far-fetching. For instance, symmetry of the Kelvin-Christoffel tensor is no longer guaranteed and wave velocities might become complex. This is characteristic of plastic behaviour –see Bigoni & Loret, 1999- and is a somewhat odd consequence of a model underpinned by wave propagation data.

This difficulties may be solved by a broadening of perspective. Up to this point we have been somewhat cavalier about and important fact mentioned in the opening chapter of this thesis: that soil behaviour is not elastic. That means that any "elastic" behaviour shall be considered within a more general framework of soil behaviour. Obviously various approaches are possible here as there is no such a thing as a generally accepted comprehensive model of soil behaviour. The one that seems more illuminating from the viewpoint here adopted is the thermodynamical elasto-plastic approach described by Collins & Houlsby (1997).The framework they describe has soils as time-independent non-conservative materials, and although much broader it has been shown to encompass models as popular as those of the Cam-clay family.

When compared with that of elastic materials the formalism for elasto-plastic materials has two new features. Apart from the externally measurable stress and strain new hidden state variables are needed and they are specified by two functions instead of one. To the energy potential, F or G, is necessary to add a dissipation function D. The basic energy relation states that the work input is shared between a variation of internal free energy and energy dissipation. It can be written in two complementary forms

$$\begin{aligned} D(\boldsymbol{\varepsilon},\boldsymbol{\alpha},\dot{\boldsymbol{\alpha}}) + \dot{F}(\boldsymbol{\varepsilon},\boldsymbol{\alpha}) &= \boldsymbol{\sigma}\dot{\boldsymbol{\varepsilon}} \\ D(\boldsymbol{\varepsilon},\boldsymbol{\alpha},\dot{\boldsymbol{\alpha}}) + \dot{G}(\boldsymbol{\sigma},\boldsymbol{\alpha}) &= \dot{\boldsymbol{\sigma}}\boldsymbol{\varepsilon} \end{aligned} \tag{146}$$

where α represents the internal variables. These are strain-like variables and have a conjugate set of stress like variables χ such that dissipation can be expressed as their product with the rate of α. Strain and stress are still related through the internal energy functions

$$\boldsymbol{\sigma}_{ij} = \frac{\partial F(\boldsymbol{\varepsilon}, \boldsymbol{\alpha})}{\partial \varepsilon_{ij}} \qquad \boldsymbol{\varepsilon}_{ij} = \frac{\partial G(\boldsymbol{\sigma}, \boldsymbol{\alpha})}{\partial \sigma_{ij}} \tag{147}$$

but now their rates have two terms, for the case of strain

$$\dot{\boldsymbol{\varepsilon}}_{ij} = \frac{\partial G(\boldsymbol{\sigma}, \boldsymbol{\alpha})}{\partial \boldsymbol{\sigma}_{ij}} \dot{\boldsymbol{\sigma}}_{ij} + \frac{\partial G(\boldsymbol{\sigma}, \boldsymbol{\alpha})}{\partial \boldsymbol{\alpha}_{ij}} \dot{\boldsymbol{\alpha}}_{ij} \tag{148}$$

The first term is called reversible strain rate and the second irreversible strain rate. The coefficient of the reversible strain rate is a compliance tensor and it will be measured with any loading that leaves the internal variables fixed. The important point, however, is that this internal variables are not particularly chimerical, Collins & Houlsby show that they can be identified with plastic strains, a rather familiar feature of soil models. When the reversible[102] compliance depends on them the model has elasto-plastic coupling. Critical state models incorporate this feature through the dependency of modulus in void ratio.

The important aspect, however, is that two tensorial variables appear in the incremental reversible relation. The modelling framework does not impose coaxiality of stress and plastic strain, a feature which will be at odds with experimental observations –e.g. Joer et al. 1998. Hence, in principle, all types of reversible stiffness anisotropy are possible.

7.3.6 Invariant formulation and representations

It is clear that the framework just presented opens new possibilities. The inclusion of void ratio effects fits perfectly well in this framework. The problems (145) that the observed stress dependency poses for the classical elastic models seem less strict, as new terms depending on plastic strain will appear on the derivatives. Any elasto-plastic model might be tested against is prediction of elastic stiffness evolution.

The formulation of general elasto-plastic coupled models is not an objective of this thesis. However it is worth mentioning that the algebraic approach to anisotropic formulations offers a second advantage at this respect. It enables the techniques employed to obtain representations of isotropic functions to be applied to anisotropic materials. As described in Appendix II, a representation, i.e. a general expression in invariant form, might be obtained for all the isotropic functions sharing the same list of arguments. For the most common types of arguments (vectors, second order tensors) those representations are already known, and some of them are summarised there.

Representations such as those are too general to be of immediate use in constitutive modelling. Nonetheless, they might provide a starting point for more concrete formulations, and this is the approach followed, or at least proposed, by many researchers. For linear elasticity Boehler (1979), Cowin (1985)

and Zysset & Curnier (1995) have presented results directly relevant for the case of stress induced anisotropy. Also isotropic representations are at the starting point of Truesdell's hypoelasticity or Kolymbas' hypoplasticity. Appendix IV presents a succinct account of sand mechanics applications of both theories, alongside with an application of one particular hypoplastic model.

[102] To achieve the identification of the internal variables with plastic strains the "elastic" strains include a irreversible part.

7.4 SUMMARY

Elastic anisotropy is a physical symmetry. It has to contain the material symmetries. In most soils direct measurement of material symmetries is problematic as they are not fixed, but evolving during loading processes. The observed elastic anisotropy is strongly dependent on the stress state, but other dependencies are also present. An algebraic approach is able to make clear what elastic symmetries are then possible. Full anisotropy may be expected for non coaxial loading. These various dependencies are still compatible with linear behaviour and acoustic tensor symmetry within the context of elasto-plastic coupled theories.

7.5 TABLES

Reference	Material	Apparatus	Material axis	Anisotropy	Strain level (%)
Graham & Houlsby (1983)	Lightly overconsolidated clay	Triaxial	Vertical	*Transverse isotropy	2-4
Kirkgaard & Lade (1991)	Normally consolidated clay	True triaxial	Vertical & horizontal	*Transverse isotropy	1-3
Hoque & Tatsuoka (1998)	Toyoura sand	Biaxial	Vertical	*Transverse isotropy	0.002
Di Benedetto et al. (1999)	Sand	Hollow Cylinder	Initially vertical	*General anisotropy	0.0001
Yamashita & Suzuki (1999)	Toyoura sand	Hollow cylinder	Initially vertical	Not specified	0.0001
*Incomplete set of stiffness constants					

Table 7-1 Experimental investigations on anisotropic elasticity: static procedures

Reference	Material	Apparatus	Material axis	Anisotropy
Roesler (1979)	Sand	Triaxial cube	Varied	Not specified
Argawal (1992)	Glass beads	True triaxial	Vertical	*Orthotropy
Lee (1993)	Dry Sand	True Triaxial (calibration chamber)	Vertical	Transverse isotropy
Jamiolkowski et al. (1995)	Six Italian clays	Oedometer	Vertical	*Transverse isotropy
Belloti et al. (1996)	Dry Ticino sand	Triaxial (calibration chamber)	Vertical	Transverse isotropy
Jovicic & Coop (1998)	NC & OC intact/reconstituted clay	Triaxial	Vertical & Horizontal	*Transverse isotropy
*Incomplete set of stiffness constants				

Table 7-2 Experimental investigations on anisotropic elasticity: dynamic procedures

Reference	Material	Apparatus	Material axis	Anisotropy	Strain level (%)
Pennington (1999)	OC clay	Triaxial	Vertical	Transverse isotropy	0.001
Kuwano (1999)	Sand	Triaxial	Vertical	Transverse isotropy	0.001

Table 7-3 Experimental investigations on anisotropic elasticity: mixed procedures

7.6 FIGURES

1-2 is a symmetry plane

$$\begin{bmatrix} d_{11} & d_{12} & d_{13} & 0 & 0 & d_{16} \\ & d_{22} & d_{23} & 0 & 0 & d_{26} \\ & & d_{33} & 0 & 0 & d_{36} \\ & & & d_{44} & d_{45} & 0 \\ & & & & d_{55} & 0 \\ & & & & & d_{66} \end{bmatrix}$$

13 parameters

Coordinate planes are symmetry planes

$$\begin{bmatrix} d_{11} & d_{12} & d_{13} & 0 & 0 & 0 \\ & d_{22} & d_{23} & 0 & 0 & 0 \\ & & d_{33} & 0 & 0 & 0 \\ & & & d_{44} & 0 & 0 \\ & & & & d_{55} & 0 \\ & & & & & d_{66} \end{bmatrix}$$

9 parameters

3 is axis of symmetry of order 3

$$\begin{bmatrix} d_{11} & d_{12} & d_{13} & d_{14} & -d_{25} & 0 \\ & d_{11} & d_{13} & -d_{14} & d_{25} & 0 \\ & & d_{33} & 0 & 0 & 0 \\ & & & d_{44} & 0 & d_{25} \\ & & & & d_{44} & d_{14} \\ & & & & & d_{66} \end{bmatrix}$$

7 parameters $\left(d_{66} = \frac{1}{2}(d_{11} - d_{12})\right)$

3 is axis of symmetry of order 4

$$\begin{bmatrix} d_{11} & d_{12} & d_{13} & 0 & 0 & d_{16} \\ & d_{11} & d_{13} & 0 & 0 & -d_{16} \\ & & d_{33} & 0 & 0 & 0 \\ & & & d_{44} & 0 & 0 \\ & & & & d_{44} & 0 \\ & & & & & d_{66} \end{bmatrix}$$

7 parameters

3 is axis of symmetry of order 6

$$\begin{bmatrix} d_{11} & d_{12} & d_{13} & 0 & 0 & 0 \\ & d_{11} & d_{13} & 0 & 0 & 0 \\ & & d_{33} & 0 & 0 & 0 \\ & & & d_{44} & 0 & 0 \\ & & & & d_{44} & 0 \\ & & & & & d_{66} \end{bmatrix}$$

5 parameters $\left(d_{66} = \frac{1}{2}(d_{11} - d_{12})\right)$

Figure 7-1 Basic linear elastic symmetries (after Lekhnitskii 1963)

Monoclinic

$$\begin{bmatrix} d_{11} & d_{12} & d_{13} & 0 & 0 & d_{16} \\ & d_{22} & d_{23} & 0 & 0 & d_{26} \\ & & d_{33} & 0 & 0 & d_{36} \\ & & & d_{44} & d_{45} & 0 \\ & & & & d_{55} & 0 \\ & & & & & d_{66} \end{bmatrix}$$

13 parameters

Orthorrombic

$$\begin{bmatrix} d_{11} & d_{12} & d_{13} & 0 & 0 & 0 \\ & d_{22} & d_{23} & 0 & 0 & 0 \\ & & d_{33} & 0 & 0 & 0 \\ & & & d_{44} & 0 & 0 \\ & & & & d_{55} & 0 \\ & & & & & d_{66} \end{bmatrix}$$

9 parameters

Hexagonal (axis 3)

$$\begin{bmatrix} d_{11} & d_{12} & d_{13} & 0 & 0 & 0 \\ & d_{11} & d_{13} & 0 & 0 & 0 \\ & & d_{33} & 0 & 0 & 0 \\ & & & d_{44} & 0 & 0 \\ & & & & d_{44} & 0 \\ & & & & & d_{66} \end{bmatrix}$$

5 parameters $\left(d_{66} = \frac{1}{2}(d_{11} - d_{12}) \right)$

Cubic

$$\begin{bmatrix} d_{11} & d_{12} & d_{12} & 0 & 0 & 0 \\ & d_{11} & d_{12} & 0 & 0 & 0 \\ & & d_{11} & 0 & 0 & 0 \\ & & & d_{44} & 0 & 0 \\ & & & & d_{44} & 0 \\ & & & & & d_{44} \end{bmatrix}$$

3 parameters

Figure 7-2 Four cases of elastic crystal symmetry (after Lekhnitskii 1963)

Anisotropic

$$\begin{bmatrix} d_{11} & d_{12} & d_{13} & d_{14} & d_{15} & d_{16} \\ & d_{22} & d_{23} & d_{24} & d_{25} & d_{26} \\ & & d_{33} & d_{34} & d_{35} & d_{36} \\ & & & d_{44} & d_{45} & d_{46} \\ & & & & d_{55} & d_{56} \\ & & & & & d_{66} \end{bmatrix}$$

21 parameters

Orthotropic

$$\begin{bmatrix} d_{11} & d_{12} & d_{13} & 0 & 0 & 0 \\ & d_{22} & d_{23} & 0 & 0 & 0 \\ & & d_{33} & 0 & 0 & 0 \\ & & & d_{44} & 0 & 0 \\ & & & & d_{55} & 0 \\ & & & & & d_{66} \end{bmatrix}$$

9 parameters

Transverse isotropic (axis 3)

$$\begin{bmatrix} d_{11} & d_{12} & d_{13} & 0 & 0 & 0 \\ & d_{11} & d_{13} & 0 & 0 & 0 \\ & & d_{33} & 0 & 0 & 0 \\ & & & d_{44} & 0 & 0 \\ & & & & d_{44} & 0 \\ & & & & & d_{66} \end{bmatrix}$$

5 parameters $\left(d_{66} = \frac{1}{2}(d_{11} - d_{12}) \right)$

Isotropic

$$\begin{bmatrix} d_{11} & d_{12} & d_{12} & 0 & 0 & 0 \\ & d_{11} & d_{12} & 0 & 0 & 0 \\ & & d_{11} & 0 & 0 & 0 \\ & & & d_{44} & 0 & 0 \\ & & & & d_{44} & 0 \\ & & & & & d_{44} \end{bmatrix}$$

2 parameters $\left(d_{44} = \frac{1}{2}(d_{11} - d_{12}) \right)$

Figure 7-3 Common elastic symmetries for non-crystalline materials

$$\mathbf{D}_0^{-1} = \begin{bmatrix} \frac{1}{E_H} & \frac{-\nu_{HH}}{E_H} & \frac{-\nu_{VH}}{E_V} & 0 & 0 & 0 \\ \frac{-\nu_{HH}}{E_H} & \frac{1}{E_H} & \frac{-\nu_{VH}}{E_V} & 0 & 0 & 0 \\ \frac{-\nu_{VH}}{E_V} & \frac{-\nu_{VH}}{E_V} & \frac{1}{E_V} & 0 & 0 & 0 \\ 0 & 0 & 0 & \frac{1}{G_{VH}} & 0 & 0 \\ 0 & 0 & 0 & 0 & \frac{1}{G_{VH}} & 0 \\ 0 & 0 & 0 & 0 & 0 & \frac{2(1+\nu_{HH})}{E_H} \end{bmatrix}$$

$$\mathbf{D}_0^{-1} = \begin{bmatrix} \frac{1}{E_H} & \frac{-\nu_{HH}}{E_H} & \frac{-\nu_{VH}}{E_V} & 0 & 0 & 0 \\ \frac{-\nu_{HH}}{E_H} & \frac{1}{E_H} & \frac{-\nu_{VH}}{E_V} & 0 & 0 & 0 \\ \frac{-\nu_{HV}}{E_H} & \frac{-\nu_{HV}}{E_H} & \frac{1}{E_V} & 0 & 0 & 0 \\ 0 & 0 & 0 & \frac{1}{G_{VH}} & 0 & 0 \\ 0 & 0 & 0 & 0 & \frac{1}{G_{VH}} & 0 \\ 0 & 0 & 0 & 0 & 0 & \frac{2(1+\nu_{HH})}{E_H} \end{bmatrix}$$

Figure 7-4 Compliance of a transverse isotropic material in engineering notation. Symmetric form above and asymmetric form below.

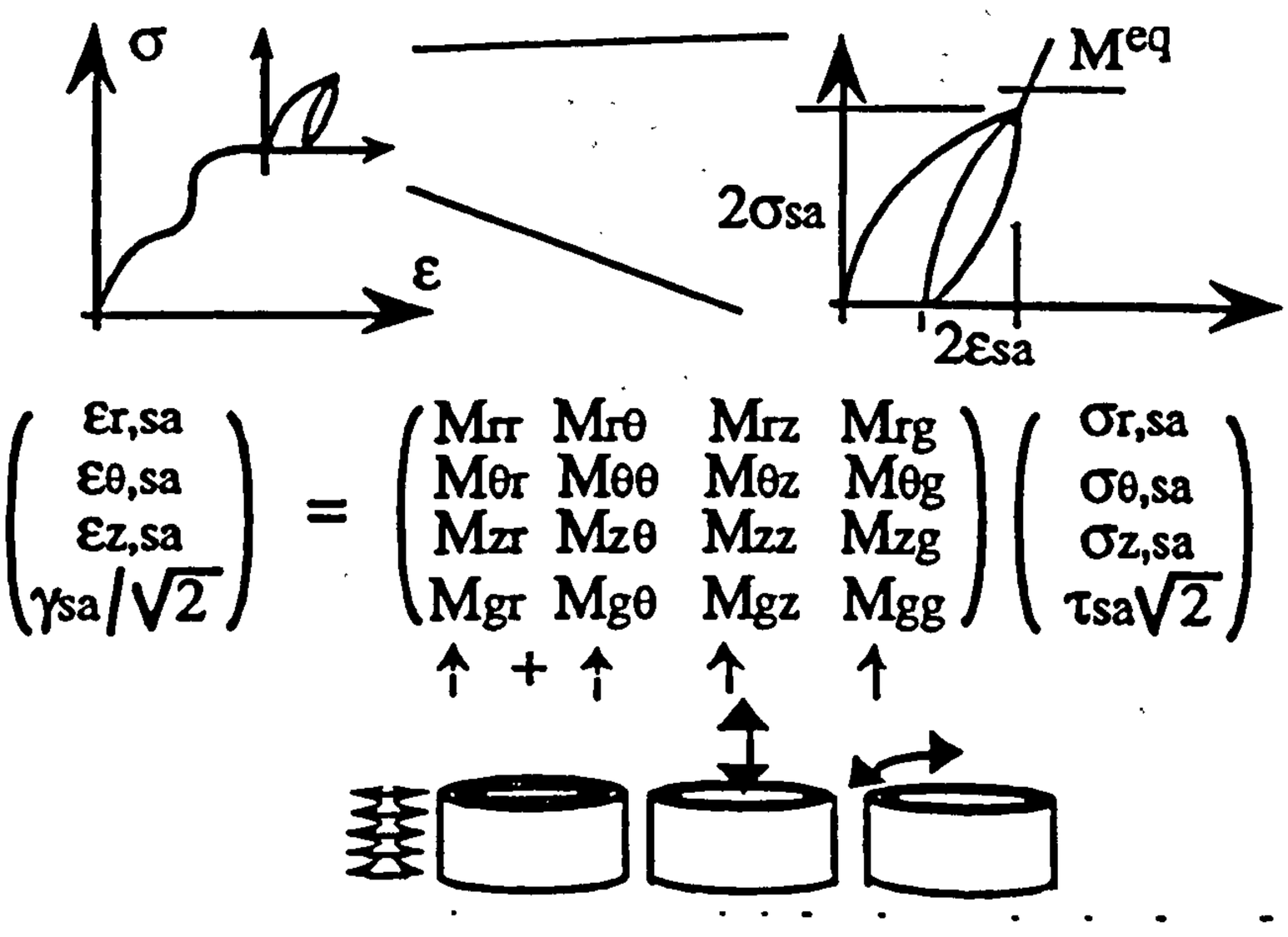

Figure 7-5 Static measurement of elastic moduli in hollow cylinder apparatus (Di Benedetto et al. 1997)

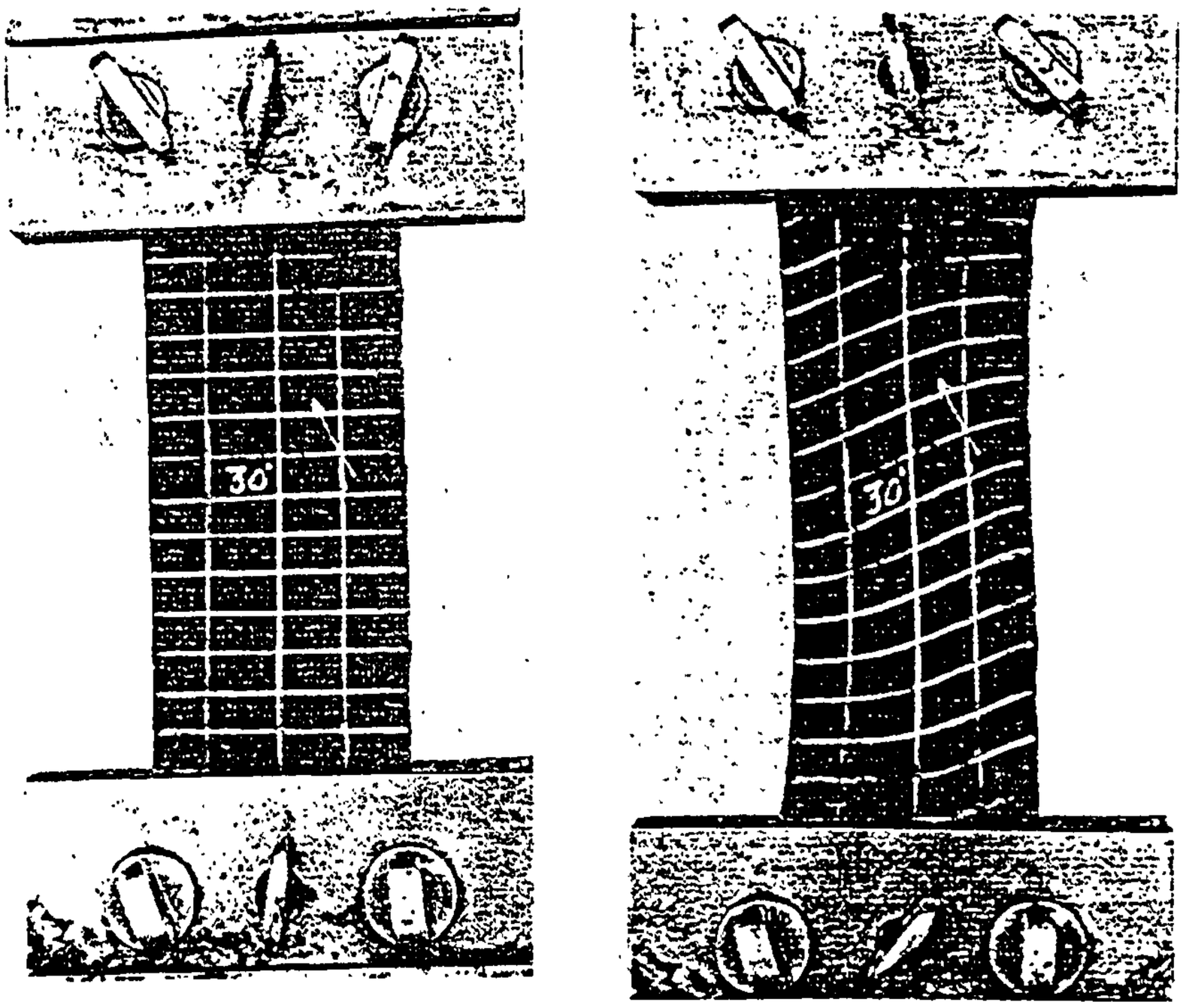

Figure 7-6 Off-axis testing in composites (after Pagano & Halpin, 1968)

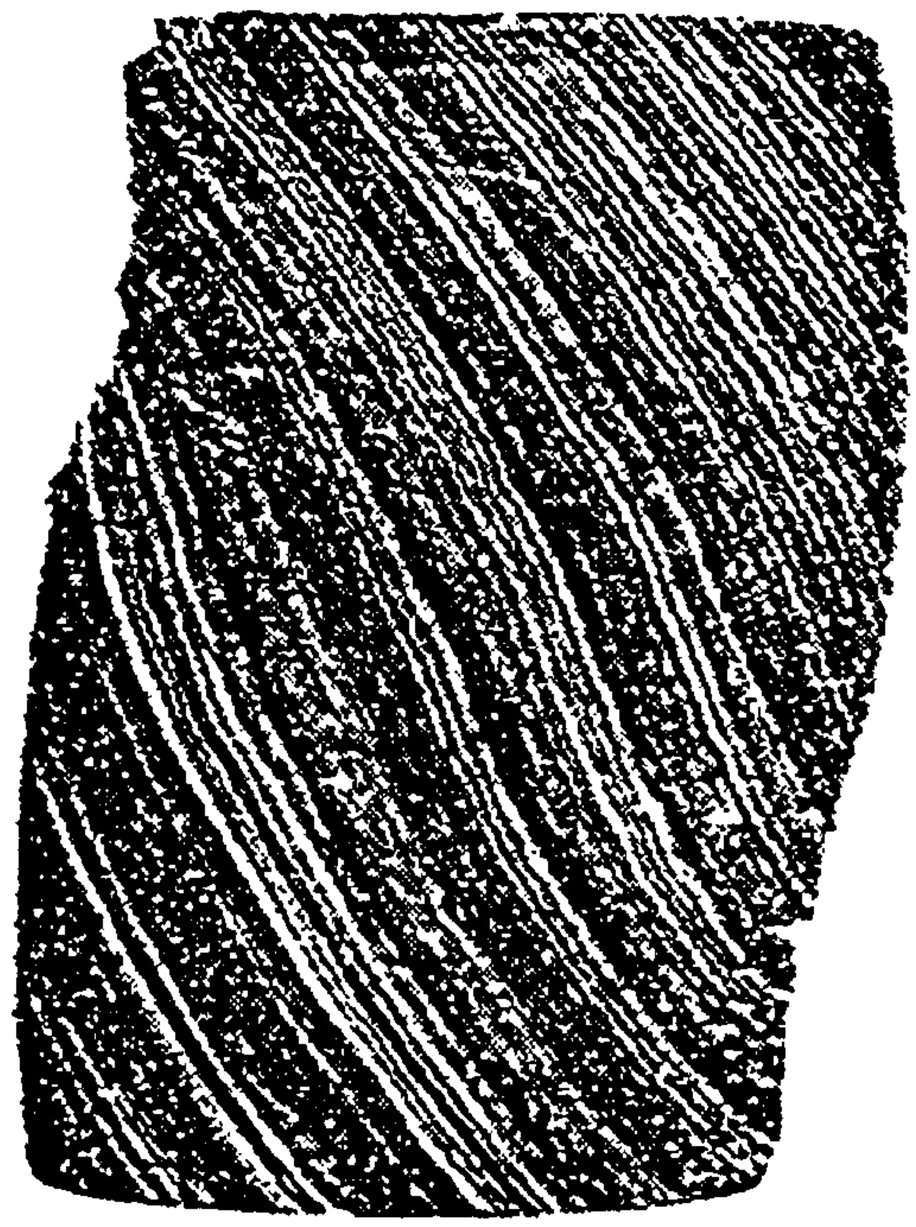

b

Figure 7-7 Off-axis testing in a cylindrical sample of stratified rock (after Boehler & Sawczuk, 1977)

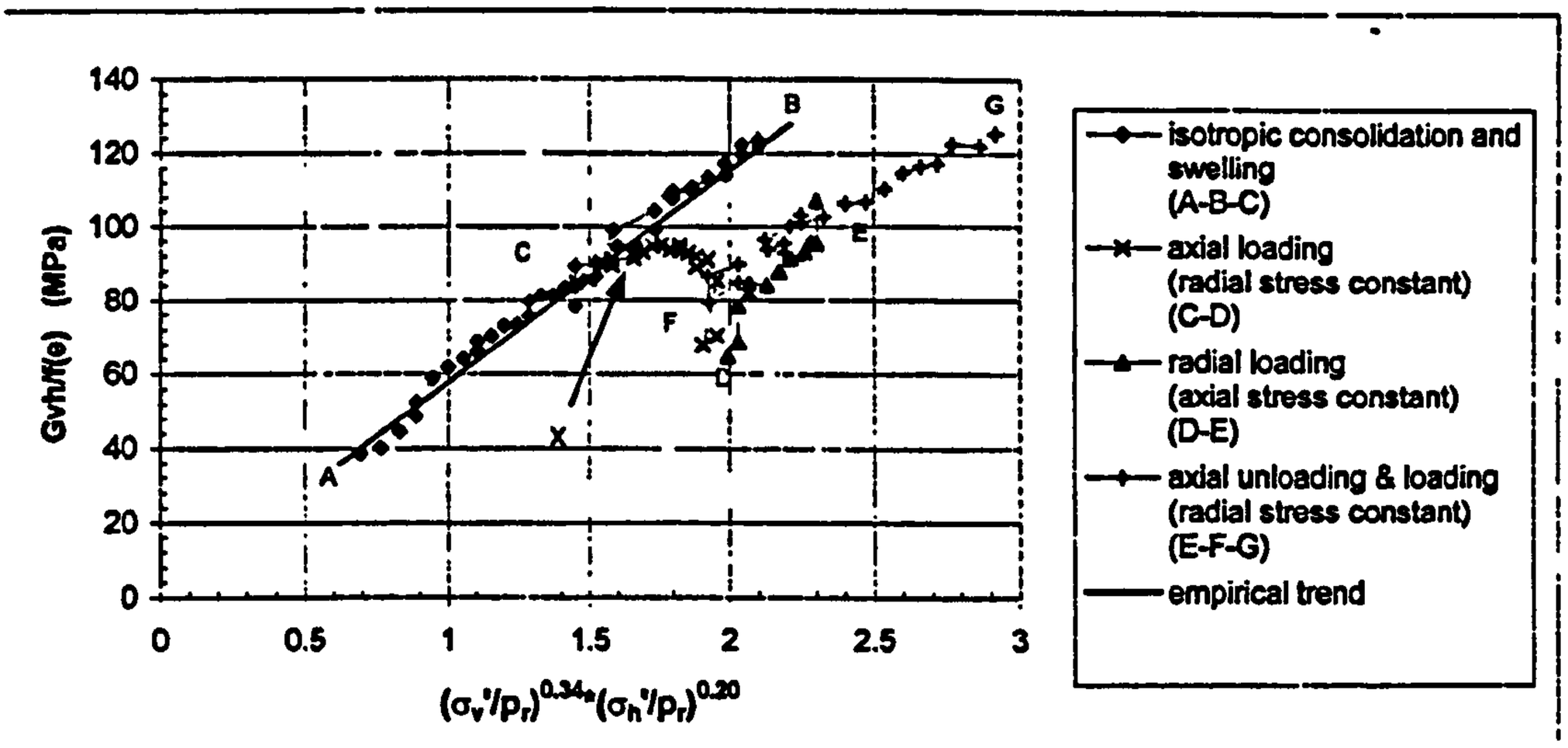

b) Change in G_{vh}

Figure 7-8 Shear modulus correlations with stress fail in general straess paths (after Kuwano, 1999)

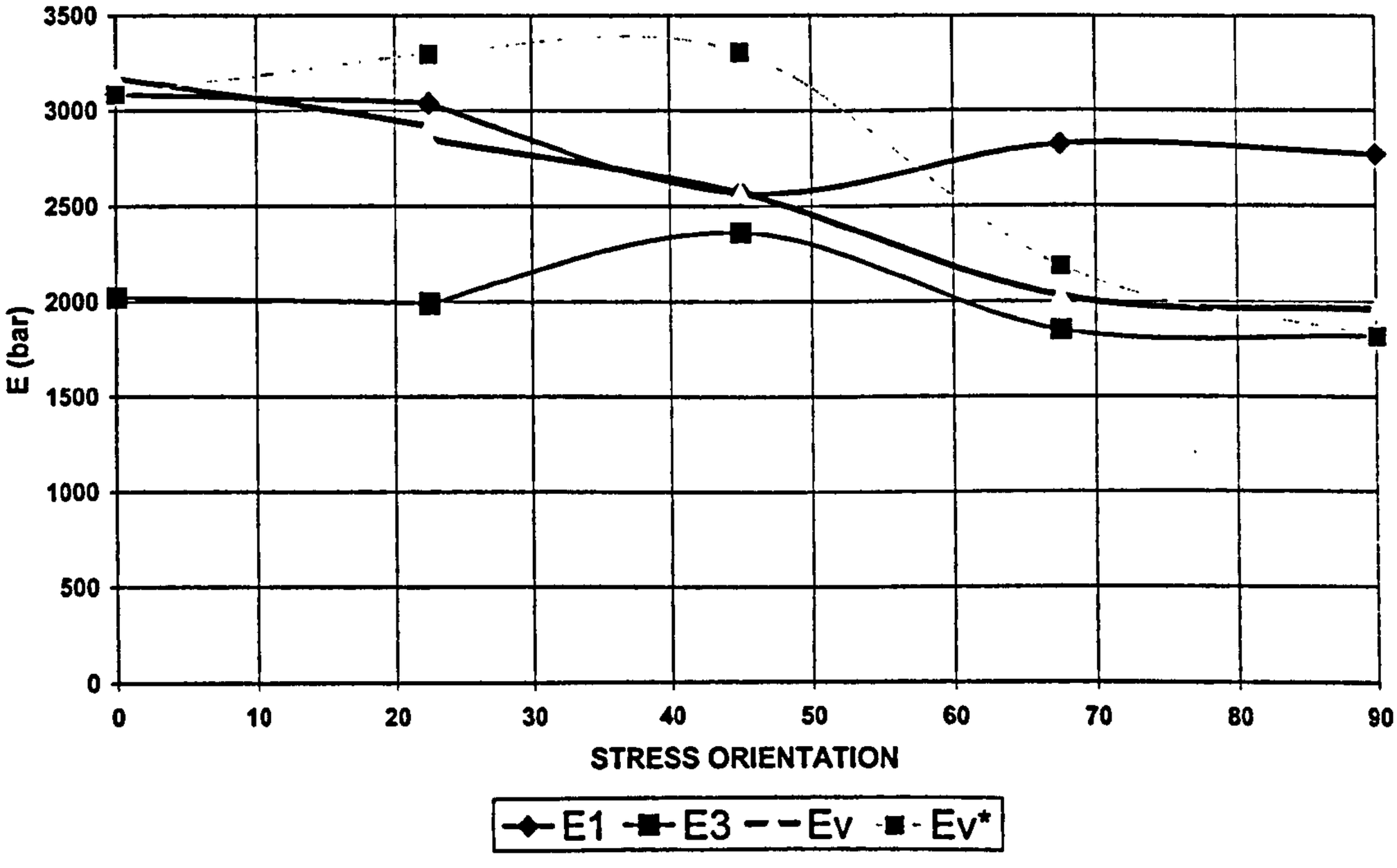

Figure 7-9 Toyoura sand. Hollow cylinder measurement of vertical modulus and prediction based in transverse anisotropy coaxial with stress

8 ANISOTROPIC ELASTIC WAVE PROPAGATION

8.1 THEORETICAL ASPECTS

8.1.1 Phase velocities and phase velocity surfaces.

As it was explained in Chapter 1 the Kelvin-Christoffel equation rules the propagation of plane waves within elastic solids. We recall here that it has the form of an eigenvalue problem relating wave polarization (**a**), its propagation direction (**p**) and its phase velocity (v).

$$\begin{aligned} \Gamma_{ij} &= D_{\theta iljk} p_l p_k \\ \left[\Gamma - \rho v^2 \mathbf{1}\right]\mathbf{d} &= \mathbf{0} \end{aligned} \tag{149}$$

and Γ was the Kelvin-Christoffel or acoustic tensor. In a generally anisotropic elastic material it is a function of direction but always positive definite. Henceforth the characteristic equation

$$\det\left[\Gamma_{ij} - \rho v^2 \delta_{ij}\right] = 0 \tag{150}$$

has three real solutions (eigenvalues), possibly different from each other, each one associated with a different direction (eigenvector). The three eigenvectors form an orthogonal set. This means that for any given elastic tensor **C** and any given propagation direction **p** there are, in general, three possible plane waves, with phase velocities v_i and polarizations $\mathbf{a}_i$. Or, using the typical names of angular spherical coordinates to emphasise this directional dependence,

$$\begin{aligned} \rho v_{(I)}^2 &= f_{(I)}(\mathbf{p}) = f_{(I)}(\theta,\varphi) \\ \mathbf{a}_{(I)} &= \mathbf{a}_{(I)}(\mathbf{p}) = \mathbf{a}_{(I)}(\theta,\varphi) \\ I &= 1,2,3 \end{aligned} \tag{151}$$

In general, and unlike the isotropic case, wave polarizations are not parallel or perpendicular to the propagation direction, i.e. the propagating plane waves cannot be classified simply as compressive or shear waves[103]. Nevertheless it is a common[104] feature in most cases to have the faster velocity (i.e. the bigger eigenvalue) associated with movement polarised in a direction closer to the propagation direction than those associated with the slower velocities. This justifies the common use of terms such as quasi-P or qP and quasi-S or qS (those are two, so qS1 and qS2 are employed).

This nomenclature also applies to the surfaces obtained by plotting the roots of the characteristic equation for every possible direction, **p**. Three surfaces are obtained, one for each solution. Those surfaces are known as phase-velocity surfaces (Crampin, 1981). This is reasonable, because, with an adequate scale factor, those plots represent the phase-velocity vectors, **c**,

$$\mathbf{c} = v(\mathbf{p})\mathbf{p} \tag{152}$$

---

[103] As we will see later, this only happens for the so called "pure mode directions", which are material-dependent.
[104] But not universal, see Auld (1973) for counterexamples.

Slowness surfaces can also be defined, by plotting the inverse of the phase velocity for each direction, and thus representing the slowness vectors. As we will see, this is more than a caprice, as these surfaces play a major role in the theory.

Classical texts on crystal acoustics such as Auld (1973) or Musgrave (1970) devote a good deal of effort and space to obtain analytical expressions and plane sections of both types of surfaces for any kind of elastic anisotropy. Today, with the aid of a mathematical program such as Maple, it is relatively easy to write a small program capable of doing exactly the same. The analytical expressions obtained are quite lengthy, and, for our purposes now, it's more interesting to include here some graphical results.

Figure 8-1, for instance, represents the complete qP surface corresponding to a particular measurement of transverse anisotropic moduli of Ham River Sand by Kuwano[105] (1999). It has a nice peanut-like shape, with the cylindrical symmetry that might be expected in a transverse anisotropic material. This shape illustrates beautifully a recurrent feature of phase-velocity surfaces (Crampin, 1981): they are not convex in general. This proviso also applies to the slowness surfaces and, as we will see later, has some interesting implications.

Figure 8-2 represents, for the same set of parameters, the two shear mode surfaces, qS1 and qS2. Lack of convexity is also evident. A back view of the first quadrant is shown, to make clear another recurrent feature of these surfaces also noted by Crampin: they intersect each other. Note that polarization changes from one surface to the other. For instance, in this case of transverse isotropy, symmetry considerations to be explained later imply that one of the shear modes is always pure, i.e. the movement is always orthogonal to the propagation direction, whereas the other is mixed, having a component also in the propagation direction. The somehow surprising implication of surface intersection is that, depending on the direction, the pure mode (the darker surface in the image) is either faster or slower than the mixed mode.

8.1.2 Ray velocities, group velocities and directional dispersion.

Up to now we have discussed plane wave propagation. But the wavefront propagating from a finite source is rather some kind of closed surface. The pulse test scheme shown in Figure 8-4 points to this. What is measured in pulse tests is the velocity of the wavefront between two points, either source and receiver or two aligned receivers. A straight line, a **ray**, can be traced from the source to the measuring point. The velocity is measured along this ray. What is the relation between plane wave velocities and the measured ray velocities?

It is quite tempting to assume that both are the same. That would mean that the ray direction is directly identifiable with **p**, the normalised slowness, and, recalling equation (152), that the wavefront surface is, but for a time factor, the same as the phase-velocity surface. That would simplify matters a great deal,

---

[105] The values correspond to test H601: E_v = 520MPa, E_h = 280MPa, ν_{vh} = 0.27, ν_{hh} = .07, G_{vh} = 154MPa

but, unfortunately, is not correct. This seems to be a fact that has been recognised long since in crystallography –e.g. Musgrave (1956)- maybe because it has close analogies with some optic phenomena. Seismologists, pioneered by Crampin (1977), followed suit. In soil mechanics literature the situation is mixed, while some researchers –e.g. Lee (1993), Stokoe et al. (1997)- seem to have an acute perception of it, others still fail to make the distinction -Argawal (1992) or Pan & Dong (1999). For this reason, and although various formal proofs can be found in the literature -for instance in Musgrave (1970) or Nayfeh (1995)- it seems necessary to restate here the argument in some albeit more informal detail.

A curved wavefront is locally identifiable with a plane wave. This local plane wave has a wave vector directed along the wavefront normal and is moving at the local phase velocity[106]. To see that look now at Figure 8-3. There T_0 and T_1 are two successive two-dimensional wavefronts, respectively corresponding to instants t_0 and $t_1 = t_0+dt$. At point P_0 the local wavefront normal is $\mathbf{dx}$. In general, this direction will not be coincident with the ray direction $\mathbf{dx'}$.

Therefore the local plane wave velocity coincides with the local ray velocity when the ray direction –a straight line traced from the source- coincides with the normal to the wavefront. The only wavefront geometry where this happens at every point is an sphere centred at the source –or the circle in our 2D sketch. In isotropic elastic solids, spherical are the phase-velocity surfaces –there is no dependency on direction- and spherical indeed are the wavefronts, both surfaces being homothetical. But in anisotropic cases we have just shown that shapes of phase-velocity surfaces, $\mathbf{c(p)}$ are quite unspherical. The phase-velocity surface and the wavefront cannot coincide then because at every point there will be two contradictory definitions of phase velocity: one given by the local normal and the other by the ray direction.

Ray velocities measured along some direction are different of plane phase velocities corresponding to that direction. This, of course, leaves unanswered the question of what is their relationship. One first answer can be obtained looking again at Figure 8-3. The unit vector normal to the wavefront has therefore the direction of the normalised slowness, $\mathbf{p}$, so we can write

$$\begin{aligned} \mathbf{dx'}\,\mathbf{p} &= dx \\ dx &= \|\mathbf{dx}\| \end{aligned} \qquad (153)$$

And dividing both sides by the time interval, we have in the limit

$$\begin{aligned} \mathbf{c}_R\mathbf{p} &= \mathbf{v} \\ \mathbf{v} &= \|\mathbf{c}\| \end{aligned} \qquad (154)$$

Where, as before, $\mathbf{c}$ represents the phase-velocity vector, $\mathbf{v}$ the phase velocity magnitude, and a new symbol, $\mathbf{c}_R$, has been introduced to represent the ray velocity vector. Still, it is clear that this relationship

---

[106] Recall the definition of this concepts in Chapter 1.

is not enough to define it completely, as only one projection or component is specified. There is need for another relationship and this is given by the concept of dispersion and group velocity.

The propagation of elastic waves in anisotropic solids is dispersive. To see that it is necessary to just look again at the Kelvin-Christoffel equation (150) and note that it has the characteristics of a dispersion relationship. To make it obvious, instead of the normalised slowness **p**, the wave vector **k** should be employed to form the acoustic tensor, thus obtaining:

$$\Gamma = \mathbf{k}\cdot\mathbf{C}\cdot\mathbf{k}$$
$$\det\left[\Gamma - \rho\,\omega^2\mathbf{1}\right] = 0 \Rightarrow \omega_i = Z_i(\mathbf{k}) \qquad (155)$$
$$i = 1,2,3$$

For each of the three propagation modes (qP, qS1, qS2) a different dispersion relation is therefore obtained. It is crucial to note that equation (155) is homogeneous in the wavenumber. Therefore the dispersion relation can be rearranged to show the frequency as the product of a constant wavenumber, k, and the direction-dependent phase velocity, v (**p**). The dispersion function is thus independent of the wave vector modulus. This is why it makes sense to talk about directional dispersion[107]. We can write this fact as follows:

$$\omega = Z(\mathbf{k}) = k\,v(\mathbf{p}) \qquad (156)$$

As we know group velocity is defined as the gradient of frequency with respect to the wavenumber. For this case of directional dispersion group velocity is a vector, $\mathbf{c}_g$, and it is shown in Appendix III that is given by the following relationships

$$\mathbf{c}_g = \frac{dZ}{d\mathbf{k}} = \frac{dv(\mathbf{p})}{d\mathbf{p}} = \frac{\nabla S}{\mathbf{q}\nabla S} = \mathrm{v}_g(\mathbf{n})\mathbf{n} \qquad (157)$$
$$\|\mathbf{n}\| = 1$$

Where S stands for the slowness surface and **q** for the slowness vector. The final identity means that group velocities are directed along the normal, **n**, of the corresponding slowness surfaces. Also note that plotting $\mathrm{v}_g(\mathbf{n})$ three group-velocity surfaces will be obtained.

Apparently we have now three velocities, the phase velocity, the geometrically defined ray velocity $\mathbf{c}_R$, and this vectorial group velocity $\mathbf{c}_g$ brought about by dispersion. Happily enough, it turns out that the last two are the same. To see this we should differentiate equation (154), and remember that the normalised slowness, **p**, is orthogonal to the tangent plane of the ray velocity surface, obtaining

$$\left.\begin{aligned}\mathbf{c}_R d\mathbf{p} + d\mathbf{c}_R\mathbf{p} &= d\mathrm{v}\\ d\mathbf{c}_R\mathbf{p} &= 0\end{aligned}\right\} \Rightarrow \mathbf{c}_R d\mathbf{p} = d\mathrm{v} \qquad (158)$$

---

[107] In other words: an hypothetical one-dimensional pulse travelling along some fixed direction of an anisotropic elastic media will not suffer any dispersion but any sort of two-dimensional or three-dimensional signal will spread and disperse.

And, looking at the first identity in equation (157) we see that is correct to identify ray and group velocity. It must be noted, finally, that as ray and group velocities are now proven to be equal[108], group velocity surfaces are directly identifiable with wavefronts, but for a time scale factor.

In Figure 8-5 the geometrical relations between the ray, phase-velocity and slowness surfaces have been illustrated[109], namely:

- There are corresponding points in each of the surfaces, in the figure are named P_W –on the ray surface-, P_V –on the phase-velocity surface- and P_S –on the slowness surface.
- The normal at P_W to the ray velocity surface, **p**, is parallel to the slowness vector **q** at P_S and to the phase velocity vector **c** at P_V.
- The normal at P_S to the slowness surface, **n**, is parallel to the ray velocity vector, $\mathbf{c_g}$ at P_W
- The phase velocity vector **c** at P_V is the projection of the ray velocity vector at P_W, $\mathbf{c_g}$ on the direction of it's normal, **p**.

.

These relationships are technically resumed by Musgrave (1970), using terminology from projective geometry: slowness and ray surfaces are polar reciprocals of each other; the ray surface is the envelope of the phase velocity surface and the phase velocity surface is the pedal of the ray surface. This has some implications that he explores at great length. One that is worth mentioning here is that non convexity of slowness surfaces produces, in turn, group velocity surfaces –and, consequently, wavefronts- that are multivalued or folded.

Figure 8-6 tries to illustrate this concept. In the slowness surface sketched (S) there are two points where the tangent planes are horizontal, as indicated. Vectors through them will obtain the corresponding points (A and B) on the phase velocity surface (V). Both these points will have corresponding points in the group velocity surface, say A' and B'. But these two points will lie on the same (vertical) ray. It is clear that along this ray there are two different values of the group velocity and the wavefront is therefore multivalued.

The consequence of a multivalued wavefront this is that two separate arrivals of the same wavefront –for instance qSH- will be expected along rays crossing the folded region. This perhaps surprising characteristic of wave propagation in anisotropic materials has been already observed in anisotropic solids. For instance, Kim et al. (1995) present measurements of this phenomena in a transverse isotropic crystal of zinc.

---

[108] From now onwards we will use freely both terms, as there is no convention established in soil mechanics, and preferences vary in other nearby fields.

[109] This representation of the surfaces assumes a convenient normalisation, by the phase (and group) value on the y axis. Slowness is multiplied by this factor, so it has similar dimensions to the others.

8.1.3 Elastic moduli and group velocities: direct and inverse problems.

Wang (1995) emphasizes the distinction between the direct and inverse problems in anisotropic elastic wave propagation. The direct problem has the elastic moduli of the material as data and then tries to build up a picture of the wavefronts. The inverse problem is posed by the experimentalist who wants to recover the elastic moduli of the material from some measured data -ray or phase velocities-. As is usually the case, the inverse problem is far harder than the direct one.

It is natural to express group and phase velocity as functions of direction with respect to the privileged material frame. Therefore we will write:

$$\begin{aligned} v &= v(\theta,\varphi) \\ V &= V(\xi,\rho) \end{aligned} \tag{159}$$

Where v is one of the phase velocities, V the corresponding group velocity, and the angle nomenclature is illustrated in Figure 8-9. This is equivalent to employ a different set of spherical coordinates to represent each vector.

The direct problem for phase velocities is straightforward indeed: for any kind of elastic anisotropy the functions giving the directional dependence of phase velocity are obtained solving the Kelvin-Christoffel equation (150) for a general unit vector. As we mentioned before this has been done a number of times since Christoffel -for instance, Auld (1974)- The resulting formulae are rather lengthy, and the general disagreement on the nomenclature of anisotropic moduli contribute to a very unappealing body of literature that we are reticent to increase.

This is even more so now that thanks to symbolic manipulation programs such as Maple, the Christoffel equation can be solved almost instantaneously for every nomenclature and every case. It is interesting, though, to have an example, and therefore we can include here the formulae obtained for the common and relatively simple case of transverse isotropy. The formulae are arranged as in Thomsem (1987) for future reference.

$$\begin{aligned} \rho v_{QP}^2(\varphi) &= \frac{1}{2}\left[D_{33}+D_{44}+(D_{11}-D_{33})\sin^2\varphi+R(\varphi)\right] \\ \rho v_{QSV}^2(\varphi) &= \frac{1}{2}\left[D_{33}+D_{44}+(D_{11}-D_{33})\sin^2\varphi-R(\varphi)\right] \\ \rho v_{QSV}^2(\varphi) &= D_{66}\sin^2\varphi+D_{44}\cos^2\varphi \\ R^2(\varphi) &= (D_{33}-D_{44})^2+2\left\{2(D_{13}+D_{44})^2-(D_{33}-D_{44})(D_{11}+D_{33}-2D_{44})\right\}\sin^2\varphi \\ &\quad +\left\{(D_{11}+D_{33}-2D_{44})^2-4(D_{13}+D_{44})^2\right\}\sin^4\varphi \end{aligned} \tag{160}$$

The symmetry axis is assumed vertical and, therefore, the formulae are independent of the azimuth. Formulae such as this were used to produce the plots in Figure 8-1 and Figure 8-2.

It is now time to go back to equation (159) and consider group velocity. It is shown in Appendix III how the dispersion equation (157) might be used to obtain a set of formal relations between the components of the group velocity vector, $\mathbf{c_g}$, and those of the corresponding phase velocity, $\mathbf{c}$. Using the nomenclature described in Figure 8-9, this formal relations read as follows:

$$V^2 = v^2 + v_\theta^2 + \frac{v_\phi^2}{\sin^2\theta}$$

$$\cos\xi = \frac{1}{V}\left[v\cos\varphi - v_\varphi \frac{\sin\varphi}{\sin\theta}\right] \qquad (162)$$

$$\tan\rho = \frac{v\sin\theta\sin\varphi + v_\theta\cos\theta + v_\phi\cos\varphi}{v\cos\theta\sin\varphi - v_\theta\sin\theta + v_\phi\cos\varphi\tan\theta}$$

Where the subscripts indicate a derivative with respect to the corresponding coordinate. These expressions offer a way to obtain ray surfaces, -and therefore wavefronts- from any given set of anisotropic moduli. Any expression of phase velocity, such as those given in equation (160) might be suitably derived and combined according to (162). Then a high enough number of group velocity vectors might be obtained and the ray velocity surface plotted along the corresponding phase velocity surface.

We have done that using a Maple-based program for the case of transverse isotropy. Due to the azimuthal symmetry of the surfaces a meridian section conveys all the information needed. An example of the results obtained is shown in Figure 8-7. The example illustrates the case of folded wavefronts that we mentioned before.

The same program might be used also to obtain the angle between any phase velocity vector and the corresponding ray velocity vector. This is illustrated in Figure 8-8 for the same example as before. It might be appreciated that even for a case of strong anisotropy such as this, the deviations are rather small.

It should be noted, of course, that what we do not have written are explicit formulae for group velocity as a function of its direction like those postulated in (159). That would involve, for instance, inverting equations (162) after substitution of a phase-velocity expression like those given in (160). The problem is that even if phase velocity expressions alone are already complicated, the expressions obtained by their substitution on equations (162) are much more so, and their inversion poses a generally horrendous problem. Already in 1970, Musgrave, based in the projective relation between slowness and ray surfaces, indicated that group velocity surfaces might be surfaces of a degree[110] as high as 150. This, in his own words "dashes any hopes of obtaining [their] equation in a general and convenient explicit form". To our knowledge, this prophecy seems to have stood the test of time.

Therefore, when the need arises to solve the inverse problem, i.e. that of recovering the set of elastic moduli from wave velocity measurements, two options are available. The first and more recent (Aristégui

& Baste, 1997) is to perform a fully numerical inversion where ray velocity surfaces numerically generated from a guess of elastic properties are matched to a set of ray velocity measurements. The second and more classical is to proceed in a step by step basis, taking profit of all known symmetries of the material under study. To understand those procedures it is first necessary to appreciate some simplifying consequences of symmetry.

8.1.4 Simplifying: consequences of symmetry.

It might be clear by now that pulse test interpretation under anisotropic elastic conditions is far more complicated than under isotropic conditions, when there are just two possible modes or phase velocities in every direction, polarizations are simply parallel or transverse to the movement, and there is no need to distinguish ray and phase velocities. It is obvious also that symmetries of the elastic tensor play a major role in establishing how complicated the problem is.

It is relatively simple to prove (see Appendix III) that two directions of propagation will have the same phase velocities if one can be transformed into the other through a rotation belonging to the symmetry group of the elastic tensor[111]. That means, basically that the phase-velocity surfaces will have the same symmetries as the elastic tensor. A transverse isotropic material will have phase-velocity surfaces with cylindrical symmetry –see Figure 8-1-. An orthotropic material will have phase-velocity surfaces with three orthogonal planes of symmetry. A monoclinic material will have phase-velocity surfaces with one plane of symmetry. A triclinic material will have phase-velocity surfaces with no symmetry whatsoever.

The same reasoning given in Appendix III is also valid for the slowness surfaces. Therefore they will have also the same symmetries as the elastic tensor. Finally, and considering its geometrical relation with the slowness surface, the same can be said about the group velocity surfaces.

An important consequence of this concerns propagation in material symmetry planes -e.g. for the common case of transverse isotropy, all planes containing the axis. They are, as we have just seen, also symmetry planes of the phase velocity and slowness surfaces. This implies that at any point on them the normal vector must also lie in the symmetry plane. In other words, the derivative of the phase-velocity function with respect the out of plane coordinate is null.

Using the same spherical coordinates of equation (162), we can choose the plane of symmetry to be a plane of constant azimuth, for instance $\theta = \pi/2$ and, imposing the condition that v_θ is null, it is shown in Appendix III that the following simplified expressions are obtained:

---

[110]The degree of a surface is roughly equivalent to the degree of the polynomial that might describe it in Cartesian coordinates.
[111] As the symmetry group defining isotropy includes all rotations this correctly implies the equivalence of all directions in the isotropic case.

$$V^2(\rho) = v^2(\varphi) + v_\varphi^2(\varphi)$$

$$\tan\rho = \frac{v_\varphi/v + \tan\varphi}{1 - (v_\varphi/v)\tan\varphi} \qquad (164)$$

$$\xi = \frac{\pi}{2}$$

It is thus evident that in symmetry planes all the points in the phase velocity surface map into points of the ray surface lying on the same symmetry plane[112]. Further manipulation of equation (164) conduces to an oft-quoted and very compact equation, relating the plane polar coordinates of the phase and group velocity vectors:

$$v = V\cos(\rho - \varphi) \qquad (165)$$

Symmetry also has interesting consequences regarding the possible polarisation of plane waves. We have mentioned before the existence of "pure mode directions", being those where the wave movement is either transverse or longitudinal. Considering also the symmetries of the elastic tensor, Auld (1973) proves some important results about pure mode directions, namely,

- If the propagation direction coincides with an axis of rotational symmetry all modes are pure, i.e. the propagating waves are either purely compressive or pure shear. Moreover, if the rotational symmetry is equal or bigger than threefold[113], the shear modes are degenerate i.e. there is only one shear velocity and the situation is the same as in the isotropic case. This is the case of propagation along the axis of symmetry in transverse anisotropy.

- If the propagation direction is contained in a plane of mirror symmetry there is always a pure shear wave polarised perpendicular to the plane, the other two modes being therefore contained in the symmetry plane.

- The precedent case is also valid when the propagation direction is contained in a plane orthogonal to a rotational symmetry axis

- Finally, and apart from those general cases, each anisotropic material has a set of pure mode directions depending on the relative values of the anisotropic elastic constants.

As might be expected, researchers using ultrasonic methods have made a systematic use of these symmetry-induced simplifications when measuring the elastic moduli of anisotropic materials (for a review, see Every, 1994). The basic idea is to increase the difficulties gradually: obtain first the maximum of information from measurements along axes of symmetry, then proceed to other directions

---

112 Kim (1994) points out that the converse is not true, as there might be points on the ray surface section that correspond to out of plane slowness vector

113 The symmetric points around the axis being spaced at 120° intervals or less

on symmetry planes, etc...We will see later on how this procedure may be applied in soil mechanics, before is convenient to look for other avenues of simplification.

8.1.5 Simplifying: weak anisotropy

The anisotropy of any elastic material could be more or less accused. Its almost intuitive that any material whose elastic properties are close to isotropy will have simpler wave propagation characteristics. This idea has been exploited mostly by geophysicists -e.g. Backus (1965), Crampin (1981) or Thomsem (1987). This is natural because, as we will see later on, crustal rocks have, generally, a much lesser degree of anisotropy than crystals or sedimentary deposits –i.e. soils. Also, as the main anisotropic system of interest for geophysicists is transverse anisotropy, most developments have focused on it.

For instance then, Thomsem (1987) examined the possible simplifications that a weak degree of anisotropy will have for the important case of transverse isotropic materials. To do that he first introduced a new set of parameters to describe a transverse isotropic material. These parameters are three adimensional ratios (ε, γ, δ) and two velocities (α_0, β_0) defined as follows:

$$\varepsilon = \frac{D_{11} - D_{33}}{2D_{33}}$$

$$\gamma = \frac{D_{66} - D_{33}}{2D_{44}} \qquad (166)$$

$$\delta = \frac{(D_{13} + D_{44})^2 - (D_{33} - D_{44})^2}{2D_{33}(D_{33} - D_{44})}$$

$$\alpha_0 = \sqrt{D_{33}/\rho} \quad \beta_0 = \sqrt{D_{44}/\rho}$$

For an isotropic material the ratios become null and the velocities become the two usual bulk plane velocities. The adimensional ratios then measure the deviation from isotropy[114]. Thomsem rewrites the phase velocity equations (164) in terms of this set of parameters. Then proceeds to linearise them in terms of the three adimensional ratios (ε, γ, δ) obtaining the following simplified expressions:

$$v_{QP}(\varphi) = \alpha_0\left[1 + \delta\sin^2\varphi\cos^2\varphi + \varepsilon\sin^4\varphi\right]$$

$$v_{QSV}(\varphi) = \beta_0\left[1 + \frac{\alpha_0^2}{\beta_0^2}(\varepsilon - \delta)\sin^2\varphi\cos^2\varphi\right] \qquad (167)$$

$$v_{QSH}(\varphi) = \beta_0\left(1 + \gamma\sin^2\varphi\right)$$

These simplified expressions make apparent the correspondence between the two velocities (α_0, β_0) and the P and S-wave velocity of an isotropic media. Anisotropy –transverse isotropy in this case- manifests itself as dip-dependent corrective terms on the isotropic velocities. Finally, Thomsem, substitutes these simplified equations in the group velocity expressions for propagation on a symmetry plane –(11)- and, again discarding higher order terms on anisotropy, obtains a much simpler set of relations.

The basic idea used by Thomsem is to linearise the quantities of interest on parameters representing deviation from isotropy. This may be restated in a more general context, for all types of anisotropy as a perturbation on an eigenvalue problem (Backus, 1965).

8.1.6 Complications: near field, fluid interaction, boundary effects

All the preceding considerations relate to plane waves propagating on the far field of a source in a purely elastic medium whose lateral boundaries are far away from the propagation direction. Anisotropic directional dispersion can, of course, combine with all the sources of isotropic dispersion mentioned in previous Chapters. Here we cannot enter in any detail about them. We would like nevertheless to mention that semi-analytical fundamental solutions for the case of transverse isotropy have been recently presented by Sáez & Domínguez (2000) using a more general technique to obtain fundamental solutions for general anisotropic materials proposed by Wang & Achenbach (1995). The generalisation of Biot theory for anisotropic materials is simpler[115], and plane wave anisotropic solutions were developed by Biot himself (see Biot 1992). We are not aware of any treatment of anisotropic cylindrical waveguides, which, for instance, are not contemplated by Disperse (Pavlakovic & Lowe, 2000).

8.2 IMPLICATIONS FOR SOIL PULSE TESTING

8.2.1 Measurable elastic anisotropy: types

The first aspect that needs to be considered is what kind of elastic anisotropy might be necessary to measure and under which conditions. According to what was said in the precedent Chapter, all kinds of elastic symmetry seem possible in soils. Those compatible with testing on currently designed sample-testing apparatus are more restricted: isotropy and transverse isotropy in triaxial apparatus, to which true triaxial apparatus add orthotropy, and hollow cylinders monoclinic symmetry.

In calibration chambers and other equally big devices –shear stack for instance- more general kinds of anisotropy may be locally generated during testing or by design. Of course self-supporting homogeneous samples of soil –clay, frozen sand- may be used for the only purpose of dynamical testing outside any apparatus. In that case general anisotropy may be again expected.

8.2.2 Measured elastic anisotropy: magnitudes

We have seen already that a substantial reduction on the complexity of the inverse problem could be achieved when the anisotropy being measured is small. It is therefore important to have an appreciation of the magnitude of the elastic anisotropy that must be dealt with in soil experiments. Our aim here is to present some data already available about this and put them in the context of other materials. Most of the data available refers to the situation of transverse anisotropy, and the comparison will therefore concentrate on this system.

---

[114] Amongst the many measures of "anisotropy" that have been proposed for this case these are perhaps the most systematic.
[115] As long as the dynamic permeability remains isotropic.

Crampin and co-workers have used extensively the following ratio to quantify the shear-wave anisotropy (SWA) of rocks as measured by phase velocities:

$$SWA = \frac{\max(v_{S1}) - \min(v_{S2})}{\max(v_{S1})} \times 100 \qquad (168)$$

Where v_{S1} refers to the faster shear wave and v_{S2} to the slower. Crampin (1994) summarises observations in rocks and concludes that values above 10% are very rare. Moreover, this limit has been related to a postulated cracking mechanism behind anisotropy and shown to be compatible with it through numerical modelling (Crampin, 1999). For comparative purposes with soil data is necessary to express the SWA in terms of the anisotropic elastic constants

$$SWA = \frac{max(D_{44}, D_{66}) - min(D_{44}, D_{66})}{max(D_{44}, D_{66})} \qquad (169)$$

Figure 8-10 presents then SWA data for various granular materials as published in the geotechnical literature. It is obvious that the values recorded are substantially higher than the 10% limit postulated for rocks. It is interesting to note here that a consistent exception to this limit has been also observed in near-surface seismic surveys (e.g. Bates & Philips, 2000) i.e. in surveys involving soils or unconfined rocks.

For the case of transverse anisotropy Thomsem parameters offer a more systematic approach to quantify anisotropy magnitude. Figure 8-11 to Figure 8-13 present histograms of the three adimensional ratios (ε, γ, δ) obtained from measurements in a number of granular materials. For comparison purposes a series corresponding to measurements in rock (Thomsem, 1987) is also included in the graphs.

Again, it is apparent that granular materials in the lab have higher degrees of anisotropy than those usually observed in seismic surveys of rock. It is noteworthy that Thomsem himself pointed to a value below 0.2 as a reasonable limit for the assumption of small anisotropy. It is clear that most rock values were well within this limit. It is clear also that this is not the case with soils.

Figure 8-14 presents again the data against the criteria $\varepsilon = \delta$ which, as can be seen from equations (167) corresponds to the assumption of an elliptical QP wavefront and to an isotropic QSV wavefront[116]. This assumption is commonly employed in seismic surveys and Thomsem observed that it was not particularly accurate for rocks. We can add that it is even much less so for soils. This is annoying as most data from calibration chambers has usually been interpreted under this assumption –Lee, 1993, Stokoe, 1996. Finally, it is worth mentioning that a point representing the zinc parameters beyond Figure 8-7 is also included in the graph. It has the higher degree of anisotropy of those included in the figure.

[116] Note that this simplified equations correspond to the phase-velocity surfaces, but if these are elliptic the geometrical relationship they have with the wavefront implies that this is also elliptic.

It is also interesting to check if the reported transverse anisotropic moduli of soils are compatible with the existence of cusps near the axis of symmetry. Musgrave (1970) shows that the condition for the existence of cusps in that location is given by

$$(D_{13} + D_{44})^2 > D_{44}(D_{11} - D_{44}) \qquad (170)$$

For the data reported by Belloti et al. (1996) this condition is not fulfilled once. For the data reported by Kuwano (1999) it is fulfilled in several occasions, for all the materials studied. The significance of this difference is still unclear, although the data reported by Kuwano are more likely to have suffered from all the parasite effects of sample size explored in Chapter 6.

8.2.3 Measuring elastic anisotropy: recommendations

Kim (1994) describes a step-by-step procedure for the determination of elastic constants in materials with orthotropic or higher elastic symmetry[117]. For orthotropic stiffness the diagonal terms D_{44}, D_{55}, and D_{66} are directly related to pure shear modes propagating along the axis of the material. The other diagonal terms are generally obtained with P measurements. Those may generally be unavailable in soils.

In that case a fitting procedure should take place using the shear modes in the symmetry planes. One of them is polarised in the symmetry plane, -although not necessarily orthogonal to the propagation direction- the other is pure transversal shear. The wavefront of both modes for, say, the 1-3 plane depends on D_{55}, D_{11}, D_{33} and D_{13} thus three more constants can be measured by fitting the measured wavefronts to a computed one. Of the three remaining constants D_{12} and D_{22} might be obtained using the same procedure in the plane 1-2 but the last one, D_{23}, will require measurements in the plane 2-3. Kim gives semi-explicit formulas for the wavefront that may be advantageously used for these fitting procedures.

The non-linearity of the fitting equations and the eventual presence of cusps near the axis of symmetry are problems that will generally require careful study of measurement direction and a certain degree of redundancy in the measurements (see e.g. Degtyar & Rokhlin, 1997). These are problems that are only more prominent in the general inversion problem for generally anisotropic materials or for materials with unknown symmetry. The kind of fixed transducers now used in soil pulse tests are ill suited for the purpose of obtaining many measurement points.

Finally it should be noted that the previous indications are based in one fundamental assumption: that it is possible to obtain measurements whose characteristics relate only to one direction in the material. The kind of sample size effects seemingly possible in current laboratory pulse testing techniques make us uncomfortable about the prospects of anisotropic measurements.

---

[117] Higher here means with less independent constants, i.e. transverse isotropic, cubic, isotropic.

8.3 SUMMARY

Anisotropic elastic plane wave propagation adds some complexities of its own to the measurement problem. There is directional dispersion and wavefronts spread out from a source in complex, sometimes folded, forms. These forms, nevertheless, retain the symmetry of the elastic tensor. Measurement along favoured axis and planes of symmetry is highly recommendable. Helpful simplifications are possible for small amounts of anisotropy, but measured soil data do not generally show small anisotropy. Measurement of orthotropic and less symmetric elastic moduli with only shear waves is theoretically possible and has been done for crystals and composites. Current testing systems for soil samples seem ill suited for the task, particularly for their inability to guarantee an accurate pulse direction.

8.4 FIGURES

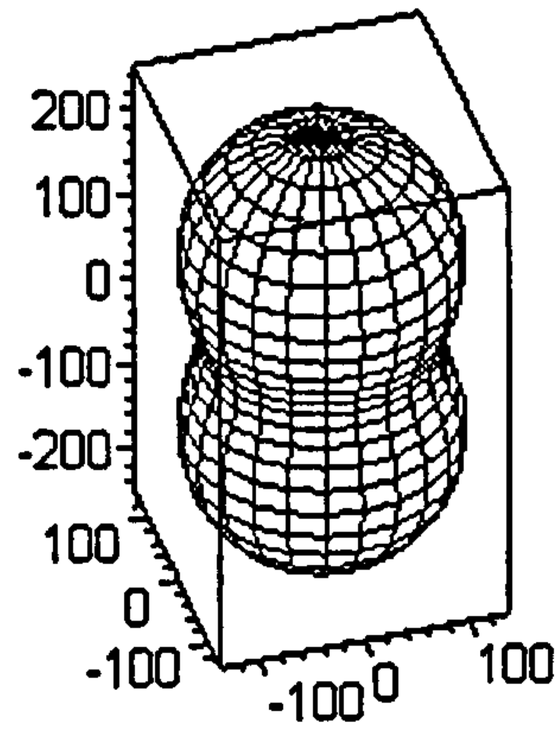

Figure 8-1 A phase-velocity surface (QP sheet) for Ham River Sand. Symmetry axis is vertical. Scale in m/s.

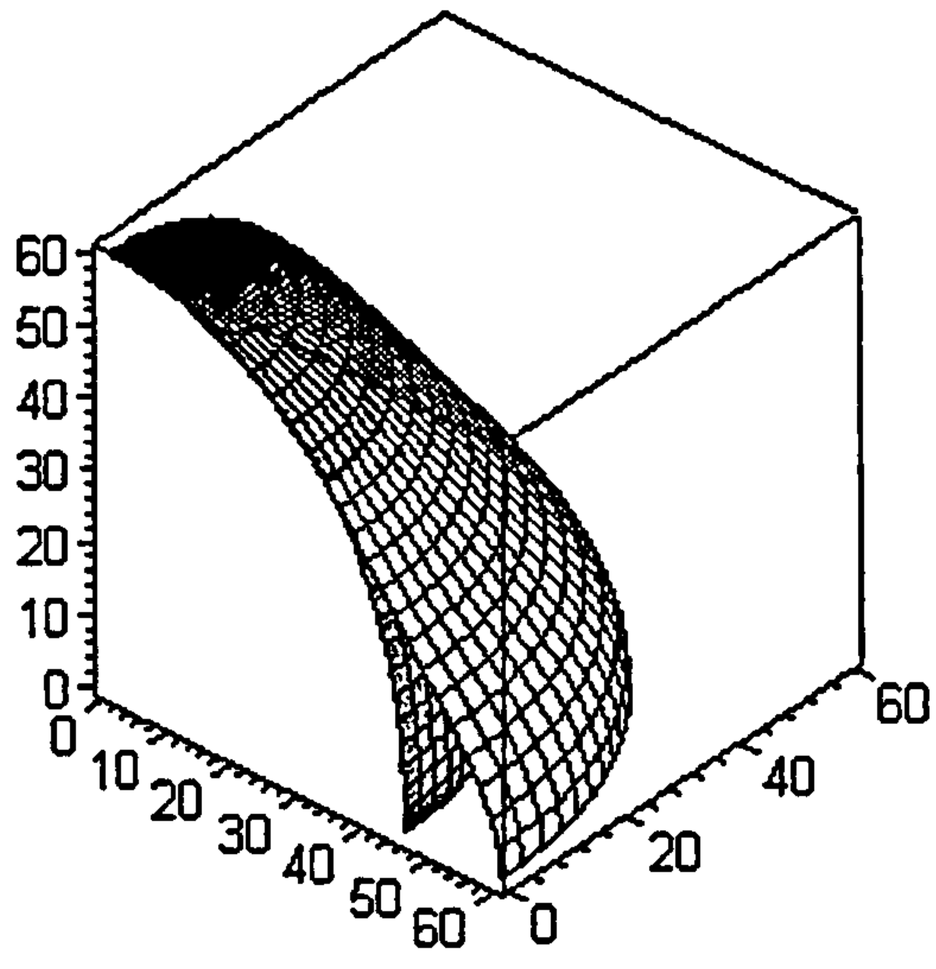

Figure 8-2 Example of phase velocity surface for Ham River Sand. qSH sheet and qSV sheet . First quadrant represented only. Scale in m/s.

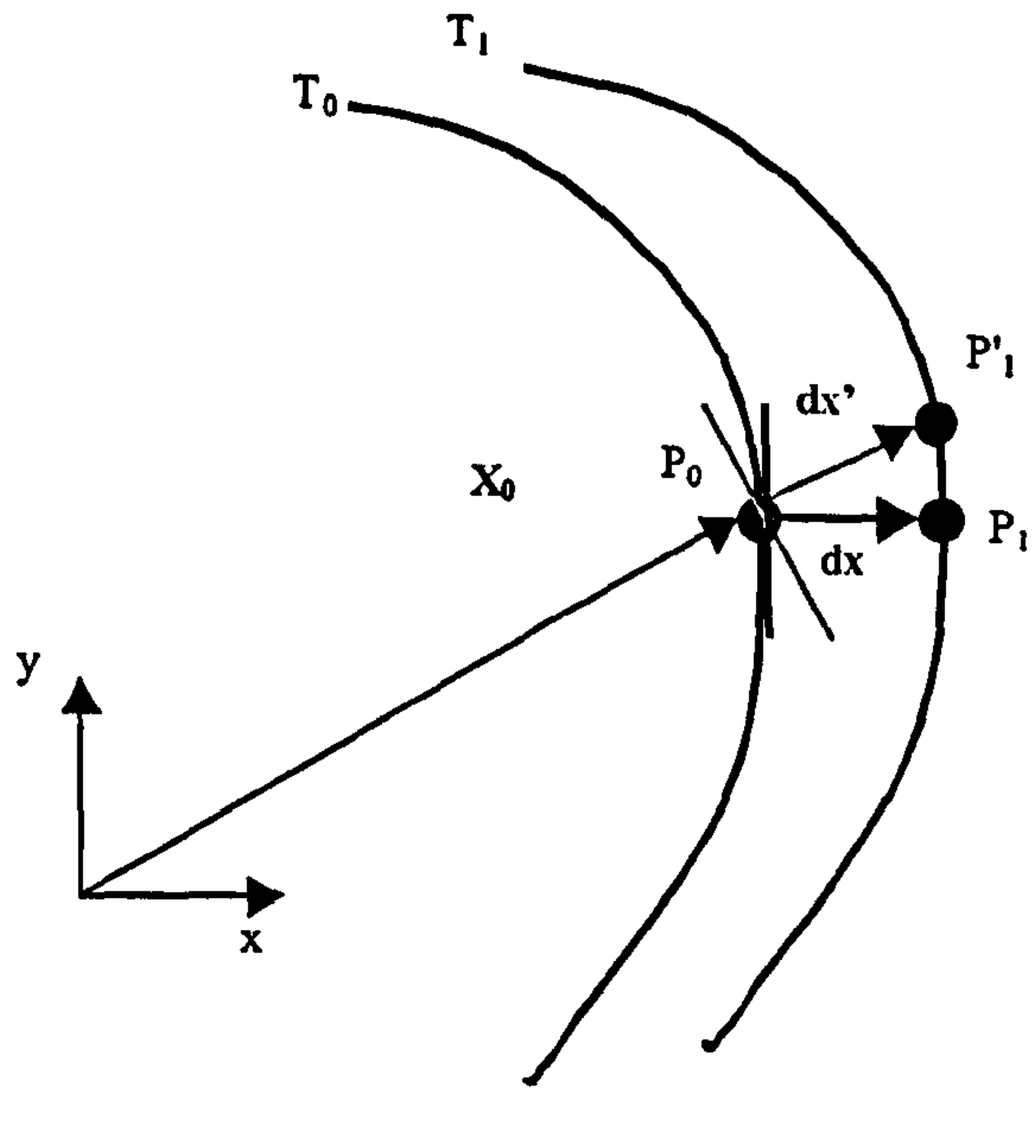

Figure 8-3 Wavefront movement and rays

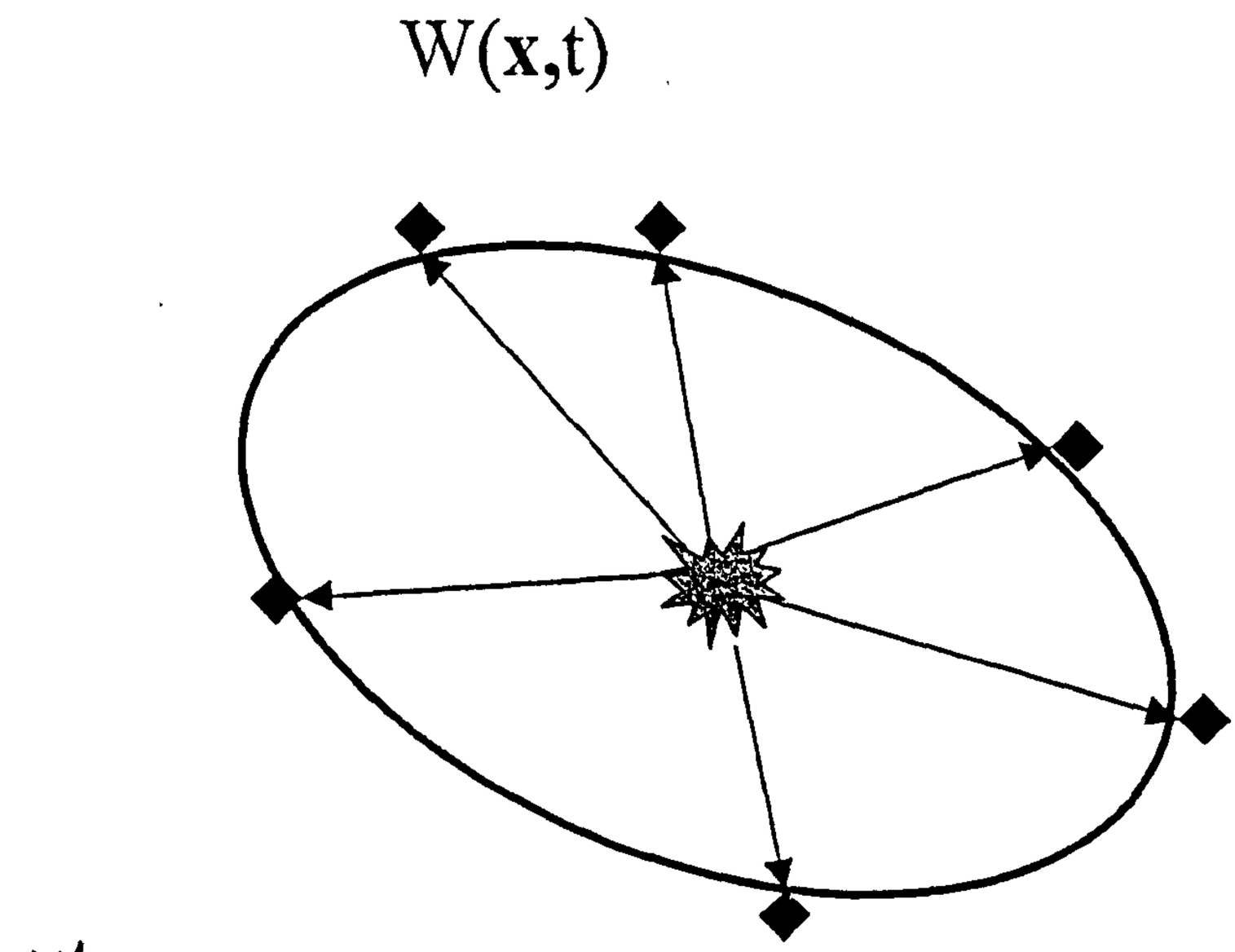

Figure 8-4 Pulse tests: conceptual scheme

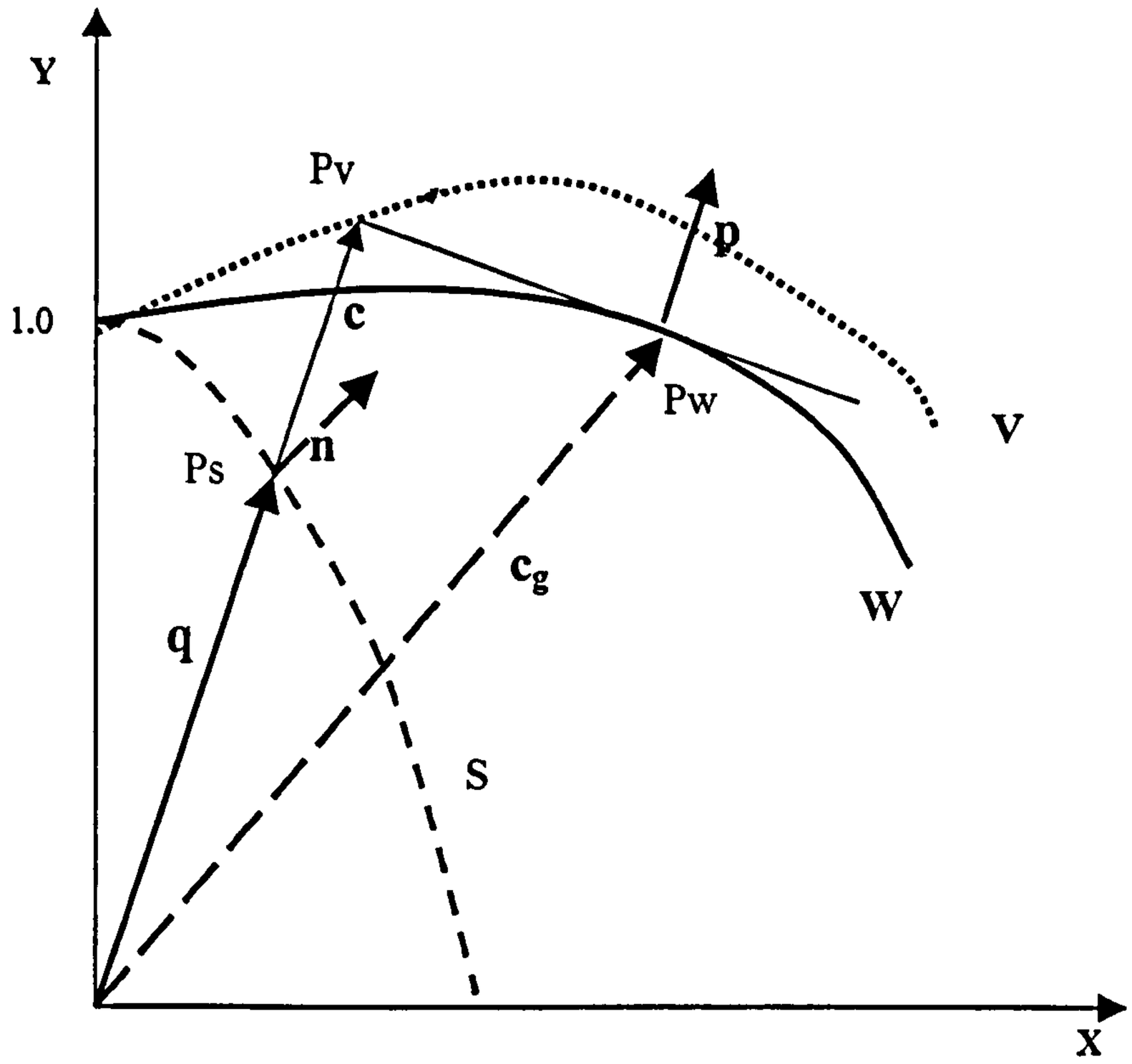

Figure 8-5 Geometrical relations between ray velocity surface (W), phase velocity surface (V) and slowness surface (S)

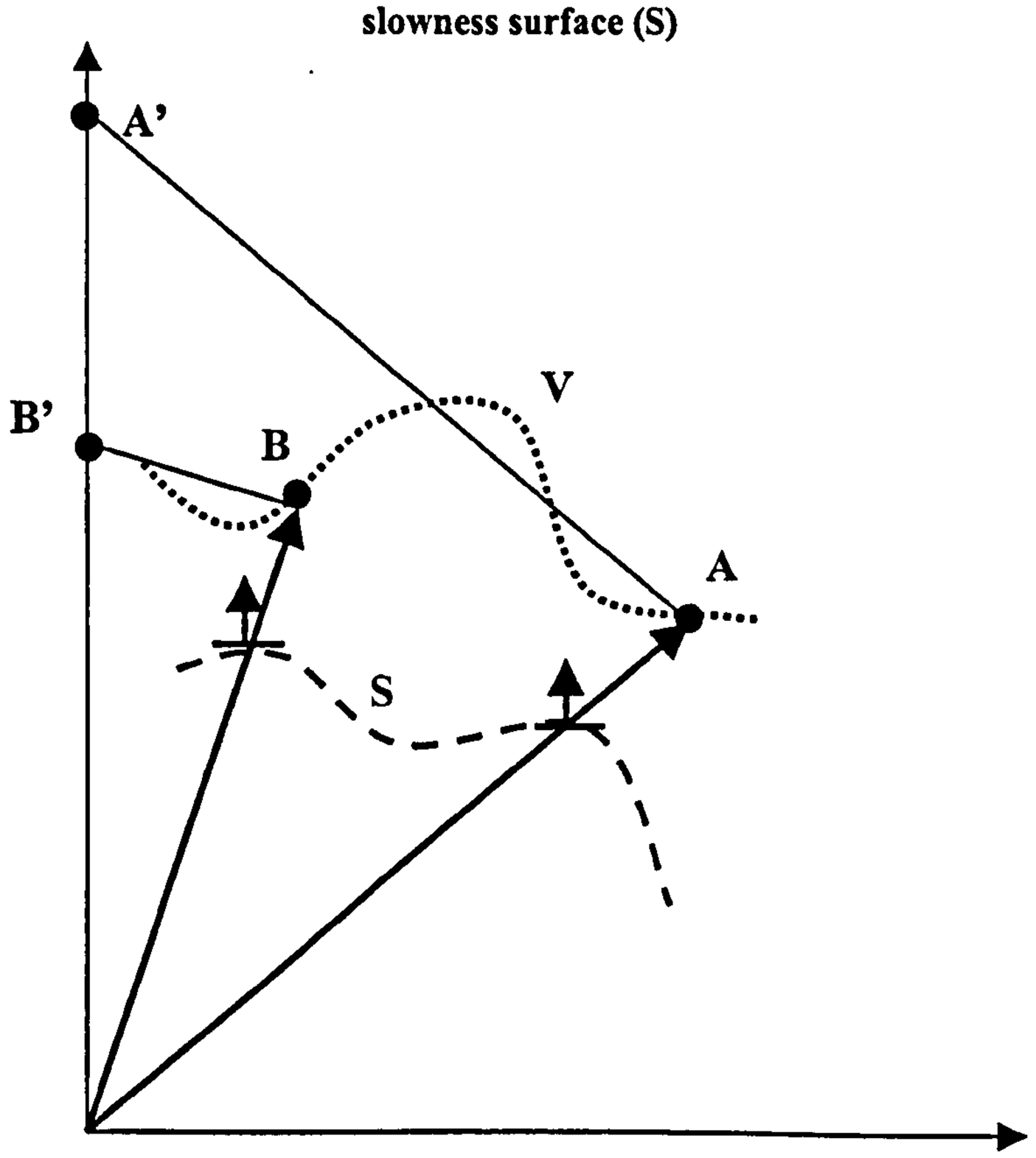

Figure 8-6 Possibility of multiple-valued wavefronts

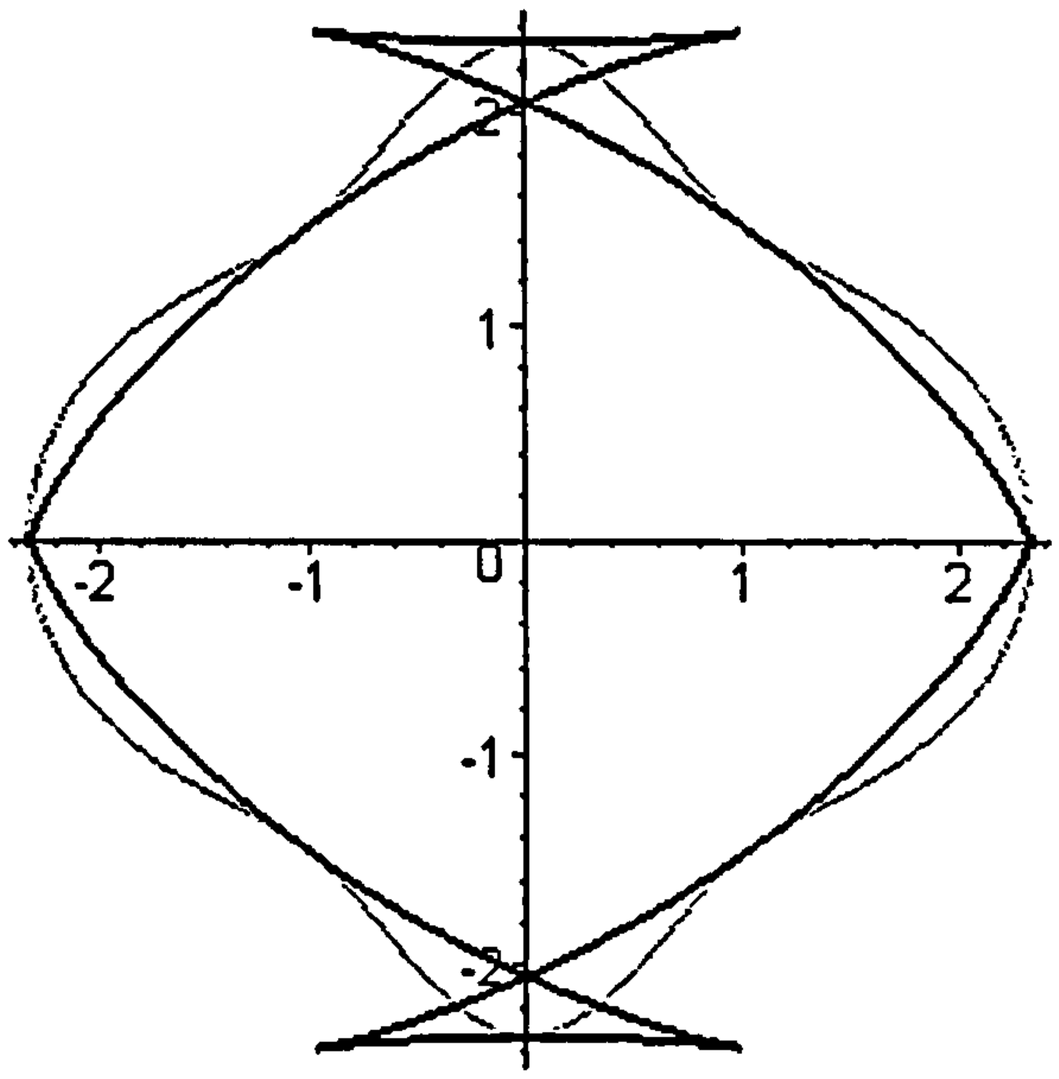

Figure 8-7 Meridian sections of phase –clear- and ray –dark- velocity surfaces for a transverse anisotropic cristal of Zinc. Data from Kim et al. (1995). Scale in km/s

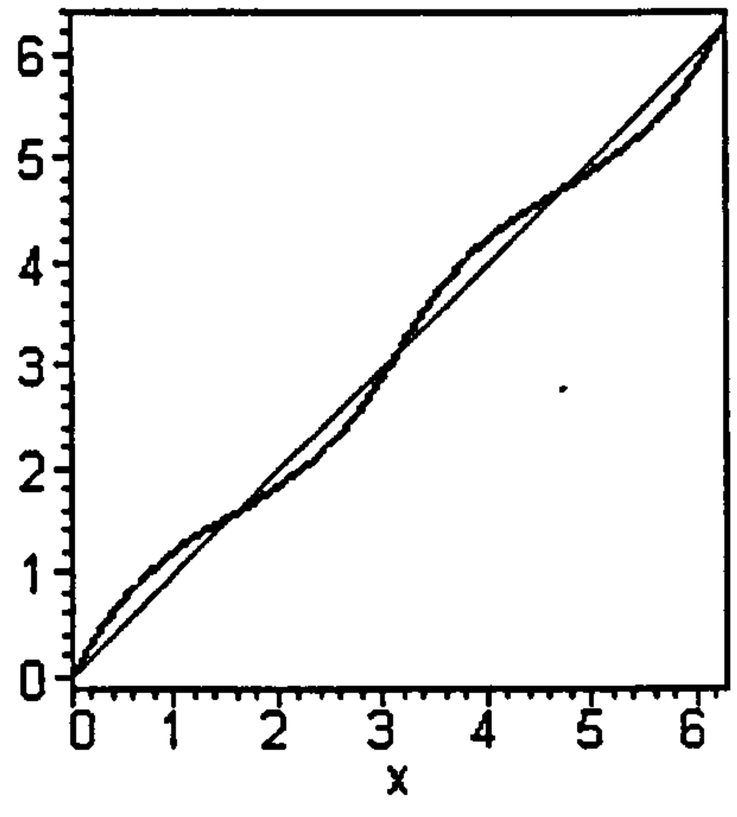

Figure 8-8 Angular deviation of corresponding ray and phase velocities from the previous figure. Horizontal axis: phase velocity dip angle. Vertical axis: ray velocity dip angle

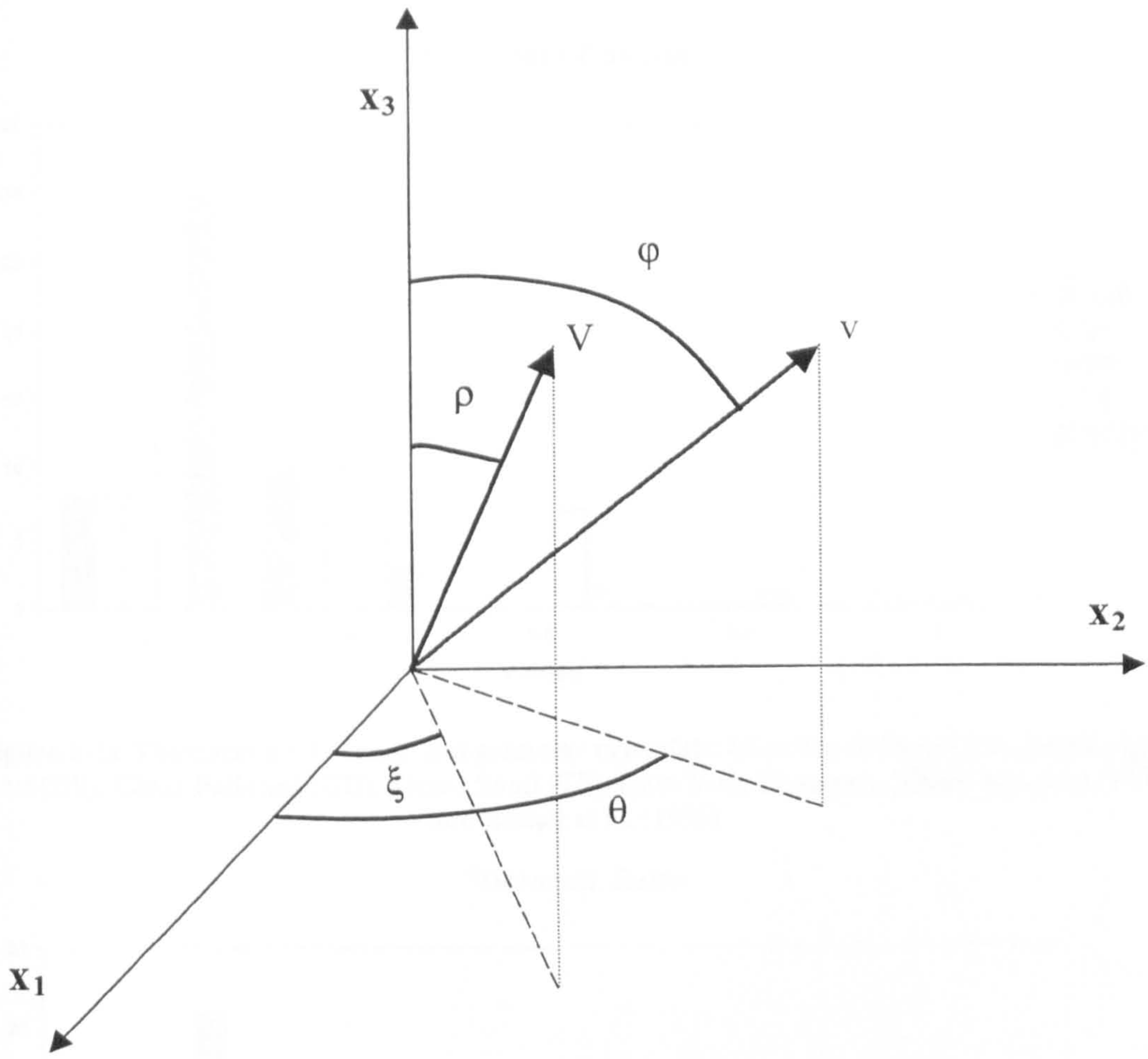

Figure 8-9 Spherical coordinates for phase velocity (v) and ray velocity (V)

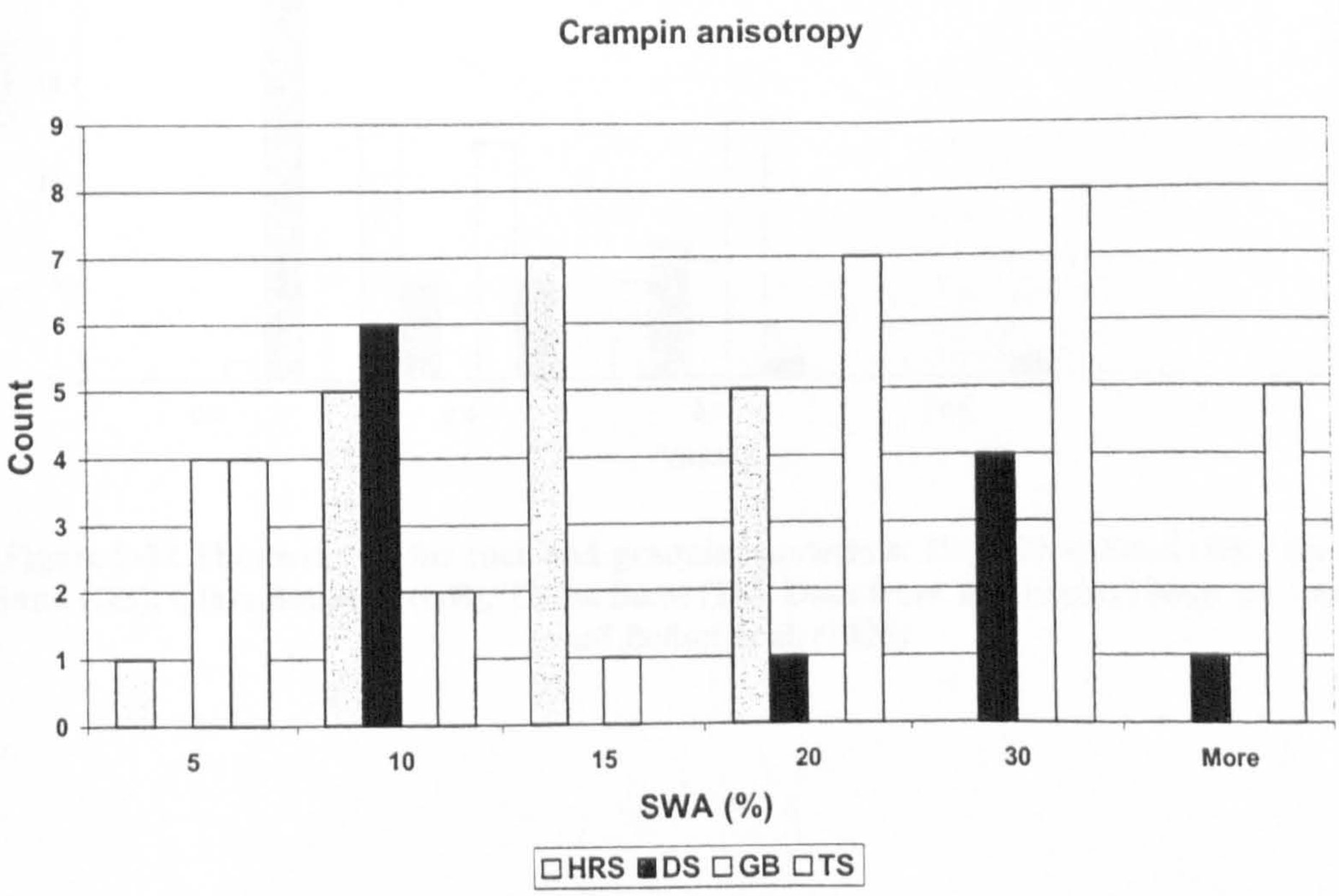

Figure 8-10 Histogram of Crampin's degree of elastic anisotropy for granular materials: Ham River Sand (HS), Dunkerque Sand (DS), Glass Ballotini (GB), Ticino Sand (TS). Data from Kuwano (1999) and Belloti et al. (1996)

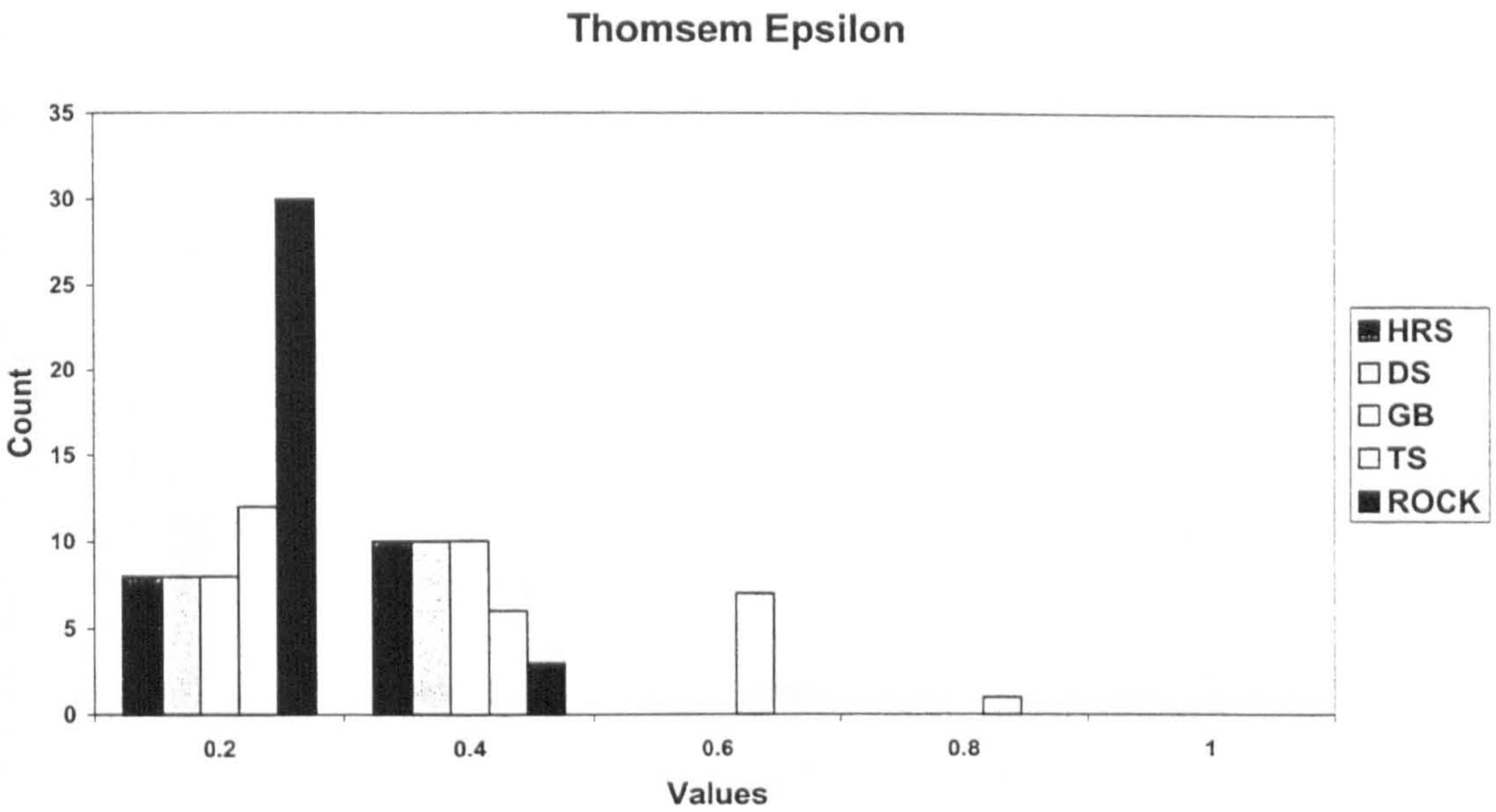

Figure 8-11 Thomsem's ε for rock and granular materials: Ham River Sand (HS), Dunkerque Sand (DS), Glass Ballotini (GB), Ticino Sand (TS). Data from Thomsem (1986), Kuwano (1999) and Belloti et al. (1996)

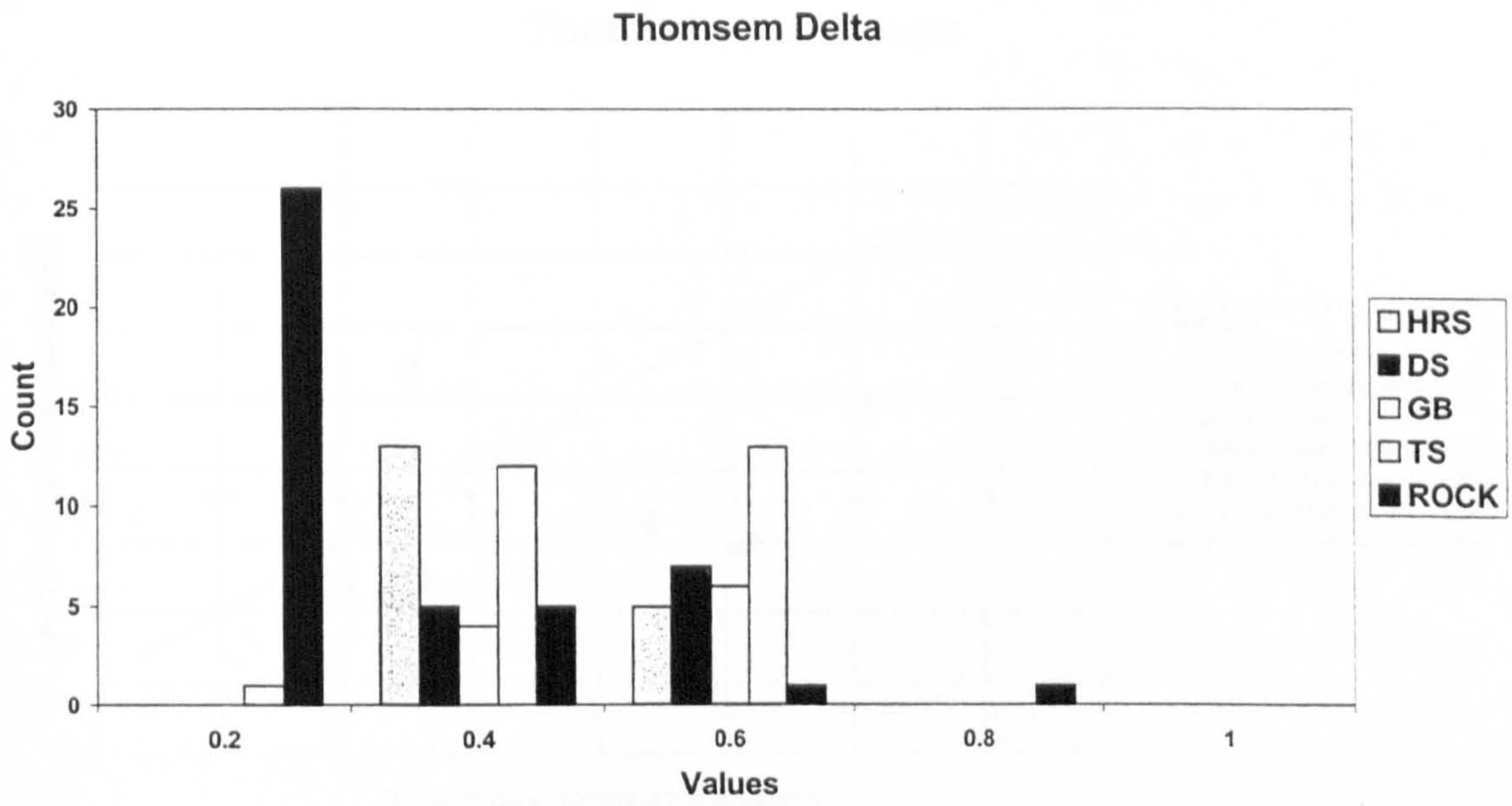

Figure 8-12 Thomsem's δ for rock and granular materials: Ham River Sand (HS), Dunkerque Sand (DS), Glass Ballotini (GB), Ticino Sand (TS). Data from Thomsem (1986), Kuwano (1999) and Belloti et al. (1996)

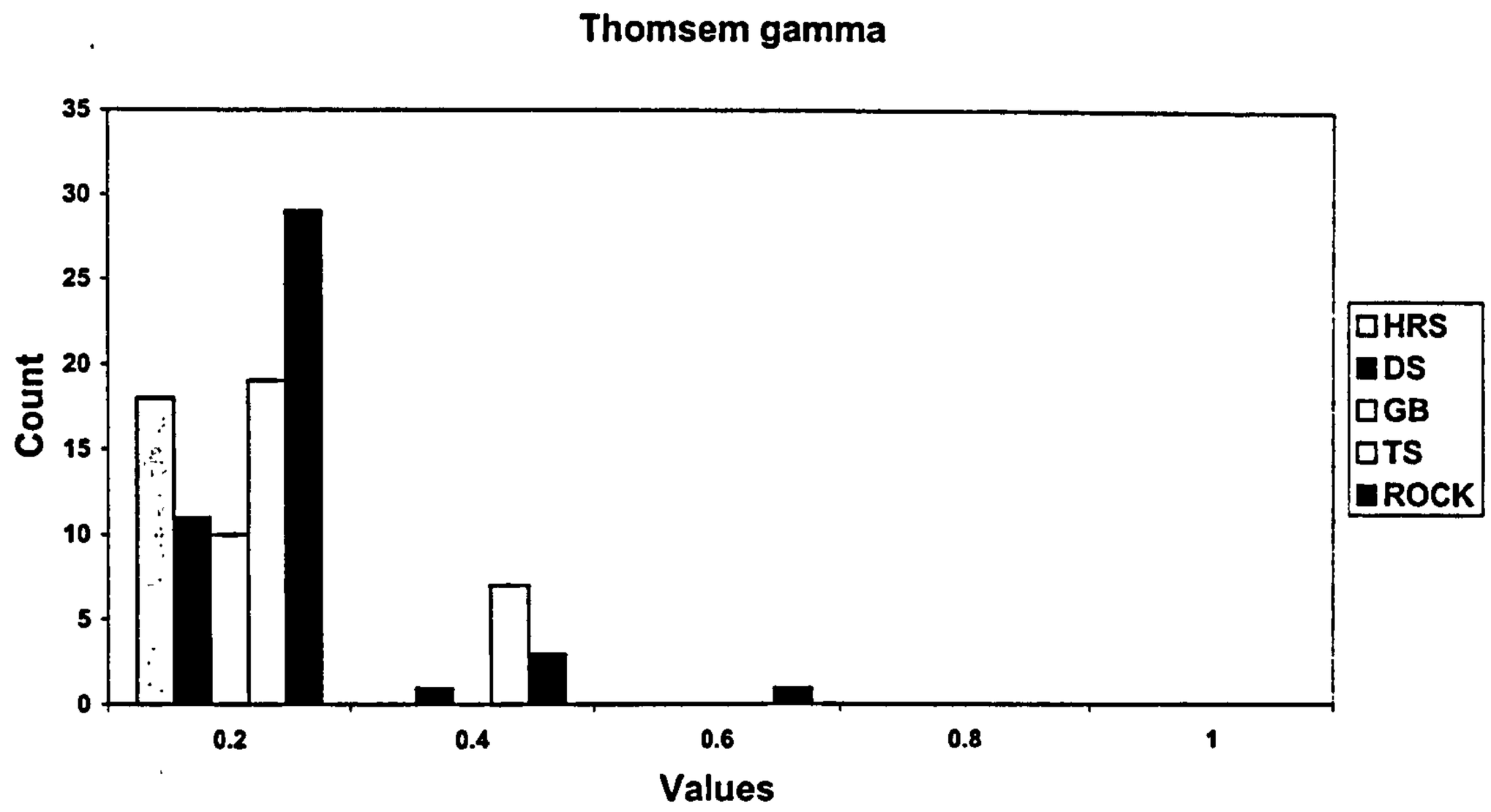

Figure 8-13 Thomsem's γ for rock and granular materials: Ham River Sand (HS), Dunkerque Sand (DS), Glass Ballotini (GB), Ticino Sand (TS). Data from Thomsem (1986), Kuwano (1999) and Belloti et al. (1996)

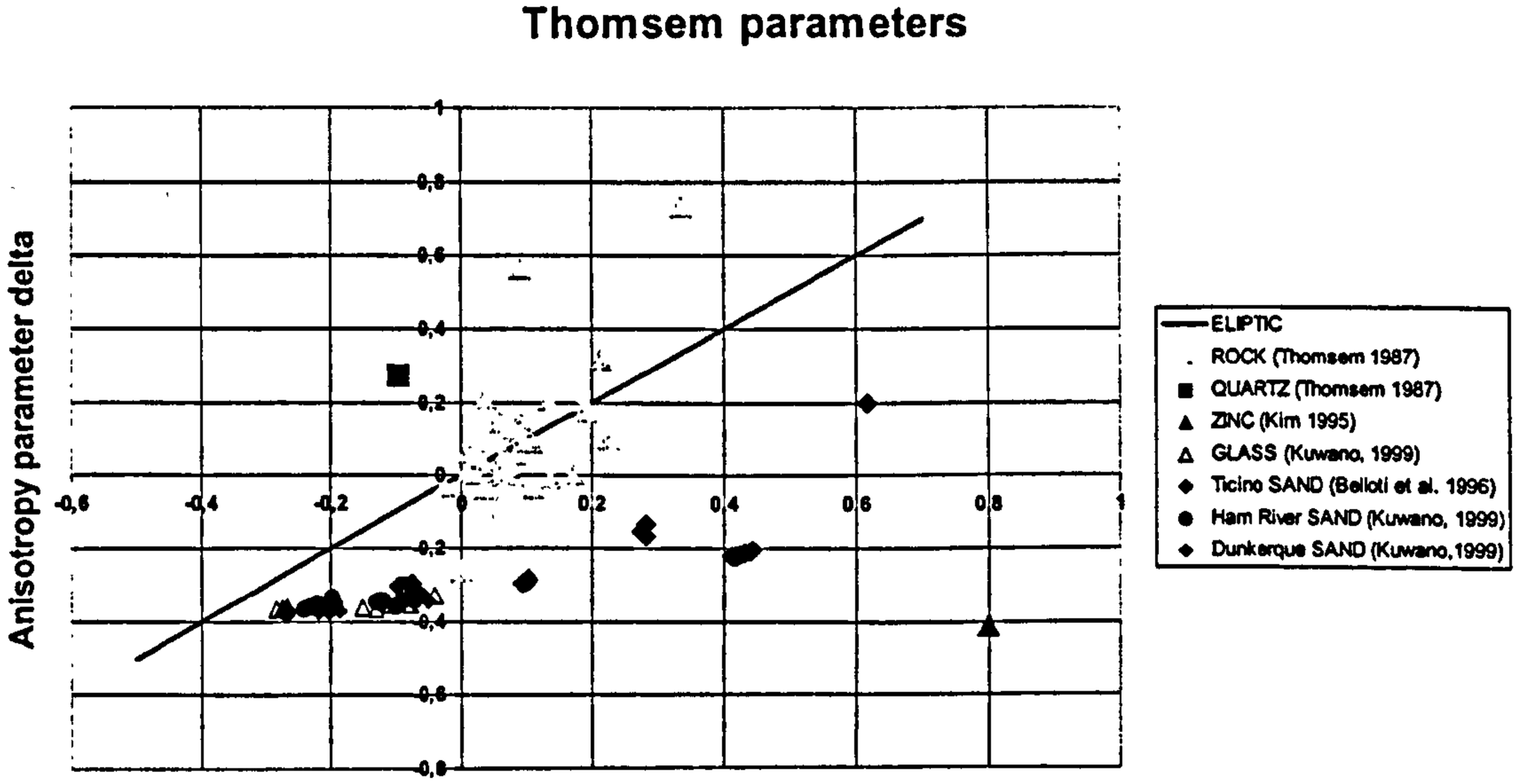

Figure 8-14 Thomsem parameters and ellipticity

9 SUMMARY AND CONCLUSIONS

This thesis set out to explore the current practice of pulse testing in soil samples, with particular emphasis on the most popular technique now in use: bender element shear testing. Our approach was mainly theoretical as it was felt that there was a gap between the increasing demands placed on the technique and its basic understanding. This gap seemed particularly relevant when anisotropic measurements were involved. Elastodynamics was the natural tool of choice as it had been used with apparent success in the nearby fields of geophysics and ultrasonic testing. This chapter summarises what has been learned on the way, comments on its relevance for geotechnics at large and offers some directions for future research.

9.1 LESSONS LEARNED

We began by reviewing the background and current practice of laboratory pulse testing in soils. Bender elements were developed to overcome the limitations posed by the typically high attenuation of soils to ultrasonic transmission. A review of current pulse testing practice revealed that arrival time selection was the most controversial aspect of the technique. The dominant interpretative framework had a plane shear wave travelling between source and receiver. Concern about near field effects had prompted various alternative suggestions for arrival selection. The effects of input signal shape on the measured arrival were not properly understood, neither was the obvious difference between input and output signals. Comparison of results with other, better understood, techniques –e.g. resonant column- was not always reassuring.

A relatively simple bench test was set up to clarify the perceived obscurities. A cylindrical sample of reconstituted Gault clay was instrumented with six bender probes, four on the side and two at each end. To explore near field effects the sample length was varied, slicing one end and reinstalling the corresponding probe five times. To explore the effects of the input signal its shape and apparent frequency were varied, employing narrow-band bursts along with more traditional wide-band signals. A total of 92 different traces were recorded. An automatic arrival time selection procedure was applied to all the traces. Six possible arrivals were selected in each trace following various previously suggested criteria, four based on characteristic points on the trace, two on signal treatment procedures of input and output: cross-correlation maxima and linear fit of cross-spectrum phase. For comparison one trained expert was asked to select the arrival points by inspection.

A statistical analysis of the results was performed. Anisotropic effects were indeed present but exclusive consideration of axially directed tests revealed much higher uncertainty than it had been previously suspected. The global variability –between different arrival selection methods- amounted to 92% of the mean shear modulus estimate. The in-method variability was also high with modulus uncertainty between 20% and 40% There were also method-dependent effects of testing distance, signal shape and apparent frequency. Close inspection of a few comparable results previously reported revealed similar orders of magnitude.

Such disparaging results further stimulated the need for deeper understanding of wave propagation in soil samples. A key concept in that respect was that of dispersion, that is of frequency-dependent propagation velocity. It was obvious that the observed propagation was dispersive and that caused problems to a naively non-dispersive model such as plane wave propagation. It was less obvious what exactly was causing that dispersion. Consideration was first made of source near field effects, as those had been previously shown to affect test results. Analytical and numerical considerations showed that near field effects can be easily discounted in pulse test interpretation. Reframing the problem as one of dispersive propagation had the advantage of obtaining results valid for all kinds of input signal. They also showed that this phenomenon was unable to explain the observed amount of dispersion both in general and in the particular case of the previously obtained bench test results.

We then moved on to consider material dispersion, that is dispersion due to properties of the material being tested. On the linear range the most important cause of that phenomenon in soils is fluid interaction. This is well described by Biot theory and we set out to examine how Biot dispersion might affect shear wave propagation. Analytical and numerical considerations showed that the problem is again relatively easy to handle and by itself unable to explain the amount of observed dispersion. Guidelines were given as to how to take it into account. For the case of impermeable materials like Gault clay Biot dispersion happens in a frequency range well above that of usual bender testing. No explanation was then forthcoming from this viewpoint either.

Finally, and still strictly within an isotropic framework, consideration was given to sample size effects. Study was restricted to the cylindrical geometry typical of triaxial tests and employed in the bench tests. Two effects were considered successively, those introduced by end rebounds and those due to the cylindrical boundary. The end rebounds were shown to introduce important interference in the received signals. With the usual rigid ends employed in triaxial samples or with the free ends employed in the bench tests end rebounds, however, are not, by themselves, a source of dispersion. They obscure the phase signature of dispersive propagation and they translate the experimental emphasis to the amplitude spectra. This is particularly so when bender length effects are taken into account. A linear system approach was employed to obtain transfer functions accounting for all rebounds and bender length effects. Results from the bench test series showed good agreement with the overall predicted shape of the amplitude spectra.

Those results, where end effects can be discounted, showed again all the features of a highly dispersive propagation still unexplained. Interaction with the cylindrical boundaries offered at last one seemingly good answer. This interaction may be treated with the tools of waveguide theory, which accounts for propagation in infinitely long cylinders. The basic tenet of this theory is that when wavelengths are comparable with the size of the propagating structure, lateral rebounds produce an interfered signal where each frequency travels at a different velocity i.e. dispersion occurs. Considering the frequency and velocity range typical of bender-based pulse tests in soils wavelengths are indeed comparable to sample

sizes. Using Disperse, a program developed for ultrasonic testing purposes, we obtained a set of dispersion curves for a Gault clay cylinder in the frequency range of testing. There were many possible dispersion curves and some geometrical considerations showed that those more likely to be excited by bender elements corresponded to flexural modes. In the frequency range of interest signals propagated with flexural modes showed an amount of dispersion compatible with the observations. For narrow-band pulses the range of likely arrival velocities varies between that of bulk compressive waves and Rayleigh waves. For wide band pulses the range is even greater. No simple recipes are available to deal with this problem, that can fool equally all the arrival selection methods currently in use. Some consideration was given to the likely range of diameter sizes and frequencies where this problem might be more intense. It shows a substantial overlap with the usual testing range.

These results made the consequent foray into anisotropic problems a more abstract endeavour than initially intended. It is obvious that, if propagation along a single direction in samples is so poorly understood and controlled, adding in the extra complications of anisotropy is somehow premature. Detailed consideration was nevertheless given to the types of elastic anisotropy that have been measured in soils and those that might be reasonably expected. This last endeavour was much helped by an algebraic approach to anisotropy that has not been given previously enough consideration in soil mechanics. The conclusion was that a much richer family of elastic anisotropies can appear in soil samples, even if current triaxial apparatuses can only cope with transverse isotropy. Some data from hollow cylinder tests were gathered to support this view.

The final chapter then went on to consider the complications that may arise when elastic anisotropic solids are tested with pulses that sample a single direction at a time. A new type of dispersion appears, directional dispersion. Symmetry plays a great simplifying role and previous knowledge of the elastic symmetry of the tested material is very helpful in designing the tests. A moderate amount of anisotropy also helps, as many simplifications are then possible. This was explored for transverse isotropy but the available data for soil show that the amount of anisotropy may be substantially higher than that guaranteed by the simplifications. However convenient, those simplifications are not always necessary, as recent research on composites and crystals shows. But research on these materials proceeds with the comfortable knowledge that each pulse traversing a sample is only affected by the traversed direction. This does not seem to be the case for current pulse testing practice in soils.

9.2 RELEVANCE OF THE RESEARCH

9.2.1 Bender testing and engineering practice

Correct estimates of structural performance are heavily dependent on soil stiffness estimates. Atkinson (2000) statement "Direct measurements of shear wave velocity using laboratory bender element tests [....] are relatively simple to perform and interpret" can be seen now as being more correct in its first part than in the second. Many results available on bender test performance have been obtained under research conditions. That is, the materials were generally well known and heavily tested. Bender measured

stiffness fitted into a big picture that many times also involved other means of stiffness estimation: resonant columns, local deformation measurements, p-wave measurements...A well informed and trained eye can see many things in the wobbly traces recorded by output benders. Many researchers happily confess to play with signal shape and frequency until "visual satisfaction" has been achieved. Then the whole set of trials is discarded and another data point is added to a well known trend.

This does not means that bender testing as it stands is useless for engineering practice. Something is better than nothing and with appropriate guidelines bender measurements might offer an adequate estimate of the small strain stiffness of soils. Much more poorly understood tests like SPT have served well the engineering profession. But this usefulness is based on a clear appreciation of the test limitations. It is reasonable for this aspect to take a second place when a new technique is developed. But design engineers need reliable tools and a level playground. Launching an uncertain technique into the realm of commercial competition without strict interpretative guidelines would be not only dangerous but unsound.

9.2.2 Laboratory pulse testing and geotechnical research

We still believe that sonic or ultrasonic testing of soils will play a fundamental role in many future research programs, in fact we give some recommendations for that in next section. Pulse tests have the potential to add some extra knowledge and not merely confirm or contrast with other measurements. But again uncertainty might ruin the purpose if it is not strictly taken into account.

Consider for instance the results presented by Jardine et al. (1999) here reproduced in Figure 1-3. They show that horizontally polarised bender inputs propagated along the vertical axis arrived systematically earlier than vertically polarised bender inputs propagated in the sample median plane. Within an assumption of elastic transverse isotropy, reasonable for triaxial tests, this result is unexplainable and they ventured a micromechanical explanation with help of some discrete element results. They may be right. But they may as well be wrong. One may argue for instance that vertical propagation is subject to guide effects to an extent that transversal propagation is not. These effects could well explain the observed difference. Also one may argue that near field effects in anisotropic samples are very poorly understood and the transversal shorter distance might be affected by them more than the larger vertical distance. Or that testing in the high frequency Biot range and using a low frequency formula to obtain the moduli may not produce the same error in all directions. More research is needed.

9.3 RECOMMENDATIONS FOR FUTURE WORK

Two different, although interacting, areas of work are now easily perceived. The first concentrates on what is likely to remain the most important test configuration for the geotechnical community: that of sonic testing along the vertical axis of a triaxial apparatus. The second should explore different testing

configurations present or foreseeable where the possibilities of sonic or ultrasonic testing of soil may be exploited.

With respect to the first area the following avenues of research are suggested

- As their consequences are so dire, there is need to confirm and explore further the extent of waveguide effects when bender elements are used along the vertical sample axis. Experimental research may proceed simply by bench-testing similar samples with different diameters.

- Numerical research should be directed to refine the location of the frequency range where multimodal transmission affects bender element operation. Account should be taken of how the confined nature of triaxial samples might affect modal characteristics. The problem would likely require a combination of various modelling levels –space discretization and modal decomposition.

- The same applies to the problem of end rebound and bender length effects or recorded modal signature. The transfer function approach developed here might be applied with numerically obtained modal reflection coefficients.

- Careful consideration should be given to the relative advantages of torsional shear-plate-based configurations for vertical testing in the triaxial apparatus. A relatively simpler interpretation might overcome the disadvantages of poorer signal quality and drainage path obstruction.

- Attention should also be paid to signal treatment procedures to obtain reliable dispersion information. The limits and relative potentials of cross-spectrum phase and amplitude techniques need to be more systematically explored. If, as it now seems, multimodal transmission is inescapable more refined techniques like time-frequency analysis or wavelet decomposition should be considered.

- Basic understanding of bender probe response while installed in the sample is lacking. Experimental research -using the self-monitoring technique or others- and numerical analysis of piezoelectric soil-embedded cantilever dynamics may be used for this purpose. A more accurate definition of installation techniques and operating frequency range should be the likely outcome of this research.

The interest of the last two items in the precedent list is not restricted to the triaxial sample-vertical testing configuration. Other ideas for research that have more general bearing or are related to different configurations are the following

- Vertical testing along oedometer axis is likely to be more affected by end rebounds than guide effects. The transfer function approach developed in this thesis should be particularly useful in these

circumstances. Attenuation measurements should also be possible from this approach if care is taken to select an adequate bender length.

- Size-induced effects need to be considered also for vertical tests along hollow cylinder walls and rectangular biaxial apparatus. Waveguide theory may be useful to explore these cases. These apparatus are likely to remain in the research realm. If, as it seems possible, guide effects are important for embedded transducers, it may be worth considering the adaptation of different ultrasonic testing techniques, particularly the refraction-based ones in use with immersed samples.

- Sample size effects for tests using lateral probes in triaxial samples have not been considered in this thesis. The same applies to cubical samples like those in use in true triaxial apparatus. Waveguide theory is unlikely to offer much insight in these cases.

- Size and near field effects have been considered in this thesis under the assumption of isotropy, it is not known how the notable anisotropy of soil samples may modify the effects described. A first step in that direction should explore systematically the extension of near field effects under various assumptions of anisotropy. This work shall be also relevant for calibration chamber and field testing.

- The possibility of obtaining permeability measurements using shear wave dispersion also deserves some consideration. To obtain only material dispersion measurements calibration chambers or field test should be considered first.

Stepping now beyond the realm of dynamic testing, other ideas spring from this research that may be interesting to follow. They are mostly related to our study of elastic anisotropy:

- Some arguments have been advanced here suggesting that elastic anisotropy in soils may have quite general forms. A more systematic combination of true triaxial and hollow cylinder testing may be employed to confirm or discard this idea.

- Elasto-plastic coupled models have the potential to predict the evolution of elastic anisotropy. The use of tensorial representation techniques seems advisable in their formulation. The apparent similitude of this approach with damage mechanics needs to be systematically examined.

The previous is a rather long list. This is mostly justified by the increasing interest in sample pulse testing. During the time employed in this research we have seen how more and more research teams have become interested in the subject. Teams from Taiwan, Portugal, Belgium, Switzerland and Spain have

started working on the subject. Closer to where these words are written, work has started already in several of the items enumerated above, both in Bristol and University College London by our research colleague Dr. Paul Greening. We hope that the work here presented will be useful for all of them.

10 APPENDIX I: SIGNAL TREATMENT CONCEPTS

10.1.1 Introduction

Some use is made in this thesis of signal treatment techniques, particularly of those based on the Fast Fourier Transform. These techniques are widespread, used in almost every work related with dynamics and have generated an extensive literature (e.g. Brigham, 1988, Balmer, 1991, Lynn & Fuerst, 1994). The first purpose of this Appendix is to recall the most important concepts for ease of reference. On the other hand, due to graphing convenience and familiarity with the Visual Basic language, many programs written for this thesis were Excel-based. This required a translation of a particular FFT Fortran-based algorithm (Press et al. 1992) whose conventions are also given here.

10.1.2 Fourier transform

The Fourier transform relates the representation of one function in time domain and in frequency domain. The definition implemented is that given –but for a sign change on the exponential- by Press et al. (1992)

$$H(f) = \int_{-\infty}^{\infty} h(t) e^{-i2\pi f t} dt$$
$$h(t) = \int_{-\infty}^{\infty} H(f) e^{i2\pi f t} df \qquad (171)$$

Even when the time domain function h(t) is real-valued, the frequency domain representation, H(f), is generally complex. Therefore it might generally be expressed as sum of real and imaginary parts or, more conveniently, in terms of its amplitude and phase,

$$H(f) = A(f) e^{\theta(f)} \qquad (172)$$

The real part of H(f) is even and the imaginary part is odd; also the amplitude spectra and phase spectra are, respectively, even and odd functions of frequency.

For notational convenience in most theoretical developments throughout the thesis the frequency domain functions are expressed in terms of the angular frequency, $\omega = 2\pi f$. The equivalent definition for this case is

$$H(\omega) = \int_{-\infty}^{\infty} h(t) e^{-i\omega t} dt$$
$$h(t) = \frac{1}{2\pi} \int_{-\infty}^{\infty} H(\omega) e^{i\omega t} d\omega \qquad (173)$$

One important property of Fourier transforms is that a time shift in the signal produces an identical phase change in its transformed counterpart. Suppose that a signal h(t) is delayed Δ to give f(t) then

$$f(t) = h(t+\Delta) \ .$$

$$F(\omega) = \int_{-\infty}^{\infty} h(t+\Delta) e^{-i\omega t} dt = \int_{-\infty}^{\infty} h(t') e^{-i\omega(t'-\Delta)} dt = H(\omega) e^{i\omega\Delta} \tag{174}$$

Note that with the transform definition here adopted a time delay results in a phase increase.

10.1.3 Convolution and correlation

Convolution and correlation are important signal treatment operations. The time domain convolution of two functions is expressed as

$$y(t) = x(t) * h(t) = \int_{-\infty}^{\infty} x(s) h(t-s)\, ds \tag{175}$$

If h(t) is taken as the impulse response of a linear system and x(t) as some input signal, then the convolution y(t) gives the corresponding output of the system. The Fourier transform of the convolution produces a simpler expression in frequency domain

$$Y(f) = X(f) H(f) \tag{176}$$

i.e. the transformed convolution is obtained just by multiplying the transformed functions.

The correlation of two signals x (t) and h(t) is a measure of their similitude for any given time shift s. The time domain correlation or of two functions is defined as

$$y(t) = Corr[x(t), h(t)] = \int_{-\infty}^{\infty} x(s+t) h(s)\, ds \tag{177}$$

More specifically, when x (t) and h(t) are different the operation is called crosscorrelation and autocorrelation when they are identical. Again, the Fourier transform of the correlation produces a much simpler expression in frequency domain, involving the product of one transformed function and the complex conjugate of the other

$$CS_{XY}(f) = X(f) Y^*(f) \tag{178}$$

The symbol employed acknowledges that the frequency domain cross-correlation function is also known as the cross-spectrum

10.1.4 Spectral power: Parseval's theorem and coherence

The modulus of the cross spectrum of two signals its known as their cross power. Also, the modulus of the autocorrelation function of a signal is known as the spectral power of the signal.

In physical applications the spectral power is shown to be directly related with the energy content of the signal. Parseval's theorem states then that the total energy content of the signal is the same in frequency and time domains. It is generally expressed equating the integral of the signal modulus in time and frequency domains

$$\int_{-\infty}^{\infty}|h(t)|^2\,dt=\int_{-\infty}^{\infty}|H(f)|^2\,df \tag{179}$$

A common measure of randomness in a series of measurements is given by the coherence function. This is defined as

$$\gamma=\frac{\left|CS_{\overline{xy}}\right|}{\sqrt{S_{\bar{x}}S_{\bar{y}}}} \tag{180}$$

The numerator is the cross power spectrum of the averaged input and averaged output. The denominator is the product of their respective spectral powers. When all measurements are completely free of random noise coherence is one, when there is some uncorrelated noise in either input, output or both coherence falls below one.

10.1.5 Discrete Fourier transform

Any continuous function of time h(t) may be digitally represented by its evaluation h_k at a finite set of N equally spaced values t_k. The spacing between these values gives the sampling rate, Δ, and, considering the number of samples, the total sampling length, T,

$$\begin{aligned} t_k &= k\Delta \qquad k=0\ldots N-1 \\ T &= (N-1)\Delta \end{aligned} \tag{181}$$

The sampled representation of h(t) is then given by a sum of equally spaced impulse functions

$$h(t)=\sum_{k=0}^{k=N-1}h_k\,\delta(t-k\Delta) \tag{182}$$

whose Fourier transform is given by

$$H(f)=\sum_{k=0}^{k=N-1}h_k\exp(-i2\pi f\,k\Delta) \tag{183}$$

This series can represent exactly any frequency domain function whose frequency range is within a certain origin centred interval. The extremes of this interval are given by the Nyquist frequency, f_{Ny} This is related to the sampling rate through

$$f_{Ny}=\frac{1}{2\Delta} \tag{184}$$

For computing convenience H(f) is evaluated at the same number of points in the frequency domain as h(t) in time domain. This gives the discrete Fourier transform as

$$H(f_n)=\sum_{k=0}^{k=N-1}h_k\exp(-i2\pi f_n\,k\Delta) \tag{185}$$

The discrete evaluation frequencies, f_n are also equally spaced, with a frequency resolution given by

$$df = \frac{2f_{Ny}}{N} = \frac{1}{N\Delta} = \frac{1}{T}$$

$$f_n = n\,df = \frac{n}{N\Delta} \qquad (186)$$

$$n = -N/2 \ldots N/2$$

Substituting this values in (185) and taking account of the periodicity of the complex exponential function a more symmetric expression of the discrete transform and its inverse is obtained

$$H_n = \sum_{k=0}^{k=N-1} h_k \exp\left(-i2\pi k \frac{n}{N}\right) \qquad n = 0..N-1$$

$$h_k = \sum_{n=0}^{n=N-1} H_n \exp\left(i2\pi k \frac{n}{N}\right) \qquad k = 0..N-1 \qquad (187)$$

Computing these equations involves the evaluation of the n*k exponential terms. When the number of data points is a power of 2 there are a number of symmetries that are systematically exploited in a class of algorithms known as Fast Fourier Transforms. As stated before, the one used in this thesis is that given by Press et al. (1992).

10.1.6 Aliasing, leakage and truncation

It is clear from (186) that there is a trade-off between time and frequency resolution for a fixed number of data points. Two problems are recurrent on this respect, leakage and aliasing. The first is due to poor frequency domain resolution, the second to poor time domain resolution. The only way out of the dilemma is to increase the number of data points.

Truncation errors are introduced when the time length record is too short and a truncated signal introduces an spurious periodicity in the signal. Artificial prolongation of the signal by zero-padding is one means out of this problem and was used here. Windowing with end-attenuating signals –gaussian, etc- is another mean.

10.1.7 Phase resolution problems

A correct estimate of phase is essential in cross-spectrum based methods of velocity estimation. This is beset with a number of problems. Usually we will compute the phase of a given complex number as

$$\theta = tan^{-1}\left(\frac{\mathrm{Im}(z)}{\mathrm{Re}(z)}\right)$$

taking the principal value of $\tan^{-1}$, which is here assumed to lay between $-\pi$ and π.

The first problem is one of numerical resolution. Whenever the complex modulus is very small the quotient giving the tangent is subject to spurious numerical fluctuations. This is illustrated in Figure 10-1 where the phase and modulus of the Fourier transform of a single sinusoidal pulse are shown.

10.2 FIGURES

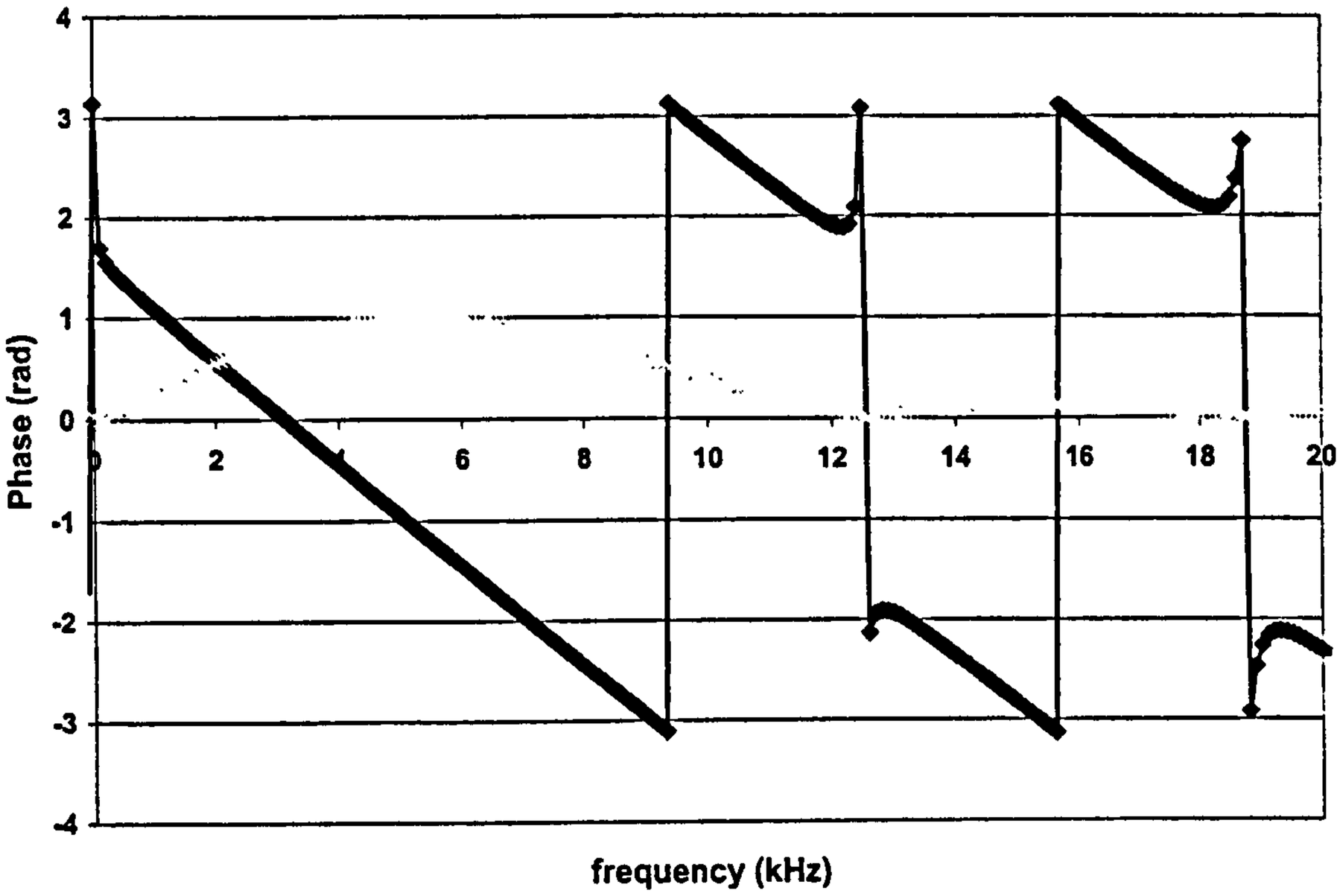

Figure 10-1 Poor numerical resolution of phase in low magnitude regions

11 APPENDIX II: CONCEPTS OF TENSORIAL FUNCTION ALGEBRA

11.1 INTRODUCTION

11.1.1 Basic definitions.

The underlying space of reference is the common three-dimensional one and Cartesian reference frames $\{\mathbf{e}_i\}$ are always assumed. Changes of reference frame, e.g. from $\{\mathbf{e}_i\}$ to $\{\bar{\mathbf{e}}_i\}$, are defined by a transformation of unit vectors $\bar{\mathbf{e}}_i = Q_{ij}\mathbf{e}_j$, which can be represented simply by a 3x3 matrix **Q**. **Tensors** are indexed collections of numbers that follow changes of reference in a very specific way, namely

$$\bar{A}_{i_1\ldots i_p} = A_{j_1\ldots j_p} Q_{i_1 j_1}\ldots Q_{i_p j_p} \tag{188}$$

All the indexes span the dimension of the space of reference, 1 to 3 in our case. The **order** of some tensor is given by the number of indexes necessary for its complete specification –p in the definition above. This definition allows scalars to be considered as zero order tensors and common vectors as first order tensors. Particularly important are second order tensors; they can be represented by a 3x3 matrix and their definition is written in matricial form as

$$\bar{\mathbf{A}} = \mathbf{Q}\mathbf{A}\mathbf{Q}^{\mathrm{T}} \tag{189}$$

As matrices and second order tensors are identifiable, changes of reference can also be considered as a peculiar set of second order tensors, the **orthogonal** second order tensors, characterised by $Q^{-1} = Q^{T}$ This set has the algebraic structure of a group, is denoted by **Orth**, and includes two important subgroups:

Rotations, Orth^{+}, reference changes defined by $\det Q = 1$

Reflections, Orth^{-}, reference changes defined by $\det Q = -1$

11.1.2 Tensorial functions

Tensorial functions are functions whose arguments include tensors. These functions could be scalar-valued or tensor-valued. In general that could be written:

$$\begin{aligned} c &= H(A_1, A_2, \ldots A_n) \\ \mathbf{T} &= F(A_1, A_2, \ldots A_n) \end{aligned} \tag{190}$$

Where the A_i stand for the arguments of the function. Examples of geotechnical relevance are provided by the yield surface in elasto-plastic models - scalar-valued function of a single tensorial argument, the stress tensor- or hypoelasticity –where the stress rate tensor is a tensorial function of the deformation rate tensor. This Appendix recalls some algebraic properties of tensorial functions like these; cases with just one or two arguments (n =1 or n = 2) are particularly important and will deserve special attention.

Tensorial arguments can be as simple as a vector or as complex as a fourth order tensor. As the number and tensorial order of arguments increase tensorial functions become more complicated. It is then

reasonable to classify them specifying their list of arguments, **L**, that is the number and tensorial order of their arguments. However, for some developments the important characteristic of the arguments is their tensorial nature and not so much the particular order of each one. In these cases we will shortly write a generic list, $\mathbf{L}_A$, as follows

$$\mathbf{L}_A \equiv \{A_1, A_2, ...A_n\} \tag{191}$$

11.2 CLASSIFYING SYMMETRY

11.2.1 Symmetry transformations

If a particular reference change, characterised by **Q**, leaves a tensorial function unchanged[118], it's called a **symmetry transformation** of the function. More specifically,

$$\begin{aligned} c &= H(A_1, A_2, ...A_n) = H(\overline{A}_1, \overline{A}_2, ...\overline{A}_n) \\ \mathbf{T} &= F(A_1, A_2, ...A_n) \Leftrightarrow \overline{\mathbf{T}} = F(\overline{A}_1, \overline{A}_2, ...\overline{A}_n) \end{aligned} \tag{192}$$

- If the function is scalar-valued this scalar would not change
- If the function is tensor-valued, the tensor itself will transform, and this transformed tensor must coincide with the one given by the transformed arguments

11.2.2 Symmetry groups

Groups are the mathematical entities employed to formalise and quantify the concept of symmetry. Jordan & Jordan (1994) give an introductory account of their properties. All the symmetry transformations of a tensorial function form a group (Zheng, 1994) called its **symmetry group**. A tensor function, f, could then be classified specifying its symmetry group, G_f. For instance:

a) An **isotropic tensor function** has the entire orthogonal group as its symmetry group
b) An **hemitropic tensor function** has the proper orthogonal group (rotations, but not reflections) as its symmetry group
c) An **anisotropic tensor function** has a symmetry group different from the precedents.

The number of possible simmetry groups is not infinite. There is a limited number of possible anisotropies, and therefore of tensor function types. Zheng & Boehler -1994- prove this extreme and give a list of just 41 different symmetry groups in 3D -for 2D the number is just 12, Zheng (1994). That list of 41 includes all the 32 crystalline classes -orthotropy being one of them- and 5 types of cylindrical symmetry including transverse isotropy.

All the transformations included in any particular symmetry group might be expressed as product of some elements within that group. These are the group **generators**. For instance, the generators of the symmetry group characterising cross anisotropy of axis $\{\mathbf{e}_1\}$ are

---

[118] Invariant is surely a nicer term, but this has here a more restricted sense explained below.

$$\left\{\begin{bmatrix}-1 & 0 & 0\\ 0 & -1 & 0\\ 0 & 0 & -1\end{bmatrix}\begin{bmatrix}1 & 0 & 0\\ 0 & \cos\theta & sin\theta\\ 0 & -sin\theta & \cos\theta\end{bmatrix}\right\} \qquad (193)$$

Where the first matrix characterises central inversion -a symmetry of all non piezoelectric materials- and the second rotations of axis $\{e_i\}$ and angle θ.

11.2.3 Structural tensors

A structural tensor, ξ, is a tensor whose components are left unchanged by a particular symmetry group. So, if ξ is an structural tensor of G,

$$\bar{\xi}_{i_1\ldots i_p} = \xi_{j_1\ldots j_p} Q_{i_1 j_1}\ldots Q_{i_p j_p} = \xi_{i_1\ldots i_p} \qquad \forall \mathbf{Q} \in G \qquad (194)$$

Zheng -1994- shows that it is always possible to find a single structural tensor for each symmetry group. As suggested by the previous equation this single structural tensor need not be of any particular order ; for instance there are symmetry groups whose structural tensor is of order two, three, four, six....The structural tensor may not be unique but even if various choices are possible they unambiguously characterise an unique symmetry group. Some examples follow.

The second order unit tensor, **1**, is the only tensor whose components are unchanged by the whole set of orthogonal transformations. It therefore characterises the isotropy group.

Cross-anisotropy of axis vector $\mathbf{e}_1$ is characterised by the following structural tensor

$$\mathbf{e}_1 \otimes \mathbf{e}_1 = \begin{pmatrix}1 & 0 & 0\\ 0 & 0 & 0\\ 0 & 0 & 0\end{pmatrix} \qquad (195)$$

Orthotropy is characterised by any one of the following structural tensors

$$\mathbf{e}_1 \otimes \mathbf{e}_1 - \mathbf{e}_2 \otimes \mathbf{e}_2 = \begin{pmatrix}1 & 0 & 0\\ 0 & -1 & 0\\ 0 & 0 & 0\end{pmatrix}$$

$$\mathbf{e}_2 \otimes \mathbf{e}_2 - \mathbf{e}_3 \otimes \mathbf{e}_3 = \begin{pmatrix}0 & 0 & 0\\ 0 & 1 & 0\\ 0 & 0 & -1\end{pmatrix} \qquad (196)$$

$$\mathbf{e}_3 \otimes \mathbf{e}_3 - \mathbf{e}_1 \otimes \mathbf{e}_1 = \begin{pmatrix}-1 & 0 & 0\\ 0 & 0 & 0\\ 0 & 0 & 1\end{pmatrix}$$

Summarising: tensorial functions have symmetries, the types of possible symmetries are limited and described by symmetry groups. All symmetry groups might be identified by their generators and/or

structural tensor. Zheng (1994) gives a complete list of all symmetry groups, indicating their generators and structural tensors.

11.3 REPRESENTATION OF TENSORIAL FUNCTIONS

11.3.1 General

As stated in precedent sections tensorial functions could be classified using two different criteria: their argument list, L_A, and their symmetry group, G_F. If these two are specified we can then talk about a particular class of tensorial functions, say $\Phi(L_A,G_F)$. The basic result of the algebraic theory of tensorial functions is that as long as the number of arguments in L_A is finite it is possible to generate all functions in the class using just a small subset of them.

For scalar valued functions in $\Phi(L_A,G_F)$ the elements of this subset are called **invariants** and the subset, say $\{I_1 \ldots I_k\}$, is called a **functional basis.** We can then write a **representation** for any function in the class as

$$c = H(A_1, A_2, \ldots A_n) = h(I_1, I_2, \ldots I_k) \tag{197}$$

For tensor-valued functions in $\Phi(L_A,G_F)$ an extra subset of tensor-valued functions is needed, and we will symbolise them by $\{S_1 \ldots S_p\}$. They are called **form-invariants.** Any function in the class $\Phi(L_A,G_F)$ may then be represented as a linear combination of this form-invariants

$$\mathbf{T} = F(A_1, A_2, \ldots A_n) = \alpha_1(I_1..I_k)S_1 + \ldots + \alpha_p(I_1..I_k)S_p \tag{198}$$

where, as indicated, the coefficients are themselves scalar-valued functions of the functional basis.

Representations could be **complete,** meaning that they are valid for each and every function in the class $\Phi(L_A,G_F)$. Representations could also be **irreducible,** meaning that the form-invariants entering in it could not be expressed as lineal function of the others and that none of the invariants in the functional basis can be expressed as a function of the others. Irreducible and complete representations are quite interesting, because they are the most simplified general expression for a certain class of functions.

To end this paragraph it's worth mentioning that representations were first developed within the narrower scope of polynomial tensorial functions, -that is $\Phi(L_A,G_F)$ were classes including only polynomials of the arguments on L_A-, being later extended to cover any kind of functions. When reading the literature, (e.g. Kolymbas 1989) this might cause some confusion because in the polynomial case the functional bases are called **integrity bases.** In general, for a given list L, its functional basis contains less elements than the corresponding integrity basis, and the number of generators is also inferior, then, the representations for general functions will differ slightly from the ones for polynomial functions[119].

[119] So to say, the price to pay for dealing only with polynomials is to have lengthier representations.

11.3.2 Isotropic functions of symmetric second order tensors

So, for any given tensorial function class it is possible in principle to find a functional basis and an irreducible representation. The problem is then solvable, but is not an easy one, being generally easier to obtain complete representations than proving those irreducible. As explained by Zheng (1994) there is a substantial increase in difficulty as the order of the arguments grows. Hence results for second order tensorial arguments are pretty much complete, but those including fourth order tensors are still being explored.

Representations of isotropic tensorial functions were the first to be explored and are also the starting point for representations of anisotropic tensorial functions. In Table 11-1, following Zheng –1994-, we collect the invariants and generators needed when the argument list is formed exclusively by second order tensors. The symbols A, B, C in the table stand for any argument in the list; that is, every argument taken in isolation introduces the three invariants and generators of the first row; every pair of arguments introduces those in the second row and every trio that in the third row. No new invariants or generators are obtained considering more than three arguments together.

Invariants are not unique. All the isotropic invariants included in the precedent basis are polynomials, defined in terms of the arguments traces. This is just a matter of convenience, partly prompted by the method employed to check the irreducible character of the base –Zheng, 1994. Any combination amongst them is also an invariant and might be substituted for any of those featuring in the list. For instance, as invariants of a single argument –those in the first row of Table 11-1- we may use instead p, q and θ defined by

$$p = \frac{1}{3} trA$$

$$q = \sqrt{\frac{3}{2}\left(trA^2 - \frac{(trA)^2}{3} \right)} \qquad (199)$$

$$\cos 3\theta = 2\sqrt{3}\, \frac{trA^3 - \frac{1}{9}(trA)^3 - \frac{2}{3}(trA)trA^2}{\sqrt{\left(trA^2 - \frac{1}{3}(trA)^2 \right)^3}}$$

As the choice of names suggest when A is identified with the stress tensor the invariants in this set are very popular: the isotropic stress, generalised deviatoric stress and Lode angle. Note that the equivalence between the definition given above and the more usual based on deviatoric stress –e.g. Jeremic & Sture, 1997- is a matter of simple algebra.

11.3.3 Isotropicization of anisotropic functions

Boehler (1979), found a simple way to develop representations for anisotropic functions starting with those corresponding to anisotropic functions. The key result is known as the **"Isotropicization theorem"**,

(Zheng, 1994). This theorem states that any anisotropic function, F, with arguments L_A and symmetry group G_F, could be treated as an isotropic function if the characteristic structural tensor of its symmetry group is added to its argument list. Formally

$$F(L_A, G_F) \equiv F(\{L_A, \xi_{G_F}\}, Orth) \tag{200}$$

This theorem provides therefore a link between the two aspects characterising any tensorial function, its argument list and its symmetry group. The function F is isotropic with respect all its arguments and anisotropic –with symmetry characterised by G_F- with respect the original argument list L_A.

Functional bases and representations for anisotropic functions can be then obtained in a two step approach. First the isotropic representation is applied to the list including the structural tensor. Then this list is simplified taking in account the simple expressions of structural tensors, -for instance in the orthotropic case -(196) above- they have zero trace, in the transverse isotropic case -(195) above- they have trace unity, etc... The resulting representations are then reduced from the equivalent isotropic case – that is, from the case of one of the arguments not being a structural tensor. For instance, in Table 11-2 we collect the functional basis and generators for transverse isotropic and orthotropic functions of a single second order symmetric tensor.

11.3.4 General vs representation-based approach to tensorial functions

Tensorial functions can be defined directly without any resource to representations. For instance, it is well known that a symmetric second order tensor has only six independent components and, consequently, the set of all them, **Symm**, corresponds exactly with a six-dimensional vector space. An obvious base for this space is given by the six following matrices $\{M_i, i = 1..6\}$

$$\{M_i\} \equiv \left\{ \begin{pmatrix} 1 & 0 & 0 \\ 0 & 0 & 0 \\ 0 & 0 & 0 \end{pmatrix} \begin{pmatrix} 0 & 0 & 0 \\ 0 & 1 & 0 \\ 0 & 0 & 0 \end{pmatrix} \begin{pmatrix} 0 & 0 & 0 \\ 0 & 0 & 0 \\ 0 & 0 & 1 \end{pmatrix} \begin{pmatrix} 0 & 1 & 0 \\ 1 & 0 & 0 \\ 0 & 0 & 0 \end{pmatrix} \begin{pmatrix} 0 & 0 & 1 \\ 0 & 0 & 0 \\ 1 & 0 & 0 \end{pmatrix} \begin{pmatrix} 0 & 0 & 0 \\ 0 & 0 & 1 \\ 0 & 1 & 0 \end{pmatrix} \right\} \tag{201}$$

In this base any symmetric second order tensor, T_{ij} can be expressed as follows

$$\mathbf{T} = T_{11}\mathbf{M}_1 + T_{22}\mathbf{M}_2 + T_{33}\mathbf{M}_3 + T_{12}\mathbf{M}_4 + T_{13}\mathbf{M}_5 + T_{23}\mathbf{M}_6 \tag{202}$$

or, briefly,

$$\mathbf{T} = t_i \mathbf{M}_i \tag{203}$$

Considering now this tensor as function of arguments given by the list L_A, the following expression is then the most general one may think of

$$\mathbf{T} = \mathbf{T}(A_1 ... A_n) = t_i(A_1 ... A_n)\mathbf{M}_i \tag{204}$$

If the list contains only one symmetric argument we will have, for instance,

$$\mathbf{T} = \mathbf{T}(\mathbf{A}) = t_i(A_{pq})\mathbf{M}_i \tag{205}$$

and this express the obvious fact that each component of T depends on each component of A, so that we need to specify six functions of six variables. For two symmetric arguments, we will instead specify six functions of twelve variables and so on...

It is interesting to compare how the problem size changes when, faced with the task of specifying a particular isotropic tensor function, we use its representation instead of the general approach above. Table 11-3 does this for the cases of one, two and three symmetric tensorial arguments. It is obvious that using a representation, does not diminish per se the size of the problem, although this is the case for a single argument. As Boehler (1979) remarks the main advantage of employing representations are then others: no hidden symmetries will appear in the formulations. Besides, their form makes easy to impose other assumptions, (e.g. linearity on one argument), realising clearly their consequences, which, of course, are mainly to prune otherwise untractable expressions.

11.4 TABLES

List elements	Functional basis	Generators
A	trA, trA^2, trA^3	I, A, A^2
A,B	$trAB, trA^2B, trAB^2, trA^2B^2$	$AB + BA, A^2B + BA^2, AB^2 + B^2A$
A,B,C	trABC	

Table 11-1 Functional basis and generators for isotropic functions of symmetric second order tensors

Symmetry	Functional basis	Generators
Isotropy	trA, trA^2, trA^3	I, A, A^2
Transverse isotropy	$trA, trA^2, trA^3, trMA, trMA^2$	$I, A, A^2, M, AM + MA, A^2M + MA^2$
Orthotropy	$trA, trA^2, trA^3, trMA, trMA^2, trM^2A, trM^2A^2$	$I, A, A^2, M, M^2, AM + MA, A^2M + MA^2$

Table 11-2 Functional basis and generators for isotropic and anisotropic functions of a single symmetric second order tensor

Arguments	General approach	Isotropic Representation
1	6 functions of 6 components	3 functions of 3 invariants
2	6 functions of 12 components	8 functions of 10 invariants
3	6 functions of 18 components	18 functions of 21 invariants

Table 11-3 Complexity of tensorial function specification

12 APPENDIX III: MISCELLANEA

The purpose of this appendix is to gather some developments that either underpin or extend results presented in the thesis and for which no appropriate reference has been found.

12.1.1 Small-strain hypothesis in bender-based pulse tests

The small strain assumption might be justified if we compare the size of the maximum bender deflection and that of typical wavelengths. We have seen in Chapter 5 that there is substantial uncertainty about the actual behaviour of a soil-embedded bender element. Nevertheless a rough estimate can still be made. The static tip displacement for a free-deflecting bender of the cantilever type is given by (Schultheiss, 1983)

$$D = 3d_{31}Vs^2 \qquad (206)$$

Where d_{31} is a piezoelectric constant of the transducer material, V is the applied voltage and s is the slenderness of the transducer. Substituting values typical of geotechnical testing practice –see Chapter 2, 3 and 6- we obtain a maximum displacement of circa 10^{-5} cm. Even assuming a dynamic gain at resonance of 100 over this free-air value, that will still be three orders of magnitude beneath a typical wavelength of 1cm. Of course, as the pulse propagates through the soil, attenuation will make this ratio even smaller.

12.1.2 A direct check on pulse superposition

We have seen thus that there are some theoretical grounds to believe that linear behaviour might be possible in soils and, furthermore, that such a linear behaviour is what pulse tests do explore. It is then interesting to try and check this linear behaviour assumption. Of course, all the results exposed in precedent chapters offer ample confirmation about the possibilities and advantages of such an approach. Nevertheless, it was thought that a direct check on linearity would also be interesting and taking advantage of ongoing research on bender element probes at Bristol such a check was performed.

A sample of Gault clay for bench testing was prepared along the lines described in Chapter 3. As illustrated in Figure 12-1, the number and disposition of bender element probes in it were nevertheless different. Single sinusoidal shots of f_{ap} 5 kHz were fired from probes A and F and recorded at probe B and G. Each source probe was first activated on isolation, then, by means of a parallel connection to the function generator, they were fired simultaneously.

Perfect linearity would imply that the simultaneous shot will be an exact copy of the result obtained by adding the two single shots. Figure 12-2 and Figure 12-3 display the recorded simultaneous trace along with the sum of equivalent consecutive shots. The level of superposition, although not perfect, seems adequate.

12.1.3 Rebound transfer function accounting for bender length

The total output can be computed as the average of those corresponding to each path between source and receiver. These in turn are computed in two steps: first separate transfer functions are obtained for the first arrival, A_i, and the rebound cycle, S_i, then these are combined to obtain O_i according to the general scheme. We have then for the first path –i.e. forward wave, front arrival-

$$A_a = I\,W^+\left(H-2l_B,0\right) = I\,e^{-ik(H-2l_B)}$$
$$S_a = W^+\left(H-l_B,H-2l_B\right)B^*W^-\left(-l_B,H\right)B'W^+\left(H-l_B,-l_B\right) = e^{-ikl_B}e^{-ik(H+l_B)}e^{-ikH} = e^{-i2kH} \qquad (207)$$
$$O_a = I\frac{e^{-ik(H-2l_B)}}{1-e^{-i2kH}}$$

for the second path –i.e. forward wave, back arrival-

$$A_b = I\,W^-\left(-l_B,0\right)B'W^+\left(H-2l_B,-l_B\right) = Ie^{-ikl_B}\,e^{-ik(H-l_B)} = Ie^{-ikH}$$
$$S_b = S_a = e^{-i2kH} \qquad (208)$$
$$O_b = I\frac{e^{-ikH}}{1-e^{-i2kH}}$$

for the third path –i.e. backward wave, front arrival-

$$A_c = I\,W^+\left(H-2l_B,0\right)B^*W^-\left(H-2l_B,H-l_B\right) = I\,e^{-ik(H-l_B)}e^{-ikl_B} = e^{-ikH}$$
$$S_c = W^-\left(-l_B,H-2l_B\right)B'W^+\left(H-l_B,-l_B\right)B^*W^-\left(H-2l_B,H-l_B\right) = e^{-ik(H-l_B)}e^{-ikH}e^{-ikl_B} = e^{-i2kH} \qquad (209)$$
$$O_c = I\frac{e^{-ikH}}{1-e^{-i2kH}}$$

and for the fourth path –i.e. backward wave, back arrival-

$$A_d = I\,W^-\left(-l_B,0\right)B'W^+\left(H-l_B,-l_B\right)B^*W^-\left(H-2l_B,H-l_B\right) = Ie^{-ikl_B}e^{-ikH}e^{-ikl_B} = Ie^{-ik(H+2l_B)}$$
$$S_d = S_c = e^{-i2kH} \qquad (210)$$
$$O_d = I\frac{e^{-ik(H+2l_B)}}{1-e^{-i2kH}}$$

Now the total output is given by

$$O = \frac{1}{4}\left\{O_a + O_b + O_c + O_d\right\}$$
$$= \frac{I}{4}\left\{\frac{e^{-ik(H-2l_B)}}{1-e^{-i2kH}} + \frac{e^{-ikH}}{1-e^{-i2kH}} + \frac{e^{-ikH}}{1-e^{-i2kH}} + \frac{e^{-ik(H+2l_B)}}{1-e^{-i2kH}}\right\} \qquad (211)$$
$$= \frac{I}{4}\frac{e^{-ikH}}{1-e^{-i2kH}}\left\{e^{i2kl_B} + 1 + 1 + e^{-i2kl_B}\right\}$$
$$= \frac{I}{2}\frac{e^{-ikH}}{1-e^{-i2kH}}\left\{\cos\left(2kl_B\right) + 1\right\}$$

12.1.4 Moduli equivalence for transverse isotropic material

The equivalence between the moduli in the symmetric engineering notation and the matrix notation is given by

$$E_V = \frac{J}{D_{11}^2 - D_{12}^2}$$
$$E_H = \frac{J}{D_{11}D_{33} - D_{13}^2}$$
$$\nu_{VH} = \frac{D_{13}}{D_{11} + D_{12}} \qquad (212)$$
$$\nu_{HH} = \frac{D_{12}D_{33} - D_{13}^2}{D_{11}D_{33} - D_{13}^2}$$
$$G_{VH} = D_{44}$$

And J represents the determinant of the principal minor of order three of $\mathbf{D_0}$. When the asymmetric engineering notation is employed the following Poisson ratio should be added

$$\nu_{HV} = \frac{E_H}{E_V}\nu_{VH} = \frac{D_{13}(D_{11} - D_{12})}{D_{11}D_{33} - D_{13}^2} \qquad (213)$$

12.1.5 Objectivity checks and anisotropy: an example

Is straightforward to apply the principle of space isotropy for isotropic materials. Classically this will be done as a check in objectivity. In a formulation whatsoever, a general reference transformation is applied to its variables, and, after some manipulation, the original form should be recovered in the new reference. As an illustration, consider the Von Mises yield criteria for plane stress

$$Y \equiv \frac{1}{2}S_X^2 + \frac{1}{2}S_Y^2\frac{1}{2}(S_X - S_Y)^2 + 3S_{XY}^2 = r^2 \qquad (214)$$

where the S_{ij} represent the components of the 2-D stress tensor. Now apply a general plane rotation of angle θ, given by

$$Q = \begin{bmatrix} \cos\theta & \sin\theta \\ \sin\theta & \cos\theta \end{bmatrix} \qquad Q \in Orth \qquad (215)$$

to the stress tensor S, obtaining a transformed stress tensor. The Mises criterion could now be written as

$$Y \equiv \frac{1}{2}\overline{S}_X^2 + \frac{1}{2}\overline{S}_Y^2\frac{1}{2}(\overline{S}_X - \overline{S}_Y)^2 + 3\overline{S}_{XY}^2 = r^2$$
$$\overline{S}_{ij} = S_{pq}Q_{pi}Q_{qj} \qquad (216)$$

Substituting the values of the transformed stresses a somehow intricate trigonometric expression is obtained -Figure 12-4. After careful consideration of the trigonometric coefficients this expression could be simplified to recover (214), thus proving the objectivity of Mises criteria.

The traditional approach to anisotropic formulations apparently precludes the application of such a check on their objectivity. Hill (1950) generalised the Mises yield criteria for anisotropic materials. The

expression proposed, for a material with general anisotropy, takes the following form in the case of plane stress

$$Y \equiv a\,S_x^2 + b\,S_y^2 + c\left(S_x - S_y\right)^2 + d\,S_{xy}^2 = r^2 \qquad (217)$$

where the coefficients a,b,c,d characterise the anisotropy. If a general transformation is applied to this formula, an intricate trigonometric expression is again obtained -Figure 12-5. But now the presence of the anisotropic coefficients, {a,b,c,d}, prevents any simplification, and, in fact, the formulation remains dependent on the angle θ, or, in other words, in the orientation of the reference system. In fact, to obtain formulations corresponding to more symmetric materials, the technique employed by Hill is to identify expressions corresponding to the rotation angles θ characterising the material symmetry. This imposes conditions on the anisotropic coefficients, reducing their number; for example, a square symmetry –symmetries given by $\theta = \pi/2$ and its integer multiples-, gives a = b, therefore reducing (217) to

$$Y \equiv a\left(S_x^2 + S_y^2\right) + c\left(S_x - S_y\right)^2 + d\,S_{xy}^2 = r^2 \qquad (218)$$

12.1.6 Collinearity

In constitutive parlance the term collinearity –or coaxiality- is frequently used to express the coincidence of principal axes of stress and strain or, in general, of an agent and a response. The theory of tensorial function representations is useful to clarify the implications of this property.

In the case of a second order tensorial function of just one tensorial second-order argument (and perhaps many scalar arguments) its representation theorem states

$$\mathbf{T} = F(\mathbf{A}) = \varphi_0\mathbf{I} + \varphi_1\mathbf{A} + \varphi_2\mathbf{A}^2 \qquad (219)$$

With φ_i functions of (trA, trA^2,trA^3). If the equation is expressed in the principal axes of A, then all the matrix are diagonal and T has the same principal axes as A i.e. T is collinear with A.

In we add any other argument to the list of F, be it a vector or another tensor, the representation will include more terms, (generators), that will not be diagonal, in the general case, when expressed in A principal axes. So T would not have, in general, the same principal axes as any of the arguments in F.

Consequently, it can be stated that for any material property that expresses one tensor as a function of just another tensor (and plenty of scalars) coincidence of principal axes is a physical requirement. Otherwise, if non-coincidence of principal axes is soughed, there is a need to include in the relation at least another argument, either a vector or a tensor.

12.1.7 Casagrande & Carrillo on induced and inherent anisotropy

A pervading feature in soil literature dealing with anisotropy is the distinction between induced and inherent anisotropy. The idea could be traced back to Casagrande & Carrillo who proposed it in 1944.

Casagrande & Carrillo dealt with strength anisotropy. It is worth to quote them exactly: "....*If the anisotropic distribution of strength, exhibited by the material at failure, is due exclusively to the strain associated with the applied stresses, the material will be said to possess induced anisotropy. If, in the other hand, the non-isotropic behaviour observed in a test is a physical characteristic inherent in the material, and entirely independent of the applied strains, the material will be said to possess inherent anisotropy.*"

This definition looks deceptively simple. In what follows it would be shown that their proponents failed to give it a precise meaning and that this purpose could be best served within the framework presented in the text.

After making this definition, they proceed to generalise the Mohr-Coulomb criteria for purely cohesive and purely frictional materials. Here we shall take a closer look to their proposal for an anisotropic cohesive material, within a plane stress context, which is simpler and good enough for our purpose.

A purely cohesive strength criterion is usually known by the name of Tresca. For an isotropic material it could be written as:

$$\max(\lambda)\ \ \mathbf{n}(\lambda)\cdot\mathbf{T}\cdot\mathbf{t}(\lambda)\leq \mathbf{c}$$

Where **T** is the stress tensor, **n** the generic unit normal to a plane (identified by λ) and **t** a generic unit vector orthogonal to **n**. What is written means that the maximum tangential stress in any plane is limited by a constant value, **c**. A straightforward development shows that this maximum corresponds to a plane at 45° with the principal axis of T.

Casagrande & Carrillo arguments are expressed in graphical form, but they could nevertheless be interpreted as follows. A "cohesion tensor", **C**, is proposed[120], such that cohesion in any plane, c_λ, will be obtained as:

$$c_\lambda = \vec{\mathbf{n}}(\lambda)\cdot\mathbf{C}\cdot\vec{\mathbf{n}}(\lambda)$$

When this equation is expressed in the principal axes of **C** the strength distribution function employed by Casagrande & Carrillo is recovered:

$$c_\alpha = c_2 + (c_1 - c_2)\ \sin^2(\alpha) \qquad (220)$$

And here α denotes the offset angle of a generic vector from the principal axes of **C**. Now, the generalised Tresca criteria proposed compares at each plane, its shear strength or cohesion, c_λ, with the tangential stress acting on that plane. This could be written as:

$$\max(\lambda)\ \ \vec{\mathbf{n}}(\lambda)\cdot\mathbf{T}\cdot\vec{\mathbf{t}}(\lambda) - \vec{\mathbf{n}}(\lambda)\cdot\mathbf{C}\cdot\vec{\mathbf{n}}(\lambda)\leq 0 \qquad (221)$$

It is at this point where the distinction between inherent and induced anisotropy is introduced. According to Casagrande & Carrillo in a material with induced anisotropy "...*the principal strengths develop in the planes*

---

[120] Although the term tensor is never used, an explicit parallel is traced with the small deformation tensor in elasticity theory.

of principal stress". We can rephrase that saying that for induced anisotropy **C** and **T** share principal axes –i.e. they are coaxial- whereas for inherent anisotropy **C** and **T** do not share principal axes -i.e. they're non-coaxial.

After maximisation of (221) some results are obtained in the paper for the coaxial or "induced" case:

- a critical value of α, angle between the failure plane and **C** principal axes
- a value c_α of cohesion in that plane
- a limit to the Mohr circle radius, r

$$\tan^2 \alpha_c = \frac{c_2}{c_1}$$

$$c_\alpha = \frac{2c_1c_2}{c_1 + c_2} \qquad (222)$$

$$r_\alpha = \sqrt{c_1c_2}$$

Note that the principal values of **C** will be obtained by measuring r_α and α_c in any test reaching failure. The initial orientation of the sample with respect to any fixed reference is immaterial. If the theory is employed to interpret the undrained strength of a clay deposit it would predict the same strength for all sample orientations. The effect of the so called "induced anisotropy" is to modify the failure angle plane and the value of the deviatoric failure stress, with respect to the case where $c_1=c_2$ but, perhaps surprisingly, the resulting failure criteria is isotropic!

12.1.8 Elastic tensor symmetries and plane wave propagation directions.

For any given elastic tensor **C** with symmetry group given by G_E, then if $\mathbf{Q} \in \mathbf{G_E}$

$$\tilde{\mathbf{C}} = \mathbf{Q}^T\mathbf{Q}^T\mathbf{C}\mathbf{Q}\mathbf{Q} = \mathbf{C} \qquad (223)$$

Consider now two different propagation directions, and form the corresponding Kelvin-Christoffel tensors

$$\Gamma = \mathbf{p}^T\mathbf{C}\mathbf{p}$$
$$\hat{\Gamma} = \hat{\mathbf{p}}^T\mathbf{C}\hat{\mathbf{p}} \qquad (224)$$

Those two directions will be related through a particular rotation, $\mathbf{Q}_p$

$$\hat{\mathbf{p}} = \mathbf{Q}_p\mathbf{p} \qquad (225)$$

and this rotation could be applied to transform any tensor. In particular we can write

$$\hat{\tilde{\Gamma}} = \mathbf{Q}_p^T\hat{\Gamma}\mathbf{Q}_p = \hat{\mathbf{p}}^T\mathbf{Q}_p^T\mathbf{Q}_p^T\mathbf{C}\mathbf{Q}_p\mathbf{Q}_p\hat{\mathbf{p}} = \mathbf{p}^T\hat{\mathbf{C}}\mathbf{p} \qquad (226)$$

Now if $\mathbf{Q}_p$ belongs to the symmetry group of **C**, i.e. if $\mathbf{Q}_p \in \mathbf{G_E}$

$$\hat{\tilde{\Gamma}} = \mathbf{p}^T\hat{\mathbf{C}}\mathbf{p} = \mathbf{p}^T\mathbf{C}\mathbf{p} = \Gamma \qquad (227)$$

$$\hat{\Gamma} = \mathbf{Q}\Gamma\mathbf{Q}^T \qquad (228)$$

Thus making similar the two Kelvin-Christoffel tensors associated with both directions. This implies (Landeman & Hestenes, 1980) that they have the same eigenvalues (phase velocities) and that their associated eigenvectors (polarizations) are related through

$$\hat{\mathbf{a}} = \mathbf{Q}_p \mathbf{a} \tag{229}$$

12.1.9 General expressions for group velocity in anisotropic elastic solids

It is convenient to work in wave vector space (**k**-space) using spherical coordinates. Therefore we have:

$$\mathbf{k} = r\begin{pmatrix}\sin\varphi\cos\theta & \sin\theta\sin\varphi & \cos\varphi\end{pmatrix} \tag{230}$$

Note that the radial coordinate, r, corresponds to the wavenumber, usually denoted by k. The dispersion relationship can be seen as describing a family of surfaces, level curves of frequency, in **k**-space.

$$D \equiv \omega - \mathrm{k}\,\mathrm{v}(\theta,\varphi) = \omega - r\,\mathrm{v}(\theta,\varphi) = 0 \tag{231}$$

The gradient of this surfaces of constant frequency is the group velocity vector. Using the gradient expression for spherical coordinates (e.g. Bourne & Kendall, 1992) we have

$$\mathbf{c_g} = \nabla D = \mathrm{v}\,\mathbf{e_r} + \frac{r\,\mathrm{v}_\theta}{r}\mathbf{e}_\theta + \frac{r\,\mathrm{v}_\varphi}{r\sin\theta}\mathbf{e}_\varphi = \mathrm{v}\,\mathbf{e_r} + \mathrm{v}_\theta\,\mathbf{e}_\theta + \frac{\mathrm{v}_\varphi}{\sin\theta}\mathbf{e}_\varphi \tag{232}$$

Where $\{\mathbf{e_r}, \mathbf{e_\theta}, \mathbf{e_\varphi}\}$ are the unit base vectors associated with the spherical coordinate system. A number of consequences follow from this expression. First, if this vector is now expressed in Cartesian coordinates we have:

$$\begin{aligned} c_{g1} &= \mathrm{v}\sin(\varphi)\cos(\theta) - \mathrm{v}_\theta\sin(\theta) + \frac{\cos(\varphi)\cos(\theta)}{\sin(\theta)}\mathrm{v}_\varphi \\ c_{g2} &= \mathrm{v}\sin(\theta)\sin(\varphi) + \mathrm{v}_\theta\cos(\theta) + \mathrm{v}_\varphi\cos(\varphi) \\ c_{g3} &= \mathrm{v}\cos(\varphi) - \frac{\sin(\varphi)}{\sin(\theta)}\mathrm{v}_\varphi \end{aligned} \tag{233}$$

Manipulation of this equations leads to expressions for the modulus, azimuth and dip angle of group velocity:

$$\begin{aligned} V^2 &= v^2 + v_\theta^2 + \frac{v_\phi^2}{\sin^2\theta} \\ \cos\xi &= \frac{1}{V}\left[v\cos\varphi - v_\varphi\frac{\sin\varphi}{\sin\theta}\right] \\ \tan\rho &= \frac{v\sin\theta\sin\varphi + v_\theta\cos\theta + v_\phi\cos\varphi}{v\cos\theta\sin\varphi - v_\theta\sin\theta + v_\phi\cos\varphi\tan\theta} \end{aligned} \tag{234}$$

Now is interesting to see the relation of the group velocity vector with the slowness surface. The phase velocity (V) and slowness (S) surfaces can be written as

$$V \equiv r - \mathrm{v}(\theta,\varphi) = 0$$
$$S \equiv r - \frac{1}{\mathrm{v}(\theta,\varphi)} = 0 \qquad (235)$$

It is readily appreciated that the slowness surface belong to the dispersion family for unit value of the parameter frequency. The gradient vector of this surface would be therefore parallel to the group velocity vector. In fact, the proportionality factor coincides with the phase velocity, as can be seen by writing:

$$\nabla S = \mathbf{e}_r + \frac{\mathrm{v}_\theta}{\mathrm{v}^2 r}\mathbf{e}_\theta + \frac{\mathrm{v}_\varphi}{\mathrm{v}^2 r \sin\theta}\mathbf{e}_\varphi = \mathbf{e}_r + \frac{\mathrm{v}_\theta}{\mathrm{v}}\mathbf{e}_\theta + \frac{\mathrm{v}_\varphi}{\mathrm{v}\sin\theta}\mathbf{e}_\varphi = \mathrm{v}\,\mathbf{c}_g \qquad (236)$$

Noting that the slowness vector can also be written as

$$\mathbf{q} = \frac{1}{\mathrm{v}}\mathbf{e}_r \qquad (237)$$

an expression for group velocity can be obtained in terms of the slowness vector, **q**, and the slowness surface (S)

$$\mathbf{c}_g = \frac{\nabla S}{\mathbf{q}\nabla S} \qquad (238)$$

12.1.10 Group and phase velocity on a plane of symmetry

In a system with planes of symmetry we can choose the plane to be one of the coordinate planes, say x_1 = 0 or, equivalently, $\theta = \pi/2$. Noting also that v_θ=0 equations (17) are reduced to:

$$c_{g1} = 0$$
$$c_{g2} = \mathrm{v}\,\sin(\varphi) + \mathrm{v}_\varphi \cos(\varphi) \qquad (239)$$
$$c_{g3} = \mathrm{v}\cos(\varphi) - \sin(\varphi)\mathrm{v}_\varphi$$

Which, in turn, are equivalent to:

$$\mathrm{V}^2(\rho) = \mathrm{v}^2(\varphi) + \mathrm{v}_\varphi^2(\varphi)$$
$$\tan\rho = \frac{\mathrm{v}_\varphi/\mathrm{v} + \tan\varphi}{1 - (\mathrm{v}_\varphi/\mathrm{v})\tan\varphi} \qquad (240)$$
$$\xi = \frac{\pi}{2}$$

12.2 FIGURES

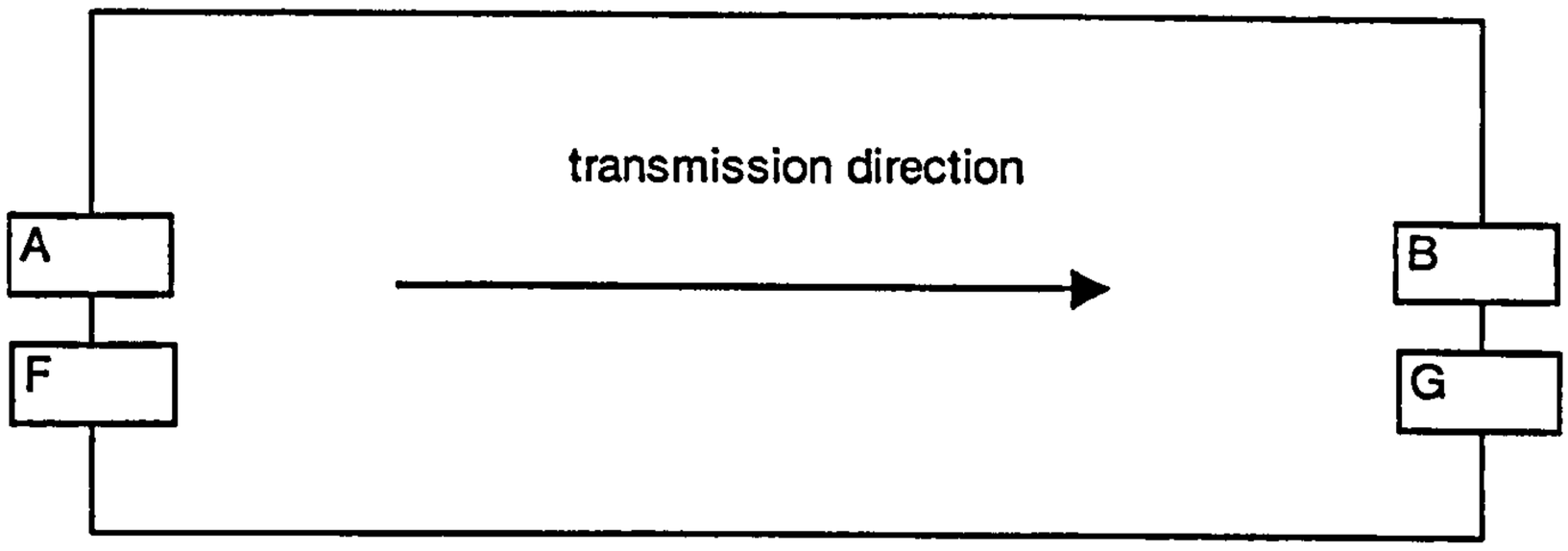

Figure 12-1 Bender set-up for linearity check

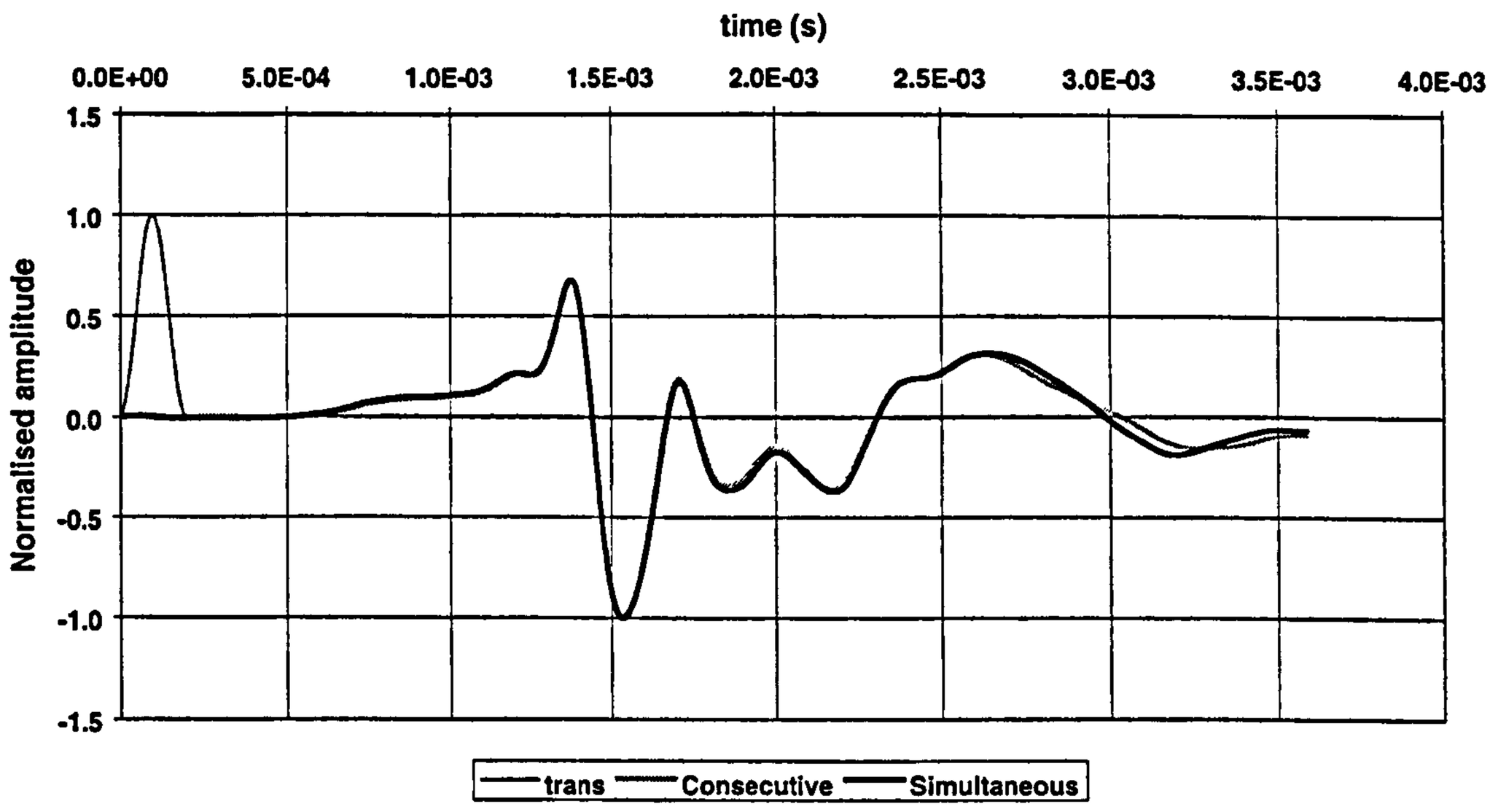

Figure 12-2 Simultaneous and consecutive transmission A+F to B

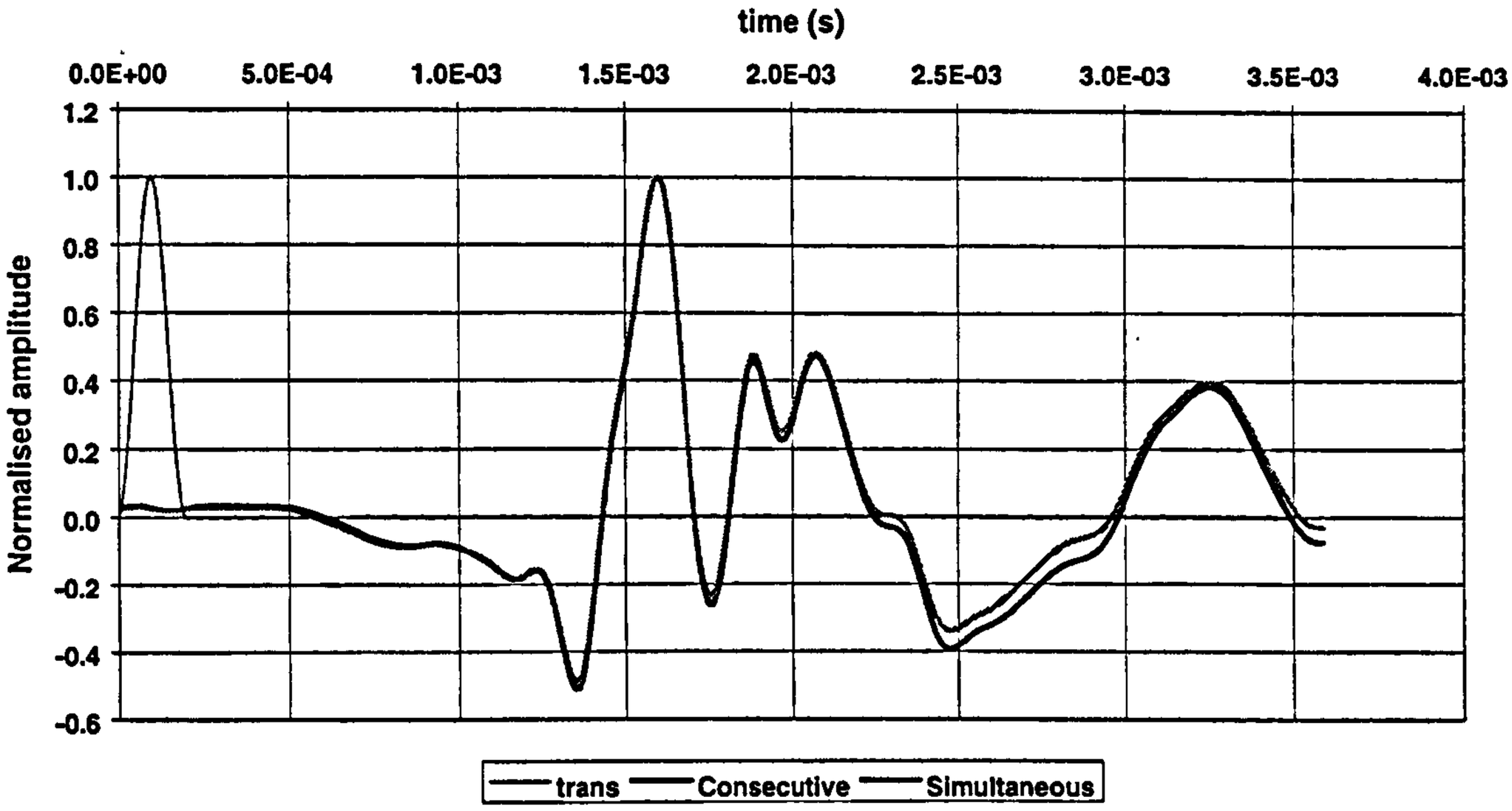

Figure 12-1 Simultaneous and consecutive transmission A+F to G

$$F = \left(\frac{1}{2}\cos(\theta)^4 + \frac{1}{2}(-\sin(\theta)^2 + \cos(\theta)^2)^2 + 3\sin(\theta)^2\cos(\theta)^2 + \frac{1}{2}\sin(\theta)^4\right) S_x{}^2$$
$$+ ((-\cos(\theta)^2 + \sin(\theta)^2)(-\sin(\theta)^2 + \cos(\theta)^2) - 4\sin(\theta)^2\cos(\theta)^2)\, S_y S_x$$
$$+ (-2\cos(\theta)\sin(\theta)(-\sin(\theta)^2 + \cos(\theta)^2) - 2\cos(\theta)\sin(\theta)^3 + 2\cos(\theta)^3\sin(\theta))\, S_{xy} S_x$$
$$+ \left(3\sin(\theta)^2\cos(\theta)^2 + \frac{1}{2}(-\cos(\theta)^2 + \sin(\theta)^2)^2 + \frac{1}{2}\sin(\theta)^4 + \frac{1}{2}\cos(\theta)^4\right) S_y{}^2$$
$$+ (4\cos(\theta)\sin(\theta)(-\cos(\theta)^2 + \sin(\theta)^2) + 2\cos(\theta)\sin(\theta)^3 - 2\cos(\theta)^3\sin(\theta) + 6\cos(\theta)\sin(\theta)(-\sin(\theta)^2 + \cos(\theta)^2))\, S_{xy} S_y - r^2$$
$$+ \left(12\sin(\theta)^2\cos(\theta)^2 + 3(-\sin(\theta)^2 + \cos(\theta)^2)^2\right) S_{xy}{}^2$$

Figure 12-4 Rotation of an isotropic failure criterion

$$F = \left(\frac{1}{2}b\sin(\theta)^4 + \frac{1}{2}a\cos(\theta)^4 + 3d\sin(\theta)^2\cos(\theta)^2 + \frac{1}{2}c(-\sin(\theta)^2 + \cos(\theta)^2)^2\right) S_x{}^2$$
$$+ (a\sin(\theta)^2\cos(\theta)^2 - 6d\sin(\theta)^2\cos(\theta)^2 + c(-\cos(\theta)^2 + \sin(\theta)^2)(-\sin(\theta)^2 + \cos(\theta)^2) + b\cos(\theta)^2\sin(\theta)^2)\, S_y S_x$$
$$+ (2a\cos(\theta)^3\sin(\theta) - 6d(-\sin(\theta)^2 + \cos(\theta)^2)\sin(\theta)\cos(\theta) + 4c\cos(\theta)\sin(\theta)(-\sin(\theta)^2 + \cos(\theta)^2) - 2b\cos(\theta)\sin(\theta)^3)\, S_{xy} S_x$$
$$+ \left(3d\sin(\theta)^2\cos(\theta)^2 + \frac{1}{2}a\sin(\theta)^4 + \frac{1}{2}b\cos(\theta)^4 + \frac{1}{2}c(-\cos(\theta)^2 + \sin(\theta)^2)^2\right) S_y{}^2$$
$$+ (2a\cos(\theta)\sin(\theta)^3 - 2b\cos(\theta)^3\sin(\theta) + 4c\cos(\theta)\sin(\theta)(-\cos(\theta)^2 + \sin(\theta)^2) + 6d(-\sin(\theta)^2 + \cos(\theta)^2)\sin(\theta)\cos(\theta))\, S_{xy} S_y - r^2$$
$$+ \left(2b\cos(\theta)^2\sin(\theta)^2 + 8c\cos(\theta)^2\sin(\theta)^2 + 3d(-\sin(\theta)^2 + \cos(\theta)^2)^2 + 2a\sin(\theta)^2\cos(\theta)^2\right) S_{xy}{}^2$$

Figure 12-5 Rotation of an anisotropic failure criterion

13 APPENDIX IV: AN EXERCISE IN HYPOPLASTIC MODELLING

13.1 INTRODUCTION

Between the years 1955 and 1970 the elasto-plastic approach to soil modelling was developed in Cambridge by Roscoe and co-workers (Wood 1990). They successfully used a particular constitutive theory, whose initial developments were guided by observations on metals, to model the behaviour of remoulded clays. Such was the success obtained that elasto-plasticity remains the standard approach of most material modelling in soils.

Nearly at the same period, a general theory of constitutive equations was being developed by Noll, Truesdell, and many others (Malvern, 1969). Their aim was to propose a two-step framework for constitutive formulations. First the basic principles of mechanics, equally relevant to all kind of materials, should be applied to obtain very general expressions. Then particular assumptions, suitable for the materials under study, would be applied, specialising step by step the general expressions

The echo of this rationalistic approach in soil mechanics was rather scarce during a long period. This has changed now. In the last fifteen years, Kolymbas, Gudehus & co-workers have used it to develop what they have called hypoplasticity. Due to their nonyielding efforts, hypoplasticity has been developed to reach the status of a sensible alternative to the more traditional elasto-plastic approach. Their very difference being strikingly present in the whole mathematical formulation from the onset, hypoplastic models look uncomfortable for the newcomer. Nevertheless the success so far obtained on modelling various different aspects of soil behaviour make worthwhile it's careful study.

The objective of this work is to obtain some familiarity with the hypoplastic approach and its possibilities. To do so we will first review the general characteristics of hypoplastic formulations, with particular emphasis on sand-related developments. Then we will explore one particular hypoplastic formulation, testing it against some features of soil behaviour recorded by Sture et al (1988) while applying complex stress paths to sand on a true triaxial apparatus.

The development of hypoplastic formulations has been frequently described by its proponents (e.g. Wu & Niemunis, 1996) as "algebraic" as opposed to the "geometric" approach which is emphasised on elasto-plastic models (with their yield surfaces, plastic potentials, bounding surfaces, etc). It is then necessary to have an understanding of the algebraic methods involved. Appendix 2 in this thesis reviews the relevant aspects of the algebra of tensorial functions.

13.2 A REVIEW OF HYPOPLASTICAL SOIL MODELLING

13.2.1 Hypoelasticity

Hypoplastic formulations are usually presented (Kolymbas 1989) as generalisations of hypoelasticity, whose applications to soil mechanics preceded those of hypoplasticity. From the rationalistic point of view they are indeed very close cousins. It is convenient then to take a look at the older to appreciate the specificity of the younger.

The concept of hypoelasticity was proposed by Truesdell (1955), as a particular class of constitutive equations where the stress rate depends only on the stress and strain rate tensors

$$\dot{\boldsymbol{\sigma}} = F(\boldsymbol{\sigma}, \dot{\boldsymbol{\varepsilon}}) \tag{241}$$

the latter is defined as the symmetric part of the velocity gradient,

$$\dot{\boldsymbol{\varepsilon}} = \frac{1}{2}\left(\nabla \mathbf{v} + \nabla \mathbf{v}^T\right) \tag{242}$$

and, within the small deformation hypothesis, it can be approximated by the rate of small-deformation tensor (Spencer, 1980). Mathematically (241) can be described as a tensorial function of two second-order symmetric tensors. Following Appendix 2, the principle of objectivity implies that the most general constitutive equations derived from it has the form

$$\begin{aligned}\dot{\boldsymbol{\sigma}} = {} & \varphi_0 \mathbf{I} + \varphi_1 \boldsymbol{\sigma} + \varphi_2 \boldsymbol{\sigma}^2 + \varphi_3 \dot{\boldsymbol{\varepsilon}} + \varphi_4 \dot{\boldsymbol{\varepsilon}}^2 + \varphi_5\left(\boldsymbol{\sigma}\dot{\boldsymbol{\varepsilon}} + \dot{\boldsymbol{\varepsilon}}\boldsymbol{\sigma}\right) \\ & + \varphi_6\left(\boldsymbol{\sigma}^2\dot{\boldsymbol{\varepsilon}} + \dot{\boldsymbol{\varepsilon}}\boldsymbol{\sigma}^2\right) + \varphi_7\left(\boldsymbol{\sigma}\dot{\boldsymbol{\varepsilon}}^2 + \dot{\boldsymbol{\varepsilon}}^2\boldsymbol{\sigma}\right) \\ \varphi_i = {} & \varphi_i\left\{tr\boldsymbol{\sigma}, tr\boldsymbol{\sigma}^2, tr\boldsymbol{\sigma}^3, tr\dot{\boldsymbol{\varepsilon}}, tr\dot{\boldsymbol{\varepsilon}}^2, tr\dot{\boldsymbol{\varepsilon}}^3, tr\boldsymbol{\sigma}\dot{\boldsymbol{\varepsilon}}, tr\boldsymbol{\sigma}^2\dot{\boldsymbol{\varepsilon}}, tr\boldsymbol{\sigma}\dot{\boldsymbol{\varepsilon}}^2\right\}\end{aligned} \tag{243}$$

Where the φ_i are, as indicated, general functions of the nine isotropic invariants listed.

According to Truesdell, hypoelastic materials are those where (241) is linear on the strain rate. This is one way, -but, as we shall see, not the only one-, of achieving rate or time-independence, a condition well adapted to sand behaviour. Such a linear relationship reduces the general expression (243) to

$$\begin{aligned}\dot{\boldsymbol{\sigma}} = {} & \varphi_0 \mathbf{I} + \varphi_1 \boldsymbol{\sigma} + \varphi_2 \boldsymbol{\sigma}^2 + \varphi_3 \dot{\boldsymbol{\varepsilon}} + \varphi_5\left(\boldsymbol{\sigma}\dot{\boldsymbol{\varepsilon}} + \dot{\boldsymbol{\varepsilon}}\boldsymbol{\sigma}\right) + \varphi_6\left(\boldsymbol{\sigma}^2\dot{\boldsymbol{\varepsilon}} + \dot{\boldsymbol{\varepsilon}}\boldsymbol{\sigma}^2\right) \\ \varphi_i = {} & \varphi_i\left\{tr\boldsymbol{\sigma}, tr\boldsymbol{\sigma}^2, tr\boldsymbol{\sigma}^3\right\} \quad i = 3,5,6 \\ \varphi_i = {} & \varphi_i\left\{tr\boldsymbol{\sigma}, tr\boldsymbol{\sigma}^2, tr\boldsymbol{\sigma}^3, tr\dot{\boldsymbol{\varepsilon}}, tr\boldsymbol{\sigma}\dot{\boldsymbol{\varepsilon}}, tr\boldsymbol{\sigma}^2\dot{\boldsymbol{\varepsilon}}\right\} \quad i = 0,1,2\end{aligned} \tag{244}$$

On the functional coefficients above the dependence on the strain rate invariants must be linear.

Further simplifications might be obtained by establishing some conditions on the stress dependency. For instance, it may be postulated that the dependency on σ is also lineal, and in that case the hypoelastic general equation reduces to

$$
\begin{aligned}
\dot{\boldsymbol{\sigma}} &= \varphi_0 \mathbf{I} + \varphi_1 \boldsymbol{\sigma} + \varphi_3 \dot{\boldsymbol{\varepsilon}} + \varphi_5 \left(\boldsymbol{\sigma}\dot{\boldsymbol{\varepsilon}} + \dot{\boldsymbol{\varepsilon}}\boldsymbol{\sigma} \right) \\
\varphi_0 &= \varphi_{0a} tr\boldsymbol{\sigma} + \varphi_{0b} tr\dot{\boldsymbol{\varepsilon}} + \varphi_{0c} tr\boldsymbol{\sigma}\dot{\boldsymbol{\varepsilon}} + \varphi_{0d} \\
\varphi_1 &= \varphi_{1b} tr\dot{\boldsymbol{\varepsilon}} + \varphi_{1d} \\
\varphi_3 &= \varphi_{3b} tr\boldsymbol{\sigma} + \varphi_{3d} \\
\varphi_5 &= \varphi_{5d}
\end{aligned}
\tag{245}
$$

And only nine independent coefficients define each material.

Note that (245) will include the following equation

$$
\dot{\boldsymbol{\sigma}} = \varphi_0 (tr\boldsymbol{\sigma}, tr\dot{\boldsymbol{\varepsilon}}) \mathbf{I} + \varphi_1 (tr\boldsymbol{\sigma}) \dot{\boldsymbol{\varepsilon}} \tag{246}
$$

which may be cast in a more familiar form like

$$
\dot{\boldsymbol{\sigma}} = \frac{E(p)}{2(1+\nu)} \dot{\boldsymbol{\varepsilon}}_v I + \frac{\nu E(p)}{(1-2\nu)(1+\nu)} \dot{\boldsymbol{\varepsilon}} \tag{247}
$$

which is the formulation of isotropic elasticity with Young modulus dependent on mean stress. This corresponds to a widely used -e.g. pavement design, interpretation of dynamic tests- proposal by Duncan & Chang (1970). Zytynski et al. (1978) famously noted that this formulation was incompatible with a strain-energy potential. But that was precisely in Truesdell mind; the existence of a strain energy potential was a restriction that hypoelastic models need not follow. If that was imposed a more restricted range of models appeared, and those were called hyperelastic to emphasise the difference.

Nevertheless, those were rather unconscious applications. Collins & Bachus (1989), while presenting their own model, made a thorough survey of conscious hypoelastic models finding that no more than two or three teams had followed that path. As stated before, in soil mechanics the elasto-plastic approach was dominating. They also weighted the pros and cons of the hypoelastic and elasto-plastic approaches to soil modelling. Their observations embrace two different aspects: implementation and modelling capabilities.

Relating to implementation they signalled that hypoelastic formulations are easier to fit into finite element codes, as they are directly written in incremental form and integration can proceed directly without extra checks on yield conditions, etc. On the wrong side they noted that parameters on hypoelastic models were quite distant from soil mechanics practice, they escaped any meaningful interpretation and there was no easy way to measure them.

They addressed themselves to solve this last problem, establishing a thorough mathematical optimisation procedure to obtain values of the parameters. The problem of interpretation, nevertheless, remained intact, and, at least in their 16-parameter model, -linear in strain and quadratic in stress-, big.

From modelling viewpoint, they noted the following interesting features of these models: nonlinearity of stress-strain response, stress-path dependence, non-coincidence of principal axes of stress and strain increment and stress-induced anisotropy.

The first two features, which might be explained just by nonlinearity, are obtained even with the simpler formulations, like (247). Non-coincidence of principal axes of increments of stress and strain requires the inclusion of at least two generators -see Appendix 2- in the formulation. For example, a formulation like (245) will be enough to provide this effect, because the increment of stress would not be, in general, collinear with either the stress or the strain increment.

These capabilities made the response thus described more similar to the one obtained with elasto-plastic models than with elastic models. In fact, hypoelastic models were even shown (Mullenger & Davis, 1981) to provide "yield points", an aspect to where we'll return later while commenting the hypoplastic results. The main limitation of the hypoelastic formulation is the linear relationship between stress and strain rates, which implies that if we apply and then retire the same strain increment no stress change is induced,

$$\dot{\boldsymbol{\sigma}} = F(\boldsymbol{\sigma}):\dot{\boldsymbol{\varepsilon}} + F(\boldsymbol{\sigma}):(-\dot{\boldsymbol{\varepsilon}}) = F(\boldsymbol{\sigma}):[\dot{\boldsymbol{\varepsilon}} - \dot{\boldsymbol{\varepsilon}}] = \mathbf{0} \qquad (248)$$

There is no unloading direction in stress space, which is a main feature of elastoplastic response. An unloading path will trace back exactly the loading path, in Figure 13-1 OAB will be followed by BAO instead of BC, and a complete unloading will not leave any trace of deformation in the material: this is why talking about **hypoelasticity** makes sense.

This feature makes hypoelastic formulations quite unsuitable to model soil behaviour in non-monotonic stress paths. Collins & Bachus (1989), tried to get round this difficulty adding a definition of elastic behaviour and a loading criteria to choose between elastic and hypoelastic response. The loading criteria was based on the sign of the stress power and, to smooth the transition from one behaviour to the other it was complemented with an interpolation rule based on the mobilised stress-ratio.

These modifications seemed to work pretty well, but on one hand they added six more parameters to the model, arriving to a total of 22, and on the other the conceptual clarity of the model suffered. The next formulations presented took a different approach to solve the linearity problem.

13.2.2 Incremental nonlinearity and hypoplasticity.

Incremental nonlinearity and hypoplasticity are concepts that have been introduced almost independently by several researchers -Dafalias (1986), Kolymbas (1989), Darve (1989). Their approaches to constitutive modelling are, nevertheless, different; it is thus not surprising that they use similar words to denote slightly varying concepts. We are here interested in the formulations by Kolymbas et al.

Kolymbas departure point is the same general constitutive equation proposed by Truesdell,

$$\dot{\sigma} = F(\sigma, \dot{\varepsilon}) \tag{249}$$

But he observes, quite accurately, that time or rate-independence could be accomplished just by making the equation homogeneous of the first degree on the strain rate, as then

$$\dot{\sigma}\Delta t = F(\sigma, \dot{\varepsilon}\Delta t) = F(\sigma, \dot{\varepsilon})\Delta t \tag{250}$$

And there is no need to keep the other condition of linearity, i.e. superposition (248), which, as seen before, is very unrealistic.

All the tensor generators are homogeneous in strain rate. Hence, this condition does not involve any term reduction in the general representation given by the application of objectivity upon (250). Only the form of the invariant functions φ_i is restricted. Kolymbas applied another general condition for sands: the equation must be homogeneous of n-degree in the stress. This (Kolymbas, 1998) was suggested by the true triaxial database accumulated in Karslruhe by Goldscheider, where a prominent feature was the observation that, for virgin loading of reconstituted samples, any maintained proportional loading resulted in a similarly maintained proportional deformation. This can be stated as

$$\dot{\sigma} = F(x\sigma, \dot{\varepsilon}) = x^{n-1} F(\sigma, \dot{\varepsilon}) \tag{251}$$

Like its strain rate counterpart, this homogeneity condition does restrict the form of the equation, but does not reduce the number of generators or invariants. All the generators and invariants might be present in the formulation; an equation such as

$$\dot{\sigma} = c_1 tr\sigma^5 (\sigma\dot{\varepsilon} + \dot{\varepsilon}\sigma) + c_2 \frac{tr\sigma^3 tr\dot{\varepsilon}\sigma^2}{tr\dot{\varepsilon}^2} (\sigma\dot{\varepsilon}^2 + \dot{\varepsilon}^2\sigma) \tag{252}$$

thoroughly non-linear, with c_i being constants, is perfectly admissible. At first sight then hypoplastic formulations encompass a fairly wider territory than hypoelastic ones. Nevertheless, the area of that territory so far explored by it's proponents has been rather reduced. The main feature of all the hypoplastic formulations reviewed here is that all the strain rate nonlinearity concentrates on a dependence on its norm,

$$\| \dot{\varepsilon} \| = \sqrt{tr\dot{\varepsilon}^2} \tag{253}$$

excluding for instance, the previous example. Moreover, the general tensorial form of the hypoplastic equations so far proposed can be written as

$$\dot{\sigma} = \underline{\mathbf{L}}(\sigma) : \dot{\varepsilon} + \mathbf{N}(\sigma) \| \dot{\varepsilon} \| \tag{254}$$

Indicating that the hypoplastic relationship can be decomposed in a hypoelastic term given by **L** underlined to emphasise its character of fourth order tensor- and a term multiplying the strain rate trace. Perhaps the main advantage of equation (254) is that could be easily inverted to give the strain increment as a function of stress and stress increment tensor. To do so its necessary to employ a two step procedure. First, the inverse of **L** is applied to both sides, and rearranging,

$$\dot{\boldsymbol{\varepsilon}} = \underline{\mathbf{L}}^{-1} : \dot{\boldsymbol{\sigma}} + \underline{\mathbf{L}}^{-1} : \mathbf{N} \| \dot{\boldsymbol{\varepsilon}} \| \tag{255}$$

and then the norm is taken, obtaining a quadratic equation,

$$\begin{aligned} x^2(\mathbf{BB}-1) - 2x\mathbf{AB} + \mathbf{AA} &= 0 \\ x &= \|\dot{\boldsymbol{\varepsilon}}\| \\ \mathbf{A} &= \underline{\mathbf{L}}^{-1} : \dot{\boldsymbol{\sigma}} \\ \mathbf{B} &= \underline{\mathbf{L}}^{-1} : \mathbf{N} \end{aligned} \tag{256}$$

Taking the positive root and substituting above the inversion equation is complete

$$\dot{\boldsymbol{\varepsilon}} = \mathbf{A} - \mathbf{B}\left[\sqrt{\frac{(\mathbf{AB})^2 - \mathbf{AA}(\mathbf{BB}-1)}{(\mathbf{BB}-1)^2}} - \frac{\mathbf{AB}}{1-\mathbf{BB}}\right] \tag{257}$$

Where again there is a linear term on the stress rate –the first- and a non-linear -the second.

13.2.3 Applications of hypoplastic formulations in sand modelling.

Even within the self-imposed strictures of (254), there is ample room for many different hypoplastic formulations. In this section we bring together some of the proposals made so far for sands, commenting also on their calibration methods and, of course, on the results so far obtained.

13.2.3.1 First proposals

Kolymbas (1989) used the following equation in the Cleveland workshop

$$\dot{\boldsymbol{\sigma}} = c_1 \frac{1}{2}(\boldsymbol{\sigma}\dot{\boldsymbol{\varepsilon}} + \dot{\boldsymbol{\varepsilon}}\boldsymbol{\sigma}) + c_2 tr(\boldsymbol{\sigma}\dot{\boldsymbol{\varepsilon}})\mathbf{1} + \left[c_3\boldsymbol{\sigma} + c_4\frac{\boldsymbol{\sigma}^2}{tr(\boldsymbol{\sigma})} + \right]\|\dot{\boldsymbol{\varepsilon}}\| \tag{258}$$

The main feature here is simplicity. Kolymbas only uses four generators and three invariants and the number of model parameters –c_i- is four. Compared with other participants, the simulation results were well on the (good) average for proportional paths on cubes and hollow cylinders, somehow over the (really poor) average for non-proportional paths and quite bad for cyclic tests.

Wu & Bauer (1994) employed a slightly modified version of (258)

$$\begin{aligned} \dot{\boldsymbol{\sigma}} &= c_1 tr(\boldsymbol{\sigma})\dot{\boldsymbol{\varepsilon}} + c_2 tr(\boldsymbol{\sigma}\dot{\boldsymbol{\varepsilon}})\frac{\boldsymbol{\sigma}}{tr(\boldsymbol{\sigma})} + \left[c_3\frac{\boldsymbol{\sigma}^2}{tr(\boldsymbol{\sigma})} + c_4\frac{\boldsymbol{\sigma}_d^2}{tr(\boldsymbol{\sigma})} + \right]\|\dot{\boldsymbol{\varepsilon}}\| \\ \boldsymbol{\sigma}_d &= \boldsymbol{\sigma} - tr(\boldsymbol{\sigma})\mathbf{1} \end{aligned} \tag{259}$$

This equation has the same number of parameters, invariants and generators as the precedent. Moreover, it also shares the same invariants and three generators. It was used to reproduce various test results of drained and undrained triaxial, oedometer and simple shear in different sands, showing good results in monotonic and single cycle cases, but –perhaps unsurprisingly- being less good in truly cyclic cases.

Calibration of these equations was rather simple. The four parameters may be determined using a conventional compressive triaxial test. In those tests all the tensors involved have their principal axes fixed and coincident during the whole test. When expressed on those axes the tensor equalities provide just two different equations due to the axial symmetry of the test. Henceforth, if stress, strain increment and stress increments are measured at any stage during a triaxial test, two linear equations in four unknowns (the parameters) are obtained.

Two such systems are enough to obtain a complete solution. Kolymbas did choose two very particular test stages: the beginning of axial load application and the end of test, when the stress deviator reaches a "limit state". It's important to appreciate here that Kolymbas "limit state" it's not the same as the more familiar critical state, because he admits eagerly that at the end of test, in the "limit state", the sand may still be dilating or contracting.

While quite straightforward, this calibration procedure has also some inconveniences. First, one may wonder what happens if, instead of the final and initial points of the triaxial test another one is chosen (the peak deviator may be an obvious candidate). It's even more puzzling to imagine what could happen if such a procedure is attempted with a true asymmetric triaxial database, where each point of a test will provide three and not just two equations, or, even worst, with a plane strain test, where each point might provide five equations...

13.2.3.2 Stress boundaries.

The surfaces pervading in elasto-plastic models convey two different types of information. They help define the incremental stress-strain relationship through their geometric characteristics and relations. But they also trace a distinction between accessible and inaccessible states -of stress, if stress is the only state variable.

In the algebraic approach of hypoplasticity, the first role is well covered by the specification of a particular form of the equation, like (259) before. The question arises about the second role, because the distinction between accessible and inaccessible states has clear physical meaning and cannot be neglected.

In hypoelasticity the problem was addressed as follows. The hypoelastic relation,

$$\dot{\boldsymbol{\sigma}} = F(\boldsymbol{\sigma}) : \dot{\boldsymbol{\varepsilon}} \tag{260}$$

could be viewed as a linear transformation between the (six dimensional) vectors of stress and strain increment. While the relationship is invertible, each stress increment determines uniquely an strain increment; when non-invertibility occurs the strain increment is undetermined. This provided a suitable definition of limit states; i.e. as the stress values, $\boldsymbol{\sigma}$, where

$$\det F(\boldsymbol{\sigma}) = 0 \tag{261}$$

Note that this is something that hyperelastic equations exclude, as there F is positive definite. Mullenger & Davis (1981) explored this approach. Their hypoelastic formulation was a seven-parameter one; application of (261) to define "yield" or "critical states" permitted the identification of those parameters. The method employed was geometrical: critical states had known traces on specific subsets of the stress space. This approach conduced to a closed smooth surface in the three-dimensional stress space very similar to the two-surface models of Lade or Matsuoka. An interesting by-product were expressions for the algebraic hypoelastic coefficients in terms of more identifiable soil-mechanics parameters, like critical friction angle in compression and extension and yield value in isotropic compression.

In the hypoplastic literature, two papers by Wu and Niemunis, (1996, 1997), are particularly concerned with this question. The exploration of this surfaces made by Wu & Niemunis is based on algebraic manipulation of equation (254) or its inverse (255) and numerical probing using (259). They looked at three different surfaces in stress space, the bounding surface $b(\sigma)$, the failure surface, $f(\sigma)$, and the stability surface, $s(\sigma)$. These are defined as follows,

$$\begin{aligned}
&\sigma \in b(\sigma) \xleftarrow{def} \nabla b(\sigma)\dot{\sigma} \le 0 \quad \forall \dot{\varepsilon} \\
&\sigma \in f(\sigma) \xleftarrow{def} \{\dot{\sigma} = 0 \ , \dot{\varepsilon} \neq 0\} \\
&\sigma \in s(\sigma) \xleftarrow{def} \{\dot{\sigma} : \dot{\varepsilon} = 0, \dot{\sigma} \neq 0 \ , \dot{\varepsilon} \neq 0\}
\end{aligned} \tag{262}$$

The bounding surface limits the accessible states of stress and is the outermost by definition; it has conical shape with the vertex on the origin of stress space, the axis coincident with the isotropic axis and circular section. This is, apparently[121], a consequence of (254) being homogeneous of the first degree on stress.

The failure surface coincides with the limit locus of invertibility of the incremental constitutive relationship (259). Looking at the inverse form this corresponds obviously to **BB = 1**. It is, thus, the same concept, as the "yield locus" of hypoelasticity. Its shape may be analytically obtained by applying condition (261) on equation (259), results on a rounded triangular shape on the deviatoric plane, and a pair of frictional straight lines as trace on triaxial (and similar) planes. The process, unlike on the Mullenger & Davis hypoelastic case, is not detailed. One may wonder if the achievement of a nice shape imposes constraints on the equation parameters or not, being just four in this particular equation

The stability surface, defined using Hill's stability criteria, was found to be the innermost, similar in deviatoric shape to the preceding ones, its isotropic trace being not quoted. The deviatoric shape was obtained by numerical testing, with a somehow restricted set of stress paths: radial excursions from the isotropic axis accepting coaxiality between stresses and strain increment. The meaning of this energetic condition in hypoplastic models was not clear even for the authors, they suggested that might be a boundary for the onset of strain softening.

---

[121] There's a somewhat obscure point in the proof.

13.2.3.3 Developments: void ratio role and critical state.

In sands, initial density is determinant of the initial and limit response in a triaxial compression test. If the calibration procedure proposed by Kolymbas is used, two sands formed at different densities will have then different parameters, and, thus, will be considered as different materials. This was to be expected, because in the basic hypoplastic equation, (258), the incremental relationship between strain and stress rates is fixed[122] for any known stress state. In other terms, there is no other state variable apart from stress and density plays no role.

As emphasised by Wood (1990) "Critical state soil mechanics is...[about] models of soil behaviour [where]..the link between volume change and effective stress history is a fundamental ingredient" and, thus, its not just another name for the Cam-clay model. The work on hypoplasticity by Bauer and Gudehus (1996, 1997), aimed at solving the preceding problem of hypoplastic formulations, it's a perfect corroboration of such idea.

To incorporate this basic idea of critical state soil mechanics, the constitutive relationship used by Truesdell and Kolymbas is modified, writing instead,

$$\dot{\boldsymbol{\sigma}} = F(\boldsymbol{\sigma}, \dot{\boldsymbol{\varepsilon}}, e) \tag{263}$$

this new state variable must be introduced along it's own evolution equation,

$$\dot{e} = (1+e)tr\dot{\boldsymbol{\varepsilon}} \tag{264}$$

where it's implicitly stated that sand grains are considered incompressible, and therefore no new material constants are introduced. Critical states are then defined as follows

$$(\boldsymbol{\sigma}, e) \in S \xleftrightarrow{def} \{\dot{e} = 0, \dot{\boldsymbol{\sigma}} = 0, \dot{\boldsymbol{\varepsilon}} \neq 0\} \tag{265}$$

This set forms a surface S in state space and this surface must be reached by any monotonically increasing shearing path.

Void ratio being a scalar variable, the general representation of (263) uses the same generators and functional basis as (249). This, as we have mentioned, may lead to very different formulations, nonetheless Bauer adhered to the restricted form proposed by Kolymbas, writing

$$\dot{\boldsymbol{\sigma}} = \underline{\mathbf{L}}(\boldsymbol{\sigma}, e) : \dot{\boldsymbol{\varepsilon}} + \mathbf{N}(\boldsymbol{\sigma}, e) \| \dot{\boldsymbol{\varepsilon}} \| \tag{266}$$

As Gudehus (e.g. 1996) has repeatedly advocated, the influence of density on the stress-strain response of sands may be concisely renamed picnotropy; the influence of stress level, barotropy. One basic tenet of critical state soil mechanics is that picnotropy and barotropy are linked together. This interaction manifest itself in the precedent formulation: **L** and **N** are postulated as functions both of the stress and the void ratio. Particularising, Bauer proposed the following equation,

---

[122] At least within the "failure surface" which, as seen before, bounds the region of invertibility.

$$\dot{\boldsymbol{\sigma}} = f_s(e,\mathrm{tr}(\boldsymbol{\sigma}))\left[a(\boldsymbol{\sigma})^2\dot{\boldsymbol{\varepsilon}} + \mathrm{tr}(\boldsymbol{\sigma}\dot{\boldsymbol{\varepsilon}})\frac{\boldsymbol{\sigma}}{[\mathrm{tr}(\boldsymbol{\sigma})]^2} + f_d(e,\mathrm{tr}(\boldsymbol{\sigma}))\cdot a(\boldsymbol{\sigma})\left[\frac{\boldsymbol{\sigma}}{\mathrm{tr}(\boldsymbol{\sigma})} + \frac{\boldsymbol{\sigma}_d}{\mathrm{tr}(\boldsymbol{\sigma})}\right]\|\dot{\boldsymbol{\varepsilon}}\|\right] \qquad (267)$$

At first glance this equation appear very similar to that presented by Wu & Bauer (259). From the algebraic viewpoint contains even less generators, dispensing with σ^2, and the invariants explicitly written are just the same {trσ, tr $\varepsilon^{\bullet 2}$, trσ $\varepsilon^{\bullet}$}. One slight difference is that the degree of homogeneity on stress is not anymore easily appreciated from that expression.

Of course, the main difference is that instead of the four constant parameters affecting the coefficients of equation (267) we have now three functions of the void ratio and the stress. The parameters of the model are provided now by the specification of these functions. The process leading to that specification is detailed by Gudehus (1996) and Bauer (1996, 1997); it is worth to consider its main ideas in some detail.

They first consider how the critical surface should look on some well explored sections of the state space. In stress space –i.e. for fixed e- the critical surface is included within the failure surface previously defined.

$$S_e(\boldsymbol{\sigma}) \subseteq f(\boldsymbol{\sigma}) \qquad (268)$$

This trace is then identified with the Matsuoka-Nakai failure surface, a successful empirical surface commonly employed in soil mechanics –e.g. Gajo & Wood, 2000. This is a one-parameter surface and this parameter could be identified with a critical state angle of friction, φ_c.

They secondly consider the critical surface trace on the p-e plane –where the second and third stress invariants are null- for which they propose an empirical expression,

$$e_c = e_{c0}\exp\left(\frac{tr(\boldsymbol{\sigma})}{h_s}\right)^n \qquad (269)$$

where three more parameters appear, the –so called- granular hardness, h_s, the critical void ratio at zero mean pressure, e_{c0}, the exponent n.

Still in the same plane, they specify on physical and empirical grounds the attainable range of states. Those limits are curves also given by expression (269), but with different values at zero mean pressure, e_{i0} and e_{d0}, maximum and minimum void ratios respectively. This adds two more parameters to the model.

These limits act as kind of bounding surface, and the distance of the actual void ratio to the critical one and to its (pressure dependent) bounds enters the equation through exponential laws, thus providing the final two parameters of the model, α and β.

A further condition is imposed. In many circumstances, -e.g. dense sands under triaxial compression- soil tests reveal a fragile behaviour with a peak on the load-response graph. Some of these peaks would also fall within the formal definition of critical state (265), however, tests do not end at peaks and it should be possible to distinguish peak states from critical states. Jefferies (1993) got rid of this problem by adding the condition

$$\ddot{e} = 0 \tag{270}$$

to the critical state definition. This is not the path followed by Bauer and Gudehus, who prefer to specify

$$f_d(e_c, \sigma_c) = 0 \tag{271}$$

The enforcement of these conditions produces the following set of expressions for the functions a, f_s and f_d.

$$\begin{aligned}
a(\sigma) &= \frac{1}{c_1 + c_2\sqrt{tr\sigma_d^2}(1+\cos 3\theta)} \\
f_d &= r_d^{\alpha} = \left(\frac{(e-e_d)}{(e_c-e_d)}\right)^{\alpha} \\
f_s &= f_e f_b \qquad f_e = \left(\frac{e_c}{e}\right)^{\beta} \\
f_b &= \left(\frac{e_{i0}}{e_{c0}}\right)^{\beta} \frac{h_s}{nh_i}\frac{1+e_i}{e_i}\left(\frac{-tr(\sigma)}{h_s}\right)^{1-n} \\
h_i &= \frac{1}{c_1^3} + \frac{1}{3} - \left(\frac{(e_{i0}-e_{d0})}{(e_{c0}-e_{d0})}\right)^{\alpha}\frac{1}{c_1\sqrt{3}} \\
c_1 &= \sqrt{\frac{3}{8}}\frac{(3-\sin\varphi_c)}{\sin\varphi_c} \quad c_2 = \frac{3}{8}\frac{(3+\sin\varphi_c)}{\sin\varphi_c}
\end{aligned} \tag{272}$$

The precedent equations lead to a different calibration procedure. In previous hypoplastic models all parameters were adjustment parameters, with no clear meaning. Now, of eight parameters employed in the model,

$$\{\varphi_c, h_s, e_{c0}, n, e_{i0}, e_{d0}, \alpha, \beta\}$$

there are just three recognised as adjustment parameters, namely the exponents n, α, β. Within the rest, four correspond to some basic soil property,

$$\{\varphi_c, h_s, e_{c0}, e_{d0}\}$$

The last two correspond approximately to the conventional minimum and maximum density. The case of the minimum void ratio e_{i0} is different, because there's no standard procedure of identification already available, but could be perhaps readily devised. This ease of parameter identification was hailed as a major achievement by Gudehus (1996) and indeed it looked so.

13.2.3.4 Developments: adding more internal variables.

Hypoplastic soil modelling has grown to be a major subspecialty of its own. Different proposals aimed at exploring or improving some particular aspects of the precedent models appear now on the literature at regular pace. Without being exhaustive we want to recall here a few united by a feature particularly interesting from our point of view: the inclusion of more state variables in the model.

In 1995 Kolymbas et al. pointed two modelling limitations of the first hypoplastic equations, like (258) or (259): lack of picnotropic-barotropic effects and lack of memory effects. The first issue is that addressed by Bauer and Gudehus critical-state models. The second issue may be also described as path-dependency. Experimental results have shown repeatedly that soil samples subject to the same incremental loading under equal stress and void ratio conditions behave differently, depending on how they have arrived at that state. This memory effect is particularly apparent under cyclic load programs but not only on them as will be shown below.

Kolymbas et al. realised that an incremental equation where stress is the only state parameter would provide an incremental response dependent only on stress: there is no way to identify how an stress state was arrived at. Their suggestion to get out of this problem was centred on the concept of back-stress, introduced as a new tensorial state variable, S, who corrected the Cauchy stress, $\boldsymbol{\sigma}$. Their difference, called corrected stress, enters the general equation (241), now written as

$$\dot{\boldsymbol{\sigma}} = F\left(\boldsymbol{\sigma} - \mathbf{s}, \dot{\boldsymbol{\varepsilon}}\right) = F\left(\boldsymbol{\sigma}_c, \dot{\boldsymbol{\varepsilon}}\right) \tag{273}$$

As before with the void ratio, a new back-stress evolution equation is needed. In general, that equation shall be written like

$$\dot{\mathbf{s}} = F\left(\boldsymbol{\sigma}, \mathbf{s}, \dot{\boldsymbol{\varepsilon}}\right) \tag{274}$$

While the concept is clear, its implementation proved much harder. As Kolymbas et al wrote "...the back stress being an internal variable is not directly accessible to measurement..." and, without any measurement to rely on, is hard to figure out what form (274) should take. This did not stop Kolymbas et al. who proceeded to simplify the problem. The first simplification suggested was quite an important one: a hydrostatic back stress was postulated. Then,

$$\mathbf{s} = s\mathbf{1} \tag{276}$$

From the algebraic viewpoint, this is just a scalar variable, and now the stress rate in (273) depends again on two tensorial variables and a scalar, having the same general representation as the previous hypoplastic equations. From this viewpoint it is just the same equation as that proposed by Bauer and Gudehus, but with a stress-dimensioned variable instead of the void ratio.

It is then not very surprising to find that the second simplifying assumption is to impose a zero back stress at the newly introduced "residual state", when the stress rate is zero. This is rather close to the critical state concept employed by Bauer and Gudehus. This careful naming is perhaps due to the author's

awareness of difficulties associated with achieving simultaneously critical state and homogeneous deformation in standard tests.

The third simplifying assumption is to substitute the (tensorial) evolution equation (274) for an (scalar) state equation (or finite equation in their terms) of the form

$$s = G(tr(\boldsymbol{\sigma}), tr(\boldsymbol{\varepsilon})) = g(p, e) \tag{277}$$

The particular development of (273) chosen is a modified eq. (259) , including now six terms "...to improve performance in non axysimmetric paths..."

$$\dot{\boldsymbol{\sigma}} = c_1 tr(\boldsymbol{\sigma}_c)\dot{\boldsymbol{\varepsilon}} + c_2 \frac{tr(\boldsymbol{\sigma}_c \dot{\boldsymbol{\varepsilon}})}{tr(\boldsymbol{\sigma}_c)} \boldsymbol{\sigma}_c + \left[c_3 \frac{\boldsymbol{\sigma}^2}{tr(\boldsymbol{\sigma})} + c_4 \frac{\boldsymbol{\sigma}_d^2}{tr(\boldsymbol{\sigma})} + c_5 \frac{\boldsymbol{\sigma}^3}{tr(\boldsymbol{\sigma}^2)} + c_6 \frac{\boldsymbol{\sigma}_d^3}{tr(\boldsymbol{\sigma}_d^2)} \right] \|\dot{\varepsilon}\| \tag{278}$$

From an algebraic standpoint again it is interesting to note that the same number of generators are employed as in the antecedent equation[123], and the only significant modification is the use of another invariant of the functional basis, $tr(\sigma^2)$. Would the back stress be generalised as a tensor, then the equation will depend on three tensorial variables, and its general representation will be a quite more complicated one.

The specification of (277) adds four parameters to the six appearing in (278), for a total of ten. In contrast with the Bauer-Gudehus proposal none of them corresponds with any basic soil property. The simulation results presented (triaxial, oedometer, simple shear) are similar in scope.

A recent paper by Niemunis and Herle (1997) addressed the problem of memory effects, but now building upon Bauer's treatment of picnotropic/barotropic features. Their proposal does not fit easily into the frame of hypoplasticity, because of its inclusion of loading/unloading criteria. The interesting point here is to note that they propose the inclusion of a tensorial variable, the intergranular strain, to deal with those pesky memory effects.

New tensorial variables were also introduced to deal with the localization problem -i.e. to reproduce the appearance and evolution of shear zones in sand. Tejchman (1994) has presented a Cosserat development of hypoplastic equations. The Cosserat approach implies the inclusion of new internal variables: microrotations and couple stresses.

13.3 HYPOPLASTIC MODELLING OF COMPLEX ELEMENT TESTS.

13.3.1 Database description

The experimental database here employed was formed at the University of Colorado at Boulder during the years 1985 to 1988. It's results have been partially presented by Alawaji et al. (1991). Full details are presented in Sture, Alawi & Ko (1988), Alawaji (1986) and Alawi (1985).

---

[123] By virtue of Cailey-Hamilton theorem.

The database comprises results from experiments on dry sand. The sand employed is Silver Leighton Buzzard, (SLB). It has a specific gravity of 2.66. It's sub-rounded and close-graded, with an uniformity coefficient of 1.48. It's maximum and minimum void ratios are $e_{max} = 0.815$ and $e_{min} = 0.516$. Samples were formed by dry pluviation from a height of 61 cm. They were cubical, with 17.8 cm side size. Specimens had 72% relative density i.e. an initial void ratio of 0.599

Two different apparatus were employed in the testing programme: the multiaxial cubical apparatus (MCA) and the directional shear cell (DSC). The MCA applies a stress-controlled true triaxial loading, applying pressure in the sample sides through flexible membranes. The DSC has mixed boundary conditions: two rigid walls ensure a null out of plane deformation i.e. a plane strain condition; the in-plane movements are stress-controlled, with normal pressure applied through flexible membranes and shear stress by pulling four textured shear pads placed between the membranes and the sample.

In the MCA, the stress paths of all[124] experiments comprised two different stages: initial isotropic loading and deviatoric loading at constant isotropic pressure. This last stage would generally include various sub-stages, varying the stress increment direction from one to another. The sub-stages ended when the accumulated deviatoric strain within them reached a previously established ceiling. Figure 13-2 is an example of how this type of loading path looks like.

The accumulated deviatoric strain ceiling was specified to be 1 or 2% in most cases. This limited deformation successfully prevented specimen failure. In some other tests, the final loading was taken up to 15% deformation, resulting in failed specimens with apparent shear bands. All throughout the experimental set the mean pressures were relatively low, between 13.8 and 69.5 kPa, to work within the range of the DSC.

The observed behaviour was interpreted within the framework of elastoplasticity. The most significant results (Alawi, 1988, Alajawi et al., 1990) are now briefly recalled.

There are grounds to propose an initial elastic response: the stiffness on unloading is very high and similar to the stiffness on initial loading. Here, unloading must be interpreted in a wide sense as any stress path corner. A nice example of this feature is given by test ACH4 on the MCA, whose deviatoric path -ACH4H- is illustrated on Figure 13-3. The deviatoric stress path has then three corners and four sections, being the last one the only proper reversal. If we graph the stress path against the accumulated strain work we obtain Figure 13-4.

There are three evident steps, indicating very small deformation, appearing after each of the stress path corners. It's nevertheless also apparent that after each plateau the deformation increases quite gradually.

---

[124] Save one isotropic test

The selection of a yield point is then a matter of convention, and the convention followed by Alawi et al used as criteria an accumulated strain after a turning point of 0.05%

From the observation of yield points thus defined (Alajawi et al., 1990) were able to establish rules for yield locus evolution. This was kinematic rather than isotropic, i.e. the yield locus did not change absolute size when dragged along the deviatoric plane. This is a result that only makes sense within the elastoplastic framework; however, other observations had wider scope.

Initial anisotropy of response was observed only on dense samples. A more general feature was volumetric densification as the stress path wandered on the deviatoric plane (Figure 13-5). This result is directly comparable to more conventional cyclic triaxial tests (Figure 13-6).

Strain increments were not simply related to either stress, stress-increment or both. This is seen very clearly in Figure 13-7, corresponding to test ACH1. The stress path goes to and fro three times on the same line and the direction of strain increments -in three different colours in the figure- are different each time. Within the elastoplastic framework this will indicate the need for a complex flow rule.

13.3.2 Hypoplastic model: description.

The hypoplastic equation here employed for the simulation was proposed by von Wolffersdorff (1996). It is written as follows

$$\dot{\boldsymbol{\sigma}} = f_s \frac{[\mathrm{tr}(\boldsymbol{\sigma})]^2}{\mathrm{tr}(\boldsymbol{\sigma}^2)}\left[\mathbf{F}^2\dot{\boldsymbol{\varepsilon}} + a^2\,\mathrm{tr}(\boldsymbol{\sigma}\dot{\boldsymbol{\varepsilon}})\frac{\boldsymbol{\sigma}}{[\mathrm{tr}(\boldsymbol{\sigma})]^2} + f_d a\,\mathbf{F}\left[\frac{\boldsymbol{\sigma}}{\mathrm{tr}(\boldsymbol{\sigma})} + \frac{\boldsymbol{\sigma}_d}{\mathrm{tr}(\boldsymbol{\sigma})}\right]\|\dot{\boldsymbol{\varepsilon}}\|\right] \qquad (279)$$

whose coefficients are given by

$$f_d = r_d^{\alpha} = \left(\frac{(e - e_d)}{(e_c - e_d)} \right)^{\alpha}$$

$$f_s = f_e f_b \qquad f_e = \left(\frac{e_c}{e} \right)^{\beta}$$

$$f_b = \left(\frac{e_{i0}}{e_{c0}} \right)^{\beta} \frac{h_s}{n h_i} \frac{1 + e_i}{e_i} \left(\frac{-tr(\boldsymbol{\sigma})}{h_s} \right)^{1-n}$$

$$h_i = a^2 + 3 - \left(\frac{(e_{i0} - e_{d0})}{(e_{c0} - e_{d0})} \right)^{\alpha} a\sqrt{3}$$

$$a = \sqrt{\frac{3}{8}} \frac{(3 - \sin\varphi_c)}{\sin\varphi_c}$$

$$\mathrm{F} = \sqrt{\frac{1}{8}\tan^2\psi + \frac{2 - \tan^2\psi}{2 + \sqrt{2}\tan\psi\cos 3\theta}} - \frac{1}{2\sqrt{2}}\tan\psi$$

$$\tan\psi = \sqrt{3}\frac{\mathrm{tr}\left(\boldsymbol{\sigma}_d^2\right)}{(\mathrm{tr}\boldsymbol{\sigma})^2} \qquad \cos 3\theta = -\sqrt{6}\frac{\mathrm{tr}\left(\boldsymbol{\sigma}_d^3\right)/(\mathrm{tr}\boldsymbol{\sigma})^3}{\mathrm{tr}\left(\boldsymbol{\sigma}_d^2\right)^{3/2}/(\mathrm{tr}\boldsymbol{\sigma})^{3/2}} \tag{280}$$

This model is very similar to that proposed by Bauer and Gudehus (272). The equation has the same structure –in terms of generators and invariants employed-, was developed using the same principles and void ratio dependency –picnotropy- is addressed in exactly the same way through factors f_e & f_d. The main changes affect the stress-dependent multiplicative factors, here named F and a, whose expressions were changed to obtain a critical surface shape more adjusted to the Matsuoka-Nakai criterion.

The parameters employed had the same name. Parameters who correspond to independently specified granular material properties should be exactly the same. Adjustment parameters may vary according to the equations shape i.e. according to their position within the equation. In this case of the adjustment parameters only α has a different position and thus it's value may change slightly.

13.3.3 Simulation procedure.

A program written by Herle (Herle, 1997) was available to solve the selected equation in some load cases . The cases included are isotropic compression, oedometric compression, triaxial compression with constant volume or constant radial pressure and, finally, biaxial compression at constant volume. The Colorado database does not fit into those categories. Therefore a new program was specifically written to simulate the tests. It's principal features will be now described.

MCA tests are among the most complex laboratory tests available. Their results could and should be displayed in a number of different ways to obtain a proper understanding of what's happening with the sample. This made attractive the idea of working within the Excel environment and writing the programme in Visual Basic.

The hypoplastic equations are formulated with the strain rate as a function of the stress and strain rate. The usual way of solving them for any element test (e.g. Kolymbas 1989) takes into account the boundary conditions of the element test, which imply constraints to either it's stress or strain path, to obtain a reduced set of equations (from the six implicit in the tensorial formulation). When constraints were enforced in the stress path the non-linearity of the hypoplastic expressions required some iteration to obtain the corresponding strain rate.

The nature of the Colorado database, (stress-controlled, but following complicated stress paths) made this approach unappealing. Instead, profit was taken of the formal inverted expression for the hypoplastic equation. This expression (257) leads in the case of Wolffersdorff formulation to

$$\dot{\varepsilon} = \frac{\mathbf{A}}{\mathrm{K}} - \frac{\mathbf{B}}{\mathrm{K}}\left[\sqrt{\frac{(\mathbf{AB})^2 - \mathbf{AA}(\mathbf{BB} - \Psi)}{(\mathbf{BB} - \Psi)^2}} + \frac{\mathbf{AB}}{\mathbf{BB} - \Psi}\right] \qquad (281)$$

$$\mathrm{K} = \frac{(tr\sigma)^2 f_b f_e}{tr(\sigma^2)} \qquad \Psi = \frac{1}{f_d a \mathrm{F}}$$

For any particular experimental step the stress-rate is fixed. Due to rate-independence the inverted hypoplastic equation is formally equivalent to a first order ordinary, non-linear differential equation, like

$$\dot{y} = h(x, y) \qquad (282)$$

where the stress length plays the role of the independent variable, x, and the strain vector the role of the dependent variable, y. Void ratio dependency explains the appearance of y on the right hand side of this equation.

Numerical integration is necessary. Roddemann (1998) has shown for a similar case that good results are obtained with an explicit Euler integration formula if the stepsize is carefully controlled. A similar approach is followed here. To do so a procedure by Press et al. (1992) was translated. The procedure uses a fifth order Runge-Kutta integration formula with adaptive stepsize control.

The inverted equation fails whenever the condition BB - Ψ = 0 is fulfilled. This means that the built in Matsuoka-Nakai failure surface is crossed. It has to be emphasised that the model is built in a way that makes this surface dependent on void ratio. In other words, the Matsuoka-Nakai criterion gives the surface shape, but its size is controlled by the void ratio. The deviatoric dependence is illustrated in Figure 13-8. Using an elastoplastic concept we would say that the model has built-in isotropic hardening.

The strenght of this hardening is controlled by all the parameters involved in the condition BB - Ψ = 0. For the set of parameters[125] given in Herle & Tejchman (1997) for SLB this implicit "hardening law" is pictured in Figure 13-9. Is apparent that the effect is substantial.

---

[125] See below for comments on this and other parameter sets.

13.3.4 Calibration.

Herle (1997) describes a simplified procedure to estimate the parameters needed by this equation:

a) The critical friction angle, φ, is the angle of repose of a heap of sand
b) The two usual limit void ratios could be employed as values of e_{c0} and e_{d0}.The correspondence is $e_{max} \approx e_{c0}$, $e_{min} \approx e_{d0}$. Alternatively, they can be estimated from the coefficient of uniformity and the grain shape.
c) The granular hardness, h_s, is obtained from an isotropic compression test.
d) An isotropic compression test provides also the parameter n, although this could also be estimated from granulometric data.
e) The exponent α is obtained through the peak friction angle of a dense sample of sand. Although not explicitly mentioned, analogy with the calibration procedure suggested by Bauer implies that this peak friction angle is to be obtained through a conventional compressive drained triaxial test.
f) Finally, two simplifications are introduced: the exponent β could be taken as 1 and the parameter e_{i0} could be approximated as 1.15 e_{i0}.

The studied database does not permit to follow exactly this calibration procedure, nonetheless some results are readily available. There are maximum and minimum density measurements, resulting on void ratios of 0.516 and 0.815; this gives e_{d0} and e_{c0}. Looking at the granulometric curve for SLB –e.g. Alawi, 1988- $d_{10} \cong 0.55$, $d_{50} = d_{60} \cong 0.8$. Thus U = 1.454 and using the regression line by Herle a value n = 0.32 is obtained.

There is one isotropic compression test done with the MCA with mean stress ranging from 13 to 173 kPa, see Figure 13-10. Following the procedure suggested by Herle (1997) and Bauer (1996) the noval compression branch is fitted very accurately with parameters h_s = 283 MPa and n = 0.741, as could be appreciated in Figure 13-11 . Is interesting to mention that extrapolating this curve to p = 0 a void ratio of 0.60 is obtained, obviously different from the ideal absolute maximum void ratio e_{i0} obtained above.

There is no standard triaxial test in the database. Moreover, the small level of deformation attained in most tests hindered the attainment of critical state. Still, there are two series, one corresponding to extension, the other to compression, of three p constant tests which were carried on to large deformations. The MCA being stress controlled there are reasonable doubts about any post-peak measurement, indeed, localization was observed in some specimens (Alawi, 1988). The data corresponding to the last register of each test of those series are collected in Table 13-1, together with the friction angle that could be estimated from them. The bigger value given by extension tests corresponds to some type of peak angle and illustrates the difficulties of recording post-peak behaviour associated with such tests.

A set of hypoplastic parameters for SLB has been produced in the literature a couple of times.

- Herle (1997), gives values for SLB sand to the parameters of the Wolffersdorff model. These parameters are estimated from a paper of Kolbuszewski (1963), who provides data on the minimum and maximum density of LBS, it's oedometric compressibility, and triaxial friction angles.
- Herle & Tejchman (1997) produced a set of parameters for SLB sand based on data by Tatsuoka. They were considering a Cosserat extension of the Bauer model. This extension introduces more parameters, while keeping the original set from Bauer (1996).

Table 13-2 collects the data from all the different sources examined. In the Colorado column there are two values for n: one from the isotropic test and another from the granulometry. Lacking conventional triaxial test data the alpha value in that column is missing. The beta value is assumed in all cases.

The calibrated values are within the (ample) range of those quoted in the literature for other granular materials. The only notable exception corresponds to the high n value, fitted to the isotropic test. This value is almost double of all the values quoted by Herle (1997) for 12 different granular materials. If this value is not accepted , and the value derived from the granulometric curve is taken instead the set of parameters from calibration are not very different from those quoted in Herle (1997).

If we look now at the two sets of literature values, although there are other differences, it is apparent that the main one corresponds to the granular hardness parameter, **hs**. The consequences of that are explored below.

13.3.5 Simulation results

13.3.5.1 A triaxial check

As explained above the newly written program differed substantially –stress driven vs strain driven integration- from that previously written by Herle. This offered an obvious opportunity to check the performance of the chosen numerical approach.

Due to the limited scope of Herle's program the Colorado database was excluded as source of comparison. Henceforth a triaxial test on Hostun sand was selected from another well-known database (Saada & Puccini, 1989). This test, named HH1, was conducted in a hollow cylinder apparatus, but the stress path imposed was exactly that of a conventional, constant σ_3, triaxial experiment. A set of hypoplastic parameters for Hostun sand was provided by Herle (Herle, 1997) and is here reproduced as Table 13-3.

The results of both simulations are displayed in Figure 13-12 -volumetric behaviour- and Figure 13-13 deviatoric behaviour. It is apparent that both programs produce the same results in the main part of the test. With the set of parameters employed the initial contraction of the sample and its stiffness are both overestimated.

Herle's strain driven program keeps integrating well beyond the actual failure of the sample until a pre-established limit of 0.1axial strain. The inverse, stress-driven solution, cannot go beyond the stress data. Both solutions diverge after the hypoplastic inversion condition, BB - ψ = 0 is attained. This can be appreciated also in Figure 13-14, where this value is plotted against the stress path. It can also be appreciated how the original data go beyond the inversion condition.

13.3.5.2 Volumetric behaviour and granular hardness

We have seen how the parameter values obtained by calibration against the Colorado database were, with one exception aligned with those quoted by Herle. On the other hand, the two sets of parameters values quoted in the literature for SLB differed substantially, particularly in the "granular hardness" value, **hs**. For this parameter we have two wildly differing values: a "small" value of 300Mpa and a "big" value of almost 9.000 MPa. This is a rather confusing result as Gudehus (1996) stated that **hs** was "proportional to the strenght of the grain material" and therefore, must not vary 30 times for the same sand, whatever the variability of it's batches. Moreover, this won't be a problem if this parameter was more or less irrelevant i.e. if the repercussions of the choice were minor. In fact they are quite spectacular, as we will see.

Figure 13-16 represents the effect of parameter choice on isotropic test simulation. Surprisingly, the "big" hardness set fits the results much more precisely[126] than the "small" one. This is a clear indication that the exponent n has bigger repercussions over isotropic paths than "hardness".

Figure 13-17 shows the effects of parameter choice on the deviatoric response of test ACH3, a typical database result (Figure 13-15) It is clear that here the "big" set provides too stiff a response. Yielding on stress reversal is almost obviated. The "small" set is clearly more adequate. This contradiction is already annoying, but there are more inconveniences. Figure 13-18 represents the volumetric behaviour measured and predicted for the precedent test. It's clear that whereas the measured response is always contracting, the predicted response shows dilatancy a short while after each stress reversal. This effect is dramatically increased if the "small" set is employed, which is bad, as that was the parameter set that best fitted the deviatoric behaviour.

It's clear that the model has an excessive built-in dilatancy. Moreover, as dilation has as result contraction of the failure surface, the possibilities of numerical failure for stress paths close but parallel to the Matsuoka-Nakai surface are apparent. This was the case for instance of test ACH3, Figure 13-7 and this numerical failure made flow comparisons difficult.

One conclusion of this work is that the so-called "granular hardness" is an adjustment parameter. This was later confirmed by Herle (1999) who recognised that it was a bit of a misnomer. It is possible that parameter optimisation of the model along the lines described by Rouainia and Wood (2000) would have produced better adjustment to the database. However, that was not the purpose of this exercise.

13.3.6 Final comments: hypoplasticity and soil modelling

It is perhaps vain and misleading to oppose the hypoplastic and elasto-plastic approaches to soil modelling. Behind their very apparent differences there are some underlying fundamental ideas (and problems). We would like to point out some of them:

- To deal with increasingly complicated problems, (cyclic versus monotonic loading, failure) models are increasingly complicated. More variables are needed to describe soil behaviour. And, along any new variable, new equations must appear.
- Whatever the model employed, there seems to be an alternative in formulations between obscure equations with clear parameters and transparent equations with opaque parameters.
- Algebraic considerations are useful to tackle some particular problems of soil modelling. An example is how to model anisotropic behaviour while attending to space isotropy requirements. Another is to explore compactly issues related with uniqueness and existence of solution for the mechanical system described by a particular formulation. These problems are, by no means, restricted to hypoplasticity and, as a consequence, hypoplasticity is not more "algebraic" than elasto-plasticity. Boehler (1987) is a good example for the first case; Imposimato & Nova, (1998) provide a nice example related with the second issue.
- Geometrical reasoning is not specific either to any model; the idea of reconstructing multidimensional figures from some specific hints of them could provide very convenient shortcuts within hypoplastic models.
- Critical states and incremental nonlinearity are very powerful ingredients in any sand model.

[126] It's noticeable, nevertheless, the poor fit to the unload-reload cycle

13.4 TABLES

TEST	TYPE	p (kPa)	q (kPa)	Friction angle
O2	COMP.	13.79	20.68	31.63
A**2	COMP.	55.16	70.33	
A*2	COMP.	68.95	86.87	
O8	EXT.	13.79	18.62	42.53
A**8	EXT.	55.16	62.05	
A*8	EXT.	68.95	74.46	

Table 13-1 Data on peak friction angle from the Colorado database

Parameter	Herle 97	Herle & Tejchman 97	Colorado database
Fi critical	30	29	31.6
ed0	0.49	0.51	0.516
ec0	0.79	0.79	0.815
ei0	0.9	0.86	0.937
hs	8,900,000	300,000	283,000
n	0.33	0.4	(0.741) 0.32
alpha	0.14	0.16	
beta	1	1	1

Table 13-2 Data available on hypoplastic parameters for SLB sand

Parameter	Value
Fi critical	31
ed0	0.61
ec0	0.91
ei0	1.09
hs	1,000,000
n	0.29
alpha	0.13
beta	2

Table 13-3 Hostun sand hypoplastic parameters (Herle, 1997)

13.5 FIGURES

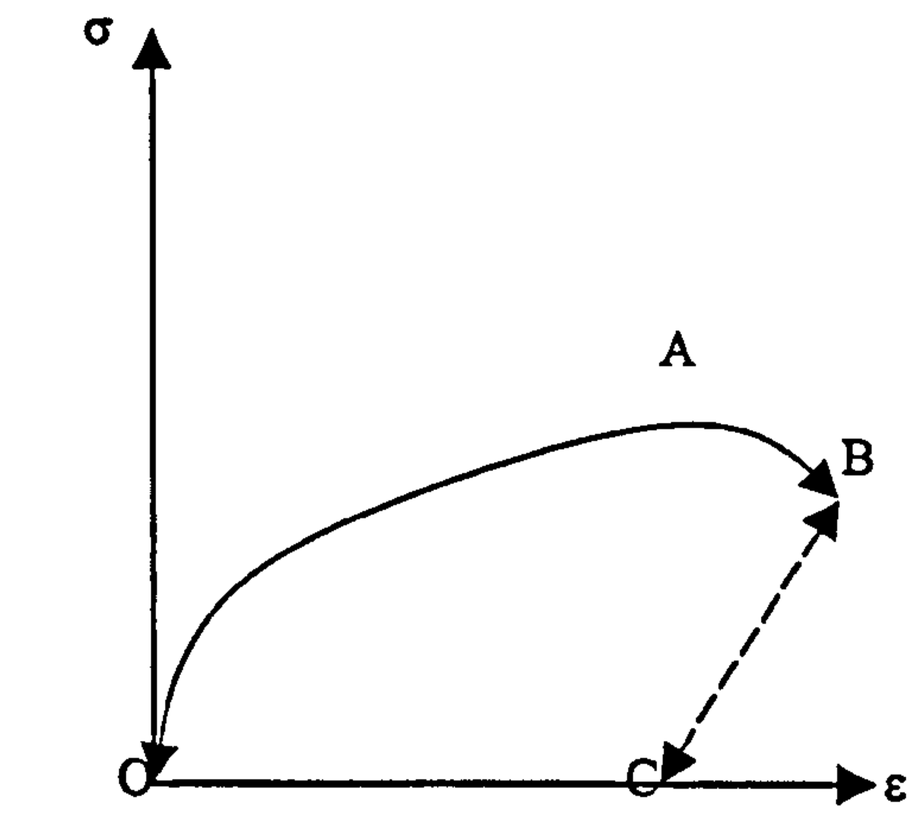

Figure 13-1 Hypoelastic vs elasto-plastic behaviour

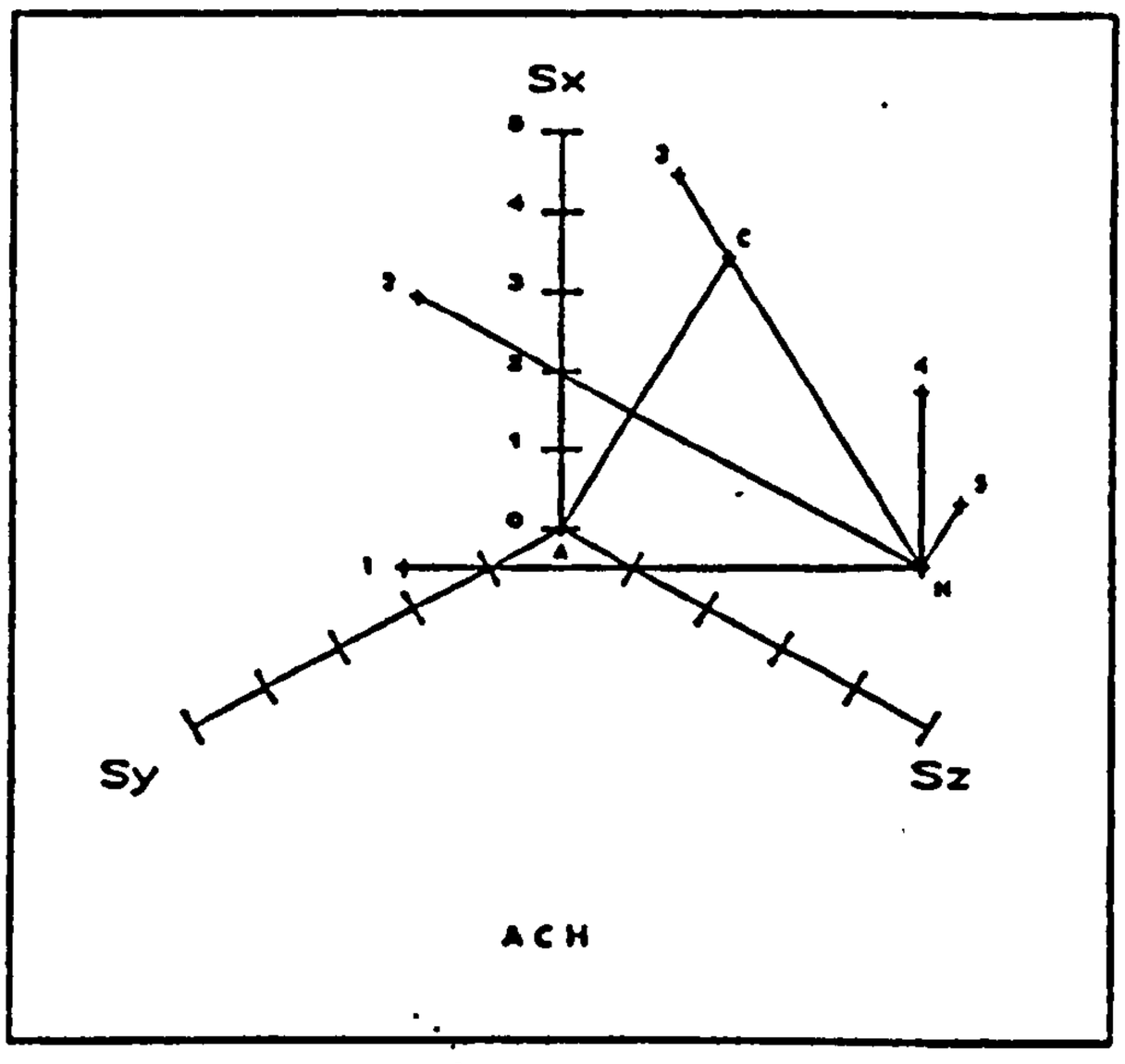

Figure 13-2 Colorado database. Deviatoric MCA paths.

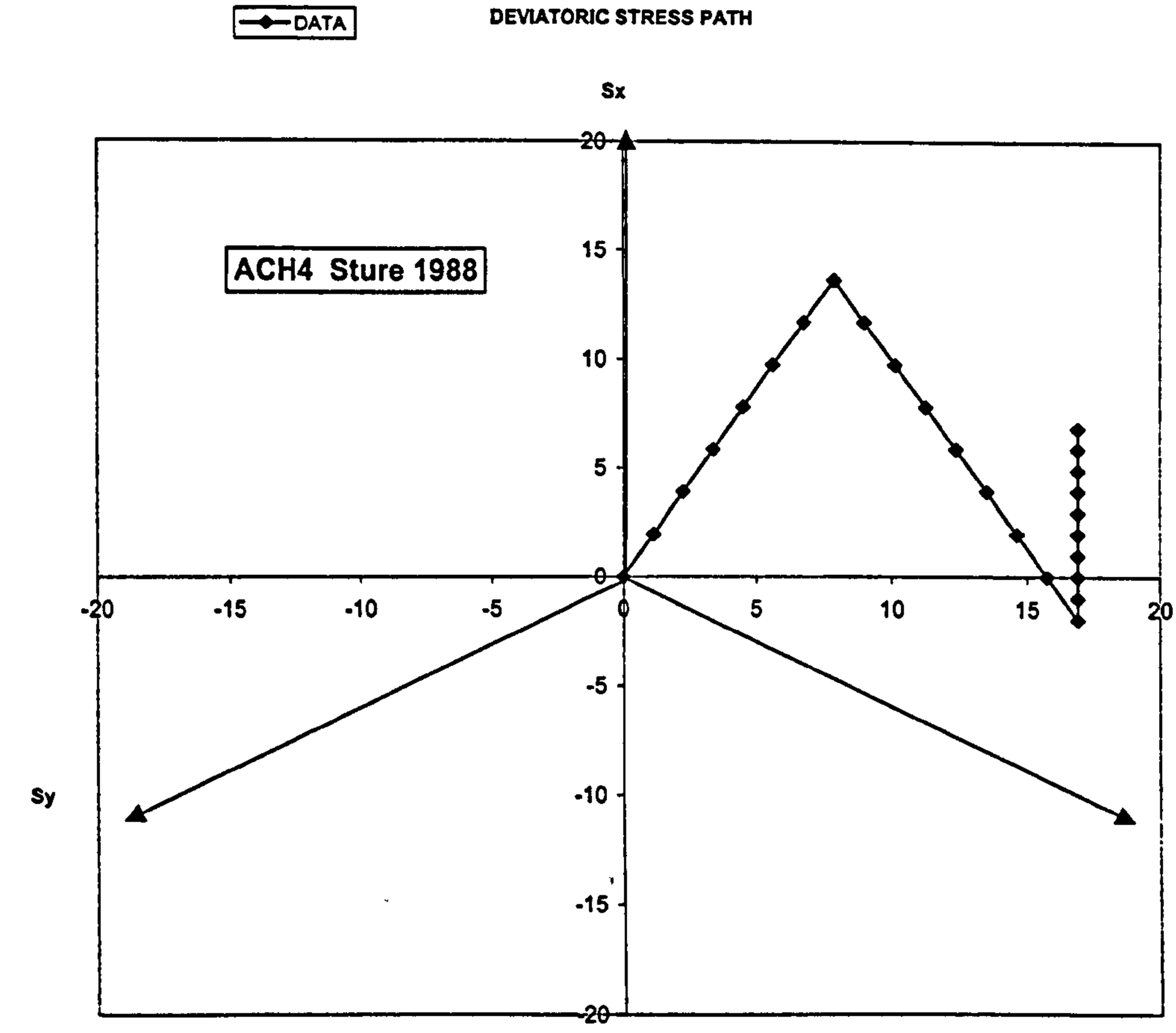

Figure 13-3 Typical MCA stress path

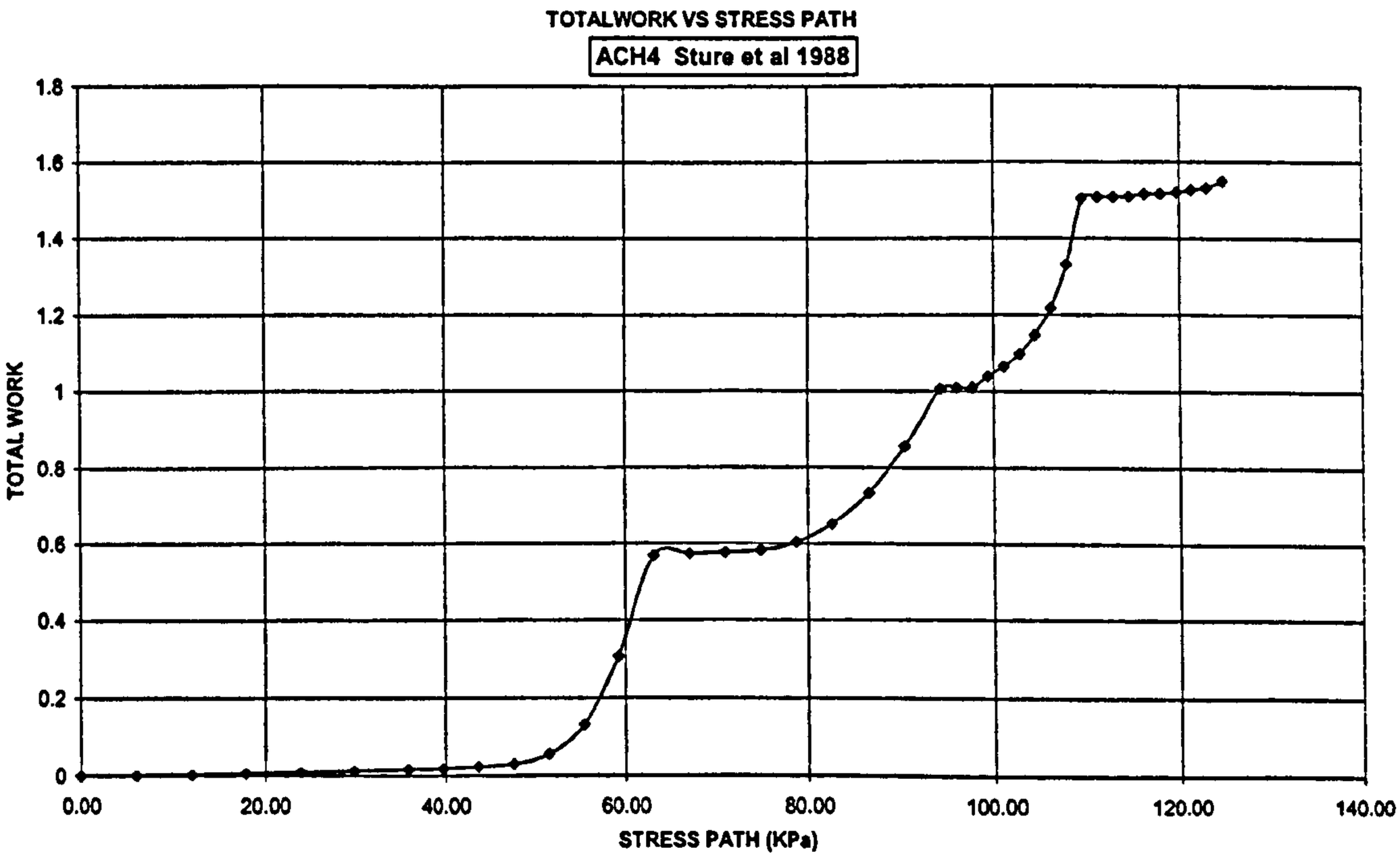

Figure 13-4 Successive yielding along MCA stress paths

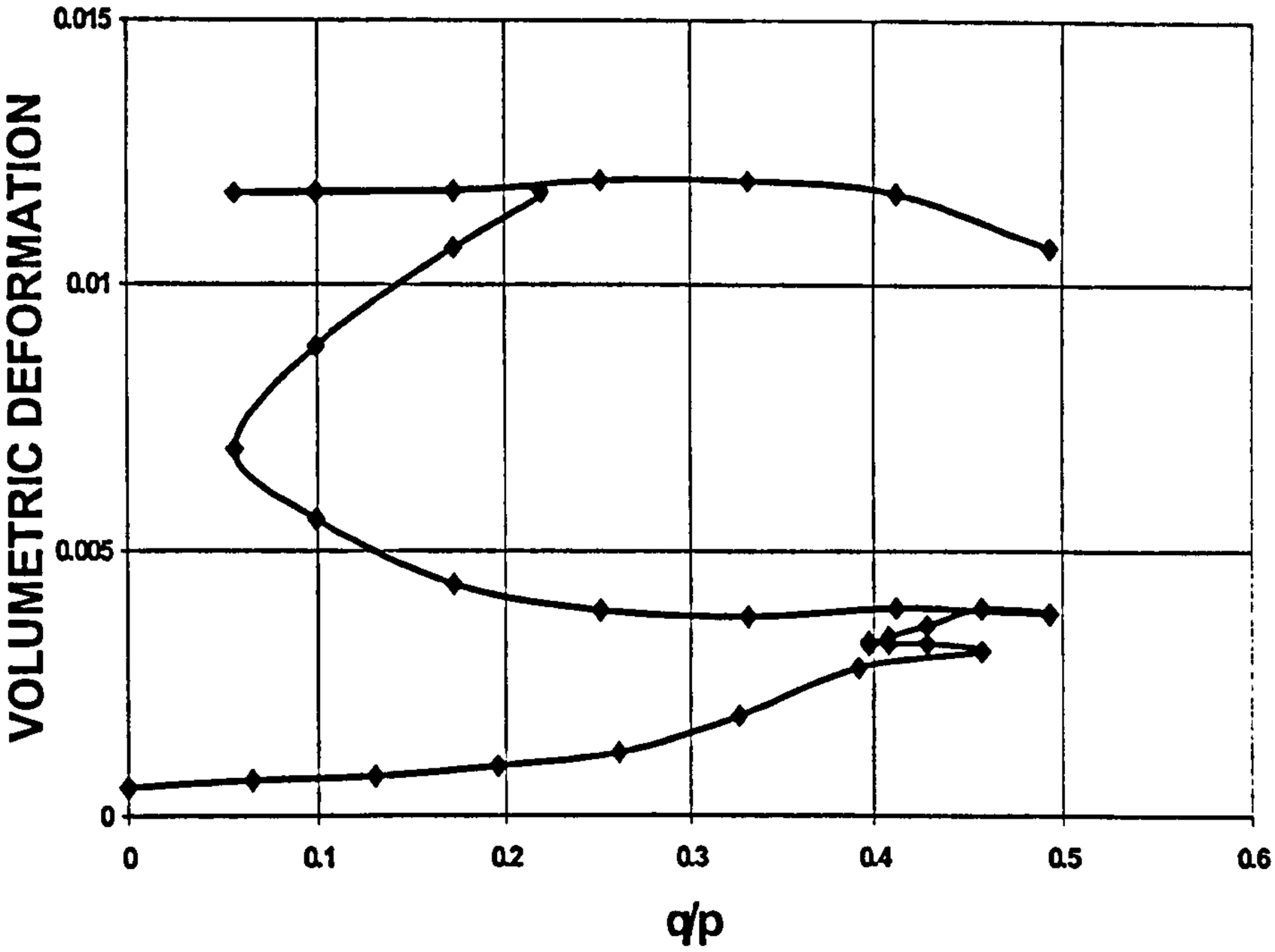

Figure 13-5 Accumulated volumatric deformation. Test ACH1

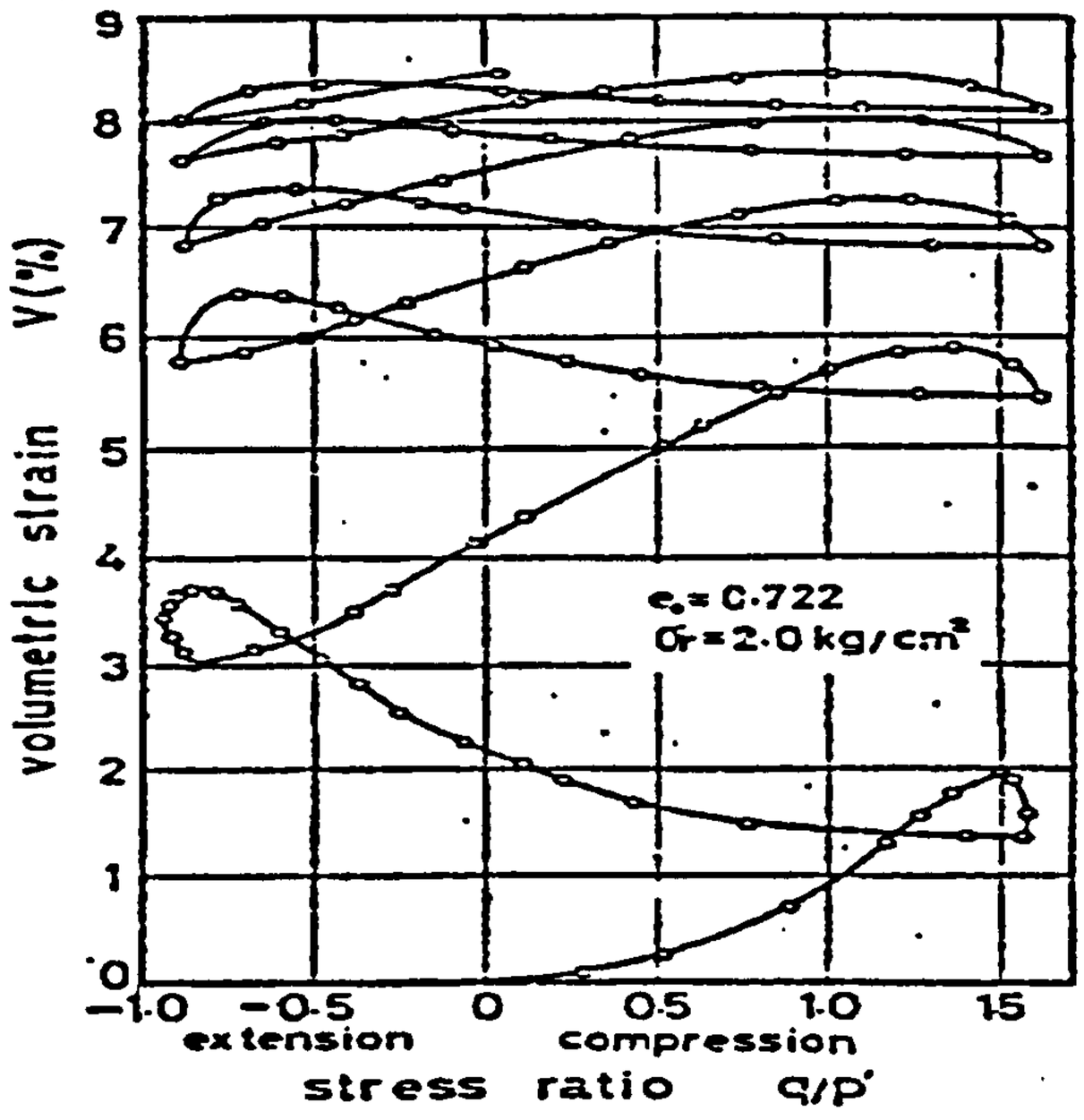

Figure 13-6 Volumetric deformation. Cyclic triaxial (Ishihara & Tatsuoka, 1974)

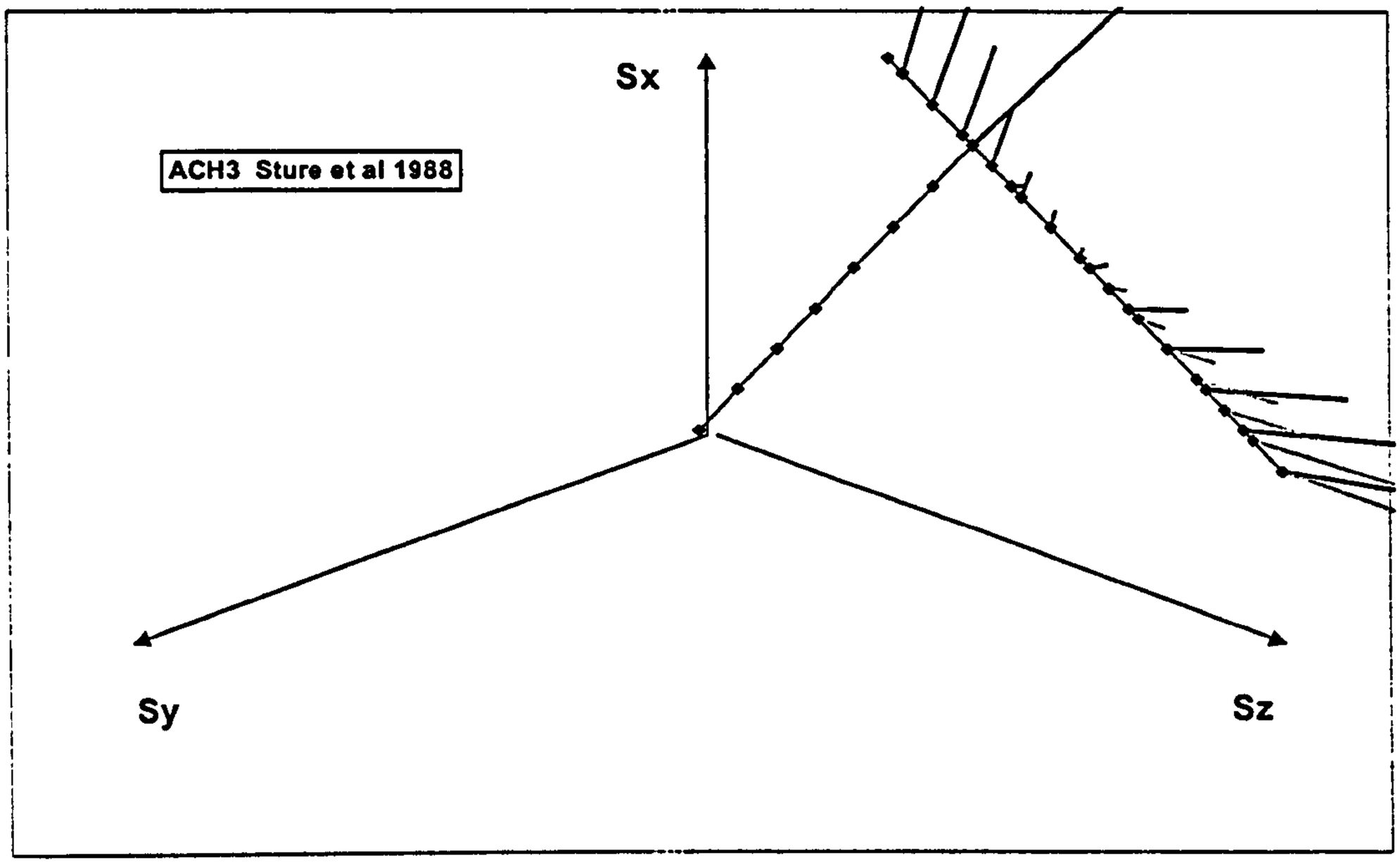

Figure 13-7 Deviatoric strain increments and repeated stress path

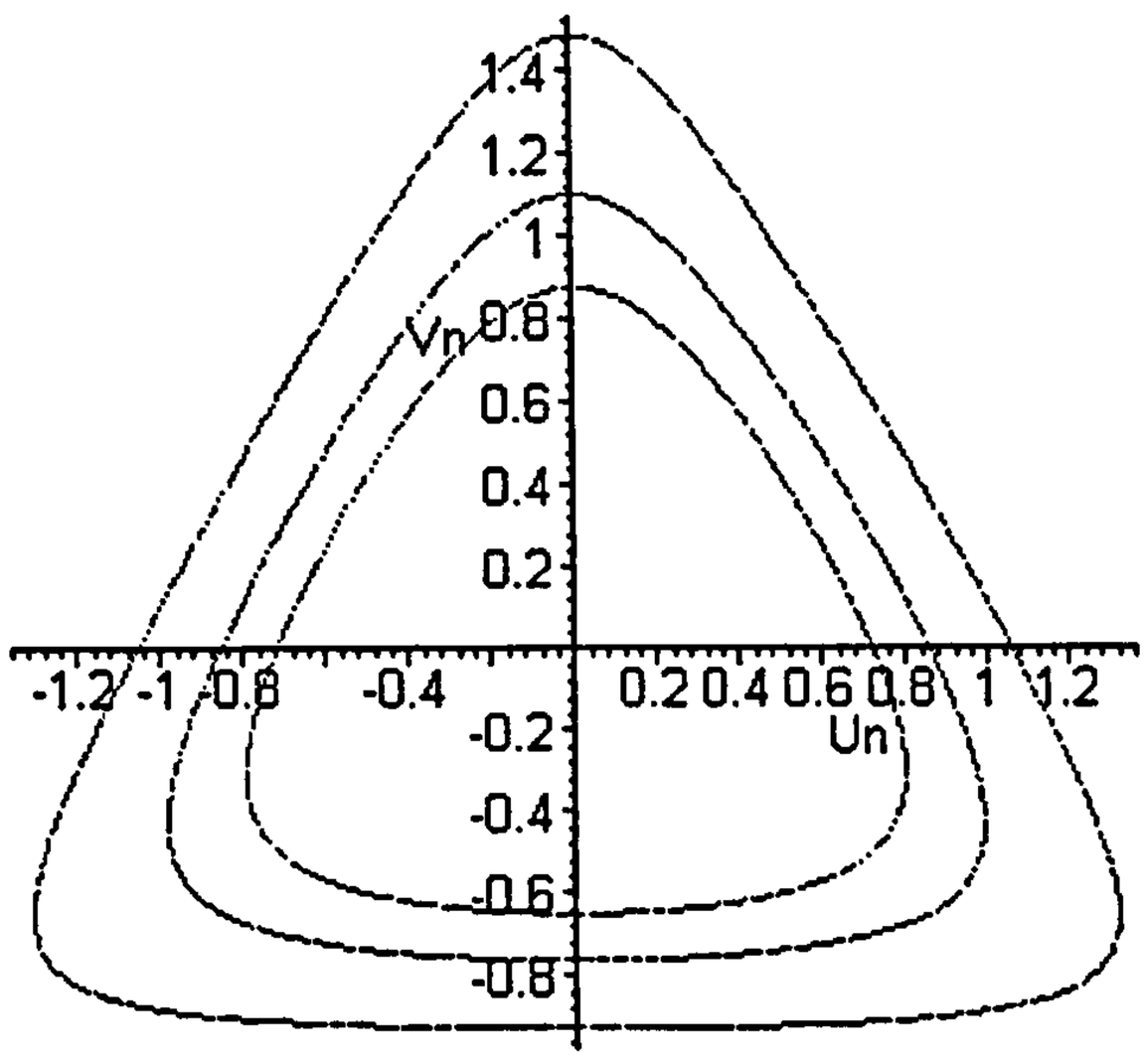

Figure 13-8 Failure surface: deviatoric dependence on void ratio

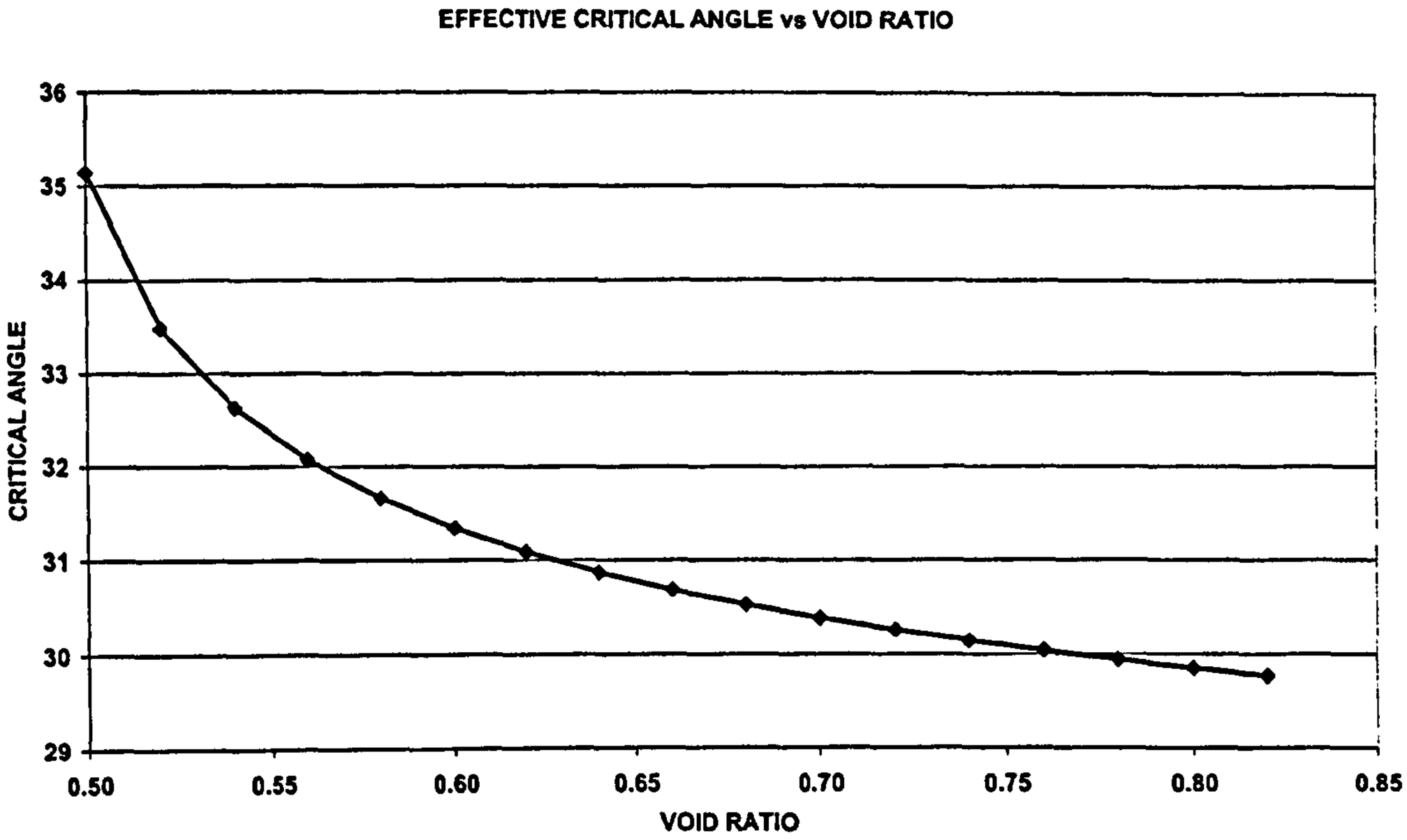

Figure 13-9 Failure surface size and void ratio

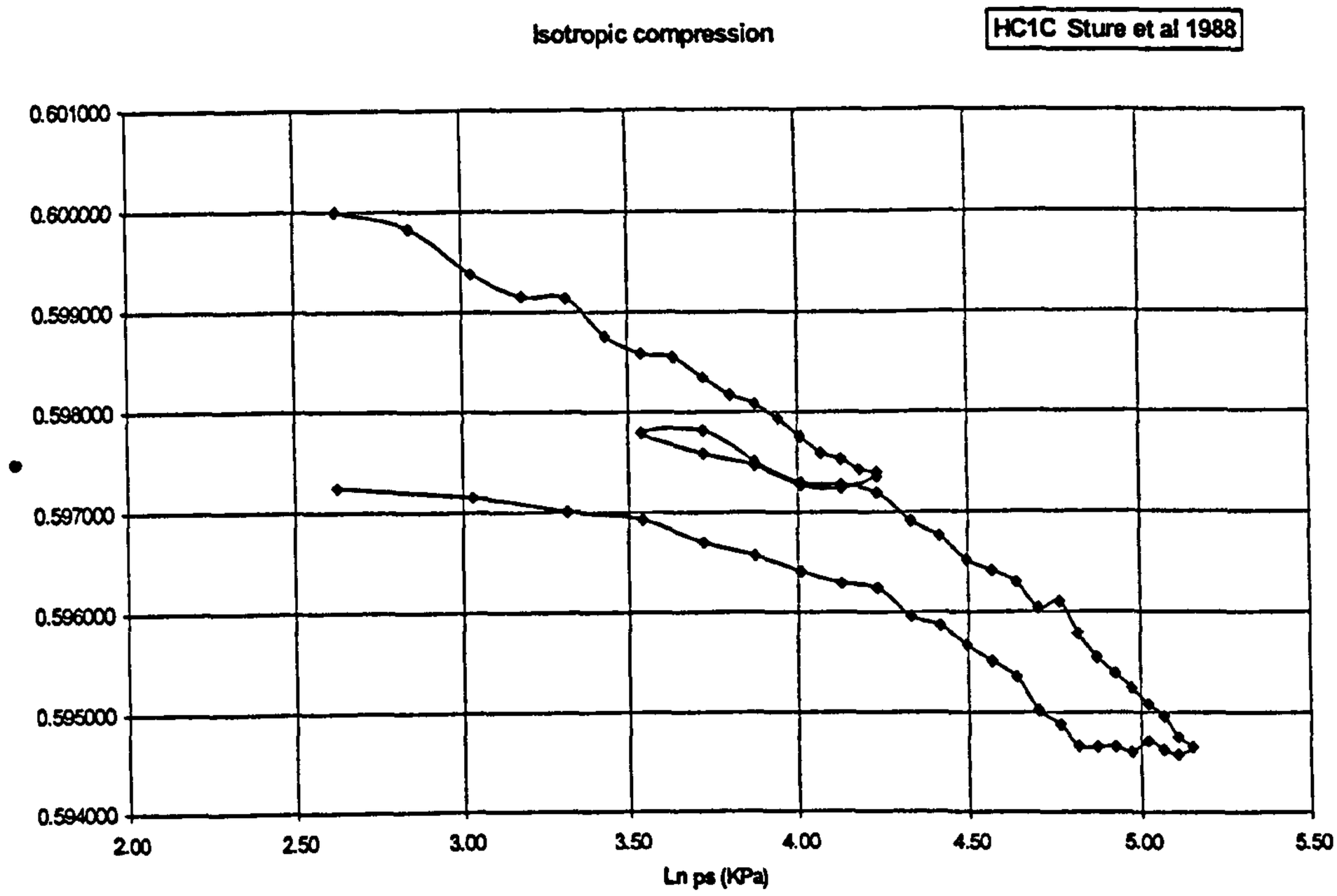

Figure 13-10 Isotropic test on MCA

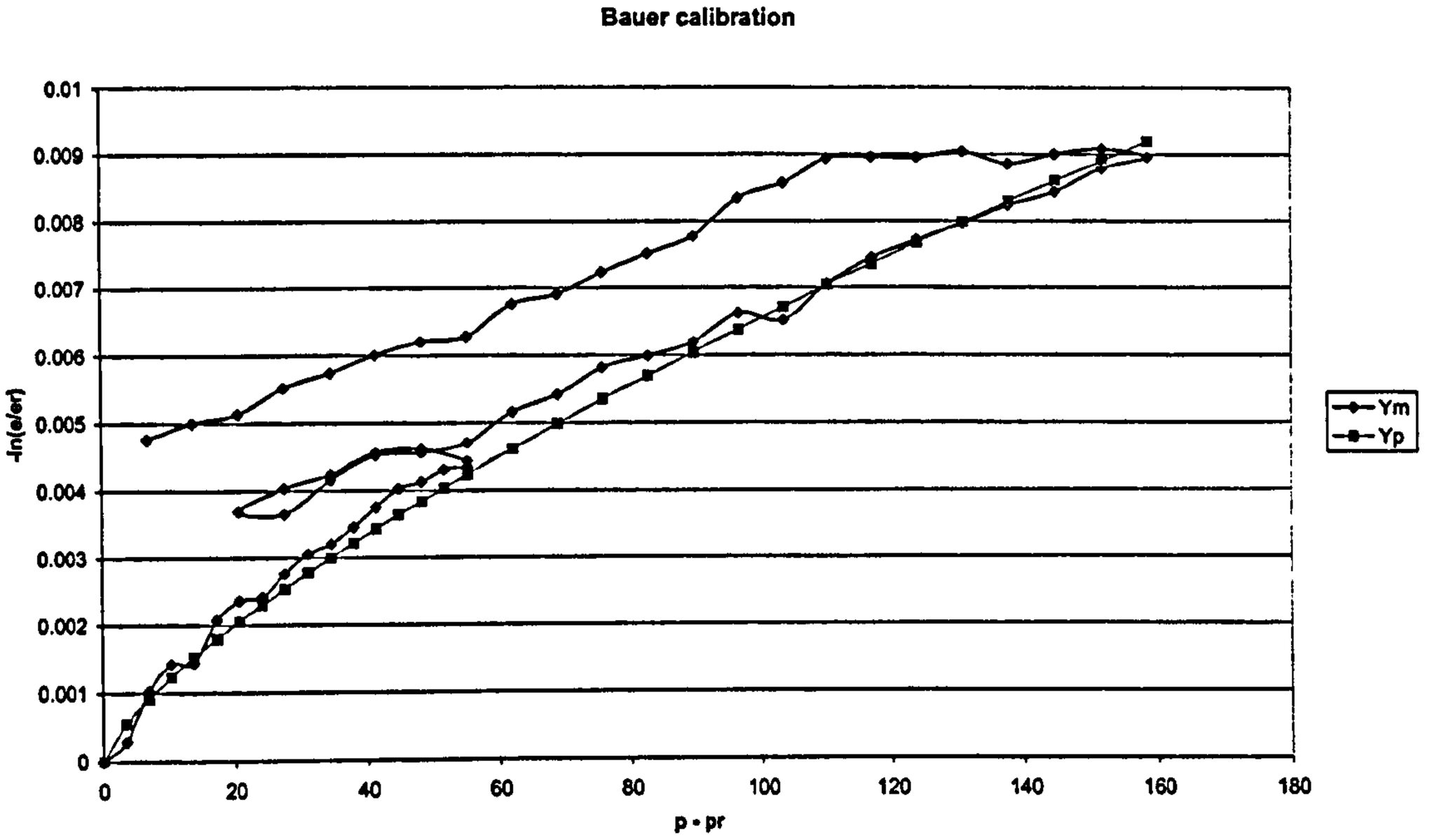

Figure 13-11 Adjusting the isotropic MCA test

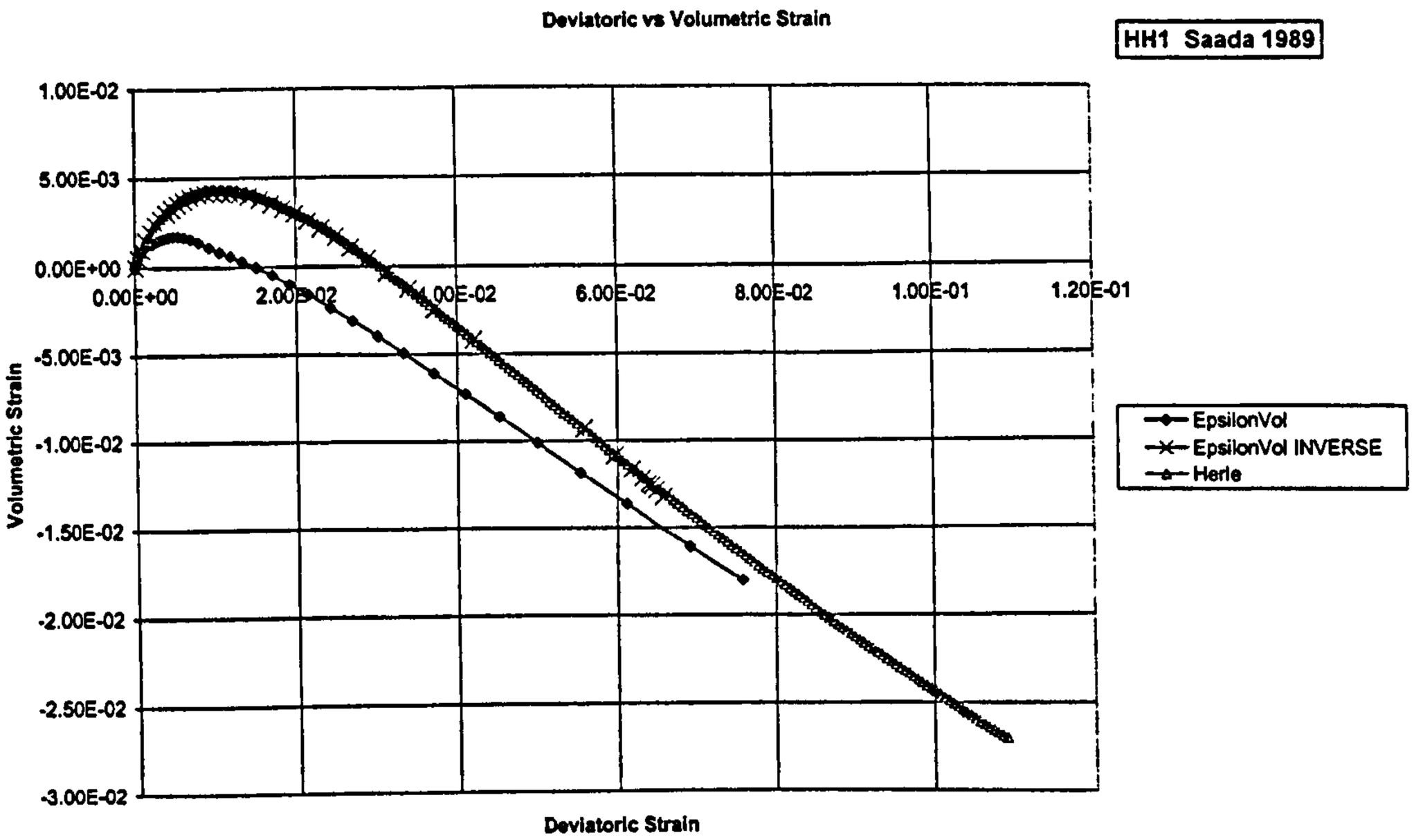

Figure 13-12 TXC Excel & Herle simulations: volumetric result

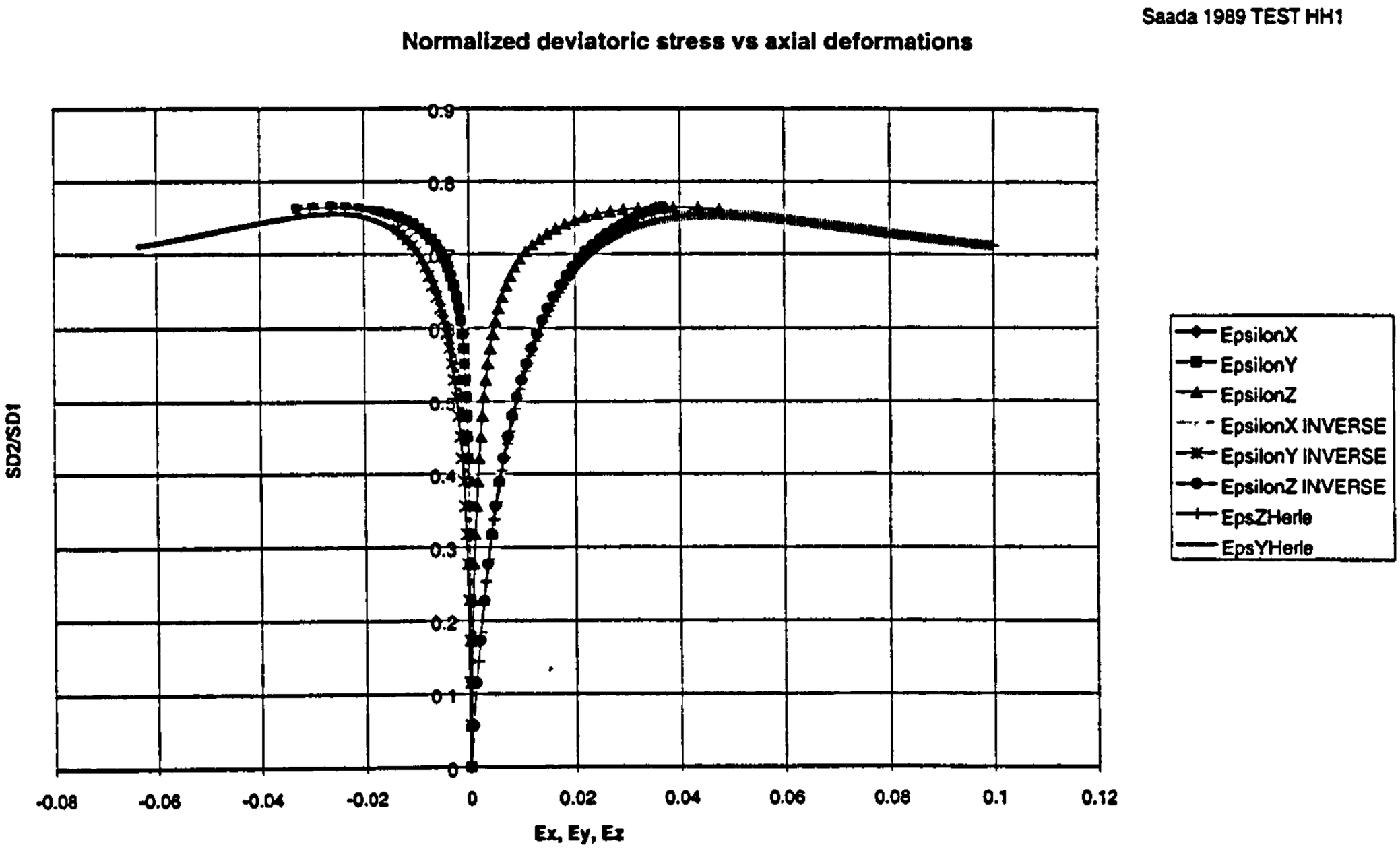

Figure 13-13 TXC Excel & Herle simulations: deviatoric results

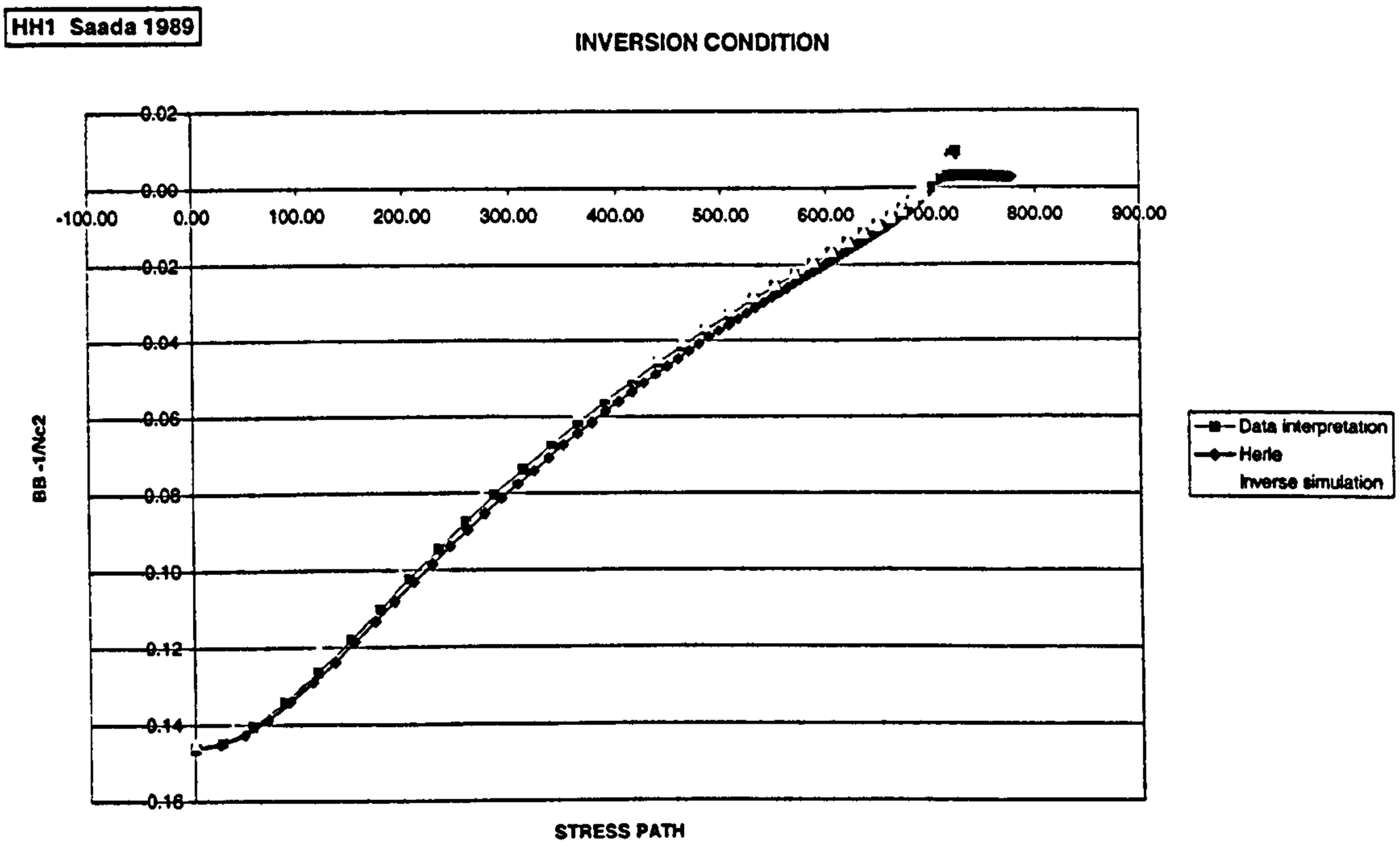

Figure 13-14 TXC Excel & Herle simulations: critical inversion condition

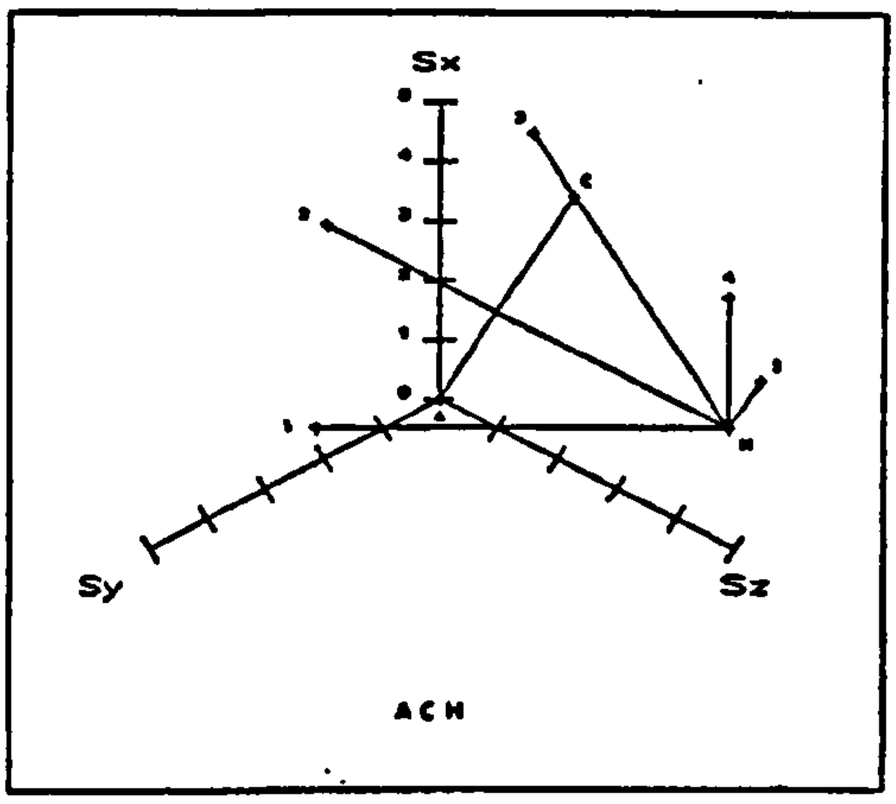

Figure 13-15 Test ACH3. Deviatoric stress path

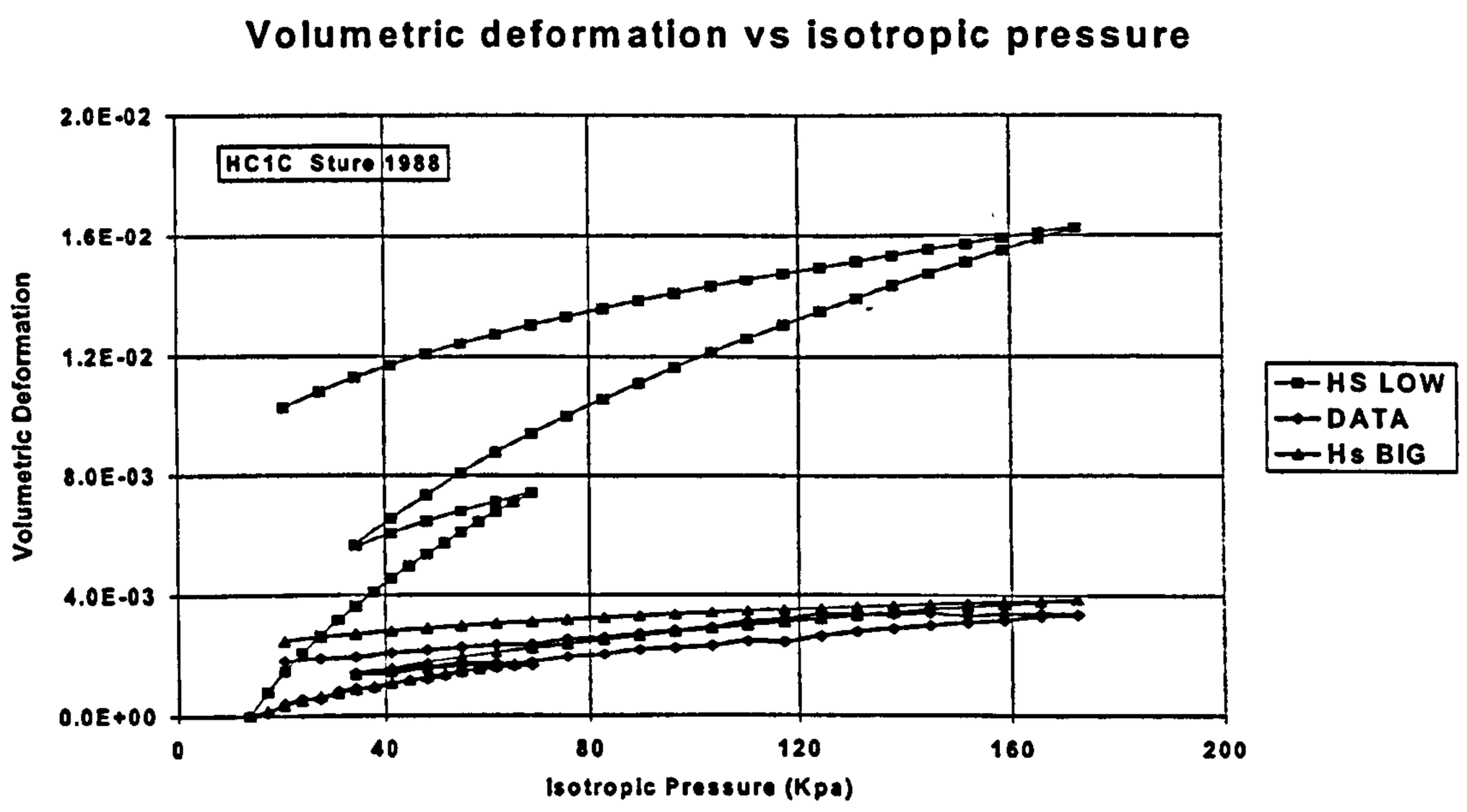

Figure 13-16 Parameter choice: effect on isotropic test results

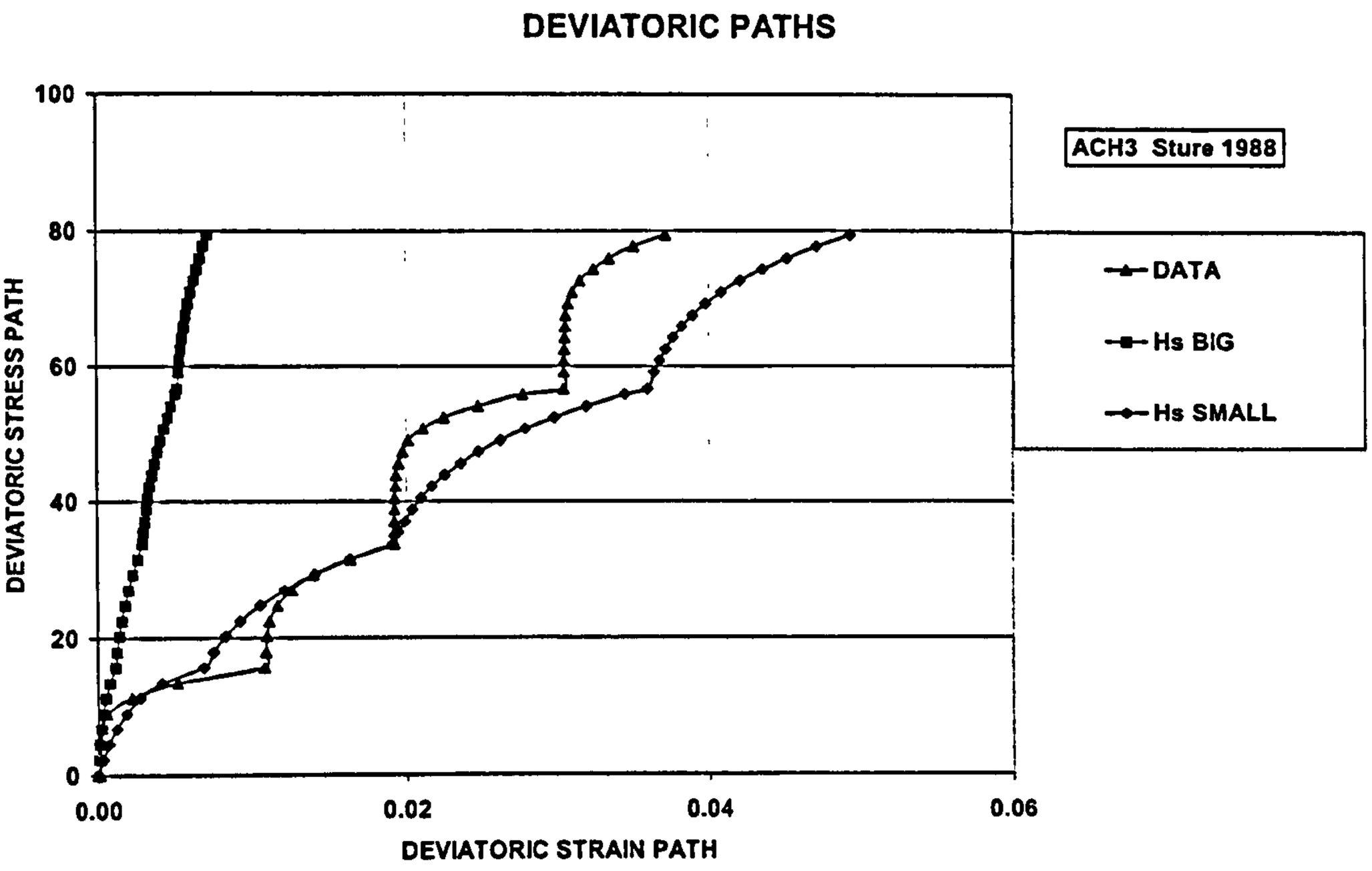

Figure 13-17 Parameter choice: effect on deviatoric response

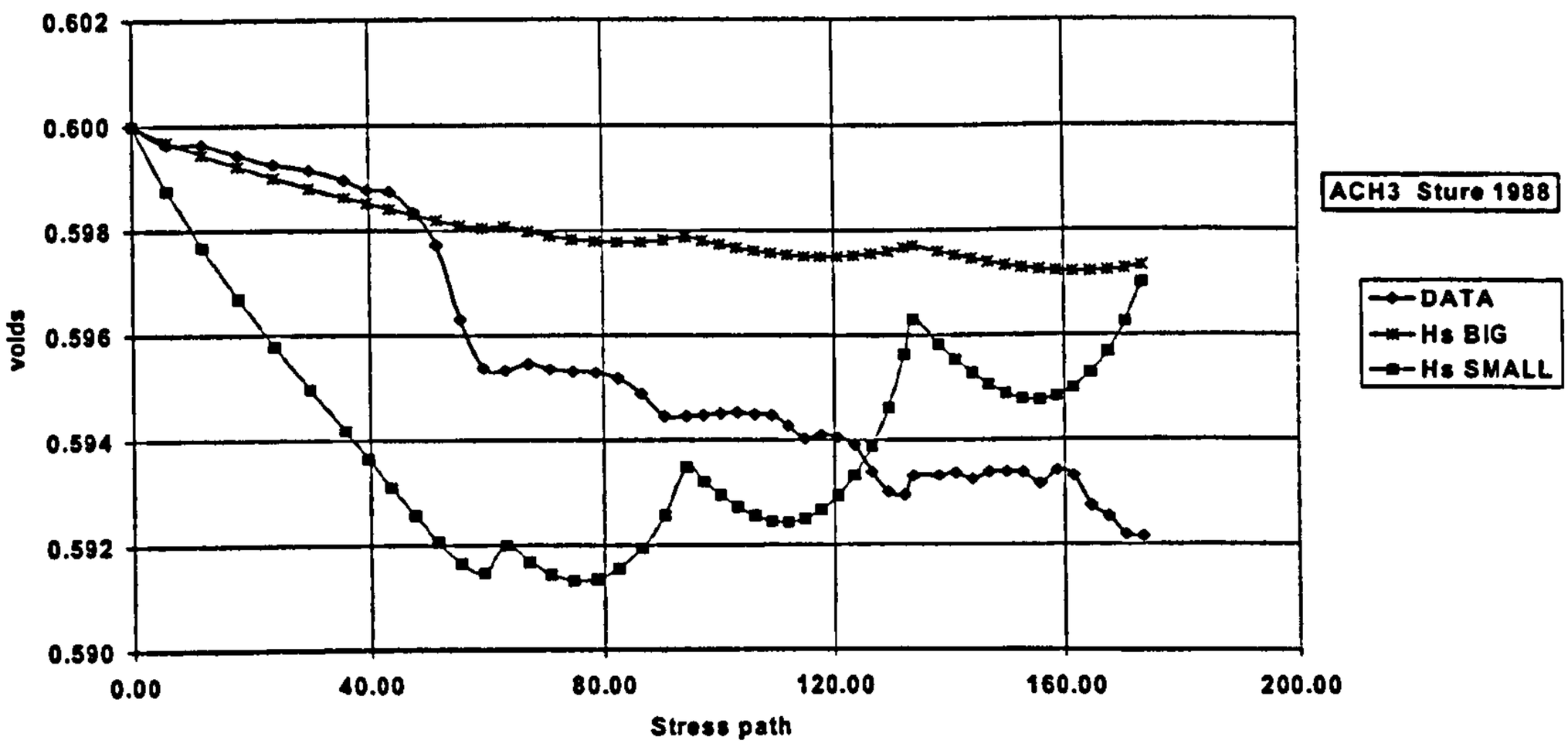

Figure 13-18 Parameter choice: effects on global volumetric behaviour

14 REFERENCES

Achenbach, J.D. (1973) "Wave propagation in elastic solids" North-Holland

Aime, J.C. & Brissaud, M. (2001) "Spatial analysis of torsional wave propagation in a cylindrical waveguide. Application to magnetostrictive generation" J. Acoust. Soc. Am. Vol 109 No.1 pp 51-58

Alajawi, H.A. (1986) "Behaviour of sand under multiaxial load histories" MSc thesis Department of Civil, Environmental and Architectural Engineering University of Colorado at Boulder

Alajawi, H., Alawi, M., Ko, H.-Y., Sture, S., Peters, J.F. & Wood, D.M. (1989) "Experimental observations of anisotropy in some stress controlled tests on dry sand" in IUTAM/ICM Symposium on Yielding, Damage and Failure of Anisotropic Solids J.P. Boehler ed.

Alawi, M. (1988) "Experimental and analytical modeling of sand behavior under nonconventional loading" PhD thesis Department of Civil, Environmental and Architectural Engineering University of Colorado at Boulder

Alleyne, D.N. & Cawley, P. (1992) "Optimization of Lamb wave inspection techniques" NDT & E International, Vol 25, No 1, 11-22

Al-Hunaidi, M.O. (1994) "Analysis of dispersed multi-mode signals of the SASW method using the multiple filter/crosscorrelation technique" Soil Dynamics and Earthquake Engineering 13, 13-24

Aki, K. & Richards, P.G. (1980) "Quantitative seismology: theory and methods" W.H. Freeman & Co. San Francisco

Anderson, O. L. & Liebermann, R.C. (1968) "Sound velocities in rocks and minerals: experimental methods, extrapolations to very high pressures, and results" Physical Acoustics, Volume IVB, 330-466

Argawal, T. K. (1991) "Micromechanics of granular materials and its relation to wave velocity" PhD thesis, Old Dominion University

Aristégui, C. & Baste, S. (1997) "Optimal recovery of the elasticity tensor of general anisotropic materials from ultrasonic velocity data" J. Acoust. Soc. Am. Vol 101, No 2, 813-833

Arulnathan, R., Boulanger, R.W. & Riemer, M.F. (1998) "Analysis of bender element tests" ASTM Geotechnical Testing Journal, Vol. 21, No. 2, 120-131

Askeland, D. R. (1996) "The science and engineering of materials" 3rd S.I. ed London Chapman & Hall

Atkinson, J.H. (2000) "Non-linear soil stiffness in routine design" Géotechnique, Vol. 50, No.5, pp 487-508

Auld B.A. (1973) "Acoustic fields and waves in solids " A Wiley-Interscience publication.

Backus, G.E. (1965) "Possible forms of seismic anisotropy of the uppermost mantle under oceans", J. Geophys. Res. 70, 3429-3439

Balmer, L. (1991) "Signals and systems: an introduction" Prentice Hall

Bates, C.R. & Philips, D.R. (2000) "Multicomponent seismic surveying for near surface investigations: examples from central Wyoming and southern England" Journal of Applied Geophysics, 44, 257-273

Bauer, E. (1997) "An objective description of critical states in hypoplasticity" in Akira, A., Adachi, T. & Oka, F. "Deformation and progressive failure in geomechanics" 347-353

Bauer, E. (1996) "Calibration of a comprehensive hypoplastic model for granular materials" Soils & Foundations Vol.36 No1, 13-26

Bedford, A. & Drumheller, D.S. (1994) "Introduction to elastic wave propagation" John Wiley & Sons

Bellotti, R., Jamiolkowski, M., Lo Presti, D.C.F. & O'Neill, D.A. (1996) "Anisotropy of small strain stiffness in Ticino sand" Géotechnique 46, No 1, 115-131

Bigoni, D. & Loret, B. (1999) "Effects of elastic anisotropy on strain localization and flutter instability in plastic solids" J. Mech. Phys. Solids 47, 1409-1436

Biot, M. (1956a) "Theory of propagation of elastic waves in a fluid saturated porous solid. I. Low frequency range" J. Acoust. Soc. Am. Vol. 28, No 2, 168-178

Biot, M. (1956b) "Theory of propagation of elastic waves in a fluid saturated porous solid. I. High frequency range" J. Acoust. Soc. Am. Vol. 28, No 2, 179-191

Biot, M. (1992) "Acoustics, elasticity and thermodynamics of porous media. Twenty-one papers by M.A. Biot" I. Tolstoy, ed. Acoustical Society of America

Blackstock, D.T. (2000) "Fundamentals of physical acoustics" Wiley-Interscience

Blewett, J., Blewett, I.J. & Woodward, P.K. (2000) "Phase and amplitude responses associated with the measurement of shear-wave velocity in sand by bender-elements" Canadian Geotechnical Journal, Vol. 37, No. 6, 1348-1357

Blewett, J., Blewett, I.J. & Woodward, P.K. (1999) "Measurement of shear-wave velocity using phase-sensitive detection techniques" Canadian Geotechnical Journal, Vol. 36, 934-939

Bodare, A. & Massarsch, K.R. (1984) "Determination of shear wave velocity by different cross hole methods" Proc. 8th WCEE, vol.III, 39-45, San Francisco

Boehler, J.P. & Sawczuk, A. (1977) "On yielding of oriented solids" Acta Mechanica 27, 185-206

Boehler, J.P. (1979) "A simple derivation of representations for non-polynomial constitutive equations in some cases of anisotropy" ZAMM 59, 157-167

Boehler, J.P. (ed.) (1987) "Applications of tensor functions in solid mechanics" CISM Series 292 Springer-Verlag

Boehler, J.P., El-Aoufi, L. & Raclin, J. (1987) "On experimental testing methods for anisotropic materials" Res. Mechanica 21, 73-95

Bolt, B.A. (ed.) (1974) "Seismology, surface waves and earth oscillations" Methods in computational physics v. 11 Academic Press

Bonnet, M. (1995) "Boundary integral equation methods for solids and fluids" John Wiley, Chichester

Boulanger, R.W., Arulnatham, R., Harder, L.F., Torres, R.A. & Driller, M.W. (1998) "Dynamic properties of Sherman Island peat" JGE, ASCE, Vol.124, No.1, 12-20

Bourne, D.E. & Kendall P.C. (1992) "Vector analysis and cartesian tensors" 3rd ed. London Chapman & Hall

BRE (1987) "Assessment of deformation properties . Stage 2: Milestone 2 report" Unpublished report

Brocanelli, D. & Rinaldi, V. (1998) "Measurement of low-strain material damping and wave velocity with bender elements in the frequency domain" Canadian Geotechnical Journal, Vol. 35, 1032-1040

Brigham, E.O. (1988) ""The fast Fourier transform and its applications" Prentice-Hall

Brignoli, E.G.M., Gotti, M. & Stokoe, K.H. (1996) "Measurement of shear waves in laboratory specimens by means of piezoelectric transducers" ASTM Geotechnical Testing Journal, Vol. 19, No. 4, 384-397

Brillouin, L. (1960) "Wave propagation and group velocity" Academic Press, New York

Burland, J.B. (1989) "Small is beautiful" –the stiffness of soils at small strains Can. Geotech. J. 26, 499-516

Casagrande, A. & Carrillo, N. (1944) "Shear failure of anisotropic materials" Proc. Boston Soc. Civ. Engrs. 31, 74-87

Chotiros, N.P. (1995) "Biot model of sound propagation in water-saturated sand" J. Acoust. Soc. Am. Vol.97 No.1 pp 199-214

Christensen, R.M. (1971) "Theory of viscoelasticity: an introduction" Academic Press, New York

Collins, S.A. & Bachus, R.C. (1988) "Use of hypoelasticity to model the behaviour of sands" in Saada & Bianchini (eds.) Constitutive Equations for Granular non Cohesive Soils, pp 201-236 Balkema

Collins, I.F. & Houlsby, G.T. (1997) "Application of thermomechanical principles to the modelling of geotechnical materials" Proc. R. Soc. Lond. A, 453, 1975-2001

Conolly, T.M. & Kuwano, R. (1999) "The measurement of G_{MAX} in a resonant column, bender element, torsional shear apparatus" in Jamiolkowski, Lancellotta & Lo Presti, *Pre-failure deformation characteristics of geomaterials. IS Torino'99* Balkema 73-80

Cowin, S.C. (1985) "The relationship between the elasticity tensor and the fabric tensor" Mechanics of Materials, Vol 4, 137-147

Crampin, S. (1999) "Calculable fluid-rock interactions" Journal of the Geological Society, London, Vol. 156, 501-514

Crampin, S. (1994) "The fracture criticality of crustal rocks" Geophys. J. Int. 118, 428-438

Crampin, S. (1984) "An introduction to wave propagation in anisotropic media", Geophysical Journal of the Royal Astronomical Society, 76, 17-28

Crampin, S. (1981) "A review of wave-motion in anisotropic and cracked elastic-media" Wave Motion, Vol 3, 343-391

Crampin, S. (1977) "A review of the effects of anisotropic layering on the propagation of seismic waves", Geophysical Journal of the Royal Astronomical Society, 49, 9-27

Crandall, S.H. (1970) "The role of damping in vibration theory" J. Sound Vib. Vol. 11, No. 1, 3-18

Dafalias, Y.F. (1986) "Bounding surface plasticity I: Mathematical Foundation and Hypoplasticity" ASCE JEM Vol. 112, No9, 967-987

Darve, F. (1987) "L'écriture incrementale des lois rhéologiques et les grandes classes de lois de comportement" in "Manuel de rhéologie des géomatériaux" F. Darve (ed.), 129-152, Presses des Ponts et Chaussées

Degtyar, A.D. & Rokhlin, S.I. (1997) "Comparison of elastic constant determination in anisotropic materials from ultrasonic group and phase velocity" J. Acoust. Soc. Am. Vol.102 No.6 pp 3458-3466

Di Benedetto, H. (2001) Personal communication

Di Benedetto, H., Geoffroy, H., Sauzéat, C. & Cazacliu, B. (1999) "Sand behavior in very small to medium strain domains" " in Jamiolkowski, Lancellotta & Lo Presti, *Pre-failure deformation characteristics of geomaterials. IS Torino'99* Balkema 89-96

Di Benedetto, H., Cazacliou, B., Boutin, C., Doanh,T. & Touret, J.P. (1997) "Comportement des sables avec rotation d'axes: nouvel appareil couvrant quatre decades de déformation" Proc. XIV ICSMFE, Hamburg, Vol. 1 279-282

Dominguez, J. (1993) "Boundary elements in dynamics" Elsevier applied science.

Doyle, J.F. (1989) "Wave propagation in structures" Springer-Verlag, New York

Duncan, J.M. & Chang, C.-Y. (1970) "Nonlinear analysis of stress and strain in soils" J. Soil. Mech. Found. Div. ASCE, Vol 96, No 5, 1629-1653

Dyvik, R. & Madshus, C. (1985) "Lab measurement of G_{max} using bender elements" in *Advances in the art of testing soils under cyclic conditions*, ASCE, New York, 186-196

Dziewonski, A.M. & Hales, A.L. (1972) "Numerical analysis of dispersed seismic waves" in Methods in computational physics, Vol. 11 Seismology: surface waves and earth oscillations, Bolt, B.A. ed. Academic Press, New York

Elices, M. & García-Moliner, F. (1968) "Wave packet propagation and frequency-dependent internal friction" Physical Acoustics, VolumeV, 163-220

Every, A.G. (1994) "Determination of the elastic constants of anisotropic solids" NDT & E International, Volume 27, No 1, 3-10

Every, A.G., Kim, K.Y. & Maznev, A.A. (1997) "The elastodynamic response of a semi-infinite anisotropic solid to sudden surface loading" J. Acoust. Soc. Am. 102 (3), 1346-1355

Ewins, D.J. (2000) "Modal testing: theory, practice and application" 2nd Ed. Research Studies Press, Baldock, England

Fioravante, V., Jamiolkowski, M., Lo Presti, D.C.F., Manfredini, G. & Pedroni, S. (1998) "Assessment of coefficient of earth pressure at rest from shear wave velocity measurements" Géotechnique 48, No 5,657-666

Foti, S. (2000) "Multistation methods for geotechnical characterization using surface waves" PhD Politécnico di Torino

Fratta, D. & Santamarina, J.C. (1996) "Wave propagation in soils: multi-mode, wide-band testing in a waveguide device" ASTM Geotechnical Testing Journal, Vol. 19, No. 2, pp 130-140

Gajo, A. (1995) "Influence of viscous coupling in propagation of elastic waves in saturated soil" ASCE J. Geoth. Eng., Vol. 121, No 9, 636-644

Gajo, A. (1996) "The effects of inertial coupling in the interpretation of dynamic soil tests" Géotechnique, Vol. 46, No 2, 245-257

Gajo, A., Fedel, A. & Mongiovi, L. (1997) "Experimental analysis of the effects of fluid-solid coupling on the velocity of elastic waves in saturated porous media" Géotechnique, Vol. 47, No 5, 993-1008

Gajo, A. & Mongiovi, L. (1994) "The effects of measure accuracy in the interpretation of dynamic tests on saturated soils" in *Shibuya, Mitachi & Miura (eds) Pre-failure deformation characteristics of geomaterials, 163-168 IS Sapporo'94* Balkema

George, D. & Mallery, P. (2000) "SPSS for Windows, step by step" 2nd Ed. Allyn & Bacon

Goddard, J.D. (1990) "Nonlinear elasticity and pressure-dependent wave speeds in granular media" Proc. R. Soc. Lond. A Vol 430, 105-131

Graff, K.F. (1975) "Wave motion in elastic solids" Clarendon Press, Oxford

Graham, J. & Houlsby, G.T. (1983) "Anisotropic elasticity of a natural clay" Géotechnique Vol. 33, No 2, 165-180

Greening, P. (2001) Personal communication

Gudehus, G. (1996) "A comprehensive constitutive equation for granular materials" Soils & Foundations, Vol. 36, No 1, 1-12

Gutierrez, M. & Lacasse, S. (1991) "Comment on the postulate of three plane strain mechanisms" IJNAMG, vol 15, 809-816

Hampton, L. (ed.) (1974) "Physics of sound in marine sediments" Marine Science 1, Plenum Press, New York

Hansen, J.B. & Gibson, R.E. (1948) "Undrained shear strenghts of anisotropically consolidated clays" Gèotechnique, Vol 1, No 3, 189-204

Hardin, B.O. & Richart, F.E. (1963) "Elastic wave velocities in granular soils" ASCE Journal of the Soil Mechanics and Foundations Division. Vol. 89, No. 1, 33-65

Hardin, B.O. & Blandford, G.E. (1989) "Elasticity of particulate materials" ASCE Journal of Geotechnical Engineering. Vol. 115, No. 6, 788-805

Herle, I (1997) "Estimation of material parameters in hypoplasticity" Lecture notes

Herle, I. & Tejchman, J. (1997) "Effects of grain size and pressure level on bearing capacity of footings in sand" in Akira, S. Asaoka, A. Adachi, T. & Oka, F. "Deformation & progressive failure in geomechanics" Balkema

Herle, I. (1999) Personal communication

Hickey, C.J. & Sabatier, J.M. (1997) "Choosing Biot parameters for modelling water-saturated sand" J. Acoust. Soc. Am. 102 (3), 1480-1484

Hitchings, D. (ed.) (1992) "A finite element dynamics primer" NAFEMS, Glasgow

Hoque, E. & Tatsuoka, F. (1998) "Anisotropy in elastic deformation of granular materials" Soils & Foundations, Vol 38, No. 1, 163-179

Houlsby, G.T. (1985) "The use of a variable shear modulus in elastic-plastic models for clays" Computers and Geotechnics, Vol 1, 3-13

Huot, F. (1999) "Caractéristiques élastiques des sols. Du comportement pseudo-statique à la propagation des ultrasons" Thése de doctorat, Université de Lausanne, Faculté des Sciences

Hutchins, D.A. & Hayward, G. (1990) "Radiated fields of ultrasonic transducers" Physical Acoustics, VolumeXIX, 1-81

Imposimato, S. (1998) "Il ruolo della variabile temporale nel comportamento meccanico delle sabbie sciolte" PhD, Politecnico di Milano, Departamento di Ingegnieria Strutturale

Imposimato, S. & Nova, R. (1998) "An investigation on the uniqueness of the incremental response of elastoplastic models for virgin sand" Mech. of cohesive-frictional materials Vol.3, No1, 65-89

Jamiolkowski, M., Lancellotta, R. & Lo Presti, D. (1999) "Pre-failure deformation characteristics of geomaterials. IS Torino'99" Balkema

Jamiolkowski, M., Lancellotta, R. & Lo Presti, D.C.F. (1995) "Remarks on the stiffness at small strains of six Italian clays" in *Shibuya, Mitachi & Miura (eds) Pre-failure deformation characteristics of geomaterials, 817-836 IS Sapporo '94* Balkema

Jardine, R.J., Kuwano, R., Zdravkovic, L. & Thornton, C. (1999) "Some fundamental aspects of the pre-failure behaviour of granular soils" Preprints of the Second International Symposium on Pre-failure Deformations Characteristics of Geomaterials. Keynote and Theme Lectures. pp 208-236

Jardine, R.J., Symes, M.J. & Burland, J.B. (1984) "The measurement of soil stiffness in the triaxial apparatus", Geotechnique 34, No.3, 323-340

Jefferies, M.G. (1993) "Nor-Sand: a simple critical state model for sand" Geotechnique 43, No 1, 91-103

Jeremic, B. & Sture, S. (1997) "Implicit integration in elastoplastic geotechnics" MCFM, Vol 2, 165-183

Joer, H.A., Lanier, J. & Fahey, M. (1998) "Deformation of granular materials due to rotation of principal axes" Geotechnique 48, No 5, 605-619

Johnson, D.L. & Plona, T.J. (1982) "Acoustic slow waves and the consolidation transition" J. Acoust. Soc. Am. Vol.72 No.2 pp 556-565

Johnson, D.L., Koplik, J. & Dashen, R. (1987) "Theory of dynamic permeability and tortuosity in fluid-saturated porous media" J. Fluid Mech. vol. 176, 379-402

Johnson, D.L., Hemmick, D.L. & Kojima, H. (1994) "Probing porous media with first and second sound. I. Dynamic permeability" J. Acoust. Soc. Am. Vol.76 No.1 pp 104-114

Jordan, C.R.J. & Jordan, D.A. (1994) "Groups" Edward Arnold

Jovicic, V. (1997) "The measurement and interpretation of small strain stiffness of soils" PhD Thesis The City University

Jovicic, V., Coop, M.R. & Simic, M. (1996) "Objective criteria for determining G_{max} from bender element tests" Géotechnique 46, No 2, 357-362

Jovicic, V. & Coop, M.R. (1999) "The influence of state on the very small strain stiffness of sands" in Jamiolkowski, Lancellotta & Lo Presti, *Pre-failure deformation characteristics of geomaterials. IS Torino'99* Balkema 175-181

Kim, D.S., Stokoe, K.H. & Roesset, J.M. (1991) "Characterization of material damping of soils using resonant column and torsional shear tests" Soil dynamics and earthquake engineering V, Karlsruhe, Computational Mechanics Publications, pp. 189-200

Kim, K.Y. (1994) "Analytical relations between the elastic constants and the group velocity in an arbitrary direction of symmetry planes of media with orthorhombic or higher symmetry" Physical Review B, Vol. 49, No.6, 3713-3724

Kim, K.Y., Sribar, R. & Sachse, W. (1995) "Analytical and optimization procedures for determination of all elastic constants of anisotropic solids from group velocity data measured in symmetry planes" J. Appl. Phys. 77, (11), 5589-5600

Kolbuszewski, J. and Frederick, M.R. (1963) "The significance ofparticle shape and size on the mechanical behaviour of granular materials" Eur. Conf. Soil Mech. Found. Eng., Wiesbaden, 253-263

Kolsky, H. (1953) "Stress waves in solids" Oxford University Press

Kolymbas, D. (1998) Personal communication

Kolymbas, D. (1989) "Generalised hypoelastic constitutive equation" in Saada & Bianchini (eds.) Constitutive Equations for Granular non Cohesive Soils, pp 349-367 Balkema

Kolymbas, D., Herle, I. & Von Wolffersdorff, P.A. (1995) "Hypoplastic constitutive equation with internal variables" IJNAMG vol 19, 415-436

Krajcinovic, D. (1998) "Selection of damage parameter – Art or science?" Mechanics of Materials 165-179

Kramer, S.L. (1996) "Geotechnical earthquake engineering" Prentice Hall

Krautkramer, J. & Krautkramer, H. (1990) "Ultrasonic testing of materials" 4th ed. Springer-Verlag

Krzanowski, W.J. (1998) "An introduction to statistical modelling" Arnold

Kuwano, R. (1999) "The stiffness and yielding anisotropy of sand" PhD Univesity of London. Imperial College of Science, Technology & Medicine.

Lade, P.V. & Nelson, R.E. (1987) "Modelling the elastic behaviour of granular matrerials" IJNAMG, Vol 11, 521-542

Landesman, E.M. & Hestenes, M.R. (1992) "Linear algebra for mathematics, science, and engineering" Prentice-Hall

Lee, N.K.J. (1993) "Experimental study of body wave velocities in sand under anisotropic conditions" PhD Thesis University of Texas at Austin

Lekhnitskii, S.G. (1963) "Theory of elasticity of an anisotropic elastic body" Holden Day, San Francisco

Liao, C.L., Chan, T.C., Suiker, A.S.J. & Chang, C.S. (2000) "Pressure dependent elastic moduli of granular assemblies" Int. J. Numer. Anal. Meth. Geomech., Vol. 24, 265-279

Lighthill, J. (1978) "Waves in fluids" CUP

Lings, M.L. (2001) "Drained and undrained anisotropic elastic stiffness parameters" Geotechnique 51, No 6, 555-565

Lings, M.L., Pennington, D.S. & Nash, D.F.T. (2000) "Anisotropic stiffness parameters and their measurements in a stiff natural clay" Geotechnique 50, No 2, 109-125

Love A.E.H. (1927) "A treatise on the mathematical theory of elasticity" 4th ed. Cambridge University Press

Lo Presti, D.C.F., Pallara, O., Jamiolkowski, M. & Cavallaro, A. (1999) "Anisotropy of small strain stiffness of undisturbed and reconstituted clays" in Jamiolkowski, Lancellotta & Lo Presti, *Pre-failure deformation characteristics of geomaterials. IS Torino '99* Balkema 3-10

Lo Presti, D.C.F., Shibuya, S. & Rix, G. J. (1999) "Innovation in soil testing" Proc. IS Torino 99

Lowe, M.J.S., Challis, R.E. & Chan, C.W. (2000) "The transmission of Lamb waves across adhesively bonded lap joints" J. Acoust. Soc. Am. Vol 107 No.3 pp 1333-1345

Lynn, P.A. (1989) "An introduction to the analysis and processing of signals. " 3rd Ed. Macmillan Education

Lynn, P.A. & Fuerst, W. (1994) "Introductory digital signal processing. Revised Edition" John Wiley & Sons. Chichester

Mancuso, C., Simonelli, A.L. & Vinale, F. (1989) "Numerical analysis of in situ S-wave measurements" Proc. 12th ICSMFE, Rio de Janeiro, Vol. 3, 277-280

Malvern, L.E. (1969) "Introduction to the mechanics of a continuous medium" Prentice -Hall

Mason, W.P. (1958) "Physical acoustics and the properties of solids" Van Nostrand

McKenna, J. & Simpkins, P.G. (1985) "Modal solutions, symmetry properties and orthogonality conditions for elastic waves in cylinders" J. Acoust. Soc. Am. Vol 78 No.5 pp 1675-1683

McSkimin, H.J. (1956) "Propagation of longitudinal waves and shear waves in cylindrical rods at high frequencies" J. Acoust. Soc. Am. Vol 28 No.3 pp 484-494

Meeker, T.R. & Meiztler, A.H. (1963) "Guided wave propagation in elongated cylinders and plates" Physical Acoustics, W. Mason ed. Vol.1A pp 112-166

Miklowitz, J. (1978) "The theory of elastic waves and waveguides" North Holland Amsterdam

Mitchell, J.K. (1991) "Fundamentals of soil behaviour" John Wiley

Moncaster, A. (1997) "The shear modulus of sand at very small strains" MSc thesis University of Bristol

Morgan Matroc Ltd (1999) "Characteristics of bimorph transducers"

Morochnik, V. & Bardet, J.P. (1996) "Viscoelastic approximation of poroelastic media for wave scattering problems" Soil Dyn. Earth. Eng. Vol. 15, 337-346

Moulin, E., Assaad, J. & Delebarre, C. (2000) "Modeling of Lamb waves generated by integrated transducers in composite plates using a coupled finite element-normal modes expansion method" J. Acoust. Soc. Am. Vol.107 No.1 pp 87-94

Moussatov, A., Guillon, L., Ayrault, C. & Castagnède, B. (1998) "Experimental study of the dispersion of ultrasonic waves in sandy sediments" C.R. Acad. Sci. Paris, Vol. 326, Serie II b, 433-439

Muhunthan, B., Masad, E. & Assaad, A. (2000) "Measurement of uniformity and anisotropy in granular materials" ASTM Geotechnical Testing Journal, Vol. 23, No. 4, 423-431

Mullenger, G. & Davis, R.O. (1981) "A unified yield criterion for cohesionless granular materials" IJNAMG Vol. 5, 285-294

Musgrave, M.J.P. (1970) "Crystal acoustics" Holden Day, San Francisco

Nash, D.F.T. (2000) Personal communication

Nakagawa, K., Soga, K. & Mitchell, J.K. (1996) "Pulse transmission system for measuring wave propagation in soils" JGE, ASCE, Vol.122, No.4, 302-308

Nayfeh, A.H. (1995) "Wave propagation in layered anisotropic media" North Holland

Needham, T. (1997) "Visual complex analysis" OUP

Nemat-Nasser S. & Hori, M. (1999) "Micromechanics: overall properties of heterogeneous materials" 2nd ed. Amsterdam Elsevier

Ng, C.W.W. (1992) "An evaluation of soil-structure interaction associated with a multi-propped excavation" PhD Thesis University of Bristol

Niemunis, A. & Herle, I. (1997) "Hypoplastic model for cohesionless soils with elastic strain range" Mech. of cohesive-frictional materials Vol.2, No4, 145-163

Oda, M. (1972) "Initial fabrics and their relations to mechanical properties of granular material" Soils and Foundations, Vol. 12, No 1, 17-37

Pagano, N.J. & Halpin, J.C. (1968) "Influence of end constraint in the testing of anisotropic bodies" J. of Composite Materials, Vol. 2, No 1, 18-31

Pan, Y.-W. & Dong, J.J. (1999) "A micromechanics-based methodology for evaluating the fabric of granular material" Géotechnique Vol. 49, No. 6, 761-775

Papadakis, E.P. (1990) "The measurement of ultrasonic velocity" Physical Acoustics, Vol XIX, 108-156

Pavlakovic, B. & Lowe, M.J.S. (2000) "Disperse: a system for generating dispersion curves. User's manual" NDT Laboratory. Dept. of Mechanical Engineering. Imperial College, London.

Pavlakovic, B., Lowe, M. & Cawley, P. (1999) "Prediction of reflection coefficients from deffects in embedded bars" Review of Progress in Quantitative Nondestructive Evaluation, Vol 18, 207-214

Pennington, D.S. (1999) "The anisotropic small strain stiffness of Cambridge Gault clay" PhD Thesis University of Bristol

Pialucha, T., Guyott, C.C.H. & Cawley, P. (1989) "Amplitude spectrum method for the measurement of phase velocity" Ultrasonics, Vol 27, 9, 270-279

Pickering, D.J. (1970) "Anisotropic elastic parameters for soil" Geotechnique 20, No 3, 271-276

Pollard, H.F. (1977) "Sound waves in solids" Pion

Prasad, M. & Meissner, R. (1992) "Attenuation mechanisms in sands: laborathory versus theoretical (Biot) data" Geophysics, Vol 57, No 5, 710-719

Press, W.H., Teukolsky, S.A., Vetterling, W.T. & Flannery, B.P. (1992) "Numerical recipes in Fortran 77. The art of scientific computing" 2nd Ed CUP

Rampello, S., Viggiani, G. & Amorosi, A. (1997) "Small-strain stiffness of reconstituted clay compressed along constant triaxial effective stress ratio paths" Géotechnique 47, No 3, 475-491

Richart, J.E. (1978) "Field and lab measurements of dynamic soil properties" in *B. Prange(ed.) Dynamic response and wave propagation in soils* A.A.Balkema

Roddeman, D. (1998) "A time integration method for hypoplasticity" Unpublished report

Rowe, P.W. (1971) "Theoretical meaning and observed values of deformation parameters for soils", Proc. Roscoe Memorial Symp. Stress-strain behaviour of soils, pp. 143-194

Roy, D. & Campanella, G. (1997) Discussion on Schanz, T. & Vermeer, P.A. (1996) "Angles of friction and dilatancy of sand" Géotechnique, Vol. 47, No. 4, 887-892

Saada, A. (1970) "Testing of anisotropic clay soils" JSMFD, ASCE, SM5, 1847-1852

Saada, A. & Puccini, P. (1989) "The development of a data base using the Case hollow cylinder apparatus" in Saada & Bianchini (eds.) Constitutive Equations for Granular non Cohesive Soils, pp 33-41 Balkema

Sachse, W. & Pao, Y.-H. (1978) "On the determination of phase and group velocities of dispersive waves in solids" J. Appl. Phys. Vol. 49, No 8, 4320-4327

Sáez, A. & Dominguez, J. (2000) "Far field dynamic Green's functions for BEM in transversely isotropic solids" Wave Motion, 32, 113-123

Sánchez-Salinero, I., Roesset, J.M. & Stokoe, K.H. (1986) "Analytical studies of body wave propagation and attenuation" (Geotechnical Engineering Report No GR86-15) Civil Engineering Department. University of Texas at Austin

Santamarina, J.C. & Cascante, G. (1996) "Stress anisotropy and wave propagation: a micromechanical view" Can. Geotech. J. Vol.33 770-782

Serrano, A.A. & Rodríguez-Ortiz, J.M. (1973) "A contribution to the mechanics of heterogeneous granular media" Proc. Symp. Plasticity and Soil Mechanics, Cambridge

Schanz, T. & Vermeer, P.A. (1996) "Angles of friction and dilatancy of sand" Géotechnique, Vol. 46, No. 1, 145-151

Schreiber, E., Anderson, O.L. & Soga, N. (1973) "Elastic constants and their measurements" McGraw-Hill

Schultheiss, P.J. (1983) "The influence of packing structure on seismic wave velocities in sediments" Marine Geological Report No. 83/1 University College of North Wales

Shatilo, A.P. (1992) "Seismic phase unwrapping: methods, results, problems" Geophysical prospecting, Vol. 40, pp 211-225

Sheriff, R.E. & Geldart, L.P. (1982) "Exploration seismology" CUP

Shibuya, S. Mitachi, T. & Miura, S. (eds) (1994) "Pre-failure deformation characteristics of geomaterials" International Symposyum Sapporo'94 Balkema

Shibuya, S., Tatsuoka, F., Abe, F. , Kim, Y.S., Park,C.S. & Mukabi, J.N. (1991) "A new look at stress-strain relations for soils and soft rocks" Proceedings 9th ARCSMFE Vol. 1, 63-66

Shirley, D.J. (1978) "An improved shear wave transducer" J. Acoust. Soc. Am. Vol. 63, No.5, 1643-1645

Shirley, D.J. & Hampton, L.D. (1978) "Shear wave measurements in laboratory sediments" J. Acoust. Soc. Am. Vol. 63, No.2, 607-613

Silvia, M.T. & Robinson, E.A. (1979) "Deconvolution of geophysical time series in the exploration for oil and natural gas" Developments in petroleum science 10. Elsevier

Simmons, G. (1964) "Velocity of shear waves in rocks to 10 kilobars, 1" Jounal of geophysical research, Vol. 69, No.6, 1123-1130

Sittig, E.K. & Coquin, G.A. (1970) "Visualization of plane strain vibration modes of a long cylinder capable of producing sound radiation" J. Acoust. Soc. Am. Vol. 48, No.5, 1150-1159

Smeulders, D.M.J., Eggels, R.L.G.M. & van Dongen, M.E.H. (1992) "Dynamic permeability: reformulation of theory and new experimental and numerical data" " J. Fluid Mech. vol. 245, 211-227

Spencer, A.J.M. (1980) "Continuum mechanics" Longman

Stephenson, R.W. (1978) "Ultrasonic testing for determining dynamic shear moduli" in *ASTM Symposium: Dynamic geotechnical testing* 179-196

Stewart, I. & Golubitsky, M. (1992) "Fearful symmetry" Penguin Books

Stokoe, K.H., Hwang, S.K., Lee, J.N.-K. & Andrus, R.D. (1995) "Effects of various parameters on the stiffness and damping of soils at small to medium strains" in *Shibuya, Mitachi & Miura (eds) Pre-failure deformation characteristics of geomaterials. IS Sapporo '94* Balkema

Stoll, R.D. & Brian, G.M. (1969) "Wave attenuation in saturated sediments" J. Acoust. Soc. Am. Vol. 47, No 5, 1440-1447

Sture, S., Alawi, M.M. & Ko, H.-Y. (1988) True triaxial and directional shear cell experiments on dry sand.

Tatsuoka, F. (1999) "Small strain behaviour of granular materials" in "Mechanics of granular materials" M. Oda & K. Iwashita, eds. pp. 299-308 A.A. Balkema, Rotterdam.

Teldorf, W.M., Geldart, L.P. & Sheriff, R.E. (1990) "Applied geophysics" 2nd Ed. CUP

Tizianel, J., Allard, J.F., Castagnède, B., Ayrault, C., Henry, M. & Moussatov, A. (1999) "Transport parameters and sound propagation in air saturated sand" J. App. Physics, Vol. 86, No. 10, 5829-5834

Thomann, T.G. & Hryciw, R.D. (1990) "Laboratory measurement of small strain shear modulus under K_0 conditions" ASTM Geotechnical Testing Journal, Vol. 13, No. 2, 97-105

Thomsen, L. (1986) "Weak elastic anisotropy" Geophysics, Vol 51, No 10, 1954-1966

Thornton, C. (2001) Personal communication

Thurston, R.N. (1978) "Elastic waves in rods and clad rods" J. Acoust. Soc. Am. Vol. 64, No 1, 1-37

Thurston, R.N. (1992) "Elastic waves in rods and optical fibers" J. Sound Vib. Vol 159, No 3, 441-467

Toki, S., Shibuya, S. & Yamashita, S. (1995) "Standardization of laboratory test methods to determine the cyclic deformation properties of geomaterials in Japan" in Pre-failure deformation of geomaterials, Shibuya, Mitachi & Miura (eds), pp 741-783, Balkema

Truesdell, C. (ed.) (1965) "Foundations of elasticity theory" International Science Review Series Gordon & Breach

Turgut, A. (2000) "Approximate expressions for viscous attenuation in marine sediments: relating Biot's "critical" and "peak" frequencies" J. Acoust. Soc. Am. Vol. 108, No 2, 513-518

Udías, A. (1999) "Principles of seismology" Cambridge University Press

Uriel, A. (1992) Personal communication

Uriel, A.O. & Cañizo, L. (1971) "On the elastic anisotropy of soil" Géotechnique, Vol 21, No 3, 262-267

Van der Grinten, J.G.M. & Van Dongen, M.E.H. (1987) "Strain and pore pressure propagation in a water-saturated porous medium" J. Appl. Phys. Vol. 62, No. 12

Veroy, K.L., Wooh, S.-C. & Shi, Y. (1999) "Analysis of dispersive waves using the wavelet transform" Review of Progress in Quantitative Nondestructive Evaluation, Vol 18, 687-694

Viggiani, G. (1992) "Small strain stiffness of fine grained soils", PhD Thesis, The City University

Viggiani, G. & Atkinson, J.H. (1995) "Interpretation of bender element tests" Géotechnique 45, No. 1, 149-154

Viggiani, G. & Atkinson, J.H. (1997) Discussion on "Interpretation of bender element tests" Géotechnique 47, No. 4, 873-877

Wang, C.-Y. & Achenbach, J.D. (1995) Three dimensional time-harmonic elastodynamic Green's functions for anisotropic solids" Proc. R. Soc. Lond. A, 449, 441-458

Wang, L. (1995) "Determination of the ray surface and recovery of elastic constants of anisotropic elastic media: a direct and inverse approach" J. Physics: Condens. Matter, Vol. 7, 3863-3880

Weidner, D.J. (1987) "Elastic properties of rocks and minerals" in *Methods of experimental physics Vol. 24 Geophysics Part A: Laboratory measurements Sammis, C.G. & Henyey, T.L. Eds.* Academic Press

Whitham, G.B. (1974) "Linear and nonlinear waves" John Wiley & Sons

Whitman, R.V. & Lawrence, F.V. (1963) Discussion on "Elastic wave velocities in granular soils" ASCE, Journal of the Soil Mechanics and Foundations Division. Vol. 89, No. 5, 112-118

Wolffersdorff, P.-A. von (1996) "A hypoplastic relation for granular materials with a predefined limit state surface" Mechanics of Cohesive-Frictional Materials, Vol. 1 251-271

Wood, D.M. (1990) "Soil behaviour and critical state soil mechanics" CUP

Wu, W. & Bauer, E. (1994) "A simple hypoplastic constitutive model for sand" IJNAMG vol 18, 833-862

Wu, W. & Niemunis, A. (1996) "Failure criterion, flow rule and dissipation function derived from hypoplasticity" Mech. of cohesive-frictional materials 1, 145-163

Wu, W. & Niemunis, A. (1997) "Beyond failure in granular materials" IJNAMG vol. 21, 153-174ki, K. & Richards, P.G. (1980) "Quantitative seismology: theory and methods" W.H. Freeman & Co. San Francisco

Yamashita, S. & Suzuki, T. (1999) "Young's and shear moduli under different principal stress directions of sand" in Jamiolkowski, Lancellotta & Lo Presti, *Pre-failure deformation characteristics of geomaterials. IS Torino'99* Balkema 149-158

Yimsiri, S. & Soga, K. (2000) "Micromechanics-based stress-strain behaviour of soils at small strains" Géotechnique Vol. 50, No. 5, 559-571

Zeng, X. (1999) "Stress-induced anisotropic G_{max} of sands and its measurement" Journal of Geotechnical and Geoenvironmental Engineering, ASCE, Vol. 125, No. 9, 741-749

Zheng, Q.-S. (1995) "On the roles of initial and induced anisotropies" Parker, D.F. & England, A.H. *IUTAM Symposium on Anisotropy, Inhomogeneity and Nonlinearity in Solid Mechanics*, 57-62

Zheng, Q.-S. (1994) "Theory of representations for tensor functions" ASME Appl Mech Rev vol 47, no 11, 545-587

Zheng, Q.-S. & Boehler, J.P. (1994) "The description, classification and reality of material and physical symmetries" Acta Mechanica 102, 73-89

Zysset, P.K. & Curnier, A. (1995) "An alternative model for anisotropic elasticity based on fabric tensors" Mechanics of Materials 21, 243-250

Zytynski, M., Randolph, M.F., Nova, R. & Wroth, C.P. (1978) "On modelling the unloading-reloading behaviour of soils" IJNAMG Vol 2, 87-94